VIP A B C

Vacuum Insulation Panels
Applied in Building Constructions

Martin Tenpierik

VIP A B C

Vacuum Insulation Panels
Applied in Building Constructions

Proefschrift

ter verkrijging van de graad van doctor
aan de Technische Universiteit Delft,
op gezag van de Rector Magnificus prof. ir. K.C.A.M. Luyben,
voorzitter van het College voor Promoties,
in het openbaar te verdedigen op maandag 1 februari 2010 om 15.00 uur

door
Martinus Johannes TENPIERIK

bouwkundig ingenieur,
geboren te De Bilt

Dit proefschrift is goedgekeurd door de promotor(en):

Prof. ir. J.J.M. Cauberg (Em.)

Copromotor: Dr. ir. W.H. van der Spoel

Samenstelling promotiecommissie:

Rector Magnificus, voorzitter
Prof. (em.) ir. J.J.M. Cauberg, Technische Universiteit Delft, promotor
Dr. ir. W.H. van der Spoel, Technische Universiteit Delft, copromotor
Prof. dr. ir. O.C.G. Adan, Technische Universiteit Eindhoven
Prof. ir. C.S. Kleinman, Technische Universiteit Eindhoven
Prof. (em.) dr.-ing. G.-W. Mainka, Universität Rostock
Prof. dr.-ing. U. Knaack, Technische Universiteit Delft
Dr.-ing. S. Brunner, Eidgenössische Materialprüfungs- und Forschungs-Anstalt

ISBN-10: 90-9024-150-0
ISBN-13: 978-90-9024-150-0

Published by M.J. Tenpierik, Singelstraat 1c, 2613 EM Delft
Printed by Wöhrmann Print Service, Loskade 4, 7202 CZ Zutphen
Layout and cover design: Martin Tenpierik
Image on cover: Remco Looman

Printed in the Netherlands

Voor jullie… mijn ouders Dik en Nini
en mijn allerliefste Karin

“Within a decade, it is going to be next to impossible for a business to be competitive without also being ‘eco-efficient’ – adding more value to a good or service while using fewer resources and releasing less pollution.”

Stephan Schmidheiney, Changing Course, 1992

Chaos theory “says that complex and chaotic systems - which means most of the systems we encounter in nature and in society - cannot accurately be predicted or exclusively controlled. Neither can rigid systems be easily budged. However, there's a loophole. What if we acted through the myriad tiny feedback loops that hold a society together? Chaos tells us that each one of us has an unrecognized but enormous influence on these loops. Chaos suggests that although we may not have power of the controller in the traditional sense, we all possess the ‘butterfly power’ of subtle influence.”

John Briggs and David Peat, Seven Life Lessons of Chaos, 1999

“Het probleem bij koudebruggen is niet alleen dat er plaatselijk een kleinere warmteweerstand aanwezig is, waardoor door dat gedeelte een groter warmtetransport optreedt. De koudebrug beïnvloedt ook zijn omgeving: vanuit de omgeving wordt warmte naar de koudebrug toegetrokken zodat het uiteindelijke warmteverlies nog groter is dan men in eerste instantie zou denken.”

Kees van der Linden, Bouwfysica, 2000

PREFACE

As everyone who did a doctoral study knows, working on a highly specialised topic for four years or more can be very challenging, both mentally and physically. Fortunately, I had the privilege to do these studies in a very lively and inspiring environment and I could also participate in several national and international research projects. At the start, you do not know how and where to begin. You listen closely to the advice of many people around you and you search along several paths finally leading you to the main road you need to take. During this process, you more and more personalise your studies and you mentally grow until finally you are considered by many to be among the experts in your specific field.

Unfortunately, however, nine months before the expected ending of my studies, fate struck; a fire caused by short-circuiting within a coffee machine entirely devastated the faculty building and consequently my office. Like many colleagues, I lost the results of numerous simulations, many books and my office. Due to the unceasing effort of our section leader, Kees van der Linden, we could temporarily be located in the building of the Faculty of Civil Engineering and Geosciences before finally arriving in our new home the former university headquarters. Fortunately, the head of our university at that time committed himself to personally help every PhD candidate and to raise funds for contract extensions; I was granted another six months to finish my work for which I am very grateful. These additional six months helped me to finish this doctoral study and to be able to present this comprehensive volume concerning the application of VIPs in buildings to you as a reader.

I hope that this dissertation will contribute to the wide-spread proliferation of vacuum insulation panels in the building sector and initiate the development of new, high performance and at the same time more robust thermal insulation materials, as a consequence enabling an energetic performance improvement of our dwellings offices and industrial buildings. By using more sustainable and efficient energy systems in combination with high performance materials, climate responsive building elements and climate adaptive skins, we might be able to increase the amount of new and refurbished carbon neutral buildings with a comfortable and healthy indoor environment. In this respect, this dissertation will hopefully contain knowledge to bring us a step closer to such buildings. Although this step in itself is rather small, a large number of such small steps make one giant leap forward.

As appropriate in a preface, I would finally like to thank several people: Hans Cauberg as promoter and Wim van der Spoel as supervisor for their support to keep me on track and for their fruitful discussions to improve the quality of my work; Olaf Adan, Cees Kleinman, Ulrich Knaack, Georg-Wilhelm Mainka and Samuel Brunner for reading and critically commenting on my dissertation; Hans Simmler, Ulrich

Heinemann, Hubert Schwab, Kumar Kumaran, Phalguni Mukhopadyaya, Daniel Quénard, Markus Erb, Armin Binz, Gregor Steinke, Thomas Thorsell and Gudni Jóhannesson for their pleasant and good co-operation during the IEA ECBCS Annex 39 research project; Harald Reiss for his pleasant co-operation during the EU Craft VACI research project and his support on running numerical simulation with ANSYS software; Roland Caps and Karl-Rudolf Friese for their inspiring co-operation and help during the EU Craft VACI research project; Renz Mets, Odin Visser, Jelle Persoon and Patrick Linthorst for their good and joyful co-operation during the SenterNovem research project into a floor heating system; Gerrit van der Ende for his endless conversations and his everlasting help with experimental work; Peter de Vries, Jan-Willem van der Kuilen, Cees van Kranenburg, Fred Veer and Gerrie Hobbelman for their deep understanding of and help on the mechanical behaviour of materials and structures; Nils Jalving for allowing me to use test equipment from the Faculty of Aerospace Engineering; Frans Biegstraaten for his support on acoustical testing and for allowing me to use the acoustics laboratories of TNO; Harjan Winter and Panelen Holland for their mechanical tests on vacuum insulation panels glued to face sheets using many adhesives; Ray Karbor for his interest in the use of vacuum insulation panels in façade constructions in hot and arid climates; Tillman Klein and Arjan van Timmeren for critically discussing with me the use of vacuum insulation panels in façade systems; Yan Ying and Karel van Went whose graduation work I could use in my own dissertation; Hans Suijkerbuijk and Jakob Fokkema for their moral and financial support after the fire; Martine Swennen for helping me improve my proficiency in English; my colleagues and former colleagues from the department of Building Technology and in specific from the section of Climate Design for their everlasting faith in me and their good fellowship; in particular I would like to thank Remco Looman and Bas Hasselaar - colleagues with whom I shared an office for quite some time - for their support, nice chitchat, fruitful discussions and extra-curricular activities; the ladies from the secretariat of Building Technology for all of their help and small-talk; of course my friends, my parents, my brother, his girlfriend and their children; and most of all my lovely and dearest girlfriend Karin without whose support and faith I could never have completed this work; thanking you here in this way is, seen in the right perspective, just a small token of my gratitude for you; all of you. Thanks!

I would finally like to wish you a pleasant and insightful journey through the depths of this book.

Martin Tenpierik

Delft, 4th of July 2009

SUMMARIES

S

VIPs Applied in Building Constructions: A Summary

Concerns regarding sustainability urge us to reduce greenhouse gas emissions drastically. One significant contributor to these emissions is the burning of fossil fuels to generate power and electricity for buildings. Buildings and building-related processes were responsible for about 40% of primary energy consumption in the European Union in 1997, of which more than half was used for space heating. Besides reduced GHG emissions, a reduction of the energy demand of buildings is important for facilitating the implementation of sustainable and renewable energy sources in the built environment; the power capacity of these sources is insufficient for their current high energy demand.

One way to lower the energy consumption of buildings in use is to reduce heat losses by improving the thermal performance of their enclosure, provided that cooling demands remain limited. Two strategies for this improvement can be followed. First, the thickness of the thermal insulation layer can be increased. Over the last decades, a huge improvement in energy performance of buildings has already been achieved in this way. Thick façade constructions however have many disadvantages: an unfavourable net-to-gross floor space area, an increased complexity of junctions and details, a reduced possibility for designing slender facades and reduced daylight penetration. Second, more effective thermal insulators can be used. One such more effective thermal insulator is a vacuum insulation panel, or abbreviated VIP.

A vacuum insulation panel is a thermal insulation component consisting of a micro-porous core material which is after evacuation tightly sealed into a barrier envelope. The vacuum inside the pores of the core reduces the thermal conductivity of the product significantly, ranging from $2 \cdot 10^{-3}$ to $8 \cdot 10^{-3}$ $W \cdot m^{-1} \cdot K^{-1}$. A VIP of only 20 mm can therefore replace a conventional mineral wool or PU-foam insulation board of 185 mm or 120 mm respectively if thermal bridge effects are neglected. This reduction of thickness is among the most interesting features for large-scale application of vacuum insulation panels in the building industry.

However, integration into the building enclosure must be performed meticulously for several reasons; first, a VIP is to be regarded as a system or component by itself, as a consequence of which it cannot be processed on site and needs careful planning in advance; second, it is very sensitive to mechanical damage thus requiring careful handling during all stages of the building process; third, careful design is required due to thermal bridges along the edges of the panel; and fourth, a decrease of its thermal performance over time needs to be considered, especially for applications with very long lifetimes or in harsh environments.

A vacuum insulation panel thus is a highly complex material of which the properties and behaviour needs to be understood clearly before a successful integration is possible. The principal objectives of this dissertation therefore are:

> *the development of calculation tools and methods regarding thermal, hygrothermal and structural aspects to support designers, engineers, manufacturers and contractors in the process of designing VIP integrated buildings components and constructions;*
>
> *and - based upon these tools and methods - the development of guidelines for a successful integration of vacuum insulation panels in building components and façade constructions regarding thermal, hygrothermal and structural aspects.*

Following from these objectives, the main research question is formulated as

> *How can relevant properties regarding thermal, hygrothermal and structural aspects of vacuum insulation panels (VIPs) be modelled and how and under what conditions can these panels be integrated successfully into building components and constructions?*

To answer this research question several aspects – thermal behaviour, service life and structural behaviour - have been researched on the level of a vacuum insulation panel and a VIP integrated building component. Moreover, three practical cases – EPS encapsulated VIPs, VIP integrated façade systems and a thin component-based floor heating and cooling system - have been studied as design and research cases. In the end this doctoral study resulted in several models and methods for calculating the overall thermal performance of VIPs and VIP integrated façade components, for estimating their service life, and for computing their structural performance under flexion. From these models and the design and research cases, several conclusions were drawn concerning important relations between parameters and concerning guidelines for a good integration of VIPs in buildings.

One important feature of vacuum insulation panels is their finite service life. It is important to realise, though, that after expiry of this service life no sudden damage occurs to the panel; it is just that slowly but gradually the thermal conductivity of its core increases due to ingress of water vapour and dry atmospheric gases and that a certain value of this thermal conductivity is said to indicate the end of life. Most researchers and manufacturers use $8.0 \cdot 10^{-3}$ $W \cdot m^{-1} \cdot K^{-1}$ as critical value for the thermal conductivity of the core. Starting from a thermal conductivity of $4.0 \cdot 10^{-3}$ $W \cdot m^{-1} \cdot K^{-1}$, this means that the service life expires if this thermal conductivity doubles, or in other words if the thermal resistance – not considering thermal edge effects – is reduced by half.

Nowadays, the most common barrier envelope around a vacuum insulation panel is a three-layered metallised polymer film laminate. If fumed silica is used as core, this type of barrier results in a sufficiently long service lifetime of a panel applied in a façade in a temperate Western-European climate, provided that these panels are larger than approximately[1] 0.4x0.3x0.02 m^3. For applications in which the panels are subjected to long-lasting high temperatures such metallised film based laminates would result in a service life too short; for the permeation rate of water vapour and dry atmospheric gases through polymer films exponentially increases with temperature. If however the barrier on the hot side of the panel is replaced by an aluminium foil or stainless steel foil laminate, it was theoretically shown that both a high thermal performance and a high service life can be achieved. For a vacuum insulation panel of 0.5x0.6x0.02 m^3 with a fumed silica core and such a combined barrier used below a floor heating system in operation 50% of a year, for instance, a service life of approximately 64 years was calculated if thermal edge effects are not considered in the calculation scheme.

Based upon mass balance equations and physical models for mass transfer, in this dissertation a method is developed with which dynamic environmental conditions can be included in service life computations. Based on these physical models and experimental data from several research institutes throughout Europe, an approximation equation for estimating the service life of a VIP with a fumed silica core was derived using regression analysis. This latter model is especially useful for design purposes.

As was already known prior to this study, the service life of a vacuum insulation panel is principally determined by the properties of the core, the presence and effectiveness of getters and desiccants, the initial vacuum and water content, degassing of the core and the laminate, the envelope's permeance for atmospheric gases and water vapour, the quality of the seam, the panel's dimensions and the environmental conditions regarding temperature, relative humidity, partial water vapour pressure and air pressure. Since, the first five factors are product-related and can hardly be influenced by architects and building engineers, especially the last two are interesting from the perspective of construction design. The environmental conditions will be discussed here first.

The most important temperature effect is the dependency of the water vapour and gas transmission rate through the barrier envelope on temperature. This effect exhibits an exponential increase for increasing temperature. The most important

[1] As service life of more than 50 years is then theoretically obtained if the Arrhenius average temperature is below 15°C and the relative humidity of the air or the materials surrounding the VIP is near 50%. In practise this relative humidity will be higher as a result of which the service life shorter. This effect might though have a strong effect on the VIP's service life.

relative humidity effect is the dependency of the water vapour and gas transmission rate through the barrier envelope on relative humidity. Here principally also holds that the higher the relative humidity, the higher the transmission rates are. The exact physical mechanisms involved in this dependency are still insufficiently clear for complex multilayered films. The partial water vapour and air pressure surrounding a VIP, finally, increase the driving potential for water vapour and dry gas permeation and thus also influence the service life.

A second important feature of vacuum insulation panels are thermal bridge effects, either caused by the laminate which entirely envelopes the core, by spacers in building components, or by other structural elements. The first and second are linear thermal bridges and can be represented by a linear thermal transmittance which reflects the additional heat flow through this thermal bridge per unit area and per unit temperature difference. As a result, the higher this linear thermal transmittance, the worse the overall thermal performance of a VIP or a building component is.

The linear thermal transmittance caused by a metallised film based laminate around a vacuum insulation panel with a thickness beyond 20 mm can be estimated with sufficient accuracy for design and engineering purposes from the product of the thermal conductivity and thickness of this envelope at the panel's edge divided by the thickness of the core. Thermal edge effects occurring in vacuum insulation panels with a thickness of more than 20 mm and enveloped by a metal foil based laminate can be estimated using the linear thermal transmittance equation presented in this dissertation for a VIP with λ_c =0 $W\cdot m^{-1}\cdot K^{-1}$. For computations required in the early stages of a design and development process, these simplified equations are sufficiently accurate. If higher accuracy is required, if the thickness of a vacuum insulation panel is less than 20 mm or if VIPs are integrated into building components, more advanced models should be used. These models were developed in the framework of this doctoral research as well.

From these models we can learn that the overall thermal performance of vacuum insulation panels or VIP integrated building components, i.e. the thermal performance in which thermal edge effects are accounted for, primarily depends on the thermal conductivity and thickness of the core, the ratio of panel circumference to surface area, l_p/S_p and the linear thermal transmittance resulting from the thermal bridge. For vacuum insulation panels, this linear thermal transmittance again is influenced by the thermal conductivity and thickness of the core, the (weighted average) thermal conductivity and thickness of the barrier envelope on either side and the type and configuration of seams and adjoining air gaps. Similar parameters influence the linear thermal transmittance of the edge of building components with spacers: thickness and thermal conductivity of the core, thermal conductivity and thickness of the face sheets on either side – or thickness weighted average thermal conductivity and total thickness of the combination of face sheet and VIP barrier – the width and thermal conductance of the edge zone.

In general, the overall thermal performance increases for decreasing thermal conductivity and thickness of the envelope and for decreasing thermal conductivity of the core. The influence of panel thickness on overall thermal performance is more complicated. In general, the linear thermal transmittance first increases from zero - or from a certain initial value in case of building components - to a maximum value and then decreases again to zero if panel thickness increases. This peak value mostly lies in the range of VIPs used in practise. An exception to this rule is a panel with a core thermal conductivity of 0 $W \cdot m^{-1} \cdot K^{-1}$.

A third important feature of VIPs applied structurally is their flexural behaviour. From this perspective, vacuum insulation panels can be considered analogously to pre-stressed reinforced concrete. The core of fumed silica is similar to the concrete matrix, the barrier to reinforcement bars and the pressure difference between environment and core to a pre-stress. Using this analogy, the entire flexural behaviour of a vacuum insulation panel with a fumed silica core and a thin film barrier can be modelled. The transitions between separate stages in its structural behaviour under flexion are: buckling of the top laminate, physical failure, yield of the lower laminate, crack formation in the tension zone of the core, up-setting in the compression zone of the core and finally structural failure. Although structural failure is the final stage in the failure process, physical failure, i.e. the formation of (micro-)cracks in the barrier envelope, strongly influences the panel's service life. Moreover, we have seen that the Young's modulus of a vented VIP is much smaller than of an intact VIP. For reasons of safety therefore, either the transition of physical failure or the behaviour of a vented VIP should be taken as limit state, the choice of which depending on which of the two poses the highest restrictions.

Moreover, experimental flexion tests on both intact and vented VIPs showed that the equivalent effective Young's modulus, which is the modulus of elasticity in which shear effects are considered, significantly reduces when a VIP is damaged. For a panel under four-point bending with a thickness of 20 mm, a width of 120 mm, a span of 200 mm and a load-to-support distance of 40 mm, this modulus approximately reduces by half after venting. The exact reduction depends on panel geometry (height and width of the core and thickness of the barrier) and on context (type of loading). This reduction in Young's modulus is caused by the structural inactivity of the laminate in the compression zone in case a VIP is vented; protective measures therefore then need to be in place to prevent a panel from collapsing.

Among the most important parameters that architects, designers and engineers can modify and that influence a component's overall thermal performance, its service life and structural behaviour are its thickness and the ratio of panel circumference to surface area, l_p/S_p.

According to an approximation model for predicting the service life of a fumed silica based vacuum insulation panel derived in this dissertation, a VIP's service life is directly proportional to its thickness, at least for practical building sizes and environmental conditions typical for the built environment; a doubling of its thickness thus results in a doubling of its service life. Besides, according to an approximation equation for calculating the linear thermal transmittance of a vacuum insulation panel with a polymeric or metallised polymer based laminate, such a VIP's overall thermal resistance is also directly proportional to its thickness, at least for a thickness beyond 20 mm; a doubling of its thickness thus results in a doubling of its thermal performance. Moreover, according a model derived for computing the equivalent Young's modulus of a vacuum insulation panel with large height to span ratio, a doubling of panel thickness results in a multiplication of the bending stiffness by a factor 8 ($=2^3$), provided that the thickness of the barrier is negligible compared to the thickness of the core. In practical situations, i.e. for small panel thickness, this multiplication factor may be significantly smaller than 8.

The second parameter influencing the panel's dimensions is the ratio of circumference to surface area l_p/S_p. This ratio also influences the panel's overall thermal performance and its service life. According to the aforementioned approximation model for predicting the service life of a fumed silica based vacuum insulation panel, a VIP's service life is proportional to this ratio to a certain power, at least for practical building sizes and environmental conditions typical for the built environment. This power was determined from a regression analysis on experimental data for two types of barrier envelope and was found to depend on temperature. For a typical three-layer metallised film envelope at 20°C, it was found to be approximately -0.78. This implies that under these conditions a division into half of the ratio l_p/S_p approximately results in an increase of the service life by a factor 1.7. Besides, the influence of the thermal bridge on the panel's overall thermal transmittance is directly proportional to this ratio of panel circumference to surface area. Since the overall thermal transmittance of a vacuum insulation panel or a VIP integrated building component is the sum of the centre-of-panel thermal transmittance and a factor representing this thermal bridge effect, one cannot conclude that the overall thermal resistance is inversely proportional to the ratio of l_p/S_p. But in any case, a decrease of this ratio, i.e. an increase in panel size and/or a decrease in aspect ratio, results in an increase in thermal performance.

Contrary to conventional thermal insulation materials, vacuum insulation panels may thus need to be larger than a certain size – length and width - owing to thermal performance requirements. This minimum size however on the one hand depends on the type of barrier which in turn determines the linear thermal transmittance of the panel's edge, and on the other hand on the performance requirement. This size can be read from surface plots in which the overall U-value is plot against both panel thickness and ratio l_p/S_p. Such plots were created in this dissertation. If for instance the overall U-value of a 40 mm thick vacuum insulation panel with a thermal conductivity of its core of $4.0 \cdot 10^{-3}$ $W \cdot m^{-1} \cdot K^{-1}$ should be limited to 0.2 $W \cdot m^{-2} \cdot K^{-1}$, the ratio of l_p to S_p should not exceed 3.8 m^{-1} – in other words the panel's size should be larger than approximately 0.90x1.25 m^2 – in case a 6 μm thick aluminium foil based barrier without seam is used.

As we have seen in this dissertation, however, it is from a combined thermal and hygrothermal perspective in general more effective and sensible to decrease the ratio of l_p/S_p than to increase the panel's thickness, except for fumed silica based vacuum insulation panels with an envelope of a metallised film based laminate applied in such a way that small thermal bridges are present. This is in accordance with the most promising feature for application of vacuum insulation panels in architectural constructions: their combination of high thermal performance with limited thickness.

To protect vacuum insulation panels against incidental damage during transportation, storage and handling on site, they should preferably be integrated in prefabricated building components. If integrated into such components, a strong relation between structural behaviour and thermal performance may be present. Depending on the type of component, i.e. an edge spacer component or a sandwich component, the structural performance of the system is mainly determined by either the outer face sheet in combination with the spacer along the component's edge or the combined action of face sheets and VIP core. In the first case, a strong spacer is required to connect both face sheets and to transmit external loads towards a secondary load-bearing structure, very often leading to high thermal edge effects. In the second case, however, no structural edge is required, on the one hand resulting in the possibility of improving the overall thermal performance of the panel, but on the other hand imposing additional structural requirements on the vacuum insulation panel itself.

In the case of structural sandwiches, a good, strong and stiff bond between face sheets and VIP barrier laminate needs to be obtained. Even if a perfect bond is obtained, sliding of this laminate over the core material cannot entirely be prevented. Since the effect of this sliding on the formation of (micro-)cracks in the barrier layer and the effect of an adhesive on service life are still unknown, vacuum insulation panels structurally applied in sandwich components subjected to bending should be considered with the highest care. Notwithstanding these issues, VIP integrated sandwich components have the highest potential for creating thin high performance façade components.

Since the application of vacuum insulation panels in sandwich components still involves solving several technical hurdles, since the risk of damage to the barrier envelope is imminent in these components and since vacuum insulation panels glued onto face sheets cannot easily be separated from these face sheets after disposal, edge spacer components might, at least temporarily, be the preferred choice. Since however these components have a high risk of large heat losses through their perimeter, their edge needs to be thermally optimised. The principal designs of two façade components presented in this dissertation showed that the potential of applying vacuum insulation panels in façades can be very high. With a thickness of the insulation layer of only 40 mm and a thickness of an entire component between 43 mm and 85 mm, an overall *U*-value less than 0.15 $W \cdot m^{-2} \cdot K^{-1}$ can be achieved. Even after 25 years the overall *U*-value of these components can be below 0.18 $W \cdot m^{-2} \cdot K^{-1}$.

If for protection a vacuum insulation panel is incorporated in an EPS insulation board, a so-called EPS encapsulated VIP or an EPS covered VIP comes into existence. If such an EPS insulation board has a fixed thickness, a maximum in thermal performance may occur at a certain thickness of the VIP inside, not being the maximum thickness of this VIP. This phenomenon was both observed in complex three-dimensional and in two-dimensional studies into EPS encapsulated VIPs with an envelope containing an aluminium layer thicker than 10 μm and having a core thermal conductivity of $4.0 \cdot 10^{-3}$ $W \cdot m^{-1} \cdot K^{-1}$. It is therefore not always best to increase the thickness of a vacuum insulation panel as much as possible. If however the total thickness of a component is not fixed but increases correspondingly with increasing thickness of the vacuum insulation panel inside, such a maximum in thermal performance does not occur. In these cases, an increased thickness of a vacuum insulation panel results in an increased thermal performance.

Large dimensional tolerances, finally, especially in length and width, should in all architectural applications involving vacuum insulation panels be accounted for. This can be achieved by reserving sufficient space between a panel and its surrounding materials and by subsequent filling of these gaps with a material that has low thermal conductivity and high compressibility (and expandability).

Martin Tenpierik

VIPs TOEGEPAST IN BOUWCONSTRUCTIES: EEN SAMENVATTING

De dreiging van klimaatverandering noodzaakt ons om de uitstoot van broeikasgassen drastisch te verlagen. Een belangrijke bijdrage aan deze emissies wordt geleverd door de verbranding van fossiele brandstoffen voor het genereren van warmte, koude en elektriciteit voor gebouwen. Gebouwen en daarmee verband houdende processen waren verantwoordelijk voor ongeveer 40% van het primaire energiegebruik in de Europese Unie in 1997, waarvan meer dan de helft werd gebruikt voor ruimteverwarming. Naast de verminderde uitstoot van broeikasgassen, is een vermindering van de energievraag van gebouwen belangrijk voor het faciliteren van de toepassing van duurzame en hernieuwbare energiebronnen in de gebouwde omgeving; het vermogen van deze bronnen is immers onvoldoende voor de huidige hoge vraag naar energie.

Een manier om het energiegebruik van gebouwen in hun gebruiksfase te verminderen kan worden gerealiseerd door verbetering van de thermische prestatie van de gebouwomhulling, op voorwaarde dat de koelbehoefte beperkt blijft. Twee strategieën voor deze verbetering kunnen worden gevolgd. In de eerste plaats kan de dikte van de warmte-isolerende laag worden vergroot. In de afgelopen decennia is langs deze weg al een enorme verbetering van de energieprestatie van gebouwen bereikt. Dikke gevelconstructies hebben echter vele nadelen: een ongunstige verhouding van het netto tot het bruto vloeroppervlak, een toegenomen complexiteit van details, een verminderde mogelijkheid voor het ontwerpen van slanke gevels en een gereduceerde daglichttoetreding. In de tweede plaats kunnen effectievere thermische isolatoren worden gebruikt. Een van deze effectievere isolatoren is een zogenaamd vacuümisolatiepaneel, of afgekort VIP.

Een vacuümisolatiepaneel is een thermische isolatiecomponent bestaande uit een micro-poreus kernmateriaal dat na vacuümzuigen wordt ingepakt in een luchtdichte verpakking. Als gevolg van het vacuüm in de poriën van de kern is de warmtegeleidingscoëfficiënt van het product sterk gereduceerd, variërend van $2 \cdot 10^{-3}$ tot $8 \cdot 10^{-3}$ $W \cdot m^{-1} \cdot K^{-1}$. Een VIP van slechts 20 mm is daardoor thermisch gelijkwaardig aan een conventionele minerale wol of PU-schuimen isolatieplaat van 185 mm of 120 mm respectievelijk, mits koudebrugeffecten worden verwaarloosd. Deze diktereductie is een van de meest interessante eigenschappen voor grootschalige toepassing van vacuümisolatiepanelen in de bouwwereld.

Echter, de integratie van deze panelen in gevels van gebouwen dient zorgvuldig te worden uitgevoerd om verschillende redenen; ten eerste, een VIP moet worden beschouwd als een systeem of component op zich, met als gevolg dat het niet kan worden aangepast op de bouwplaats en een zorgvuldige planning vooraf is vereist; ten tweede, een paneel is zeer beschadigingsgevoelig waardoor een zorgvuldige behandeling tijdens alle fasen van het bouwproces vereist is; ten derde, vanwege koudebruggen langs de randen van het paneelis een goed ontwerp vereist; en ten vierde, er dient rekening gehouden te worden met een afname van de thermische prestatie in de tijd, vooral voor toepassingen met een zeer lange levensduur of onder 'agressieve' omgevingscondities.

Een vacuümisolatiepanel is dus een zeer complex materiaal waarvan de eigenschappen en het gedrag moet worden begrepen voordat een succesvolle integratie mogelijk is. De voornaamste doelstellingen van dit proefschrift zijn dus:

> *de ontwikkeling van rekenhulpmiddelen en -methoden ter bepaling van thermische, hygrothermische en constructieve aspecten van vacuümisolatiepanelen en bouwcomponenten met VIPs ter ondersteuning van ontwerpers, ingenieurs, fabrikanten en aannemers gedurende het ontwerpproces;*
>
> *en - op basis van deze instrumenten en methoden - de ontwikkeling van richtlijnen voor een succesvolle integratie van vacuümisolati panelen in bouwcomponenten en gevelconstructies met betrekking tot thermische, hygrothermische en constructieve aspecten.*

Naar aanleiding van deze doelstellingen, volgt de belangrijkste onderzoeksvraag als

> *Hoe kunnen de relevante eigenschappen van vacuümisolatiepanelen (VIPs) met betrekking tot thermische, hygrothermische en constructieve aspecten worden gemodelleerd en hoe en onder welke voorwaarden kunnen deze panelen met succes worden geïntegreerd in bouwelementen en -constructies?*

Om deze onderzoeksvraag te kunnen beantwoorden zijn verschillende aspecten - thermisch gedrag, levensduur en constructief gedrag - onderzocht op zowel het niveau van een vacuümisolatiepanel als een met VIP geïntegreerde bouwcomponent. Bovendien zijn drie concrete gevallen - EPS ingekapselde VIPs, met VIP geïntegreerd gevelsystem en een dun vloerverwarmings- en vloerkoelingsysteem - bestudeerd vanuit het perspectief van ontwerp en onderzoek. Al deze studies hebben geresulteerd in diverse modellen en methoden voor de berekening van de totale thermische prestatie van VIPs en met VIP geïntegreerde gevelcomponenten, voor het schatten van hun levensduur, en voor de berekening van hun constructieve prestaties onder buiging. Op basis van deze modellen en de drie casus zijn diverse conclusies getrokken aangaande verbanden tussen diverse parameters en aangaande richtslijnen voor een goede integratie van de VIPs in gebouwen.

Een eerste belangrijk kenmerk van vacuümisolatiepanelen is hun beperkte levensduur. Het is echter belangrijk te beseffen dat na het verstrijken van deze levensduur geen plotselinge schade ontstaat aan het paneel; er is alleen maar sprake van een langzame maar gestage stijging van de warmtegeleidingscoëfficiënt van de kern met verstrijken van de tijd door het binnendringen van waterdamp en droge atmosferische gassen; daarbij is tevens afgesproken dat de levensduur is verstreken als een bepaalde grenswaarde van deze warmtegeleidingscoëfficiënt wordt overschreden. De meeste onderzoekers en fabrikanten hanteren $8\cdot10^{-3}$ $W\cdot m^{-1}\cdot K^{-1}$ als grenswaarde. Uitgaande van een initiële warmtegeleidingscoëfficiënt van $4\cdot10^{-3}$ $W\cdot m^{-1}\cdot K^{-1}$ betekent dit dat de levensduur verstreken is indien de warmtegeleidingscoëfficiënt is verdubbeld, of anders gezegd indien de thermische weerstand - thermische randeffecten buiten beschouwing latend - met de helft is verminderd.

Tegenwoordig is de meest voorkomende omhulling rondom een vacuümisolatiepaneel een drie-laags laminaat van gemetalliseerd polymeerfolie. Als pyrogene kiezelzuur wordt gebruikt als kern, resulteert een dergelijke barrièrefolie in een voldoende lange levensduur van een paneel toegepast in een gevel in een gematigd West-Europees klimaat, op voorwaarde dat deze panelen groter zijn dan ongeveer 0.4x0.3x0.02 m^3. Voor toepassingen waarin de panelen langduring worden blootgesteld aan een hoge temperatuur resulteert een dergelijk laminaat in een te korte levensduur; de diffusiesnelheid van waterdamp en droge atmosferische gassen door polymeerlagen stijgt immers exponentieel met de temperatuur. Indien echter de folie aan de warme kant van het paneel wordt vervangen door een laminaat met een aluminium of roestvrij staal folie is het in theorie mogelijk zowel een hoge thermische prestatie als een hoge levensduur te bereiken. Voor een vacuümisolatiepanel van 0.5x0.6x0.02 m^3 met een kern van pyrogene kiezelzuur en een dergelijke gecombineerde enveloppe toegepast onder een vloerverwarmingssysteem dat 50% van het jaar in bedrijf is, is in dit proeschrift bijvoorbeeld een levensduur van ongeveer 64 jaar berekend op voorwaarde dat thermische randeffecten niet in de berekening zijn meegenomen.

Gebaseerd op massabalansvergelijkingen en fysische modellen voor de massatransport is in dit proefschrift een methode ontwikkeld waarmee dynamische omgevingscondities kunnen worden opgenomen in levensduurberekeningen. Op basis van deze fysische modellen en experimentele gegevens van verschillende onderzoeksinstellingen in Europa, is op basis van regressieanalyse een formule afgeleid voor het schatten van de levensduur van een VIP met een kern van pyrogene kiezelzuur. Deze vergelijking is handig voor gebruik in een ontwerpproces.

Zoals reeds bekend was voorafgaand aan deze studie, wordt de levensduur van een vacuümisolatiepaneel voornamelijk bepaald door de eigenschappen van de kern, de aanwezigheid en effectiviteit van gasabsorptie- en droogmiddelen, de initiële gasdruk en het vochtgehalte, ontgassing van de kern en het laminaat, de permeantie van de omhulling, de kwaliteit van de naad, de afmetingen van het paneel en de omgevingscondities met betrekking tot temperatuur, relatieve luchtvochtigheid, partiële waterdampspanning en luchtdruk. Aangezien de eerste vijf factoren productgerelateerd zijn en nauwelijks kunnen worden beïnvloed door architecten en bouwkundigen, zijn met name de laatste twee interessant vanuit bouwkundig perspectief. De invloed van deze omgevingscondities zal hieronder allereerst worden besproken.

Het belangrijkste temperatuurseffect is dat de waterdamp- en gastransmissiesnelheid door de omhulling een functie is van de temperatuur. Deze snelheden vertonen een exponentiële toename bij verhoging van de temperatuur. Het belangrijkste effect van de relatieve luchtvochtigheid is dat de waterdamp- en gastransmissiesnelheid door de omhulling een functie is van de relative luchtvochtigheid. Ook hier geldt dat een toename van de relatieve luchtvochtigheid leidt tot een toename van de transmissiesnelheden. De exacte fysische mechanismen die betrokken zijn bij deze afhankelijkheid zijn echter nog onvoldoende duidelijk voor complexe meerlaagse laminaten. De partiële waterdampspanning en luchtdruk rondom een VIP ten slotte vergroten de drijvende kracht voor waterdamp- en gaspermeatie en beïnvloeden op deze manier dus ook de levensduur.

Een tweede belangrijk kenmerk van vacuümisolatiepanelen zijn koudebrugeffecten, hetzij veroorzaakt door de folielaminaat die volledig rondom de kern loopt, hetzij door afstandhouders langs de rand van bouwcomponenten, hetzij door andere constructieve elementen. De eerste twee zijn zogenaamde lineaire thermische bruggen en kunnen worden beschreven door een lineaire warmtedoorgangs-coëfficiënt die de extra warmtestroom als gevolg van deze dit effect per oppervlakte-eenheid en per eenheid temperatuurverschil weergeeft. In rpincipe geldt dat hoe hoger deze lineaire warmtedoorgangscoëfficiënt, hoe slechter de totale thermische prestaties van een VIP of een bouwcomponent.

De lineaire warmtedoorgangscoëfficiënt als gevolg van een laminaat van gemetalliseerde kunststoffolie rond een vacuümisolatiepaneel met een dikte van meer dan 20 mm kan met voldoende nauwkeurigheid voor ontwerp- en engineeringdoeleinden worden geschat uit het product van de warmtegeleidingscoëfficiënt en de dikte van de laminaat gedeeld door de dikte van de kern. Indien bij een identieke vacuümisolatiepaneel de barriere enveloppe wordt vervangen door een laminaat met een metalen folie kan deze coëfficiënt met voldoende nauwkeurigheid worden geschat met behulp van de formule ter berekening van de warmtedoorgangscoëfficiënt van een VIP met $\lambda_c = 0\ \mathrm{W{\cdot}m^{-1}{\cdot}K^{-1}}$. Voor berekeningen in de beginfase van een ontwerpproces, zijn deze vereenvoudigde vergelijkingen voldoende nauwkeurig. Als een grotere nauwkeurigheid gewenst is, als de dikte van een VIP minder is dan 20 mm of als VIPs zijn geïntegreerd in componenten, kunnen meer geavanceerde modellen worden gebruikt. Ook deze modellen zijn afgeleid in dit proefschrift.

Deze modellen tonen ons dat de totale thermische prestatie van vacuümisolatiepanelen of bouwcomponenten met VIPs, ofwel de thermische prestatie waarin thermische randeffecten zijn verdisconteerd, voornamelijk wordt bepaald door de warmtegeleidingscoëfficiënt en de dikte van de kern, de verhouding van paneelomtrek tot oppervlak, l_p/S_p, en de lineaire warmtedoorgangscoëfficiënt. Voor vacuümisolatiepanelen wordt deze warmtedoorgangscoëfficiënt op zijn beurt beïnvloed door de warmtegeleidingscoëfficiënt en de dikte van de kern, de (gewogen gemiddelde) warmtegeleidingscoëfficiënt en dikte van de folielaminaat aan beide zijden van het paneel en het type en de configuratie van naden en aangrenzende luchtlagen. Vergelijkbare parameters bepalen de lineaire warmtedoorgangscoëfficiënt van de rand van bouwcomponenten met afstandhouders: de warmtegeleidingscoëfficiënt en de dikte van de kern, de warmtegeleidingscoëfficiënt en de dikte van de bekledingsplaten aan beide zijden van de component - of de op basis van dikte gewogen gemiddelde warmtegeleidingscoëfficiënt en de totale dikte van de combinatie van plaat en folie - de breedte van de randzone en de warmtedoorgangscoëfficiënt van deze rand.

Over het algemeen verbetert de totale thermische prestatie als gevolg van een daling van de warmtegeleidingscoëfficiënt en de dikte van de folielaminaat en als gevolg van een afname van de warmtegeleidingscoëfficiënt van de kern. De invloed van de paneeldikte op de totale thermische prestatie is ingewikkelder. Over het algemeen neemt de lineaire warmtedoorgangscoëfficiënt eerst toe van nul - of van een bepaalde initiële waarde in geval van bouwcomponenten - tot een maximum waarde waarna zij vervolgens weer daalt tot nul bij toenemende paneeldikte. Deze piekwaarde ligt meestal in het diktebereik relevant voor de bouw. Een uitzondering hierop vormt een paneel met een kern met $\lambda_c = 0\ \mathrm{W{\cdot}m^{-1}{\cdot}K^{-1}}$. Bij een dergelijk paneel daalt de lineare warmtedoorgangscoëfficiënt altijd bij toenemende dikte.

Een derde belangrijk kenmerk van vacuümisolatiepanelen, die constructief zijn toegepast, is hun gedrag onder een buigbelasting. Vanuit dit perspectief kunnen vacuümisolatiepanelen worden beschouwd analoog aan voorgespannen gewapend beton. De kern van pyrogene kiezelzuur is vergelijkbaar aan de cementmatrix, de barrièrefolie aan de wapeningsstaven en het drukverschil tussen omgeving en kern aan de voorspanning. Met behulp van deze analogie kan het gehele buiggedrag van een vacuümisolatiepaneel met een kern van pyrogene kiezelzuur en een dunne barrièrefilm worden gemodelleerd. De transities tussen de afzonderlijke fasen in het constructieve gedrag onder buiging zijn: knik van de folie aan de bovenzijde, fysisch bezwijken, plastische deformatie van de folie aan de onderzijde, scheurvorming in de trekzone van de kern, stuik in de drukzone van de kern en tot slot constructief bezwijken. Hoewel constructief falen het laatste stadium van bezwijken is, is fysisch bezwijken, dat wil zeggen de vorming van (micro-)scheuren in de barrierelaag, sterk van invloed op de levensduur van het paneel. Bovendien hebben we waargenomen dat de elasticiteitsmodulus van een beschadigde VIP aanzienlijk kleiner is dan van een intact VIP. Uit oogpunt van veiligheid dienen daarom beide hiervoor genoemde processen te worden beschouwd.

Bovendien is uit buigtests op zowel intacte als beschadigde VIPs gebleken dat de equivalente effectieve elasticiteitsmodulus, waarin afschuivingseffecten meegenomen zijn, aanzienlijk vermindert als een VIP beschadigd raakt. Voor een paneel met een dikte van 20 mm, een breedte van 120 mm, een overspanning van 200 mm en een belasting-tot-steunpuntsafstand van 40 mm onder vier-puntsbuiging, halveert deze modulus ongeveer na druknivellering. De exacte reductie is afhankelijk van de geometrie van het paneel (lengte en breedte van de kern en dikte van de barrièrefolie) en van de context (soort belasting). Deze afname van de elasticiteitsmodulus wordt veroorzaakt door de constructieve inactiviteit van het folie in de drukzone in het geval een VIP beschadigd raakt; beschermende maatregelen moeten dan dus worden genomen om te voorkomen dat een paneel van volledig bezwijkt of van de constructie loskomt.

Twee belangrijke parameters die door ontwerpers en ingenieurs kunnen worden aangepast en die van invloed zijn op de totale thermische prestatie, de levensduur en het constructieve gedrag zijn de dikte van een bouwcomponent en zijn verhouding van het paneelomtrek tot oppervlakte, l_p/S_p.

Volgens een benaderingsmodel voor het voorspellen van de levensduur van een vacuümisolatiepanel met een kern van pyrogene kiezelzuur afgeleid in dit proefschrift, is de levensduur van een VIP recht evenredig met de paneeldikte, ten minste voor praktische afmetingen en omgevingscondities kenmerkend voor de gebouwde omgeving; een verdubbeling van deze dikte resulteert dus in een verdubbeling van de levensduur. Tevens is volgens een benaderingsformule ter berekening van de lineaire warmtedoorgangscoëfficiënt van een vacuümisolatiepaneel met een (gemetalliseerde) kunststoffolielaminaat de totale thermische weerstand ook recht evenredig met de paneeldikte, ten minste voor een paneeldikte van meer dan 20 mm, een zeer dunne barrièrefolie en verwaarloosbare overgangscoëfficiënten; een verdubbeling van de dikte resulteert in dat geval dus ook in een verdubbeling van de thermische prestatie. Bovendien resulteert volgens een model afgeleid voor de berekening van de equivalente elasticiteitsmodulus van een vacuümisolatiepaneel met grote dikte-tot-overspanningsratio een verdubbeling van paneeldikte in een vermenigvuldiging van de buigstijfheid met een factor 8 ($=2^3$), op voorwaarde dat de dikte van de barrièrefolie te verwaarlozen is in vergelijking met de dikte van de kern. In de praktijk echter, dat wil zeggen voor kleine paneeldiktes, kan deze factor aanzienlijk kleiner zijn dan 8.

De tweede hiervoor genoemde parameter is de verhouding van omtrek tot oppervlak, l_p/S_p. Ook deze verhouding is van invloed op de totale thermische prestatie van het paneel en zijn levensduur. Volgens het eerder genoemde benaderingsmodel voor het voorspellen van de levensduur van een VIP met een kern van pyrogene kiezelzuur is de levensduur evenredig met deze ratio tot een zekere macht, ten minste voor praktische afmetingen en omgevingscondities kenmerkend voor de gebouwde omgeving. Deze macht is bepaald met behulp van een regressieanalyse met experimentele gegevens van twee soorten barrièrefolies en blijkt afhankelijk te zijn van temperatuur. Voor een typisch drielaags gemetalliseerde kunststoffolielaminaat bij 20°C, is zij bepaald op ongeveer -0.78. Dit houdt in dat onder deze omstandigheden een halvering van de verhouding l_p/S_p ongeveer resulteert in een stijging van de levensduur met een factor 1.7. Daarnaast is de invloed van de koudebrug op de totale warmtedoorgangscoëfficiënt van het paneel recht evenredig met deze ratio l_p/S_p. Aangezien de totale warmtedoorgangscoëfficiënt van een vacuümisolatiepanel of een met VIP geïntegreerd bouwcomponent de som is van de warmtedoorgangscoëfficiënt over het midden van het paneel en een factor die het koudebrugeffect vertegenwoordigt, kan men niet concluderen dat de totale thermische weerstand omgekeerd evenredig is aan de verhouding van l_p/S_p. Maar in ieder geval leidt een daling van deze ratio, dwz een stijging van de paneelomvang en/of een afname van de lengte-breedteverhouding, tot een toename van de thermische prestatie.

In tegenstelling tot conventionele thermische isolatiematerialen, kunnen vacuümisolatiepanelen dus een minimale omvang nodig hebben - lengte en breedte – om aan de thermische prestatie-eisen te voldoen. Deze grenzen worden aan de ene kant bepaald door het type barrièrefolie, dat op zijn beurt de lineaire warmtedoorgangscoëfficiënt van de rand van een component bepaalt, en aan de andere hand door de prestatie-eis. Deze minimale maat van een VIP kan worden bepaald met behulp van grafieken waarin de U-waarde is uitgezet als functie van zowel de paneeldikte en de ratio l_p/S_p. Dergelijke grafieken zijn weergegeven in dit proefschrift. Indien bijvoorbeeld de totale U-waarde van een 40 mm dik VIP met een warmtegeleidingscoëfficiënt van de kern van $4 \cdot 10^{-3}$ $W \cdot m^{-1} \cdot K^{-1}$ moet worden beperkt tot 0.2 $W \cdot m^{-2} \cdot K^{-1}$, mag de verhouding van l_p tot S_p niet meer bedragen dan 3.8 m^{-1} - met andere woorden het panel moet groter zijn dan ongeveer 0.90x1.25 m^2 - in het geval een 6 μm dikke aluminiumfolie zonder naad wordt gebruikt.

Zoals we gezien hebben in dit proefschrift is het echter vanuit het gecombineerde perspectief van zowel thermische prestatie als levensduur in het algemeen efficiënter en verstandiger om de verhouding van de l_p/S_p te verkleinen dan om de paneeldikte te vergroten, behalve voor VIPs met een kern van pyrogene kiezelzuur en een enveloppe van een gemetalliseerde folie toegepast op een zodanige wijze dat geringe thermische bruggen aanwezig zijn. Dit eerste is in overeenstemming met de veelbelovende eigenschap van VIPs voor gebruik in de bouw: de combinatie van hoge thermische prestatie met beperkte dikte.

Ter bescherming van VIPs tegen incidentele beschadiging tijdens transport, opslag en gebruik op het bouwterrein moeten zij bij voorkeur worden geïntegreerd in geprefabriceerde bouwcomponenten. Geïntegreerd in zulke componenten is er veelal een sterk verband tussen het constructieve gedrag en de thermische prestatie. Afhankelijk van het type component, dat wil zeggen een component met afstandhouder langs de rand of een sandwichcomponent, wordt de constructieve prestatie voornamelijk bepaald door ofwel de bekledingsplaat aan de buitenzijde in combinatie met de afstandhouder of het synergetische samenspel tussen bekledingsplaten en VIP. In het eerste geval is een sterke en buigstijve afstandhouder vereist om een verbinding te maken tussen de bekledingsplaten en om externe krachten over te brengen naar de hoofddraagconstructie; vaak leidt een dergelijke randverbinding tot sterke thermische randeffecten. In het tweede geval echter is geen constructieve rand vereist, hetgeen aan de ene kant resulteert in de mogelijkheid om de totale thermische prestatie van het panel te verbeteren, maar aan de andere kant resulteert in constructieve vereisten voor het VIP zelf.

In geval van een constructieve sandwich dient een goede, sterke en stijve verbinding te worden verkregen tussen bekledingsplaten en de folie van het VIP. Zelfs echter als een perfecte hechting is verkregen, kan afschuiven van de folie over de kern van het VIP niet geheel worden voorkomen. Omdat de invloed van deze afschuiving op de vorming van (micro-)scheuren in de barrièrelaag en het effect van een kleefmiddel op de levensduur nog onbekend zijn, dienen vacuümisolatiepanelen met de nodige omzichtigheid te worden toegepast in sandwichcomponenten onderworpen aan buiging. Ondanks deze uitdagingen hebben sandwich-componenten waarin VIPs zijn geïntegreerd het grootste potentieel voor het maken van dunne gevelcomponenten met hoge thermische prestatie.

Aangezien voor de toepassing van VIPs in sandwichcomponenten nog de nodige technische hindernissen opgelost moeten worden, aangezien het risico van schade aan de barrièrelaag in dergelijke componenten aanzienlijk kan zijn en aangezien VIPs verlijmd aan bekledingsplaten niet gemakkelijk hiervan kunnen worden gescheiden aan het einde van hun gebruiksfase, hebben componenten met een randverbinding momenteel, althans tijdelijk, de voorkeur. Aangezien er bij deze componenten echter grote energieverliezen kunnen optreden langs de rand, moet deze rand thermisch worden geoptimaliseerd. Op basis van twee ontwerpen van gevelcomponenten gepresenteerd in dit proefschrift kan worden geconcludeerd dat het potentieel van toepassing van vacuümisolatiepanelen in gevels zeer hoog is. Met een dikte van de isolatielaag van slechts 40 mm en een dikte van het gehele component tussen 43 mm en 85 mm, kan een effectieve *U*-waarde van minder dan 0.15 $W{\cdot}m^{-2}{\cdot}K^{-1}$ worden bereikt. Zelfs na 25 jaar kan de effectieve *U*-waarde van de componenten nog minder zijn dan 0.18 $W{\cdot}m^{-2}{\cdot}K^{-1}$.

Als uit oogpunt van bescherming een vacuümisolatiepaneel is opgenomen in een EPS isolatieplaat ontstaat een zogeheten 'met EPS ingekapselde VIP' of een 'met EPS beklede VIP'. Indien een dergelijke EPS isolatieplaat een vaste dikte heeft kan een maximum in thermische prestaties optreden bij een bepaalde dikte van dit VIP, niet zijnde de maximale dikte van het VIP. Dit verschijnsel is waargenomen zowel in complexe driedimensionale en in eenvoudigere tweedimensionale studies naar 'met EPS ingekapselde VIPs' met een barrierelaminaat met aluminium folie dikker dan 10 μm en een warmtegeleidingscoëfficiënt van de kern van het VIP van $4 \cdot 10^{-3}$ $W \cdot m^{-1} \cdot K^{-1}$. Het is dus niet per definitie het beste om de dikte van een vacuümisolatiepaneel zo groot als mogelijk te maken. Indien echter de totale dikte van een 'met EPS ingekapselde VIP' niet van tevoren is vastgelegd maar toeneemt met toenemde dikte van het VIP doet een dergelijk verschijnsel zich niet voor. In dat geval leidt een grotere dikte van een vacuümisolatiepaneel tot een verhoogde thermische prestatie.

Grote maattoleranties, ten slotte, vooral in lengte en breedte, moeten in alle bouwkundige toepassingen met VIPs kunnen worden opgenomen. Dit kan worden bereikt door het reserveren van voldoende ruimte tussen een paneel en de omliggende materialen en door de zo ontstane gaten te vullen met een materiaal met lage warmtegeleidingscoëfficiënt en hoge samendrukbaarheid.

Martin Tenpierik

TABLE OF CONTENTS

T

TABLE OF CONTENTS

Thermal Behaviour of Vacuum Insulation Panels

3. ***Study into the Effect of the Barrier Laminate on the Overall Thermal Performance of VIPs***

Thermal Behaviour of Building Panels

4.

Study into the Thermal Bridging Caused by the Combined Effect of VIP's Barrier Envelope and Spacers of Building Components

Service Life of VIPs and Components

5.

Study into the Fundamentals of Service Life Prediction and into Models for Estimating such Values

R/ Case: EPS Encapsulated VIPs

7. *Research Case Study into the effects of incorporating a VIP into an EPS Insulation Board on Overall Thermal Performance*

D/ Case: VIP Integrated Façade Panels

8. *Design Case Study: Principal Designs of High Performance, Slim, Prefabricated Façade Components*

Conclusions and Recommendations

10.

Outlook

O.

Past, present and future

References

R.

Appendixes

A.

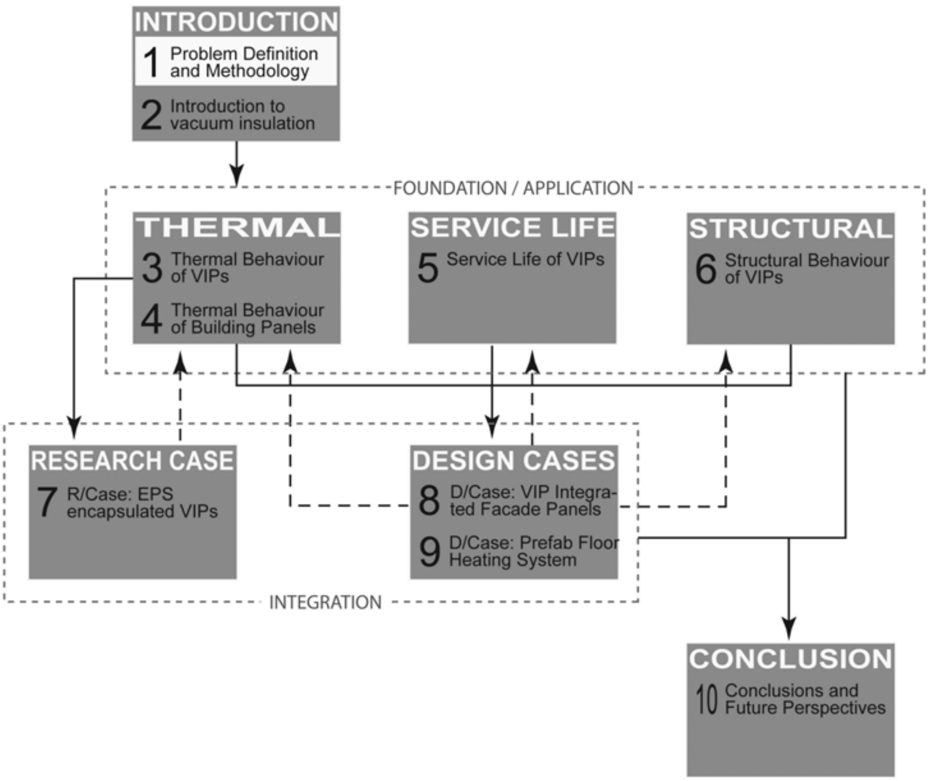
INTRODUCTION
1 Problem Definition and Methodology
2 Introduction to vacuum insulation
FOUNDATION / APPLICATION
THERMAL
3 Thermal Behaviour of VIPs
4 Thermal Behaviour of Building Panels
SERVICE LIFE
5 Service Life of VIPs
STRUCTURAL
6 Structural Behaviour of VIPs
RESEARCH CASE
7 R/Case: EPS encapsulated VIPs
DESIGN CASES
8 D/Case: VIP Integrated Facade Panels
9 D/Case: Prefab Floor Heating System
INTEGRATION
CONCLUSION
10 Conclusions and Future Perspectives

PROBLEM DEFINITION AND METHODOLOGY 1

INTRODUCTION INTO 'VACUUM INSULATION PANELS APPLIED IN BUILDING CONSTRUCTIONS'

1.1 PROBLEM DEFINITION

Due to sustainability and due to international treaties (UNFCCC, 1997), it is desired and required to reduce greenhouse gas emissions drastically[1], among which are carbon dioxide, methane, water vapour, nitrous oxide and ozone. Although methane is a gas with a stronger greenhouse effect, carbon dioxide emissions by man-made equipment, vehicles, industrial and power plants are often considered the major cause for anthropogenic climate change due to the sheer amount of their annual emissions. One contributor to these emissions is the burning of fossil fuels to generate power and electricity to be used in and for buildings.

Buildings and building-related processes are responsible for about 40% of primary energy consumption in the European Union in 1997 (European Parliament and Council, 2002). About 57% and 52% of this energy is applied for heating systems in the residential and commercial sector respectively[2]. The European Union therefore has laid down new energy performance requirements for buildings in the European Directive on the Energy Performance of Buildings (European Parliament and Council, 2002). Moreover, a reduction of energy losses of buildings during their occupational phase is important for facilitating the implementation of sustainable and renewable energy sources in the built environment, since the power capacity of these energy systems is insufficient for the current high energy demand of buildings.

In 1989, Duijvestein (Duijvestein, 1989) proposed a strategy to deal with (future) energy-problems. This strategy was later adopted by Lysen under the term *Trias Energetica* (Lysen, 1996). It consists of three principal steps: 1.) reduce the required amount of energy consumed by stimulating energy conservation and energy

---

[1] The Netherlands have committed themselves to a reduction of greenhouse gas emissions in 2008-2012 by 8% with reference to 1990 according to Kyoto Protocol (UNFCCC, 1997). Besides, in February 2007 the 27 EU member states have agreed upon reducing CO_2 emissions by 20% in 2020 with reference to 1990 (EU, 2007). Moreover, around the same date the European Committee proposed to challenge other 'rich' nations to join the EU in achieving even a 30% CO_2-reduction in 2020 relative to 1990 by increasing the energy efficiency (of the EU) with 20%, by increasing the amount of renewable energy sources within the energy mix with 20%, by raising the share of bio fuels by 10% of total petrol and diesel consumption for transportation within the EU and by developing technology for carbon capture and sequestration (EU, 2007). With respect to energy savings it was estimated that within the building sector a reduction potential of primary energy use of 27% to 30% existed (EU, 2006).

[2] According to Earthtrends (2008), the residential sector and the commercial sector within Europe were in 2001 responsible for 27.5% and 8.7% resp. of the total energy consumed within this area. Total final consumption was approximately 1.859 million metric toe. Within the Netherlands both sectors within that year used 17.3% and 13.3% of in total 60 million toe.

efficiency; 2.) maximize the amount of energy generated from renewable energy sources; 3.) use non-renewable energy sources as efficiently as possible. According to this strategy, one way to lower the environmental impact of the energy consumption of buildings during their functional lifetime is to reduce heat losses by improving the thermal performance of the building enclosure[3]. Two strategies for this improvement can be followed. The first strategy is increasing the thickness of thermal insulation materials. Until recently, this strategy has primarily been followed. As a result, a huge increase in energy performance of buildings has already been achieved (Figure 1.2). In the Netherlands currently, a thermal resistance of 2.5 $m^2 \cdot K \cdot W^{-1}$ is required for opaque climate-separating elements or components (VROM, 2001), resulting in insulation layer thicknesses of typically 8 to 10 cm for mineral fibre insulation in traditional Dutch cavity walls. Especially for residential buildings this thermal performance requirement is likely to become more stringent with time[4]. Current practise for building sustainable housing, already implements a thermal resistance of 3.0 to 4.0 $m^2 \cdot K \cdot W^{-1}$ (Hameetman, 2005). If, however, German or Swiss Passivhaus[5] standards are applied, thermal insulation thickness would increase to about 30 cm or even more, resulting in thick building constructions with a number of possible disadvantages. Thick façade and wall constructions …

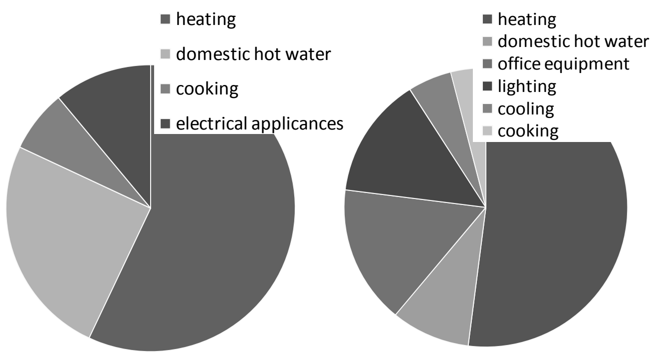

Figure 1.1

Indication of the distribution of total primary energy end-use for a.) the entire EU residential sector, b.) the EU commercial sector; total energy consumption for both residential and commercial sector is 378.5 Mtoe in 1997 (Simmler et al., 2005)

[3] It should be noted that increasing the thermal performance of building enclosures may lead to an increase in cooling demand. With respect to reducing the energy consumption of buildings, both heating and cooling – and all other energy use – should be considered.

[4] Currently, the cost optimum value for the thermal conductance of the enclosure of buildings, which depends on climate, energy prices, insulation cost and interest rates, lies at 0.17 and 0.21 $W \cdot m^{-2} \cdot K^{-1}$ for roofs and walls resp. in Amsterdam (Boermans and Petersdorff, 2008).

[5] A Passivhaus is defined as a residential dwelling in which a comfortable interior climate is achieved a.) without the use of a traditional heating and air conditioning system, b.) of which the annual energy demand for heating and cooling is less than 15 $kWh \cdot m^{-2} \cdot yr^{-1}$, and c.) of which the total primary energy demand is less than 120 $kWh \cdot m^{-2} \cdot yr^{-1}$ (Graf, 2003). For achieving this standard, the *U*-value of the opaque elements of a façade is often set to a limit of 0.15 $W \cdot m^{-2} \cdot K^{-1}$ (Kalkman, 2008).

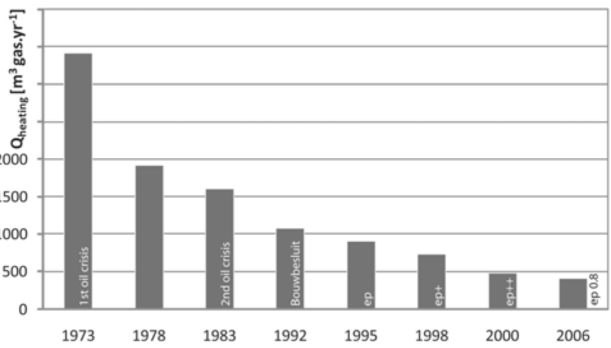

Figure 1.2

Average annual consumption of natural gas used for space heating by newly built dwellings in the Netherlands. (Hameetman, 2005) 'ep' stands for energy performance demands.

1. result in an unfavourable net-to-gross floor space area, conducing to less usable space or a larger required building area, in most cases leading to higher building costs per floor area;
2. may result in an increased complexity of junctions and details within and between building components and parts, leading to increased risk of design errors;
3. impede the possibility for architects and designers to create slender facades;
4. conduce to an increase in material use and result in heavier load transmitting cantilevers to connect the outermost façade layer to the load bearing system;
5. reduce the amount of daylight penetrating the façade since the projected area onto the part of the atmosphere with high illuminance reduces (Wollensak, 2003; Cremers, 2006c).

The second, more innovative, strategy for reducing energy losses through the building enclosure is the application of more effective thermal insulators. The phenomenological material property that represents the effectiveness of a thermal insulator is its thermal conductivity. The lower the thermal conductivity, the less heat is flowing through the material per unit thickness and per unit temperature difference, thus the better its thermal effectiveness. Figure 1.3 presents the thermal conductivity of several conventional and non-conventional thermal insulators.

Since the first and the second oil crises in 1973/1974 and 1979/1980, energy performance regulations for buildings have been developed and have gradually grown into important and stringent requirements for facades, necessitating the continuous improvement of thermal insulators. Most developments, however, aimed at improving the quality and performance of existing materials on their thermal behaviour. Polyurethane foam, for instance, evolved gradually from foam without additional blowing agent into foam with CFC11-filled (trichlorofluoromethane) pores and finally into foam with ozone layer friendly low thermal conductivity gases as blowing agents (liquid carbon dioxide, acetone, and methylene chloride), reducing the overall thermal conductivity with approximately 25% to 30%. Some years ago, resol foams have been developed which even have a lower thermal conductivity than polyurethane foams.

Recently, Aspen Aerogel introduced aerogel insulation blankets (Spaceloft™), which have been commercialised in the offshore industry several years before, to the building market. This composite material composed of aerogel pressed into a fibre glass insulation blanket has a thermal conductivity of about $13.5 \cdot 10^{-3}$ $W \cdot m^{-1} \cdot K^{-1}$ at room temperature and ambient pressure (Aspen Aerogel, 2007). A Spaceloft™ insulation blanket can however still be considered as a conventional thermal insulator since it is a homogeneous, flexible and easily processed material.

The logical, however not chronological, next step in the development of highly performing thermal insulators is evacuating open-porous materials or gaps. Over the last few years, the interest in vacuum insulation has considerably increased and the need for volume efficient means of insulation has led to the development of new techniques among which vacuum insulation panels are one of the promising candidates. A vacuum insulation panel consists of an open-celled core material which is evacuated and then tightly sealed into a barrier envelope to maintain this vacuum. The vacuum inside the pores of the core material reduces the thermal conductivity of the product significantly (Brodt, 1995; Caps et al., 2001; Rath, 1989), varying between $2 \cdot 10^{-3}$ and $8 \cdot 10^{-3}$ $W \cdot m^{-1} \cdot K^{-1}$. A vacuum insulation panel of only 20 mm can therefore replace a conventional mineral wool or PU-foam insulation board of 185 mm or 120 mm respectively. This reduction of thickness is among the most interesting features for large-scale application of vacuum insulation panels in the building industry.

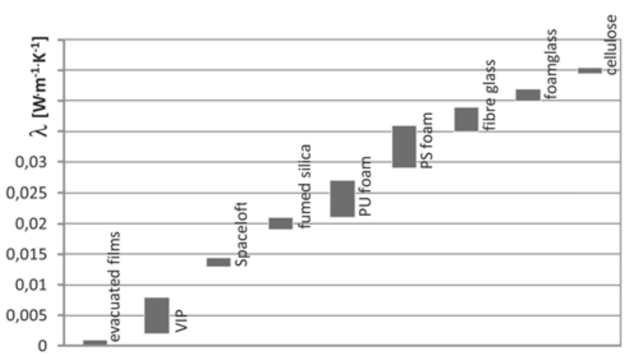

Figure 1.3

Comparison of the thermal conductivity of vacuum insulation panels to other thermal insulators. Divided by the thickness of the material, it provides a measure for the thermal performance of the insulation layer.

Evacuated multilayered foil insulations, which consist of a multitude (30 to 80 layers) of highly reflecting metal foils, metallized polyimide or PET films and thin fibrous separating layers put together in a thin evacuated cavity, have the lowest thermal conductivity at the moment technically achievable (Degen et al., 1994; Timmerhaus, 2007; Scurlock and Saull, 1976). The large number of radiation shields, kept at a fixed distance from each other by spacers, significantly reduces radiative heat transfer. This heat transfer is directly proportional to the emissivity of both the cold and warm surface and inversely proportional to the number of layers[6] (Timmerhaus, 2007). Since at ambient pressure such a layered system performs poorly as thermal insulator – its thermal conductivity is above 0.1 $W \cdot m^{-1} \cdot K^{-1}$ – evacuation is required. But although their thermal conductivity can then be as low as $0.04 \cdot 10^{-3}$ $W \cdot m^{-1} \cdot K^{-1}$, the very high vacuum needed (below 10^{-8} bar) is not practical and feasible for application in buildings (Green, 1998). VIPs therefore currently are the best performing thermal insulators available to the building industry.

Since VIPs combine high thermal performance with limited material thickness due to their very low thermal conductivity, which is about a factor 5 to 10 lower than that of mineral fibre insulation, they do not have the possible disadvantages mentioned earlier. However, integration of VIPs into the building enclosure must be performed very meticulously for several reasons; first, a VIP is to be regarded as a system or component by itself, as a consequence of which it cannot be processed on site and needs careful planning in advance; second, it is very sensitive to mechanical damage thus requiring careful handling during production, transportation, storage and installation; third, careful design is required due to thermal bridges along the edges of the panel; fourth, a decrease of its thermal performance over time needs to be considered, especially for applications with very long lifetimes.

Despite that VIPs are currently being used successfully in several applications, like refrigerators and shipping containers, acceptation of VIPs by the building industry - contractors, architects and engineers - is rather slow owing to lack of proven reliability (gaps in knowledge, lack of calculation tools, lack of long-term on-site measurements, liability issues), too high production costs, difficult handling, and the highly traditional attitude of the building industry in general (Binz et al., 2005).

---

[6] Yoon and Song (2009) report the development of a so-called vacuum insulation chip. This device can be considered a combination of evacuated multi-foil insulation and vacuum glazing. It consists of three layers of metal-coated LCD glass chips separated by two 5 μm wide evacuated gaps. Support pillars in these gaps are used for keeping the glass chips separated. They report an effective thermal conductivity of $1.0 \cdot 10^{-3}$ to $1.5 \cdot 10^{-3}$ $W \cdot m^{-1} \cdot K^{-1}$ at a pressure of 0.24 to 1.33 Pa for chips with a size of 32x32x1.88 mm^3.

1.2 A THERMOS FLASK AND A PACK OF COFFEE

Vacuum insulation can be differentiated into three different types: foil or film based vacuum insulation panels (film-VIP), sheet based vacuum insulation panels (sheet VIP)[7] and vacuum insulating glass (VIG). Each of these has its own areas of application and specific features. Film-VIPs, for instance, are especially interesting for applications in which the panel does not have to transmit forces that cause flexion. They can therefore be applied on floors, roofs, in front of massive walls or in building components. Sheet-VIPs on the other hand can be applied in more demanding structural situations, like self-bearing façade components. And VIG can typically be applied in situations when transparency is required.

Film-VIPs (Figure 1.5) consist of a meso-porous[8] core material, after evacuation tightly sealed into a thin high barrier envelope, conceptually similar to a typical evacuated pack of coffee. The evacuated core material not only functions as a thermal resistance, but also needs to counteract the pressure difference generated over the barrier envelope resulting from evacuation. For applications in the building sector mostly fumed silica, originally a by-product from the micro-chip industry, has been used as core owing to its non-flammability and favourable material properties. Fumed silica however is an expensive material, as a consequence of which less expensive materials with less favourable properties, like open-cell PS foam, open-cell PU foam and mineral fibre insulation, have been applied for consumer goods and transport containers, as well. Currently, some research is directed towards finding less expensive alternative core materials with desired properties.

---

[7] Sheet based VIPs are sometimes also named vacuum insulating sandwiches (VIS) (Willems and Schild, 2005). In this dissertation however the term vacuum insulating sandwich is not applied, since it does not consider the similarities between sheet and film based panels and since it may cause confusion with sandwich building components with VIP as a core material.

[8] Porosity of a porous material is a property that describes the ratio of void spaces to the total volume of the material. These voids can either be filled by gases or liquid water. Regarding the size of pores, generally three types of porosity are distinguished: macro porosity, meso porosity and micro porosity. Macro porosity normally is used to describe pores bigger than 50 nm in diameter; micro porosity for pores smaller than 2 nm; and meso porosity for pores with a size between 2 nm and 50 nm. A meso-porous material thus is a porous material for which the main peak(s) of pore size distribution lie between 2 nm and 50 nm (Aysen, 2002). In chapter 3 and 5 it will be shown that there exists a relation between this pore size, the thermal behaviour of a material and a VIP's service life.

Sheet-VIPs primarily differ from film based panels in their barrier envelope. Instead of a thin barrier laminate, a relatively thick stainless steel casing (Figure 1.6) is used to keep atmospheric gases and water vapour outside as much as possible. Because of this hardly permeable barrier layer, the thickness of which is determined by the structural loads acting upon the panel in application, the service life of sheet based VIP is significantly longer than that of film based VIPs. Because of this hardly permeable barrier layer, less expensive core materials with less favourable properties, like fibre glass blankets, can be applied.

Vacuum insulating glass (Figure 1.7) finally consists of a thin evacuated space sandwiched between two perpendicular or concentric glass plates. So, it differs from the aforementioned panels in that it does not consist of a load transmitting and cavity filling core material, thus resembling a thermos flask. To counteract the pressure difference over the glass envelope small spacers are added to this cavity, connecting both glass plates to one another (Collins and Simko, 1998; Güttler et al., 2007; Schultz and Jensen, 2008). From a phenomenological point of view vacuum insulating glass is therefore quite similar to vacuum insulation panels, since the glass variant can be considered as having a core material with very large macro-pores inside. Vacuum glass will however not be studied in this dissertation since it is actually used to replace a typical single-pane or double-pane glazing. It thus follows the rules and application procedures of regular glass systems. Due to the higher thermal performance, though, thermal bridge effects resulting from window frames need important consideration.

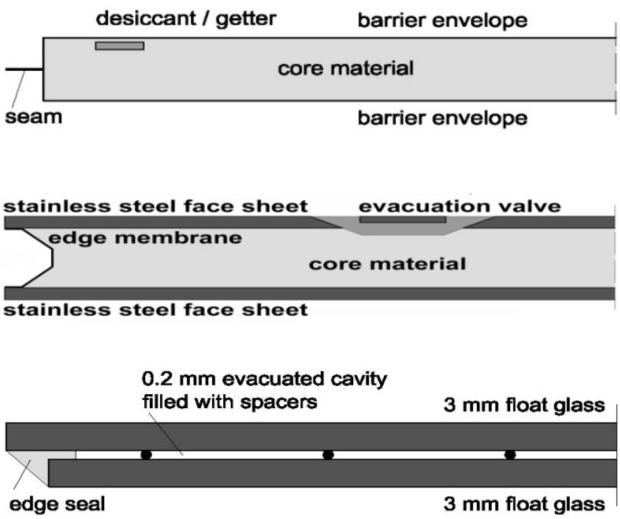

Figure 1.4

Cross-section of a film-based VIP (top), a sheet-based VIP (middle) and vacuum insulation glass (bottom).

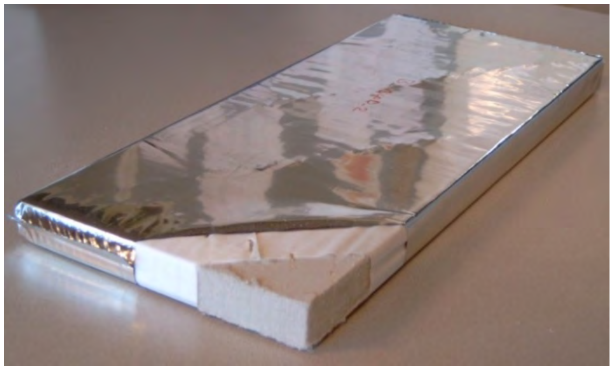

Figure 1.5

Example of a film based vacuum insulation panel, consisting of a fumed silica core which is after evacuation tightly sealed into a high barrier envelope of a three-layer metallized polymer film.

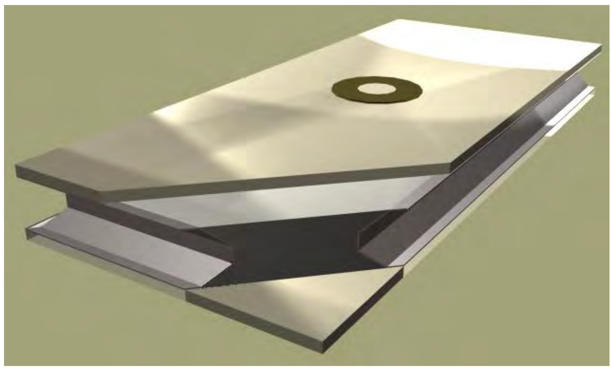

Figure 1.6

Example of a sheet based vacuum insulation panel with a relatively thick stainless steel encasing as once were produced by Lambdasave GmbH and ThyssenKrupp Tempsafe GmbH.

Figure 1.7

Example of vacuum insulating glass from Osaka Sheet Glass.

1.3 Research Objectives and Questions

A vacuum insulation panel is a highly complex material, of which the properties and behaviour needs to be understood clearly before a successful integration is possible. The principal objectives of this dissertation therefore are:

> *the development of calculation tools and methods regarding thermal, hygrothermal and structural aspects to support designers, engineers, manufacturers and contractors in the process of designing VIP integrated buildings components and constructions;*
>
> *and - based upon these tools and methods - the development of guidelines for a successful integration of vacuum insulation panels in building (façade) components and façade constructions regarding thermal, hygrothermal and structural aspects including their interrelationships.*

Following from these objectives, the main research question is

> *How can relevant properties regarding thermal, hygrothermal and structural aspects of vacuum insulation panels (VIPs) be modelled and how and under what conditions can these panels be integrated successfully into building components and constructions?*

This research question suggests investigating the material and constructional properties of vacuum insulation panels and VIP integrated building components, developing methods and tools for facilitating the design processes of VIP incorporated products, and testing these methods and tools by designing solutions for several (semi-)practical cases. This main research question will always be seen in the context of designing building components and façade constructional systems. Three important research sub questions can now be developed that structure this study into three elements, or research domains:

FOUNDATION: MATERIAL PROPERTIES AND BEHAVIOUR ON THE LEVEL OF VIP

> *How and to what extent influence thermal, hygrothermal and structural factors the overall performance of vacuum insulation panels and how can these factors be modelled with sufficient accuracy for design purposes on the level of a vacuum insulation panel?*

APPLICATION: CONSTRUCTION PROPERTIES AND BEHAVIOUR ON THE LEVEL OF COMPONENT

How and to what extent influence thermal, hygrothermal, structural factors the overall performance of VIP integrated building components and constructions and how can these factors be modelled with sufficient accuracy for design purposes on the level of VIP integrated building components?

INTEGRATION: MATCHING PROPERTIES AND REQUIREMENTS

How, taking into account their specific properties and behaviour, can vacuum insulation panels be integrated successfully into building components and constructions?

1.4 RESEARCH SCOPE: DOMAINS AND ASPECTS

The previously named research domains not only indicate different parts of this study, but also indicate the transition from applied fundamental research to design related research. While fundamental research typically is object driven, design related research is context driven. In fundamental research, the subject is separated from its surroundings and can thus be studied as a single object on its own. This typically implies that the number of aspects studied is reduced to the minimum to have a clear focus on the object studied. In design related research on the other hand, the subject is always seen in its context (spatial, historical, societal, technical, judicial, etc.), as a consequence interacting with elements outside its boundary, as demonstrated in Figure 1.8. These aspects are however too many to be studied within the scope of this research. So, what aspects are studied within this dissertation?

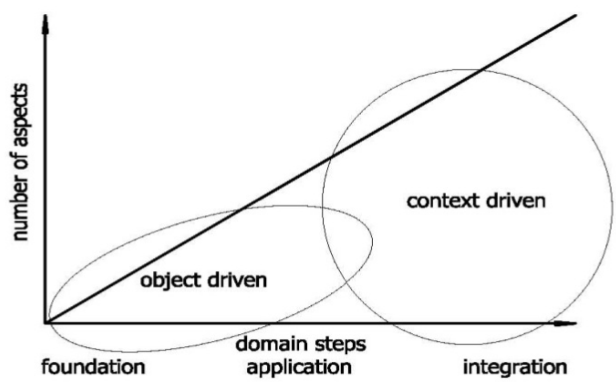

Figure 1.8

Figure indicating the increase in the number of aspects when the research progresses from the domain of foundation towards integration.

The application of VIPs in buildings puts specific requirements on this panel, in most cases heavier than the requirements for traditional VIP applications, like refrigerators and transport boxes. Based on the European Construction Products Directive (European Council, 1988), seven product-related technical requirements on building products in general and thus VIPs in specific can be distinguished[9, 10]: 1.) thermal requirements (energy economy and heat retention)[11]; 2.) structural requirements (mechanical resistance and stability); 3.) fire protection requirements (safety in case of fire); 4.) requirements regarding hygiene, health and environment; 5.) application safety and fitness for use (safety in use); 6.) acoustical requirements (protection against noise); 7.) service life requirements. Besides these requirements, customer's desires can influence the success of integration as well. These customer's desires can be specified as follows: 1.) cost-efficiency; 2.) appearance.

Since this set of requirements and desires is still too large for a complete detailed and in-depth analysis within the domains of *foundation* and *application*, the principal requirements need to be selected for a comprehensive analysis. As will be shown in chapter 8, it can be argued that especially two relations between properties or behaviour of VIPs and as a result three properties are particularly important when integrating them in building components and constructions:

- The relation between the thermal performance of a VIP-incorporated building component on the one hand and its structural performance on the other hand.
- The relation between the thermal performance of a VIP-incorporated building component on the one hand and its service life on the other hand.

The domains of foundation and application will be limited to these properties.

Within the domain of *integration* several (semi-)practical cases will be studied for which will show how VIPs can be integrated into building constructions and components. In this domain knowledge obtained from the domains foundation and application will be used. The aspects studied within this domain are however no longer limited to thermal, hygrothermal and structural behaviour but studied integrally as part of three cases involving all aspects required. The research and design cases will be discussed in the next section.

---

[9] The requirement of service life is not explicitly mentioned in annex 1 on essential requirements of this directive but follows from the sentence: "such requirements must, subject to normal maintenance, be satisfied for an economically reasonable working life" (European Council, 1988, annex 1).

[10] In this list of requirements only product-related requirements and not process-related requirements are considered. For an elaborate discussion on these latter requirements, it is referred to IEA ECBSC Annex 39 (Binz et al., 2005).

[11] The phrases between brackets denote the original description from the European Construction Products Directive.

1.5 RESEARCH SCOPE: Research and Design Cases

The design of this doctoral study follows a sequence from more fundamental to applied research. The results obtained through the fundamental research are applied and validated using several cases. These cases will be studied using the method of research by design (de Jong and van der Voordt, 2002) by which possible solutions for building constructions incorporating vacuum insulation panels are proposed[12]. These cases are studied based upon a central question, which is the third sub question presented in section 1.3.

For the selection of cases, several variables have been considered with the aim of obtaining a range of application areas[13]. Using these cases the potential and possibilities for VIPs in buildings are investigated. The main selection criterion is:

- Limited availability of space for building constructions.

As will be explained in chapter 2, limited thickness is an inherent advantage of vacuum insulation panels. By thus using this criterion for selecting cases, one of the advantages of VIPs is coupled to a practical need or desire.

Within the solution space of practical cases that pass this first criterion three cases are selected that give a variation of application possibilities. The secondary selection criteria then are:

- Type of constructional part according to the classification system of Eekhout (1997) and Moonen (2001);
- Potential for both newly erected buildings and refurbishments;
- Availability of projects in practise.

It is important to realise that the criterion of potential success in application is not set prior to selection. It might thus occur that certain application areas selected to be studied will not result in successful solutions[14].

---

[12] VIP integrated applications can be subdivided into already existing demonstration buildings and cases designed and studied during this doctoral research. The results of the first are extensively published in Binz et al. (2005), while the latter will be presented in this thesis.

[13] The advantage of choosing a multitude of constructional elements as design cases is that the potential of VIPs for a broad range of applications can be tested. However, conclusions can only be drawn for these individual cases solely. No generalised conclusions are then possible.

[14] Due to future developments however solutions with vacuum insulation panels which are currently considered to be unsuccessful might be successful in the years to come.

For a solution to be successful it is important to first define the term success. For the sake of this dissertation, success is defined as having three general components:

- Technical: the solution must meet the (legal) technical requirements from the European Construction Products Directive (European Council, 1988) and the Dutch Building Decree (VROM, 2001) for period as long as its required service life;
- Financial: The solution must be economically feasible;
- Societal: the solution must have reduced environmental impact compared to similar existing solutions and must be socially acceptable.

In this dissertation however primarily the technical component is studied in detail.

Besides these general issues, several specific requirements are set for the solution obtained to be designated successful:

- Thermal performance: the solution must meet the requirement that the overall thermal performance meets Passivhaus standard: $U_{overall} < 0.15\ W \cdot m^{-2} \cdot K^{-1}$;[15]
- Service life: the service life of the vacuum insulation panel in solution must at least equal the desired functional or economic lifetime of the application;
- Protection: the risk of mechanical damage of the panel must be limited or measures should be taken to replace or repair broken panels.

Based upon the previously defined variables and considerations, the following design cases will be studied:

1. *EPS encapsulated VIPs:* This research-based case-study resulted from a question from industry. This question related to the thermal improvement of EPS insulation boards using vacuum insulation panels and resulted in a parameter study into the overall thermal performance of such EPS encapsulated VIPs.

---

[15] It is important to note that this high thermal performance requirement is set here as a prerequisite for solutions to be successful since the use of vacuum insulation panels allows the creation of high thermal performance facades having limited construction thickness. In practice, however, many solutions for buildings have already been developed with vacuum insulation panels of 20 to 30 mm thickness having higher central *U*-value than promoted here. In fact, these thicknesses are ordered from VIP manufacturers most often. Still, with future developments of energy performance standards in mind a lower *U*-value is advocated here.

2. *VIP integrated façade panels:* This design-based case-study resulted from interest from several manufacturers from the building industry. It aims at principally designing slim, high performance façade systems. These systems should have potential for both newly erected and refurbished buildings.

3. *A slim prefabricated floor heating system:* This design-based case-study is performed within a collaborative research and development project under auspices of SenterNovem with several partners: Well Design, BouwhulpGroep, Cauberg-Huygen raadgevend ingenieurs, Metz Consult and Delft University of Technology. It aims at developing a thin, prefabricated, dry, high performance floor heating and cooling system.

1.6 Scale of Study: Components and Façade Constructions

Façade components and constructions can be classified according to a classification system. An example of such a system is the system initially developed by Eekhout (Eekhout, 1997) and later extended by other researchers (Moonen, 2001), based on a subdivision from a low to a high level, as depicted in Figure 1.9. To clarify the relationship between these different aggregation levels, the following example is very insightful. If an aluminium glass façade is taken with the emphasis on the aluminium frame in this facade, then the natural resource would be bauxite, the raw material aluminium, the composite material an aluminium alloy (billets for extrusion machines), the trade material extruded profiles, the elements complete mullions or window frames, the components a façade module, and finally the part of building under consideration would be the complete aluminium glass façade. This example also identifies the position of a façade within this system.

In this classification system, a building component is defined as the aggregation level between a building element and a building part. A component is therefore defined as a combination and composition of elements (and/or trade materials). Since a VIP consists of a core (trade material level), which is after evacuation tightly sealed into, for example, a thin barrier envelope (element level), they thus form a composite system in themselves. They can therefore be classified on the aggregation level of a subcomponent (Lichtenberg, 2002).

It is finally important to note that this dissertation deals with the aggregation levels from subcomponent to part of the building only; it does not seek to improve the materials and elements of which VIPs are composed of (materials research) nor does it attempt to study complete buildings. It only deals with VIPs as a composite system and the way they are integrated into components and the building enclosure.

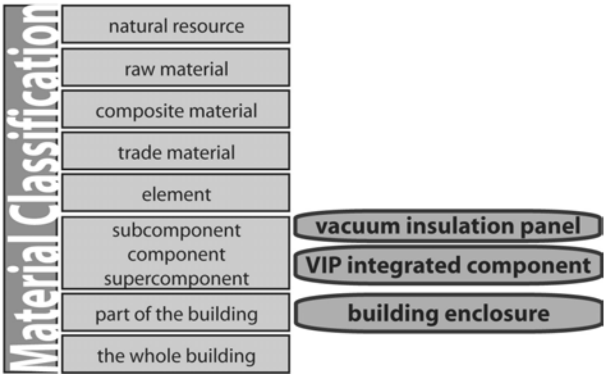

Figure 1.9

Material classification system according to Eekhout (1997).

1.7 ORIGINALITY: RELEVANCE FOR SCIENCE AND SOCIETY

This dissertation can be relevant to science, technology and society because it

a.) adds to the scientific knowledge in the field of building physics in general and in the field of advanced thermal insulation systems specifically, in that it develops new methods and mathematical models for assessing parameters relevant to estimate thermal bridging, service lives and structural behaviour;

b.) in the end integrates existing and new knowledge from different fields into practical solutions for a successful application of vacuum insulation panels in architectural constructions;

c.) not only looks into the application of vacuum insulation panels in building components and constructions in general but also takes the specifics of the climate, the building industry and Building Codes into account.

With this dissertation, scientific knowledge in the fields of building physics and advanced thermal insulation systems is expanded. For the research aspect of thermal bridging, for instance, two new mathematical models are derived for estimating the linear thermal transmittance arising from a thin high film barrier envelope around a VIP. An extended version capable of handling more complex geometries is derived as well, on the one hand enabling scientists, architects and engineers to estimate thermal shunting by the edge of building component and on the other hand showing relations between relevant geometric and material parameters. As a result, a tool is provided to designers for thermally optimizing VIP integrated building components. These thermal models, however, are not only applicable to thermal bridge effects related VIPs and VIP included building components, they can also be applied to building panels in general, elevating this research to a higher level of abstraction (external validity and generalizability). And if they are incorporated into an easy to handle (spread sheet based) software tool, their use can be facilitated.

Within the research domain of integration, this dissertation also synthesizes knowledge from different scientific fields to show how vacuum insulation panels can be integrated successfully into building constructions. Not only the research aspects specifically mentioned in the section on methodology, but also other aspects, are included in the optimisation process of successfully integrating VIPs. Since these tertiary aspects will not be investigated in full detail in this dissertation, only qualitative information can be used as input for this design optimisation.

Moreover, this dissertation not only gives general insights into specific physical phenomena but also relates these insights to legal standards, to climatic conditions and to building practice. VIPs have until recently only been applied primarily in appliances and consumer goods, like refrigerators and mobile organ boxes. Several years ago, some preliminary studies on the applicability of VIP in the building industry have been performed, indicating the high potential of this new product for reducing the energy consumption of buildings (Eicher et al., 2000; NAHB, 2002). This dissertation attempts to continue generating knowledge on how to integrate VIPs in buildings according to systematic and scientific methods.

As a consequence of developing and then disseminating this knowledge, one principal implication for society can be distinguished: a reduction of primary energy consumption of buildings. The impact of this reduction in primary energy consumption can be very significant. The task group Annex 39 of the International Energy Agency estimated that it is possible to fulfil the requirement of 8% reduction in CO_2 gas emissions for the European Union member states, set by the Kyoto protocol, by merely insulating the existing non-insulated and poorly insulated EU building stock with 2 cm of vacuum insulation (Simmler et al., 2005). Vacuum insulation can thus in this sense significantly contribute to a more sustainable and less energy-intensive society.

1.8 Some Definitions

Throughout this dissertation, several types of building components are mentioned. To prevent confusion these components will be named and defined here:

Film-VIP or VIP: vacuum insulation panel with an evacuated open-porous core and a relatively thin laminate-based barrier envelope.

(VIP integrated) (edge) spacer panel: a VIP integrated building component with a strong spacer along its perimeter and with unconnected face sheets.

(VIP integrated) sandwich panel: a VIP integrated building component in which the face sheets are structurally adhered to the VIP.

Sheet-VIP or VIS: vacuum insulation panel (sandwich) with an evacuated open-porous core and a relatively thick metal-based encasing as barrier.

VIG: vacuum insulation glass consisting of two glass sheets encompassing an evacuated cavity filled with small spacers.

VIP integrated building component: Building component consisting of a film-VIP at its centre, two face sheets on either side of the VIP and a spacer or thin profile along its perimeter.

VIP integrated building panel: VIP integrated building component.

1.9 Selection of Past Research Projects

This PhD research can be considered as a follow-up project of an international collaborative research project under the IEA ECBCS implementing agreement: Annex 39 “High Performance Thermal Insulation in Buildings and Building Systems”. This project aimed especially at generating knowledge on the long-term thermal performance of VIPs. Other spin-off research projects are:

- Fachhochschule Nordwestschweiz, Basel, prof. dr. A. Binz and dipl.-ing. G. Steinke: Advising on the application of VIPs in the building sector and monitoring applied constructions with integrated VIPs.
- Royal Institute of Technology, Stockholm, prof. G. Jóhannesson and T.I. Thorssell Msc: “Bättre värmeisolering av byggnader” - Licentiate research into the optimization of the edge of vacuum insulation panels and into the permeation of dry gases and water vapour trough multi-layered barrier skins.

TU Delft also participated in the “Vacuum insulation Applications for the Cooling Industry” project (VACI) from January 2004 till December 2005. This project was a Co-operative Research Project (Craft) under supervision of the European Union (EU). Despite that this project, which was a collaboration between universities and SME’s, was not directly related to buildings, it generated information that is not only relevant for industrial but also for architectural applications.

Five other foreign research projects into vacuum insulation panels related to buildings need to be mentioned, as well. These research projects, however, do not have collaborative relationships with this dissertation.

- PhD research (2004) by prof. dr. H. Schwab at Universität Würzburg, titled “Vakuumsolationsaneele – Gas- und Feuchteeintrag sowie Feuchte- und Wärmetransport“, supervised by prof. dr. J. Fricke.
- PhD research (2006) by dr.-ing J. Cremers at Technische Universität München, titled “Architektonische Einsatzmöglichkeiten von Vakuum-Dämmsystemen im Bereich der Gebäudehülle”, supervised by prof. dr. Th. Herzog.
- Research at Universität Rostock by prof. dr.-ing. G.-W. Mainka into vacuum insulation glass: thermal and structural behaviour.
- Research at Ruhr-Universität Bochum by prof. dr.-ing. W.M. Willems and dr.-ing. K. Schild into the use of sheet-based vacuum insulation panels.
- MSc research (2009) by R. Baetens at Katholieke Universiteit Leuven, titled “Properties, Requirements and Possibilities for Highly Thermal Insulating Materials and Solutions in Buildings – State-of-the-Art and Beyond”, supervised by dr. S. Roels and dr. B.P. Jelle.
- ROBUST project at SINTEF and NTNU into the development of innovative, adaptive, dynamic/controllable, multifunctional, tailor-made materials.

On a national level, both TU Delft and Cauberg-Huygen consulting engineers are actively involved in research into vacuum insulation panels for buildings and building systems. The following projects need to be mentioned in this respect:

- Went, K. van (2000), “Vacuum Isolatie Panelen”, Master’s thesis, Faculty of Civil Engineering and Geosciences, TU Delft.
- Y. Yan (2006) “Vacuum Insulation Panels: thermal bridge effects of building panels and junctions”, Master’s Thesis, Faculty of Civil Engineering and Geosciences, TU Delft.
- Three research projects from 2002 till 2006 commissioned by SenterNovem related to the use of VIPs in building panels or in heating systems for buildings.

1.10 Dissertation Outline

The outline of this dissertation logically follows the structure of the underlying research. It can therefore be subdivided into the two specified main domains, an introductory part and a concluding part:

- Introduction and methodology;
- Part A: Foundation/Application: material properties and behaviour on the level of VIPs and construction properties and behaviour on the level of VIP integrated building components and façade constructions;
- Part B: Integration: Matching properties and requirements;
- Conclusion, evaluation and future prospect.

Based upon these main divisions, the separate chapters can be grouped as in the dissertation outline on the next page. Chapter 2 starts with an introduction into vacuum insulation panels and some concepts to understand this dissertation and the underlying study. Following chapter 2, the main body of the text is grouped into aforementioned research domains and research aspects studied. Chapters 3 and 4 will deal with separate issues of thermal bridging related to either vacuum insulation panels or VIP integrated building components. Chapter 5 subsequently discusses the service life of VIPs (and building panels). In this chapter thermal bridge effects are also included in service life estimations, indicating one of the principal relations put forward in section 1.4. Chapter 6 presents results of studies into the structural behaviour of VIPs. Chapters 3 to 6 thus form a comprehensive discussion of the behaviour of vacuum insulation panels and VIP integrated building components that comprise VIPs on the domain levels foundation and application. Each group of chapters dealing with one research aspect can be read independently from the other chapters, which allows professionals solely interested in a specific issue to rapidly obtain all relevant knowledge.

In the third part of this research (integration), the focus changes from scientific inquiry into separated research aspects to research or research by design of cases in which VIPs have been integrated. It presents possible solutions for a successful integration of VIPs in buildings. In this respect, chapters 7, 8 and 9 deal with three cases studied.

Based upon all studies performed within the three domains, chapter 10 finally answers the research questions put forward in this chapter on methodology. It also presents an overview of recommended future research together with a prospect into the future on a broader scope.

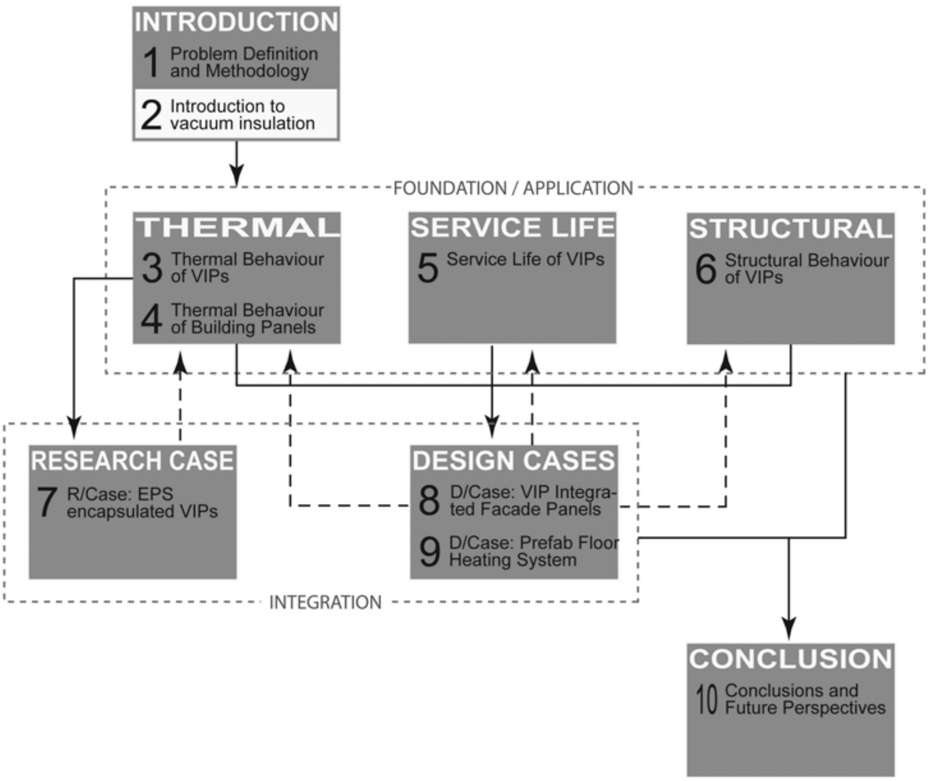
INTRODUCTION
1 Problem Definition and Methodology
2 Introduction to vacuum insulation
FOUNDATION / APPLICATION
THERMAL
3 Thermal Behaviour of VIPs
4 Thermal Behaviour of Building Panels
SERVICE LIFE
5 Service Life of VIPs
STRUCTURAL
6 Structural Behaviour of VIPs
RESEARCH CASE
7 R/Case: EPS encapsulated VIPs
DESIGN CASES
8 D/Case: VIP Integrated Facade Panels
9 D/Case: Prefab Floor Heating System
INTEGRATION
CONCLUSION
10 Conclusions and Future Perspectives

2 INTRODUCTION TO VACUUM INSULATION PANELS

GENERAL OVERVIEW OF ADDED VALUES, DESIGN ISSUES AND MATERIALS

Vacuum Insulation Panels (VIPs) are thermal insulators consisting of an evacuated core material enveloped by a high barrier film or casing required to maintain the vacuum for a long period of time. In the evacuated state, the thermal conductivity of the core material ideally is a factor 5 to 10 lower than that of insulators under atmospheric conditions. As a consequence, vacuum insulation panels combine high thermal performance with limited material thickness. This space-saving potential is among the most interesting features for large-scale application of VIPs in architectural applications. Not only this space-saving potential, but also high thermal performance, low effective weight and possibly in some situations image proclamation, design potential and cost-effectiveness may be considered as advantages or added values over conventional thermal insulators. Application of these panels in building constructions, however, is not without risks regarding barrier envelope damage, service lifetime and thermal bridging. This chapter therefore first identifies and elucidates the intrinsic added values (section 2.2), extrinsic added values (section 2.3) and design issues (section 2.4) for application of vacuum insulation in buildings before discussing several aspects in more detail in the subsequent chapters. After a discussion on these aspects, the materials from which vacuum insulation panels are constructed are discussed in section 2.5. Section 2.6 finally gives some recommendations for how to use vacuum insulation panels by the construction sector.

2.1 INTRODUCTION

Although vacuum insulation panels (VIPs) have widely been used in refrigerators and transport containers for a long time, they have only recently been discovered by the building sector. Concerns for a sustainable future necessitate the reduction of greenhouse-gas emissions and thus primary energy generation by means of fossil fuels. Beside the search for alternative energy sources, a reduction of energy consumption of buildings is an important element in developing a sustainable energy provision. As a consequence, more efficient thermal insulation materials, like vacuum insulation, have been identified for application in building constructions.

Due to the 'absence' of gas inside the voids of a VIP core material and due to added opacifiers[1], gas conduction on the one hand and thermal radiation on the other hand are significantly reduced or even eliminated. As a result, the total thermal conductivity of a vacuum insulation panel with a core of fumed silica is reduced to approximately $4 \cdot 10^{-3}$ $W \cdot m^{-1} \cdot K^{-1}$ directly after production. If we compare this value to the thermal conductivity of mineral fibre insulation, which typically is $37 \cdot 10^{-3}$ $W \cdot m^{-1} \cdot K^{-1}$, or of polyurethane foam, which approximately is $24 \cdot 10^{-3}$ $W \cdot m^{-1} \cdot K^{-1}$, we observe a significant reduction of this thermal conductivity. A vacuum insulation panel of only 20 mm can therefore ideally replace a mineral fibre board or polyurethane board of about 185 mm and 120 mm respectively.

Although VIPs are thermally well-performing thermal insulators suitable for architectural application, actual application will either take place only if a client or a (sub)contractor is prepared to willingly take the risk resulting from a new and practically untested product or system, or if this new product or system has a distinguished added value over alternative conventional products or systems. The first application strategy will normally only be present during the initial phases of introduction of a new product on the building market, in which phase a client or a contractor either hopes to gain (empirical) knowledge on the performance and expertise in the implementation of a new product or system in a specific application, or hopes to create or maintain a certain desired image, in both cases resulting in an advantage over potential competitors. Because of the high material cost of a VIP[2] and its special required treatment during the construction process due to its fragility, it is necessary that these panels have an added value over conventional

[1] An opacifier is a substance added to a material in order to make this material opaque in the infrared frequency range. Typical opacifiers used for fumed silica are silicon carbide, carbon black or TiO_2. These opacifiers cause the material fumed silica to colour grey in stead of white (Randel, 2003; Wacker-Ceramics, 2003).

[2] The current average prize (2008) of a film-VIP lies between 80 to 130 euro$\cdot m^{-2}$, the exact price depending on panel dimensions.

insulators, if VIPs are considered to become a prevailing (generally applicable) product or system among a broad assortment of thermal insulators.

Intrinsic added values (limited thickness, high thermal resistance, low effective weight) and extrinsic added values (image, design potential, cost effectiveness) can be distinguished. At this point it is important to realize that intrinsic added values, which relate to physical or technological advantages, are a direct result of material properties and are thus practically valid for all applications. Extrinsic added values, however, relate to psychological and societal advantages and thus also depend on the context in which VIPs are applied. They are thus not always an advantage.

Since VIPs, at least the film-based panels, are very fragile and prone to thermal conductivity ageing[3] (Binz et al., 2005; Simmler et al., 2005; Schwab et al., 2005c), application in buildings needs to be planned carefully. The most important critical factors are: thermal bridge effects, the hygrothermal micro-environment and service life, and mechanical damage.

2.2 INTRINSIC ADDED VALUES

2.2.1 Limited thickness

Since typical VIPs initially have a centre-of-panel thermal conductivity, i.e. a thermal conductivity in which thermal bridge effects are not accounted for, approximately 5 to 10 times as low as the thermal conductivity of conventional insulators, like mineral wool or polymer foams, the thickness required for a certain thermal resistance is this same factor smaller. If, for instance, a thermal resistance of 3.5 $m^2 \cdot K \cdot W^{-1}$ (excluding boundary resistances) is required for the opaque elements in a façade and if the building construction without thermal insulation has a thermal resistance of 0.3 $m^2 \cdot K \cdot W^{-1}$, a mineral wool insulation board of 12 cm thick is required. This same thermal resistance, however, can also be achieved with a VIP of only 1.3 cm based on initial value calculation to 2.6 cm based on design value calculation[4], not considering thermal edge effects. As a consequence, a space-saving potential of 9.4 to 10.7 cm for each façade arises.

---

[3] Thermal conductivity ageing is the degradation of a VIP's thermal performance over time due to the uptake of water and atmospheric gases, especially nitrogen and oxygen.

[4] As initial value a thermal conductivity of the core material of $4 \cdot 10^{-3}$ $W \cdot m^{-1} \cdot K^{-1}$ is used, which is the thermal conductivity of the core material directly after production. Because of ageing effects, Simmler and Brunner (2005) declare a design value of $6 \cdot 10^{-3}$ $W \cdot m^{-1} \cdot K^{-1}$ or of $8 \cdot 10^{-3}$ $W \cdot m^{-1} \cdot K^{-1}$ of a 20 mm thick VIP of at least 250 mm wide with a fumed silica core and with an aluminium foil laminate or a metallised film laminate as barrier envelope respectively.

Figure 2.1 shows the one-dimensional space-saving potential of a VIP, δd [m], i.e. the potential reduction of the thickness of the building enclosure, relative to a mineral fibre board. As can be seen, the space-saving potential increases for increasing required thermal resistance. Especially, if in the (near) future thermal performance criteria for buildings increase, this space-saving potential due to limited insulation thickness may become an important incentive for application of VIP in architectural constructions; a doubling in required thermal resistance conduces to a doubling of space-saving potential in one direction or a quadrupling of space-saving potential in two directions.

As an example, the area space-saving potential, δA [m²] for a rectangular building plan, can be estimated in a simple way[5] as

$$\begin{aligned}\delta A &\approx 2 \cdot \delta d \cdot n \cdot \left[\left(w_e - 2d + \delta d\right) + \left(l_e - 2d + \delta d\right)\right] \\ &= 2 \cdot \delta d \cdot n \cdot \left[\left(w_i + \delta d\right) + \left(l_i + \delta d\right)\right]\end{aligned} \qquad (2.1).$$

In this equation, w_e [m] and l_e [m] are the outer dimensions of the building plan while w_i [m] and l_i [m] are the width and length measured between the inner surfaces of the facades in case traditional insulation material has been used, n [-] is the number of stories and d [m] is the thickness of the facades with traditional thermal insulation. For a typical office building with internal floor plan dimensions of 14.4x36 m², with six stories and a required thermal resistance of 5.0 $m^2 \cdot K \cdot W^{-1}$ for the opaque elements in the facades, the total area space-saving potential of VIPs relative to mineral fibre insulation would be between 89 and 102 m² (2.9 to 3.2%), again based upon design value and initial value calculation. For a smaller building, like a single-family house, however, this percentile space-saving is much higher. In case of a square 2-storey detached house with inner dimension 8x10 m² and having the same R-value as previously specified, δA would be between 10.6 and 12.1 m² (6.6% to 7.5%). Even higher percentile space gains are obtained if the required R-value increases. If we take the previous example of a 2-storey detached house with a R-value increased to 10.0 $m^2 \cdot K \cdot W^{-1}$, δA increases to between 21.6 and 24.6 m² (13.5% to 15.4%). Concluding, the percentile space-saving potential increases with

---

Moreover, the German Institute for Building Technology (DIBt) gave a technical approval for vacuum insulation panels specifying a declared thermal conductivity of $8 \cdot 10^{-3}$ $W \cdot m^{-1} \cdot K^{-1}$ (Va-Q-vip®) or of $11 \cdot 10^{-3}$ $W \cdot m^{-1} \cdot K^{-1}$ (Vacupor®) for a VIP with a fumed silica core and a metallized film envelope, provided that the size is larger than 300x400 mm² (DIBt Z-23.11.1658, 2007; DIBt Z-23.11.1662, 2007). These values are to be used as value for thermal calculations in practise. It is important to note that these declared values include both ageing effects and thermal bridge effects.

[5] It is assumed that the entire building enclosure reduces with a δd as specified by Figure 2.1 since transparent elements are not considered. It is a rough estimate only.

Figure 2.1

1D space saving potential of a VIP relative to mineral fibre insulation. The grey area indicates the range for this saving potential and the values along the lines denote the equivalent thermal conductivity of the VIP core material. ($\lambda_{minwool}$ = 0.037 W·m^{-1}·K^{-1}).

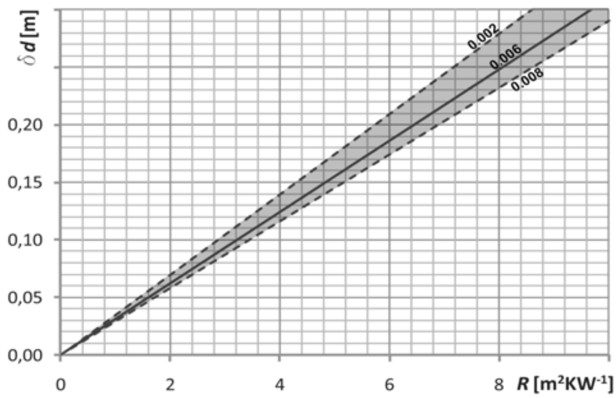

decreasing floor plan area and increasing thermal performance of the building enclosure. Because of these dimensional advantages, a VIP is not only of interest for newly built architectural constructions, but can also be helpful in facilitating the possibilities of re-use and retrofitting of existing buildings.

2.2.2 High thermal resistance

The added value of *high thermal performance* is closely related to the previously discussed *limited insulation layer thickness,* since the thermal resistance equals the material layer thickness divided by its (equivalent) thermal conductivity. While limited material thickness is especially interesting from an architectural or a retrofitting point of view, high thermal performance of building envelopes during their service life on the other hand contributes to a reduction in primary energy consumption, as a consequence reducing CO_2-emissions and facilitating the implementation of renewable and sustainable energy sources. These high thermal performances are on the one hand important for a general energy-reduction of buildings, but on the other hand also for special applications like refrigerated storage rooms, in which a stable temperature far below ambient is continuously required. Figure 2.2 presents a visualisation of the effect of thermal conductivity (and thus type of insulator) on the thermal resistance of an insulation layer.

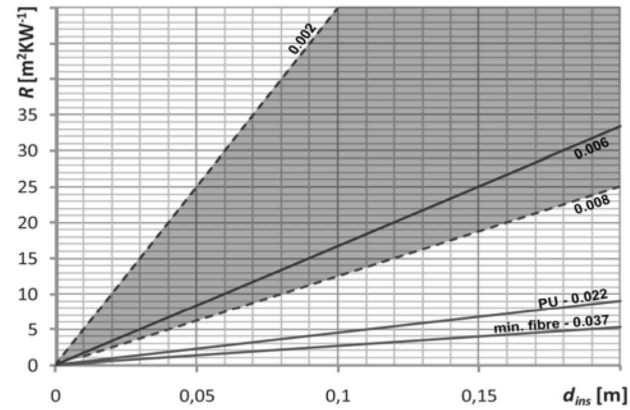

Figure 2.2

Comparison of the thermal resistance of different thermal insulators, boundary resistances not included. The grey area indicates the range in the thermal resistance of VIP. The values along the lines denote the equivalent thermal conductivity of the VIP.

2.2.3 Low effective weight

Despite the high material density of fumed silica, which is the most widely applied and for architectural applications most suited core material (160 - 200 kg·m^{-3} (Simmler et al., 2005)), the mass of a silica-based VIP in a specific application, however, is typically considerably lower than the mass of a thermally equivalently performing conventional alternative. For a required thermal resistance of 2.5 m^2·K·W^{-1}, for example, the mass of a mineral wool insulation panel with thermal conductivity of 37·10^{-3} W·m^{-1}·K^{-1} and density of 35 kg·m^{-3} would equal 3.2 kg·m^{-2}, while the mass of a VIP (including barrier envelope) with effective thermal conductivity of 4·10^{-3} W·m^{-1}·K^{-1} and density of 180 kg·m^{-3} would be about 2.0 kg·m^{-2} which is approximately 38% less. This reduced weight might contribute to a reduction of transportation energy and cost[6]. In case the design value of the thermal conductivity is used, 8·10^{-3} W·m^{-1}·K^{-1}, the mass would be about 3.8 kg·m^{-2} which is approximately 17% more. For buildings, however, the weight of insulation material is negligible compared to other building materials, as a consequence of which its relevance is limited to the transportation phase. But for other applications, like transport containers, appliances and airplanes, it may be of importance.

Different insulation materials can easily be compared to one another on their combined thermal and weight-related performance by introducing a specific thermal conductivity, defined as the product of (equivalent) thermal conductivity, λ

[6] Moreover, since a VIP is a volume-efficient thermal insulator, fewer trucks are required to transport this material to the construction site, compared to conventional thermal insulators. If the thickness of insulation material is five times less than that of a conventional alternative, only 20% of truck volume is required. This even further reduces transportation cost and petrol use.

Table 2.1 - *Typical values of the specific thermal conductivity for several conventional thermal insulators and of different vacuum insulation panels. Values are calculated for panel sizes of 1x 1x0.02 m³, include thermal edge effects and core material density increase after evacuation.*

Material	$\lambda \cdot \rho$ (kg·W·m^{-4}·K^{-1})
Cellulose	2.7-3.2
PS-foam	0.5-1.9
Flaxen wool	0.9-1.3
Cork	3.8-4.6
Mineral fibre	0.9-3.9
PU-foam	0.3-1.6
Foam glass	4.8-8.4
Sheep wool	0.9-1.4

Material	Envelope [b]	Core	$\lambda \cdot \rho$ [a] (kg·W·m^{-4}·K^{-1})
Foil-VIP	6 μm AF	Glass fibre	0.8 ± 0.5
		XPS-foam	1.0 ± 0.5
		Fumed silica	1.5 ± 0.6
	50 μm SSF	Glass fibre	0.8 ± 0.5
		XPS-foam	1.0 ± 0.5
		Fumed silica	1.5 ± 0.6
Film-VIP[d]	97 μm MF	Glass fibre	0.6 ± 0.4
		XPS-foam	0.8 ± 0.5
		Fumed silica	1.1 ± 0.5
Sheet-VIP	2.5/0.8 mm steel	Glass fibre	34.5 ± 0.7

[a] Variations in specific thermal conductivity arise due to increase of internal pore gas pressure during the service life of a VIP and/or variation in core material density.

[b] AF, SSF and MF stand for aluminium foil laminate, stainless steel foil laminate and metallised film laminate respectively. The latter film is a three layer metallized polymer film.

[c] Direct comparison of the specific thermal conductivity of sheet-based VIP with film-based VIP and conventional thermal insulators is not always possible, since sheet-based VIP can be directly applied as building component, while film-based VIP and conventional thermal insulators in most applications need a protective layer, which increases the weight of the material or component.

[d] It is important to note that in case of VIPs, some of the combinations of barrier envelope and core result in very short service lives and are therefore not used in practice. These combinations include the Film-VIPs with a core of glass fibres and XPS foam.

[W·m^{-1}·K^{-1}], and (average) density or specific mass, ρ [kg·m^{-3}]. Table 2.1 shows this specific thermal conductivity for some thermal insulators often applied in building construction and for several VIPs respectively. The specific thermal conductivity of a VIP includes thermal bridge effects. As can be seen, a typical metallized film covered VIP with an initial specific thermal conductivity of approximately 0.6 kg·W·m^{-4}·K^{-1} performs slightly better than polymeric foams and sheep wool with respect to density related specific thermal conductivity and can thus be classified among the light-weight thermal insulators. Due to thermal bridge effects, metal-foil covered VIPs, however, have a small disadvantage regarding weight and are therefore only interesting for applications in which very long service lives of for example more than

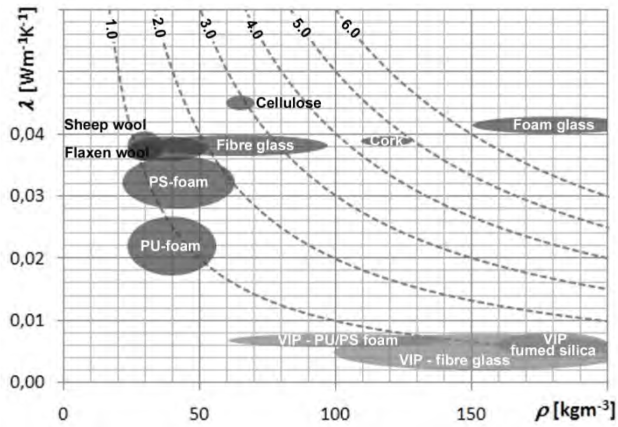

Figure 2.3

Conventional and vacuum insulation materials classified according to their thermal conductivity and density. The broken lines indicate a constant product of λ and ρ.

50 years are required or for applications in which very large panel dimensions are allowed (Simmler and Brunner, 2005). For the VIPs, the values in these tables are based upon thermal conductivity values that apply to new panels. Due to thermal conductivity ageing, the thermal conductivity increases over time, as a result of which the specific thermal conductivity increases alike.

2.2.4 Daylight penetration and view

In case a VIP results in thin wall constructions, the amount of solar radiation and daylight entering through this wall will be larger than through a similar insulating but thicker wall. Moreover, the amount of view, i.e. the viewing angle, is larger too.

Solar radiation can be considered as parallel rays of electromagnetic waves. The thinner the wall, the larger the width of the beam and thus the larger the amount of solar radiation penetrating this wall, as can be seen from Figure 2.4. Solely considering the 2D-case, the width of the beam, s [m], can be obtained from

$$s = (a - d \tan\gamma)\cos\gamma \qquad (2.2),$$

provided that $\gamma < \arctan(a/d)$. In this equation, a [m] is the height of the opening, d [m] is the thickness of the wall and γ [rad] is the angle of incidence of the light beam. If now the difference in thickness between two walls, Δd, is 15 cm and if $\gamma = 45^{\circ}$, then the difference in beam width, Δs, is approximately 11 cm.

The view out of a building and the amount of daylight penetrating is also affected by the width of the wall. If this width increases then the viewing angle and daylight penetration decreases, as can be seen from Figure 2.5. The exact change in viewing

Figure 2.4

Diagrams showing the effect of wall thickness on daylight and solar radiation penetration.

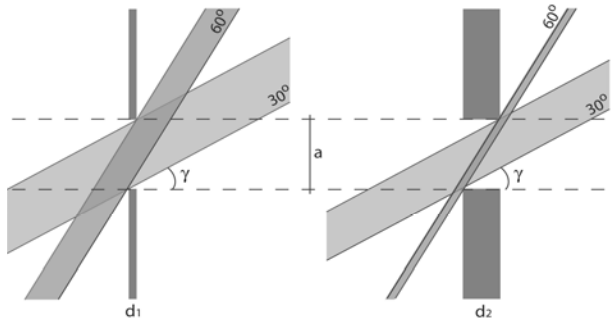

Figure 2.5

Diagrams showing the effect of wall thickness on view angle.

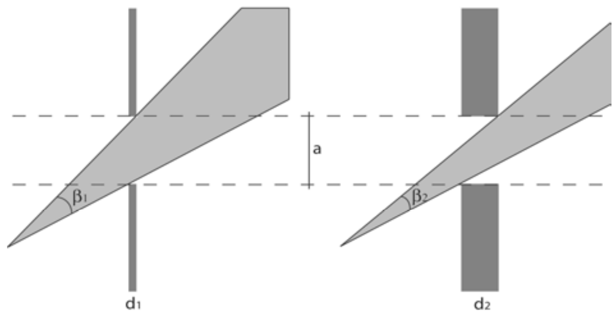

angle depends on the distance from the observer to the façade and the height of this observer relative to the opening in the wall; the closer to the façade this observer is and the larger the vertical distance between the observer and the opening, the larger the effect of thickness on viewing angle (Cremers, 2006c). A complete mathematical description of this phenomenon however is outside the scope of this study. Using simulation results, Wollensak (2003) however showed that especially beyond a distance of about 5 meters behind the façade lighting levels are positively influenced. Closer to the façade, the influence of width is less relevant.

2.3 Extrinsic Added Values

2.3.1 Image

Since VIPs have the appearance of a futuristic and high-tech building component, they can play a role, although modest, in the establishment or the maintaining of a certain desired *image* for the client or (sub)contractor of an constructional project. These images can be classified as high-tech, innovative or environmentally

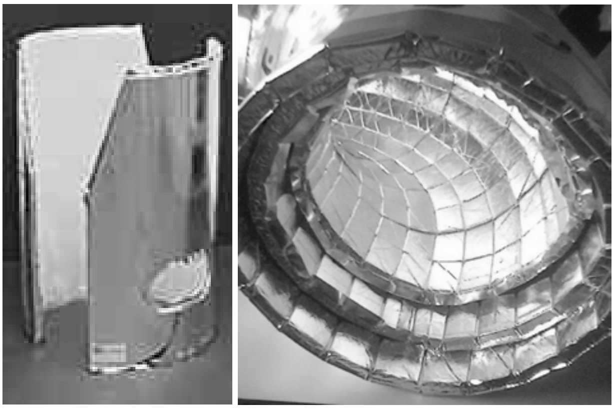

Figure 2.6

Single curved film-VIP from SAES Getters with holes and openings (Manini et al., 2003) (left) and three layers of double curved film-VIPs forming an elbow piece developed during the VACI project (Caps, 2006) (right).

concerned. If the client of an architectural construction for example is a commercial company, a real-estate developer or a large institutional investor, this desired image may lead to a marketing advantage over competitive companies, since innovation or environmental concern are nowadays accepted marketing instruments. For a (sub)contractor, however, the marketing advantage is not solely a commercial advantage he can acquire from implementing VIPs in a building project. From his planning and installation experience he increases his knowledge on the possibilities of, the conditions for, the problems with and the process of VIP application in constructional projects, establishing him as the most suited partner when building with VIP. The advantages arising from the image of a VIP will, however, only have effect in the early phases after the introduction of VIP to the building market. Since for some countries this market introduction has already taken place several years ago, this advantage apparently may not always be effective.

2.3.2 Design potential

For architects and building designers, *design potential* is interesting. In certain respects, the design freedom of VIPs, however, is restricted due to production methods. Because of a pressure of about 1 bar acting on the core material after evacuation, for example, the core thickness reduces, the amount of which is still difficult to predict adequately. As a consequence, production tolerances of +2 to -5 mm in length or width and +1 to –1 mm in thickness for film-based VIPs[7] result (Va-

[7] Production tolerances for sheet-based VIPs are smaller (± 1.5 mm), since the panel dimensions are not determined by the core material (dimensional changes due to evacuation) (ThyssenKrupp tempsafe, 2003).

Q-tec AG, 2008). These tolerances need certainly be accounted for in the design process and may put restrictions on certain desired solutions[8].

Another production difficulty, which may also lead to a challenge for designers, arises from directional forces acting on the VIP, if non-flat products are developed. These directional forces need to be accommodated in the shape of the panel or need to be balanced by external (or internal) constraints. Despite these difficulties[9], several manufacturers have shown the possibility of developing complex dimensionally stable single and double-curved shapes, in some cases even with holes inside the system (Manini et al., 2003). This may result in design freedom for architects and building engineers since the aforementioned directional forces, although leading to complex production processes, could be exploited in creating dimensionally stable curved panels. By carving small triangular gaps in the core material, the position and size of which are determined using form-finding software, these complex shaped VIPs are dimensionally stable and can thus be used without a structural support. Moreover, although film-VIPs are not designed for carrying loads, curved panels, like panels in a wave form or cylinders, can due to increased stability as shown in Figure 2.7.

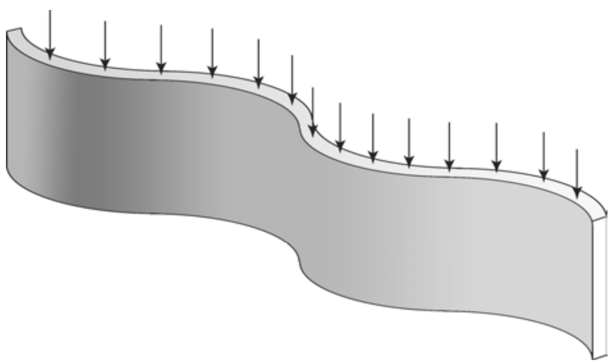

Figure 2.7

Curving and shaping film-VIPs increases their ability to sustain structural loads in in-plane direction.

[8] Due to the production process of film-VIPs, the panel's dimensions are also restricted, either by practical considerations or the size of the vacuum chamber. The minimum and maximum size of Va-Q-vips®, manufactured by Va-Q-tec AG, for example are 300x400 mm^2 and 1200x1000 mm^2 respectively (Va-Q-tec, 2008). As with all film-VIPs, this maximum size is limited to the size of the vacuum chamber. The minimum and maximum size of Tempsafe® VIPs, once produced by ThyssenKrupp tempsafe GmbH, were 500x500 mm^2 and 3000x8000 mm^2 respectively (ThyssenKrupp tempsafe, 2003). Because in this case an evacuation valve is used to evacuate the panel, its maximum dimension is limited by transportation constraints.

[9] Manini et al. (2003) mention three additional challenges to overcome in designing complex shaped VIPs: difficulty of keeping sealing parameters under control for complex sealing areas; difficulty of integrating the panel sealing process into the complete VIP manufacturing cycle; difficulty of scaling prototype manufacturing process to large volumes without increasing cost beyond acceptable.

Besides, due to their inherit slenderness, VIPs open up possibilities for designing very thin high performance façade constructions, like membrane walls. Cremers (2006c), for example, designed for his PhD studies at TU München a façade which mainly consists of two layers of vacuum insulation protected by polymer face sheets and stabilised by either a cable stay structure or a membrane structure. Such a design concept enables the spanning of large facades for example for industrial buildings.

2.3.3 Cost-effectiveness

Whether a VIP has the added value of *cost-effectiveness* depends on the rent per square meter floor area[10] of the building in which a VIP is applied, and upon the energy-saving potential in a certain application[11].

The first criterion applies to the case in which the thermal requirements of the building skin are used as a minimum performance level or if the thermal resistance is a fixed value, resulting in layer thicknesses that differ for each alternative insulator. This first criterion therefore strongly relates to the intrinsic added value of *limited thickness*. If now for example the square meter prize of 20 mm thick VIPs lies between 80,- and 145,- €·m^{-2} including transportation, installation and VAT (Binz et al., 2005), which for a floor space height of 3.6 m equals between 288,- and 522,- €·m^{-1} façade length, and if the costs of a conventional insulator is between 15,- €·m^{-2} for mineral wool and 26,- €·m^{-2} for polystyrene[12], or between 54,- and 94,- €·m^{-1} façade length respectively, the difference in cost between vacuum insulation and conventional thermal insulation varies between 194,- and 468,- €·m^{-1} façade length. The minimum required annual rent, C_t [€·m^{-2}·year^{-1}] can now be estimated for a rectangular building plan based on net present value calculations as (npv ≥ 0)

$$\sum_{t=1}^{n} \frac{C_t}{(1+i)^t} \geq \frac{\Delta K_A \cdot h_{storey}}{\delta d} \qquad (2.3),$$

in which i is the interest rate [-], t is the time [years], ΔK_A is the difference in cost of thermal insulation per square meter [€·m^{-2}], i.e. the difference in cost between VIPs and conventional insulators) and h_{storey} is the façade height per storey [m]. Based

---

10 Or alternatively, the investment cost per square meter of a parcel of land.

11 Besides these factors, other factors may also play an important role, such as a change of building costs due to a technical simplification of building constructions and details and a change of costs due to modifications of the building process, for example the need for skilled personnel for installing VIPs on site.

12 The thickness of the conventional thermal insulators used here is assumed to result in similar thermal performance.

Figure 2.8

Indication of the pay back time of VIPs relative to mineral fibre insulation. The values along the lines denote the R-value [$m^2 \cdot K \cdot W^{-1}$] of the insulation layer. The continuous lines represent a price of 130 euro·m^{-2} VIP while the broken lines represent a price of 50 euro·m^{-2} VIP. ($K_{A;minfibre}$ = 16 euro·m^{-2}; $\lambda_{vip} = 8 \cdot 10^{-3}$ $W \cdot m^{-1} \cdot K^{-1}$; $\lambda_{minfibre} = 40 \cdot 10^{-3}$ $W \cdot m^{-1} \cdot K^{-1}$; i = 5%; h_{storey} = 3.6 m). C_t is the annual rent.

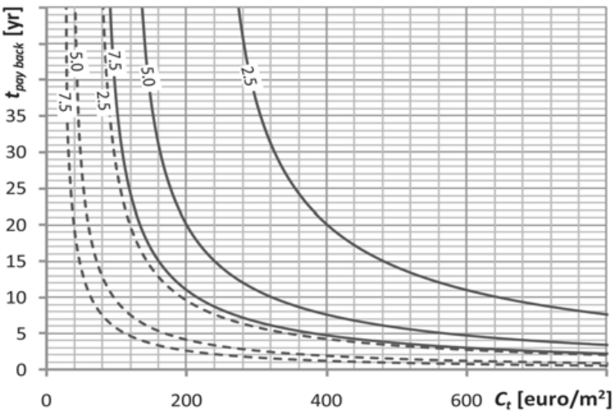

upon this equation and for the typical office building introduced in subsection 2.2.2, an interest rate of 5% and a building lifetime of 25 years, the annual rent per floor area of the building needs to be higher than about 80,- to 160,- €·m^{-2} to make VIPs cost-effective relative to conventional thermal insulators. This rough calculation indicates that VIPs may even be cost-effective in office buildings today. Using a similar procedure, an indication of the pay-back-time of VIPs relative to conventional thermal insulators can be determined as well, if the annual rent per square meter floor space is known, as can be seen from Figure 2.8.

The second criterion for cost-effectiveness applies to the situation in which the thickness of the insulation layer is kept constant for different materials, thus conducing to differences in energy transfer through the building enclosure. Different thermal insulators can be compared to one another based on their specific thermal insulation cost, $K_{R;spec}$ [€·W·m^{-4}·K^{-1}], defined as

$$K_{R;spec} = K_A / R_{eff} = K_V \cdot \lambda_{eff} \qquad (2.4),$$

with K_V the cost of thermal insulation per cubic meter [€·m^{-3}] and R_{eff} the effective thermal resistance, as defined by Eicher et al. (2000) and λ_{eff} [W·m^{-1}·K^{-1}]the effective thermal conductivity of a material, which includes thermal bridge effects. They give some typical values for this specific thermal insulation cost. Some of these values are presented in Table 2.2. As can be seen, VIPs are still among the most expensive thermal insulators. It is however expected that production cost will decrease if VIPs are produced on a larger scale.

Table 2.2 *- Indicative values of the specific thermal insulation costs of different insulation materials. Values are taken from Binz et al. (2005). Price base: October 2004. Figures are without installation and support structure.*

Material	$K_{R;spec}$ (€·W·m^{-4}·K^{-1})
Cellulose (70 kg·m^{-3})	5.28
EPS-foam (20-30 kg·m^{-3})	5.03 – 7.62 [a]
Cork (120 kg·m^{-3})	12.75
Mineral fibre (32-100 kg·m^{-3})	2.90 – 7.90 [a]
PU-foam	6.70 – 7.34
Foam glass (130 kg·m^{-3})	13.83
XPS-foam (33 kg·m^{-3})	11.95
Film-based VIP (silica core)	21.45 – 34.32 [b]

[a] Variations in specific thermal insulation cost arise due to differences in material densities.

[b] Thermal conductivity of VIP core varies from 0.005 to 0.008 W·m^{-1}·K^{-1}.

2.3.4 Eco-efficiency

According to Stephan Schmidheiny (1992), eco-efficiency equals adding more value to a good or service while using fewer resources and releasing less pollution. McDonough and Braungart (2002), actually preferring eco-effectiveness to eco-efficiency, summarize it as doing more with less. This maxim could typically apply to vacuum insulation panels, as well; less material is used to obtain higher insulation quality. Whether however a VIP really is sustainable depends on its factual environmental impact; it is among others important that the manufacture of a VIP does not consume more energy than the amount finally saved by building services due to this VIP and that preferably an entire VIP or its constituents can be re-used.

Schönhardt (2003) performed life cycle analysis (LCA) studies into the environmental impact of film-VIPs using three methods of assessment: Eco-indicator 99, the method of ecological scarcity UBP97 and method of Cumulated Energy Consumption CEC. The environmental impact of a film-VIP with a fumed silica core was assessed by comparing it to fibre glass and polystyrene insulation board, or actually to 1 m^2 of a façade construction with a U-value of 0.15 W·m^{-2}·K^{-1}. From these studies[13] it was concluded in general that the effect of a thermal insulator on the

[13] One important assumption for this study was the exact allocation of the environmental pollution of silicon tetrachloride to the VIP. Fumed silica is by-product of the manufacture of

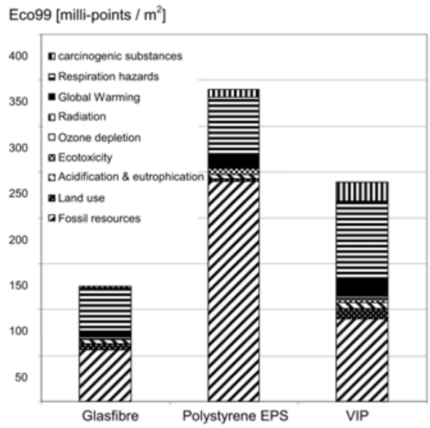

Figure 2.9a

Environmental impact of a film-VIP with a fumed silica core compared to fibre glass and Styrofoam according to the method of eco-indicator 99 (Schönhardt, 2003).

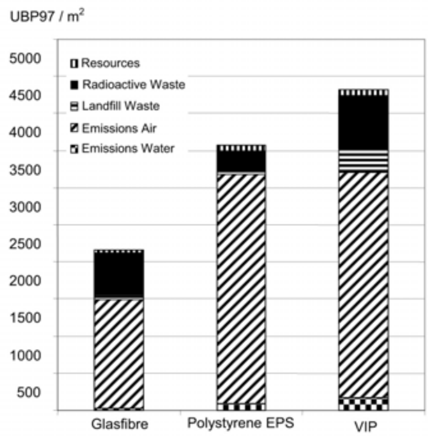

Figure 2.9b

Environmental impact of a film-VIP with a fumed silica core compared to fibre glass and Styrofoam according to the method of ecological scarcity (Schönhardt, 2003).

total eco-balance of a façade is insignificant compared to the impact of other building materials since insulators are lightweight materials. As a consequence, the benefits outweigh the ecological disadvantages; this applies to all thermal insulators, including vacuum insulation panels.

Figure 2.9 presents two figures from Schönhardt (2003) showing the comparison of a film-VIP to fibre glass and polystyrene foam. As can be seen, according to the Eco-indicator 99 method VIP performs ecologically slightly better than EPS but poorer than fibre glass insulation while according to the method of

high-purity silicon for microchip fabrication. The precursor for this production process is silicon tetrachloride which has very high embodied energy (Binz et al., 2005). It was assumed by Schönhardt (2003) that the environmental pollution should be allocated to both the VIP and microchip manufacture process pro rata to their market prices.

ecological scarcity its performance is slightly worse than that of both conventional materials. It is however important to realise that these differences are marginal when put into the perspective of the entire building envelope. The environmental impact of a VIP is dominated by the high consumption of energy during manufacture, especially during the manufacture of fumed silica (Schönhardt, 2003). As a result, the impact of the thin barrier envelope is only marginal. Alternative core materials having less embodied energy would thus be favourable from a sustainable perspective. However, almost all currently existing alternatives have less favourable thermal properties, see also chapter 3.

2.4 DESIGN ISSUES

2.4.1 Thermal bridge effects

Since VIPs are high performance insulators, thermal bridge effects may strongly affect the overall hygric and thermal performance of façades. Due to the low centre-of-panel thermal conductivity of a VIP, differences in local *U*-values between areas with VIPs and thermal bridges are very big, resulting on the one hand in a higher average *U*-value and on the other hand in an increased risk of surface and interstitial condensation. Several levels of thermal bridgies may be distinguished: due to VIP envelopes, due to component edge constructions and due to mounting systems.

The favourable thermal properties of a VIP are primarily obtained by evacuating the pores of its core material. To sustain this state of vacuum for long periods however a barrier envelope is needed. This envelope has a thermal conductivity by far exceeding that of the core material; the thermal conductivity of the core initially lies within the range from $3 \cdot 10^{-3}$ to $5 \cdot 10^{-3}$ $W \cdot m^{-1} \cdot K^{-1}$ while the thermal conductivity of the barrier is higher than approximately 0.5 $W \cdot m^{-1} \cdot K^{-1}$ for a polymer laminate up to about 200 $W \cdot m^{-1} \cdot K^{-1}$ for an aluminium foil based laminate. Since this barrier completely and continuously envelops the core, a thermal bridge arises at the edges and corners of the panel. Despite its very high centre-of-panel thermal performance, the overall thermal performance of a VIP may thus be considerably less owing to its envelope, to the amount depending on envelope thickness and thermal conductivity, panel dimensions, core material thermal conductivity and seam dimensions (Binz et al., 2005; Ghazi Wakili et al., 2004). The centre-of-panel thermal conductivity of a VIP thus does not reflect its overall thermal performance. As will be shown in chapter 3, for a typical panel of 0.6x1.2x0.02 m^3 with a metallized or an aluminium foil based barrier laminate, this results in a rise in thermal conductivity of $0.2 \cdot 10^{-3}$ (+5%) and $4.0 \cdot 10^{-3}$ $W \cdot m^{-1} \cdot K^{-1}$ (+100%) respectively. Especially for the latter type, this effect needs consideration.

Since VIPs are very sensitive to damage, protection by incorporating them in a prefabricated building component may reduce this sensitivity significantly. Although favourable to the structural capabilities of the material, the component edge constructions increase the total heat flow through the building façade as they act as a thermal bridge. In case of a building panel with an aluminium edge profile, the overall *U*-value of the panel may increase with more than 800%, as will be shown in chapter 4. For building panels it is thus of paramount importance to know what parameters influence this thermal edge effects and how to thermally improve edge designs.

Finally, the systems that connect VIPs or building components to a supporting structure may also reduce the overall thermal performance of the façade. Mounting systems, however, are a necessity for connecting a façade to its main load-bearing structure. Since mounting systems form a complex subject on their own they are outside the scope of this dissertation, except when they become part of the design themselves as with sandwich façade panels.

2.4.2 Service life

The thermal performance of a VIP is subjected to so-called thermal conductivity ageing. As a result of a gas and water-vapour pressure difference over the barrier envelope water vapour and atmospheric gases permeate through this envelope into the core, the rate of which primarily depends on envelope properties and the hygrothermal environment, as will be discussed thoroughly in chapter 5. Since the thermal conductivity of a porous material depends on pore gas pressure and water content, an increase of these parameters results in an increase of thermal conductivity. The service life is defined as the time elapsed from the moment of production until the moment the centre-of-panel thermal conductivity has increased to a certain limit often set at $8{\cdot}10^{-3}$ $W{\cdot}m^{-1}{\cdot}K^{-1}$ (Simmler and Brunner, 2005). It depends on the properties of the barrier envelope, the size, aspect ratio and thickness of the panels and the environment.

Studies into this ageing effect have shown that an increase of centre-of-panel thermal conductivity of about $2.3{\cdot}10^{-3}$ $W{\cdot}m^{-1}{\cdot}K^{-1}$ over a period of 25 years may be considered typical for fumed silica based VIPs with a three fold metallized polymer film, dimensions of 0.6x1.0x0.02 m^3 and applied as terrace-roof insulation in a Swiss climate (Brunner and Simmler, 2005). The higher the temperature and relative humidity, the shorter the service lifetime is, as will be shown in chapter 5.

2.4.3 Mechanical damage

Sensitivity to mechanical damage may be an important critical factor for film-VIP application as well[14]. This sensitivity only applies to film-based VIPs and not to sheet-based VIPs. Due to the very thin barrier envelope of film-based VIPs, puncture of this barrier by sharp objects can easily occur. Moreover, too high stresses in the barrier laminate resulting from bending might cause rupture of the barrier laminate. Despite that the thermal conductivity of a vented VIP still is as low as about $20 \cdot 10^{-3}$ $W \cdot m^{-1} \cdot K^{-1}$ (about half the value of mineral fibre insulation), the *U*-value then increases to higher values[15]. In this case the small thickness of a VIP is counter-productive. For a typical 2 cm thick VIP with a centre-of-panel thermal conductivity of $4 \cdot 10^{-3}$ $W \cdot m^{-1} \cdot K^{-1}$, the mid-section *U*-value will increase from 0.19 $m^2 \cdot K \cdot W^{-1}$ to 0.85 $m^2 \cdot K \cdot W^{-1}$.

For a successful VIP application, it is thus imperative that all possible causes of damage are identified in advance and that sufficient preventive measures are taken. In the subtask b report written in the of IEA ECBCS Annex 39 HiPTI (Binz et al., 2005), potential hazards have been identified and described in detail. Because of protection, integrating VIPs into prefabricated building components has advantages over in-situ application.

2.4.4 Sound attenuation and absorption

Sound waves need a medium to propagate. If this medium is removed, the sound transmission should theoretically reduce to zero; we all remember our physics classes where the teacher puts an alarm clock in a bell jar and then evacuates the interior of the jar; slowly but gradually the sound fades away according as the internal gas pressure decreases. Removing the gases from a material might thus prove effective acoustically. However, a VIP not only consists of evacuated pores but also of a matrix of still present material, i.e. the core material, and an envelope completely surrounding this core. Both strongly influence the acoustic behaviour of a VIP or a VIP integrated construction.

---

[14] Regarding mechanical damage, sheet-VIPs have a significant advantage over film-VIPs since sheet-VIPs have a thick metal encasing in stead of thin film barrier laminate. According to Keitzl (2003), it is possible, by choosing the right thickness of stainless steel encasing, to have a small fork-lift driving over a sheet-VIP. Experiments conducted by Willems (2003a) showed that an incidental load causing a pit with a depth of about 40% of the thickness of the panel did not penetrate the barrier itself.

[15] German technical approval from the DIBt (DIBt Z-23.11.1658, 2007) states that a building construction with VIPs should always fulfil energy performance requirements from Building Codes, even if the VIPs applied are vented.

Figure 2.10

Comparison of sheet-VIPs – sometimes called VISs - to a variety of building panels on their mass versus sound attenuation behaviour. The continuous line depicts the mass law for single leaved panels; the dots denote a very broad range of existing panel constructions (single leaved panels, cavity panels and sandwich panels) while the squares depict two sheet-VIPs (Lenz et al., 2005).

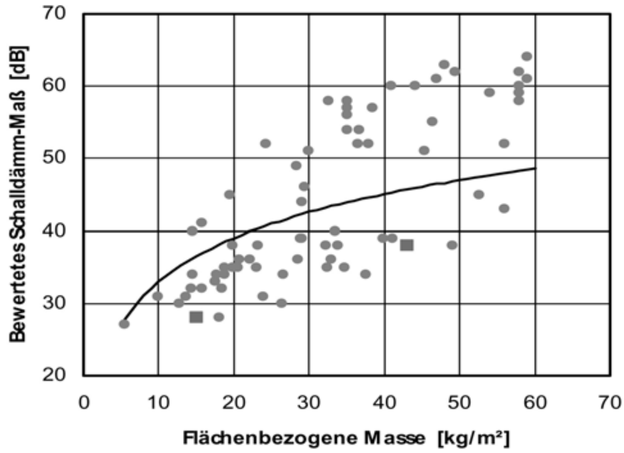

From an acoustics perspective two situations are interesting: a VIP in a façade where it is part of the sound attenuating system and a VIP as insulation below a floating screed where it acts an acoustic spring. For these situation, the panel's thickness, d_c [m], its dynamic Young's modulus [MN·m^{-3}], the core's density, ρ_c [kg·m^{-2}], its sound absorption coefficient, a [-] and the mass of the barrier laminates or the face sheets in case of double-leafed constructions m'_f [kg·m^{-2}] are relevant. Still, little is known about the exact acoustic properties of both sheet-VIPs and film-VIPs.

Until recently, only Lenz et al. (2005) and Maysenhölder (2008a; 2008b) have studied some of the acoustical properties of sheet-VIPs and film-VIPs while Boetker Metallbau GmbH (Cremers, 2006b) has investigated the effect of filling the cavity of double-glazing with film-VIP. Lenz et al. (2005) also discuss that the behaviour of a VIP is far from ideal behaviour among others due to the introduction of dimension effects resulting from the barrier envelope along the panel's edge. They also compare a sheet-VIP to a variety of existing panel constructions on their mass per square meter[16] and sound attenuation, R_w [dB], as presented in Figure 2.10. As can be seen, the sound reduction performance of sheet-VIPs is among the poorest of building panels. It is important to note that the collection of panel constructions depicted consists of all kinds of panel typologies, like single leaved constructions, double-leaved constructions and sandwich constructions. They attribute this poor performance to the presence of resonance within the frequency range relevant in building acoustics and to the influence of the transmissions along the panel's edge.

[16] The mass per square meter of a single material or the mass per square meter of the face sheets of double-leafed panels with a cavity in-between.

The façade panels developed by Boetker Metallbau GmbH consist of a 18 to 20 mm thick film-VIP loosely put into an encasing of face sheets (6 or 8 mm glass and/or 2 or 3 mm lightweight metal) and an edge profile. The mass of the face sheets varies between 5 and 20 $kg \cdot m^{-2}$ while the panels' sound reduction coefficients vary between 39 and 43 dB (Cremers, 2006b). These values are significantly higher than the values found by Lenz et al. (2005) for sheet-VIPs and by Maysenhölder (2008b) and Cauberg and Tenpierik (2007) for VIP integrated building panels. They showed that façade panels and sandwich panels with a core of 20 mm film-VIP and wood or Trespa based face sheets have an R_w-value in the order of 28 dB.

2.4.5 Fire resistance

Fumed silica - the material most widely used as core material for VIPs applied in buildings - is classified as category A1 according to DIN4102-6 with respect to its fire behaviour. This implies that it is non-flammable. Also other potential core materials, like aerogel and glass fibre board have this same fire classification while polymer foams are classified as B3 (Cremers, 2006c). The fire behaviour of VIPs with non-flammable core materials however is primarily determined by the behaviour of the envelope. In case of sheet-VIPs, the thick steel covering is incombustible, too[17]. The thin barrier laminates enveloping Film-VIPs on the other hand, are less reliable regarding fire. In general, the polymer layers melt at a temperature far below the maximum temperature during fire. This results in a loss of thermal performance conducing to higher heat transfer rates through the construction, i.e. the heat of the fire is more easily transferred to the other side, and might also result in loss of integrity of the core material. Wipak, a manufacturer of packaging materials, claims to have developed a barrier laminate for VIPs that is non-flammable (Wipak, 2008).

With respect to fire behaviour, however, it is important to realise that in general complete building components or systems need to be classified regarding their fire proofing qualities. For vacuum insulation panels hardly any tests have been performed until now. It is expected, though, that their behaviour will not be beyond category B2 (normal flammable) (Cremers, 2006c).

[17] According to Keitzl (2003), sheet-VIPs can withstand a maximum temperature of 1000 K for a period of at least 90 minutes.

2.5 MATERIALS USED FOR VIPS

2.5.1 Potential core materials

Different materials can be used as a core material for vacuum insulation panels. These materials need to fulfil four principal requirements:

- It should be able to withstand a 1 bar pressure difference without dimensional changes beyond unacceptable;
- It should inhibit the movement of gas molecules in its voids to suppress gas conduction by having a very small pore size, as will be explained in chapter 3;
- It should block infrared radiation with use of IR-reflectors or IR-absorbers to suppress radiation heat transfer, as will be explained in detail in chapter 3;
- It should have an open cell structure to be able to be evacuated easily - a quick evacuation procedure (less than 500 s)[18] makes a large production possible and economically feasible. Besides, the presence of some closed cells would raise the pressure inside the core material slightly because of permeation of the gas in the closed cells to the evacuated cells.

Besides these principal requirements, there are different less important requirements to be fulfilled by the filler material: a.) Ability to withstand different forces acting during production, storage, transport, implementation and use without breaking down or losing its primary function; b.) Ease of production (pre-treatment (tempering (time and temperature)[19], flushing with dry nitrogen to remove water), formability, ease of sawing or cutting, evacuation time, ease of evacuation, etc.); c.) Low gas emissions after production; d.) Low mass; e.) Non-flammability; f.) Low environmental impact (recycling, toxicity, etc.); g.) Low cost

[18] Evacuation times are determined by the type of filler material, the presence of getters and/or desiccants, the required vacuum, pre-treatments (drying) and the evacuation procedure (use of evacuation ducts). This last requirement poses heavy restrictions on the applications of polymer foams. These foams normally consist of closed cells to keep the low thermal conductivity gases, i.e. the so-called blowing agents, inside the cells.

[19] Most materials need tempering (drying) before evacuation. During the tempering process, a material is heated to between 70°C and 200°C for about 15 to 60 minutes. The ideal combination of time and temperature depends on the specific material (Cremers, 2006c).

Table 2.3 *- Properties of potential core materials (van Went, 2002; Brodt, 1995; Cremers, 2006c; Simmler et al., 2005; manufacturer's information).*

property		Aerogel - Nanogel® Cabot Corp.	Fumed silica – WDS® Wacker Chemie
Thermal conductivity	0.1mbar	3.4 – 3.6	3.6 - 4.2
at 25°C	1.0 mbar	4	4 - 5
[x10^{-3} W·m^{-1}·K^{-1}]	1.0 bar	18	20
Density [kg·m^{-3}]		90 - 100	160 - 200
Average pore size [μm]		0.2	0.2 – 0.3
Porosity [%]		> 90	91 - 95
Compressive strength [kPa]			> 521
Fire classification (DIN4102-6)		A1	A1
Getter/desiccant required		desiccant opt.	desiccant opt.
VIP production cycle time		slow	medium
Pre-drying requirements		yes	yes
Recyclability		possible	possible
Price information [€·m^{-3}]		1800 - 2500	500 - 1000

property		XPS – Instill® Dow Chemicals	PU – Elastocool® Elastogran GmbH	Glass fibre Johns Manville
Thermal conductivity	0.1mbar	4.8 – 5.8	8 - 9	1.5
at 25°C	1.0 mbar	7	16	4 - 5
[x10^{-3} W·m^{-1}·K^{-1}]	1.0 bar	29	33 - 34	30
Density [kg·m^{-3}]		80 - 144	62	100 - 400
Average pore size [μm]		20 – 100	100 – 300	30 – 100
Porosity [%]				
Compressive strength [kPa]		340 - 410		
Fire classification (DIN4102-6)		B3	B3	A1
Getter/desiccant required		both	both	both
VIP production cycle time		fast	medium	slow
Pre-drying requirements		optional	optional	yes
Recyclability		possible	difficult	possible
Price information [€·m^{-3}]		250 - 500		2000 - 3000

The most widely used core materials are silica-based materials (aerosil, fumed silica, aerogel, perlite)[20]. However, sometimes fibre-based materials (mineral fibre) or micro porous open-porous polymer foams (polystyrene, polyurethane, polyimide) are used. Moreover, new alternative core materials are searched as well (Mukhopadyaya et al., 2008; 2009). Due to its very fine pore structure, and thus high allowed pressure increase (see section 3.1), fumed silica is most widely used as filler material for architectural applications. As with the other potential core materials, this material is briefly described in appendix A21.

2.5.2 Potential barrier materials

The barrier envelope is an important constituent of a vacuum insulation panel; it assures that a low gas pressure in the panel is maintained for a long period of time. This barrier needs to fulfil different primary requirements:

- Low Water Vapour Transmission Rate (WVTR) and Oxygen Transmission Rate (O_2TR)[21] in relation with expected lifetime and application conditions. The barrier envelope is required to keep the pore gas pressure in and water content of the core below a critical value. If these critical values are exceeded, the service life of a VIP is said to have expired. Regarding gas and vapour tightness, metals are favourable over polymers. In thin aluminium (below 12 μm) or stainless steel (below 25 to 50 μm) foils gas and water vapour primarily penetrates though so-called pinholes, i.e. macroscopic defects. The metal itself is not permeable (Jacobsen, 2003). The transmission rates of atmospheric gases and water vapour though the laminate, together with the quality of the seal, thus significantly influence the service lifetime of the product. According to Fricke et al. (2006) and Simmler et al. (2005) a pressure increase rate of less than 1 $mbar \cdot yr^{-1}$ is desired for VIPs with a fumed silica core. This tolerable pressure increase rate however cannot easily be translated into a requirement for aforementioned transmission rates since the heat seal and defects in the barrier at the panel's corners also strongly affect the pressure increase rate of a

---

[20] Although Zeolites can nowadays be manufactured with an engineered pore size distribution and small average pore size (Cheetham et al., 1999; Davis, 2002), they are generally considered as having too high a density for application in vacuum insulation panels.

[21] Water vapour and oxygen transmission rates not only give the values for the amount of water vapour (kg) or oxygen (cm^3) that is transmitted though the film per unit area, unit time and unit pressure difference but also give an indication of the ease with which other gases are transmitted. The water vapour transmission rate is indicative for polar gases and the oxygen transmission rate for non polar gases (Jacobsen, 2003).

panel[22,23]. Besides, emissions from the barrier or the core also influence this increase rate, especially during the first weeks after evacuation. Moreover, the transmission rates declared by manufacturers finally are measured at a certain temperature and relative humidity, e.g. at 23°C and 50% RH, while in fact they depend on these environmental properties (Simmler and Brunner, 2005);

- Low thermal conductivity (λ_f) and small thickness (t_f), or in fact a small value of $\lambda_f \cdot t_f$, to minimise thermal bridge effects. As explained previously, thermal bridge effects influence the overall thermal performance of a complete panel. It is therefore important to minimise this edge effect by reducing the thermal conductivity and thickness of the barrier. Although metals have very promising barrier properties, they have a relatively high thermal conductivity as well. Polymers on the other hand have relatively low thermal conductivity but unfavourable barrier properties. The right trade-off between thermal and barrier properties thus needs to be found;

- Ability to be (heat) sealed or otherwise closed (welded, glued) with high quality. Since the quality of the seal or closure influences the service life of a VIP, sealing/closing needs to be performed very meticulously. An aluminium foil for example cannot be sealed, as a result of which a sealing layer is added to the foil. Stainless steel foils cannot be sealed either but are welded. Polymer films, though, are heat sealed. As sealing layer most of the time a polyethylene (PE), a polyethylene terephthalate (PET) or a polyvinylidene chloride (PVDC) film is used. A seal of 2x50 μm PE for example has a WVTR and O_2TR of the order of $6.25 \cdot 10^{-2}$ g·cm·m^{-2}·day^{-1}·bar^{-1} and 15.5 cm^3·cm·m^{-2}·day^{-1}·bar^{-1} (Kücükpinar et al., 2001). Moreover, the sealing process needs to be performed in a clean environment since dust particles might reduce the gas tightness of the seal strictly. An extensive overview of possibilities of, materials for and configurations for closing vacuum insulation panels is given by Cremers (2006c);

---

22 Cremers (2005) states that the oxygen and water vapour transmission rate of VIP barrier materials may not exceed $1 \cdot 10^{-2}$ cm^3·m^{-2}·day^{-1}·bar^{-1} at 23°C and $1 \cdot 10^{-2}$ to $5 \cdot 10^{-2}$ g·m^{-2}·day^{-1}·bar^{-1} at 38°C / 90% RH respectively.

23 It is also important to realise that the values declared are solely valid directly after production, not considering ageing and damaging factors. Among these ageing and damaging factors are delaminating, hydrolysis, foil degradation (crystallization of polymers), corrosion of the metallic parts, damage of the foil due to external forces (puncture, stresses near edges and folding), inhomogeneities or defects in the seal due to the production process (temperature, pressure and time), discontinuities in the seal due to powder or small particle contamination (Simmler et al., 2005).

Besides these primary needs, secondary objectives may be relevant as well:

- Ease of production, formability, ease of cutting;
- Low gas emissions;
- High mechanical robustness (puncture resistance, abrasion resistance, flexibility, strength, UV-radiation resistance, tearing strength);
- Incombustibility;
- Low environmental impact (recycling, toxicity, etc.) and low health risk;
- Low cost and good availability;
- Longevity and long term stability of the barrier must be of the same order as the expected functional lifetime of the panel;
- Compatibility with other adjoining materials;

Several materials can potentially be used as VIP barrier. Besides glass and metal sheets, the most common barriers are constructed out of thin films and foil laminates. Since many requirements must be met and hardly any single polymer scores high on low permeability, polymers are always laminated. Laminated barrier

***Table 2.4** – Basic properties of thin film barrier laminates (Reisacher, 2003).*

Property	Aluminium foil laminate	Metal deposition film (Al_2O_3)	Deposition film (SiO_x)	Polymer laminate
Constituents	Al, PA, HDPE, PET	deposited al. or al. oxide, PET, PE, PA	deposited SiOx, PET, PE, PA	PVDC, EVOH, PVOH, PET, PE, PA
WVTR [$g{\cdot}m^{-2}{\cdot}day^{-1}$] (38°C; 90% RH)	< 0.05	< 0.1	< 0.1	< 0.1
O_2TR [$cm^3{\cdot}m^{-2}{\cdot}day^{-1}{\cdot}bar^{-1}$] (23°C)	< 0.005	< 0.01	< 0.01	approx. 0.01
Climatic influences on TR	none	moderate	moderate	high
Thermal Conduction at standard t_f	high	low	low	low
Formability	low	low	low	high, thermo-formable
Risk of damage	damage of seal, corrosion, low flex crack resistance	delaminating, moderate tearing strength, low flex crack resistance	delaminating, moderate tearing strength, low flex crack resistance	
Risk of pinholes	yes	none	none	none
Transparency	no	no	yes	possible

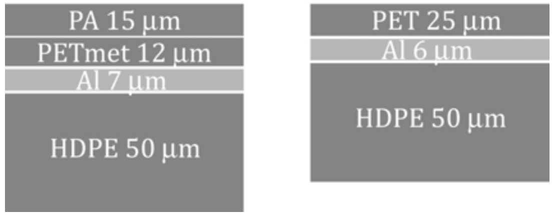

Figure 2.11a

Typical constructions of metal foil laminates.

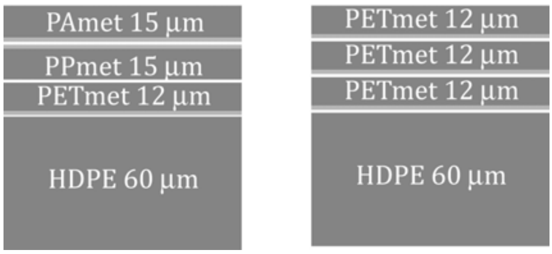

Figure 2.11b

Typical constructions of metallised film laminates. The metal oxides in these figures are light grey.

Figure 2.11c

Example of a polymer film laminate.

envelopes combine the positive effects of each layer into a synergetic barrier. Each layer has its own purpose: the innermost layer is a sealing layer, the outermost layer a protective layer and the layers in-between gas and vapour barriers. The following materials are mostly used to make up these layers: aluminium (Al), stainless steel, silicon oxide (SiO_x), aluminium oxide (Al_2O_3), polyamide (PA), polyethylene (HDPE, LDPE), polypropylene (PP), polyethylene terephthalate (PET) and in some rare cases polyvinylidene chloride (PVDC), polyvinyl alcohol (PVOH) and ethylene vinyl alcohol (EVOH). In general, the following types of envelopes are distinguished:

- metal foil based laminates (aluminum foil or stainless steel foil based barriers);
- metal deposition films / metallised film laminates (laminated polymer films with aluminium, aluminium oxide or silicon oxide depositions);
- laminated polymer films.

The first and second type of laminate is most commonly used as barrier for VIPs. In appendix A22 a thorough description of all three laminate types is given. Table 2.4 presents an overview of some properties of these laminate types. Figures 2.11a, b and c present some typical examples. More information on other materials used in combination with VIPs, like getters, is given in appendixes A23 and A24.

2.6 APPLICATION GUIDELINES

Since VIPs have specific properties and are very prone to damage during production, storage, transportation, installation and use, special care has to be taken when applying these panels. During the research project ‘Annex 39 - High Performance Thermal Insulation for Buildings and Building Systems’ under the auspices of the IEA ECBCS implementing agreement, several practical guidelines for the design and installation of constructions with vacuum insulation panels have been determined based on an evaluation of case studies (Binz et al., 2005). Some of these guidelines relevant for design will be discussed briefly below.

Thermal edge effect: Due to the high barrier film, additional heat losses through the VIP edge occur, resulting in an effective thermal conductivity significantly higher than the centre-of-panel thermal conductivity, especially for metal-foil based laminates. This thermal bridge effect is not only affected by the high barrier envelope, but can be increased considerably due to ill-considered application.

Detail processing: For damage protection, VIPs should be positioned in building structures and systems in such a way that mechanical damage of the high barrier envelope due to puncture is limited as much as possible.

Replaceability / repairability: Despite that VIPs for building applications nowadays have a laboratory service life of more than 25 years, damage to the gas and vapour barrier may result in serious deterioration of their thermal performance. It is therefore important that these damaged panels can either be repaired or replaced easily. This inherently introduces the requirement for regular non-destructive inspection of the thermal quality, for instance using infrared thermography. This however is not possible if VIPs are applied between two relatively well-conducting heavy layers or behind a ventilated air cavity.

UV-radiation: Since the effect of UV-radiation on the long-term stability of the high barrier envelope, and thus on the service life, is still unknown, VIPs should be cleared from direct solar radiation as much as possible.

Delivery and storage: For reasons of damage protection, VIPs and VIP integrated building components should be delivered just-in-time and arranged in the correct sequence exactly before installing them in the building. If, however, delivery takes place prior to installation, these components should be stored under dry conditions to prevent contact between the integrated VIP and liquid water, which may result in deterioration of the barrier envelope.

Tolerances: Since the production dimensions of VIPs currently may vary within an interval of +3 to -6 mm in length for large panels and an interval of ± 1 mm in thickness (Va-Q-tec AG, 2008), sufficient space should be reserved in a building component or an on-site application to accommodate these variations.

protection against internal forces: To allow the integrated VIP to expand due to temperature differences, movement of this panel should be unrestricted as far as possible. According to Simmler et al. (2005), the thermal expansion coefficient of fumed silica lies between $10 \cdot 10^{-6}\ K^{-1}$ and $15 \cdot 10^{-6}\ K^{-1}$, which is in the same order as that of steel. For a temperature difference of 40 K, thermal expansion thus amounts to about 0.4 to 0.6 $mm \cdot m^{-1}$. This dilation can easily be accounted for.

load diffusion: To protect the VIP inside a building construction assembled on-site, the top layer of this construction, i.e. its surface finish, should be able to diffuse (accidental) point loads.

Preparation: As for every building component that cannot be changed in dimensions on-site, exact parts lists and a detailed laying plan need to be prepared in advance. Tolerances and construction irregularities should be taken into account.

Cleaning: With respect to preparing the design, materials that come in contact with the VIP should have a soft or a flat surface without sharp surface irregularities. Besides, a floor or a wall onto which VIPs will be positioned should be cleaned in advance of installation.

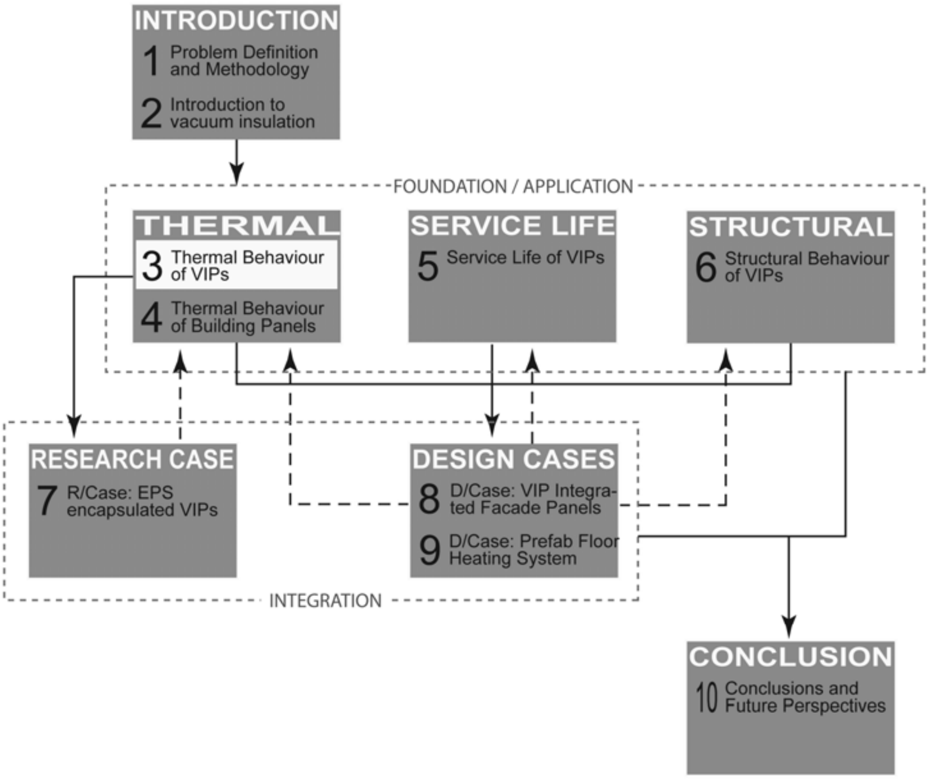
INTRODUCTION
1 Problem Definition and Methodology
2 Introduction to vacuum insulation
FOUNDATION / APPLICATION
THERMAL
3 Thermal Behaviour of VIPs
4 Thermal Behaviour of Building Panels
SERVICE LIFE
5 Service Life of VIPs
STRUCTURAL
6 Structural Behaviour of VIPs
RESEARCH CASE
7 R/Case: EPS encapsulated VIPs
DESIGN CASES
8 D/Case: VIP Integrated Facade Panels
9 D/Case: Prefab Floor Heating System
INTEGRATION
CONCLUSION
10 Conclusions and Future Perspectives

3

Thermal Behaviour of VIPs

Study into the Effect of the Barrier Laminate on the overall Thermal Performance of VIPs

In the previous chapters on methodology, it was explained that this dissertation can be subdivided into two main research domains: foundation/application and integration, and that each of these domains contains several research aspects. This chapter 3 focuses on the aspect of thermal behaviour within the domain of foundation/application, or more specific it focuses on the thermal behaviour on the level of a vacuum insulation panel. It gradually evolves from ideal, or centre-of-panel, behaviour via models to calculate overall thermal behaviour including thermal shunting effects towards practical implications of the overall thermal behaviour of VIPs compared to conventional insulation materials.

Section 3.1 therefore presents a brief introduction into the fundamental heat transfer properties of porous media in general and evacuated porous media in particular. The centre-of-panel thermal conductivity resulting from those properties forms the basis for estimating overall thermal performance of VIPs. Due to the high barrier envelope, necessary to maintain the state of vacuum inside the pores for a relatively long period of time, thermal bridge effects arise. As a consequence, the centre-of-panel performance of a VIP differs from the overall or actual thermal performance, which is discussed in more detail in section 3.2. To calculate overall thermal performance, a measure, named linear thermal transmittance, must be known. This linear thermal transmittance can be calculated numerically for different high barrier envelopes which is however tedious and does not produce insight into the effect of relevant parameters. Therefore analytical (approximation) models to determine this linear thermal transmittance are introduced and tested in section 3.3. In Section 3.4, finally, some practical implications of this edge effect are discussed while VIPs are compared to conventional thermal insulators.

3.1 CENTRE-OF-PANEL THERMAL CONDUCTIVITY OF VIPS

3.1.1 Total centre-of-panel thermal conductivity (core material)

Heat transfer through porous media in general occurs in four main modes: conduction through the solid matrix, conduction through and convection by the gases in the voids, and radiation. Solid skeleton conduction is heat transfer through the solid particles via small point-like contacts between spheres or fibres for a powder or fibre-based core material or through the solid matrix for a foamed core material. In thermal insulators, this process of heat transfer is mainly determined by the effectiveness of energy transfer from molecule to molecule resulting from mutual collisions, especially between molecules of different grains or fibres. The main resistance against solid skeleton heat conduction in porous materials is found at these contact points (Brodt, 1995). Like solid conduction, gas conduction is also a result of molecular collisions. Since, however, gases lack a crystal structure or other structural constraints, collision chances are much lower under atmospheric pressure and at ambient temperature. As a result, they have a lower thermal conductivity than solids. While gas conduction is a result of individual molecular interactions, gas convection results from bulk movement of molecules, i.e. fluid flow. The energy stored in a fluid in the form of internal and kinetic energy moves from one place to another along with the movement of a molecule. Radiative heat transfer, finally, is the net exchange of energy between surfaces of different temperature through electromagnetic waves, thus not necessitating the presence of a medium.

Due to a temperature gradient over a material, a heat flux[1], q [$W \cdot m^{-2}$], is generated directed from a high to a low temperature. In building practise, this total heat flux consisting of the four modes of transfer described above, however, is phenomenologically typified as a ‘conductive’ heat flux. From this phenomenological perspective, we then may consider this total heat flux directly proportional to a temperature gradient according to Fourier’s law with the proportionality constant being the thermal conductivity of the material. This overall thermal conductivity thus also consists of the four main heat transfer modes in porous materials.

It has been demonstrated by several researchers (Achtziger, 1960; Zehender, 1964; Rath, 1989) that (free) convection through the gas phase is negligible in porous materials having small pores, a sufficient thickness and a low gas pressure, as a consequence conducing to only three heat transfer modes significant for vacuum insulation panels. These remaining modes, however, cannot simply be

[1] Heat flux is defined as the heat flow per unit area normal to the direction of this heat flow.

superposed; interactions and coupling effects between the different modes may occur, as a result of which

$$q > q_s + q_g + q_r \qquad (3.1),$$

in which *s* stands for solid skeleton conduction, *g* for gas conduction and *r* for radiation. In some cases, the coupling terms can raise the heat flux considerably[2,3]. Dividing equation (3.1) by the temperature gradient and adding an individual term for interactions and coupling effects results in an expression for the overall thermal conductivity, λ_c, as

$$\lambda_c \approx \lambda_s + \lambda_g + \lambda_r - \frac{dx}{dT} q_{coupling} \qquad (3.2).$$

For standard thermal insulators, the solid skeleton conductivity in this equation varies between $1{\cdot}10^{-3}$ and $30{\cdot}10^{-3}$ $W{\cdot}m^{-1}{\cdot}K^{-1}$; the gas conductivity is approximately $25{\cdot}10^{-3}$ $W{\cdot}m^{-1}{\cdot}K^{-1}$ at ambient pressure and temperature; and the contribution of radiation at room temperature varies between $1{\cdot}10^{-3}$ and $10{\cdot}10^{-3}$ $W{\cdot}m^{-1}{\cdot}K^{-1}$. For Polystyrene, for example, we obtain a total thermal conductivity at room temperature and atmospheric pressure of $2{\cdot}10^{-3}$ (λ_s) + $25{\cdot}10^{-3}$ (λ_g) + $10{\cdot}10^{-3}$ (λ_r) = $37{\cdot}10^{-3}$ $W{\cdot}m^{-1}{\cdot}K^{-1}$ (van Went, 2002). For dried and evacuated opacified fumed silica at room temperature, for instance, we get $3{\cdot}10^{-3}$ to $4{\cdot}10^{-3}$ (λ_s) + $0{\cdot}10^{-3}$ (λ_g) + $1{\cdot}10^{-3}$ (λ_r) = $4{\cdot}10^{-3}$ to $5{\cdot}10^{-3}$ $W{\cdot}m^{-1}{\cdot}K^{-1}$. These examples clearly demonstrate the influence of gas conduction on the total thermal conductivity; it is responsible for approximately 67% of the heat transported through Styrofoam. If, however, the gas pressure in the insulator is reduced to below a certain value, as will be explained in the next subsection, gas conduction can be reduced to almost zero thus reducing the total conductivity considerably. This is the fundamental principal of vacuum insulation technology[4].

---

[2] This, for example, occurs with powder- and fibre-based materials, which have many point-like contacts. Here, the thermal conduction through the gas phase more-or-less thermally bridges the point contacts. In polymer foams and aerogels with a coherent internal structure, however, these coupling terms may be neglected.

[3] While for polymer foams and aerogels interactions and coupling effects may be neglected, for powder-based materials, like fumed silica, and fibre-based materials, like mineral wool, they may not, resulting in complex relationship between solid skeleton conduction, gas conduction and radiation. From literature many models are known which in some way try to calculate the overall thermal conductivity from the different partial conductivities (Rath, 1989). Since it is beyond the scope of this dissertation to present and discuss some or all of these models, it is referred to the dissertation by Rath (1989) for a more detailed introduction.

[4] A thorough description of the different components of the thermal conductivity are presented in appendix A34.

3.1.2 Gas conduction thermal conductivity

From kinetic gas theory several theoretical relationships for the unrestricted[5] gas thermal conductivity, $\lambda_{g;0}$, can be derived (Rath, 1989). This gas thermal conductivity is independent of gas pressure. Rath (1989) explains that the number of molecules, and thus the number of collisions, is directly proportional to pressure while the mean free path of these molecules[6], and thus the amount of energy transferred per collision, is inversely proportional to this pressure. Consequently, both effects cancel each other out. For air at atmospheric pressure and at 10 °C $\lambda_{g;0}$ approximately equals $25.3 \cdot 10^{-3}$ W·m^{-1}·K^{-1}.

If, however, a gas is placed between two parallel flat plates with an intermediate distance δ [m], which is in the same order of magnitude as the mean free path of the gas molecules, the molecules near the edges are restrained in their movement (Smoluchowski effect (Smoluchowski, 1898)) and almost all collisions are between gas molecule and boundary, which are highly elastic. As a result, the gaseous thermal conductivity reduces in magnitude. In such situations the gas conductivity, λ_g, does depend on pressure and can, according to McAdams (1954), be expressed as

$$\lambda_g = \frac{\lambda_{g;0}}{1 + \dfrac{2X \cdot mfp}{\delta}} \tag{3.3}$$

provided that no convection occurs. For the gas thermal conductivity, this equation shows that besides the unrestricted gas thermal conductivity three parameters are of importance: a dimensionless variable X (with a value of approximately 1.6 for the combination of air and fumed silica (Fricke et al., 2006; 2008)), the mean free path of the considered gas, *mfp* [m] and the distance between the boundaries, δ [m].

This mean free path of the unrestricted molecules is the average distance a gas molecule travels between two collisions, being a function of gas pressure, p_g [Pa]. This pressure dependency can easily be explained by looking at the number of gas molecules per unit of volume present at different pressures. The lower the pressure, the fewer molecules per unit of volume and thus the larger the distance travelled between collisions. The mean free path can be expressed as (Simmler et al., 2005)

$$mfp = \frac{k_B \cdot T}{\sqrt{2} \cdot \pi d_c^2 p_g} = c\frac{T}{p_g} \tag{3.4}$$

[5] Unrestricted means that the gas is not limited in its movement by boundaries or other obstacles.

[6] The mean free path of a gas is the average distance a molecule traverses before it collides with another gas molecule.

With k_B [J·K^{-1}] the Boltzmann constant (k_B = 1.38·10^{-23} J·K^{-1}), T [K] the absolute temperature and d_c [m] the collision diameter of the molecule (for air 3.53·10^{-10} m at ambient pressure and 298 K). The proportionality constant in the second part of Equation (3.4), c, differs for each type of gas. For air[7], for example, this constant equals 2.49·10^{-5} m·Pa·K^{-1}, at ambient pressure resulting in a mean free path of 7·10^{-8} m and at a pressure of 1 mbar in a value of 7·10^{-5} m.

Although Equation (3.3) is only valid for a gas between two parallel plates, it can be used to estimate the gas conductivity in a void of a micro porous thermal insulating material. The distance, δ, in that case is not the distance between two parallel plates, but an average distance between the surfaces of two spheres for powder insulation or an equivalent average void diameter for foamed or fibre-based insulation materials. This average distance, or mean chord distance, is a function of mean particle diameter, d_p, or mean fibre diameter, d_f, and of porosity, ε.

Combining Equations (3.3) and (3.4), we can now rewrite Equation (3.3) as (Simmler et al., 2005; Caps et al., 2001)

$$\lambda_g = \frac{\lambda_{g;0}}{1 + C\dfrac{T}{\delta \cdot p_g}} = \frac{\lambda_{g;0}}{1 + \dfrac{p_{1/2}}{p_g}} \qquad (3.5),$$

clearly showing that four properties are relevant in developing vacuum insulation panels: the type of gas (first gas property), the gas pressure (second gas property), the temperature (environmental property), and an equivalent pore diameter (insulation material property). In this equation C is a constant, which depends on the type of gas. This second equation expresses the gas conductivity among others as a function of pore gas pressure, p_g, and a typical gas pressure at which one half of the gas conductivity $\lambda_{g;0}$ has developed, $p_{1/2}$. From this equation, we can learn that, if the gas pressure is reduced, gas conductivity will be reduced as well. In Table 3.1 values for $\lambda_{g;0}$ and $p_{1/2}$ are given for some material-gas-combinations.

Based upon the basic physics of gas conduction through porous insulator materials, a description of the effect of reducing gas pressure in vacuum insulation panels can be presented. Figure 3.1 demonstrates how for different potential VIP core materials the thermal conductivity is reduced due to a reduction of internal gas pressure. As can be seen, three different pressure regions can be distinguished: low pressure region, intermediate pressure region and high pressure region.

[7] To calculate the constant for air, the properties of nitrogen are used.

Table 3.1 -Parameters determining the thermal conductivity / gas pressure curve at 20°C.

core	gas	λ_0 [$\cdot 10^{-3}$ W$\cdot$m$^{-1}\cdot$K^{-}	$\lambda_{g;0}$ [$\cdot 10^{-3}$ W$\cdot$m$^{-1}\cdot$K^{-1}]	$p_{1/2}$ [mbar]
fumed silica	Air[a,c,e]	4-5	26.0	600-800
	water[b,e]	4.2	16.0	120
Perlite powder	air[a]	6-8	26.0	2-10
Elastogran PU	air[d]	7.0	26.0	1.8
glass fibre board	air[a]	1.5-3	35.2	1-5

NB: According to theory, $\lambda_{g;0}$ should only depend on the type of gas. For air at room temperature, this value equals $26.0\cdot 10^{-3}$ W$\cdot$m$^{-1}\cdot$K^{-1}, as can be seen for fumed silica and PU foam. In the case of glass fibre insulation however the value for $\lambda_{g;0}$ is higher than the value for unrestricted still air at room temperature. This is caused by the coming into existence of contact bridges between the glass fibres and the gaseous phase inside the pores. These bridges thermally shortcut the heat flows thus increasing the thermal conductivity. This shortcut effect is incorporated into the $\lambda_{g;0}$ for air within glass fibre insulation.

[a] Caps et al., 2008; [b] Fricke et al., 2006; [c] Simmler et al., 2005; [d] Elastogran, 2005; [e] Schwab, 2004.

In the low pressure region, a plateau exists for which gas conduction is practically non-existent, as a result of which reducing gas pressure does not have any significant further effect. This occurs if the so-called Knudsen-number, which is the ratio of *mfp* to δ, has become much larger than 1. In this low pressure region, the mean free path of the gas molecules is much larger than the size of the voids in which the gas in trapped. This implies that collisions between gas molecules hardly occur. In the remaining collisions between gas molecules and the void surrounding solid material, which are almost completely elastic, hardly any energy is transferred.

In the high pressure region, i.e. for $Kn << 1$, a second plateau exists at which changes in gas pressure do not influence gas conduction inside the material pores. Here, the mean free path is less than the void size and lateral collisions between molecules are dominant. The gas conductivity in this region takes on a constant value, which equals the unrestricted gas thermal conductivity, $\lambda_{g;0}$.

In the intermediate range, finally, where $Kn \approx 1$, the transition between high gas conductivity and practically zero gas conductivity occurs. In this intermediate pressure region, changes in gas pressure strongly affect gas conductivity.

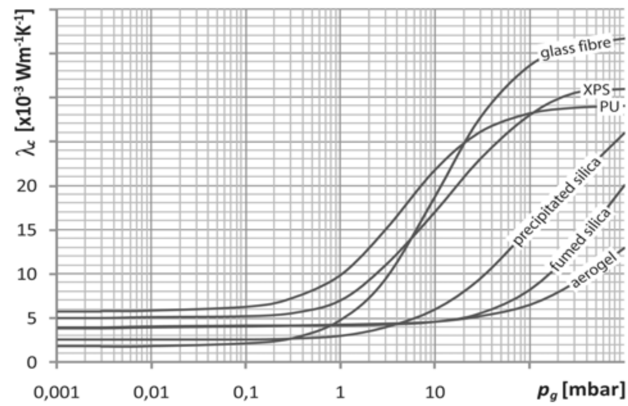

Figure 3.1

Effective thermal conductivity of different potential VIP core materials as function of internal gas pressure. Based on Cabot (2003) and Simmler et al. (2005).

Since in the definition of the Knudsen-number the mean free path, *mfp*, and the void size, expressed by δ, are present, both factors can influence the gas thermal conductivity. Reducing this void size has a similar effect as reducing the internal gas pressure. For vacuum insulation technology, therefore, materials with small pore sizes and a pressure reduced to below the Knudsen region should be taken. For building applications, fumed silica is therefore the most widely used and most suited core material since it allows a large pressure increase before its thermal conductivity increases. Kaganer (1969) was one of the first to conduct extensive thermal conductivity measurements on fibrous and powdery materials. He measured the thermal conductivity as function of pore gas pressure, external load and temperature. Several decades later more accurate measurements have been conducted by Caps and Fricke (2000), Caps et al. (2001) and Simmler et al. (2005).

3.1.3 Moisture

Moisture can have a significant influence on the thermal conductivity of a vacuum insulation panel in several ways. Water vapour that has permeated through the high barrier laminate into the core material will be present as vapour in the pores and as capillary condensed and/or molecularly adsorbed water. Water vapour influences the thermal conductivity by increasing the pore gas pressure, p_g. The effect of water vapour pressure on thermal conductivity however differs from the effect of dry gas pressure on thermal conductivity, i.e. the values $\lambda_{g;0}$ and $p_{1/2}$ differ. The adsorbed water on the other hand increases the solid conductivity of the core material considerably by modifying the contact between solid grains and by creating water bridges between these grains.

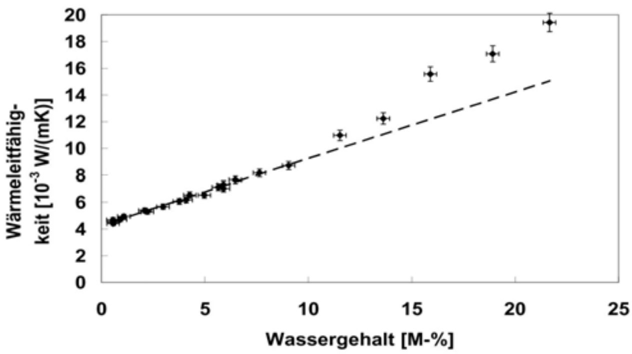

Figure 3.2

Effect of water content, u [mass%], on thermal conductivity for fumed silica samples (Schwab, 2004).

Investigations at CSTB in France (Quenard and Sallée, 2004) and at ZAE-Bayern in Germany (Schwab, 2004; Schwab et al., 2005) have shown that the effect of water content, u [kg·kg^{-1}], on thermal conductivity at a mean temperature of 10°C, for a panel thickness of 20 mm[8] and for a maximum water content of 5 m% can be approximated sufficiently accurately by[9]:

$$\lambda_c = \lambda_{c;dry} + a_m u \qquad (3.6).$$

In this equation, $\lambda_{c;dry}$ [W·m^{-1}·K^{-1}] is the thermal conductivity of the completely dry core material, u [kg·kg^{-1}] the water content and a_m [W·m^{-1}·K^{-1}] a proportionality factor. Although Schwab (2004) determined this proportionality factor from gravimetric measurements and estimated it to be 4.8·10^{-2} W·m^{-1}·K^{-1} for tested fumed silica samples up to a water content of 10 mass%, he also showed in his dissertation that it actually should be corrected for the effects of water vapour on thermal conductivity. After correction, this value was found to be 2.9·10^{-2} W·m^{-1}·K^{-1}. Although this approximation is factually solely valid for the conditions specified, it can be used as a rough estimate for other conditions as well provided that the conditions stay within standard limits for architectural applications. Moreover, by fitting a theoretical model to experimental results Beck et al. (2007b) derived a value of 5.0·10^{-2} W·m^{-1}·K^{-1} for this proportionality factor and a value of 2.4·10^{-2} W·m^{-1}·K^{-1} after regression analyses in which also latent heat transport effects due to liquid and vapour flow were accounted for[10,11]. Quenard and Sallée (2004) finally

[8] At one side of the panel the temperature was 0°C, at the other side 20°C. Panel dimensions were 30x30x2 cm^3.

[9] For many more materials, this effect can be approximated using a linear function.

[10] As shown by Beck et al. (2007b, 2009), Heinemann (2008) and Platzer (2007a) the presence of water inside a VIP core might have several additional effects on its apparent thermal conductivity. Water affects the structure of the core resulting in increased irreversible shrinkage when an external load is applied. This shrinkage results in a smaller thickness and higher density resulting in higher apparent thermal conductivity values. Moreover, a

found for fumed silica a value between $19.0 \cdot 10^{-3}$ and $20.7 \cdot 10^{-3}$ $W \cdot m^{-1} \cdot K^{-1}$ for λ_{dry} at ambient pressure and temperature and between 1.36 and 1.70 $W \cdot m^{-1} \cdot K^{-1}$ for a_m, which considerably exceeds the values from Schwab and Beck et al[12]. Although equation (3.6) is factually solely valid for the conditions specified, it can be used as a rough estimate for other conditions as well provided that the conditions stay within standard limits for architectural applications.

3.2 Overall Thermal Performance of VIPs

3.2.1 Previous research

As explained in the previous section, the vacuum inside the pores of the core material reduces the thermal conductivity of the product significantly (Brodt, 1995; Caps et al., 2001; Rath, 1989). A VIP of only 20 mm can therefore replace a conventional mineral wool or PU-foam insulation of 185 mm or 120 mm respectively. This reduction of thickness is among the most interesting features for large-scale application of vacuum insulation panels in the building industry.

To maintain the vacuum inside the core material for a period as long as possible (at least 25 years but preferably 50 years or more for architectural applications), a barrier material with very low water vapor and gas permeance is required. This barrier laminate completely surrounding the evacuated core, however, forms a thermal bridge between both sides of the panel. This edge effect is particularly important for metal-based barrier envelopes. A VIP of 1x1 m^2 with a

---

temperature gradient over a vacuum results in water vapour and liquid water flow. Suppose on one side, the temperature is increased. At this place the relative humidity within the pores will suddenly drop resulting in desorption according to the material's sorption isotherm. As a result, the partial water vapour flow will increase resulting in vapour flow from the hot to the cold side. At the cold side, the partial water vapour pressure and relative humidity will thus increase resulting in adsorption here. Due to this desorption and adsorption a water content gradient will appear over the panel resulting in liquid water flow back from the cold to the hot side. A temperature gradient thus results in water vapour flow from the hot to the cold side and liquid water flow in the reverse direction. This in turn leads to an increase in apparent thermal conductivity of about 0.5 to $1.7 \cdot 10^{-3}$ $W \cdot m^{-1} \cdot K^{-1}$ (Beck et al., 2007b).

[11] It is important to realise that the micro-structure of fumed silica might be modified if much water is present in its pores. Morel et al. (2007; 2009) observed that when fumed silica samples were subjected to a combination of a high temperature (35°C-60°C) and high relative humidity (80%) hydroxylation of the surface occurred leading to an increased capacity to take up water. At the same time, they observed a reduction of the specific surface area of these samples.

[12] Regarding these differences it must be noted that the values by Beck et al. (2007b) and Schwab (2004) were determined for evacuated VIPs while the value from Quenard and Sallée (2004) was determined for VIPs at ambient conditions.

centre-of-panel U-value of 0.2 $W \cdot m^{-2} \cdot K^{-1}$, for example, has an ideal[13] effective thermal transmittance (U_{eff}-value) of approximately 0.33 (=+64%), 0.32 (=+60%) or 0.21 (=+4%) $W \cdot m^{-2} \cdot K^{-1}$ for a 6 μm aluminium based foil, a 50 μm stainless steel based foil or a 97 μm laminated metallized polymer film respectively[14] (van Went, 2002). If the effect of a seam at the panel edge is considered as well, this effective thermal transmittance even increases to approximately 0.36 (=+80%), 0.35 (=+75%) or 0.23 (=+15%) $W \cdot m^{-2} \cdot K^{-1}$ respectively for the aforementioned barrier laminates. From these values, it is clear that the thermal bridge effect cannot always be neglected and is most significant for aluminium and stainless steel barrier foils.

Several investigations into the thermal conductivity of VIPs have already been performed. Glicksman (1991) and di Gregorio (2003) were among the first to mathematically define thermal bridge effects that occur on vacuum and reflective insulations. The first studies were mainly limited to centre-of-panel values (Stovall and Brzezinski, 2002). As shown in the previous paragraph, however, these values are not representative for the panel as a whole, resulting in too optimistic values for the overall thermal performance. Most researchers therefore used numerical calculation techniques for estimating thermal edge effects of VIPs, in which the laminate or encasing was schematised as either a single layer with averaged thermal conductivity (Brodt and Bart, 1994; Brodt, 1995; van Went, 2002; Bundi, 2003; Willems et al., 2005, Gudmundsson, 2009) or as a multi-layered structure, each layer having its own thermal conductivity (Ghazi Wakili et al., 2004). Ghazi Wakili et al. (2004) also performed experimental studies to investigate the effect of the heat flows through the panel edge. They, for example, found a value for the linear thermal transmittance of a 18 mm VIP with a fumed silica core and a metallized high barrier film including seam of $(6.96 \pm 1.63) \cdot 10^{-3}$ $W \cdot m^{-1} \cdot K^{-1}$. Simmler and Brunner (2005) and Baetens (2009) also declare some thermal design values for VIPs based upon both thermal considerations and service life estimates. Moreover, Nussbaumer et al. (2005, 2006), Schwab et al. (2005e) and Grynning et al. (2009) investigated thermal bridge effects of VIP integrated building systems. And Thorsell and Källebrink (2005) and Thorsell (2006b) finally studied the possibility of reducing thermal shunting in VIPs covered with stainless steel foil based laminates by introducing a so-called serpentine edge.

All previously mentioned studies have in common that they have led to a better understanding of the thermal bridge effect of VIPs and of the importance of minimising this effect. The presented experimental and numerical data, for example,

---

13 Ideal in this context is defined as not having a seam at the edge of the VIP.

14 These values are calculated for a panel size of 1 x 1 m^2, a panel thickness of 20 mm and a core thermal conductivity of $4 \cdot 10^{-3}$ $W \cdot m^{-1} \cdot K^{-1}$.

are very useful for analysing the quantitative deviation between centre-of-panel thermal conductivity and effective panel thermal conductivity, which value is higher due to the thermal bridge. The procedures and methods described and demonstrated, however, are accurate but quite laborious and time-consuming and thus not suitable for practical purposes, e.g. for application in a design and manufacturing process.

The remaining sections of this chapter, therefore, lead to the introduction of analytical models for easily calculating thermal shunting of VIP high barrier envelopes within a single step. They not only facilitate the calculation process, but by varying individual parameters also generate knowledge and insight into the significance of these thermal bridge influencing parameters, as a result enabling VIP manufacturers and designers to improve their products. Numerical data will be used to validate the proposed models and to give an indication of the error made. Only thermal shunting due to the vacuum insulation high barrier envelope and not due to edges of building panels, in which vacuum insulated panels are integrated, is considered in this chapter. Thermal bridge effects in building panels will be discussed and modelled in the next chapter.

3.2.2 Effective thermal conductivity and thermal conductance

While the centre-of-panel thermal properties characterize the whole thermal behaviour of conventional homogeneous insulators, they are not able to do so for vacuum insulation panels, since they do not take into account additional thermal flows at the edges of these panels. These additional heat flows result from the high thermal conductivity of gas and vapour barriers completely enveloping a VIP, or more accurately from the difference in thermal resistance between centre-of-panel region and panel edge region. This high barrier film thus forms a thermal bridge between both sides of the panel. As can be seen from Figure 3.3, the heat flux towards a conventional homogeneous thermal insulator is constant over the entire surface of the panel, while that flux increases near the edge for materials enveloped by a thermally highly conducting barrier. Since the total heat flow towards (or from) an insulation panel, $\phi_{q;total}$ [W·m^{-1}], equals the integral of that heat flux over the length of the panel, or in symbols

$$\phi_{q;total} = \int_0^L q \cdot dx \qquad (3.7),$$

which equals the surface area below the lines in Figure 3.3, the total heat flow through a material with a thermal short-cut at its edge is higher than the heat flow through the same material without this edge effect.

For characterizing the overall thermal performance of non-homogeneous materials, European and Dutch standards (NEN-EN-ISO 10077-1, NEN-EN 13947, NEN 1068) introduce the concept of linear thermal transmittance, ψ [$W \cdot m^{-1} \cdot K^{-1}$]. The linear thermal transmittance is defined as the additional amount of heat transferred through a panel or construction with thermal bridges related to the same panel or construction without these bridges, which actually is a difference in surface area between the two graphs in Figure 3.3 divided by the temperature difference.

For an accurate description of the overall thermal performance of a VIP, we have to distinguish between the linear thermal transmittance of a panel edge, $\psi_{vip,edge}$ [$W \cdot m^{-1} \cdot K^{-1}$], and the corner thermal transmittance[15], $\chi_{vip,corner}$ [$W \cdot K^{-1}$]. As demonstrated in Figure 3.4, presenting a schematic representation of a VIP, $\psi_{vip,edge}$ defines the additional heat flow as a consequence of a material thermal bridge (laminate at the edge), while $\chi_{vip,corner}$ defines the additional heat flow as a result of a geometric thermal bridge alone (corner).

Based upon these thermal transmittances, it is possible to determine two quantities to characterize the overall thermal performance of a vacuum insulation panel. The first quantity, the effective thermal conductivity, λ_{eff} [$W \cdot m^{-1} \cdot K^{-1}$], can be approximated as (Schwab et al., 2005; Simmler et al., 2005)

$$\lambda_{eff} \approx \lambda_{cop} + \frac{d_p l_p}{S_p} \psi_{vip,edge} + \frac{d_p}{S_p} \sum_{i=1}^{n} \chi_{vip,corner,i} \qquad (3.8),$$

with λ_{cop} [$W \cdot m^{-1} \cdot K^{-1}$] the centre-of-panel thermal conductivity, d_p [m] the panel thickness of the core, l_p [m] the panel circumference, S_p [m^2] the surface area of one side of a panel, and n the number of corners. The second quantity is the effective thermal transmittance, U_{eff} [$W \cdot m^{-2} \cdot K^{-1}$], which is determined from

$$U_{eff} = U_{cop} + \frac{l_p}{S_p} \psi_{vip,edge} + \frac{1}{S_p} \sum_{i=1}^{n} \chi_{vip,corner,i} \qquad (3.9).$$

Assumed that in most circumstances the corner thermal bridge effect is significantly smaller than the effect of the panel edge, the third term on the right hand side of Equations (3.8) and (3.9) may be neglected[16].

---

[15] It is important to realize that both the linear and the corner thermal transmittance depend on boundary heat transfer coefficients.

[16] To check this assumption, both the corner and edge thermal transmittance of a 20 mm thick VIP with an 8 μm thick aluminium foil and a thermal conductivity of its core of $4 \cdot 10^{-3}$ $W \cdot m^{-1} \cdot K^{-1}$ have been calculated according to the procedures described below. A ψ-value of $3.9 \cdot 10^{-2}$ $W \cdot m^{-1} \cdot K^{-1}$ and a χ-value of $-4 \cdot 10^{-4}$ $W \cdot K^{-1}$ were computed numerically. This very small χ-value is below the inaccuracy limits of the computation. Even for very small panels, it is negligible compared to the linear thermal transmittance.

Figure 3.3

Schematic representation of the heat flows through a homogeneous thermal insulation panel and a panel with a thermal bridge arising from a barrier envelope. Note: the arrows in the figure only indicate the direction and not the magnitude of the heat flow.

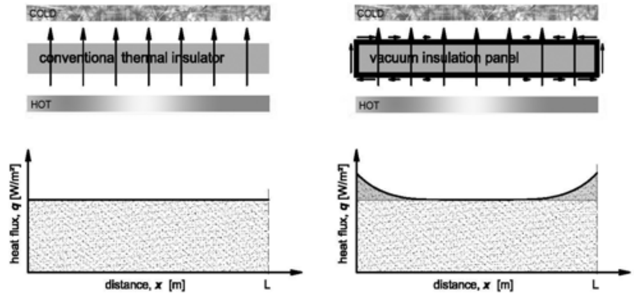

Figure 3.4

Schematic representation of a vacuum insulation panel indicating the difference between linear thermal transmittance and corner thermal transmittance.

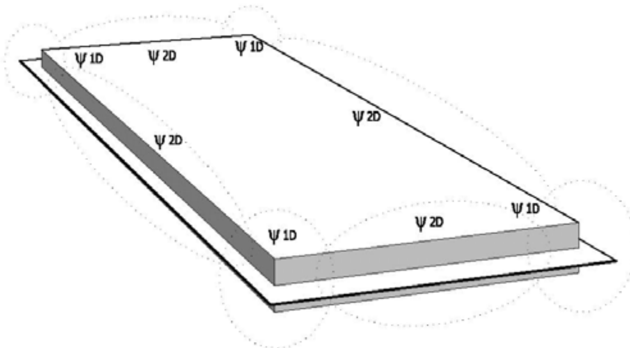

Both equations clearly show the difference between a homogeneous insulation material, for which the effective thermal conductivity equals the centre-of-panel thermal conductivity, and a VIP, for which the centre-of-panel thermal conductivity needs to be modified to obtain the effective thermal conductivity. As a result of the linear thermal transmittance, the effective thermal conductivity of a VIP is increased, the amount of which depends on the thickness and the thermal conductivity of the barrier envelope, the type of seam, the panel size, the centre-of-panel thermal conductivity and the panel thickness, as will be discussed in section 3.3. It is, however, sufficiently clear that, if the type of insulator material cannot be changed, the lowest value for U_{eff} is generated with a linear thermal transmittance as low as possible and a more-or-less square panel of large dimensions.

3.2.3 Thermal transmittances: determination

Having introduced the linear thermal transmittance and the corner thermal transmittance in the previous section, we must now establish a method to determine these transmittances. Generally, three approaches are distinguished: experimental procedure, numerical calculation and analytical modelling. The second and the third approach are adopted for investigating VIP thermal bridge effects more thoroughly.

For numerical thermal simulations in this dissertation, the thermal analysis software package Trisco developed by Physibel is used. This is a simulation tool able to calculate 3D steady-state heat transfer phenomena through rectangular materials and constructions respectively using the energy balance technique (Physibel, 2002). In concordance with the discussion in subsection 3.2.2, a 2D analysis is performed to calculate the linear thermal transmittance of panel edges (thus only ψ-value and not χ-value). Numerical computations are used to verify and validate the model which will be proposed in the next section.

When applying thermal analysis software for calculating heat flows and temperature fields within façade constructions, several parameters need to be specified, among others the boundary conditions, the desired accuracy and the panel dimensions.

The boundary conditions represent the inside climate on the one hand and the outside climate on the other hand. Since according to European standards (NEN-EN-ISO 10077-1, 2004; NEN-EN-ISO 10211, 2008; NEN-EN 13947, 2000) a steady-state analysis is required to calculate thermal transmittances, the actual climates are reduced to a stead-state temperature, T [K], and a boundary heat exchange coefficient, α [W·m^{-2}·K^{-1}], as specified in Table 3.2.

The required accuracy for the simulation is specified in the international standard NEN-EN-ISO 10211 (2008). This standard states the requirement that the grid applied to the constructions needs to be this fine that for a doubling of the number of gridlines the heat flow does not change with more than 2%. Under this condition a sufficiently accurate result is obtained. Because of large differences in thermal conductivity between adjacent material layers, for instance between core material with $\lambda_c = 4.0 \cdot 10^{-3}$ W·m^{-1}·K^{-1} and aluminium foil with $\lambda_f = 225$ W·m^{-1}·K^{-1}, and because of the presence of very thin material layers, the grid required to fulfil the specified condition would be very dense. As a consequence, not all envelope material layers are modelled separately but are combined into groups of equal thermal conductivity, thus reducing the number of grids and calculation time considerably[17].

The panel width, b_p [m] and panel length, l^{2D} [m] are chosen to be 200 mm and 1000 mm respectively. Since it is desired to have values for the linear thermal transmittance that are independent of panel width, these dimensions need to be outside the range influenced by the thermal bridge. Van Went (2002) showed that for vacuum insulation panels a panel width of 200 mm satisfies this condition. As a

[17] This assumption is justified since, if the direction of heat flow is perpendicular to the surface of the laminate, all layers act as a thermal resistance and the sequence of these resistances is irrelevant and since, if the direction of heat flow is parallel to the surface of the laminate, the difference between the product of thickness and thermal conductivity of each layer is small (at most a factor of 5 to 6 in case of a metallised film).

__Table 3.2__ - Boundary conditions.

climate	T [K]	α [W·m^{-2}·K^{-1}]
inside	293	7.8
outside	263	25

__Table 3.3__ - Thermal conductivity of barriers.

material	λ [W·m^{-1}·K^{-1}]
aluminium foil laminate	225[a]
stainless steel foil laminate	25[a]
metallized film lam.: HDPE	0.32[b]
metallized film lam.: PET	0.28[b]
metallized film lam.: alu.	200[b]
2-layer met. lam.: average	0.39[c]
3-layer met. lam.: average	0.54[c]

[a] van Went (2002);
[b] Ghazi Wakili et al. (2004);
[c] The thickness of these laminates is 84 μm (60 μm HDPE, 2x12 μm PET and 40 nm met.) and 97 μm (60 μm HDPE, 3x12 μm PET and 120 nm met.) respectively.

result of this condition, however, the numerically calculated (and analytically modelled) transmittance values are strictly solely valid for panels longer and wider than the thermal bridge influence length. Notwithstanding this effect, they can also be used to indicate the edge effect for smaller panels, however with less accuracy.

The values obtained from a guarded hot plate experiment or numerical simulations represent total heat flows, thus including both centre-of-panel heat flows and additional edge (and/or corner) flows. Both the linear thermal transmittance and the corner thermal transmittance, however, can be computed from these total values. Based upon the total heat flow, $\phi_{q;total}$ [W], the linear thermal transmittance can be obtained from

$$2\psi_{vip,edge} = \frac{\phi_{q;total} - 2\phi_{q;cop}}{l^{2D}\Delta T} = \frac{\phi_{q;total}}{l^{2D}\Delta T} - 2U_{cop}b_p \quad (3.10),$$

with $\phi_{q;cop}$ [W] the central heat flow, ΔT [K] the applied temperature difference, l^{2D} [m] the simulated panel length, typically set at 1 m, and U_{cop} [W·m^{-2}·K^{-1}] the centre-of-panel thermal transmittance. The factor 2 on both the right and the left side of the equation is a result of the geometry defined for numerical simulation. As demonstrated in Figure 3.5, two identical vacuum insulation panels are placed in adjacent position. If, based on symmetry considerations, only one panel is calculated and an adiabatic condition is forced on the plane of symmetry, both factors 2 in Equation (3.10) would become unity[18].

[18] A similar equation can be derived for calculating the χ-value from a three dimensional numerical model. Since these values are not further used in this dissertation, this equation is not presented here.

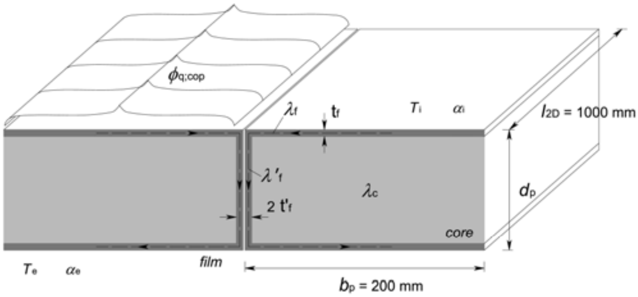

Figure 3.5

Model for numerical calculation of $\psi_{vip,edge}$ -values (2D-model of two edges).

3.3 THERMAL BRIDGING OF VIPS: ANALYTICAL APPROXIMATION MODELS

3.3.1 Analytical models for calculating thermal bridge effects due to envelopes

The approximating models presented in this section are based on an approach generally used for calculating the thermal behaviour of linear thermal bridges, like protruding balcony floor slabs. The representation of the thermal bridge effect induced by a high barrier foil or film is shown in Figure 3.5. For the derivation of these models the following are assumed:

- The length of the vacuum insulation panel is presumed infinite. At a defined distance x and y from the origin the temperature of the foil at surface i, therefore, equals the surrounding air temperature, T_i. At that point the influence of the thermal bridge on the temperature of the foil has diminished (Figure 3.6).
- The boundary heat transfer coefficient α_i is constant across the surface of surface i and the temperature T_i is constant over the cross-section through this barrier laminate.
- Additional radiative heat transfer processes not covered by the boundary heat transfer coefficients, α_i, are not considered.
- No lateral heat exchange between VIPs in the panel edge region occurs.

Considering the preceding assumptions, the linear thermal transmittance of the thermal bridge as a result of the high barrier envelope of a VIP can be estimated with the following equation, the derivation of which is presented in appendix A32[19]:

---

[19] Regarding the models presented in this section one remark must be posed. Both equations yield the linear thermal transmittance of the edge of just one panel. If thus two panels are closely adjoined, the linear thermal transmittance of the combined junction equals the sum of both individual transmittances, at least for equal panels.

Figure 3.6

Schematic representation of the thermal bridge arising from the thin film high barrier envelope around a vacuum insulation panel

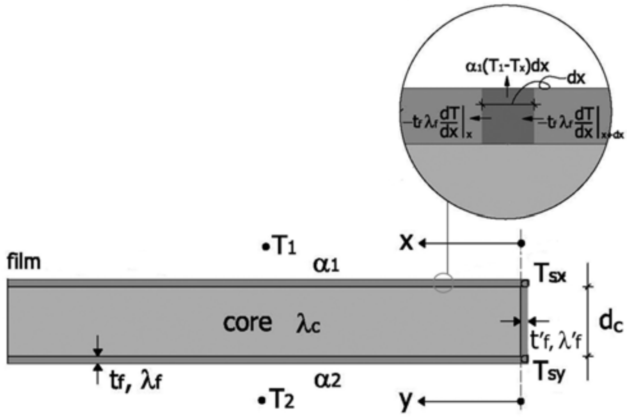

$$\psi_{vip,edge} = \frac{1}{1+\frac{\lambda_c}{\alpha_1 d_p}+\frac{\lambda_c}{\alpha_2 d_p}} \cdot \left[\frac{\alpha_1 (N_2^2 - B)}{\frac{d_p t_f \lambda_f}{t_f^{'} \lambda_f^{'}}\left(N_1^2 N_2^2 - B^2\right) - \lambda_1 \sqrt{N_1^2 N_2^2 - B^2}\left(1+\frac{2B}{\sqrt{D}}\right) - \lambda_2 \sqrt{N_1^2 N_2^2 - B^2}\left(1-\frac{2B}{\sqrt{D}}\right)}\right] \quad (3.11),$$

provided that the envelope consists of the same barrier laminate on both sides of the panel. In appendix A33, an equation is presented that is able to estimate the linear thermal transmittance of the edge of a VIP with different barrier laminates on each side. The parameters N_1, N_2 and B are calculated as

$$N_i = \sqrt{\frac{\alpha_i}{t_f \lambda_f} + \frac{\lambda_c}{t_f \lambda_f d_p}} \quad (3.12a),$$

$$B = \frac{\lambda_c}{t_f \lambda_f d_p} \quad (3.12b),$$

while λ_1 and λ_2 in Equation (3.11) are the eigenvalues of the linear system of differential equations derived to represent the thermal phenomenon. They are calculated as

$$\lambda_1 = -\sqrt{\frac{(N_1^2 + N_2^2) - \sqrt{(N_1^2 - N_2^2)^2 + 4B^2}}{2}} \quad (3.13a),$$

$$\lambda_2 = -\sqrt{\frac{(N_1^2 + N_2^2) + \sqrt{(N_1^2 - N_2^2)^2 + 4B^2}}{2}} \qquad (3.13b),$$

D is the discriminator of the second square root of the eigenvalues, which equals

$$D = \left(N_1^2 - N_2^2\right)^2 + 4B^2 \qquad (3.14).$$

In these equations, α_i [W·m^{-2}·K^{-1}] is the heat transmission coefficient at boundary surface i (i=1 or 2), d_p [m] is the thickness of the vacuum insulation panel, t_f [m] is the thickness of the barrier laminate, t'_f [m] is the thickness of this laminate at the panel's edge, λ_f [W·m^{-1}·K^{-1}] is the laminate thermal conductivity and λ'_f [W·m^{-1}·K^{-1}] is the laminate thermal conductivity at the panel's edge.

If now the limit for $\lambda_c \downarrow 0$ is taken for Equation (3.11), an equation for calculating the linear thermal transmittance due to the barrier laminate surrounding a VIP with a thermal conductivity of its core of 0 W·m^{-1}·K^{-1} arises[20]:

$$\psi_{vip,edge,0} = \frac{1}{\frac{d_p}{t'_f \lambda'_f} + \frac{1}{\sqrt{\alpha_1 t_f \lambda_f}} + \frac{1}{\sqrt{\alpha_2 t_f \lambda_f}}} \qquad (3.15).$$

The advantage of this equation, which was already previously presented by Cauberg (2002), is its simple form and ease for making computations by hand. Besides, it looks very similar to a model developed by Collins and Simko (1998) for the thermal edge effect of vacuum glazing. It, however, also includes a term for the thermal conductance of the thermal bridge, i.e. the panel edge. For differences between the properties of the edge and of the barrier laminate along surface, a ratio φ [-] can be introduced defined as $\lambda_f t_f / \lambda'_f t'_f$. Later it will be used to estimate the influence of a seam on the linear thermal transmittance.

One of the assumptions for this second model is that the thermal conductivity of the core material, λ_c, equals 0 W·m^{-1}·K^{-1}. This assumption is valid as long as λ_c is sufficiently small. For higher values of λ_c, or actually a higher ratio of λ_c to λ_f, this assumption results in excessive deviations between analytically and numerically determined values because envelope and core interactions are neglected.

---

[20] Since Equation (3.15) is a special case of Equation (3.11), only the general Equation (3.11) is tested and compared to numerical data in the next section.

3.3.2 Model tests: comparative testing

The analytical model, Equation (3.11), is tested by comparing the calculated results of this equation with numerical data available through previous research (van Went, 2002) and new simulations. Figures 3.7 and 3.8[21] show some of the results of numerical and analytical linear thermal transmittance calculations for VIPs with an aluminium foil based and a metallized film based high barrier envelope as a function of panel and envelope thickness. It is important to notice that the simulations are run for idealized VIPs, which implies that at their edge neither a seam is present nor a difference in laminate thickness occurs. For each envelope type, fives different core material thermal conductivity values have been investigated: $2 \cdot 10^{-3}$, $4 \cdot 10^{-3}$, $6 \cdot 10^{-3}$, $20 \cdot 10^{-3}$ and $40 \cdot 10^{-3}$ $W \cdot m^{-1} \cdot K^{-1}$. Some results are presented in the figures. In these figures, the markers represent the results of numerical simulations, while the continuous lines are based upon analytical modelling with Equation (3.11). The results of numerical simulation according to section 3.2 are also presented in Appendix A39.

As can generally be seen from these figures, the difference between the analytically calculated and numerically simulated results is small, as a result of which the analytical model presented can be used as a tool to estimate ψ-values due to continuously enveloping thin high barrier laminates. For a VIP with a 6 μm thick aluminium based foil and a core material thermal conductivity of $4 \cdot 10^{-3}$ $W \cdot m^{-1} \cdot K^{-1}$, for instance, this deviation is $-2 \cdot 10^{-4}$ $W \cdot m^{-1} \cdot K^{-1}$ (-0.4%), $-2 \cdot 10^{-4}$ $W \cdot m^{-1} \cdot K^{-1}$ (-0.7%), $3 \cdot 10^{-5}$ $W \cdot m^{-1} \cdot K^{-1}$ (0.1%) and $-4 \cdot 10^{-4}$ $W \cdot m^{-1} \cdot K^{-1}$ (-1.8%)[22] for a panel thickness of 10 mm, 20 mm, 30 mm and 40 mm respectively. For a similar VIP with a 50 μm stainless steel foil based covering, these deviations amount to approximately $-7 \cdot 10^{-4}$ $W \cdot m^{-1} \cdot K^{-1}$ (-1.7%), $4 \cdot 10^{-4}$ $W \cdot m^{-1} \cdot K^{-1}$ (-1.3%), $-3 \cdot 10^{-4}$ $W \cdot m^{-1} \cdot K^{-1}$ (-1.2%) and $-2 \cdot 10^{-4}$ $W \cdot m^{-1} \cdot K^{-1}$ (-1.2%) for a panel thickness of 10 mm, 20 mm, 30 mm and 40 mm respectively. Even if a low thermal conductivity barrier, like a three-layer metallized film, is applied, deviations between analytical and numerical results are small as well[23]: $-2 \cdot 10^{-4}$ $W \cdot m^{-1} \cdot K^{-1}$ (-6.7%), $-7 \cdot 10^{-5}$ $W \cdot m^{-1} \cdot K^{-1}$ (- 3.3%), $-4 \cdot 10^{-5}$ $W \cdot m^{-1} \cdot K^{-1}$ (-2.8%) and $-3 \cdot 10^{-5}$ $W \cdot m^{-1} \cdot K^{-1}$ (-2.4%) for a panel thickness of 10 mm, 20 mm, 30 mm and 40mm respectively. These very small deviations thus seem to indicate that the proposed model is a tool sufficiently accurate to calculate the thermal bridge effect induced by the high barrier envelope, at least for the studied panel variants. These very small deviations not only occur for low centre-of-panel thermal conductivities but also for higher thermal conductivities.

---

[21] Appendix A35, A36 and A37 include more results.

[22] Differences in percentile deviations in this paper are based upon non-rounded values.

[23] Percentile deviations are higher due to the low linear thermal transmittance values.

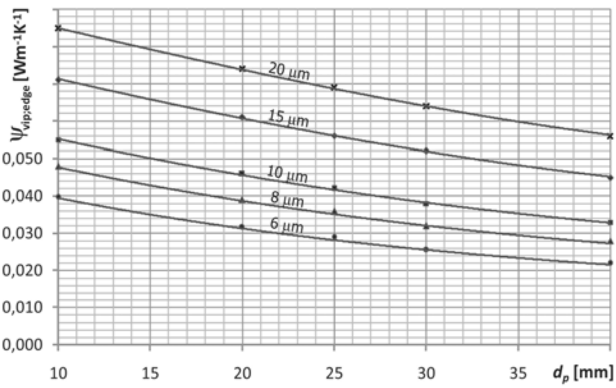

Figure 3.7

Comparison of numerical data (markers) to analytical model (continuous lines) of the linear thermal transmittance as function of panel thickness for a VIP with an AF barrier with different foil thicknesses

$\lambda_f = 225\ W{\cdot}m^{-1}{\cdot}K^{-1}$;
$\lambda_c = 4{\cdot}10^{-3}\ W{\cdot}m^{-1}{\cdot}K^{-1}$;
$\varphi = 1$ (ideal seam);
$\alpha_1 = 7.8\ m^2{\cdot}K{\cdot}W^{-1}$;
$\alpha_2 = 25\ m^2{\cdot}K{\cdot}W^{-1}$.

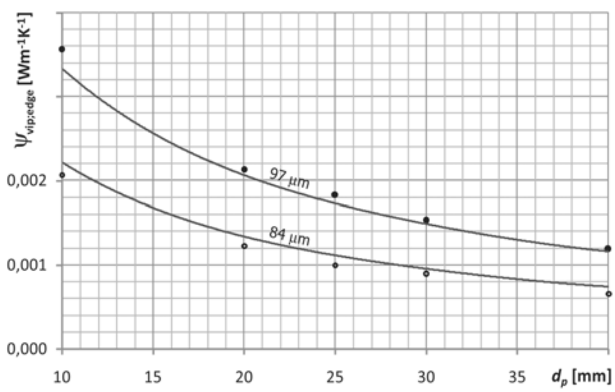

Figure 3.8a

Comparison of numerical data (markers) to analytical model (continuous lines) of the linear thermal transmittance as function of panel thickness for a VIP with a MF barrier with film thickness of 84 μm and 97 μm for a two fold and three fold metallised film laminate respectively.

film: MF; $\lambda_c = 4{\cdot}10^{-3}\ W{\cdot}m^{-1}{\cdot}K^{-1}$; $\varphi = 1$ (ideal seam); $\alpha_1 = 7.8\ m^2{\cdot}K{\cdot}W^{-1}$; $\alpha_2 = 25\ m^2{\cdot}K{\cdot}W^{-1}$.

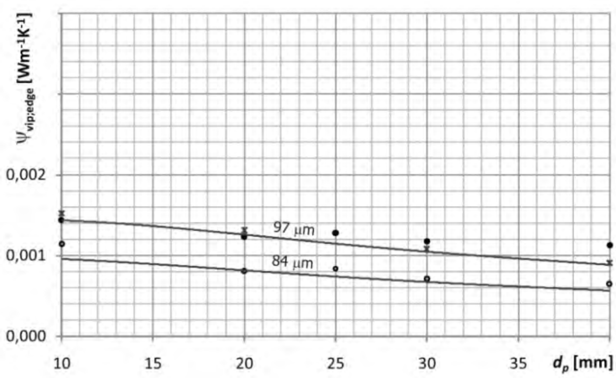

Figure 3.8b

Comparison of numerical data (markers) to analytical model (continuous lines) of the linear thermal transmittance as function of panel thickness for a VIP with a MF barrier with different film thickness of 84 μm and 97 μm for a two fold and three fold metallised film laminate respectively.

film: MF; $\lambda_c = 40{\cdot}10^{-3}\ W{\cdot}m^{-1}{\cdot}K^{-1}$; $\varphi = 1$ (ideal seam); $\alpha_1 = 7.8\ m^2{\cdot}K{\cdot}W^{-1}$; $\alpha_2 = 25\ m^2{\cdot}K{\cdot}W^{-1}$.

Although the absolute difference between numerical and analytical results is small for all variants tested, percentile differences are relatively high for thick VIPs with a low thermal conductivity barrier, like metallised film laminates, and with high thermal conductivity of the core. For a panel of 40 mm thick enveloped by a three-layer metallized film of 97 μm thick and with a centre-of-panel thermal conductivity of $40 \cdot 10^{-3}$ $W \cdot m^{-1} \cdot K^{-1}$, the deviation amounts to about $-2 \cdot 10^{-4}$ $W \cdot m^{-1} \cdot K^{-1}$ (-21.3%). These high percentile differences of course result from low ψ-values combined with the inaccuracy of both models. To check whether the numerical models developed with the software tool Trisco are accurate enough when computing low ψ-values, VIP models with a three-layer metallized film of 97 μm thick and with a centre-of-panel thermal conductivity of $6.0 \cdot 10^{-3}$, $20 \cdot 10^{-3}$ and $40 \cdot 10^{-3}$ $W \cdot m^{-1} \cdot K^{-1}$ have been developed with Comsol Multiphysics as well. The results of these simulations are added to Figure 3.8b and to Figures A37c/d/e in appendix A37 marked with asterisks[24]. As can be seen, the numerical results obtained with Comsol Multiphysics are even closer to the values obtained with the analytical model than the values obtained with Trisco. With Comsol Multiphysics, the difference between numerical and analytical model only amounts to $-2 \cdot 10^{-5}$ $W \cdot m^{-1} \cdot K^{-1}$ (=-2.7%) for a panel of 40 mm thick enveloped by a three-layer metallized film of 97 μm thick and with a centre-of-panel thermal conductivity of $40 \cdot 10^{-3}$ $W \cdot m^{-1} \cdot K^{-1}$. So, we might say that even for these panels absolute differences are still small.

3.3.3 Parameters influencing the $\psi_{vip;edge}$-value

The presented numerical data and analytical model can also be used to investigate the parameters influencing the thermal bridge effect of a high barrier laminate enveloping a VIP. As can be seen from the figures discussed in the previous section, the linear thermal transmittance on the level of a VIP primarily depends on five parameters: envelope thickness, t_f [m], envelope thermal conductivity, λ_f [$W \cdot m^{-1} \cdot K^{-1}$], thermal conductivity of core material, λ_c [$W \cdot m^{-1} \cdot K^{-1}$], panel thickness, d_p [m] and seam type and configuration. The first four parameters are discussed in this section while the last property is addressed in the next section.

The laminate thickness, t_f, is an important parameter influencing the overall thermal performance of a VIP. As demonstrated in Figures 3.7 and 3.8, the linear thermal transmittance increases for increasing laminate thickness, for all simulated and calculated variants. For a VIP of 20 mm thick with a core thermal conductivity of $4 \cdot 10^{-3}$ $W \cdot m^{-1} \cdot K^{-1}$ and an aluminium high barrier foil (Figure 3.7), for instance, an increase in foil thickness from 6 μm to 20 μm results in an increase in linear thermal transmittance of $4.2 \cdot 10^{-2}$ $W \cdot m^{-1} \cdot K^{-1}$ (= $7.4 \cdot 10^{-2} - 3.2 \cdot 10^{-2}$ $W \cdot m^{-1} \cdot K^{-1}$), which

[24] The numerical results obtained with Trisco are marked with open and closed circles.

approximately equals an increase of 130%. For stainless steel and metallized barrier envelopes similar results are found. For a metallized film enveloping the aforementioned VIP, for example, Figure 3.8a displays an increase of $0.9 \cdot 10^{-3}$ $W \cdot m^{-1} \cdot K^{-1}$ (= $2.1 \cdot 10^{-3} - 1.2 \cdot 10^{-3}$ $W \cdot m^{-1} \cdot K^{-1}$) if the film changes from a two-layer metallized film (84 μm) to a tree-layer metallized film (97 μm). This increase is small in absolute terms but is 73% in relative terms.

The envelope thermal conductivity, λ_f, is a second important parameter influencing the linear thermal transmittance of a VIP edge. Comparison of Figures 3.7 and 3.8a demonstrates that, similar to the effect of laminate thickness, the linear thermal transmittance increases for increasing laminate thermal conductivity as well[25]. If again the example of a VIP of 20 mm thick with a core thermal conductivity of $4.0 \cdot 10^{-3}$ $W \cdot m^{-1} \cdot K^{-1}$ is taken, Figure 3.7 shows a linear thermal transmittance of $7.4 \cdot 10^{-2}$ $W \cdot m^{-1} \cdot K^{-1}$ for a 20 μm aluminium foil, while a value of $1.8 \cdot 10^{-2}$ $W \cdot m^{-1} \cdot K^{-1}$ is found for a 25 μm stainless steel foil. Although both values cannot be compared directly because of a small difference in thickness, comparison of both values clearly indicates that an aluminium foil with a simulated thermal conductivity of 225 $W \cdot m^{-1} \cdot K^{-1}$ creates a stronger thermal bridge effect than an equivalently thick stainless steel foil with a simulated thermal conductivity of 25 $W \cdot m^{-1} \cdot K^{-1}$.

The third parameter that influences the linear thermal transmittance of a VIP edge is the thermal conductivity of the core material, λ_c. In general, the linear thermal transmittance decreases with increasing core material thermal conductivity, the effect of which is stronger according as the panel thickness is smaller. Due to an increased thermal conductivity, more heat is ‘conducted’ through the centre-of-panel region, as a result of which the amount of heat flowing through the thermal bridge decreases relative to this centre-of-panel heat flow and also in absolute terms as can be seen from among others Figure 3.10.

Finally, Figures 3.7 and 3.8 demonstrate that within the studied thickness range the linear thermal transmittance of the edge of a VIP can both increase and decreases with increasing panel thickness. For the studied panel variants, local maximum values for this transmittance are found to exist between a panel thickness of 5 and 25 mm for aluminium and stainless steel based VIPs. These maximum values thus lie in the range for practical application of VIPs. Figure 3.9 displays the general behaviour, based upon Equation (3.11), of the linear thermal transmittance of a VIP with a 6 μm aluminium foil, a 25 μm thick stainless steel foil and a three-layer metallized film (centre-of-panel thermal conductivity of $4.0 \cdot 10^{-3}$ $W \cdot m^{-1} \cdot K^{-1}$)

---

[25] This is not surprising, since, if the thickness or the thermal conductivity of the envelope increases, on the one hand more heat is deflected towards the edge (the envelope at the VIP’s surface more strongly acts as a thermal collector) while on the other hand more heat is transferred through this edge relative to the central area (edge conductance has increased).

Figure 3.9

General behaviour of the linear thermal transmittance as a function of panel thickness for a 6 μm AF foil (λ_f = 225 W·m⁻¹·K⁻¹), a 25 μm SSF foil (λ_f = 25 W·m⁻¹·K⁻¹) and a 3-layer MF film (λ_f = 0.54 W·m⁻¹·K⁻¹). Broken lines represent Equations (3.17) and (3.19).

$\lambda_c = 4\cdot10^{-3}$ W·m⁻¹·K⁻¹;
$\varphi = 1$; $\alpha_1 = 7.8$ m²·K·W⁻¹;
$\alpha_2 = 25$ m²·K·W⁻¹.

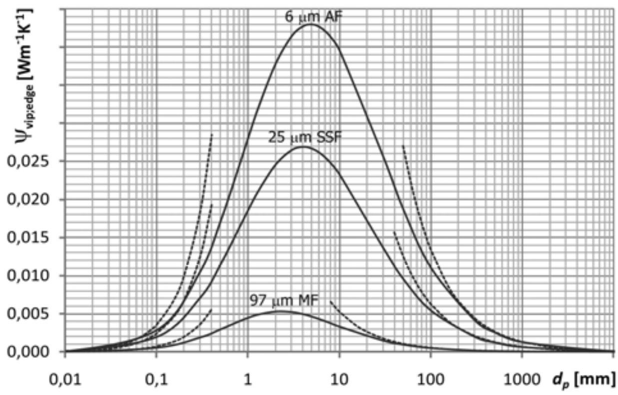

Figure 3.10

General behaviour of the linear thermal transmittance of a 6 μm AF foil as a function of panel thickness and thermal conductivity of the core material. The values in the graph denote the thermal conductivity of the core material.

λ_f = 225 W·m⁻¹·K⁻¹;
$\lambda_c = 4\cdot10^{-3}$ W·m⁻¹·K⁻¹;
$\varphi = 1$; $\alpha_1 = 7.8$ m²·K·W⁻¹;
$\alpha_2 = 25$ m²·K·W⁻¹.

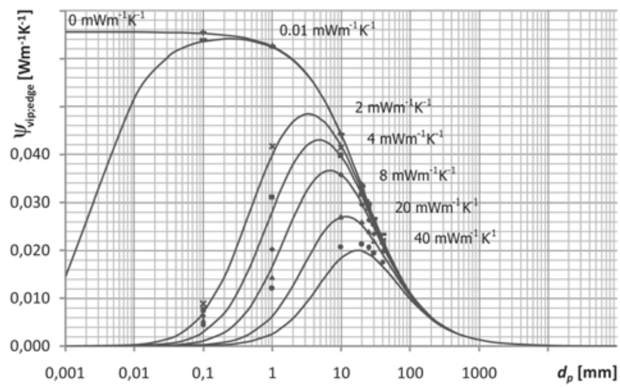

Figure 3.11

General behaviour of the linear thermal transmittance of a 3-layer MF film as a function of panel thickness and thermal conductivity of the core material. The values in the graph denote the thermal conductivity of the core material.

λ_f = 0.54 W·m⁻¹·K⁻¹;
$\lambda_c = 4\cdot10^{-3}$ W·m⁻¹·K⁻¹;
$\varphi = 1$; $\alpha_1 = 7.8$ m²·K·W⁻¹;
$\alpha_2 = 25$ m²·K·W⁻¹.

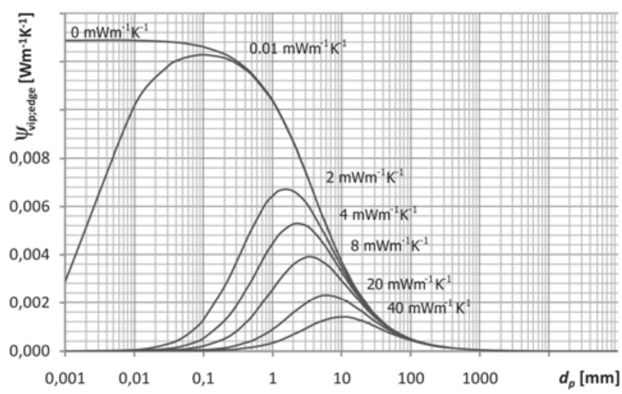

as function of panel thickness, while Figures 3.10 and 3.11 present this transmittance as a function of panel thickness for a VIP with a 6 μm thick aluminium barrier and a three layer metallized envelope respectively for varying core material thermal conductivity[26]. As can be seen, local maximum values do exist for all film-VIPs, as long as the thermal conductivity of the core material is larger than zero. As can be seen, the higher the thermal conductivity of the core material the lower the linear thermal transmittance. This statement is valid for all panels.

The analytical model derived in this chapter allows a closer look at the influence of panel thickness on the linear thermal transmittance. First, it is interesting to see what happens if the panels thickness goes to a large value. If we take the limit for d_p to infinity of equations (3.11) and (3.15), we obtain

$$\lim_{d_p \to \infty} \psi_{vip,edge} = \lim_{d_p \to \infty} \psi_{vip,edge,0} = 0 \tag{3.16}$$

which we already observed from Figures 3.10 and 3.11. For very large values of d_p it is also possible to simplify equations (3.11) and (3.15) resulting in

$$\psi_{vip,edge} = \psi_{vip,edge,0} = \frac{t_f' \lambda_f'}{d_p} \tag{3.17}$$

This equation elucidates that for large panel thickness the linear thermal transmittance, or the extent of the thermal bridge, is determined mainly by the thermal conductance of the edge, i.e. the thermal properties and geometry of the thermal bridge. The thermal conductivity of the core and the properties of the barrier laminate on top and at the bottom of the panel are no longer relevant. This can also be seen from Figures 3.10 and 3.11 since at large panel thickness all lines denoting different thermal conductivity of the core converge to a single curve.

Second, it is interesting to see what happens if the panels thickness goes to zero. It must then be distinguished between zero and non-zero thermal conductivity of the core; panels with zero core material thermal conductivity have a different

[26] In Figure 3.10 markers that represent numerical computations are added to the figure. These added markers indicate similar general behaviour of the linear thermal transmittance as equation (3.11) does. The differences between the numerical model and the analytical equation however become bigger as the panel thickness decreases. Based upon this comparison, however, it is impossible to tell whether the numerical or the analytical results are closer to reality. For this, experimental results should be taken as reference. Due to limited resources and unavailability of equipment such experimental data is unavailable. Therefore only differences between two mathematical computations are presented.

behaviour from panels with non-zero core material thermal conductivity. If we now take the limit for d_p towards zero of the linear thermal transmittance, we obtain

$$\lim_{d_p \downarrow 0} \psi_{vip,edge} = 0 \qquad \text{if } \lambda_c >> 0 \text{ W·m}^{-1}\text{·K}^{-1} \qquad (3.18a),$$

$$\lim_{d_p \downarrow 0} \psi_{vip,edge,0} = \frac{1}{\frac{1}{\sqrt{\alpha_1 \lambda_f t_f}} + \frac{1}{\sqrt{\alpha_2 \lambda_f t_f}}} \qquad (3.18b),$$

the latter of which is a non-zero constant value. For small values of the panel thickness, the equation for the linear thermal transmittance can also be simplified yielding[27]

$$\psi_{vip,edge} = \frac{d_p \sqrt{d_p}\, \alpha_1^2 \alpha_2^2 \sqrt{\lambda_f t_f}}{\lambda_c \sqrt{2\lambda_c}\, (\alpha_1 + \alpha_2)^2} \qquad \text{if } \lambda_c >> 0 \text{ W·m}^{-1}\text{·K}^{-1} \qquad (3.19a),$$

$$\psi_{vip,edge,0} = \frac{1}{\frac{1}{\sqrt{\alpha_1 \lambda_f t_f}} + \frac{1}{\sqrt{\alpha_2 \lambda_f t_f}}} \qquad (3.19b),$$

which again is consistent with Figures 3.9 to 3.11. These two equations show that if the panel thickness is very small, then the linear thermal transmittance is dominated by the thermal resistance of the core, by the boundary heat resistances and the properties of the barrier laminate on top and at the bottom of the panel, as long as the thermal conductivity of the core is non-zero, or by the properties of the barrier laminate on top and at the bottom of the panel, if the thermal conductivity of the core is zero. The thermal properties of the thermal bridge itself no longer matter.

Unfortunately, however, the range of panel thickness for which equations (3.17) and (3.19) are sufficiently accurate is either well above or well below the range of panel thickness of VIPs in practise, except for VIPs with a metallised barrier laminate and a panel thickness of 20 mm or more. For such panels equation (3.17) produces good results as can be seen from Figure 3.9.

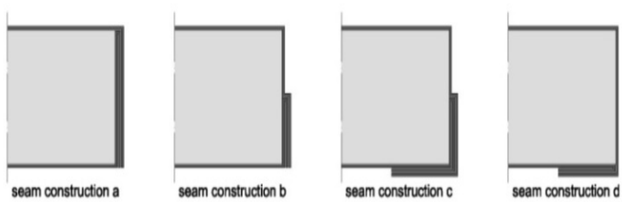

Figure 3.12

Different seam configurations.

---

[27] Differences between both equations result from the simplifications made.

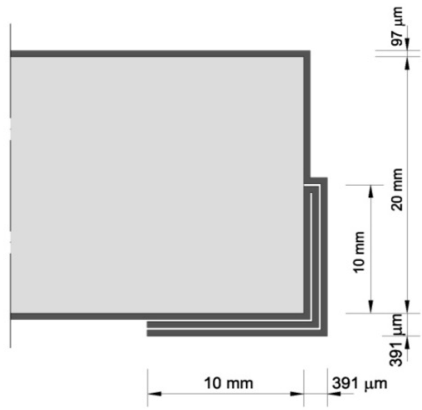

Figure 3.13

Detailed representation of seam construction type c with a 3-layer MF film.

3.3.4 Seam modelling

The analytical model cannot only be used to predict thermal shunting for idealized, envelopes but also for realistic ones with seams. The ratio φ in Equations (3.11) and (3.15) can then either be used to incorporate a difference in laminate thickness, or to compensate for a seam at its edge. Figure 3.12 shows four different types of seams to indicate how Equation (3.11) can model these geometries. Table 3.4 shows the results of a comparison between numerically and analytically calculated values for the ψ-value of aforementioned configurations. As can be seen, for metal foils with seams, deviations between Equation (3.11) and numerical calculations are small, except for seam type c (about -14.5%). Although this value is larger than the deviations found for idealized laminates, it is still acceptably small. Since, however, seam type c is larger than seam type b, the ratio φ should be chosen somewhat smaller than 0.75 (near 0.5), improving the transmittance prediction by Equation (3.11) as well. With the right choice of φ, Equation (3.11) can thus be used to estimate realistic VIPs, too.

It is, however, important to mention that the seams modelled and calculated numerically are idealized as well. Figure 3.13 shows a detailed drawing of seam type c; air gaps between the seam and the remaining laminate are not modelled. Ghazi Wakili et al. (2004) experimentally found a ψ-value of (6.96 ± 1.63) $\cdot 10^{-3}$ W$\cdot$m$^{-1}\cdot$K^{-1} for a three-layer metallized film (3x30 nm metallization) with a seam similar to type c around a 18 mm thick VIP with central thermal conductivity of (4.14±0.08)$\cdot 10^{-3}$ W$\cdot$m$^{-1}\cdot$K^{-1}. For this type of film and VIP combination, Table 3.4 presents a value of 4.5$\cdot 10^{-3}$ W$\cdot$m$^{-1}\cdot$K^{-1}. This deviation on the one hand results from differences in geometry (the absence of air spaces and a somewhat shorter seam length) and on the other hand from differences in boundary conditions (α_i and α_e are used in the calculations while in a guarded hot plate rubber sheets flank the VIP on both sides changing the conditions from an air to a material boundary).

***Table 3.4** - Comparison of numerical data to Equation (3.11) for different edge seam constructions. (d_p=0.02 m; λ_c=4.0·10^{-3} W·m^{-1}·K^{-1}; α_i=7.8 W·m^{-2}·K^{-1}; α_e =25 W·m^{-2}·K^{-1}).*

	seam type	$\psi_{vip,edge}$ [·10^{-3} W·m^{-1}·K^{-1}]			φ [-][a]
		numerical analysis		Eq. (3.11)	
		seam folded to inside surface	seam folded to outside surface		
6 µm AF	no seam	32	32	31	1
	a	48	48	47	0.33
	b	37	37	36	0.75
	c	42	40	36	0.75
	d	34	33	31	1
50 µm SSF	no seam	30	30	30	1
	a	46	46	45	0.33
	b	36	36	34	0.75
	c	40	39	34	0.75
	d	32	31	30	1
3-layer MF	no seam	2.0	2.0	2.0	1
	a	5.6	5.5	4.6	0.33
	b	2.8	2.7	2.6	0.75
	c	4.5	3.6	2.6	0.75
	d	2.6	2.3	2.0	1

[a] Seam construction a can easily be calculated by using the value 0.33 ($\varphi = \lambda_f t_f / \lambda'_f t'_f = 1/3$) for φ. Seam construction b and c must be estimated by considering two conductances arranged in series. φ is than computed as $1/(\varphi_1+\varphi_2)$ if both conductances cover half the thickness of the panel. In this equation, φ_1 and φ_2 are the local φ-values of each conductance. For seam type b (and c) this yields $\varphi = 1/(1+1/3)=0.75$. Since however contact between all conductances is not perfect as a result of which an additional resistance is introduced between both conductances, the φ–value estimated with this equation is slightly overestimated.

***Table 3.5** - Comparison of numerical data (Beck and Frank, 2005) to analytical model for added insulation layers (d_p=20 mm; λ_c=5.0·10^{-3} W·m^{-1}·K^{-1}; φ=1).*

	$\psi_{vip,edge}$ [·10^{-3} W·m^{-1}·K^{-1}]								
	metallised film			aluminium foil					
				5 µm			10 µm		
R_{ins} [m^{2}KW^{-1}]	0.00	0.25	0.50	0.00	0.25	0.50	0.00	0.25	0.50
numerical	1.4	1.1	0.90	22	13	8.8	36	20	13
analytical	1.6	1.1	0.90	21	12	8.3	35	19	13
difference	14.3%	0.3%	0.4%	-4.1%	-10.7%	-5.7%	-2.8%	-6.5%	-2.3%

3.3.5 Additional insulation layers, thin air gaps and laminate combinations

Additional insulation layers on top of the vacuum insulation panel are modelled by modifying the boundary heat transfer coefficient, α_j, so that this coefficient not only includes the conductance of the air layer adjacent to the barrier laminate but also includes the additional insulation layer. A thermal network analysis with two serial resistances results in the following modified boundary heat exchange coefficient

$$\alpha_j^* = \frac{1}{1/\alpha_j + d_{ins}/\lambda_{ins}} \quad (3.20),$$

with α^*_j [$W\cdot m^{-2}\cdot K^{-1}$] the modified boundary heat exchange coefficient, d_{ins} [m] the insulation layer thickness, and λ_{ins} [$W\cdot m^{-1}\cdot K^{-1}$] the thermal conductivity of the insulation material. If on both sides of the panel an insulation layer is added, then both boundary heat transfer coefficients need to be modified according to Equation (3.20). Table 3.5 shows a comparison of numerical data obtained from Beck and Frank (2005) and data obtained with Equation (3.11) and (3.20). As can be seen, the deviation between both methods is very small.

Very thin air gaps between adjacent panels can be modelled by modifying the thickness and thermal conductivity of the edge, t'_f [m] and λ'_f [$W\cdot m^{-1}\cdot K^{-1}$]. The thickness in that case is the sum of the thickness of the VIP barrier laminate at the side of the panel including seam and half the width of the air gap between the two

***Table 3.6** - Comparison of numerical data (Beck and Frank, 2005) to analytical model for air gaps between two panels and added insulation layers (d_p=20 mm; λ_c=5.0·10^{-3} W·m^{-1}·K^{-}; φ=1).*

$t_{gap}/2$	$\psi_{vip,edge}$ [$\cdot 10^{-3}$ $W\cdot m^{-1}\cdot K^{-1}$]					
[mm]	metallised film			aluminium foil 10 μm		
	numerical	analytical	difference	numerical	analytical	difference
2	2.7	2.6	-2.9%	14	14	-1.0%
4	3.9	2.9	-26%	15	14	-1.9%
6	4.9	3.0	-39%	15	15	-2.8%
8	5.7	3.0	-47%	16	15	-4.1%
10	6.5	3.1	-53%	16	16	-5.7%
12	7.2	3.1	-57%	17	16	-7.7%

NB: The thermal conductivity of the air gap is calculated according NEN-EN-ISO 10211 (2008).

Table 3.7 - *Comparison of numerical data to analytical model for VIP with envelopes containing a combination of two barrier laminates (λ_c=4.0·10^{-3} W·m^{-1}·K^{-1}; φ=1; MF3-barrier on cold side).*

d_p	$\psi_{vip,edge}$ [·10^{-3} W·m^{-1}·K^{-1}]					
[mm]	combi-laminate MF3-8 μm AF			combi-laminate MF3-25 μm SSF		
	numerical	analytical	difference	numerical	analytical	difference
10	7.2	6.6	-8.6%	6.7	6.1	-9.1%
20	4.8	4.0	-15.9%	4.3	3.8	-12.1%
30	3.7	2.9	-22.7%	3.2	2.7	-16.3%
40	3.0	2.3	-24.7%	2.7	2.1	-20.0%
50	2.7	1.8	-31.8%	2.4	1.7	-26.6%

VIPs[28]. The thermal conductivity of the edge is determined from a resistance network model of the edge consisting of two parallel resistances, i.e. a resistance of the barrier laminate and one of the air gap. This thermal conductivity thus equals

$$\lambda_f^{'*} t_f^{'*} = \lambda_f^{'} t_f^{'} + \frac{\lambda_{airgap} t_{airgap}}{2} \qquad (3.21),$$

in which t'^*_f [m] and λ'^*_f [W·m^{-1}·K^{-1}] are the modified thickness and thermal conductivity and t_{airgap} [m] and λ_{airgap} [W·m^{-1}·K^{-1}] are the thickness and thermal conductivity of the air gap.

Table 3.6 presents a comparison of results obtained from analytical analysis among others using Equation (3.21) and numerical results from Beck and Frank (2005)[29]. As can be seen, again the difference between numerical and analytical results is relatively small for VIPs enveloped by aluminium laminates, even up to a gap of 12 mm. This difference however increases with increasing gap width. The differences between both calculation methods are however considerably bigger for VIPs enveloped by a metallised laminate, especially for a gap width beyond 4 mm.

The reason why this difference increases for increasing gap width is that owing to the increased width of the edge an additional heat flow from the environment is transferred to this edge. This additional heat flow, which is neglected using Equation (3.11), equals α_j·(t'_f+t_{airgap})·(T_j-T_{si}), with T_{si} [K] the temperature of the barrier laminate at the corner of the panel on the warm side (i=x) or at the cold side (i=y).

[28] The other half is attributed to the second VIP.

[29] A comparison of more numerical data to the advanced analytical model that will be introduced in the next chapter is presented in appendix A43.

The larger the air gap, the larger the effect of this additional heat flow on the total heat flow over the edge is and thus the larger the differences between numerical and analytical results are. For VIPs with wide air gaps but also for sheet-VIPs (VISs) and building panels, the analytical approximation equations derived need to be modified to account for this additional width. This modified analytical equation will be presented in the next chapter.

For VIPs having a combined barrier envelope of both a metal-based laminate on one side and a metallised laminate on the other side, the ψ-value can finally be calculated using the equations presented in appendix A33. Numerical computations for combined barrier laminates have been performed using Trisco. VIPs with two types of combined barrier laminates have been studied. A VIP with on the cold side a 3-layer metallised film (MF3) and on the warm side an 8 μm thick aluminium foil laminate (AF:8) and a VIP with on the cold side a 3-layer metallised and on the warm side a 25 μm thick stainless steel foil laminate (SSF:25). For both variants, the laminate of each type continues till half the thickness of the panel at the panel's sides. Due to the difference in thickness of both barrier laminates, though, a small air gap exists at this edge next to the thinnest laminate. The thermal conductance of this edge, K, can be modelled by a thermal resistance network with the thermal conductivity of the air gap obtained from NEN-EN-ISO 10211 (2008).

The results of the computations are presented in Table 3.7 and compared to results obtained with the approximation model presented in appendix A33. As can be seen, the relative difference between numerical and analytical computations is big. For a 20 mm thick VIP with a MF3-AF:8 laminate and a central thermal conductivity of $4 \cdot 10^{-3}$ $W \cdot m^{-1} \cdot K^{-1}$, it amounts to about -15.9%. For thicker panels, the difference even becomes bigger up to about -31.8% for a 50 mm thick VIP. Although the relative difference between numerical and analytical results is big, the absolute difference is not; it is less than $0.9 \cdot 10^{-3}$ $W \cdot m^{-1} \cdot K^{-1}$ which is in the same order of magnitude as the difference found for ideal VIPs with metal-based barrier envelopes (subsection 3.3.2).

3.3.6 Limitations

From an analysis of the deviations between analytically calculated and numerically modelled panel variants, it can be concluded that the error made with the approximating models increases with decreasing thermal resistance of the core, i.e. increasing thermal conductivity and decreasing thickness of this core. A dependence of the absolute and/or relative error on the conductance of the barrier envelope, $\lambda_f \cdot t_f$ [$W \cdot K^{-1}$], and thermal bridge, K [$W \cdot m^{-1} \cdot K^{-1}$], was not found within the range of panels

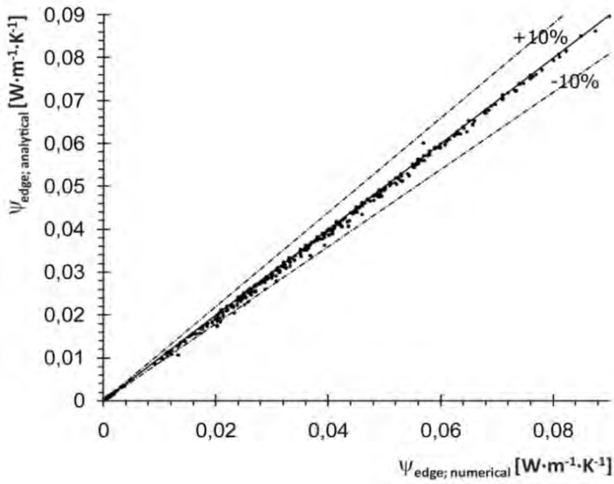

Figure 3.14

Error plot: plot of numerical results (Trisco) versus analytical results.

studied mainly due to large scatter in this error. However, as is indicated by Figure 3.14, the difference between analytical and numerical results in 80% of the cases simulated is less than 5% and in 94% of the cases simulated less than 10%[30]. As a result, it can be concluded that for almost all VIPs encountered in practise the model will yield sufficiently accurate results.

One limitation, however, must be specified; a limitation regarding the thickness of the panel edge. For the derivation of both approximation equations in the appendix, the laminate thickness at the edge of a VIP was assumed to be in the same thickness range as the complete envelope. If this thickness, however, increases significantly beyond this thickness range (from the micrometer scale level to the millimetre level) an additional heat flow over the width of this edge needs to be considered. Such an advanced model will be derived, tested and discussed in the next chapter.

[30] These percentages are solely determined from a comparison of the results obtained by the analytical model and by Trisco. The results from Comsol Multiphysics, which are even closer to the analytical results, are not included in the calculation.

3.4 Comparison of VIPs to Conventional Thermal Insulators

A comparison of VIP with conventional thermal insulators on their overall thermal performance is made[31]. Table 3.8 shows the U_{eff}-value of two types of film-based VIPs of 0.6x1.2 m^2 and 0.3x0.6 m^2, all at start and end of service life[32], and four conventional thermal insulators. As can be seen, the effective thermal transmittance of all large VIPs presented and almost all small VIPs is lower than the values for conventional thermal insulators. Thus, even if the thermal edge effect happening for VIPs is considered, their overall thermal performance is still better than the performance of cellulose, mineral fibre, Polyurethane foam (PU) and aerogel insulation blankets. Only small VIPs with a 6 μm aluminium foil laminate as barrier envelope perform worse than aerogel insulation blankets if its thickness increases to beyond approximately 20 to 30 mm. For a typical 20 mm thick vacuum insulation panel, for instance, the effective thermal transmittance varies between 0.21 and 0.73 $W{\cdot}m^{-2}{\cdot}K^{-1}$, depending on the selected barrier envelope, the thermal conductivity of the core material and the panel size, while this transmittance varies between 0.63 and 1.63 $W{\cdot}m^{-2}{\cdot}K^{-1}$ for the presented conventional thermal insulation materials.

Table 3.8a *- Effective thermal transmittance of typical large VIPs and several conventional thermal insulators for different panel thicknesses.*

d_p	U_{eff} [$W{\cdot}m^{-2}{\cdot}K^{-1}$] - panel size of 0.6x1.2 m^2							
[mm]	VIP - initial [a]		VIP – after 25 yr [a]		Cellulose	Mineral fibre	PU	aerogel
	AF 6 μm	MF3	AF 6 μm	MF3				
10	0.60	0.40	0.76	0.72	2.55	2.38	1.85	1.13
20	0.38	0.21	0.47	0.39	1.63	1.49	1.10	0.63
30	0.29	0.14	0.35	0.27	1.20	1.09	0.78	0.43
40	0.24	0.11	0.28	0.20	0.94	0.85	0.61	0.33
50	0.20	0.09	0.24	0.16	0.78	0.70	0.49	0.27

NB: φ=0.67; α_1=7.8 $W{\cdot}m^{-2}{\cdot}K^{-1}$; α_2=25 $W{\cdot}m^{-2}{\cdot}K^{-1}$; $\lambda_{cellulose}=45{\cdot}10^{-3}$ $W{\cdot}m^{-1}{\cdot}K^{-1}$; $\lambda_{minwool}=40{\cdot}10^{-3}$ $W{\cdot}m^{-1}{\cdot}K^{-1}$; $\lambda_{PU}=27{\cdot}10^{-3}$ $W{\cdot}m^{-1}{\cdot}K^{-1}$; $\lambda_{aerogel}=14{\cdot}10^{-3}$ $W{\cdot}m^{-1}{\cdot}K^{-1}$.

[a] Initial condition of all VIPs (fumed silica core): $\lambda_c = 4{\cdot}10^{-3}$ $W{\cdot}m^{-1}{\cdot}K^{-1}$; conditions after 25 years (fumed silica core): AF 6 μm: $\lambda_c = 6{\cdot}10^{-3}$ $W{\cdot}m^{-1}{\cdot}K^{-1}$; MF3: $\lambda_c = 8{\cdot}10^{-3}$ $W{\cdot}m^{-1}{\cdot}K^{-1}$.

---

[31] A selection of thermal performance plots showing either the overall thermal transmittance or effective thermal conductivity as function of panel thickness and ratio of perimeter to surface area is presented in appendix A38.

[32] The thermal conductivity of a VIP at the start of service life is approximately $4{\cdot}10^{-3}$ $W{\cdot}m^{-1}{\cdot}K^{-1}$ when a fumed silica core is used. In Chapter 5, it will be explained that the thermal conductivity at the end of service life is defined as $8.0{\cdot}10^{-3}$ $W{\cdot}m^{-1}{\cdot}K^{-1}$.

Table 3.8b - *Effective thermal transmittance of typical small VIPs and several conventional thermal insulators for different panel thicknesses.*

d_p [mm]	U_{eff} [$W\cdot m^{-2}\cdot K^{-1}$] - panel size of 0.3x0.6 m^2							
	VIP - initial [a]		VIP – after 25 yr [a]		Cellulose	Mineral fibre	PU	aerogel
	AF 6 μm	MF3	AF 6 μm	MF3				
10	0.82	0.42	0.97	0.74	2.55	2.38	1.85	1.13
20	0.57	0.22	0.65	0.40	1.63	1.49	1.10	0.63
30	0.45	0.15	0.51	0.28	1.20	1.09	0.78	0.43
40	0.38	0.11	0.42	0.21	0.94	0.85	0.61	0.33
50	0.32	0.09	0.36	0.17	0.78	0.70	0.49	0.27

NB: φ=0.67; α_1=7.8 $W\cdot m^{-2}\cdot K^{-1}$; α_2=25 $W\cdot m^{-2}\cdot K^{-1}$; $\lambda_{cellulose}=45\cdot 10^{-3}$ $W\cdot m^{-1}\cdot K^{-1}$; $\lambda_{minwool}=40\cdot 10^{-3}$ $W\cdot m^{-1}\cdot K^{-1}$; $\lambda_{PU}=27\cdot 10^{-3}$ $W\cdot m^{-1}\cdot K^{-1}$; $\lambda_{aerogel}=14\cdot 10^{-3}$ $W\cdot m^{-1}\cdot K^{-1}$.

[a] Initial condition of all VIPs (fumed silica core): $\lambda_c = 4\cdot 10^{-3}$ $W\cdot m^{-1}\cdot K^{-1}$; conditions after 25 years (fumed silica core): AF 6 μm: $\lambda_c = 6\cdot 10^{-3}$ $W\cdot m^{-1}\cdot K^{-1}$; MF3: $\lambda_c = 8\cdot 10^{-3}$ $W\cdot m^{-1}\cdot K^{-1}$ (Simmler and Brunner, 2005).

Since at this moment Dutch Building Codes (VROM, 2001) still require a thermal resistance of the opaque elements of building facades of at least 2.5 $m^2\cdot K\cdot W^{-1}$, which more-or-less equals a requirement for a thermal transmittance of less than 0.37 $W\cdot m^{-2}\cdot K^{-1}$, the thickness required to fulfil this demand would be approximately 20 mm for a VIP with a metallized film using end of life thermal performance as criterion. For mineral fibre insulation board in contrast, a thickness of at least 100 mm is necessary, not considering thermal resistances due to additional material (and boundary) layers.

In Chapter 5, it will be explained that due to permeation of water vapour and dry atmospheric gases through the high barrier envelope the internal pore gas pressure and the water content of the core material will increase over time, as a result of which the (centre-of-panel) thermal conductivity will increase likewise. Considering this thermal conductivity ageing, Simmler and Brunner (2005) suggest for a VIP with initial centre-of-panel thermal conductivity of $4\cdot 10^{-3}$ $W\cdot m^{-1}\cdot K^{-1}$, design values of $6\cdot 10^{-3}$ $W\cdot m^{-1}\cdot K^{-1}$ and $8\cdot 10^{-3}$ $W\cdot m^{-1}\cdot K^{-1}$ for the centre-of-panel thermal conductivity of aluminium foil based and metallized film based VIPs respectively. Baetens (2009) on the other hand recommends a time-average value of $6\cdot 10^{-3}$ $W\cdot m^{-1}\cdot K^{-1}$ for the central thermal conductivity of metallised film based VIPs including edge effects[33]. Based

[33] Baetens (2009) also adds the notes that this value was determined for an initial central thermal conductivity of $4\cdot 10^{-3}$ $W\cdot m^{-1}\cdot K^{-1}$ while manufacturers currently state an initial value of

upon the design values by Simmler and Brunner, the effective thermal conductivity of a 20 mm thick panel becomes $8.2 \cdot 10^{-3}$ $W \cdot m^{-2} \cdot K^{-1}$ for both a 6 μm aluminium foil based VIP and a three-layer metallized film based VIP, at least for l_p / S_p = 3 m^{-1} (=1.2x1.5 m^2)[34] with l_p the panel circumference [m] and S_p the surface area of one side of the panel. This implies that due to this ageing effect the thermal disadvantage of a metal foil based barrier envelope is more-or-less counterbalanced by its superior barrier properties. Since, however, the linear thermal transmittance of the thermal bridge, which is larger for metal based foils than for metallized films, more significantly affects the overall thermal performance for small panel sizes, it can be recommended that for panels having a ratio of l_p / S_p larger than 3 m^{-1} only metallized films be used, while for larger panels, i.e. smaller ratio of l_p / S_p, both aluminium foils and metallized films are applied. The ratio that divides between both types of envelopes can also be estimated for other panel thicknesses: 5.2 m^{-1} (≈0.6x1.0 m^2), 2.3 m^{-1} (≈1.5x2.0 m^2), 2.0 m^{-1} (=2.0x2.0 m^2) and 1.8 m^{-1} (=2.0x2.5 m^2) for a panel thickness of 10, 30, 40 and 50 mm. For a 40 mm thick VIP this for instance implies that if the panel is larger than 2.0x2.0 m^2, a metal foil based laminate is preferred to a metallised film laminate while for smaller panels the opposite applies. As will be explained in Chapter 5, if extremely high service life requirements are in place or if very harsh environments are to be expected, metal foil based VIPs are preferred to metallized film based VIPs, while under heavy thermal performance requirements metallised film based VIPs may be advantageous.

3.5 CONCLUSIONS AND SUMMARY

The objective of this chapter was to introduce analytical models for approximating thermal bridge effects of thin barrier laminates around VIPs. By comparing model predictions to numerical data, it was shown that the proposed model in about 80% of all cases studied deviates by less than 5% and in about 94% by less than 10% from numerical data for idealized envelopes (within the limitations specified). The proposed models on the one hand complement existing numerical and experimental data and on the other hand show the effect of laminate thickness, laminate thermal conductivity, core thermal conductivity and panel thickness on the ψ-value. These

---

$5 \cdot 10^{-3}$ $W \cdot m^{-1} \cdot K^{-1}$; and that manufacturers, although all stating the same design value of a VIP, use different types of barrier envelope (Grynning et al., 2009) as a result of which differences in design values should occur.

[34] This separating variable can be calculated from equating formula (3.8) for a VIP with an aluminium barrier laminate and a VIP with a metallised film laminate. Rearranging this equation yields $(l_p / S_p)_{boundary} = (\lambda_{c;el;AF} - \lambda_{c;el;MF})/d_p/(\psi_{AF} - \psi_{MF}) = (0.008 - 0.006)/d_p/(\psi_{AF} - \psi_{MF})$.

models thus clearly explicate the relations between parameters influencing the thermal performance of VIPs. Contrary to numerical tools, which in fact are black boxes, such explicit relations facilitate design and engineering processes in a way that they show us in advance what will happen if a certain parameter is changed. Thus without needing to perform actual computations, designers and engineers are able to improve their engineered designs and create optimised products.

From these models, it readily becomes clear that the ψ-value representing the thermal edge effect depends on the thermal conductivity and thickness of the barrier at the surface, the thermal conductivity and thickness of the core and the properties and configuration of the seam. The linear thermal transmittance increases for increasing thermal conductivity and thickness of the barrier envelope along the surface, for decreasing ratio φ ($=\lambda_f t_f / \lambda'_f t'_f$) and for decreasing thermal conductivity of the core. The influence of panel thickness on linear thermal transmittance is more difficult. In general, the ψ-value first increases from zero to a maximum value and then decreases again to zero if the panel thickness increases. This peak value mostly lies in the range of VIPs used in practise.

A seam or a difference in laminate thickness between the edge region and surface region can be included into the models by introducing the ratio φ ($=\lambda_f t_f / \lambda'_f t'_f$). It was shown that the difference between analytical model and numerical data is less than approximately 7% for realistic seam containing envelopes, except for seams continuing to outside the panel edge region (seam type c).

Moreover, it was shown that the model is also applicable with sufficient accuracy if a small air gap is present between two adjoining VIPs or if additional insulation layers are added. Such an air gap can be modelled by changing the product of thickness and thermal conductivity of the edge, while additional insulation is modelled by changing the boundary heat transfer coefficients. It is important to note that the error made with the model increases with increasing thickness of the air gap because an additional heat flow from the environment is transferred to and through this edge. The maximum air gap width for which the approximation equation yields a difference with numerical computations of less than 10% therefore is about 25 mm for a 10 μm aluminium foil laminate and 5 mm for a metallised film laminate.

The linear thermal transmittance of non-vented vacuum insulation panels with a thickness of more than 20 mm and a metallised barrier envelope can be approximated with sufficient accuracy by calculating the thickness of the barrier laminate at the panel's edge multiplied by the laminate's thermal conductivity at this edge and divided by the thickness of the VIP (core). Moreover, the linear thermal transmittance of practically all non-vented VIPs - including those with a metal foil based barrier laminate – with a thickness of more than 20 mm can be sufficiently approximated by the analytical model for λ_c = 0 W·m^{-1}·K^{-1} presented in this chapter.

The approximation models presented show that the best barrier laminate from a thermal performance point of view is a metallized barrier laminate, followed in this order by a combined envelope of metallized film on one side and a 8 μm aluminium foil laminate on the other side, a 25 μm thick stainless steel foil laminate, a 6 μm thick aluminium foil laminate, a 50 μm thick stainless steel foil laminate and a 8 μm thick aluminium foil laminate. Besides, these thermal performance plots show that the thermal performance of a VIP with a metal-foil based barrier strongly depends on the perimeter to surface area ratio while this performance of a VIP with a metallized barrier is only moderately influenced by this ratio.

A comparison with conventional thermal insulators shows that in almost all cases a VIP thermally outperforms conventional insulators, even aerogels. Thus, even if the thermal edge effect for VIPs is considered, their overall thermal performance is still better than the performance of cellulose, mineral fibre, Polyurethane foam (PU) and aerogel. Only small VIPs with a 6 μm aluminium foil laminate as barrier perform worse than aerogel if its thickness increases to beyond approximately 20 to 30 mm, both at initial and end of life thermal conditions.

By equating the effective thermal transmittance of a VIP with a metallized barrier laminate and a 6 μm aluminium foil laminate, finally, a perimeter to surface area ratio can be determined which indicates the boundary between when a metallized film is preferred to an aluminium foil based laminate and vice versa. This boundary ratio is computed as 5.2 m^{-1}, 3.0 m^{-1}, 2.3 m^{-1}, 2.0 m^{-1} and 1.8 m^{-1} for a panel thickness of 10, 20, 30, 40 and 50 mm respectively, using $\lambda_c = 6\cdot10^{-3}$ W·m^{-1}·K^{-1} and $\lambda_c = 8\cdot10^{-3}$ W·m^{-1}·K^{-1} for aluminium foil and a metallised film based VIP respectively.

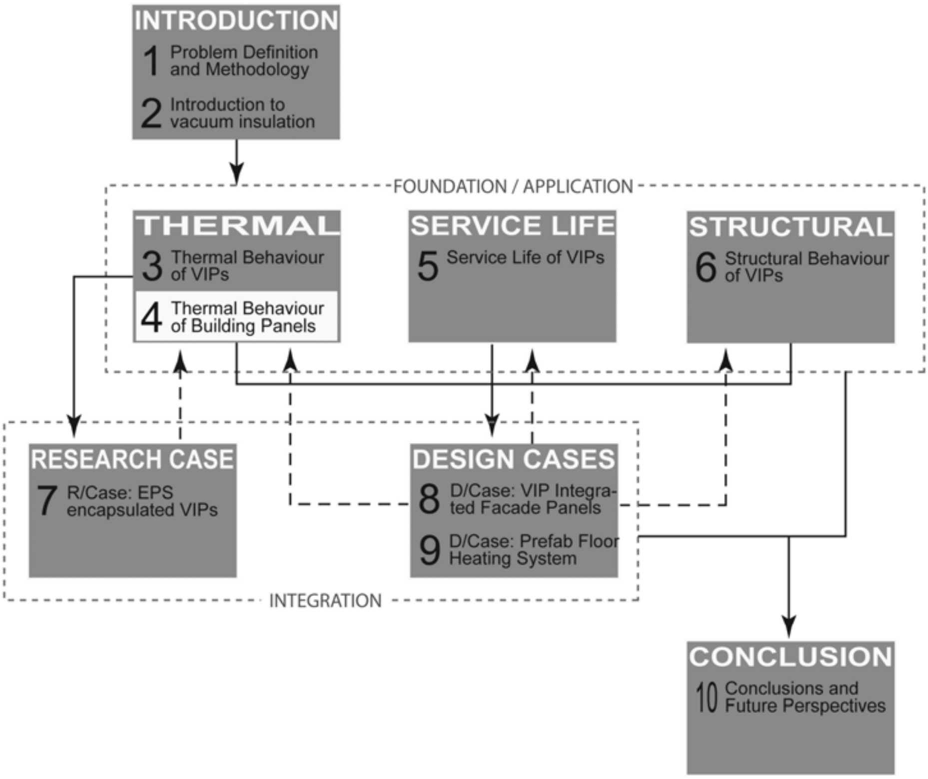

INTRODUCTION
1 Problem Definition and Methodology
2 Introduction to vacuum insulation
FOUNDATION / APPLICATION
THERMAL
3 Thermal Behaviour of VIPs
4 Thermal Behaviour of Building Panels
SERVICE LIFE
5 Service Life of VIPs
STRUCTURAL
6 Structural Behaviour of VIPs
RESEARCH CASE
7 R/Case: EPS encapsulated VIPs
DESIGN CASES
8 D/Case: VIP Integrated Facade Panels
9 D/Case: Prefab Floor Heating System
INTEGRATION
CONCLUSION
10 Conclusions and Future Perspectives

THERMAL BEHAVIOUR OF BUILDING PANELS 4

STUDY INTO THE THERMAL BRIDGING CAUSED BY THE COMBINED EFFECT OF VIP'S BARRIER ENVELOPE AND SPACERS OF BUILDING COMPONENTS

Although vacuum insulation panels (VIPs) are excellent thermal insulators, edge effects decrease their overall thermal performance. Moreover, they are often used with protections such as face sheets and profiles along their edge. These panels typically use spacers that cause a significant additional thermal bridge. The effect of this thermal bridge is either determined accurately with numerical simulation tools or estimated with simple thermal resistance networks. The first approach is laborious, while the latter approach lacks accuracy. This chapter therefore presents and tests an analytical approximation model for calculating this thermal edge effect.

While in the previous chapter the thermal behaviour of VIPs within the domain of foundation was discoursed about, the current chapter discusses thermal bridge effects occurring in VIP integrated building components and façade panels. This chapter continues the discussion started before, however changing the perspective from the level of a subcomponent (VIP) to the level of a full component (VIP integrated building component). The properties and behaviour discussed in chapter 3 are the fundaments for the discussion in the current chapter.

The structure of chapter 4 is therefore similar to the structure of chapter 3. It starts with an introduction into previous research and the basic centre-of-panel thermal behaviour of building components and façade constructions in section 4.1. Based on these centre-of-panel properties, the overall thermal performance can be estimated in section 4.2 introducing the concept of linear thermal transmittance for building panels and building components. For this linear thermal transmittance, the analytical model presented in chapter 3 is modified to include computations for building panels. This elaborated model is presented and tested in section 4.3 for different load bearing and non-load bearing panel edge spacers. Section 4.4 finally discusses practical implications of the thermal edge effects for realistic building panels.

4.1 INTRODUCTION

Vacuum insulation panels (VIPs) have been introduced to the construction sector as an alternative to conventional thermal insulation materials. Vacuum insulation panels can be subdivided into two main categories: foil (film) or sheet-encapsulated VIPs, the latter are also called vacuum insulating sandwiches (VIS). While both types use open-celled core materials, the latter is enclosed by a relatively thick metal sheet. Moreover, film-VIPs are often used in a protective enclosure, like in a building panel. These typically use spacers that cause a significant additional thermal bridge.

Glicksman (1991) was among the first to mathematically define thermal bridge effects that occur on vacuum and reflective insulations. Other researchers addressed experimental determination of thermal performance of a VIP (Stovall and Brzezinski, 2002; Ghazi Wakili et al., 2004) or of a VIP assembly (Brodt and Bart, 1994; Bundi et al., 2005; Nussbaumer et al., 2006; Grynning et al., 2009). Different studies aimed at investigating the influence of the barrier envelope and edge on thermal performance of a VIP (Ghazi Wakili et al., 2004; Nussbaumer et al., 2005; Nussbaumer et al., 2006; Went, 2002; Gudmundsson, 2009) or to investigate edges of building panels (Bundi, 2003; Schwab et al., 2005e), all applying numerical simulations. Based upon previous numerical studies, Simmler and Brunner (2005) declared design values for VIPs including thermal bridge and ageing effects. Besides, Thorsell (2006b) theoretically succeeded in reducing thermal bridge effects in VIPs with stainless steel coverings by proposing a new shape of the panel's edge, the so-called serpentine edge. Although both experimental and numerical studies generated a significant amount of knowledge, they are very time-consuming and labour-intensive. Moreover, these studies did not clearly define relationships between relevant parameters influencing thermal bridging. Because of these issues an analytical equation that predicts the effect of the thermal bridge induced by a VIP barrier laminate was derived and verified in the previous chapter. This equation, however, is derived for film based vacuum insulation panels, i.e. panels with a very thin envelope and edge (approximately 10 to 300 μm). It cannot be applied to VIP incorporated building panels, which have broader edges and often thick facings.

This chapter expands the aforementioned equation to also include building panels. It modifies the derivation of this equation in such a way that an additional heat flow over the surface of the panel's edge is also considered. Furthermore, it will be shown that it is not only applicable to VIP integrated building panels but practically to all building panels within specified conditions. It can thus also be used as a more accurate alternative to 'thermal bridge' calculations according to NEN-EN-ISO 6946 (2005). Data obtained through numerical simulations are used to test the proposed model and to indicate the error generated using this model.

4.2 OVERALL THERMAL PERFORMANCE AND TESTING PROCEDURE

Typically, building constructions, including building panels, are characterized by their thermal transmittance through the central area, U_{cop} [W·m^{-2}·K^{-1}]. Due to differences in geometry and thermal properties of the edge in respect to the centre-of-panel region, the overall or effective thermal transmittance of a building panel as a whole differs from the centre-of-panel thermal transmittance. According to standards (NEN-EN-ISO 10077, 2004) and neglecting geometric thermal bridges at the corners, this effective thermal transmittance can be estimated as

$$U_{eff} = \frac{U_{cop} S_{cop} + U_{edge} S_{edge} + \psi^{(a)}_{edge} l_p}{S_{cop} + S_{edge}} \qquad (4.1).$$

In this equation S_{cop} [m^2] is the central area, S_{edge} [m^2] the edge surface area, U_{edge} [W·m^{-2}·K^{-1}] the thermal transmittance of the edge, $\psi^{(a)}_{\text{edge}}$ [W·m^{-1}·K^{-1}][1] the linear thermal transmittance of the edge and l_{p} [m] the length of the panel perimeter. In this equation, the linear thermal transmittance is defined according to Figure 4.1 (left), only comprising the additional heat flow due to centre-of-panel-edge-interactions.

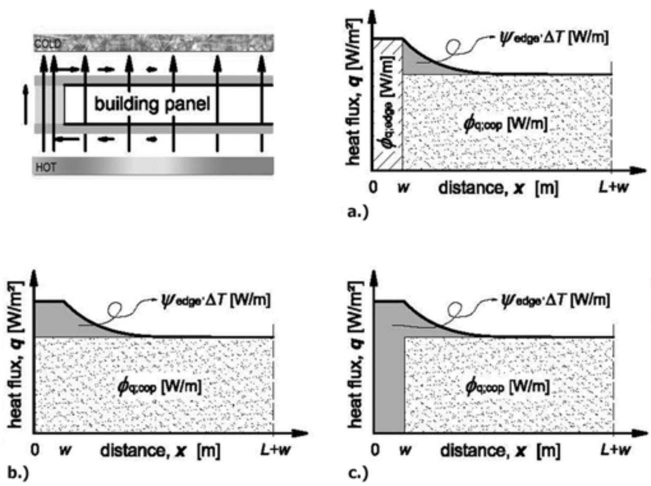

Figure 4.1

Idealised representation of the heat flows through a building panel for three definitions of the linear thermal transmittance: a.) ψ_{edge} only includes centre-of-panel-edge-interactions (top right); b.) ψ_{edge} includes both centre-of-panel-edge-interactions and the difference in heat flux between centre-of-panel region and edge over the width of the edge (bottom left); c.) ψ_{edge} includes both centre-of-panel-edge-interactions and the edge heat flow (bottom right).

[1] For the purpose of clarity, the linear thermal transmittance will be designated with an additional index to distinguish between the three definitions according to Figure 4.1. The indexes *(a), (b)* and *(c)* thus refer to definition 1, 2 and 3 respectively.

To be able to use equation (4.1), however, the thermal behaviour of the panel edge needs to be known and specified in a single parameter (U_{edge}). For many panel edges, like the edge of a double-glazing panel, it is not always practical or possible to determine this parameter with sufficient accuracy. In this chapter therefore the overall thermal transmittance is calculated based upon a slightly different definition of the linear thermal transmittance. Two different options for this definition then exist, as shown in Figure 4.1 (top right and bottom right). In the first alternative definition b), the linear thermal transmittance comprises both centre-of-panel-core-interactions and the difference in heat flux between centre-of-panel region and edge over the width of this edge, while in the latter definition c), the linear thermal transmittance includes both centre-of-panel-edge-interactions and the total edge heat flow. Since the first alternative definition still requires knowledge of the thermal conductance of the edge and since the second alternative definition more-or-less equals the definition employed previously in chapter 3, this second definition is also used in this chapter to derive a model for building panels. These three differently defined linear thermal transmittances are related to one another according to the following equations:

$$\psi_{edge}^{(a)} = \psi_{edge}^{(c)} - U_{edge} w \tag{4.2a}$$,

$$\psi_{edge}^{(b)} = \psi_{edge}^{(c)} - U_{cop} w \tag{4.2b}$$,

with w [m] the width of the edge. Using the third definition of the linear thermal transmittance, $\psi^{(c)}_{edge}$, the overall or effective panel thermal transmittance can now be calculated as[2]

$$U_{eff} = \frac{U_{cop} S_{cop} + \psi_{edge}^{(c)} l_p}{S_{cop} + S_{edge}} \tag{4.3}$$.

Based on the third definition of the linear thermal transmittance, this property can now be derived from numerical simulations or experimental measurements using an equation identical to equation (3.10) from the previous chapter with a geometry as defined in Figure 4.2.

[2] It is important to realise that the equation mentioned in NEN-EN-ISO 10077 (2004), which is equation (4.1) or equation (4.3) in modified form, specifically holds for 2-dimensional geometries. If however the U_{eff}-value of 3-dimensional panels is wanted, then two additional terms in the numerator of equation (4.3) need to be added: $-4U_{edge}w^2$ and $+4\chi$, provided that the panel has 4 corners and that the width of each edge is equal. χ [WK^{-1}] is the thermal transmittance of the corner of the panel which is negative for an outer corner. Since however both terms reduce the U_{eff}-value of such panels, equation (4.3) gives an upper estimate for 3-dimensional panels.

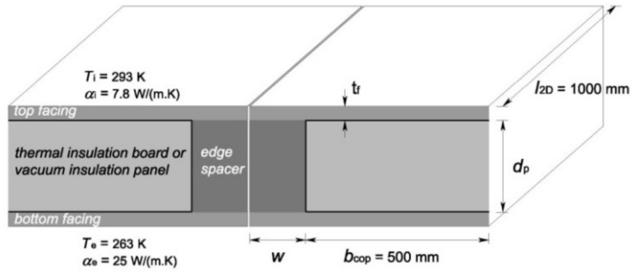

Figure 4.2

Schematic representation of the geometry used in numerical simulations for ψ_{edge} calculations.

Equations (4.1) and (4.3) already clearly show that the thermal performance of a building panel including edge effects increases for increasing panel dimensions and decreasing edge width. Moreover, the thermal properties of the edge and the centre-of-panel-edge-interaction, determined by either U_{edge} and ψ_{edge} for equation (4.1) or by ψ_{edge} for equation (4.3), can strongly affect the overall thermal performance of a building panel. These properties can be determined accurately using numerical simulation software or experimental set-ups. In this chapter a model is presented and tested to analytically estimate the linear thermal transmittance of building panels (and sheet-encapsulated VIPs) with sufficient accuracy. To test this analytical model, the 3D steady-state heat transfer simulation tool TRISCO, which uses the energy balance technique, has been employed (Physibel, 2000). For the simulations, the same (boundary) conditions and accuracy requirements as were used in chapter 3 have been used here, too.

4.3 THERMAL BRIDGING OF BUILDING PANELS: ANALYTICAL MODEL

4.3.1 Analytical model for computing thermal bridge effects in Building Panels

Since the analytical model presented in this section is based upon the model for edge effects on VIPs presented in chapter 3, the assumptions made are the same as for this earlier model and will therefore not be discussed here. Moreover, the differential equations and boundary conditions governing the heat flows through the face sheets are the same and will therefore be omitted as well. Due to the increased width of the edge of a building panel relative to a VIP edge, however, additional heat flows over the width of this edge need to be considered. Consequently, two modifications in the derivation of the original equation need to be made[3].

---

[3] The complete derivation of this approximation model is presented in appendix 41.

First, the heat balance at the corners of the building component (Equation (A32.16) in appendix 32) needs to be modified as

$$-t_{f1}\lambda_{f1}c_1\lambda_1 - t_{f1}\lambda_{f1}c_2\lambda_2 + K(T_{sx}-T_{sy}) - \alpha_1 w(T_1 - T_{sx}) = 0 \qquad \text{for } x=0 \qquad (4.4a),$$

$$-t_{f2}\lambda_{f2}c_1\lambda_1 \frac{B_2}{N_2^2-\lambda_1^2} - t_{f2}\lambda_{f2}c_2\lambda_2 \frac{B_2}{N_2^2-\lambda_2^2} - K(T_{sx}-T_{sy}) + \alpha_2 w(T_2 - T_{sy}) = 0$$

$$\text{for } y=0 \qquad (4.4b),$$

with w [m], $t_{f;j}$ [m], d_c [m], $\lambda_{f;j}$ [W·m^{-1}·K^{-1}] and λ_c [W·m^{-1}·K^{-1}] dimensional or material properties of the building component. w is the width of the panel edge, $t_{f;j}$ is the thickness of the facing or the combined thickness of the facing and the high barrier film (on side 1 or 2), d_c is the thickness of the panel core, $\lambda_{f;j}$ is the equivalent thermal conductivity of the facing (or facing plus barrier film) (on side 1 or 2), λ_c is the thermal conductivity of the panel core and c_1 and c_2 are variables defined in appendix 41. T_j is the boundary temperature on side 1 or 2 respectively. The remaining variables are explained below. Second, the equation for the linear thermal transmittance (Equation (A32.28) in the aforementioned appendix) needs to be expanded to include the additional heat flow through the edge.

Based upon both modifications, the linear thermal transmittance of the thermal bridge due to the edge of a building component is now computed analytically as

$$\psi_{edge}^{(c)} = \frac{\alpha_1}{(T_1 - T_2)} \cdot \left[w\cdot(T_1 - T_{sx}) - \frac{B_1(T_{sy}-c_{0y})(\lambda_1-\lambda_2) + B_1B_2(T_{sx}-c_{0x})\left(\dfrac{\lambda_2}{(N_2^2-\lambda_2^2)} - \dfrac{\lambda_1}{(N_2^2-\lambda_1^2)}\right)}{\sqrt{CD}} \right]$$

$$(4.5).$$

In this equation, (N_1), N_2, B_1, B_2, C and D are calculation parameters, which are defined as

$$N_j = \sqrt{\frac{\alpha_j}{t_{f;j}\lambda_{f;j}} + \frac{\lambda_c}{t_{f;j}\lambda_{f;j}d_c}} \qquad (4.6a),$$

$$B_j = \frac{\lambda_c}{t_{f;j}\lambda_{f;j}d_c} \qquad (4.6b),$$

$$C = N_1^2N_2^2 - B_1B_2 \qquad (4.6c),$$

$$D = \left(N_1^2 - N_2^2\right)^2 + 4B_1B_2 \qquad (4.6d),$$

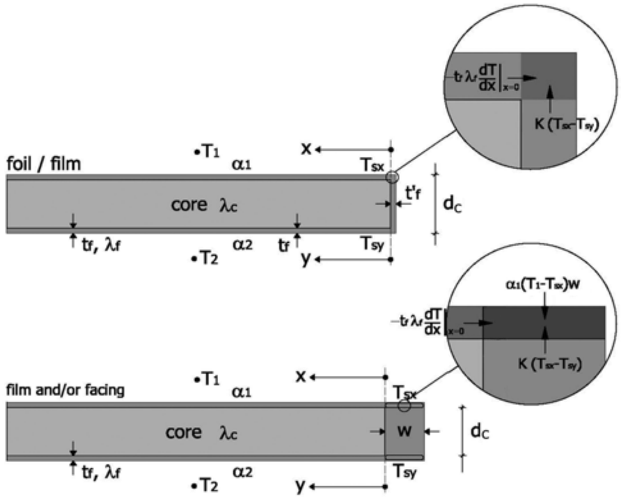

Figure 4.3

Energy balance of the edge of a film-VIP (top) and a building panel (bottom).

c_{0x} [K] and c_{0y} [K] are the temperatures of the face sheets (or face sheet and laminate) at large distance from the thermal bridge where only 1D effects occur. They are calculated as

$$c_{0x} = \frac{A_1 N_2^2 T_1 + B_1 A_2 T_2}{N_1^2 N_2^2 - B_1 B_2} \qquad (4.7a),$$

$$c_{0y} = \frac{A_2 N_1^2 T_2 + B_2 A_1 T_1}{N_1^2 N_2^2 - B_1 B_2} \qquad (4.7b).$$

T_{sx} [K] and T_{sy} [K] are (fictive or average) temperatures of the face sheet (or face sheet and laminate) right in front of the thermal bridge, determined from

$$\begin{aligned} T_{sx} &= \frac{\left[e_4(K+e_2)+e_1(K-e_3)+e_4\alpha_2 w\right]c_{0x} - \left[e_3(K+e_2)+e_2(K-e_3)+e_3\alpha_2 w\right]c_{0y}}{(K-e_3)(K+e_1)-(K+\alpha_2 w+e_2)(K+\alpha_1 w-e_4)} \\ &\quad - \frac{(K-e_3)\alpha_2 w T_2 + \left[(K+e_2)\alpha_1 w+\alpha_1\alpha_2 w^2\right]T_1}{(K-e_3)(K+e_1)-(K+\alpha_2 w+e_2)(K+\alpha_1 w-e_4)} \end{aligned}$$

(4.8a/b),

$$\begin{aligned} T_{sy} &= \frac{\left[e_4(K+e_1)+e_1(K-e_4)+e_1\alpha_1 w\right]c_{0x} - \left[e_3(K+e_1)+e_2(K-e_4)+e_2\alpha_1 w\right]c_{0y}}{(K-e_3)(K+e_1)-(K+\alpha_2 w+e_2)(K+\alpha_1 w-e_4)} \\ &\quad - \frac{(K+e_1)\alpha_1 w T_1 + \left[(K-e_4)\alpha_2 w+\alpha_1\alpha_2 w^2\right]T_2}{(K-e_3)(K+e_1)-(K+\alpha_2 w+e_2)(K+\alpha_1 w-e_4)} \end{aligned}$$

In equation (4.8), the parameters e_1, e_2, e_3, e_4 are defined as

$$e_1 = +\frac{B_1(\lambda_1 - \lambda_2)}{\sqrt{D}}\lambda_{f2}t_{f2} \qquad (4.9a),$$

$$e_2 = -\frac{2B_1B_2}{\sqrt{D}}\left(\frac{\lambda_1}{N_2^2 - N_1^2 + \sqrt{D}} - \frac{\lambda_2}{N_2^2 - N_1^2 - \sqrt{D}}\right)\lambda_{f2}t_{f2} \qquad (4.9b),$$

$$e_3 = -\frac{B_1(\lambda_1 - \lambda_2)}{\sqrt{D}}\lambda_{f1}t_{f1} \qquad (4.9c),$$

$$e_4 = -\frac{2B_1B_2}{\sqrt{D}}\left(\frac{\lambda_1}{N_2^2 - N_1^2 - \sqrt{D}} - \frac{\lambda_2}{N_2^2 - N_1^2 + \sqrt{D}}\right)\lambda_{f1}t_{f1} \qquad (4.9d),$$

with λ_1 and λ_2 the eigenvalues of the linear system of differential equations derived to represent this thermal phenomenon. They are defined by

$$\lambda_1 = -\sqrt{\frac{(N_1^2 + N_2^2) - \sqrt{(N_1^2 - N_2^2)^2 + 4B_1B_2}}{2}} \qquad (4.10a),$$

$$\lambda_2 = -\sqrt{\frac{(N_1^2 + N_2^2) + \sqrt{(N_1^2 - N_2^2)^2 + 4B_1B_2}}{2}} \qquad (4.10b).$$

K [W·m^{-1}·K^{-1}] finally is the thermal conductance of the edge defined as

$$K = \frac{1}{\frac{R_{edge}}{w} + \frac{R_{f1}}{w + w_{eff;1}} + \frac{R_{f2}}{w + w_{eff;2}}} \qquad (4.11).$$

In this equation, R_{edge} [m^2·K·W^{-1}] is the thermal resistance of the edge spacer, which can be estimated using a thermal resistance network of this edge, R_{f1} and R_{f2} [m^2·K·W^{-1}] are effective thermal resistances of facing 1 and 2 respectively and $w_{eff;1}$ and $w_{eff;2}$ [m] are effective widths of the facings. From the edge resistance, R_{edge}, an equivalent edge thermal conductivity, λ_{edge} [W·m^{-1}·K^{-1}], can be determined as well:

$$\lambda_{edge} = \frac{d_c}{R_{edge}} \qquad (4.12).$$

The thermal resistances of the facings are defined as

$$R_{f;j} = \frac{t_{facing;j}}{\lambda_{facing;j}} \qquad (4.13),$$

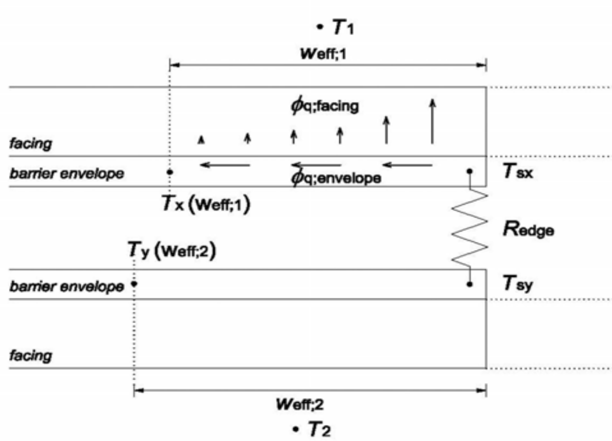

Figure 4.4

Schematic representation of a building panel edge including a definition of the facing effective width.

The effective width, finally, is (arbitrarily) defined as the distance from the edge of the VIP to the point at which the lateral heat flow in the barrier laminate equals the perpendicular heat flow through the face sheet and boundary layer, as explained in Figure 4.4. This width is added to the equation because heat flows deflect at the transition between edge spacer and facing, prolonging the heat flow paths and thus influencing the resistance of the edge. Equating both thermal flows results in an equation for the effective width of a facing as[4]

$$w_{eff;ij} = \sqrt{\frac{T_{si} - T_i(w_{eff})}{\overline{T}_i - T_j} \lambda_{film;j} t_{film;j} \left(\frac{t_{facing;j}}{\lambda_{facing;j}} + \frac{1}{\alpha_j} \right)} \qquad (4.14).$$

In this equation[5] T_{si} [K] is the temperature of the barrier envelope near the panel edge, T_i (w_{eff}) [K] is the temperature of the barrier envelope at w_{eff}, $\overline{T}_i$ [K] is the average envelope temperature between edge and w_{eff}, T_j [K] is the temperature of the environment. λ_{film} [W·m^{-1}·K^{-1}], λ_{facing} [W·m^{-1}·K^{-1}], t_{film} [m] and t_{facing} [m] are the thermal conductivity and thickness of the barrier envelope and facing respectively. The index i can be either x or y, while the index j can either be 1 (corresponding to x) or 2 (corresponding to y) denoting both sides of the building panel.

[4] The derivation of this equation is presented in appendix 42.

[5] During the simulations, we observed that deflection of heat flows was especially relevant for an alu. foil based laminate in combination with a face sheet with low thermal conductivity and least important for the combination of an alu. foil based laminate and an alu. face sheet. If w_{eff} is not included in the analytical calculation, the difference between numerical and analytical results is also largest for the first combination and smallest for the latter one. Although $w_{eff;ij}$ for both combinations practically has the same value, the correction made to the analytical model by the combination of eq. (4.11) and (4.14), i.e. $R_{f;j}$ / $w_{eff;ij}$, is largest for the first combination and smallest for the latter one. This is in agreement with the correction desired.

The temperature ratio in equation (4.14) can be computed very precisely using the equations from appendix 41. Calculations, however, showed that variation in this ratio is very small; it varies between about 0.30 and 2.2 for the warm side of the panel and between 0.49 and 2.3 for the cold side of the panel. For ease of calculation, this ratio is assumed to be 2 for all calculations in this chapter[6].

Although it may seem as if the linear thermal transmittance depends on the temperatures T_1 and T_2, this is actually not true. If equations (4.6) to (4.10) are inserted into equation (4.5), it can be proven, that these temperatures are eliminated from the equation. The resulting equation however is impractically complex and is therefore not presented here but solely in the appendix. Moreover, if the limit for $w \downarrow t_{film}'$ (= the thickness of the high barrier film at the panel edge) is taken for equations (4.5) to (4.11) using the assumption that t_{film}' is very small (approaches zero, except for the edge thickness used in K), equation (3.11) arises.

4.3.2 Studied building component types

To test equation (4.5), four edge spacers types have been used (Figure 4.5a): 1.) an aluminium spacer typically used for double-glazing; 2.) a panel edge construction with an inwards folded facing and a silicone sealant; 3.) an optimized thermoplastic spacer and 4.) a reinforced non-metallic tape. The thermal properties of the materials used are in Table 4.1. Beside these edge construction types, three different facings and two VIP barrier envelopes have been applied, the types and properties of which are shown in Tables 4.2 and 4.3 respectively. Although polymers typically depict anisotropic thermal conductivity, this is not considered in the simulations. Moreover, one type of sheet-based vacuum insulation panel has been simulated.

Based upon these edge spacer types, facing materials and barrier envelopes, 24 component variants and 1 type of sheet-VIP have been composed (with 6 variations in thickness of the top facing)[7]. For each of these component types, a parameter study has been performed using 0, $4.0 \cdot 10^{-3}$, $8.0 \cdot 10^{-3}$, $20 \cdot 10^{-3}$ and $40 \cdot 10^{-3}$ $W \cdot m^{-1} \cdot K^{-1}$ and 10, 20, 30 and 40 mm for the thermal conductivity of the VIP core and its thickness respectively. In total thus 480 simulations on VIP integrated building components and 120 on sheet-based VIPs have been conducted to test the analytical equation. Some results will be presented in the next section.

---

[6] This value is chosen since it corresponds to a linear decrease of temperature in the barrier laminate from T_{si} at x=0 towards T_j at $x=w_{eff}$.

[7] The sheet-VIPs simulated were always composed of stainless steel face sheets and edge profile both having a thermal conductivity of 16.2 $W \cdot m^{-1} \cdot K^{-1}$. The thickness of the bottom face sheet and edge profile always equalled 0.8 mm and 0.3 mm respectively while the thickness of the top face sheet – on the cold side of the panel – varied from 1.5 to 2.0, 2.5, 3.0, 3.5 and 4.0 mm. In practice this thickness is determined by structural requirements.

First however, we will explain how the effective thermal conductivity of the facing and the edge spacer are calculated. Since the heat flow in the facings is mainly directed in the in-plane direction, the combination of facing and film can be seen as two parallel thermal resistances. The equivalent thermal conductivity of the facing λ_f, is therefore estimated as a thickness-weighted thermal conductivity as

$$\lambda_{f;j} = \frac{t_{facing;j}}{t_{f;j}} \lambda_{facing;j} + \frac{t_{film}}{t_{f;j}} \lambda_{film} \tag{4.15}$$

with t_{facing} [m] and t_{film} [m] the thickness of the facing and of the VIP barrier, t_f [m] the sum of t_{facing} and t_{film}, λ_{facing} [W·m^{-1}·K^{-1}] the thermal conductivity of the facing and λ_{film} [W·m^{-1}·K^{-1}] the thermal conductivity of the VIP barrier envelope. In case of sheet-VIPs, t_{film} equals zero as a consequence of which λ_f equals λ_{facing}.

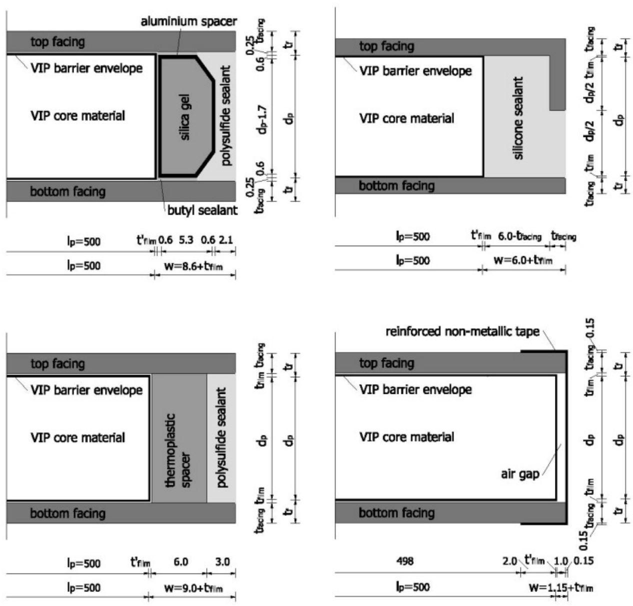

Figure 4.5a

Four edge spacer construction types: a.) double-glazing aluminium spacer (top left); b.) inwards folded edge construction (top right); c.) improved thermoplastic spacer (bottom left); d.) reinforced non-metallic tape (bottom right).

Dimensions in mm.

Appendix A48 contains an enlarged version of these drawings.

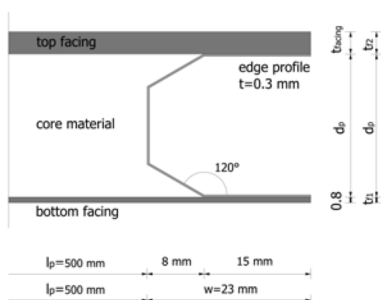

Figure 4.5b

Edge configuration of a sheet-based vacuum insulation panel. Dimensions in mm.

Table 4.1 *- Thermal conductivity of edge construction materials (van Went, 2002).*

material	λ [W·m^{-1}·K^{-1}]
aluminium spacer	
aluminium	160
silica gel	0.12
polysulfide sealant	0.24
butyl sealant	0.40
air gap	0.07
inwards folded spacer	
silicone sealant	0.35
thermoplastic spacer	
thermoplastic spacer	0.25
polysulfide sealant	0.24
non-metallic tape	
non-metallic tape	0.33
air gap d_c = 10mm	0.06
air gap d_c = 20mm	0.07
air gap d_c = 30mm	0.07
air gap d_c = 40mm	0.08

Table 4.2 *- Thermal conductivity of facing materials (Yan, 2006).*

material	t_{facing} [mm]	λ [W·m^{-1}·K^{-1}]
aluminium facing	2	160
polyester facing	3	0.25
stainless steel facing	1.5	16.2

Table 4.3 *- Thickness-averaged thermal conductivity of VIP barrier materials.*

material	t_{film} [mm]	λ [W·m^{-1}·K^{-1}]
aluminium laminate	0.006	160
metallized film	0.097	0.54
edge film/foil	$t'_{film} = 3*t_{film}$	

Table 4.4 *- Thickness-averaged thermal conductivity of face sheets [W·m^{-1}·K^{-1}].*

material	aluminium foil	metallized film
aluminium facing	160.0	152.6
polyester facing	0.569	0.259
stainless steel facing	16.77	15.25

Table 4.5 *- Equivalent thermal conductivity values of edge construction types, λ_{edge} [W·m^{-1}·K^{-1}].*

edge construction		aluminium foil	metallized film
aluminium spacer	d_c = 10 mm	3.75	3.33
	d_c = 20 mm	6.21	5.71
	d_c = 30 mm	8.11	7.55
	d_c = 40 mm	9.61	9.01
folded edge construction	with aluminium facing	0.813	0.359
	with polyester facing	0.727	0.263
	with stainless steel facing	0.791	0.337
thermoplastic spacer	-	0.569	0.259
non-metallic tape	-	2.72	0.317
Sheet-VIPs	d_c = 10 mm	0.249 – 0.258 [a]	
	d_c = 20 mm	0.288 – 0.300 [a]	
	d_c = 30 mm	0.315 – 0.330 [a]	
	d_c = 40 mm	0.326 – 0.342 [a]	

[a] Variations in λ_{edge} arise from differences in thermal conductivity of the core material. The first value applies to λ_c = 0·10^{-3} W·m^{-1}·K^{-1} and the second to λ_c = 40·10^{-3} W·m^{-1}·K^{-1}

Figure 4.6

Thermal resistance networks for a.) the aluminium double-glazing spacer (left) and b.) the inwards folded edge construction (right).

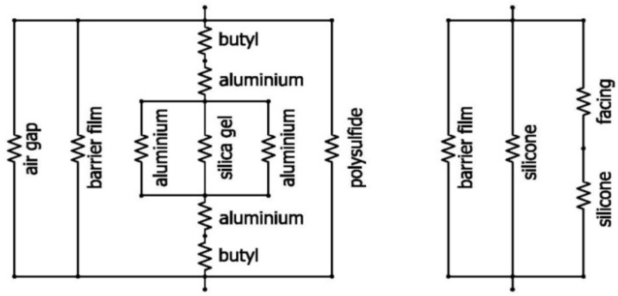

As an approximation for the edge region, the heat streamlines are considered to be parallel and primarily in a direction perpendicular to the panel's surface, which is plausible as long as K is much higher than λ_c / d_c and the panel consists of highly conducting face sheets. The spacer types *improved thermoplastic spacer* and *reinforced non-metallic tape* can thus, similarly to the facings, be considered as parallel resistances. Their equivalent thermal conductivity can then be estimated with a procedure identical to equation (4.15). The types *alu. double-glazing spacer* and *inwards folded spacer* are geometrically more complex. Their thermal resistance networks are shown in Figure 4.6a and b. Table 4.4 and 4.5 present the results of the equivalent thermal conductivity calculations for the facings and the spacers respectively. These values can be used in equations (4.5) to (4.11) for λ_f and λ_{edge}.

4.3.3 Comparative model testing using symmetrical building components

The derived analytical model is tested by comparing its results to numerical simulations of the building component types previously discussed. Figures 4.7 and 4.8 show some of the results[8,9]. In the figures, continuous lines represent predictions according to equation (4.5), while the markers represent the results of numerical calculations. Moreover, the numbers accompanying the continuous lines denote the thermal conductivity of the core material.

---

[8] A complete overview of the results can be found in appendix A43.

[9] The components are designated with a number and a character. The number represents the type of spacer: *1.)* alu. double-glazing spacer; *2.)* folded edge spacer; *3.)* reinforced non-metallic tape and *4.)* improved thermoplastic spacer. The character behind the number represents the combination of laminate and face sheets: *a.)* 2 mm thick alu. face sheets with 6 μm thick alu. based laminate; *b.)* 2 mm thick alu. face sheets with a three layer metallised film based laminate; *c.)* 3 mm thick polyester face sheets with 6 μm thick alu. based laminate; *d.)* 3 mm thick polyester face sheets with a three layer metallised film based laminate; *e.)* 1.5 mm thick stainless steel face sheets with 6 μm thick alu. based laminate; *f.)* 1.5 mm thick stainless steel face sheets with a three layer metallised film based laminate. The figures in the appendix are arranged in the following order: from component 1a to 1f, 2a to 2d, 3a to 3f, 4a to 4d.

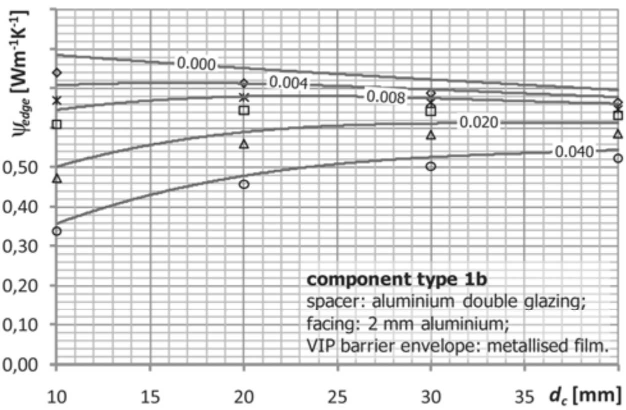

Figure 4.7a

Comparison of numerical (markers) to analytical (lines) data of the linear thermal transmittance as function of panel thickness for a VIP integrated building panel.

<u>Spacer: alu. double-glazing;</u>
<u>Face sheets: 2 mm aluminium;</u>
VIP barrier: metallised film;
$\varphi = 0.67$;
$\alpha_1 = 7.8\ m^2{\cdot}K{\cdot}W^{-1}$;
$\alpha_2 = 25\ m^2{\cdot}K{\cdot}W^{-1}$.

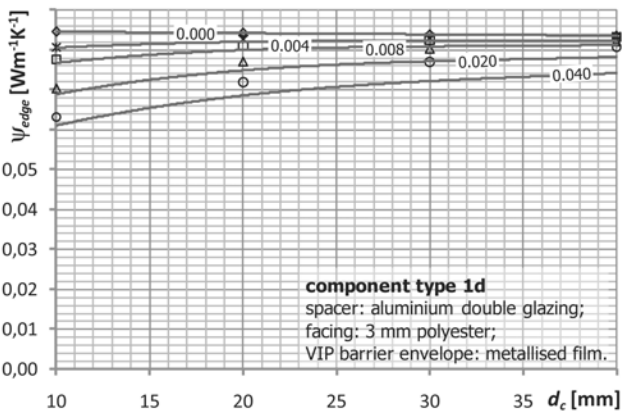

Figure 4.7b

Comparison of numerical (markers) to analytical (lines) data of the linear thermal transmittance as function of panel thickness for a VIP integrated building panel with improved face sheets compared to Figure 4.7a.

<u>Spacer: alu. double-glazing;</u>
<u>Face sheets: 3 mm polyester;</u>
VIP barrier: metallised film;
$\varphi = 0.67$;
$\alpha_1 = 7.8\ m^2{\cdot}K{\cdot}W^{-1}$;
$\alpha_2 = 25\ m^2{\cdot}K{\cdot}W^{-1}$.

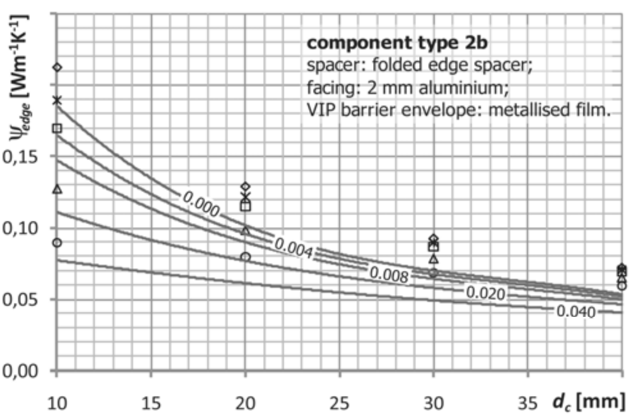

Figure 4.8

Comparison of numerical (markers) to analytical (lines) data of the linear thermal transmittance as function of panel thickness for a VIP integrated building panel with different spacer compared to Figure 4.7a.

<u>Spacer: folded edge spacer;</u>
<u>Face sheets: 2 mm aluminium;</u>
VIP barrier: metallised film;
$\varphi = 0.67$;
$\alpha_1 = 7.8\ m^2{\cdot}K{\cdot}W^{-1}$;
$\alpha_2 = 25\ m^2{\cdot}K{\cdot}W^{-1}$.

As observed from the comparison of analytical to numerical data, the linear thermal transmittance prediction of equation (4.5) is quite well for the aluminium (and stainless steel) facing combinations with an aluminium spacer, an optimized thermoplastic spacer and a non-metallic tape. Differences are however bigger for the inwards folded edge construction. As will be shown in the before last section, this is to a large extent caused by the approximation of the panel edge to a resistance network. Significant errors are introduced in the calculations due to this edge approximation. For panels with a 'high' thermal conductivity facing, deviations between analytical model and numerical data are thus small, even for the folded edge spacer if the thermal conductance of the edge can be estimated with higher accuracy. A building component with a 20 mm thick core of an aluminium foil based VIP, having a central thermal conductance of 0.2 $m^2 \cdot K \cdot W^{-1}$ and having a 2 mm thick aluminium facing and an aluminium edge spacer has a linear thermal transmittance of 0.750 $W \cdot m^{-1} \cdot K^{-1}$ according to numerical simulations, and of 0.725 $W \cdot m^{-1} \cdot K^{-1}$ according to equation (4.5). This is a difference of only $-2.5 \cdot 10^{-2}$ $W \cdot m^{-1} \cdot K^{-1}$, or of -3.3%. As a second example, a building panel with the same VIP core and the same facing, but having an edge consisting of a non-metallic tape can be mentioned. According to numerical simulations its linear thermal transmittance value is 0.129 $W \cdot m^{-1} \cdot K^{-1}$, while equation (4.5) predicts a value of 0.129 $W \cdot m^{-1} \cdot K^{-1}$ as well.

For low thermal conductivity facings, like polyester, however, the relative deviations between modelled and simulated results are moderately bigger, at least if a polyester face sheet is combined with an aluminium foil based VIP. For an optimized thermoplastic spacer in a building component with an aluminium foil based VIP of 20 mm and a 3 mm thick polyester facing, for instance, the deviation between numerical and analytical data amounts to $6 \cdot 10^{-3}$ $W \cdot m^{-1} \cdot K^{-1}$ (= $76 \cdot 10^{-3}$ $W \cdot m^{-1} \cdot K^{-1}$ - $70 \cdot 10^{-3}$ $W \cdot m^{-1} \cdot K^{-1}$), which corresponds to 8.5%. For the same building panel but now with a metallized film based VIP, the deviation is $1 \cdot 10^{-3}$ $W \cdot m^{-1} \cdot K^{-1}$ (2.3%) (=$50 \cdot 10^{-3}$ $W \cdot m^{-1} \cdot K^{-1}$ - $49 \cdot 10^{-3}$ $W \cdot m^{-1} \cdot K^{-1}$). The largest deviations are thus primarily restricted to panels with a polyester facing and an aluminium foil based VIP.

4.3.4 Model testing using sheet-VIPs

In this section the model will be tested furthermore using sheet-VIPs. Two types of sheet-VIPs exist: sheet-VIPs with 2 stainless steel facings and a thin flat edge membrane, and sheet-VIPs with 2 stainless steel face sheets and a thin folded edge membrane. The thermal edge effect of the first type can accurately be predicted using the theory developed in chapter 3 while the latter should be estimated using the equations from this chapter. Due to the edge geometry of those sheet-VIPs, the model presented in chapter 3 is not suitable for determining the linear thermal transmittance of these VIPs. For comparative testing purposes, this latter type of

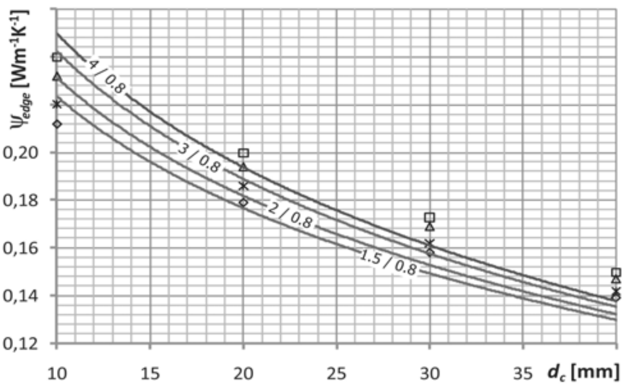

Figure 4.9

Comparison of numerical (markers) to analytical (lines) data of the linear thermal transmittance as function of panel thickness of a sheet-VIP. The numbers accompanying the lines denote the thickness [mm] of facing 1 and 2 respectively.

λ_c =4.0·10^{-3} W·m^{-1}·K^{-1};
α_1 = 7.8 m^2·K·W^{-1};
α_2 = 25 m^2·K·W^{-1}.

sheet-VIP is modelled numerically and computed analytically. The geometry of this VIP was defined in subsection 4.3.2. The thickness of the edge membrane and bottom face sheet equals 0.3 mm and 0.8 mm respectively. The thickness of the top face sheet was chosen to be 1.5, 2, 3 and 4 mm. Moreover, the thickness of the core material, d_c, was selected to be 10, 20, 30 and 40 mm while its thermal conductivity varied from 0, 4.0·10^{-3}, 8.0·10^{-3}, 20·10^{-3} and 40·10^{-3} W·m^{-1}·K^{-1}. A parameter study with in total 80 variants has thus been performed. Some results of this study are presented in Figure 4.9; all results are available in appendix A45.

As observed, the difference between the analytical and numerical computation of the $\psi^{(c)}_{\text{edge}}$–value of a sheet-VIP is small as long as the thermal conductivity of the core is below 8.0·10^{-3} W·m^{-1}·K^{-1}. The $\psi^{(c)}_{\text{edge}}$–value of a sheet-VIP with a thickness d_c of 20 mm, a thermal conductivity of its core of 4.0·10^{-3} W·m^{-1}·K^{-1} and stainless steel face sheets of 0.8 and 3.0 mm thick is 0.194 W·m^{-1}·K^{-1} and 0.190 W·m^{-1}·K^{-1} according to numerical and analytical computations respectively; a relative difference of -2.1%.

However, if is 20·10^{-3} W·m^{-1}·K^{-1} or more, the differences increase. The maximum difference is found for a sheet-VIP with a thickness d_c of 10 mm, λ_c of 40·10^{-3} W·m^{-1}·K^{-1} and stainless steel face sheets of 0.8 and 1.5 mm thick. In that case numerical calculations predict a ψ_{edge}-value of 0.126 W·m^{-1}·K^{-1} while the analytical approximation method results in a value of 0.152 W·m^{-1}·K^{-1}, which is a deviation of +20.8%. As will be shown in section 4.3.5, however, this difference is largely caused by the schematisation of the edge into a single parameter K using thermal resistance networks. The type of network developed for the edge of the panel influences the outcome of this K-value and thus the results of the prediction[10].

---

[10] If the error introduced by this resistance network is separated from the error induced by the analytical model for estimating ψ_{edge} of the previously mentioned sheet-VIP, this results in an error of about +3.1% by the analytical model and of about 17.7% by the schematisation. The maximum error due to the approximation model thus stays below about 3%.

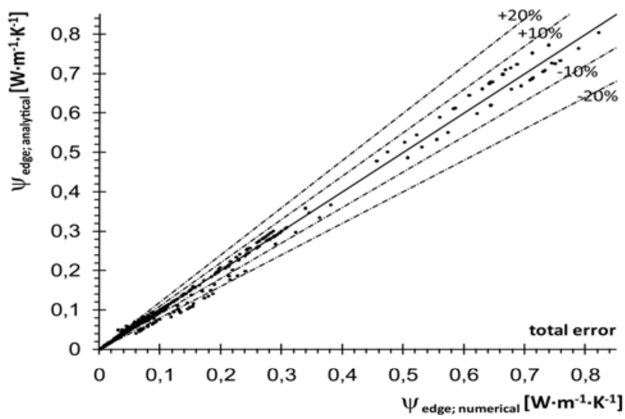

Figure 4.10

Total deviation between analytically calculated and numerically simulated linear thermal transmittance values for all studied panel variants.

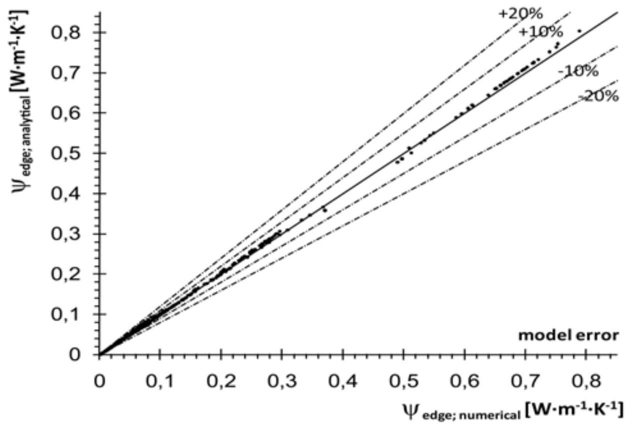

Figure 4.11a

Model deviation between analytically calculated and numerically simulated linear thermal transmittance values for all studied panel variants.

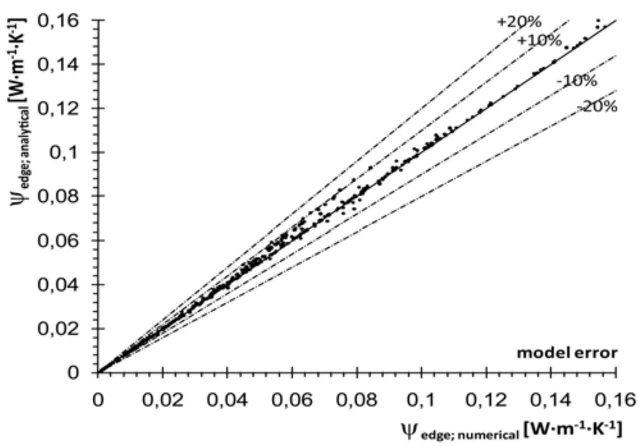

Figure 4.11b

Detail of Figure 4.11a.

4.3.5 Error analysis and model limitations

In the previous sections, analytically calculated ψ-values have been compared to numerically determined values. For these numerical calculations, realistic panel geometries have been taken as models. Figures 4.10 and 4.11 show an overview of the difference between both numerical and analytical values for all studied building panel variants and sheet-VIPs. As can be seen, for high linear thermal transmittance values the approximation of the thermal bridge effect by equation (4.5) is sufficiently accurate, while for smaller linear thermal transmittance values, the differences are bigger.

To be able to use the analytical equation (4.5), however, the edge construction needed to be characterized by only two parameters: the equivalent edge thermal conductance, K, and the edge width, w. This edge thermal conductance was calculated based upon thermal resistance network representations. Since very simple networks were applied, a schematization error occurred. This schematization error must not be attributed to the model itself, but separated from the total error, resulting solely in a model error. To determine this model error, the panel edge constructions and spacers have been schematized as a single material block at the edge of the building component, having a width equal to the width of the original edge and a thermal conductivity equal to the equivalent edge thermal conductivity. Comparing the results of these numerical simulations with the analytical results from equation (4.5) produces Figure 4.11. As demonstrated by this figure, the model error is significantly smaller than the total error presented in Figure 4.10. For 90% of all components studied[11], the difference between analytical model and numerical simulations is smaller than 5% while even for 99% of all these components the difference is smaller than 10%. Now thus also for smaller linear thermal transmittance values, the deviations are in many cases below 5%.

A more detailed error analysis reveals that the largest differences between the analytical model and numerical simulations exist for components having a combination of 3 mm thick polyester face sheets and an aluminium barrier envelope. If all components with this combination of face sheet and barrier laminate are excluded from the error analysis, then in 96% of all components studied the difference between numerical and analytical model is less than 5% and even in 100% of all components less than 10%. Based upon this observation, we may state that the analytical model is in any case sufficiently accurate for all components studied with the exception of components having a polymer face sheet combined with a VIP with an aluminium barrier envelope.

---

[11] This applies to all components studied, thus the components of section 4.3.3, the asymmetrical components of appendix A44 and the sheet-VIPs of section 4.3.4. In total the number of components studied was 580.

The different combinations of face sheet and barrier laminate can be distinguished among each other either by their thermal conductance, calculated as the product of average thermal conductivity of face sheet and barrier laminate and their combined thickness, $\lambda_f t_f$, or by the ratio of the thermal conductance of each layer separately. This latter ratio, ξ, is calculated as

$$\xi = \frac{\lambda_{film} t_{film}}{\lambda_{facing} t_{facing}} \tag{4.16}$$

Table 4.6 presents the values of both $\lambda_f t_f$ and ξ for all laminate and face sheet combinations. As can be seen, ξ can be used to unequivocally distinguish the combination of polymer face sheet and aluminium barrier laminate from the other combinations since it produces the highest value for this factor. The separation between both groups of combinations may arbitrarily be set at a ξ–factor of 1[12].

Based upon the previous analyses, it can be stated that the model is practical for almost all building components that might be used in reality. The analysis shows that for all panels studied for which ξ<1 the difference between numerical and analytical results is less than 10% in all cases. For building components for which ξ>1 the error is moderately bigger but still acceptably small with a maximum error observed of 10.7%.

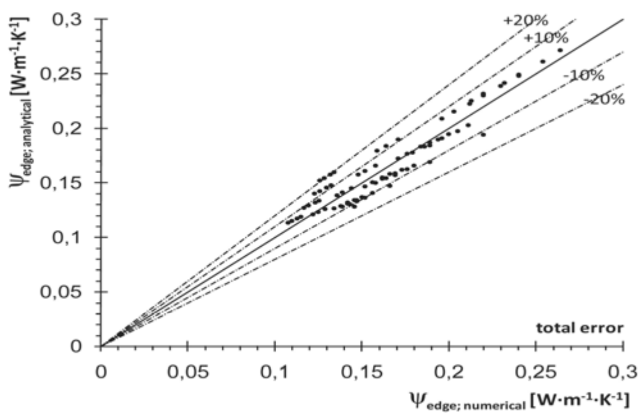

Figure 4.12

Total deviation between analytically calculated and numerically simulated linear thermal transmittance values for all studied sheet-VIPs.

[12] Since the error apparently increases if this ξ-factor increases, additional insulation layers as face sheets cannot be modelled as part of $\lambda_f t_f$. In chapters 3 and 7 it is shown that such layers can be modelled as a modification of the boundary heat transfer coefficients α_1 and α_2. It is difficult to give strict boundaries but as a rough indication this can be done if ξ>1.

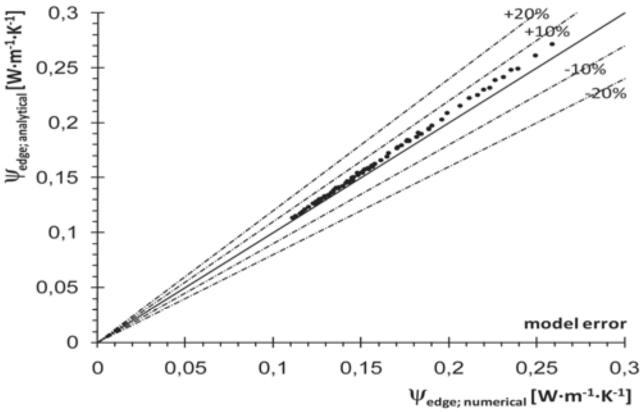

Figure 4.13

Model deviation between analytically calculated and numerically simulated linear thermal transmittance values for all studied sheet-VIPs.

Table 4.6a *– ξ-factor for the combination of face sheets and barrier laminates used.*

		barrier laminate	
		6 μm AF	97 μm MF
face sheet	2 mm aluminium	$4.2 \cdot 10^{-3}$	$1.6 \cdot 10^{-4}$
	1.5 mm stainless steel	$5.6 \cdot 10^{-2}$	$2.2 \cdot 10^{-3}$
	3 mm polyester	1.8	$7.0 \cdot 10^{-2}$

Table 4.6b *– $\lambda_f t_f$ for the combination of face sheets and barrier laminates used.*

		barrier laminate	
		6 μm AF	97 μm MF
face sheet	2 mm aluminium	$3.2 \cdot 10^{-1}$	$3.2 \cdot 10^{-1}$
	1.5 mm stainless steel	$2.6 \cdot 10^{-2}$	$2.4 \cdot 10^{-2}$
	3 mm polyester	$2.1 \cdot 10^{-3}$	$8.0 \cdot 10^{-4}$

4.3.6 General behaviour of the linear thermal transmittance

The presented analytical model can now be used to investigate the parameters influencing the thermal bridge effect resulting from spacers. The linear thermal transmittance on the level of a VIP integrated building component primarily depends on five parameters: product of thermal conductivity and thickness of either face sheet (or combination of face sheet and barrier laminate), $\lambda_{f;j}\, t_{f;j}$ [W·K-1], thermal conductivity of the core, λ_c [W·m-1·K-1], thickness of the core, d_c [m], thermal conductance of the edge, K [W·m-1·K-1], and width of the edge, w [m].

Similar to the conduct of VIPs, the ψ-value increases for increasing thermal conductivity and thickness of the face sheets (Figure 4.15), for increasing edge thermal conductance (Figure 4.16), and width, and for decreasing thermal conductivity of the core (Figures 4.14 to 4.16). The influence of the thickness of the core on the linear thermal transmittance is more difficult again. In general, the ψ-

Figure 4.14

General behaviour of the linear thermal transmittance of a VIP integrated panel as a function of panel thickness and thermal conductivity of the core material. The values in the graph denote the thermal conductivity of the core.

<u>Spacer: alu. double-glazing with constant λ_{edge}=6 W·m-1·K-1;</u>
<u>Face sheets: 2 mm aluminium;</u>
<u>VIP barrier: aluminium foil;</u>
α_1 = 7.8 $m^2·K·W^{-1}$;
α_2 = 25 $m^2·K·W^{-1}$.

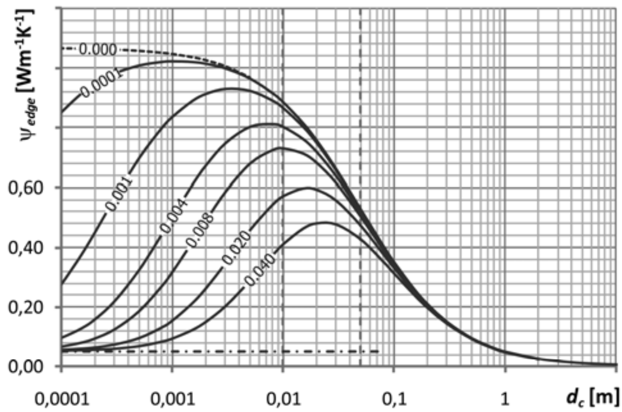

Figure 4.15

General behaviour of the linear thermal transmittance of a VIP integrated panel as a function of the product of thermal conductivity and thickness of face sheets. Face sheets on both sides identical. The values in the graph denote the thermal conductivity of the core.

K=2.67 $W·m^{-1}·K^{-1}$; w= 8.62 mm;
d_c = 20 mm;
VIP barrier: 6 μm alu. foil;
α_1 = 7.8 $m^2·K·W^{-1}$;
α_2 = 25 $m^2·K·W^{-1}$.

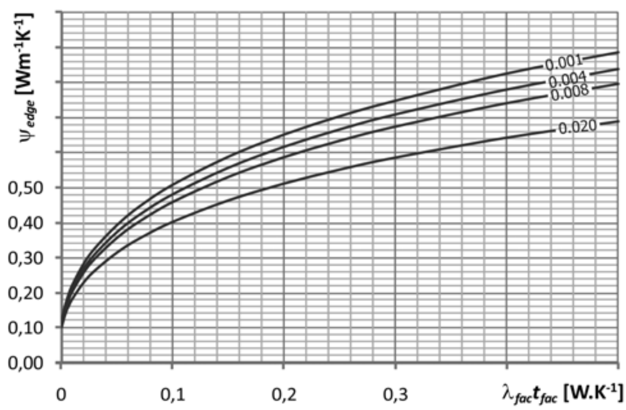

Figure 4.16

General behaviour of the linear thermal transmittance of a VIP integrated panel as a function of the thermal conductance of the edge. Face sheets on both sides identical. The values in the graph denote the thermal conductivity of the core.

w= 8.62 mm; d_c = 20 mm;
face sheets: 2 mm aluminium;
VIP barrier: 6 μm alu. foil;
α_1 = 7.8 $m^2·K·W^{-1}$;
α_2 = 25 $m^2·K·W^{-1}$.

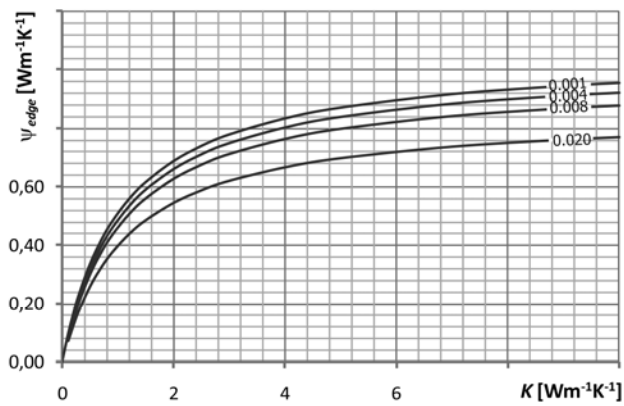

value first increases from a certain value to a maximum value and then decreases asymptotically to zero if the panel thickness increases. Figure 4.14 depicts this general behaviour of a building panel with an aluminium based spacer, 2 mm thick aluminium face sheets and a VIP with aluminium foil based laminate and a thermal conductivity between 0 and $40 \cdot 10^{-3}$ W·m^{-1}·K^{-1}. From this figure it readily becomes clear that the linear thermal transmittance does not start at 0 W·m^{-1}·K^{-1} at very low panel thicknesses but at a higher value. This higher value equals

$$\lim_{d_c \downarrow 0} \psi_{edge}^{(c)} = \lim_{d_c \downarrow 0} w\alpha_1 \frac{T_1 - T_{sx}}{T_1 - T_2} = w\frac{\alpha_1\alpha_2}{\alpha_1 + \alpha_2} \qquad (4.17),$$

which is the heat flow towards the panel's edge from side one divided by the total temperature difference[13]. In general, the conduct is identical to that of VIPs, though.

4.4 Overall Thermal Performance: Practical Considerations

Having given a theoretical discussion and having presented an analytical model to determine the value of the linear thermal transmittance with high accuracy, in this section several effective panel thermal transmittance values are discussed and compared to effective transmittances of a typical 3-layer metallized film based vacuum insulation panel and a conventional mineral fibre board[14]. Table 4.7 presents the results of the effective transmittance value calculations for several building components. As can be seen, the effective thermal transmittance varies significantly among others depending on the type of edge construction and the type of face sheet.

---

[13] This value results from the choice for the definition of $\psi^{(c)}_{edge}$. Since it is defined in this dissertation as the heat flow through an entire component with thermal bridge minus the heat flow through the central area of this same panel, thus not including the edge of the component, the linear thermal transmittance both includes the additional heat flow due to centre-of-panel-edge interactions and the heat flow over the edge of the panel (section 4.2). If d_c reduces in a limit to zero, centre-of-panel-edge interactions diminish because the central region has become identical to the edge region – the difference was caused by the VIP and the spacer which are now gone since d_c = 0 m. The flow through the edge still remains. This is reflected by the equation neglecting resistances of the face sheets.

[14] In addition to this investigation the panels presented in section 4.3.2 have also been studied in more detail. All panels studied consisted of a VIP core with a metallised barrier envelope. Based on the model presented in the previous sections, the U_{eff}-value (equation (4.3)) can be plotted as function of panel thickness and ratio of perimeter to surface area for the selected panels. These plots can be very useful for designers and manufacturers and are therefore presented in appendix A47 giving the U_{eff}-values of panels with VIPs as core with a thermal conductivity, λ_c, of either $4.0 \cdot 10^{-3}$ W·m^{-1}·K^{-1} or $8.0 \cdot 10^{-3}$ W·m^{-1}·K^{-1}.

Figure 4.17

Surface plot of the linear thermal transmittance [W·m⁻¹·K⁻¹] of a symmetrical VIP-integrated building panel due to its edge as function of K [W·m⁻¹·K⁻¹] and $\lambda_{f;j}\, t_{f;j}$ [W·K⁻¹].

w = 0.01 m;
d_c = 0.02 m;
$\lambda_c = 4{\cdot}10^{-3}$ W·m⁻¹·K⁻¹;
$\alpha_1 = 7.8$ m²·K·W⁻¹;
$\alpha_2 = 25$ m²·K·W⁻¹.

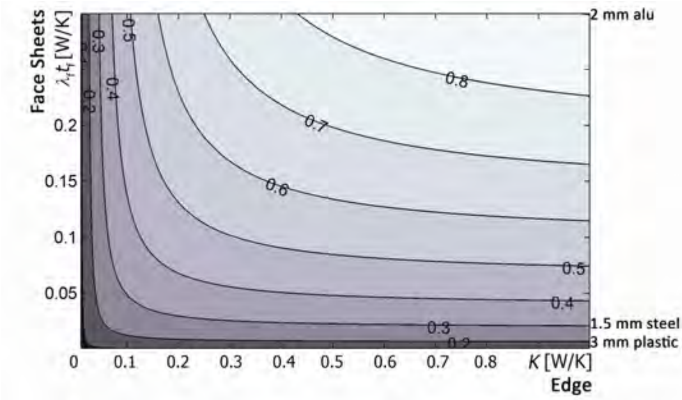

The thermal behaviour of the face sheet (or face sheet + laminate) can be characterized by the product of its thickness and thermal conductivity, $\lambda_{f;j}\, t_{f;j}$. According to Table 4.7a and b and Figure 4.17, the overall thermal behaviour of a building panel improves if $\lambda_{f;j}\, t_{f;j}$ reduces. For instance, the overall thermal transmittance of a 20 mm thick building panel with an aluminium spacer and λ_c of $4.0{\cdot}10^{-3}$ $W{\cdot}m^{-1}{\cdot}K^{-1}$ reduces from 2.8 via 1.2 to 0.5 $W{\cdot}m^{-2}{\cdot}K^{-1}$, if the face sheet changes from 2 mm aluminium via 1.5 mm stainless steel to 3 mm polyester.

The thermal behaviour of the panel edge can be characterized by its thermal conductance, *K*. Regarding this edge thermal behaviour, Table 4.7b shows that the overall panel thermal transmittance decreases for decreasing *K*. A building panel with a 20 mm thick VIP core with $\lambda_c = 4.0{\cdot}10^{-3}$ $W{\cdot}m^{-1}{\cdot}K^{-1}$, 2 mm thick aluminium facing and an aluminium spacer edge construction, for example, has an overall thermal transmittance of 2.8 $W{\cdot}m^{-2}{\cdot}K^{-1}$, while the same panel but now with an thermoplastic spacer has an overall thermal transmittance of 0.6 $W{\cdot}m^{-2}{\cdot}K^{-1}$ and with a reinforced non-metallic tape even of 0.3 $W{\cdot}m^{-2}{\cdot}K^{-1}$.

Moreover, the overall thermal performance of a VIP integrated building component depends on the thickness of the core and the ratio l_p / S_p[15]. The thickness of the building component influences its overall thermal performance in two ways. First, due to variation in panel thickness, the thermal conductance of the central region changes; the thicker the building panel, the smaller its central thermal conductance is. Second, the thickness of the panel also affects the ψ-value of its edge; the thicker the building panel, the lower this value in most cases is[16]. Since the effect

[15] Note that S_p as used to create the plots in appendix A47 is the surface area of the entire panel on one side and thus comprises both the centre-of-panel and the edge surface area.

[16] As we have seen previously, the linear thermal transmittance due to the thermal bridge caused by the edge of many building components increases for decreasing panel thickness, at

of panel thickness on centre-of-panel U-value is stronger than on linear thermal transmittance, the overall thermal performance increases with increasing panel thickness[17]. The dependency of U_{eff} on the ratio l_p / S_p can also be explained clearly. If the ratio l_p / S_p decreases, thus if the panel becomes larger, the influence of the thermal bridge relative to the centre-of-panel area decreases. The effective thermal transmittance decreases asymptotically to the value of U_{cop} for decreasing l_p / S_p. So, with decreasing l_p / S_p U_{eff} decreases as well, which is especially discernible for components with highly conducting face sheets and spacer.

***Table 4.7a** - Effective thermal transmittance of VIP integrated panels with central thermal conductivity of $4{\cdot}10^{-3}$ W·m^{-1}·K^{-1}, metallised film VIP with the same central thermal conductivity and a conventional thermal insulator, all for different panel thicknesses and a panel size of 0.5 x 0.5 m^2.*

d_c [mm]	U_{eff} [W·m^{-2}·K^{-1}]								
	aluminium spacer			thermoplastic spacer		non-metallic tape		VIP[4]	fibre glass[4]
	A[1]	B[2]	C[3]	A	C	A	C	MF	
10	5.7	2.5	1.0	1.7	0.9	0.7	0.5	0.4	4.0
20	5.6	2.4	0.9	1.0	0.6	0.4	0.3	0.2	2.0
30	5.4	2.3	0.8	0.7	0.5	0.2	0.2	0.1	1.3
40	5.3	2.2	0.8	0.5	0.4	0.2	0.2	0.1	1.0

[1] 'A': a panel with 2 mm thick aluminium face sheets; [2] 'B': a panel with 1.5 mm thick stainless steel face sheets; [3] 'C': a panel with 3 mm thick polyester face sheets; [4] The thickness of a VIP panel and a mineral fibre board equals the thickness of the building component core, d_c.

---

least within the range of practical architectural application, i.e. a VIP thickness lying between 10 and 50 mm. However, for building components with a highly conducting edge, like an aluminium double-glazing spacer, this linear thermal transmittance may decrease for decreasing panel thickness. From a thermal perspective however this is not a recommended solution. Such a decrease in ψ_{edge} -value is also visible for component type 3c with $\lambda_c \geq 20{\cdot}10^{-3}$ W·m^{-1}·K^{-1} and $d_c \leq 0.02$ m. Type 3c consists of panel with a non-metallic tape as spacer, a 6 µm thick aluminium barrier envelope around the VIP and 2 3 mm thick Polyester face sheets.

[17] If the thickness of the VIP decreases, the centre-of-panel thermal transmittance increases while in most cases the linear thermal transmittance of the panel's edge increases too. The relative effect of d_c on U_{cop} is however stronger than its effect on ψ_{edge}, as a consequence of which the ratio of $\psi_{edge}{\cdot}l_p$ to $U_{cop}{\cdot}S_{cop}$ decreases. This implies that the relative effect of the thermal bridge decreases and thus the importance of centre-of-panel region increases. Since the thermal behaviour of the central region does not depend on panel size and aspect ratio, the effect of these factors should reduce too with decreasing panel size. In the surface plots in appendix A47, this effect is visible in the fact that the lines denoting equal U_{eff} become more horizontal for decreasing d_c. Thus the smaller the panel size, the less pronounced the dependency of U_{eff} on l_p / S_p and the more pronounced its dependency on d_c.

***Table 4.7b** - Effective thermal transmittance of VIP integrated panels with central thermal conductivity of $4\cdot10^{-3}$ $W\cdot m^{-1}\cdot K^{-1}$, metallised film VIP with the same central thermal conductivity and a conventional insulator, all for different panel thicknesses and a panel size of 1 x 1 m^2.*

d_c [mm]	U_{eff} [$W\cdot m^{-2}\cdot K^{-1}$]								
	aluminium spacer			thermoplastic spacer		non-metallic tape		VIP[4]	fibre glass[4]
	A[1]	B[2]	C[3]	A	C	A	C	MF	
10	2.9	1.4	0.7	1.0	0.6	0.5	0.4	0.4	4.0
20	2.8	1.2	0.5	0.6	0.4	0.3	0.2	0.2	2.0
30	2.7	1.2	0.4	0.4	0.3	0.2	0.2	0.1	1.3
40	2.6	1.1	0.4	0.3	0.2	0.1	0.1	0.1	1.0

Finally, as can be seen from the tables, it is difficult to achieve 'Passivhaus standard' ($U_{eff} < 0.15$ $W\cdot m^{-2}\cdot K^{-1}$) with building panels with a VIP core having a thickness d_c of less than 4 cm[18], even at the beginning of service life. Only building panels with a reinforced non-metallic tape at their edges are more-or-less able to perform according to this standard with VIPs thinner than 4 cm. This result implies that sandwich panels, which do not need a strong and stiff edge profile, are to be preferred to other building components, at least from a thermal perspective.

4.5 Conclusions and Summary

The objective of this chapter was to present an analytical model for studying and approximating thermal edge effects due to spacers in thermally highly performing building panels. Through a comparison of this model with numerical simulations of several building components and sheet-VIPs (VISs), it was shown that the analytical model can be used to estimate the linear thermal transmittance of these spacers with sufficient accuracy. For 99% of all components studied, the analytical model deviates from numerical results by less than 10% (model error). For 90% of all components, differences were found to be even less than 5% (model error). It was found that especially components with a combination of a highly conducting barrier envelope, like a metal foil based laminate, and low conducting face sheets, like polyester, the differences were moderately bigger. If these results are excluded from the analysis, then even in 100% of all components studied the deviations were found to be less than 10% and in 96% less than 5%.

[18] One manufacturer has limited the thickness of producing VIPs to 40 mm (Va-Q-tec, 2008).

It is important to keep in mind that the total error not only consists of the model error but also involves a schematization error resulting from the use of resistance network models for estimating the equivalent edge thermal conductance. This additional error does increase the prediction error but should not be attributed to the proposed model. Moreover, the differences specified are deviations of the analytical model from numerical simulations and not from laboratory tests.

The proposed model must be considered as an extension to the model for estimating the linear thermal transmittance of VIP edges presented in the previous chapter. This model thus explicates the relations between parameters influencing the thermal performance of (VIP integrated) components. As already stated in the previous chapter, such explicit relations facilitate design and engineering processes in a way that they show us in advance what will happen if a certain parameter is changed. It thus increases our understanding of the thermal behaviour of complete building panels and enables product designers to improve or optimize spacers of building components on the one hand and facilitates architects and façade engineers with estimating the thermal performance of building skins on the other hand.

From this model and the figures produced with it, it readily becomes clear that the ψ-value depends on the product $\lambda_{fj}t_{fj}$ of each face sheet, the boundary heat transfer coefficients, α_j, the width of the edge, w, the equivalent thermal conductance of the edge, K, and the thermal conductivity and thickness of the core material. It is important to realise that the thickness of the core might also influence K.

Similar as was found in the previous chapter, the linear thermal transmittance increases for increasing thermal conductivity and thickness of the face sheets, for increasing edge thermal conductance, K, and width, w, and for decreasing thermal conductivity of the core, λ_c . The reasons for this are that more heat is collected and transferred to the edge by the face sheets if their thickness and thermal conductivity increase while also more heat is transferred through the thermal bridge if this becomes wider or more conducting relative to the central region. The influence of the thickness of the core on the linear thermal transmittance is more difficult. In general, the ψ-value first increases from a certain value to a maximum value and then decreases asymptotically to zero if the panel thickness increases.

Moreover, from simulations on several building components it became clear that it is difficult to achieve 'Passivhaus standard' with building panels with a VIP core having a thickness of less than 40 mm, even at the beginning of service life. This result implies that, if such high standards are desired, sandwich panels, which do not need a strong and stiff edge profile, are the preferred choice from a thermal perspective.

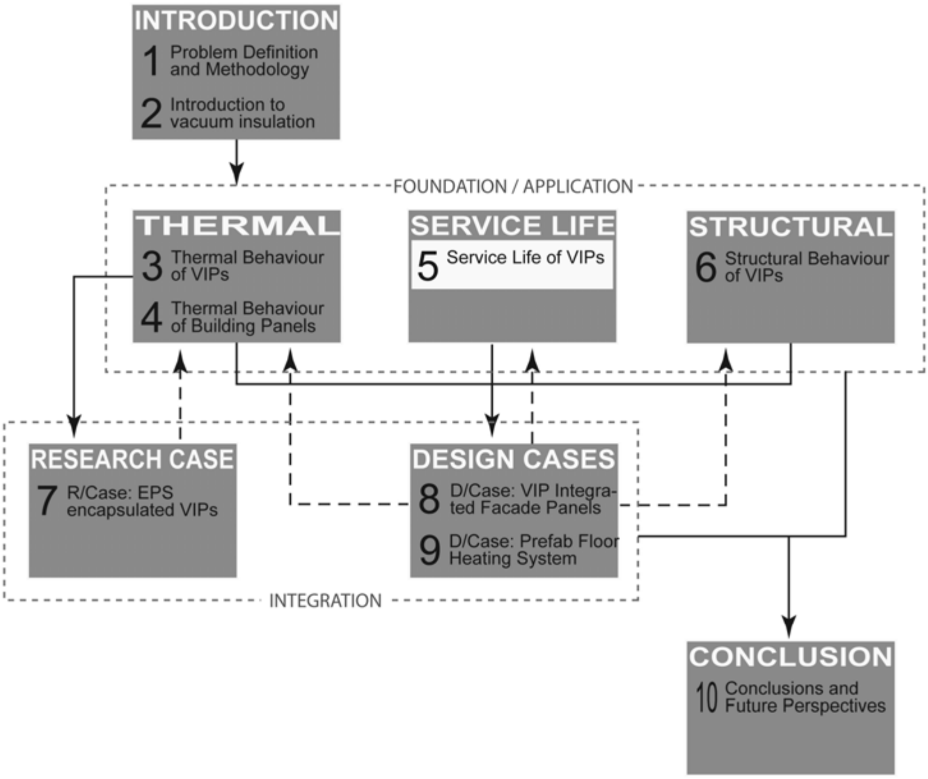
INTRODUCTION
1 Problem Definition and Methodology
2 Introduction to vacuum insulation
FOUNDATION / APPLICATION
THERMAL
3 Thermal Behaviour of VIPs
4 Thermal Behaviour of Building Panels
SERVICE LIFE
5 Service Life of VIPs
STRUCTURAL
6 Structural Behaviour of VIPs
RESEARCH CASE
7 R/Case: EPS encapsulated VIPs
DESIGN CASES
8 D/Case: VIP Integrated Facade Panels
9 D/Case: Prefab Floor Heating System
INTEGRATION
CONCLUSION
10 Conclusions and Future Perspectives

Service Life of VIPs and Components 5

Study into the Fundamentals of Service Life Prediction and into Models for Estimating such Values

While the two previous chapters discussed the first research aspect, thermal behaviour, this chapter elaborates on the aspect of service life properties of vacuum insulation panels and VIP integrated building components on a fundamental and applicational level. This chapter investigates the effects of different environmental conditions, like temperature, relative humidity, partial water vapour pressure and atmospheric pressure on service life. Both static and transient environmental conditions are studied and modelled. Moreover, models for approximating service lives are derived and based upon these models, the effects of temperature, panel thickness, panel dimensions and thermal bridge effects on the service life of vacuum insulation panels and building components are studied.

However, to be able to study the aforementioned effects, it is necessary to introduce the phenomenon of thermal conductivity ageing and present definitions of service life in section 5.1. Thermal conductivity ageing causes the centre-of-panel thermal conductivity to increase over time due to water vapour and gas pressure increase. Based on this ageing concept, it is possible to define the service life of a vacuum insulation panel under laboratory conditions and under applied or built-in conditions. Moreover, the discussion on thermal conductivity ageing enables the introduction of physical models that predict the service life under constant conditions (section 5.2) and the development of service life influencing functions and factors that approximate transient effects for each of the aforementioned environmental conditions, as is demonstrated in section 5.3. After the position of assumptions and the derivation of relations, an (approximation) model for VIPs with a core of either polyurethane foam, glass fibre board or compressed fumed silica powder board are presented in section 5.4. Since the model for a SiO_x*-VIP is a semi-empirical model, several parameters are derived from a regression analysis using experimental data from EMPA or ZAE-Bayern. Based on these models, the effects of environmental conditions, size and thermal bridge effects on the service life of VIPs and VIP incorporated building panels can finally be studied in section 5.5, 5.6 and 5.7.*

5.1 INTRODUCTION

5.1.1 Service life definitions

In a previous chapter, it was explained that the thermal conductivity of the core of a vacuum insulation panel significantly depends on the gas pressure and the amount of water absorbed. Because the gas pressure and partial water vapour pressure in the panel surrounding air are higher than in the core material itself, a difference in chemical potential occurs. To block or at least to reduce the ingress of gases and water vapour, it is necessary to separate the core from the surrounding air by a barrier laminate, which should be able to maintain a low gas pressure and water content in this core for as long as possible. The barrier, however, is not completely gas and water vapour tight. As a result, atmospheric gases and water vapour will migrate into the core, slowly but gradually increasing its thermal conductivity. This increase of the thermal conductivity over time is called thermal conductivity ageing.

The functional service life of a VIP or a VIP incorporated building component mainly depends on this ageing, since the properties of the remaining materials and elements used do not seriously deteriorate over time with respect to their thermal behaviour, provided that the component is designed properly. The definition of the functional service life, t_{sl}, of a VIP integrated building component is therefore more-or-less equal to the service life definition of the VIP itself. Two different service life definitions can be distinguished, the first of which is the most widely used with respect to vacuum insulation, at least if thermal bridge effects are excluded[1].

Service life definition 1: *The time elapsed from the moment of manufacturing (t=0) until the moment the effective thermal conductivity of the vacuum insulation panel[2], λ_{eff}, has exceeded a certain critical value, λ_{cr}, ($t=t_{sl}$); or in other words, the service life has expired if the following condition has been reached:*

$$\left.\lambda_{eff}\right|_{t=t_{sl}} = \lambda_{cr} \qquad (5.1).$$

[1] In the construction industry, service life is generally defined as 'the period of time after installation during which a building or its parts meet or exceed the performance requirement(s)' (NEN-ISO 6707-1, 2004, p. 86). According to aforementioned standard, loss of thermal performance in this case is the degradation indicator; the increase of thermal conductivity is called the performance characteristic in this case also being the terminal critical property.

[2] In most literature concerning VIPs, the thermal conductivity of the core is used in stead of the effective thermal conductivity of the VIP. If the first is used, thermal bridge effects are neglected. If the latter is used, these effects are included.

This critical thermal conductivity can be set at an arbitrary value, but is mostly set at $8 \cdot 10^{-3}$ $W \cdot m^{-1} \cdot K^{-1}$ (Simmler and Brunner, 2005) or sometimes at $11 \cdot 10^{-3}$ $W \cdot m^{-1} \cdot K^{-1}$ (ASTM C1484, 2001). It is also important to note that in general the thermal conductivity limit is set for the core material alone (λ_c), thus not considering thermal bridge effects. Unless specified otherwise, in this dissertation service life definitions explicitly comprise thermal bridge effects since only then a valid comparison between barrier envelopes for VIPs is attainable.

> Service life definition 2: *The time elapsed from the moment of manufacturing (t=0) until the moment the time-averaged effective thermal conductivity of the vacuum insulation panel equals some critical value, λ_{cr} (t=t_{SL}); in other words, the service life has expired if*

$$\left.\bar{\lambda}_{eff}\right|_{t=t_{SL}} = \lambda_{cr} \qquad \text{with} \qquad \bar{\lambda}_{eff} = \frac{1}{t}\int_0^t \lambda_{eff}(t)dt \qquad (5.2).$$

This second definition results in the possibility to set a limit for the total heat loss through the building construction including thermal bridges during the entire VIP service life, while the first definition just limits the instantaneous heat loss[3,4,5].

The service life demands on a VIP depend on the application. Actually, the service life defined on the VIP itself is not so important, but the service life for the entire product or component incorporating a VIP is. The service life of a transport container, e.g., is approximately 2 years. The service life of refrigerators is about 15

[3] The service life defined using the effective thermal conductivity of a VIP can for instance be used for engineering purposes, like guaranteeing that a certain performance is always achieved during the entire life of a panel and testing façade constructions against worst-case scenarios, while the service life defined using the time average thermal conductivity can be used for calculations involving costs, like energy cost calculations and feasibility studies.

[4] According to standards for mineral wool and mineral fibre insulation (NEN-EN 13162:2009 and NEN-EN 13171: 2009), the declared value of the thermal conductivity should be based on measurements using a 90% upper boundary, i.e. 90% of the tested samples should have a thermal conductivity below the declared value. This would fit with definition 1 rather than definition 2. Erb and Simmler (2008) also use this method to define a declared thermal conductivity value of a VIP. The so-called $\lambda_{90,90,0}$ is then used to determine the thermal conductivity of a VIP after 25 years which includes aging effects, $\lambda_{90,90,25a}$. From this last value then a declared value is computed, λ_D, in which thermal edge effects are also considered. This

[5] For determining design values of the thermal resistance of polymeric foams, like polyiso insulation, this second definition of service life, named long-term thermal resistance (LLTR), has been introduced in the USA and Canada several years ago. For such insulation materials, a 15 year weighted average thermal resistance is then used (Clinton, 2002). For vacuum insulation panels currently the first definition is most common.

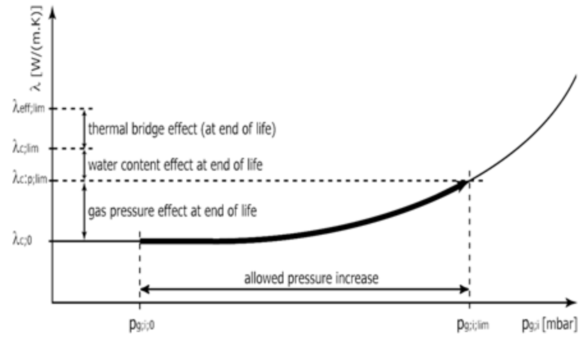

Figure 5.1

Service life definition of a vacuum insulation panel. Note: the x-axis has logarithmic scale.

INTERLUDE

As explained in the previous paragraph, the thermal conductivity of a VIP core material both depends on the pore gas pressure and the water content. Due to a pressure difference over the high barrier envelope, both the pore gas pressure and water content will increase over time. If it is now assumed that the partial water vapour pressure inside the pores (and thus the water content) reaches equilibrium with the panel surrounding air before the expiration of the service, which applies to thin VIP sizes, the criterion for a limiting value of the effective VIP thermal conductivity can be translated into a limiting value for the gas pressure. Figure 5.1 shows the thermal conductivity of a core material (fumed silica) as function of pore gas pressure. Thermal edge effects must be subtracted from the effective thermal conductivity limit, resulting in a critical value for the thermal conductivity of the core material or centre-of-panel thermal conductivity, $\lambda_{c;cr}$ or $\lambda_{cop;cr}$. By subtracting the effect of water content at the end of service life from $\lambda_{c;cr}$, we obtain a thermal conductivity criterion for the effect of pore gas pressure, $\lambda_{c;p;cr}$. This thermal conductivity criterion can now directly be related to a pore gas pressure limit and thus a maximum allowed pressure increase, as demonstrated in Figure 5.1.

years. The service life of office buildings, façade systems and building services ranges from 20 to 30 years and of residential houses from 50 to 100 years for contemporary buildings[6]. This wide range creates room for different combinations of core material, getter/desiccant and barrier. Especially for applications with a long service life (residential buildings), gas and water vapour transmission rates should be kept minimal. This implies that metal-foil based barrier laminates are advocated from this point of view, resulting however in significant thermal bridge effects. For household appliances and facades of office buildings, however, metallized polymer laminates or laminated polymer films can be used, which do not significantly have the problem of thermal shunting. It is thus important that a VIP is designed with respect to the required service life, the service conditions and thermal requirements.

[6] It is important to stress here that most common thermal insulation materials have a service life below 50 years. Normalised values in Switzerland for instance are 25 years for EPS, 30 years for mineral fibre insulation (HEV Schweiz, 2009).

5.1.2 Effects influencing the service life

The increase in thermal conductivity, or actually the increase in pore gas pressure and water content, is principally determined by the properties of the core material (1) as explained in previous paragraph, the presence of getters and desiccants (2), the initial vacuum and water content (3), degassing of the core material and the barrier laminate (4), the envelope permeance for atmospheric gases and water vapour (5), the panel's dimensions (6) and the environmental conditions, like temperature, relative humidity and partial water vapour pressure (7) (Porextherm, 2004). Since, the first five factors are product-related and can hardly be influenced by architects and building engineers, especially the last two are interesting from the perspective of construction design. These two and the gas and vapour tightness of the barrier will briefly be discussed. More information is in appendix A55.

GAS AND VAPOUR TIGHTNESS OF THE BARRIER LAMINATES AND SEAMS

The change in thermal conductivity over time, $\mathrm{d}\lambda/\mathrm{d}t$, and as a consequence the service life depends on the rate at which the gas pressure in the core, $\mathrm{d}p_{g;i}/\mathrm{d}t$, and the water content of this core, $\mathrm{d}u/\mathrm{d}t$, increase. These rates in turn depend for a large part on the permeability properties of the barrier envelope. Manufacturers specify a water vapour transmission rate (WVTR in $g \cdot m^{-2} \cdot day^{-1}$) and an oxygen transmission rate (O_2TR in cm^3 (STP)$\cdot m^{-2} \cdot day^{-1} \cdot bar^{-1}$ or cm^3 (STP)$\cdot m^{-2} \cdot day^{-1}$)[7]. These rates are defined as the amount of water vapour or oxygen respectively which comes through the laminate per unit area, per day (and per bar pressure difference)[8,9].

In general, however, permeation rates are measured for the laminate itself and not for an entire envelope around a VIP. This is the principal reason that the values for the transmission rates declared by manufacturers are not quite representative for the amount of gases and water vapour penetrating a complete barrier envelope of a vacuum insulation panel. Not only are the seals weak spots in this envelope but also the corners at which the laminate is folded. These effects must certainly be accounted for when considering the total transmission through this envelope.

[7] STP stands for standard temperature and pressure. It is important to realise that during O_2TR or WVTR measurements other gases than oxygen and water vapour respectively are not included in the measurements. Detection occurs on the molecules and not on pressure.

[8] The values stated by manufacturers must be treated with caution, because they strongly depend on the environmental conditions under which the tests have been conducted (relative humidity and temperature). Standard measurement conditions are a temperature of 23°C and a relative humidity of 90% on one side and of 0% on the other side of the laminate.

[9] These two rates, however, stand for more than water vapour and oxygen alone. The water vapour transmission rate is representative for water vapour and all polaric gases present in air, while the oxygen transmission rate represents all non-polaric gases. Often foils that have high barrier qualities against polaric gases are less optimal for non-polaric gases, vice versa.

Other reasons that the transmission rates specified by manufacturers cannot always directly be used for service life estimates are (Brunner and Simmler, 2003):

- The presence of non-linear behaviour in permeation mechanisms. Permeation rates strongly depend on relative humidity and temperature (Brunner and Simmler, 2005a). With increasing temperature or relative humidity the permeation rates for polymers increase (van 't Hoff, 1884; Arrhenius, 1889).
- The water vapour transmission rate normally is not constant during the service life of a vacuum insulated panel. Water vapour permeation is a fast process relative to gas permeation and on a long-term basis equilibrium of the internal partial water vapour pressure with the environment may be reached well within the range of standard service lives for thin vacuum insulation panels.
- On a long-term basis physical and mechanical ageing mechanisms occur as well. Polymer degradation, delaminating, corrosion, UV-radiation and mechanical stresses can have a profound influence on transmission rates.

PANEL DIMENSIONS

For the effect of panel dimensions on service life, both the thickness and the ratio of panel circumference to surface area need to be considered, since both factors influence the volume in which gases can be stored and the envelope or edge area through which gases can permeate. In general, thick and large panels have a longer expected service life than thin and small panels. So, in the design process of building constructions with vacuum insulation panels, panels need to be designed as large as possible with an aspect ratio, which is the ratio of length to width, close to one; also because of the reduction of the thermal edge effect[10].

---

[10] To discuss the effect of panel dimensions on service life in more detail, we must distinguish between the effect of water vapour and the effect of atmospheric gases. Since the permeance of high barrier films for oxygen and nitrogen is very low (in the order of $5 \cdot 10^{-4}$ $cm^3 \cdot m^{-2} \cdot day^{-1}$ for oxygen for a triple layer metallized film) (Hanita, 2004), oxygen and nitrogen permeation primarily occurs through the seam, implying that both panel thickness and the ratio of circumference to surface area are important. In case of very large panels, though, the amount of dry gas permeating through the surface of a VIP and through its seam can be in the same order of magnitude. With respect to water vapour, however, permeation through the surface area and through the seam are of equal importance for typical panel sizes due to the higher permeance for water vapour through barrier laminates (in the order of $1 \cdot 10^{-2}$ $g \cdot m^{-2} \cdot day^{-1}$ for a triple layer metallized film) (Hanita, 2004). This implies that especially for larger panels the thickness is important, while for small panels both the thickness and the panel's circumference (or ratio of circumference to surface area) are equally important.

ENVIRONMENTAL OPERATING CONDITIONS

The most important environmental conditions are the temperature and the moisture conditions directly outside the VIP.

Temperature can have several effects on a VIP, the most important of which are:

- with increasing temperature, the gas and water vapour permeability of barrier laminates and seams increases according to an Arrhenius equation;
- with increasing temperature, in general the relative humidity of air decreases because of increased vapour saturation pressure;
- with increasing temperature, the rate of degradation processes on barrier films and seams might increase as well. These degradation processes are corrosion on metal foils, polymer degradation and delaminating.

The partial water vapour pressure and relative humidity also have several effects:

- with increasing relative humidity, the permeability of barrier laminates and seams for atmospheric gas but especially for water vapour permeation increases;
- with increasing water vapour pressure, the driving potential Δp increases as well;
- with increasing moisture levels, the rate of corrosion processes on non-protected metal foils increases. This is not a linear relation.

5.2 (ADVANCED) SERVICE LIFE PREDICTION MODEL

5.2.1 Assumptions

Regarding the service life prediction model presented in the next sections, the following are assumed:

- No fluctuations in the environmental conditions (temperature, relative humidity and air pressure) around a vacuum insulation panel occur;

- Degassing effects of the barrier envelope and the core material and (de)sorption effects of getters and desiccants are not present (no production or annihilation of gas and water inside the core material).

5.2.2 *Physical model for gas pressure increase*

In the previous section, the service life of a vacuum insulation panel has been defined. This service life can be determined accurately from laboratory measurements[11]. The disadvantage of this method, however, is that these measurements have to continue for a very long time since VIPs for buildings have life spans of several decades. By increasing the test temperature the testing time can be reduced considerably. Combining the initial results[12] of gas pressure and water content increase measurements and physical models, a service life estimate can be given without doing long-lasting measurements. In this section a model to predict the gas pressure increase is introduced, while in the next section the model for water content increase is presented.

In general, the change of a property over time within a defined volume can be described with a balance equation. For pore gas pressure and for negligible production or annihilation of gas, this can be converted into

$$\frac{dm_{g;i}}{d(t-t_{get})} = \frac{\delta S}{t_f} \cdot \left(p_{g;e} - p_{g;i}\right) \qquad (5.3a),$$

in which $m_{g;i}$ [kg] is the mass of the pore gas, δ [kg·m^{-1}·s^{-1}·Pa^{-1}] is the permeability of the barrier, S [m^2] is the surface area through which permeation occurs, t_f [m] is the barrier thickness, $p_{g;i}$ [Pa] is the internal pore gas pressure, $p_{g;e}$ [Pa] is the external gas pressure, t_{get} [s] is the time shift due to a getter and t [s] is time. If the mass of the pore gas is reformulated into a gas pressure, then Equation (5.3a) changes into

$$\frac{dp_{g;i}}{d(t-t_{get})} = \frac{\delta S}{\varepsilon V t_f} \cdot \frac{RT}{M} \cdot \left(p_{g;e} - p_{g;i}\right) \qquad (5.3b),$$

with ε [-] the porosity, V [m^3] the volume, R the universal gas constant (R=8.31 J·mol^{-1}·K^{-1}), T [K] the temperature and M the mean molar mass of air (M=2.9·10^{-2} kg·mol^{-1}). This equation, however, does not consider gases permeating through the seam region of a VIP and should therefore be modified so as to incorporate this effect. For VIPs without additional getter, which is common for a VIP with a pyrogenic silica core, Schwab et al. (2005b, 2005c, 2005d) write this equation as

---

[11] More information on these experimental procedures can for instance be found in Schwab (2004) and Simmler and Brunner (2005) and Brunner and Simmler (2005a; 2008).

[12] Initial results in this respect are defined as the results obtained from gas pressure and water content increase measurements during the first year after production of the panel. During this first year, the water content and gas pressure increase rate can be considered constant.

$$\frac{dp_{g;i}}{dt} = \frac{GTR}{\varepsilon V} \cdot \frac{p_0 T}{T_0} \cdot \left(p_{g;e} - p_{g;i}\right) \quad (5.3c),$$

in which GTR [m^3(STP)·s^{-1}·Pa^{-1}][13] is the atmospheric gas transmission rate, p_0 [Pa] and T_0 [K] are the gas pressure and temperature at standard conditions.

If both GTR and $p_{g;e}$ are assumed constant and if the initial internal pressure is denoted $p_{g;i;0}$, then the following solution can be obtained for equation (5.3c)

$$p_{g;i} = p_{g;e} - (p_{g;e} - p_{g;i;0}) \cdot e^{-(t-t_{get})/\tau_g} \quad (5.4),$$

with the time constant τ_g defined as

$$\tau_g = \frac{\varepsilon V}{GTR} \cdot \frac{T_0}{p_0 T} \quad (5.5).$$

The atmospheric gas transmission rate, GTR, is an overall transmission rate including both the effects of area-related permeation and edge-related permeation. This overall transmission rate is calculated from the surface permeance, $Q_{k;g}$ [m^3(STP)·m^{-2}·s^{-1}·Pa^{-1}] and the edge permeance, $Q_{L;g}$ [m^3(STP)·m^{-1}·s^{-1}·Pa^{-1}] as

$$GTR = Q_{L;g} l_p + \sum_{k=1}^{2} Q_{k;g} S_k \quad (5.6).$$

In this equation, l_p [m] is the panel's perimeter length and S_k [m^2] is the panel's surface area at the front side (k=1) or at the back side (k=2). The different components making up the gas transmission rate can be determined from gas pressure increase measurements on real VIPs of different sizes (and under different environmental conditions) over a period of several months.

To be able to estimate the getter time shift, it is assumed that, before the maximum capacity of the getter is reached, the atmospheric gas pressure inside the core remains at low level. Then, the getter time shift is calculated as

$$t_{get} = \frac{c_{get} m_{get}}{GTR(T,\phi) \cdot \left(p_{g;e} - p_{g;i;0}\right)} \quad (5.7),$$

with c_{get} [m^3·kg^{-1}] the maximum capacity of the getter and m_{get} [kg] its mass.

---

[13] Film and foil manufacturers normally specify this transmission rate with the units cm^3·day^{-1}·bar^{-1}. The following factor should be used to this transmission rate to a value with the proper SI units: 1 m^3·s^{-1}·Pa^{-1} ≡ 87.5·10^{14} cm^3·day^{-1}·bar^{-1}.

5.2.3 Physical model for water content increase

For the water content increase a differential equation similar to equation (5.3) can be derived. Modified from Simmler and Brunner (2005), it is written as

$$\frac{du}{d(t-t_{des})}=\frac{WVTR}{\rho_{dry}V}\cdot\left(p_{wv;e}-p_{wv;i}\right) \qquad (5.8a),$$

in which u [kg·kg^{-1}] is the water content of the core, $WVTR$ [kg·s^{-1}·Pa^{-1}][14] is the water vapour transmission rate, ρ_{dry} [kg·m^3] is the dry density of the core, $p_{wv;i}$ [Pa] and $p_{wv;e}$ [Pa] are the internal and external partial water vapour pressure and t_{des} [s] is the desiccant time shift. For a constant slope of the sorption-curve of the core[15], $du/d\phi$, and for constant temperature, equation (5.8a) can be rewritten as

$$\frac{du}{d\phi}\frac{1}{p_{sat}}\frac{dp_{wv;i}}{d(t-t_{des})}=\frac{WVTR}{\rho_{dry}V}\cdot\left(p_{wv;e}-p_{wv;i}\right) \qquad (5.8b),$$

with p_{sat} [Pa] the saturation vapour pressure of air and ϕ its relative humidity. For constant $p_{wv;e}$ and with $p_{wv;i;0}$ as initial condition, the solution to this equation is

$$p_{wv;i}=p_{wv;e}-(p_{wv;e}-p_{wv;i;0})\cdot e^{-(t-t_{des})/\tau_w} \qquad (5.9),$$

in which the time constant τ_w [s] is defined as

$$\tau_w=\frac{\rho_{dry}V}{WVTR(T,\phi)}\frac{1}{p_{sat}(T)}\frac{du}{d\phi} \qquad (5.10).$$

The water vapour transmission rate is calculated from the surface permeance, $Q_{k;w}$ [kg·m^{-2}·s^{-1}·Pa^{-1}] and the edge permeance, $Q_{L;w}$ [kg·m^{-1}·s^{-1}·Pa^{-1}] as

$$WVTR(T,\phi)=Q_{L;w}(T,\phi)l_p+\sum_{k=1}^{2}Q_{k;w}(T,\phi)S_k \qquad (5.11).$$

To estimate the desiccant time shift, it is assumed that, before the maximum capacity of the desiccant is reached, the water vapour pressure and water content of the core remains equal to their initial values. Then, the desiccant time shift is calculated as

$$t_{des}=\frac{c_{des}m_{des}}{WVTR(T,\phi)\cdot\left(p_{wv;e}-p_{wv;i;0}\right)} \qquad (5.12),$$

with c_{des} [kg·kg^{-1}] the maximum capacity of the desiccant and m_{des} [kg] its mass.

---

[14] Film and foil manufacturers normally specify this transmission rate with the units g·day^{-1}·bar^{-1}. The following factor should be used to this transmission rate to a value with the proper SI units: 1 kg·s^{-1}·Pa^{-1} ≡ 87.5·10^{11} g·day^{-1}·bar^{-1}.

[15] The sorption-curve of fumed silica and glass fibre insulation is given in appendix A51.

5.2.4 *Physical model for thermal conductivity increase*

The service life of a vacuum insulation panel is defined based upon the thermal conductivity of the core material, or its effective thermal conductivity including thermal edge effects. In the previous sections, prediction models for pore gas pressure and water content as function of time have been discussed. Based upon these models, it is now possible to compute the increase of thermal conductivity with time as well. To be able to do so, the relation between thermal conductivity and pore gas pressure on the one hand and between thermal conductivity and water content on the other hand needs to be known. These relations have already been presented in form of equations (3.5) and (3.6).

Combining these equations finally results in a model to calculate the thermal conductivity of the core material if the pore gas pressure and water content are known. Based upon this combined equation, the thermal conductivity of the core material as a function of time can be plotted. Figure 5.2 a/b shows as an example of thermal conductivity increase of a SiO_2-VIP of 0.6x0.6x0.02 m^3 with a typical three layer metallised barrier envelope (MF3[16]) or an aluminium-foil based barrier laminate (AF:8) based upon data from Simmler et al. (2005).

We can now finally also compare the results from measurements by Simmler and Brunner (2005) at EMPA in Switzerland, which formed the basis for semi-empirical regression parameters in the service life approximation tools, to predictions by the service life models developed in this (and the previous) chapter. Simmler and Brunner (2005) derived from measurements an increase in thermal conductivity of a SiO_x-VIP of 0.5x0.5x0.02 m^3 with a MF3 barrier envelope of $1.58 \cdot 10^{-3}$ and $0.93 \cdot 10^{-3}$ $W \cdot m^{-1} \cdot K^{-1}$ due to gas pressure and water content increase respectively at a temperature of 23°C and a relative humidity of 50% (if the values from the tables are used). For the same panel and under the same environmental conditions, the service life prediction model presented in this chapter predicts an increase of $1.47 \cdot 10^{-3}$, $0.47 \cdot 10^{-3}$ and $1.05 \cdot 10^{-3}$ $W \cdot m^{-1} \cdot K^{-1}$ due to gas pressure, water vapour and water content increase respectively. The prediction model presented in this section thus produces somewhat higher thermal conductivity values and thus shorter service life values for this example. Although not proven here, this observation is generally valid for this prediction model.

---

[16] The designation MF3 comes from the work of Simmler et al. (2005) in which four types of metallised laminates were mentioned. The number 3 was arbitrarily chosen to distinguish among all types; it is a three layer metallised barrier envelope. It is important to note here that this same barrier film was designated MF1 in Simmler and Brunner (2005). The number 8 in designation AF:8 comes from the thickness of the aluminium foil in this laminate: 8 mm.

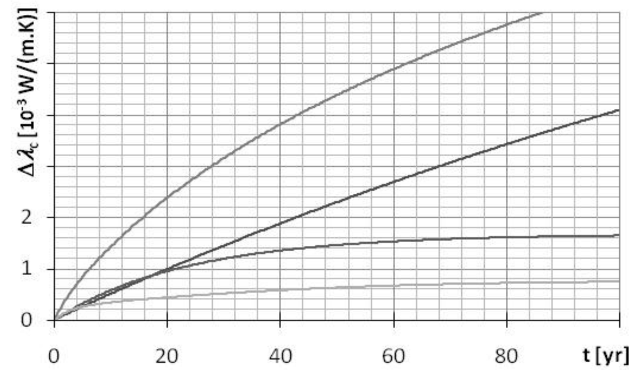

Figure 5.2a

Increase of the thermal conductivity of the core as function of time - SiO_x-VIP of 600x600x20 mm^3 with a MF3 envelope. (T=296K; RH=50%).

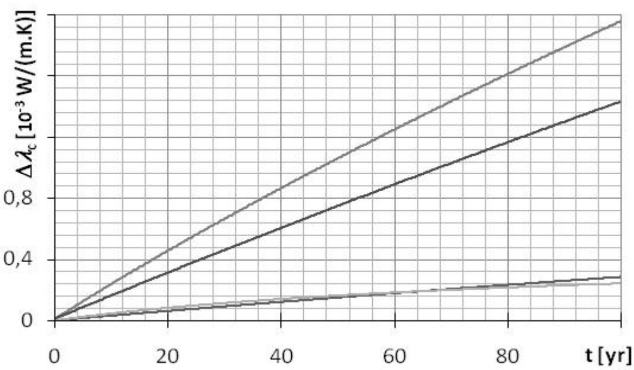

Figure 5.2b

Increase of the thermal conductivity of the core as function of time - SiO_x-VIP of 600x600x20 mm^3 with a AF:8 envelope. (T=296K; RH=50%).

5.3 Service life influencing factors

5.3.1 Assumptions

In the previous section, a service life prediction model that assumes constant boundary conditions has been introduced. In practise however these boundary conditions are not constant. Moreover, the service life of a VIP is typically ascertained from lab measurements under typical constant conditions (Simmler et al., 2005). None of these testing conditions, however, takes actual fluctuating environmental conditions in building constructions into account. A method therefore needs to be developed to incorporate these effects of environmental conditions inside building components on VIP service lives. As a consequence, in this section service-life influencing factors will be derived with which the original service-life prediction model from section 5.2 can be modified to include fluctuating boundary conditions (temperature, relative humidity and pressure).

For these service-life influencing factors the following are assumed:

- Degassing effects of the barrier envelope and the core material and (de)sorption effects of getters and desiccants are not present (no production or annihilation of gas and water inside the core material);
- Mechanical stresses inside the barrier envelope and film degradation due to chemical or physical 'attack' (adhesives, solvents, UV-radiation, etc) are not considered;
- Fluctuations in relative humidity and temperature on short time-scales (temperature and humidity cycling) do not influence the service life more significantly than fluctuations in relative humidity and temperature on large time-scales do (Brunner and Simmler, 2008);
- For the service-life influencing factor incorporating the effects of both temperature and relative humidity, it is assumed that these effects are statistically independent of each other. Since however temperature, relative humidity and partial water vapour pressure are related, a small and acceptable error is introduced by this assumption;
- Using the modified service life prediction models, it is not allowed to study the increase of gas pressure and water content in detail on short time-scales since fluctuations in environmental service conditions are averaged by introducing annual average partial service life influencing factors.

5.3.2 Overall service life factor

To characterise the service life of a vacuum insulation panel, the actual service life will be normalised by introducing an overall service life factor, f_{sl}, defined as

$$f_{sl} = \frac{t_{sl}}{t_{lab}} \qquad (5.13),$$

with t_{lab} [years] the service life of a panel measured experimentally under laboratory conditions determined by a reference temperature, T_0 [K], reference water vapour pressure, $p_{v;0}$ [mbar] and reference atmospheric pressure, $p_{g;0}$ [mbar] and t_{SL} [years] the actual service life of the vacuum insulation panel or VIP integrated building component calculated using modified service-life prediction models. The service-life prediction models presented in section 5.2 are modified so as to incorporate service conditions deviating from laboratory conditions. In section 5.2, we distinguished explicitly between gas pressure and water content increase. This distinction must also be upheld if the effect of temperature on the permeation rates, the effect of relative humidity on the permeation rate and the effect of external pressure on the permeation driving-force are introduced into the service life prediction models[17].

The water content increase rate, du/dt [kg·kg^{-1}·s^{-1}] and consequently the water vapour pressure increase rate, dp_{wv}/dt [mbar·s^{-1}], is influenced in three ways. First, the water vapour transmission rate, *WVTR** [g·day^{-1}·bar^{-1}], is influenced by the relative humidity (or actually the water activity) inside this envelope. In general, the water vapour transmission rate of laminates increases with increasing relative humidity, at least up till about 80%. This is known for pure polymeric laminates and will be discussed in detail later (subsection 5.3.6). Second, since a water vapour pressure difference is the driving force behind water vapour permeation, changing this potential influences the water content increase rate. Third, the water vapour transmission rate is also affected by the temperature of the laminate, according to a well-established Arrhenius equation (van 't Hoff, 1884; Arrhenius, 1889).

The gas pressure increase rate[18], dp_g/dt [mbar·s^{-1}], is also influenced in three ways[19]. First, the gas transmission rate, *GTR* [cm^3·day^{-1}], is influenced by the relative humidity (or actually the water activity) inside this envelope. In general, the gas transmission rate of high barrier films increases with increasing relative humidity, at least up till about 75% to 80%. Second, since a gas pressure difference is the driving force behind atmospheric gas permeation, changing this pressure difference influences the gas pressure increase rate. Third, the gas transmission rate is also affected by the temperature of the laminate, according to the aforementioned Arrhenius equation. This latter effect is the strongest of these influences.

[17] For all effects it is assumed that safety limits are not exceeded during the service life. Since, if such limits are exceeded, immediate failure is imminent. For example, if the stresses in the metal or metallized layer of the envelope due to whatever cause increase to beyond its strength, (micro)cracks will occur in this layer resulting in a significant increase in gas and water vapour permeation rate. Rapid pressure equalization will result in a defective product.

[18] The total gas pressure inside the pores of the core is the sum of all separate gas components, including water vapour. With gas pressure in this dissertation primarily dry gases are meant unless otherwise specified. It thus incorporates all atmospheric gases except water vapour.

[19] Two additional factors influencing both the water vapour and gas transmission rate must be mentioned as well: mechanical stresses in the barrier envelope and temperature and humidity cycling. The precise effect of mechanical stresses in the envelope on water vapour and gas transmission rates is still unknown. For the effect of temperature and humidity cycling, a similar lack of knowledge exists. Investigations at EMPA in Switzerland did show that a cycle in which a specimen was subjected to a relative humidity of 80% at 80^{o}C for 8 hours subsequently and consecutively followed by a relative humidity of 50% at 23^{o}C resulted in a gas pressure increase rate a factor of 1.5 higher than under constant 80% RH and 80^{o}C conditions (Simmler et al., 2005). It remains however unclear whether this high increase rate is caused by 'condensation' of water vapour directly after cooling the specimen or by thermal stresses and relaxation phenomena. Since generating knowledge on these effects would require a thorough study beyond the objectives of this thesis and since no absolute but relative service life estimates are pursued, both effects will be neglected in the estimations.

Based upon the previous discussion, four separate partial service-life influencing factors can be defined, which will be discussed more thoroughly in the next paragraphs:

- $f_{w;T+\phi}$ the factor incorporating the effect of temperature and relative humidity on the water vapour transmission
- $f_{w;p}$ the annual average relative load due to water vapour
- $f_{g;T+\phi}$ the factor incorporating the effect of temperature and relative humidity on the atmospheric gas transmission[20]
- $f_{g;p}$ the annual average relative load due to atmospheric gases.

It is important to realise that the factors defined above are annual average factors thus involving a time-integral.

Since the effects of temperature and relative humidity influence the water vapour and atmospheric gas transmission rates, they also influence the rate of gas pressure and water content increase. External atmospheric gas pressure and external partial water vapour pressure, however, influence the driving-force behind the permeation processes, as a result of which they in addition influence the final level of pore gas pressure and water content of the core material. For the internal pore gas pressure, the service life prediction model can therefore be modified as[21]

$$p_{g;i} = f_{g;p} \cdot p_{g;e;lab} - (f_{g;p} \cdot p_{g;e;lab} - p_{g;i;0}) \cdot e^{-f_{g;T+\phi} \cdot \frac{t-t_{get}}{\tau_g}} \quad (5.14).$$

For the internal pore water vapour pressure (and thus the water content) similar considerations apply, resulting in the following modified service life prediction model:

$$p_{wv;i} = f_{w;p} \cdot p_{wv;e;lab} - (f_{w;p} \cdot p_{wv;e;lab} - p_{wv;i;0}) \cdot e^{-f_{w;T+\phi} \cdot \frac{t-t_{des}}{\tau_w}} \quad (5.15).$$

---

[20] For reasons of simplicity, the effects of temperature and relative humidity on the transmission rate of water vapour or dry gas are combined into one factor for each type of transmission being aware of possible different behaviour. Both affect the rate at which gas pressure and water content increase, contrary to the effect of external gas pressure or external partial water vapour pressure which affects the final pore gas and water content level.

[21] Modifying the original service life prediction model for constant boundary conditions in this way is allowed since the time constant τ_g (and τ_w) is much larger (in the order of 25 to 75 years for τ_w (Schwab, 2005c; Simmler and Brunner, 2005) and much larger for τ_g because of low GTR-values) than the timescale used to determine the service-life influencing factors (one year). In the interlude an example in which the partial water vapour pressure is the only fluctuating condition is shown.

Imagine as a hypothetical situation that a vacuum insulation panel is subjected to a constant temperature, a constant relative humidity and fluctuating partial water vapour pressure (notice that this is not a realistic case since physics states that the partial water vapour pressure cannot fluctuate if both the temperature and relative humidity are constant). The actual external partial water vapour pressure is assumed to fluctuate according to

$$p_{w;e} = \overline{p}_{w;e} + \hat{p}_{w;e} \cos(\omega t) \qquad \text{(A).}$$

The actual partial water vapour pressure inside the pores of the core material can now be calculated using differential equation (5.8b) combined with equation (A) above. The partial water vapour pressure inside the pores of the core material under constant laboratory conditions can be calculated from equation (5.9) with $p_{w;e} = p_{w;e;lab}$. The partial water vapour pressure inside the pores can also be estimated from equation (5.15) with $f_{w;T+\phi} = 1$ and $f_{w;p}$ determined from equation (5.16a). Figure (5.3) presents these three different internal pore water vapour pressure computations for a vacuum insulation panel of 0.6x1.0x0.02 m^2 with a typical three-layer metallized high barrier envelope (τ_w = 40 years). The following input parameters have been used: $\omega = 2\pi$ rad·year^{-1}; $p_{w;i;o}$ = 10 Pa; $p_{w;e;lab}$ = 1440 Pa; $\overline{p}_{w;e}$ = 2304 Pa; $\hat{p}_{w;e}$ = 576 Pa. As can be seen, the modified service-life model predicts the gas pressure increase on large timescales quite well, but does not take into account small timescale fluctuations.

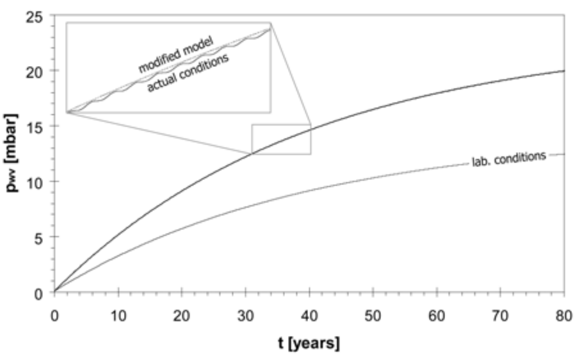

Figure 5.3

Internal pore water vapour pressure as function of time according to three different models or conditions. The panel and boundary conditions are specified in the text of this interlude.

INTERLUDE

Based upon equations (3.5), (3.6), (5.14) and (5.15) and a service life criterion, it is now possible to estimate the actual service life of a vacuum insulation panel (or VIP integrated building component), t_{sl} and to compute the overall service life influencing factor, f_{sl}. Still remaining is the question how to determine the previously defined partial influencing factors, $f_{w;T+\phi}$, $f_{w;p}$, $f_{g;T+\phi}$ and $f_{g;p}$. They will be defined in the next sections.

5.3.3 *Partial service-life influencing factors*

As previously mentioned, the partial service life influencing factors still need to be defined. Each factor is defined as an annual average value of the instantaneous effect, which can be described mathematically for the gas-related factors as

$$f_{g;p} = \frac{1}{t_2 - t_1} \int_{t_1}^{t_2} a_{g;p}(t) dt \quad (5.16a),$$

and as

$$f_{g;T+\phi} = \frac{1}{t_2 - t_1} \int_{t_1}^{t_2} a_{g;T}(t) \cdot a_{g;\phi}(t) dt \quad (5.16b),$$

in which $a_{g;i}$(t) is some function of either T, p_g or ϕ. Contrary to the service-life influencing factor, this variable is named a service-life influencing function. The time difference $t_2 - t_1$ [h] represents a period of one year. For calculation purposes it is often easier to discretise this year into small time intervals Δt_i and calculate the annual average service life factor as

$$f_{g;p} = \frac{1}{t_n - t_1} \sum_{j=1}^{n} a_{g;p}(t_j) \cdot \Delta t_j \quad (5.17a),$$

and as

$$f_{g;T+\phi} = \frac{1}{t_n - t_1} \sum_{j=1}^{n} a_{g;T}(t_j) \cdot a_{g;\phi}(t_j) \cdot \Delta t_j \quad (5.17b).$$

For the partial factors incorporating the environmental effects on water content increase, similar equations are valid. In the next subsections the functions $a_{g;i}$(t) and $a_{w;i}$(t) are discussed in more detail.

5.3.4 *Partial service-life influencing function: temperature effect*

Since the diffusion coefficient of a gas or of water vapour through or in a polymer follows the Arrhenius law, and since the permeation coefficient equals the product of the diffusion and solubility coefficient, the effect of temperature on envelope permeance, Q [m^3(STP)·m^{-2}·s^{-1}·Pa^{-1} for gas or kg·m^{-2}·s^{-1}·Pa^{-1} for water vapour], can be formulated according to such a law as well (Arrhenius, 1889; Simmler et al., 2005; Simmler and Brunner, 2005):

$$Q = Q_0 \cdot e^{-\frac{E_a}{R}\left(\frac{1}{T} - \frac{1}{T_0}\right)} \quad (5.18),$$

with Q_0 the permeance at temperature T_0, E_a [J·mol^{-1}] an activation energy for permeation (Table 5.1), R [J·mol^{-1}·K^{-1}] the universal gas constant, T [K] the absolute temperature and T_0 [K] a reference laboratory temperature.

Since the effect of temperature on gas permeance at a certain instant in time equals the permeance at that certain instant divided by the reference laboratory permeance, the instantaneous temperature induced service life factor equals this same ratio. With the temperature, T, as a function of time, the temperature induced service life function then becomes

$$a_{g;T} = e^{-\frac{E_{a;g}}{R}\left(\frac{1}{T(t)}-\frac{1}{T_0}\right)} \tag{5.19a}$$

However, equation (5.19a) only applies, if the environmental conditions around a vacuum insulation panel are equal in each point, i.e. no temperature gradients exist alongside the panel. If, however, these gradients do exist, equation (5.19a) needs to be modified so as to incorporate temperature differences alongside the surface and around the perimeter of this panel, resulting in the following general equation for the temperature induced service life function for atmospheric gases

$$a_{g;T} \approx \frac{1}{GTR_o}\left[Q_{L;0;g}\, l_p e^{-\frac{E_{a;L;g}}{R}\left(\frac{1}{T_L(t)}-\frac{1}{T_0}\right)} + \sum_{k=1}^{2} Q_{k;0;g} S_k e^{-\frac{E_{a;k;g}}{R}\left(\frac{1}{T_k(t)}-\frac{1}{T_0}\right)}\right] \tag{5.19b}$$

The first term between the brackets in this equation represents gas permeation through the seam and edge of a panel (subscript L). The edge permeance, $Q_{L;0;g}$ in this term is a length-related permeance and is therefore multiplied with the panel perimeter length, l_p, to obtain a transmission rate. The second term between the brackets in this equation represents gas permeation through the front and backside of a panel (k=1 or 2 respectively). The corresponding laminate permeances, $Q_{k;0;g}$ are area-related and thus multiplied with the surface area, S_k. GTR_0 finally is the gas transmission rate [m^3(STP)· s^{-1}·Pa^{-1}] under laboratory conditions:

$$GTR_0 = Q_{L;0;g}\, l_p + \sum_{k=1}^{2} Q_{k;0;g} S_k \tag{5.20}$$

For the temperature induced service life function for water vapour transmission an equation more-or-less identical to equation (5.19b) can be derived. This analysis yields

$$a_{w;T} \approx \frac{1}{WVTR_o}\left[Q_{L;0;w} l_p e^{-\frac{E_{a;L;w}}{R}\left(\frac{1}{T_L(t)}-\frac{1}{T_0}\right)} + \sum_{k=1}^{2} Q_{k;0;w} S_k e^{-\frac{E_{a;k;w}}{R}\left(\frac{1}{T_k(t)}-\frac{1}{T_0}\right)}\right] \quad (5.21),$$

with $WVTR_0$ [g·day^{-1}] the reference laboratory water vapour transmission rate determined by

$$WVTR_0 = Q_{L;0;w} l_p + \sum_{k=1}^{2} Q_{k;0;w} S_k \quad (5.22).$$

The values for $Q_{L;0;w}$, $Q_{k,0,w}$, $Q_{L;0;g}$ and $Q_{k,0,g}$ are derived from the IEA Annex 39 report (Simmler et al., 2005) and tabulated in Table 5.1b.

A final remark on the activation energies for permeation is still required. In practise, barrier envelopes for VIPs are multilayered laminates consisting of both organic and inorganic layers. Permeation through polymers in general can be described by the solution-diffusion theory, while permeation through metallic and metallisation layers mainly occurs through microscopic defects, or so-called pinholes (langowski,

Table 5.1a *- Typical values for the activation energy of metallized films and aluminium based foils for dry-gas and water vapour transmission.*

	MF3	MF4	AF:8
$E_{a;k;g}$ [kJ·mol^{-1}]	50 ± 2 [a,d]	47 ± 3 [b,d]	26 ± 2 [b,d]
$E_{a;L;g}$ [kJ·mol^{-1}]	50 ± 2 [a,d]	47 ± 3 [b,d]	26 ± 2 [b,d]
$E_{a;k;w}$ [kJ·mol^{-1}]	n/a	n/a	n/a
$E_{a;L;w}$ [kJ·mol^{-1}]	49.5 ± .. [c]	49.5 ± .. [c]	49.5 ± .. [c]

[a] Simmler and Brunner, 2005; [b] Schwab et al., 2005b; [c] Rowe et al., 2009.

[d] These values were determined for ATR_{total} (Air Transmission Rate – transmission rate in which all atmospheric gases are included). They were thus determined including both the permeation through the surfaces and the seams of the VIP. Due to lack of data it is not possible to separate both area and edge related effects for the activation energies. These values are therefore inserted for both $E_{a;k;g}$ and $E_{a;L;g}$.

NB: Subscript *k* relates to the surface area of a VIP, *L* to the perimeter or seam of the VIP; *g* relates to atmospheric gases while *w* relates to water vapour.

NB: Since permeation of gases and water vapour through the seam principally occurs through the HDPE sealant layer, it is assumed that activation energies of HDPE apply to the seam.

Table 5.1b *- Values for the area and length related reference permeances for two metallized high barrier films at 23⁰C and 50% relative humidity and an 8 μm thick aluminium foil at 25°C and 45% relative humidity, recalculated from Simmler et al. (2005).*

	MF3	MF4	AF:8
$Q_{k;0;g}$ [$m^3(STP)\cdot m^{-2}\cdot s^{-1}\cdot Pa^{-1}$][a]	$3.9\cdot 10^{-19}$	$9.9\cdot 10^{-19}$	0
$Q_{L;0;g}$ [$m^3(STP)\cdot m^{-1}\cdot s^{-1}\cdot Pa^{-1}$][a]	$1.0\cdot 10^{-18}$	$2.1\cdot 10^{-19}$	$3.3\cdot 10^{-19}$
$Q_{k;0;w}$ [$kg\cdot m^{-2}\cdot s^{-1}\cdot Pa^{-1}$][b,c]	$2.7\cdot 10^{-14}$	$4.3\cdot 10^{-14}$	$1.7\cdot 10^{-15}$
$Q_{L;0;w}$ [$kg\cdot m^{-1}\cdot s^{-1}\cdot Pa^{-1}$][b,c]	$7.2\cdot 10^{-15}$	$5.4\cdot 10^{-15}$	$1.5\cdot 10^{-16}$

[a] The values for $Q_{k;0;g}$ and $Q_{L;0;g}$ can easily be computed from Simmler et al. (2005) by using a conversion factor for recalculating to the units from the table: $m^3(STP)\cdot m^{-2}\cdot s^{-1}\cdot Pa^{-1} = 1/1\cdot 10^6/24/3600/1.013\cdot 10^5\ cm^3\cdot m^{-2}\cdot dag^{-1} = 1.14\cdot 10^{-16}\ cm^3\cdot m^{-2}\cdot dag^{-1}$.

[b] For the recalculation of the $Q_{k;0;w}$ and $Q_{L;0;w}$ values, the relative humidity inside the core material is assumed to be 4%, which value is considered to be the production limit for VIPs.

[c] The values for $Q_{k;0;w}$ and $Q_{L;0;w}$ can be computed in a similar way as in table footnote a: $kg\cdot m^{-2}\cdot s^{-1}\cdot Pa^{-1} = 1/1\cdot 10^3/24/3600/\Delta p_{wv}\ g\cdot m^{-2}\cdot dag^{-1} = 1.16\cdot 10^{-8}/\Delta p_{wv}\ g\cdot m^{-2}\cdot dag^{-1}$. An additional difficulty here consists in determining the pressure difference over the laminate. This can easily be computed from the external relative humidity and partial saturation pressure of water vapour in air at the respective temperature and the production limit of the relative humidity inside the VIP (table footnote b) and the aforementioned saturation pressure.

2005)[22]. The activation energy for dry-gas permeation through the surface of several multilayered barrier envelopes has been measured by Simmler et al. (2005) and Schwab (2004). These values are presented in Table 5.1a. These values were determined for the total gas transmission rate through both the surface and the seam of a VIP. Due to lack of data it is not possible to separate both area and edge related effects for the activation energies. The measured values are therefore inserted for both $E_{a;k;g}$ and $E_{a;L;g}$. Concerning water vapour permeation through the seams of the VIP envelope, finally, permeation mainly occurs through the sealant layer of the laminate. This sealant layer almost always consists of either HDPE of LDPE. Activation energies for water vapour permeation through this material are added to Table 5.1a (Rowe et al., 2009).

[22] According to Langowski (2005; referring to Hanika (2004)), the permeance of a polymer barrier film with a thin vacuum coated inorganic layer remains constant with in creasing substrate thickness beyond a certain critical substrate thickness. He concludes that for a typical PET layer with 35 nm aluminium metallisation this critical thickness is less than 4 μm. As a result, in case of a 12 μm thick PET layer, the permeance of this barrier is primarily determined by the number of defects per unit area and their size distribution (Miesbauer et al., 2008). However, the influence of temperature on this process is hardly known.

5.3.5 *Partial service-life influencing function: external pressure effect*

Since permeation processes are driven by a partial pressure (or concentration) gradient, fluctuations in this driving force may change the rate at which gases enter the core material. The relative load due to atmospheric pressure (function) can therefore be written as

$$a_{g;p} = \frac{p_{g;e}(t) - p_{g;i}(t)}{p_{g;e;0} - p_{g;i;0}} \approx \frac{p_{g;e}(t)}{p_{g;e;0}} \approx 1 \qquad (5.23),$$

with $p_{g;e}$ [mbar] the exterior atmospheric pressure (outside the VIP), $p_{g;e;0}$ [mbar] the reference (laboratory) exterior atmospheric pressure, $p_{g;i}$ [mbar] the interior gas pressure (inside the VIP) and $p_{g;i;0}$ [mbar] the reference (laboratory) internal gas pressure. It is assumed that $p_{g;i;0} << p_{g;e;0}$ and $p_{g;i}(t) << p_{g;e}(t)$.

Equation (5.23) is also solely applicable if the atmospheric pressure of the air surrounding the VIP does not vary across the entire surface of the vacuum insulation panel. If it is assumed that the atmospheric pressure is a constant at the front, the back and the edges of a panel, equation (5.23) must be modified to compensate for these differences in pressure as

$$a_{g;p} \approx \frac{1}{S_{tot}} \sum_{k=1}^{3} \frac{p_{g;e;k}(t)}{p_{g;e;0}} \cdot S_k \qquad (5.24).$$

With regard to the load function due to water vapour, the instantaneous relative load due to water vapour must be defined. This relative load is specified as

$$a_{w;p} = \frac{p_{w;e}(t) - p_{w;i;0}(t)}{p_{w;e;0} - p_{w;i;0}} \qquad (5.25).$$

Similarly as with atmospheric gas pressure, this equation needs to be modified to include differences in water vapour along the panel surface, resulting in

$$a_{w;p} \approx \frac{1}{S_{tot}} \sum_{k=1}^{3} \frac{p_{w;e;k} - p_{w;i;0}}{p_{w;e;0} - p_{w;i;0}} S_k \qquad (5.26).$$

5.3.6 *Partial service-life influencing function: relative humidity effect*

To be able to indicate the service life of a vacuum insulation panel based upon service life influencing factors, it is important to know the dependency of atmospheric gas and water vapour permeation on relative humidity. According to Kundu and Choe (2003) four basic mechanisms of transport of gaseous molecules through thin films can be distinguished: viscous flow (Poiseuille flow), Knudsen flow/diffusion, molecular sieving (surface diffusion) and solution diffusion (Fickian diffusion). The type of mechanism that dominates the diffusion process mainly depends on the mean free path of the diffusing gas molecules, *mfp* [m], and the (average) pore diameter/void size, δ. For large pore sizes relative to the mean free path of the diffusing molecules, Knudsen diffusion or even Poiseuille flow predominates, while for small pore sizes relative to the mean free path of the diffusing molecules, Fickian diffusion is the dominant contributor to gas transport (Kundu and Choe, 2003; Hale et al., 2001). According to Hale et al. (2001) the predominating diffusion process of water vapour through PE films is Fickian. It can be expected that this same mechanism is the most important for water vapour diffusion through PET films. For metallized films however the diffusion process through the metallization layers must be considered as well. Diffusion through those layers is mainly through pinholes and other microscopic defects in this layer (Thorsell, 2006, Langowski, 2005, Miesbauer et al., 2008).

In general under isothermal conditions, the water vapour transmission or gas transmission rate through many materials as function of relative humidity can be described as (Galbraith and Mclean, 1990; Galbraith et al., 1998; Burch et al., 2002)[23]

$$TR = k_1 + k_2 e^{k_3 \phi} \qquad (5.27)^{24},$$

in which k_1, k_2 and k_3 are experimental parameters and ϕ [-] is the relative humidity, or actually the water activity inside the pores of the polymer. To determine the parameters k_1, k_2 and k_3 for VIP barrier films with sufficient accuracy, experimental

[23] Galbraith et al (1998) also propose a different model (power law model), which even more accurately describes the effect of relative humidity on water vapour transmission for many building materials. In this dissertation however the exponential function is adopted for its simplicity. Moreover, Guevara-Arauza et al. (2006) suggest using the water vapour pressure deficit (VPD) instead of using the relative humidity since VPD also includes the effect of temperature. In their equation the effect of temperature and relative humidity are combined into one equation. Since in this dissertation the effect of temperature is separated from the effect of relative humidity, RH and not VPD is used in the equations. In general, a diffusion coefficient decreases with increasing relative humidity. Due to capillary condensed water at higher relative humidity values, the number of paths (continuous pore systems) through which vapour can diffuse decreases as a result increasing the tortuosity. Vapour diffusion coefficients that do exhibit this increase do not only include water vapour transport but also liquid water transport. Since however the solution coefficient does increase with increasing relative humidity and since the permeation coefficient is the product of the diffusion and solution coefficient, the permeation coefficient may also increase with increasing RH.

[24] This equation can be split into the length-related transmission rate through the panel seam and the area-related transmission rate through the panel surfaces as

$$TR = k_1 + S \cdot k_{2S} e^{k_{3S} \cdot \phi} + l_p k_{2L} e^{k_{3L} \cdot \phi}.$$

It is important to consider that by doing this the units of the regression parameters change.

data are required. It must be noted that these parameters may be different depending on the type of gas that is permeating through the film, thus resulting in a distinction between parameters for dry gas and water vapour permeation. Since temperature and relative humidity are assumed to be independent influences, the regression parameter k_3 is a constant independent of temperature[25]. The parameters k_1 and k_2 however do depend on temperature according to Arrhenius's equation.

Despond et al. (2001) report that, for the permeation of oxygen and carbon dioxide through Chitosan films, the increase in gas permeance or gas transmission rate can be explained by an increase in sorption of the permeant in water. An increase in the amount of water in the material pores thus increases the amount of atmospheric gas that can be solved in the film layer. Zhang et al. (2001) explain in the introduction to their paper on the permeation of oxygen and water vapour through EVOH films that hydrophobic polymers like PE and PET do not exhibit an increase in permeation coefficient for increasing water activity because these polymers lack the capacity to absorb enough water to plasticize these polymers. Such a dependency of both the gas and water vapour transmission rate for metallised barrier laminates was however found by Simmler et al. (2005); with increasing relative humidity GTR but especially WVTR increases[26].

Due to lack of experimental data at the moment of writing this dissertation and since it is outside the scope and possibilities of this thesis to do extensive hygrothermal laboratory experiments, no equations and regression parameters for these equations are determined to model the effect of relative humidity on water vapour and dry gas permeation through barrier films. This relative humidity effect is therefore neglected in all service life calculations in this dissertation, except for the influence of relative humidity on the water vapour pressure difference across the barrier envelope as driving-potential for water vapour permeation. The service life influencing function for the effect of RH on the barrier properties is shown below just as an example if Equation (5.27) split for edge and surface-related effects were used:

[25] Zhang et al. (2001) and Marais et al. (2002) showed that the effects of relative humidity and temperature cannot be considered completely independent for permeation of gases and water vapour through EVOH and EVA copolymer films.

[26] For many polymers above 80% RH a decrease of transmission rate with increasing RH is discernible. Zhang et al. (2001), e.g., found this behaviour for the permeation of oxygen through EVOH films. According to Marais et al. (2002), this decrease in transmission rate with increasing RH can be ascribed to the clustering of water molecules inside the pores increasing the permeant size (negative plasticization effect in non-polar polymers). They also present an equation that describes their results quite well. Due to lack of experimental data, it is however questionable if this equation may be used for VIP metallised laminates as well. Moreover, this model does not accurately predict the behaviour found by Zhang et al. (2001) above 77% RH.

$$a_{g;\phi} \approx \frac{1}{GTR_0^*}\left[k_{1;g} + l_p k_{2L;g} e^{k_{3L;g}\cdot\phi_{iL}} + \sum_{k=1}^{2} S_k k_{2S;g} e^{k_{3S;g}\cdot\phi_{ik}}\right] \quad (5.28a),$$

$$a_{w;\phi} \approx \frac{1}{WVTR_0^*}\left[k_{1;w} + l_p k_{2L;w} e^{k_{3L;w}\cdot\phi_{iL}} + \sum_{k=1}^{2} S_k k_{2S;w} e^{k_{3S;w}\cdot\phi_{ik}}\right] \quad (5.28b).$$

In these equations, $WVTR_0^*$ [kg·s^{-1}·Pa^{-1}] and GTR_0^* [m^3·s^{-1}·Pa^{-1}] are a reference rates determined under lab conditions using ϕ_0 [-] as a reference laboratory RH and

$$GTR_0^* = k_{1;g} + l_p k_{2L;g} e^{k_{3L;g}\cdot\phi_0} + \sum_{k=1}^{2} S_k k_{2S;g} e^{k_{3S;g}\cdot\phi_0} \quad (5.29a),$$

$$WVTR_0^* = k_{1;w} + l_p k_{2L;w} e^{k_{3L;w}\cdot\phi_0} + \sum_{k=1}^{2} S_k k_{2S;w} e^{k_{3S;w}\cdot\phi_0} \quad (5.29b).$$

INTERLUDE

The regression parameters k_1, k_2 and k_3 can be obtained from pressure and water content increase measurements on actual VIPs. If even measurements on different panel sizes under different conditions are available, k_2 and k_3 can be split into edge-related and area-related regression parameters.

The following four steps can be used to determine the regression parameters for the gas transmission rate. First, the measured pressure and water content increase rates need to be recalculated using Arrhenius's equation with the proper values for activation energy and reference temperature so that all values are at the same temperature. This is needed to exclude temperature effects from the computations. Since it is assumed that the effects of both the relative humidity and the temperature are independent, this recalculation is allowed. Second, the water content increase rate needs to be converted into a pressure increase rate using the sorption-curve. Third, since the total gas pressure inside the pores of the core equals the sum of the pore gas pressure due to atmospheric gases and water vapour, the atmospheric gas pressure increase rate can now be separated from the total gas pressure increase rate. Fourth, since the atmospheric pressure difference across the laminate is generally constant during measurements, equation 5.3c should be used to compute *GTR*. These *GTR* values can finally be fitted to

$$TR = k_1 + S \cdot k_{2S} e^{k_{3S}\cdot\phi} + l_p k_{2L} e^{k_{3L}\cdot\phi} \quad (a),$$

for several panel sizes using a multi-curve fit, resulting in values for k_1, k_{2S}, k_{2L}, k_{3S} and k_{3L}.

To determine the parameters for the water vapour transmission rate, *WVTR*, a slightly different approach of four steps is needed. First, the water content increase rate needs to be plotted versus the partial water vapour pressure difference across the laminate for the different measurement conditions. A curve then needs to be fitted through the data points, from which the derivative can be determined. This derivative is necessary since both the WVTR and the partial water vapour pressure difference across the barrier laminate influence the water vapour pressure increase rate. Second, using this derivative, the water vapour transmission rate can now be determined from

$$WVTR = \frac{d(du/dt)}{d\Delta p_w}\rho_{dry}V \quad (b).$$

Third, the *WVTR* values are corrected for temperature influences by recalculating all of them to 23^{o}C using the Arrhenius equation with the proper values for the activation energy. These corrected *WVTR* values can in the last step finally be fitted to equation (a).

5.4 APPROXIMATION MODEL FOR SERVICE LIFE PREDICTION

5.4.1 Introduction

Simmler et al. (2005), Simmler and Brunner (2005), Schwab (2004) and Schwab et al. (2005a, b and c) showed how to estimate service lives based upon the method described in section 5.2 by determining the thermal conductivity as function of time. The determination of the service life using these equations is accurate, as far as the measurements are accurate, but requires an iterative procedure. This section therefore derives simplified closed analytical equations to determine the service life directly from input values.

Based upon these new models, it is possible to estimate the service life without first calculating and plotting the thermal conductivity of the core as a function of time. Depending on the type of equation, several semi-experimental parameters need to be determined from laboratory measurements on VIPs for different barrier envelope and core combinations. In this chapter, these semi-experimental parameters for VIP combinations of a metallised and an aluminium-based barrier envelope and a core of fumed silica, XPS foam and glass fibre insulation are determined. It is shown that the difference between this simplified analytical model and the more advanced iterative model is less than approximately 9% for a thermal conductivity criterion of $8 \cdot 10^{-3}$ $W \cdot m^{-1} \cdot K^{-1}$ or higher. Moreover, it is shown how thermal edge effects can be considered when determining the service life.

These models then allow rapid estimation of the service life of a VIP or of a VIP integrated building component if average environmental conditions are known or specified and explicate to what extent certain parameters influence the service life of a vacuum insulation panel.

5.4.2 Assumptions

Based upon the physical models described in the previous sections, an approximating model for estimating the service life of a vacuum insulation panel under constant climatic conditions can be developed. This approximating model allows a rapid estimation of the service life, solely using the panel dimensions, the temperature, the relative humidity, some properties of the barrier envelope and three regression parameters.

For this approximating model the following are assumed:

- The sorption-isotherm of the VIP core material is linear in the range 0% < ϕ < X%, with X% the relative humidity (or actually the water activity) of the core material at the end of the panel service life. For fumed silica the slope of the sorption-isotherm can be approximated as $du/d\phi$ = (7.1 ± 0.5) $\cdot 10^{-2}$ $kg \cdot kg^{-1}$ up till approximately 80% relative humidity. For glass fibre insulation (and PU-foam), this slope can be approximated as $du/d\phi = 1.3 \cdot 10^{-2}$ $kg \cdot kg^{-1}$ (and as $du/d\phi$ = 0 $kg \cdot kg^{-1}$) up till approximately 95% relative humidity. More information in Appendix A51.

- The curve representing the gaseous thermal conductivity of the core material, λ_g, as a function of the pore gas pressure, p_g, is linear in the range 0 mbar < p_g < Y mbar, with Y mbar the pore gas pressure inside the core material at the end of the panel service life. Up to a pore gas pressure of approximately 100 mbar, the slope of this (λ_g,p_g)-curve of fumed silica can be approximated as $\partial \lambda_c / \partial p_g$ = (3.5 ± 0.7)$\cdot 10^{-7}$ $W \cdot m^{-1} \cdot K^{-1} \cdot Pa^{-1}$. (Simmler et al., 2005; Simmler and Brunner, 2005; Schwab et al., 2005a; Schwab et al., 2005c). Up to a pressure of 0.3 mbar the slope of the (λ_g,p_g)-curve of Elastogran polyurethane foam can be approximated as $\partial \lambda_c / \partial p_g$ = (1.2 ± 0.1)$\cdot 10^{-4}$ $W \cdot m^{-1} \cdot K^{-1} \cdot Pa^{-1}$ (Elastogran, 2005). Up to a pressure of 1 mbar the slope of the (λ_g,p_g)-curve of glass fibre board can be approximated as $\partial \lambda_c / \partial p_g$ = (5.1 ± 0.9)$\cdot 10^{-5}$ $W \cdot m^{-1} \cdot K^{-1} \cdot Pa^{-1}$ (Simmler et al., 2005).

- The thermal conductivity of the core material is linearly dependent on the water content, u. Schwab et al. (2004) found for fumed silica that $\partial \lambda_c / \partial u$ = $2.9 \cdot 10^{-2}$ $W \cdot m^{-1} \cdot K^{-1}$ up till about 5 mass%. Up to a volumetric water content of approximately 0.1 vol%, the thermal conductivity of glass fibre insulation does not depend on water content (Hokoi and Kumaran, 1993), so $\partial \lambda_c / \partial u$ = 0 $W \cdot m^{-1} \cdot K^{-1}$. Since for polyurethane foam board it is assumed that $du/d\phi$ = 0, $\partial \lambda_c / \partial u$ is not relevant.

- Since the pore gas pressure and water content at the end of service life are much higher than at the beginning, the initial pore gas pressure and water content of the core can be neglected in case of fumed silica as core material.

- The service life is defined according to definition 1 (section 5.1.1).

- Getters and desiccants have a certain specified capacity. Before this capacity is reached, the atmospheric gas pressure, partial water vapour pressure and water content of the core are equal to their initial values.

- The relative humidity has no effect on the water vapour and gas permeability of the barrier laminate. Although this is not entirely correct, for reasons of simplicity and due to lack of scientific data it is however assumed.
- Water vapour and other atmospheric gases can simply be superposed. Theoretically this is solely valid at low gas pressure (Schwab, 2004). Since vacuum insulation panels are characterized by this low gas pressure even at the end of service life, this assumption is plausible.

5.4.3 Model derivation

For constant environmental conditions and using the assumptions stated in the previous section, changes in the thermal conductivity of a VIP core material can be written as (based upon Simmler and Brunner, 2005; Schwab, 2004; Schwab et al., 2005c and section 5.2)

$$\begin{aligned}\Delta\lambda_c &= \frac{\partial\lambda_c}{\partial p_g}\Delta p_g + \frac{\partial\lambda_c}{\partial p_{wv}}\Delta p_{wv} + \frac{\partial\lambda_c}{\partial u}\Delta u \\ &\approx \frac{\partial\lambda_c}{\partial p_g}\left(p_{g;e} - p_{g;i;0}\right)\left(1 - e^{-(t-t_{get})/\tau_g}\right) \\ &+ \frac{\partial\lambda_c}{\partial p_{wv}}\left(p_{wv;e} - p_{wv;i;0}\right)\left(1 - e^{-(t-t_{des})/\tau_w}\right) \\ &+ \frac{\partial\lambda_c}{\partial u}\frac{du}{d\phi}\left(\phi_e - \phi_{i;0}\right)\left(1 - e^{-(t-t_{des})/\tau_w}\right)\end{aligned} \quad (5.30a).$$

with p_g [Pa] the pore gas pressure, $p_{g;e}$ [Pa] the atmospheric gas pressure, $p_{wv;e}$ [Pa] the partial water vapour pressure outside the VIP, ϕ_e [-] the relative humidity of the air outside the VIP, u [kg·kg^{-1}] the water content of the core material, t [s] the time, t_{get} [s] the time shift due to a getter, t_{des} [s] the time shift due to a desiccant, τ_g [s] the time constant for gas pressure increase, τ_w [s] the time constant for water increase and λ_0 [W·m^{-1}·K^{-1}] the initial thermal conductivity of the core. Since in principal all parameters are 'known' and the critical value for λ_c can be chosen freely, the service life, t_{sl}, of a VIP can thus be estimated from

$$\begin{aligned}\lambda_{cr} - \lambda_0 &\approx \frac{\partial\lambda_c}{\partial p_g}\left(p_{g;e} - p_{g;i;0}\right)\left(1 - e^{-(t_{sl}-t_{get})/\tau_g}\right) \\ &+ \frac{\partial\lambda_c}{\partial p_{wv}}\left(p_{wv;e} - p_{wv;i;0}\right)\left(1 - e^{-(t_{sl}-t_{des})/\tau_w}\right) \\ &+ \frac{\partial\lambda_c}{\partial u}\frac{du}{d\phi}\left(\phi_e - \phi_{i;0}\right)\left(1 - e^{-(t_{sl}-t_{des})/\tau_w}\right)\end{aligned} \quad (5.30b).$$

It is important to realise that Equation (5.30) is only valid as long as $t > t_{get}$ and/or $t > t_{des}$. If either $t < t_{get}$ or $t < t_{des}$ the corresponding term in Equation (5.30) needs to be set to zero. Since τ_g and τ_w are defined according to Equations (5.5) and (5.10) and since according to the assumptions, the service life, t_{sl}, is defined as the time elapsed from the moment of production until the moment the thermal conductivity of the core material has reached a certain critical value, the following relations can be derived with as long as no getter and desiccant are present or they are saturated:

$$t_{sl} \sim d_p$$

Since the panel volume is the product of the panel thickness and surface area, the service life is linearly proportional to the panel thickness.

$$t_{sl} \sim \frac{T_0}{T} e^{\frac{E_a}{R}(\frac{1}{T}-\frac{1}{T_0})}$$

If it is assumed that water vapour inside the core material has reached equilibrium before the end of service life[27], then the service life is directly proportional to the time constant for gas pressure increase, τ_g. According to equation (5.5) this time constant is inversely proportional to GTR and directly proportional to the ratio of T_0 / T. Because GTR of the barrier envelope depends on temperature according to a (van't Hoff-)Arrhenius type equation[28] (Arrhenius, 1889), the service life depends on temperature according to the equation beside.

$$t_{sl} = f\left(\frac{l_p}{S_p}\right)$$

Moreover, since both the WVTR and GTR can be separated into a part involving the edge transmission and a part concerning the area-related transmission, the ratio l_p / S_p (panel perimeter length to surface area ratio) plays an important role. Due to different values for GTR and WVTR, however, it is not possible to derive a relation for this ratio at this stage. A relation between t_{SL} and this ratio will therefore be proposed based on a regression analysis.

[27] See comments accompanying relation between t_{sl} and $\lambda_{cr} - \lambda_0$ on the next page.

[28] The activation energy for water vapour permeation and for dry gas permeation is not equal. Moreover, it differs for both the surface area and the seam area of a panel. Since however an approximation tool is derived here for which parameters are derived from regression analysis, this effect is neglected in the approximation models. Here the activation energy for atmospheric gas permeation should be taken.

$t_{sl} = f(\lambda_{cr} - \lambda_0)$

Besides, equation (5.30b) indicates a relation between the service life and the critical value of the thermal conductivity minus the initial thermal conductivity, λ_{cr}-λ_0. Although the equation (5.30b) suggest a relation of the form –ln(1-ax), a regression analysis has shown that this type of equation does not produce high accuracy. Therefore a different relation will be proposed using a Naperian base. For a core of fumed silica it is additionally assumed that water vapour has reached equilibrium before the end of service life. In that case the service life becomes a function of λ_{cr}-λ_0-λ_w. This last assumption however is not entirely correct (but holds for thin VIPs), as a consequence of which the relation based upon a natural logarithm does not produce accurate results.

To derive approximation models, several practical situations now need to be distinguished. These will be discussed in the next sections.

VACUUM INSULATION PANELS WITH A CORE OF POLYURETHANE FOAM OR GLASS FIBRE BOARD

Since the thermal conductivity of PU-foam and glass fibre board starts increasing already below 0.1 mbar gas pressure and since especially for metallized films water vapour permeation is the strongest contributor to pore gas pressure increase in the early stages after production, a desiccant is always added to a these VIPs. For the first model for estimating the service life of a VIP, it is therefore assumed that a desiccant with infinite capacity is available. In that case water and water vapour effects can be neglected, resulting in the following equation for the service life, t_{sl} [s], of a VIP:

$$t_{sl} = t_{get} - \tau_g \ln\left(\frac{p_{g;e}}{p_{g;e} - p_{g;i;0}} - \frac{\lambda_{cr} - \lambda_0}{\left.\frac{\partial \lambda_c}{\partial p_g}\right|_{\lambda=\lambda_{cr}} \left(p_{g;e} - p_{g;i;0}\right)} \right)$$

$$\approx t_{get} - \tau_g \ln\left(1 - \frac{\lambda_{cr} - \lambda_0}{\left.\frac{\partial \lambda_c}{\partial p_g}\right|_{\lambda=\lambda_{cr}} p_{g;e}} \right) \qquad (5.31a),$$

which equals

$$t_{sl} \approx t_{get} - \tau_g \ln\left(1 - \frac{(\lambda_{cr} - \lambda_0)\lambda_{g;0}}{(\lambda_{g;0} - \lambda_{cr} + \lambda_0)^2} \frac{p_{1/2}}{p_{g;e}}\right) \qquad (5.31b).$$

In the practise of buildings (with service lives of 25 years or more), this equation implies that for a VIP with a core of PU-foam or glass fibres and a metallized barrier envelope, the service life is almost completely determined by the life of the getter since t_{sl} without a getter would only be a few years at most. The exact time depends on the type of barrier, panel size, temperature and relative humidity. In case no desiccant but a getter with infinite capacity is available within the VIP, an equation similar to Equation (5.31a) can be obtained. From this equation we would draw a similar conclusion that the service life is largely determined by the life of the desiccant. A VIP with a core of glass fibres of 600x1200x20 mm^3 with an MF3 envelope without getter and desiccant, for example, would have a service life of only 4.4 months at 296 K and 50% RH and with $\lambda_{cr} = 8.0\cdot10^{-3}$ W·m^{-1}·K^{-1}. The same VIP with an AF:8 barrier would have a service life of about 4 years under the same environmental conditions. In case of the use of both a getter and a desiccant, t_{sl} is therefore mainly determined by the shortest life of either the getter or the desiccant, as a consequence of which a safe estimate would be

$$t_{sl} \approx t_{get} \qquad \text{for } t_{get} < t_{des} \qquad (5.32a),$$

$$t_{sl} \approx t_{des} \qquad \text{for } t_{des} < t_{get} \qquad (5.32b).$$

VACUUM INSULATION PANELS WITH A CORE OF COMPRESSED FUMED SILICA POWDER BOARD

Since the thermal conductivity of compressed fumed silica powder board starts increasing only above approximately 20 mbar and since the primary agglomerates of fumed silica have reactive isolated Silanol-groups (SiOH) that are able to bind water (Randel, 2003), getters and desiccants are hardly ever added to SiO_x-VIPs. No getter and desiccant time shifts are then present. Since both water and atmospheric gas effects need to be considered when determining the service life, no exact closed analytical equation for t_{sl} can be determined.

Proceeding from the considerations above, the service life of a SiO_x-VIP under constant climatic conditions can be estimated using

$$t_{sl} = a \cdot e^{b(\lambda_{cr} - \lambda_0 - \lambda_w)} \cdot d_p \cdot \left(\frac{l_p}{S_p}\right)^c \cdot \frac{T_0}{T} e^{\frac{E_a}{R}\left(\frac{1}{T} - \frac{1}{T_0}\right)} \qquad (5.33),$$

with a [s·m^{-1-c}], b [m·K·W^{-1}] and c [-] regression parameters or functions and λ_w [W·m^{-1}·K^{-1}] the thermal conductivity of the liquid water and water vapour when it is at equilibrium with ambient conditions. The thermal conductivity of the liquid water and water vapour when it is at equilibrium with ambient conditions, λ_w, is obtained from (Simmler et al., 2005; Schwab, 2004)

$$\lambda_w = 0.029u(\phi_e) + \frac{\lambda_{wv;0}}{1 + \frac{p_{1/2}}{\phi_e p_{sat}(T)}} \quad (5.34).$$

The parameters *a* and *b* only depend on the type of barrier envelope (and core material), while *c* also depends on temperature. For *c* a quadratic regression function is used:

$$c = c_0 + c_1\left(\frac{T_0}{T}\right) + c_2\left(\frac{T_0}{T}\right)^2 \quad (5.35).$$

with the parameters c_0, c_1 and c_2 determined from a regression analysis of service life values derived from computations using the service life prediction model of section 5.2 and experimental results (Simmler et al, 2005; Simmler and Brunner, 2005; Schwab et al., 2005c). For the reference temperature T_0 a value of 296 K should be used, since measured data obtained at these conditions were used for the regression analysis. A regression analysis yields the values for *a*, *b* and *c* for a metallized film (MF3) and an aluminium-foil laminate (AF: 8 μm) as stated in Table 5.2. This analysis has been performed within the following boundaries: 0.01 m < d_p < 0.05 m; 268 K < T < 318 K; 2 m^{-1} < l_p / S_p < 12 m^{-1}.

***Table 5.2** – Regression parameters a, b and c and activation energy E_a for a SiO_x-VIP.*

core	envelope	*a* [yr·m^{c-1}]	*b* [m·K·W^{-1}]	E_a [kJ·mol^{-1}]
SiO_x	MF 3	(5.174 ± 0.802)·10^3	333.4 ± 0.8	50 ± 2
	AF: 8 μm	(3.614 ± 0.395)·10^4	270.3 ± 0.4	26 ± 2

core	envelope	c_0 [-]	c_1 [-]	c_2 [-]
SiO_x	MF 3	15.41 ± 2.60	-31.32 ± 5.25	15.14 ± 2.64
	AF: 8 μm	8.76 ± 1.38	-17.76 ± 2.77	8.16 ± 1.38

NB: The values are stated for a 95% confidence interval.

5.4.4 Comparison of approximation to advanced model for SiO_x-VIPs

The model presented in the previous section is compared to the more advanced service life prediction model described in section 5.2 using experimental data for the transmission properties of the barrier envelope and properties of fumed silica; the same properties as were used for determining the regression parameters. Figure 5.4[29] presents an overview of the results of this comparison for a SiO_x-VIP with either a MF3 or an AF:8 envelope and a thermal conductivity criterion of $8.0 \cdot 10^{-3}$ $W \cdot m^{-1} \cdot K^{-1}$. Plots for a thermal conductivity criterion of $7.0 \cdot 10^{-3}$ and $11 \cdot 10^{-3}$ $W \cdot m^{-1} \cdot K^{-1}$ are presented in appendix A56. The ratio of l_p to S_p was varied from 2 to 12 m^{-1}, the thickness of the VIP from 0.01 to 0.05 m and the temperature from 278 to 318 K [30]. The relative humidity was kept constant at 50%, as a result of which the effect of relative humidity on the permeation properties of the barrier is neglected. Due to a varying temperature and a constant RH, however, the partial water vapour pressure outside the VIP does vary. For this analysis no thermal edge effects are considered.

As can generally be seen from the figures, the difference between both models is acceptably small, as a consequence of which the approximation model is sufficiently accurate for application in practical situations or in the early stages of a design process. For a SiO_x-VIP of 0.67x0.67 m^2 with an aluminium foil based laminate (AF:8), a thermal conductivity criterion of $8 \cdot 10^{-3}$ $W \cdot m^{-1} \cdot K^{-1}$ and at a temperature of 288 K, the difference between the advanced model (section 5.2) and the approximation tool (section 5.4) amounts to 15 (+6.7%), 30 (+6.7%), 45 (+6.7%), 60 (+6.7%) and 76 (+6.7%) years for a panel of 10, 20, 30, 40 and 50 mm thick respectively. If we now change the barrier to a metallised laminate (MF3), the difference approximately is 6.8 (+11%), 14 (+11%), 20 (+11%), 27 (+11%) and 34 (+11%) years for a panel thickness of 10, 20, 30, 40 and 50 mm respectively.

The largest percentile deviations are found for a thermal conductivity critical value of $7.0 \cdot 10^{-3}$ $W \cdot m^{-1} \cdot K^{-1}$ at high temperature for large panel sizes. For a SiO_x-VIP of 2.00x2.00 m^2 with an aluminium foil based barrier laminate (AF:8), a thermal conductivity criterion of $7.0 \cdot 10^{-3}$ $W \cdot m^{-1} \cdot K^{-1}$ and at a temperature of 318 K, the difference between the advanced model (section 5.2) and the approximation tool (section 5.4) amounts to 9.5 (+18%), 19 (+18%), 28 (+18%), 38 (+18%) and 47

[29] The highest values in each of these plots are for a VIP of size 2.0x2.0x0.05 m^2 at 5°C.

[30] In total 450 simulations have been performed.

Figure 5.4a MF3

Error plot: plot of the service life calculated with the approximation model as function of the service life calculated with the advanced model for film-based vacuum insulation panels with a ***core of fumed silica and an MF3 barrier****. No thermal bridging.*

λ_{cr} = 8.0·10^{-3} W·m^{-1}·K^{-1};
ϕ = 50%; thickness: 1 to 5 cm;
size: 0.25x0.25 m^2 to 2x2 m^2;
T: 5°C to 45°C.

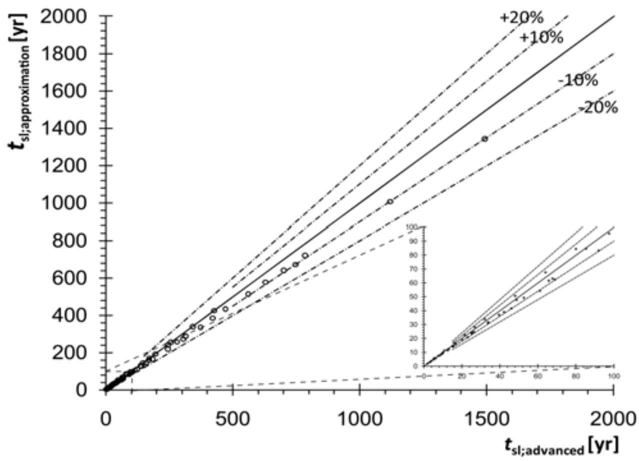

Figure 5.4b AF:8

Error plot: plot of the service life calculated with the approximation model as function of the service life calculated with the advanced model for film-based vacuum insulation panels with a ***core of fumed silica and an AF:8 barrier****. No thermal bridging.*

λ_{cr} = 8.0·10^{-3} W·m^{-1}·K^{-1};
ϕ = 50%; thickness: 1 to 5 cm;
size: 0.25x0.25 m^2 to 2x2 m^2;
T: 5°C to 45°C.

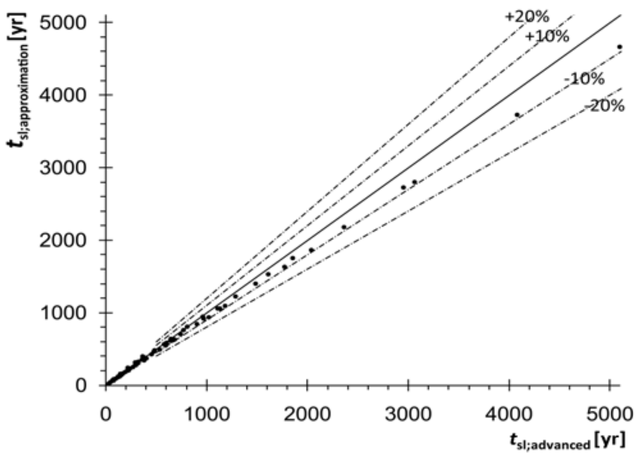

(+18%) years for a panel thickness of 10, 20, 30, 40 and 50 mm respectively. For the same panel but now with a metallised barrier laminate (MF3) and under the same conditions, the difference between both models approximately is 0.5 (+15%), 1.0 (+15%), 1.5 (+15%), 2.0 (+15%) and 2.5 (+15%) years for a panel thickness of 10, 20, 30, 40 and 50 mm respectively. Although these differences are bigger, still the model is sufficiently accurate for application in design and engineering practise.

5.4.5 Model limitations

The application range of the approximation model presented in this chapter for estimating the service life of SiO_x-VIPs is limited owing to the boundaries that were used for performing the regression analysis. These limits can be summarised as

$0.01 \text{ m} < d_p < 0.05 \text{ m}$;

$268 \text{ K} < T < 318 \text{ K}$;

$2 \text{ m}^{-1} < l_p / S_p < 12 \text{ m}^{-1}$;

$\phi = 50\%$.

Outside of these boundaries, the prediction model can however still be used but with unspecified accuracy. Since the effect of relative humidity on dry gas and water vapour permeation through the barrier envelope is not considered, the model is strictly solely valid for a relative humidity of 50%. Since this effect might be expressed by an exponential curve, changing the relative humidity might have a strong influence on the inaccuracy of the prediction model (Galbraith and Mclean, 1990; Galbraith et al., 1998; Burch et al., 2002).

Within these boundaries the maximum difference between the advanced model, equation (5.30b), and the approximation model, equation (5.33), is less than 18%. For $\lambda_{cr} > 8.0 \cdot 10^{-3}$ W·m^{-1}·K^{-1} the difference even goes to below 8%. It is however important to realize that these differences are between two mathematical models and not between a model and reality. This implies that the difference between the approximation tool and reality might be even bigger but might be smaller as well. More experimental data are required to validate and verify the model more thoroughly.

Moreover, the approximation model was derived for constant climatic conditions. In reality however such conditions only apply to laboratory (or inside) situations. Brunner and Simmler (2008) showed that as an approximation an effective temperature, which is the annual average temperature using the Arrhenius function for the applicable barrier as weighting function, can be used to include temperature fluctuations in the prediction. Due to this weighting function, high temperatures have a stronger effect on the service life than low temperatures. They obtained good results when comparing predictions of the gas pressure increase rate using this effective temperature to actual in-situ measurements on vacuum insulation panels of 25x25x2 cm^3 and of 50x50x2 cm^3 with a metallised barrier envelope. A similar Arrhenius weighting might also be used for temperature difference on both sides of the vacuum insulation panel.

5.5 SERVICE LIFE PLOTS OF VIPS WITHOUT THERMAL BRIDGING

Based upon equation (5.33) service life plots can be created in which the service life of a SiO_x-VIP is plotted against panel thickness and the ratio of circumference to surface area. Two plots are shown in Figures 5.5 and 5.6 for a VIP with an aluminium foil based barrier laminate and a metallized film envelope respectively for a temperature of 293 K and for a thermal conductivity criterion of $8.0 \cdot 10^{-3}$. More plots are presented in appendix A52.

These plots can be used to rapidly determine the service life during the different stages of the design process. Moreover, since in practice very often a minimum requirement for the service life is specified in advance, these plots can also be used to determine the minimum size to fulfil service life demands. If, for instance, a thermal resistance of 5.0 $m^2 \cdot K \cdot W^{-1}$ is required for the insulation layer in the façade of a building immediately after construction, a thickness of about 20 mm VIP would fulfil this demand, not considering thermal edge effects. If now a service life of 70 years is needed, if the annual average temperature around the VIP is 293 K and if the thermal conductivity criterion is $8.0 \cdot 10^{-3}$ $W \cdot m^{-1} \cdot K^{-1}$, the minimum ratio of l_p to S_p would be about 4.5 m^{-1} if a three-layer metallised film were used (Figure 5.6). This would equal a panel size of 0.8x1.0 m^2. In this case, it is however better to choose the required dimensions of the panel based on the thermal conductivity at the end of life: $8.0 \cdot 10^{-3}$ $W \cdot m^{-1} \cdot K^{-1}$. Using the previously stated conditions, a thickness of 40 mm would be needed to fulfill the thermal requirements. For this panel then the minimum of the ratio of l_p to S_p would be about 10.8 m^{-1}, which would equal a panel size of approximately 0.3x0.5 m^2. Due to thermal edge effects however a slightly larger panel would be required. The combined effect of thermal bridging and service life will be discussed in the next sections.

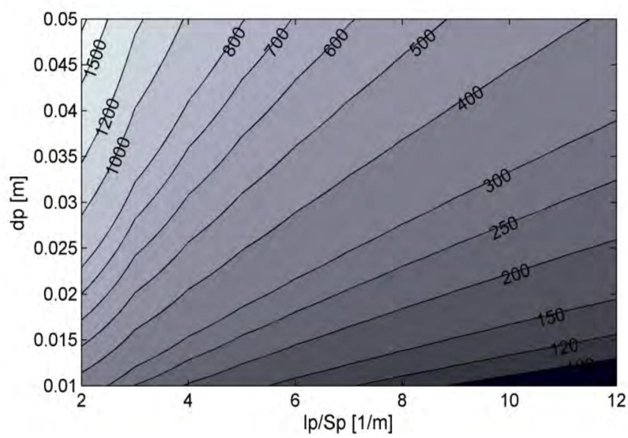

Figure 5.5

Service life plot of a SiO_x-VIP as function of panel thickness and of panel perimeter to surface ratio.

Barrier: AF:8
T = 293 K
RH = 50%
$\lambda_{cr} = 8.0 \cdot 10^{-3}$ $W \cdot m^{-1} \cdot K^{-1}$

Numbers on lines are t_{sl} [yr].

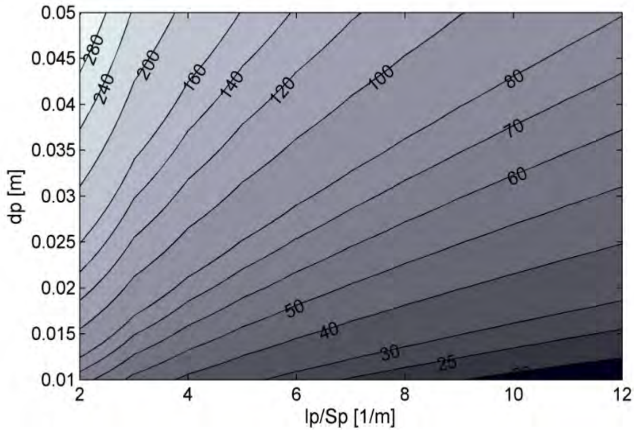

Figure 5.6

Service life plot of a SiO_x-VIP as function of panel thickness and of panel perimeter to surface ratio.

Barrier: MF3
T = 293 K
RH = 50%
$\lambda_{cr} = 8.0 \cdot 10^{-3}\ W \cdot m^{-1} \cdot K^{-1}$

Numbers on lines are t_{sl} [yr].

5.6 Service Life Plots of VIPs With Thermal Bridging

For determining the service life of a vacuum insulation panel which includes both the effects of thermal conductivity ageing and thermal bridging due to the barrier envelope, the same equation can be used as for determining the service life of a VIP solely including ageing (Equation 5.33) for SiO_x-VIPs). The thermal conductivity criterion, λ_{cr}, now no longer is a constant value but must be reduced for thermal shunting effects. Using knowledge from Chapter 3 and neglecting corner thermal transmittances, this thermal conductivity criterion can then be written as

$$\lambda_{cr} = \lambda_{eff;cr} - \psi_{vip;edge} d_p \frac{l_p}{S_p} \qquad (5.36),$$

with $\lambda_{eff;cr}$ [$W \cdot m^{-1} \cdot K^{-1}$] the critical value of the effective thermal conductivity, thus including the thermal edge effect and $\psi_{vip;edge}$ [$W \cdot m^{-1} \cdot K^{-1}$] the linear thermal transmittance calculated according to the approximation models (or numerical procedure) described in Chapter 3.

Using the considerations from the previous paragraph, plots can now be drawn representing the service life that results from considering both thermal conductivity ageing and thermal bridge effects. Two of such plots are presented in Figures 5.7 and 5.8 for a SiO_x-VIP with either an aluminium foil based laminate (AF:8) or a metallised film laminate (MF3) respectively for a temperature of 293K and an effective thermal conductivity criterion of $8.0 \cdot 10^{-3}\ W \cdot m^{-1} \cdot K^{-1}$. More plots are presented in appendix A53.

As can be seen, changes in the service life plots are relatively small for VIPs with metallized film laminates but are large for VIPs with aluminium foil laminates, as can be expected. For VIPs with a metallized barrier laminate, the linear thermal transmittance is small as a result of which λ_{cr} almost equals $\lambda_{eff;cr}$ and thus the service life including both thermal shunting and ageing almost equals the service life solely based on ageing.

Moreover, according to equation (5.36), the influence of thermal edge effects should be bigger according as the panel is smaller and/or deviates more from a square panel. A comparison of Figure 5.8 to Figure 5.6 indeed indicates this behaviour. The service life of a square VIP of 1.0x1.0x0.02 m^3 with a MF3 barrier at 293K and 50% RH, for instance, changes from about 75 years to about 70 years (-6.7%) if thermal bridging is considered while in case of a square VIP of 0.4x0.4x0.02 m^3 it shifts from approximately 37 years to about 31 years (-16%) ($\lambda_{eff;cr} = \lambda_{cr} = 8.0 \cdot 10^{-3}$ W·m^{-1}·K^{-1}). Since the linear thermal transmittance resulting from an aluminium based barrier laminate is much larger than from a metallized film based barrier, the difference between the service life including both thermal shunting and thermal conductivity ageing should be larger for this metal layer barrier envelope. As an example, the service life of a square VIP of 1.0x1.0x0.02 m^3 with a AF:8 barrier at 293 K and 50% RH changes from about 390 years to about 185 years (-53%) if thermal bridging is considered and from 180 years to 28 years (-84%) if the size of the VIP were 0.4x0.4x0.02 m^3. These significant changes in service life for a VIP with an AF:8 barrier if thermal bridge effects are taken into account are also clearly observed from changes in the path of the lines with equal service life.

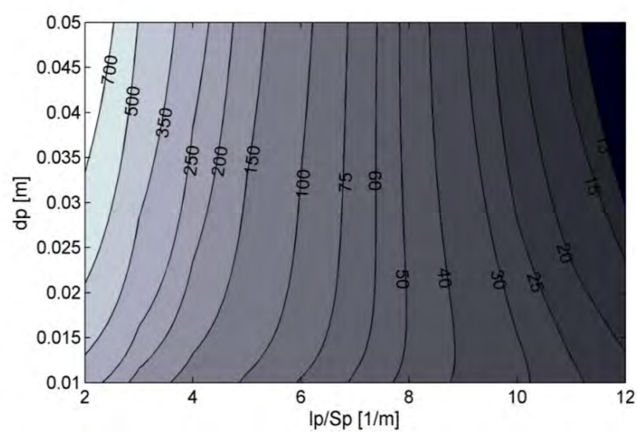

Figure 5.7

Service life plot of a SiO_x-VIP as function of panel thickness and of panel perimeter to surface ratio including thermal edge effects.

Barrier: AF:8
Seam: type b ($\varphi = 0.67$)
T = 293 K; RH = 50%
$\lambda_{eff;cr} = 8.0 \cdot 10^{-3}$ W·m^{-1}·K^{-1}
$\alpha_1 = 7.8$ m^2·K·W^{-1}
$\alpha_2 = 25$ m^2·K·W^{-1}

Numbers on lines are t_{sl} [yr].

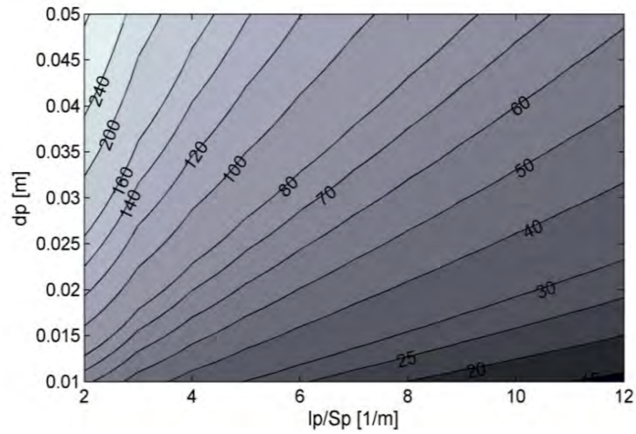

Figure 5.8

Service life plot of a SiO_x-VIP as function of panel thickness and of panel perimeter to surface ratio including thermal edge effects.

Barrier: MF3
Seam: type b ($\varphi = 0.67$)
$T = 293$ K; $RH = 50\%$
$\lambda_{eff;cr} = 8.0 \cdot 10^{-3}$ W·m^{-1}·K^{-1}
$\alpha_1 = 7.8$ m^2·K·W^{-1}
$\alpha_2 = 25$ m^2·K·W^{-1}

Numbers on lines are t_{sl} [yr].

For estimating the service life of VIP integrated building components both including thermal conductivity ageing and thermal edge effects, a similar procedure as explained at the start of this section can be used. The calculation of λ_{cr} however is more complicated. In appendix A54 this procedure is explained in more detail. In this appendix also service life plots of many VIP integrated building components are presented. Concerning these plots, only one remark will be made here.

As can be seen from Table A54.1 in this appendix, a VIP integrated building component with an aluminium spacer, a folded edge spacer or an optimized thermoplastic spacer in combination with two 2 mm thick aluminium facings (or facings having a $\lambda_{f;j}\, t_{f;j}$ higher than approximately 0.3 W·K^{-1}) are not suitable for application in building panels if λ_{cr} is chosen $8.0 \cdot 10^{-3}$ W·m^{-1}·K^{-1} or below and if thermal edge effects are considered in the service life computation. Within the range of panels tested[31], the critical value of the thermal conductivity of the core was always lower than its initial thermal conductivity. As a consequence, their service life is 0 years.

Within the same range of panels and temperature conditions, the aluminium double-glazing spacer is even practically hardly suitable in combination with low thermal conductivity facings like polyester ($\lambda_{f;j}\, t_{f;j} = 8 \cdot 10^{-3}$ W·K^{-1}). Only very large and thin panels have a service life which goes beyond that required for office buildings (25 to 30 years).

[31] 0.01m < d_p < 0.05 m; 268 K < T < 318 K; 2 m^{-1} < l_p / S_p < 12 m^{-1}; ϕ = 50%.

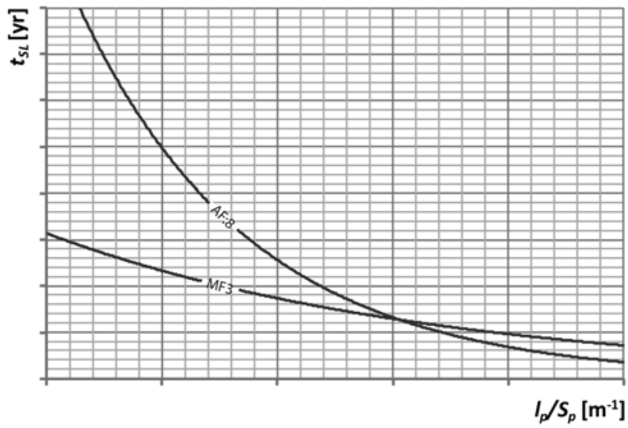

Figure 5.9

Typical plot of the service life of a VIP with a fumed silica core and either an aluminium-based or metallised barrier envelope as function of VIP perimeter to surface ratio. ***Thermal edge effects included.***

5.7 Practical Consideration: Choosing a Barrier Laminate

As we have seen in the previous and in this chapter, a criterion for either the thermal conductivity of the core or for the effective thermal conductivity of the entire VIP can be set to define the panel's service life. If thermal bridge effects are accounted for in service life predictions, i.e. if a criterion is set for the effective thermal conductivity of the entire VIP, then the thermal conductivity criterion for the core material becomes dependent on the type of barrier laminate chosen in accordance with equation (5.36). This equation implies that the bigger the ratio of l_p/S_p, the lower the critical value of the thermal conductivity of the core, λ_{cr}. Since the linear thermal transmittance resulting from the barrier laminate at the panel's side is higher for an aluminium-foil based barrier envelope than for a metallised film based envelope, λ_{cr} is influenced more strongly by l_p/S_p in case of an aluminium-foil based envelope than in case of a metallised-film based envelope.

Figure 5.9 presents a typical plot of the service life of VIP with either an aluminium-foil based or a metallised-film based envelope as function of l_p/S_p. The service life predictions presented in this plot include the effect of thermal bridging. As can be seen from this plot, the curve representing the service life of a VIP with an aluminium-foil based barrier decreases more steeply than the curve representing a VIP with a metallised-film based barrier, which is in accordance with the reasoning from the previous paragraph. At a certain ratio l_p/S_p, the service life of both VIPs is equal. This implies that for panels with a high ratio, i.e. small panels, metallised barrier envelopes are preferred to aluminium-based barriers. This argument principally holds for all temperature and humidity conditions. The position of this transition, though, among others depends on panel thickness, temperature and relative humidity. For a VIP with a fumed silica core and a thickness of 20 mm in an environment with a constant temperature of 288 K and relative humidity of 50%, this transition[32,33], for instance, takes place at a ratio l_p/S_p of approximately 3.6 m^{-1}, if the effective thermal conductivity criterion is a priori set to $8.0 \cdot 10^{-3}$ $W \cdot m^{-1} \cdot K^{-1}$. This implies that under these conditions, a metallised-film based barrier envelope is preferred to an aluminium-foil based barrier for panels smaller than approximately 1.0x1.25 m^2. The ratios determining these boundaries can be calculated using the service life prediction model from this and the previous chapter combined with equation (5.36).

5.8 CONCLUSIONS AND SUMMARY

The functional service life of a VIP and a VIP incorporated component can be defined using either an absolute thermal performance criterion or a time-averaged thermal performance criterion. For vacuum insulation panels and VIP integrated building components, the absolute thermal performance criterion may be formulated either as an effective thermal conductivity of for instance $8.0 \cdot 10^{-3}$ $W \cdot m^{-1} \cdot K^{-1}$ (or of $11 \cdot 10^{-3}$ $W \cdot m^{-1} \cdot K^{-1}$) or as a thermal conductivity of the VIP's core of the same value.

In general, a service life of 30 to 100 years should be guaranteed for application of VIPs in commercial or residential buildings respectively.

The functional service life of a vacuum insulation panel, is principally determined by the properties of the core material, the presence and effectiveness of getters and desiccants, the initial vacuum and water content, degassing of the core material and the barrier envelope, the envelope's permeance for atmospheric gases and water vapour, the panel's dimensions and the environmental conditions regarding temperature and relative humidity (and partial water vapour pressure). Since, the first five factors can hardly be influenced by architects and building engineers, especially the last two are of interest from the perspective of construction design and architectural practise.

---

[32] A 97 μm thick three-layer metallised film (MF3) envelope is compared to a 6 μm thick aluminium-foil based envelope (AF:6). Regarding the barrier properties (GTR and WVTR) of the AF:6 envelope, the properties of an AF:8 envelope are assumed.

[33] At a temperature of 296 K, a r.H. of 50%, with a fumed silica core and a thickness of 20 mm, this transition would be near 3.8 m^{-1} (panel size: 1.0x1.1 m^2). Increasing the temperature to 303 K increases this ratio l_p / S_p to 4.0 m^{-1} (panel size: 1.0x1.0 m^2).

Since the seam or the edge of a vacuum insulation panel has a non-negligible permeance for water vapour and dry atmospheric gases, size effects concerning its service life occur. Since aluminium foil based envelopes in their flat surfaces are almost impermeable to atmospheric gases, these size effects are stronger for these envelopes than for metallised film based envelopes. Moreover, the time constants for atmospheric gases and for water are both directly proportional to panel volume, as a consequence of which the service life is also directly proportional to panel thickness.

The most important temperature effect on the service life of a vacuum insulation panel or a VIP integrated building component is the dependency of water vapour and gas transmission rate of the barrier envelope on temperature. This effect can be modelled using an Arrhenius type of equation which exhibits an exponential increase of the transmission rate for increasing temperature. The activation energy required in this Arrhenius equation differs for water vapour and dry gas permeation and depends on the type of material used for the barrier or the seam.

The most important relative humidity effect on the service life of a vacuum insulation panel or a VIP integrated building component is the dependency of water vapour and gas transmission rate of the barrier envelope on relative humidity. The exact physical mechanisms involved in this dependency are still insufficiently clear for complex multilayered barrier films. As a result, insufficient data are available to accurately model this. Simmler et al. (2005), though, showed that this effect is stronger for WVTR than for GTR.

The partial water vapour pressure of the air surrounding a vacuum insulation panel finally increases the driving-potential for water vapour permeance through the barrier envelope and thus influences the service life by speeding up the permeation process.

Using mass balance and transfer equations for water vapour and dry gas permeation in conjunction with the properties of the core material[34], the service life of a VIP can be estimated for constant climatic conditions. For these estimations experimental data on complete intact VIPs are required.

Service life factors in conjunction with aforementioned mathematical models can be used to approximate the influence of variation in environmental conditions

[34] Its sorption-isotherm, the relation between thermal conductivity and gas pressure for both air and water vapour, and the relation between thermal conductivity and water content.

on the service life. Two factors are distinguished: a factor considering the effect of temperature and relative humidity fluctuations which more-or-less influences the time constants, τ_g and τ_w; and a factor considering the effect of external partial water vapour or atmospheric gas pressure fluctuations which influences the value of the thermal conductivity at $t = \infty$.

Moreover, in this chapter analytical models with which the service life of a VIP can be estimated without using iterative or numerical procedures were derived. Differences between the advanced service life model from section 5.2 and this approximation model for SiO_x-VIPs have been found to be less than 18% for very low thermal conductivity critical values. If this criterion increases to beyond $8.0 \cdot 10^{-3}$ $W \cdot m^{-1} \cdot K^{-1}$ differences reduce to below 8% making it a tool sufficiently accurate for the building practise. As was shown, based upon these approximation models, service life plots can easily be drawn. Based upon these plots finally the service life of a VIP can be determined graphically facilitating the selection process in a design phase.

Since thermal bridge effects are considerable both for VIPs with a large ratio of circumference to surface area (small VIPs) or VIPs with a metal-based barrier envelope and since the service life of a VIP was defined using a criterion for the effective thermal conductivity, thermal bridge effects should be considered when VIP service lives are computed. The inclusion of these effects into service life prediction models can be done by making λ_{cr} a function of the linear thermal transmittance, panel thickness and the ratio of circumference to surface area[35] according to the models presented in chapter 3. This can be done as long as $\lambda_{cr} > \lambda_0$.

As can be expected, the effect of thermal shunting on the service life is smallest for large panels and panels having a small linear thermal transmittance, i.e. VIPs with a MF3 barrier. The service life of a small VIP with a metal-based barrier envelope is significantly reduced due to a strong thermal bridge effect if t_{sl}-values including thermal edge effects are compared to t_{sl}-values not considering this effect. A reduction of the service life with more than 50% is quite normal.

Besides, if the critical value for the effective thermal conductivity is set at $8.0 \cdot 10^{-3}$ $W \cdot m^{-1} \cdot K^{-1}$, a VIP integrated building component with facings for which $\lambda_{f;j} \, t_{f;j} \geq 0.3$ $W \cdot K^{-1}$ combined with either an aluminium double-glazing spacer, a folded edge spacer or an optimised thermoplastic spacer is never suitable for application in buildings since $\lambda_{cr} < \lambda_0$, except for extremely large panels (l_p / $S_p < 2$ m^{-1}).

---

[35] and in case of building panels, additional resistances and the width of the spacer.

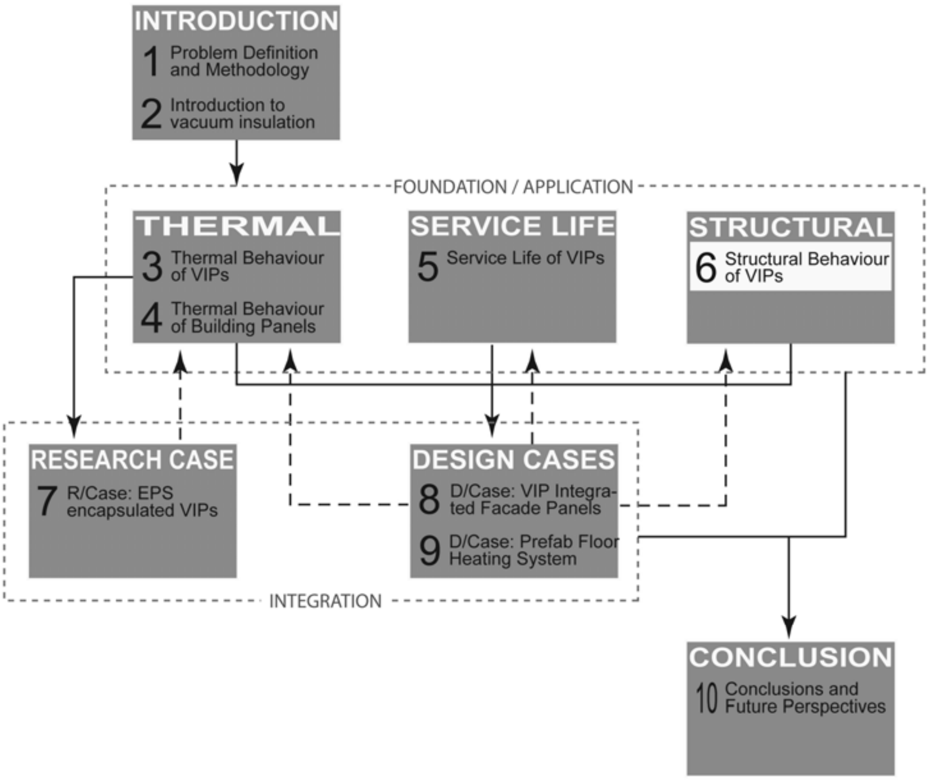
INTRODUCTION
1 Problem Definition and Methodology
2 Introduction to vacuum insulation
FOUNDATION / APPLICATION
THERMAL
3 Thermal Behaviour of VIPs
4 Thermal Behaviour of Building Panels
SERVICE LIFE
5 Service Life of VIPs
STRUCTURAL
6 Structural Behaviour of VIPs
RESEARCH CASE
7 R/Case: EPS encapsulated VIPs
DESIGN CASES
8 D/Case: VIP Integrated Facade Panels
9 D/Case: Prefab Floor Heating System
INTEGRATION
CONCLUSION
10 Conclusions and Future Perspectives

STRUCTURAL BEHAVIOUR OF VIPS 6

STUDY INTO THE YOUNG'S MODULUS AND FAILURE BEHAVIOUR OF VIP

In the previous chapters on thermal behaviour and service life of VIPs two out of four research aspects within the domains of foundation and application were discussed. In this chapter, the third aspect within these domains is investigated: structural behaviour of vacuum insulation panels. The objective of this chapter is to obtain values for relevant mechanical properties of VIPs and to develop insights into the structural behaviour of these panels.

Since a VIP is a composite system, the mechanical properties of both barrier laminate and fumed silica are therefore introduced. In the next section, the Young's modulus of intact and damaged VIPs is studied experimentally and theoretically. Using sandwich theory, a model for calculating an equivalent effective Young's modulus, which includes shear effects, is derived. In section 6.4, finally, a model for estimating the complete flexural behaviour of a vacuum insulation panel is developed and verified experimentally. Using this model it is also possible to estimate the panel's modulus of elasticity during the entire process of bending up till structural failure.

Since the compressive strength of typical core materials, like fumed silica, is sufficiently high to withstand a pressure difference of approximately 1 bar from core centre to surrounding air and to withstand a distributed load typically acting on floors, these properties are not investigated in detail in this dissertation. The flexural properties are the main focus of this chapter.

6.1 INTRODUCTION

Although vacuum insulation panels are primarily used for their excellent thermal performance, structural use might be interesting in case of VIP integrated facade panels. In case of sandwich panels, thermal performance is combined with structural performance to obtain a façade panel with minimised thermal bridges. The structural behaviour of a VIP must be known if such panels are to be constructed. This chapter therefore presents a first study into the structural behaviour of vacuum insulation panels. The mechanical properties of fumed silica and several barrier envelopes are studied experimentally, the Young's modulus of a complete VIP system is investigated experimentally and theoretically and the failure behaviour finally is primarily studied theoretically. Moreover, the effect of damage, i.e. loss of vacuum, on the Young's modulus is studied as well. This chapter should not be considered as a complete and in-depth analysis of the structural behaviour of vacuum insulation panels but as a first introduction.

A vacuum insulation panel cannot be considered as a single material but must be regarded as a composite system. A pressure difference over the barrier laminate causes the film to adhere to the core material; high shear stresses along the interface between barrier laminate and core are needed to overcome the resulting friction. As a consequence, the barrier envelope and core material co-operate to form a composite system that exhibits similar behaviour as a sandwich panel. This sandwich action improves the flexural stiffness of a VIP composite considerably as will be observed from the difference in Young's modulus of an intact and vented VIP.

Not only can a vacuum insulation panel be considered as exhibiting sandwich behaviour, it can also be compared to reinforced (pre-stressed) concrete. In this analogy the core material is analogous to concrete while the barrier envelope is similar to the steel reinforcement bars; fumed silica, like concrete, is weak in tension but strong in compression especially due to the outside/inside air pressure difference whereas the barrier envelope at the panel's top, bottom and sides, like steel, is relatively strong in tension and ductile. This analogy is used to qualitatively describe and quantitatively determine the flexural behaviour of a VIP. Using this knowledge and these models then allows the design of sandwich panels. Such panels are presented in chapter 8 of this dissertation.

6.2 MECHANICAL PROPERTIES OF VIP CONSTITUENTS

6.2.1 Mechanical properties of fumed silica: flexion

During the IEA Annex 39 project (Simmler et al., 2005), flexion tests on two types of fumed silica (specimen sizes: 300x110x20 mm^3) according to standard NF T 56 102 (1976) have been conducted at CSTB (Table 6.1). The samples were tested at two conditions as specified in appendix A613. For condition 1, four-point flexion tests on fumed silica samples (SIL3) of different sizes according to ASTM C393 (1992) have also been conducted at TU Delft (Table 6.2 and Figure 6.1).

From Table 6.1 and 6.2 again two effects are discernible. First, water and/or water vapour affect the strength and Young's modulus of fumed silica by reducing their values. So, the deflection of a fumed silica board loaded in bending will increase due to the uptake of water. This will lead to an increase in deflection by a factor of about 3. As will be explained later in this chapter, the deflection of a complete VIP will hardly be influenced by this water uptake since the bending stiffness is mainly determined by the properties of the laminate and the distance between the centroids of this laminate. Second, as can be seen from Table 6.2, size effects on the properties of fumed silica are not significant, at least within the size ranges studied.

Table 6.1 *- Three-point flexion behaviour of two types of fumed silica (Simmler et al., 2005).*

Cond.	Mat.	d_p [mm]	l_{span} [mm]	w_p [mm]	a [mm]	$f_{c;u}$ [kPa]	$E_{c;0}$ [MPa]	$\varepsilon_{c;u}$ [%]
1	SIL1	20	230	110	-	28.7	8.9	0.6
1	SIL2	20	230	110	-	38.6	2.3	3.2
2	SIL1	20	230	110	-	13.3	2.9	0.8
2	SIL2	20	230	110	-	20.7	-	-

NB: test speed is 5 mm·min^{-1}; d_p is specimen thickness, l_{span} is the span of the specimen in the test assembly, w_p is the width of the specimen, a is the load-to-support distance, $f_{c;u}$ is the ultimate strength, $E_{c;0}$ is the tangential Young's modulus at ε=0 and $\varepsilon_{c;u}$ is the strain at $f_{c;u}$.

Table 6.2 *- Four-point flexion behaviour of a compressed fumed silica powder board.*

Cond.	Mat.	d_p [mm]	l_{span} [mm]	w_p [mm]	a [mm]	$f_{c;u}$ [kPa]	$E_{c;0}$ [MPa]	$\varepsilon_{c;u}$ [%]
1	SIL3	150	690	20	190	47 ± 7	7.2 ± 1.4	1.6 ± 0.3
1	SIL3	20	200	120	40	47 ± 18	7.0 ± 1.3	2.2 ± 0.4

NB: test speed is 10 mm·min^{-1}; see also remarks accompanying Table 6.1.

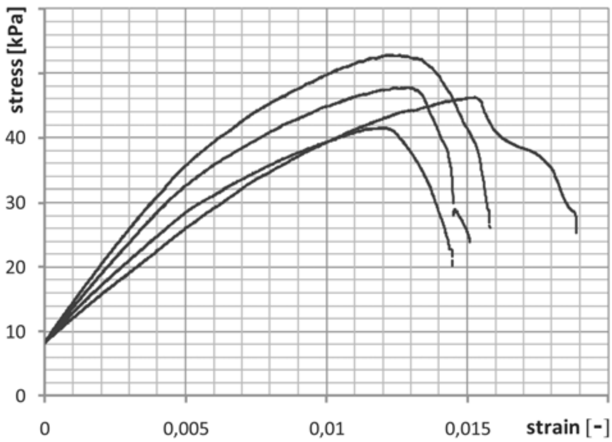

Figure 6.1

Flexion behaviour of fumed silica samples SIL3 (d_p=150mm; l_{span}=750mm) for condition 1.

6.2.2 Mechanical properties of barrier envelopes

The barrier envelope of a VIP should fulfil several requirements, two of which will be mentioned. First, it should have low GTR and WVTR (chapter 5). Second, it should have sufficient mechanical strength to withstand stresses resulting from evacuation, from temperature differences or from structural loading. If this barrier envelope is subjected to mechanical stresses due to a cooling from room to cryogenic temperature (liquid natural gas) or due to solar radiation, failure may endanger the application of VIPs. Moreover, the mechanically weakest spot in the barrier envelope is the heat seal at which point two envelope parts are welded together. In this respect, it is important to realise that on the one hand the geometric shape of the seal provides stress concentrations and on the other hand this seal itself consists of the weakest material of the laminate, polyethylene.

Table 6.3 *- List of the laminate types under consideration (data specified by manufacturers).*

Name [a]	t_f [µm]	area yield [m^2kg^{-1}]	tensile strength [MPa]	*HSS* [Nmm^{-1}]	max. strain [%]	lam. (PEtoPET) strength [Nmm^{-1}]	puncture resistance [N]	O_2TR [ccm^{-2} day^{-1}]	WVTR [gm^{-2} day^{-1}]
Lam 1	97	9.25	MD: 83 TD: 90	>4.4	MD: 60 TD: 59	>0.39	92	$<5\cdot10^{-4}$	$1\cdot10^{-2}$
Lam 2	81	n.a.	81	2.3	75	n/a	10	$<5\cdot10^{-4}$	$<5\cdot10^{-3}$

[a] The layout of the laminates is as follows:

Lam 1: 60 µm HDPE – 12 µm alPET – 12 µm alPET – 12 µm alPET

Lam 2: 50 µm HDPE – 6 µm Al – 25 µm PET

Between the different layers of polymer or aluminium, a polyurethane adhesive layer of about 2 µm is present; Note: *HSS* is the heat seal strength of a seal

__Table 6.4__ - Characteristic stress and strain values for laminate 1 and 2 at room temperature.

laminate	$\varepsilon_{f;pl}$	$f_{f;y}$	$\varepsilon_{f;u}$	$f_{f;u}$	$E_{f;o}$
	[%]	[MPa]	[%]	[MPa]	[MPa]
lam. 1 (MF3)	4.6 ± 0.9	46.8 ± 0.2	128 ± 40	87.1± 6.9	1355 ± 15
lam. 2 (AF:6)	5.2 ± 1.2	50.7 ± 0.8	145 ± 13	75.8 ± 0.9	1189 ± 49

Note: $\varepsilon_{f;pl}$ is the strain at which plastic deformation start to occur; $f_{f;y}$ is the yield strength; $f_{f;u}$ is the ultimate strength, $E_{f;0}$ is the tangential Young's modulus at ε=0 and $\varepsilon_{f;u}$ is the strain at $f_{f;u}$.

This section explores mechanical properties of some laminates at room temperature. More information on their behaviour at cryogenic temperature and of seals at room and cryogenic temperature is given in Malsen et al. (2008). The results presented in this section were obtained in the framework of the VACI (Vacuum Insulation for the Cooling Industry) research program, a joint EU/CRAFT-funded project that took place from 2003 until 2005. The objective of part of this research has been to test materials suitable for application as barrier laminate for vacuum insulation panels. Two types of barrier laminate have been tested. The first type is typified as a metal-polymer laminate; the second type is a metallised polymer barrier laminate. The specific details of the laminates are listed in Table 6.3. The samples for testing the strength, strain and Young's modulus were cut out of sheets of laminate material into rectangular samples of 12.5 mm wide and 230 mm long according to ASTM E345 type 2 specimens (ASTM, 2002). The samples were tested at a temperature of approximately 21°C at a strain rate of 4 mm/min using a tensile testing machine and of each laminate several duplication tests are performed (in most cases 5 tests)[1].

Since for VIPs in buildings especially the behaviour near room temperature is relevant (-5°C to +40°C), Figure 6.2 displays the stress-strain curves of the tensile tests on laminate 1 and 2 as measured at room temperature. Both laminates more-or-less behave similarly with respect to tension loading at room temperature. Although the curve of laminate 1 (MF3) exhibits some curvature especially during plastic behaviour, both stress-strain curves can be schematised as bi-linear elasto-plastic with the characteristic transition points tabulated in Table 6.4. ε_{pl} [%] and f_y [MPa] represent the strain and stress for the transition between elastic and plastic behaviour while ε_u [%] and f_u [MPa] represent the ultimate strain and stress.

[1] During the VACI research projects in total four laminates have been tested - two variants of each laminate type – within a temperature range from -196°C to +70°C. Only the results of two laminates at room temperature are presented in this dissertation. More information can be found in Malsen et al. (2008) and in Cauberg et al. (2006).

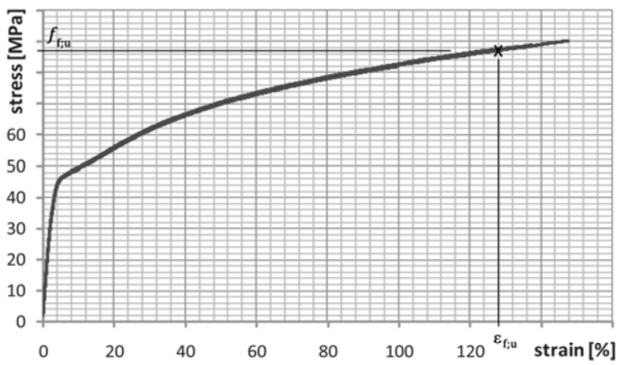

Figure 6.2a

Stress-strain curves of four laminate 1 samples at room temperature.

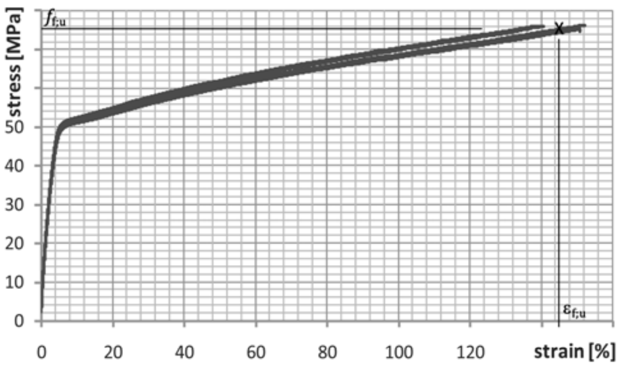

Figure 6.2b

Stress-strain curves of four laminate 2 samples at room temperature .

6.3 YOUNG'S MODULUS OF A VIP (FLEXION)

The Young's modulus is among the most important structural properties of materials, since combined with the area moment of inertia it principally determines the flexural behaviour of beams and plates. In general, the Young's modulus of a homogeneous material is a statistic material property representing an average resistance against deformation. Since VIPs consist of a combination of a core material under vacuum and an enveloping barrier film, a Young's modulus for a VIP defined as a material property does not exist. It is however possible to define an equivalent Young's modulus as the total bending stiffness of the VIP, $(EI)_{\text{vip}}$ [N·m²], divided by the area moment of inertia of the VIP, I_{vip} [m⁴]

$$E_{eq} = \frac{(EI)_{vip} \cdot (1 - \overline{\nu^2})}{I_{vip}} \tag{6.1}$$

As a result, the equivalent Young's modulus not only depends on the Young's moduli of the core material and the barrier envelope but also on the thickness of the core material and the thickness of the barrier envelope; it thus becomes panel specific.

Due to the complexity of vacuum insulation panels, E_{eq} however is not representative for the Young's modulus as it is measured in experiments. Four important influences will be discussed and modelled in the next two sections:

- shear deformations
- sandwich behaviour
- buckling of barrier laminate for damaged VIPs
- second-order-effects

6.3.1 Shear deformation, sandwich behaviour and buckling

By a comparison with experimental results later in this section, it will be shown that a vacuum insulation panel under vacuum can be considered as having similar behaviour as a sandwich panel. It is thus important to realise that shear deformations need to be accounted for, as well. One way of dealing with shear deformations is splitting the total deflection of a beam or plate into a part resulting from pure bending and a part resulting from shear. The equations describing these parts are well-known and covered in many textbooks; they will therefore not be discussed here. A second way of dealing with shear deformations is incorporating them into an effective equivalent Young's modulus, $E_{eq;eff}$ [Pa] (Ashby, 2005). By doing this, deflections of vacuum insulation panels under different loads are calculated by solely using the equations for pure bending. A consequence however is that the effective equivalent Young's modulus not only depends on the cross-sectional properties of the VIP but also on the span and the way the panel is loaded; it thus becomes panel and context specific.

Equating the formulae for both deflection due to pure bending and shear deformation with the formula for pure bending alone results in a model for determining $E_{eq;eff}$. This model can generally be written as[2]

$$E_{eq;eff} = \frac{(EI)_{vip} \cdot (1-\overline{\nu^2})}{I_{vip}} \cdot \frac{1}{1+\xi \dfrac{(EI)_{vip}}{(GA)_{vip}}} \quad (6.2),$$

[2] A derivation of this equation for a four point bending test as an example is presented in appendix 610.

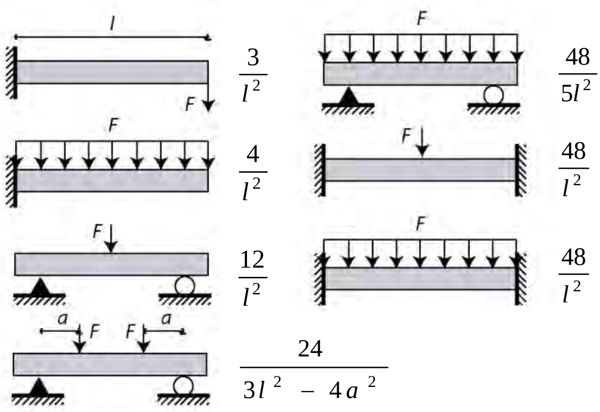

Figure 6.3

Factor ξ in equation (6.2) for several panel loading cases (partly derived from (Ashby, 2005).

in which ξ [m^{-2}] is a factor determined by the span and the way the panel is loaded as can be seen from Figure 6.3 (partly derived from Ashby (2005)), $\bar{\nu}$ is a weighted average Poisson's modulus of the core and the barrier film, and $(GA)_{vip}$ is the shear stiffness of the composite VIP system, calculated as (ASTM C 393, 1992)[3]

$$(GA)_{vip} = G_c \frac{(d_c + t_f)^2}{d_c} w_c + 2G_f \frac{(d_c + t_f)^2}{d_c} t_f \qquad (6.3),$$

with G_c [Pa] the shear modulus of the core, G_f [Pa] the shear modulus of the laminate, d_c [m] the thickness of the core, t_f [m] the thickness of the barrier envelope and w_c [m] the width of the core. The area moment of inertia of the VIP is determined from

$$I_{vip} = \frac{w_p d_p^3}{12} \qquad (6.4),$$

in which d_p [m] and w_p [m] are the panel thickness and width respectively (thus including thickness of barrier laminate).

[3] If a vacuum insulation panel structurally acts as a plate, then the structural parameters are mostly determined per square meter of plate. As a result, the effect of the barrier laminate at the panel's edges needs to be omitted. The parameters, w_c and w_p are then both set to unity in equations (6.3) to (6.7) and the terms that represent the influence of the barrier laminate at the panel's edges must be omitted in the equations (the second term of equation (6.3), the third and fourth terms of equation (6.6) and the third term in both the numerator and the denominator of equation (6.7)).

Assumed that the laminate is completely adhered to the core by means of friction due to a pressure difference over this barrier, the bending stiffness of an intact VIP, finally, is primarily determined by the Young's modulus of the laminate and the distance between its centroids on top and at the bottom; it is determined from

$$(EI)_{vip} = E_f \frac{\left(w_p d_p^3 - w_c d_c^3\right)}{12\cdot(1-\nu_f^2)} + E_c \frac{w_c d_c^3}{12\cdot(1-\nu_c^2)} \tag{6.5}$$

with E_c [Pa] the Young's modulus of the core, E_f [Pa] the Young's modulus of the barrier film, ν_c the Poission's ratio of the core and ν_f the Poission's ratio of the film.

In case of a vented VIP, the laminate is no longer 'adhered' to the core by friction. Consequently, the barrier on top of the VIP will almost immediately buckle after loading. The top barrier thus no longer partakes in structural action and must thus be omitted from the stiffness calculation. Moreover, the barrier envelope at the panel's sides above the neutral axis of the panel is assumed to also immediately buckle. The stiffness must therefore now be calculated using Steiner's rule as

$$\begin{aligned}(EI)_{vip,dam} &= E_f \frac{w_p t_f^3}{12\cdot(1-\nu_f^2)} + E_f \frac{w_p t_f}{(1-\nu_f^2)}\left[\frac{t_f}{2}+d_c-z_0\right]^2 + E_f \frac{t_f\left(d_c-z_0\right)^3}{6\cdot(1-\nu_f^2)} \\ &+ E_f \frac{t_f\left(d_c-z_0\right)^3}{2(1-\nu_f^2)} + E_c \frac{w_c d_c^3}{12\cdot(1-\nu_c^2)} + E_c \frac{w_c d_c\left(z_0-d_c/2\right)^2}{(1-\nu_c^2)}\end{aligned} \tag{6.6}$$

with z_0 [m] the distance from the top of the core material to the neutral plane of the entire cross-section of the damaged VIP. This distance is computed as

$$z_0 = \frac{E_c w_c d_c^2/2 + E_f w_p t_f\left(d_c + t_f/2\right) + E_f t_f\left(d_c^2 - z_0^2\right)}{E_c w_c d_c + E_f w_p t_f + 2E_f t_f\left(d_c - z_0\right)} \tag{6.7}$$

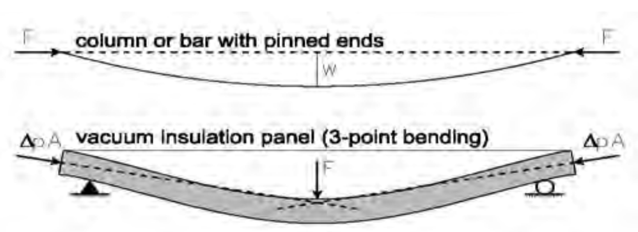

Figure 6.4

Second order effects for a pin-ended column and a VIP under flexion.

6.3.2 Second-order-effects

The Young's modulus of a VIP predicted with equation (6.2) may be slightly over- or underestimated since a deflection of the plate combined with a pressure force induced by the vacuum introduces an additional bending moment in the panel. In general mechanics theory this so-called second-order bending moment almost always results in an additional deflection, as a result increasing the second-order moment, which in turn increases the deflection, etc., etc. This second-order effect can directly be accounted for by reducing the Young's modulus (not reduced with shear effects) with a factor (n-1)/n (Gere and Timoshenko, 1999). In this factor, n is defined as the buckling force divided by the actual pressure load, or for a VIP as

$$n = \frac{F_{buc}}{N_d} = \frac{\pi^2 E_{eq;eff;vip} I_{vip}}{l_{buc}^2 \cdot \Delta p \cdot w_p \cdot d_p \cdot (1-\overline{\nu^2})} \qquad (6.8),$$

in which l_{buc} [m] is the buckling length of the VIP and Δp [Pa] is the pressure difference between the core and the surrounding atmosphere.

In case of VIPs, however, the external atmospheric pressure force always acts perpendicular to the outer shape of the panel, as shown in Figure 6.4. As a consequence, the lines of action of both atmospheric pressure forces do not coincide but intersect at mid span at a certain distance from the neutral plane, the exact position of which depending on the shape of the panel during bending. The influence of second-order-effects is thus smaller than in the case of a column with pinned ends as shown in Figure 6.4. Since the shape of a VIP during bending is hardly predictable and since, due to perpendicular action of the pressure force, second-order-effects are small, they are not considered when modelling the Young's modulus of a VIP.

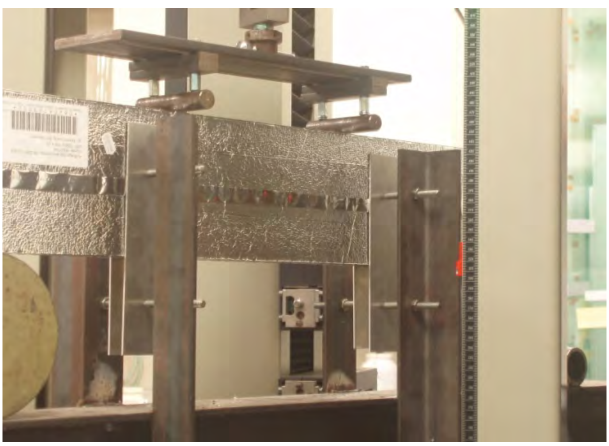

Figure 6.5

Four-point flexion testing of a vacuum insulation panel with a thickness of 20 mm, a panel height of 150 mm and a span of 690 mm.

Table 6.5 - Experimental and theoretical flexion modulus of VIPs evacuated and vented.

	d_p [mm]	l_{span} [mm]	w_p [mm]	a [mm]	E_0 [a,c,d,g] [MPa]	E_{eq} [b,c,e,f] [MPa]	$E_{eq;eff;i}$ [b,c,e,f] [MPa]
VIP: vacuum	20	300	150	75	38.5 ± 6.8	47.4 ± 1.6	44.8 ± 1.8
	150	690	20	190	17.2 ± 1.2	25.3 ± 1.5	22.1 ± 1.3
	20	200	120	40	32.9 ± 6.8	47.8 ± 1.6	42.6 ± 1.9
VIP: vented	20	300	150	75	20.9 ± 3.7	17.2 ± 2.2	16.9 ± 2.1
	150	690	20	190	13.6 ± 1.6	12.7 ± 1.7	11.8 ± 1.6
	20	200	120	40	16.6 ± 6.2	17.3 ± 2.2	16.5 ± 2.2
core	150	690	20	190	7.2 ± 1.4	-	-
	20	200	120	40	7.0 ± 1.3	-	-

[a] E_0 is determined from regression between a panel deflection from 1 to 3 mm during 4 point-bending tests. For the experiments on VIPs and core materials at least 4 panels and in some cases 6 panels have been tested for each panel dimension.

[b] Uncertainties in the values calculated with equation (6.2) arise from uncertainties in material data.

[c] Specified uncertainties are for a 95% reliability interval.

[d] In E_0 shear effects are included.

[e] From experiments into acoustical properties of VIPs, Maysenhölder (2008b) concluded that the Poisson's ratio of fumed silica lies between 0.3 and 0.4. A ratio of 0.4 is therefore used in the calculations. For the Poisson's ratio of the barrier laminate 0.4 is taken as well.

[f] The experimental values are corrected for deformations near load points and supports (Figure 6.6).

[g] The VIPs tested have very small seams at two edges and one at a surface. These small seams hardly influence the results. However, VIPs with larger taped flaps do exist as well. This additional material might increase the bending stiffness of a VIP to a small extent. These have not been tested though.

6.3.3 *Experimental results*

To determine this effective equivalent Young's modulus of a VIP and to check whether this theoretical model is valid for VIPs, four-point bending tests according to ASTM C 393 (1992) on several panel sizes have been conducted. The results of these tests with respect to VIP Young's moduli are summarised in Table 6.5 and compared to $E_{eq;eff;i}$ as calculated from equation (6.2). As can be seen from this comparison, the uncertainty intervals for both the measured and calculated Young's modulus in most cases partly while the average values are relatively close to one another, indicating that equation (6.2) predicts the Young's modulus of a VIP sufficiently accurately. The largest absolute difference between experimental data and measured data occurs for an intact VIP of 20x200x120 mm^3; the deviation between the average values is about 9.7 MPa (=29%). In all cases, model predictions yield somewhat higher values than measurements. This may indicate that the adherence between barrier envelope and core is not perfect enabling a small but discernible sliding between both elements, which may have occurred when the shear stresses along the interface between the film and the core increased to beyond a certain lower friction limit.

Moreover, a comparison between equivalent effective Young's moduli for VIPs under vacuum and damaged shows that the Young's modulus of a damaged VIP (no vacuum) is less than the Young's modulus of an undamaged VIP. This can be expected since the barrier envelope on top of the panel does partake in structural action if the core is under vacuum but does not partake in this action if there is no friction between core and envelope; in the latter case, the top film immediately buckles after loading. As an example, for the panel of 20 mm thick and 150 mm wide spanning 200 mm this reduction in $E_{eq;eff;vip}$ is almost 50%. It is however important to notice that the reduction factor depends on panel dimensions, on span and on loading situation.

A last effect that is indicated by the data in Table 6.5 is the reduction in Young's modulus for increasing panel thickness, d_p. Since the width of each measured panel differs, a realistic comparison is not possible based upon this data. However, the data does indicate that the Young's modulus decreases for increasing panel thickness. Figures 6.7a and 6.7b present the effective equivalent Young's modulus of an intact and vented VIP as function of span and panel thickness for a distributedly loaded and simply supported VIP of 1 m wide, computed according to section 6.3.1. These figures also indicate this effect.

The reason for this lies in the presence of shear deformations and in fact that a VIP is a composite system. With increasing panel thickness, the bending stiffness of the panel increases more rapidly than its shear stiffness since the bending and shear stiffness are proportional to the thickness to the third power and to the first power respectively. Shear therefore becomes relatively more important, i.e. the difference between E_{eq} and $E_{eq;eff}$ increases, if the thickness increases. Moreover and more importantly, if the thickness of a panel increases, the relative influence of the core material and the barrier envelope on the bending stiffness of a VIP composite changes. The equivalent Young's modulus was defined as bending stiffness $(EI)_{vip}$ divided by area moment of inertia I_{vip}. Neglecting the Poisson's ratio and substituting the equations for $(EI)_{vip}$ and I_{vip}, equation (6.1) can also be written as

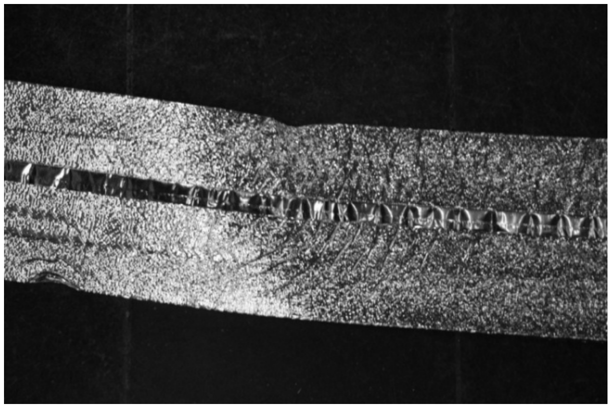

Figure 6.6

Deformations near the load points and supports.

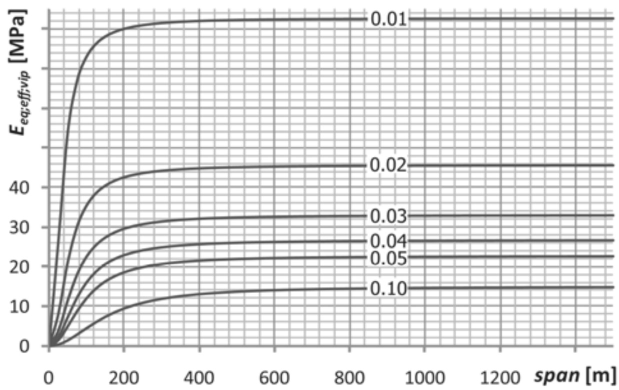

Figure 6.7a

Effective equivalent Young's modulus of an intact VIP having a width of 1000 mm (distributedly loaded and simply supported) as a function of span for several panel thicknesses (thickness is given in m).

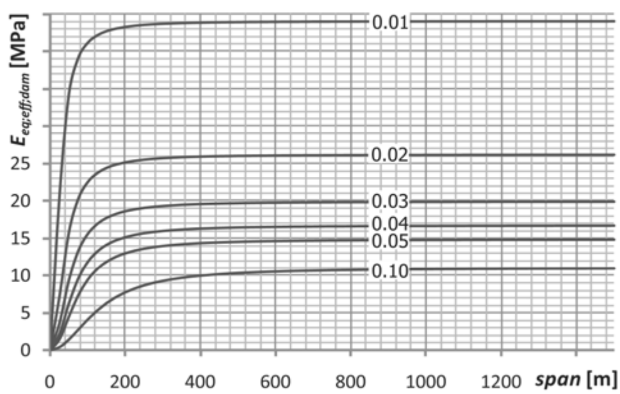

Figure 6.7b

Effective equivalent Young's modulus of a damaged VIP having a width of 1000 mm (distributedly loaded and simply supported) as a function of span for several panel thicknesses (thickness is given in m).

$$E_{eq} = E_f + \left(E_c - E_f\right)\frac{w_c d_c^3}{w_p \left(d_c + 2t_f\right)^3} \quad (6.9),$$

In the situation that $d_c >> t_f$ (and $w_c >> t_f$) the term $d_c^3/(d_c+2t_f)^3$ equals one and thus E_{eq} equals E_c. For all other situations the term $d_c^3/(d_c+2t_f)^3$ is smaller than one and thus E_{eq} is higher than E_c. With constant t_f one could say that the smaller d_c, the higher E_{eq} as can be seen from the figures as well. Especially this latter effect, i.e. the composite nature of a panel, strongly influences the value of the equivalent (effective) Young's modulus of a VIP. It is however important to realise that only the equivalent effective modulus decreases with increasing panel thickness and not the bending stiffness of the panel since the area moment of inertia plays a role too[4].

6.4 VIP Failure Behaviour (Flexion)

6.4.1 Assumptions and schematisation

Before a model that describes the failure behaviour of a VIP can be developed, first several assumptions and schematisations of the material behaviour and the geometry of a VIP must be made.

First, it is assumed that the failure behaviour of a VIP is analogous to that of reinforced concrete. This analogy implies that the core, which is similar to concrete weak in tension but strong in compression, is reinforced by the barrier envelope, which is similar to steel relatively strong in tension. However, from a certain critical stress in the top film onwards, this top barrier laminate starts to buckle and from then onwards only partly partakes in structural action.

Second, adhesion between the barrier envelope and the core material is assumed to be perfect as long as the VIP is intact. This adhesion results from (pressure-induced) friction between the 'rough' surfaces of the core and the barrier. The pressure normal to the surface of friction derives from the pressure difference between the inside of a VIP (vacuum) and its surroundings (atmospheric pressure) and approximately equals 1 bar. Since the aforementioned adhesion is perfect, no sliding of surfaces along each other is occurring.

[4] In appendix A611 some ideas on how to improve the bending stiffness of a vacuum insulation panel are given including their consequences on thermal performance.

Figure 6.8

Schematised stress-strain diagrams for a.) fumed silica core under compression and b.) fumed silica core under tension.

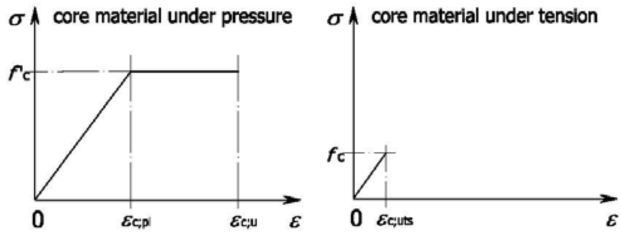

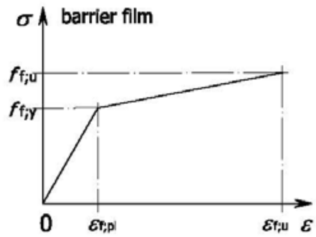

Figure 6.9

Schematised stress-strain diagrams for a three layer metallized high barrier film.

Table 6.6 – *Characteristic stress and strain values of the constituents of a VIP.*

constituent	$\varepsilon_{i;pl}$ [%]	$f_{i;y}$ [MPa]	$\varepsilon_{i;u}$ [%]	$f_{i;u}$ [MPa]
barrier laminate lam. 1[a,e]	4.6 ± 0.9	46.8 ± 0.1	128 ± 40	87.1± 3.6
metallisation layer[b]	-	-	4.0 ± 0.5	-
core material – compression[c, d]	40	0.73	n/a	n/a
core material – tension[c]	-	-	1.9 ± 0.4	$(4.7 \pm 1.3)\cdot 10^{-2}$

[a] Cauberg et al., 2006; [b] http://www.matweb.com; [c] Simmler et al., 2005 (measured at CSTB).

[d] Although the exact values of $\varepsilon'_{c;pl}$ and $f'_{c;y}$ are not available since the experiments presented in appendix A613 were terminated at $\varepsilon'_{c;pl}$ = 40%, these values are still used in computations in this chapter. This is acceptable since these properties only affect the final two stages in the failure behaviour of a vacuum insulation panel under flexion (start of up-setting in core compression zone and structural failure).

[e] Laminate type lam. 1 is the same as the MF3 laminate from previous chapters.

Third, since a VIP is a composite system, the failure behaviour of this system is determined by the mechanical behaviour of each constituent and the way these are attached to each other. As core fumed silica is used. This material is assumed to be linear elastic in tension and bi-linear elasto-plastic in compression. In section 6.2.1 the behaviour of fumed silica under static loading is presented in detail. Figure 6.8 and Table 6.6 present the schematised stress-strain diagrams of fumed silica and the characteristic stress and strain values. A three layer metallized polymer laminate is used as barrier envelope. The stress-strain diagram of this composite material is schematised according to Figure 6.9 as bilinear behaviour. The characteristic stress and strain values of this laminate are also displayed in Table 6.6.

Fourth, the model describing VIP failure is valid for VIPs loaded flexurally and is assumed to be force-controlled. This implies that no instant changes in load bearing capacity occur. As a result, however, instant changes in deflection and thus curvature can occur. If a certain constituent of the composite VIP system fails at a certain curvature or moment capacity, this constituent can no longer partake in structural action. As a consequence, either the moment capacity of the system immediately reduces or the deflection increases in order to find a new static equilibrium. Since the model is assumed to be force-controlled, the first cannot happen so the latter will occur.

6.4.2 Model describing VIP failure behaviour

Based upon the schematized diagrams and considering the behaviour of concrete, the failure process of a vacuum insulation panel can now be described concisely. This failure process needs to be subdivided into eight stages, the transitions between each of which describing a characteristic point in this failure process. Each characteristic transitions and the accompanying characteristic normal stresses and strains can be described by stress and strain diagrams through a cross-section of a VIP. These diagrams are shown in Figure 6.10, each displaying one of the transitions[5]:

- buckling of top barrier laminate (immediately before buckling)
- buckling of top barrier laminate (immediately after buckling)
- physical failure – rupture of metallization layer(s)
- start of yield of lower barrier laminate
- rupture of core material in tension zone (immediately before rupture)
- rupture of core material in tension zone (immediately after rupture)
- start of upsetting of core material in compression zone
- structural failure - failure of core material in compression zone

[5] The equations describing the stresses, strains, forces and moments in the VIP's cross-section during each transition are presented in appendixes A61 to A68. Using these equations, the curvature of a VIP and the load bearing capacity during each stage of the loading process can be estimated.

It is important to note that due to the pressure difference between the interior of the VIP and its surroundings, the core material is under hydrostatic compression when the VIP is not 'loaded'.

The first transition, buckling of top barrier laminate, is marked by the loosening of part of the barrier laminate at the top of the VIP. As long as the compressive stress in this top barrier laminate stays below a critical value, the pressure exerted by the atmosphere onto the VIP causes the barrier laminate to stick onto the core material. However, if a certain critical stress is exceeded, small discontinuities in the flatness of the barrier envelope, due to irregularities in the surfaces of both the laminate and the core, cause the barrier laminate to buckle. This situation of barrier envelope attached to core material can be schematised as a very thin plate supported by a bed of springs. Davies (2001) derives an equation for this critical stress for buckling of thin face sheets of sandwich panels. It is calculated as

$$\sigma_{buc} = \frac{3}{2}\left[\frac{2(1-\nu_c)^2}{3(1+\nu_c)^2(3-4\nu_c)^2(1-\nu_f^2)}\right]^{1/3}\left(E_c^2 E_f\right)^{1/3} \tag{6.10}$$

in which ν_c [-] is the Poisson's ratio of the core material, ν_f [-] is the Poisson's ratio of the barrier laminate, E_c [N·m^{-2}] is the Young's modulus of the core material and E_f [N·m^{-2}] is the Young's modulus of the barrier laminate. This buckling stress defines the strain of the barrier laminate, ε_{buc}, and thus also the strain in the topmost layer of the core material, the latter of which equals the sum of ε_{buc} [-] and ε_p [-], the compressive strain resulting from atmospheric compression (=Δp / E_c = 1,013·10^5 / E_c = 5.48·10^{-2}). Using force equilibrium within the cross-section then results in the unknown strain in the bottommost layer of the core and the bottom barrier envelope, which due to symmetry equals the equivalent values in the top barrier and topmost layers of the core. Based upon these strains, the maximum bending moment the VIP can uptake, M_{buc} [N·m], as well as the curvature, κ_{buc} [m^{-1}], can be calculated. The governing equations are presented in appendix A61.

Immediately after buckling, the second transition must be discerned. Right before buckling, the cross-section of the VIP can still be considered symmetric. However, after buckling most of the load bearing capacity of the top barrier laminate diminishes as a consequence of which the curvature increases instantly, at least theoretically[6]. Since the model is assumed to be force-controlled, the bending

[6] This immediate increase of the curvature of the loaded VIP results from the assumption that the model is force-controlled. In practical situations, however, these step changes will be concealed by more gradual behaviour.

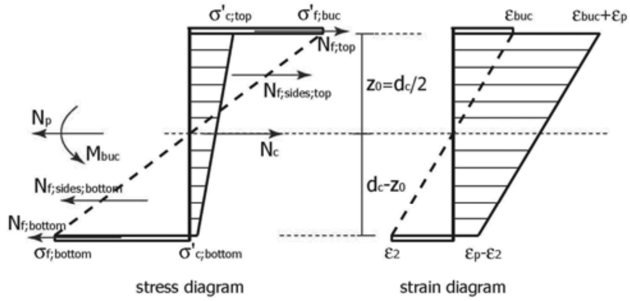

Figure 6.10a

Stress and strain diagrams for the load case buckling of top barrier laminate (right before buckling).

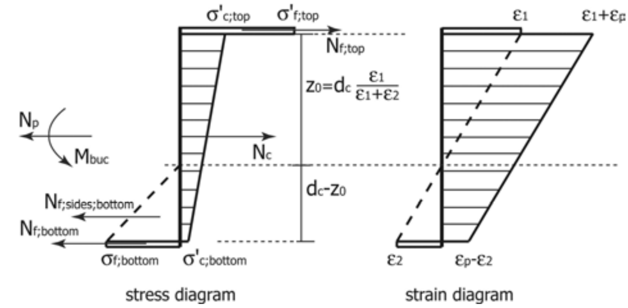

Figure 6.10b

Stress and strain diagrams for the load case buckling of top barrier laminate (right after buckling).

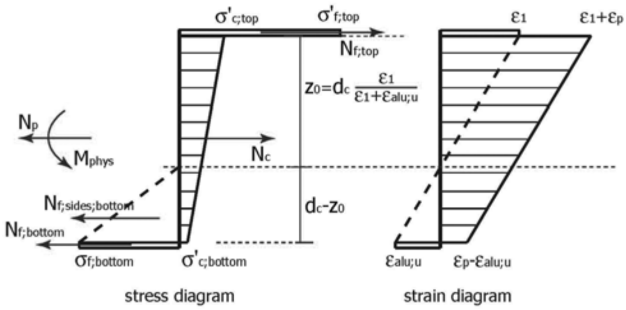

Figure 6.10c

Stress and strain diagrams for the load case physical failure (crack initiation in metallic barrier layer).

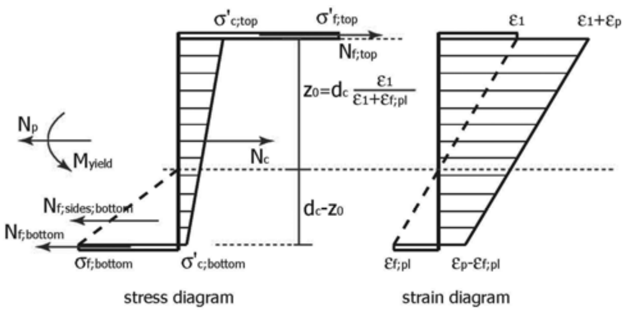

Figure 6.10d

Stress and strain diagrams for the load case start of yield in lower barrier laminate. Diagrams are valid before the occurrence of cracks in the core material.

Figure 6.10e

Stress and strain diagram for the load case crack initiation in the tension zone of the core material (immediately before rupture). Diagrams are valid after start of yield in lower barrier envelope.

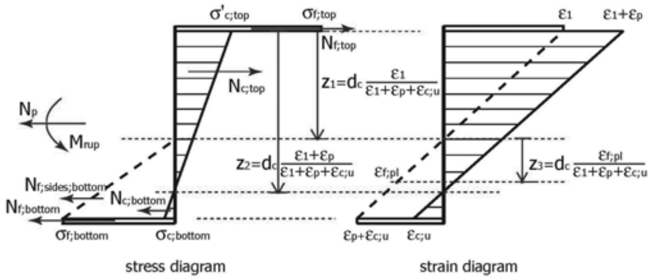

Figure 6.10f

Stress and strain diagram for the load case crack initiation in the tension zone of the core material (immediately after rupture). Diagrams are valid after start of yield in lower barrier envelope.

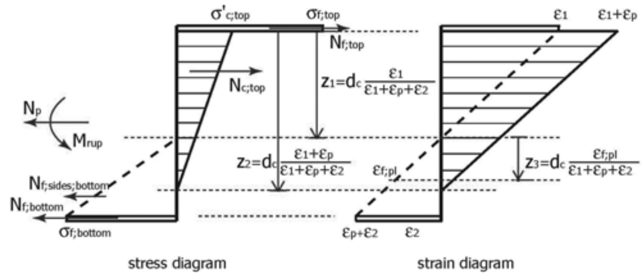

Figure 6.10g

Stress and strain diagram for the load case upsetting of the core material in the compression zone. Diagrams are valid after start of yield in lower barrier envelope and crack occurrence in core material.

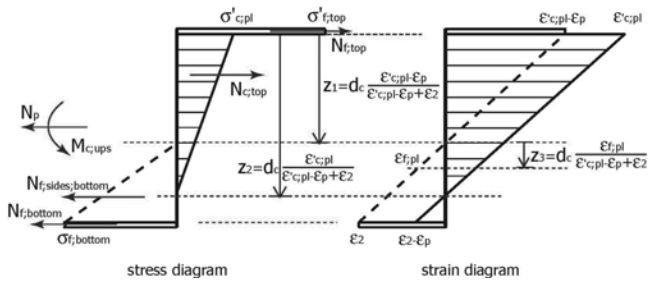

Figure 6.10h

Stress and strain diagram for the load case structural failure of the core material in the compression zone. Diagrams are valid after start of yield in lower barrier envelope and crack occurrence in core material.

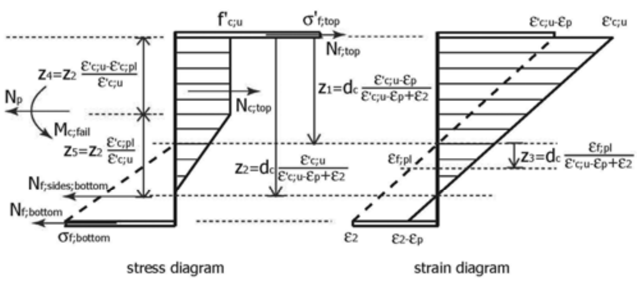

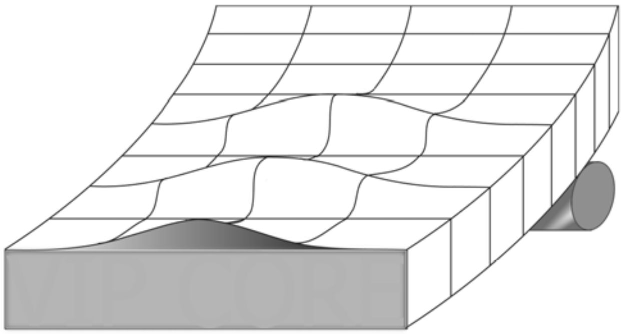

Figure 6.11

Visualisation of the effect of local buckling in the top barrier laminate.

moment the VIP is able to uptake must equal the one calculated for the previous transition, M_{buc}. Both force and moment equilibrium then yields the unknown stains at the top and bottom of the cross-section. The equations describing the forces, bending moments, strains and curvature are presented in appendix A62. It is important to note two observations. First, at this transition the stresses everywhere in the core material are still tensile, as long as fumed silica and a metallized polymer barrier laminate are used. Second, four-point bending experiments described in section 6.4.3, showed that buckling in the top barrier laminate does not occur over the complete width of this top barrier laminate but is localised to only a small part of this width, approximately 50%. The reason for this is that at the edges of the panel where the laminate goes from the top to the sides of the panel (Figure 6.11), the laminate is restricted in its movement due to its shape. Therefore, it is assumed in the model that only a part of the top barrier buckles. The width of this top barrier is therefore reduced to $c_{\text{buc}} \cdot w_c$, with c_{buc} [-] a factor describing the ratio of the width that does not buckle to the total width of barrier laminate, or in other words it is a measure for the amount of the top barrier laminate that still partakes in structural action. w_c is the width of the core material, or the width of the total VIP, w_p, minus two times the width of the barrier laminate at the panel's sides[7].

The third transition is factually not a big change in structural behaviour of the VIP; it is determined by crack initiation in the aluminium or the metallization layer of the bottom barrier laminate. Since this aluminium or this metallization is the

[7] At the sides of the vacuum insulation panel, the barrier envelope might also buckle partly in the zone above the neutral plane where the barrier envelope is under compression. For these buckling effects, also local buckling might occur. In the VIP failure model developed, it is assumed that the entire barrier envelope at the sides of the panel above the neutral plane - thus the barrier envelope under compression – buckles and no longer partakes in structural action. Effects of local buckling at the panel's sides are included in the factor c_{buc} since this factor is determined from data fitting to experimental results.

principal barrier against water vapour and atmospheric gas permeation, cracks in this layer may significantly increase the permeance, thus reducing the VIP's service life. As a consequence, the vacuum inside the system will be lost more quickly changing the mechanical properties of the bond between core and envelope on the long run as well. Since cracks will presumably be small, the rate of vacuum loss, however, is considered to be small enough so that resulting changes in structural behaviour may be neglected. This step can be characterised as the beginning of physical failure, in contrary to structural failure being the final step. At this point of physical failure, the strain in the laminate in the tension zone equals the fracture strain of the aluminium or metallization layer, $\varepsilon_{\mathrm{alu;u}}$. Although the laminate consists of several material layers, each of which having its own mechanical behaviour, it is assumed to act as one material having average stress and strain characteristics. Based upon that assumption, the tensile stress in the bottom film at this stage equals a stress between 0 MPa and the yield strength of the laminate, $f_{\mathrm{f;y}}$ [N·m^{-2}]. Force equilibrium results in knowledge of the strain in the topmost barrier laminate and the core material. From these strains the maximum bending moment, $M_{\mathrm{phys,}}$ and the curvature, κ_{phys}, can be determined. The equations are presented in appendix A63.

When after continuous loading the stress in the lower barrier laminate reaches its yield strength, $f_{\mathrm{f;y}}$, the lower barrier starts to yield, which is the fourth transitions. The strain in bottom laminate than equals its yield strain, $\varepsilon_{\mathrm{f;pl}}$, while the strain in the lowest layers of the core equals $\varepsilon_{\mathrm{f;pl}}$ - ε_{p}. Since $\varepsilon_{\mathrm{p}} = 5.48 \cdot 10^{-2}$ (atmospheric pressure difference and fumed silica core) and $\varepsilon_{\mathrm{f;pl}} = 4.6 \cdot 10^{-2}$ (three layer metallised film), the strain in the lowest layers of the core material is always negative (upsetting), for all panel geometries. The strain in the topbarrier laminate and the topmost layers of the core material can be obtained from force equilibrium within the cross-section. The bending moment that the panel can uptake, M_{yield}, and the curvature at this transition, κ_{yield}, can be calculated from the equations in appendix A64.

When in the core material in the lowest layers tensile stresses start to occur and when these stresses increase to the tensile strength of the core material, the next transition has arrived. Cracks in the core material start to occur. As with concrete, these cracks immediately grow towards the neutral plane where the stress in the material is zero. As a consequence, from this point onwards, that part of the core material below the neutral plane (of the core material) will no longer participate in structural action since it has already lost cohesion. Immediately before crack initiation, the tensile stress in the lowest layers of the core material equals, its tensile strength, $f_{\mathrm{c;u}}$ [N·m^{-2}] and the strain equals the strain at rupture, $\varepsilon_{\mathrm{c;u}}$ [-]. As a result, the strain in the bottom barrier laminate equals $\varepsilon_{\mathrm{c;u}} + \varepsilon_{\mathrm{p}}$. The strains in the top barrier laminate and the topmost layers of the core materials can again be obtained from force equilibrium. . The bending moment that the panel can uptake, M_{rup}, and the curvature at this transition, κ_{rup}, can be calculated from the equations in appendix A65. It is important to note that, with the material used (Table 6.6), this transition always succeeds yield in the lower barrier envelope since the sum of $\varepsilon_{c;u}$ + ε_{p} equals $1.9 \cdot 10^{-2} + 5.48 \cdot 10^{-2} = 7.4 \cdot 10^{-2}$ while the strain at which yield in the barrier laminate occurs, $\varepsilon_{f;pl}$, equals $4.6 \cdot 10^{-2}$.

Due to the aforementioned instantaneous crack growth towards the neutral plane, the curvature of the panel will increase without a change in structural capacity, i.e. the internal moment will remain constant, M_{rup}. This is defined as the sixth transition. Since in this case all strains are unknown, force and moment equilibrium are required to obtain the unknown strains in the core and barrier. The equations governing this stage are presented in appendix A66. It is important to realise that in the model developed from this point onwards, that part of the core material below its neutral plane no longer partakes in structural action. In reality however, fibres within the core material are able to bridge the cracks and still partly contribute to the structural behaviour of the vacuum insulation panel as a whole. This effect is however assumed to be marginal and therefore neglected.

Stresses in and strains of the constituents of a VIP will continue to increase until the core material reaches its elastic limit from which point onwards upsetting starts to occur. This point is the next transition in the failure model of a vacuum insulation panel. This upsetting is the beginning of plastic behaviour in the compression zone of the core material. The strain in the outermost top layer of the core material then equals the strain at upsetting, $\varepsilon'_{c;pl}$, while the corresponding stress in this layer equals the upsetting stress of fumed silica, $f'_{c;y}$. The strain in the top barrier laminate equals the difference of this strain at upsetting, $\varepsilon'_{c;pl}$, and ε_{p}. The unknown strains at the bottom of the cross-section can be obtained again from force equilibrium, for which the equations are presented in appendix A67.

This process of upsetting in the core continues until the maximum upsetting has been reached. This point is defined arbitrarily and designated transition 8; it corresponds to complete structural failure of the VIP system[8]. At this point it is assumed that the stress distribution through a cross-section of the core material equals the shape of its stress-strain diagram (Figure 6.8a). This same assumption is used for the definition of structural failure of reinforced concrete. The strain of the topmost layer of the core material then equals the fracture strain, $\varepsilon'_{c;u}$, while the strain in the top barrier laminate again equals the difference between this strain and ε_{p}. Force equilibrium then again results in knowledge of the unknown strains at the bottom of the cross-section. The equations are presented in appendix A68.

---

[8] Structural failure might also occur earlier if a non-ductile barrier material is used. In that case failure occurs because the barrier envelope is loosing its integrity due to crack initiation and rupture. However, the VIPs tested and modeled had a ductile barrier envelope as a result of which failure of the core material preceded failure of the lower barrier envelope.

Figure 6.10a to h show the development of the stresses and strains through a cross-section of the VIP composite system. It must be noted however that these diagrams are indicative and do not show correct proportions. The position of the neutral plane within the core material and the barrier envelope, for instance, changes from transition to transition. The position of the neutral plane in the barrier envelope measured from the top layer of the core material - z_1 [m] is the distance from the interface between core material and top barrier laminate to the neutral plane in the barrier envelope - first moves downwards until yield in the bottom barrier laminate (transition 4) and then moves upwards again. Also the position of the neutral plane in the core material – z_2 [m] is the distance from the interface between core material and top barrier laminate to the neutral plane in the core material - moves upwards from core rupture onwards (transition 5). The stress and strain diagrams presented in Figure 6.10 do not clearly indicate this behaviour. The position of both neutral planes can be calculated using the geometric relations presented in Figure 6.10.

Based on the equations presented in appendixes A61 to A68 and the stress-strain diagram displayed in Figure 6.10, the complete structural behaviour of a vacuum insulation panel under bending can be plotted in a moment – curvature diagram, or a (M-κ)-diagram. Figure 6.12 presents a typical example of such an (M-κ)-graph of a VIP flexurally loaded[9]. As can be seen, the defined transitions are clearly discernible and reflect a change in structural behaviour, represented by a change in slope of the graph. Since the constitutive relation for flexed beams tells us that bending moment divided by curvature, i.e. the slope of the graph, equals flexural stiffness, the transitions defined in the failure model thus indicate changes in flexural stiffness, $(EI)_{vip}$. Determining (M-κ)-diagrams thus enables engineers to estimate the flexural stiffness of a VIP composite during every stage of the loading process.

***Table 6.7** – Overview of calculated moment capacity and curvature at physical failure.*

	d_p [mm]	l_{panel} [mm]	w_p [mm]	l_{span} [mm]	a [mm]	M_{phys} [N·m]	κ_{phys} [N·m]
VIP: vacuum	20	350	150	300	75	11.3	8.6
	150	750	20	690	190	29.5	1.0
	20	250	120	200	40	9.1	8.6

[9] The continuous lines in Figure 6.13 are calculated using the equation from the appendixes A61 to A68. These calculations show a jump in curvature when buckling of the top high barrier laminate and rupture of the core material occurs. In practice, however, such jumps are not likely to occur; a more gradual transition will take place. Therefore broken lines are added to the graph representing such gradual transition.

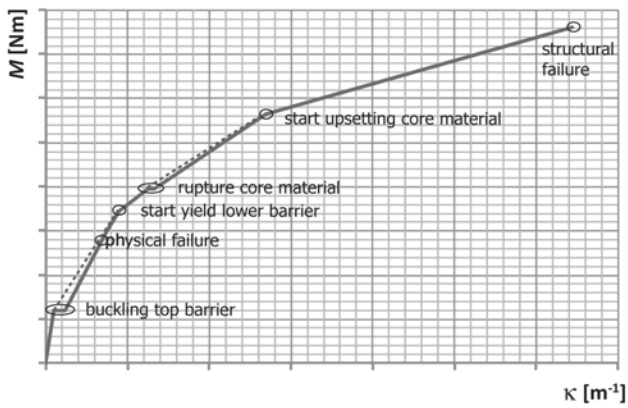

Figure 6.12

Typical moment-curvature diagram for a vacuum insulation panel loaded in bending calculated with the failure model.

6.4.3 Comparison of model to experimental results

To validate the failure model presented in the previous section, several four-point bending tests according to ASTM C393 (1992) have been conducted on intact VIPs. Table 6.8 gives an overview of the tests conducted and the Young's modulus derived from the first part of the (M,κ)-diagrams and from the model developed in section 6.3. As can be seen, the Young's modulus directly derived from the (M,κ)-diagrams differs from the Young's modulus determined by the model developed in section 6.3. This difference results from several effects:

- Shear effects: In the E-model (section 6.3), the Young's modulus was corrected for shear effects, while these effects are not accounted for in the failure model. As shown in appendix 69, both methods should result in the same values for the bending stiffness and thus Young's modulus of a VIP if in both models shear effects are not considered, if no Poisson's ratios are used and if $t_f << d_c$.
- Different values for the Young's modulus of the core material and the barrier envelope are used. For the E-model (section 6.3), the tangent moduli at ε=0 are used. These tangent moduli, or actually secant moduli with a very short interval near ε=0, were determined in section 6.2. For the failure model secant moduli determined within the interval from ε=0 to $\varepsilon=\varepsilon_{pl}$ were used. These secant moduli can be calculated from the properties presented in Table 6.6. It turns out that these secant moduli are somewhat smaller than the the tangent moduli at ε=0 ($E_{f;tan}$ = 1355 MPa; $E_{f;sec}$ = 1017 MPa; $E_{c;tan}$ = 7.0 MPa; $E_{c;sec}$ = 1.8 MPa). Especially this effect has a significant effect on the aforementioned differences.
- The failure model does not include the influence of Poisson's ratios while the E-model does. In case of the E-model both the Poisson's ratio of the barrier envelope and the core material were set to 0.4.

Table 6.8 *– Overview of conducted flexion tests and initial Young's modulus according to (M,k)-diagram.*

	d_p [mm]	l_{panel} [mm]	w_p [mm]	l_{span} [mm]	a [mm]	$E_{eq;eff;vip}$ [MPa]		
						Experiments	*failure model*	*E-model*
VIP: vacuum	20	350	150	300	75	38.5 ± 6.8	31.9	41.7 ± 7.3
	150	750	20	690	190	17.2 ± 1.2	15.4	22.2 ± 2.1
	20	250	120	200	40	32.9 ± 6.8	32.2	38.9 ± 7.3

A second observation from the table is that the experimental values of the Young's modulus in all cases lie between the values determined with the E-model and with the failure model. The values of the experimental Young's moduli and the modeled moduli are relatively close to one another for both the E-model and the failure model. It can therefore be concluded that both models predict the modulus of elasticity of a VIP with sufficient accuracy to be used in building practice.

A comparison of the experimental (M,κ)-diagrams to the calculated ones (Figures 6.13 to 6.15) shows that the failure model quite accurately predicts the behaviour of the VIPs under bending. The deviations between both are very small. The experiments on VIPs with a width of 150 mm, a height of 20 mm and aspan of 300 mm even clearly show a short plateau where buckling of the top barrier envelope occurs. During the experiments this buckling was visually observed as well. The deflection from the straight line the experiments on these panels show after a strain of about 6% results from sliding of the test specimen over the supports and must therefore not be contributed to the behaviour the bending behaviour of the panel[10].

However, due to limitations (safety and geometrical limits) in the testing apparatus only the first part of the (M,κ)-diagram could be experimentally verified. The analogy to reinforced (pre-stressed) concrete, however, indicates that the behaviour beyond this first part is likely to happen the way it is presented. The exact location of transitions, though, should be used carefully since no verification is available of yet.

[10] The experiments on VIPs with a width of 150 mm, a height of 20 mm and a span of 300 mm were conducted on a testing machine different from the one used for the other panels. The 300 mm spanning panels were tested using a 10 kN Instron tester at the faculty of Civil Engineering and Geosciences (TUDelft) while the other panels were tested with a 1 kN Zwick tester at the faculty of Architecture (TUDelft). The 10 kN tensile testing machine in fact was too heavy as a consequence of which the results from this machine are less accurate.

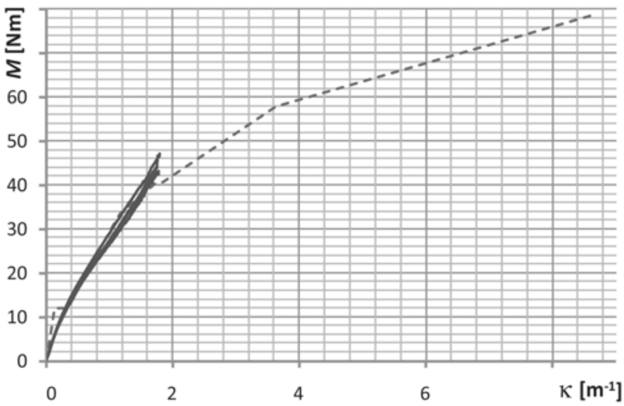

Figure 6.13

(M,k)-diagram for a vacuum insulation panel with a fumed silica core and a three layer metallized film. The continuous lines represent experimental results while the broken line is a calculated result.

load type: 4-point bending
height: d_c = 150 mm
width: w_c = 20 mm
span: l_{span} = 690 mm
load-to-span dist.: a = 190 mm

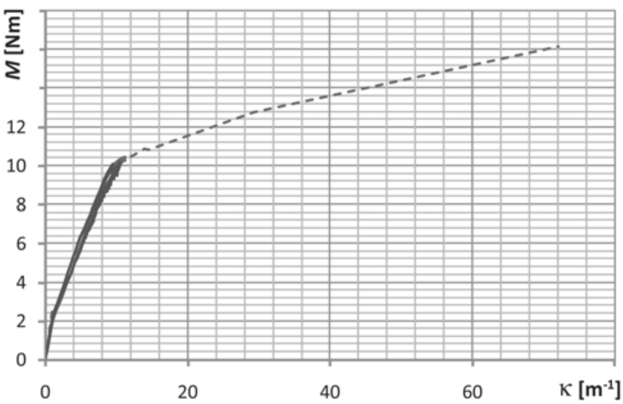

Figure 6.14

(M,k)-diagram for a vacuum insulation panel with a fumed silica core and a three layer metallized film. The continuous lines represent experimental results while the broken line is a calculated result.

load type: 4-point bending
height: d_c = 20 mm
width: w_c = 120 mm
span: l_{span} = 200 mm
load-to-span dist.: a = 40 mm

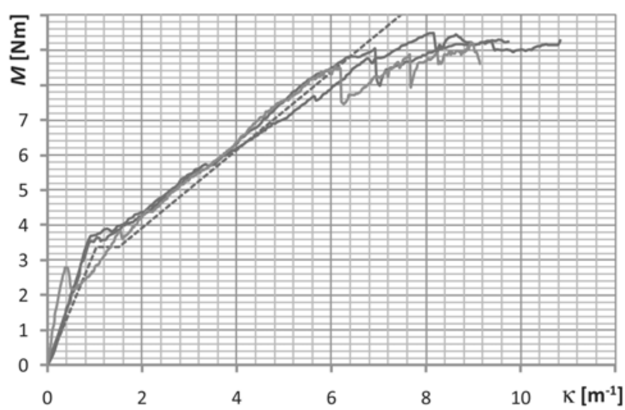

Figure 6.15

(M,k)-diagram for a VIP with a fumed silica core and a three layer metallized film. The continuous lines represent experimental results while the broken line is a calculated results. Only first part of (M,k)-diagram shown.

load type: 3 + 4-point bending
height: d_c = 20 mm
width: w_c = 150 mm
span: l_{span} = 300 mm
load-to-span dist.: a = 75 mm

6.4.4 Limitations and remarks

Regarding the failure model, several limitations need to be specified and remarks be made. First, the model is solely valid for the specified sequence of transitions. As was tested extensively, the sequence always occurs in this order if the specified materials, or in fact material properties, are used. If, however, different materials are used as VIP constituents then the sequence might change. In that situation it is important to realise that the methodology used to derive the equations and to determine the transitions is still valid. The exact equations, though, slightly change and must therefore be derived again for that specific sequence.

Second, shear effects are not considered in the model. As explained in section 6.3 such shear effects do influence the deflection of a beam or plate and can be incorporated in an effective Young's modulus. Especially with squat beams these shear effects can be significant. In case of thin beams of plates with a large span, these effects are rather small. Moreover, in the models secant moduli within the interval from ε=0 to $\varepsilon=\varepsilon_{\text{pl}}$ were used. These moduli of elasticity are smaller than the tangent moduli used for the E-model.

Third, the failure model uses a correction factor, c_{buc}, which includes local buckling of the barrier laminate at the panel's top. In the model, this correction factor solely represents local buckling phenomena in the top barrier while in reality such buckling might also occur in the compression zone of the barrier laminate at the panel's sides, in these areas in which the compressive stress increases to beyond the buckling stress as calculated according to the model by Davies (2001). The value of c_{buc} however was determined by fitting the failure model (beyond buckling) to the experimental data and might thus also include other effects than solely local buckling of the top barrier laminate, like local buckling of the side laminates and shear (after buckling). A regression analysis on this data showed that the value of c_{buc} was between 0.48 and 0.51 for all panels studied which does indicate that using c_{buc} is a valid way of dealing with these effects[11].

Fourth, the failure model assumes perfect sandwich behaviour. This implies that a perfect connection exists between the barrier envelope and the core material, except for buckling. Due to this perfect connection the barrier envelope does not

[11] This buckling effect of the top (and probably side) barrier laminate was not studied in more detail experimentally. Additional four point bending tests should then be executed in which either a high resolution camera, high accuracy distance meters using laser beams or a set of small displacement meters attached to the top surface of a panel should be used. These additional tests were not performed since the experiments into the mechanical behavior of VIPs were meant as getting a first good impression of their structural behaviour. Moreover, in case a VIP is not structurally loaded as in façade panels with a spacer along their edge, this behavior is no longer relevant and if a VIP is used in a sandwich panel, buckling of the top barrier film can only occur at high stresses due to its connection to a face sheet.

slide over the core material but is always fixed to it. In the experiments however such sliding is likely to have occurred when the shear stresses along the interface between the film and the core increase to beyond a certain lower friction limit. Since the value of c_{buc} however was determined from experiments, this correction factor does also take sliding into account.

6.5 CONCLUSIONS AND SUMMARY

The mechanical properties of fumed silica as core material for VIPs loaded in bending have been studied experimentally. These tests showed that the Young's modulus of the fumed silica samples tested was approximately 7 MPa which is somewhat higher than the Young's modulus of most plastic foams. These values are in the same order of magnitude as found by Simmler et al. (2005). The flexural strength was found to be around 47 kPa.

The mechanical properties of two potential barrier laminates – an aluminium foil laminate and a three layer metallised laminate - have been tested in a tensile testing machine as well. These materials exhibited plastic behaviour and strain hardening beyond the plastic limit. For a three layer metallised film commonly used with commercially available VIPs this plastic limit was at a tensile stress around 47 MPa and strain around 5% while failure occurred at a stress of about 87 MPa and at a strain of about 130% (Table 6.6). This laminate can thus be characterised a ductile. It is here important to mention that the plastic limit should normally be used in failure analyses since it indicates functional failure.

A vacuum insulation panel is a composite system and must therefore be regarded as such. For this composite system the analogy to reinforced (pre-stressed) concrete is applicable. The core material then is analogous to the concrete matrix, the barrier envelope surrounding this core is the reinforcement and the atmospheric pressure causes a pre-stress in the core material. Moreover, the mechanical behaviour of the constituents of a VIP resembles the constituents of reinforced concrete. Similar to the concrete matrix, fumed silica can withstand a very small tensile but high compressive stress. Like steel reinforcement bars, the barrier envelope on the other hand can uptake high tensile stresses.

Experimental flexion tests on both intact and vented VIPs showed that the Young's modulus significantly reduces when a VIP is damaged. For a panel with a height of 150 mm, a width of 20 mm and a span of 300 mm, the Young's modulus, in which shear effects are considered, approximately halves when it gets damaged. The exact reduction of the flexion modulus depends on panel geometry (height and width of core material and thickness of barrier envelope) or on panel geometry and context (type of leading) if the shear effects are also considered in the Young's modulus. The reduction in Young's modulus is caused by the structural inactivity of the barrier envelope in the compression zone in case a VIP is vented.

Considering its cross-sectional geometry and assuming a perfect interface between the barrier laminate and the core (no sliding), the Young's modulus of a VIP composite system can be modelled as an equivalent Young's modulus, E_{eq}, which considers the composite nature of a VIP, or as an equivalent effective Young's modulus, $E_{eq;eff}$, which also includes shear effects. It is important to realise that both E_{eq} and $E_{eq;eff}$ are not material properties but depend on the material properties of the constituents of the composite, the cross-sectional geometry and, in case of $E_{eq;eff}$, also on the type of loading and span.

As was verified both by experiments and by the aforementioned *E*-model, the higher, i.e. the thicker, the vacuum insulation panel (d_p), the lower the equivalent effective flexion modulus; and the shorter the span, the lower the equivalent effective flexion modulus. It must be noted again that E_{eq} solely depends on the cross-sectional geometry of a VIP and thus not on span and loading type.

A comparison between experimental results and the *E*-model showed that the *E*-model is a model sufficiently accurate to predict the flexion modulus of a VIP. The relative difference between both results was largest for a VIP with a thickness of 20 mm, a width of 120 mm and a span of 200 mm and amounts to approximately 29%. The absolute difference between both moduli for this panel is 6 MPa.

Using the analogy of reinforced (pre-stressed) concrete, the entire flexural behaviour of a vacuum insulation panel can be modelled. The transitions between the separate stages in the structural behaviour of a VIP under flexion are: buckling of the barrier laminate at the panel's top (immediately before and immediately after buckling), physical failure, yield of the barrier laminate at the panel's bottom, crack formation in the tension zone of the core material (immediately before and immediately after rupture), up-setting in the compression zone of the core material and finally structural failure. Although structural failure is the final stage in the failure process of a VIP, physical failure, i.e. the formation of (micro-)cracks in the aluminium or metallisation layer of the barrier laminate, strongly influences the panel's service life. Moreover, we have seen in this chapter that the Young's modulus of a vented VIP is much smaller than of an intact VIP. For reasons of safety therefore, either the transition of physical failure or the behaviour of a vented VIP should be taken as limit state, the choice of which depending on which of the two poses the highest restrictions.

The sequence of transitions presented in the previous section, is valid for the combination of materials used: fumed silica as core material and a three layer metallised film as barrier laminate. In case of other materials, i.e. different material properties, are used, the sequence might change. As a result, the equations determining the stress, strain, moment and curvature might slightly change, too. The methodology used to determine the transitions, however, remains the same.

Using the failure model, so-called (M,κ)-diagrams can be constructed, depicting the bending moment capacity and the curvature of a panel loaded flexurally. The slope of such (M,κ)-lines equals the bending stiffness of a panel during each stage of the process. From this bending stiffness, a Young's modulus can be obtained as well. Comparison of this Young's modulus to the moduli derived from experiments and the E-model shows that they are relatively close to one another. The differences between the Young's modulus derived from the (M,κ)-diagram and the E-model arise from several effects: shear effects, which are included in the E-model but not in the failure model; the use of different values for the Young's modulus of the core material and the barrier envelope in both models, i.e. tangent modulus versus secant modulus; and the inclusion or otherwise of Poisson's ratios.

Notwithstanding simplifications and despite the limitations specified in section 6.4.4, the failure model is a model sufficiently accurate to be used for determining the bending behaviour of a vacuum insulation panel. It enables designers and engineers to estimate the moment capacity of a panel at both physical and structural failure.

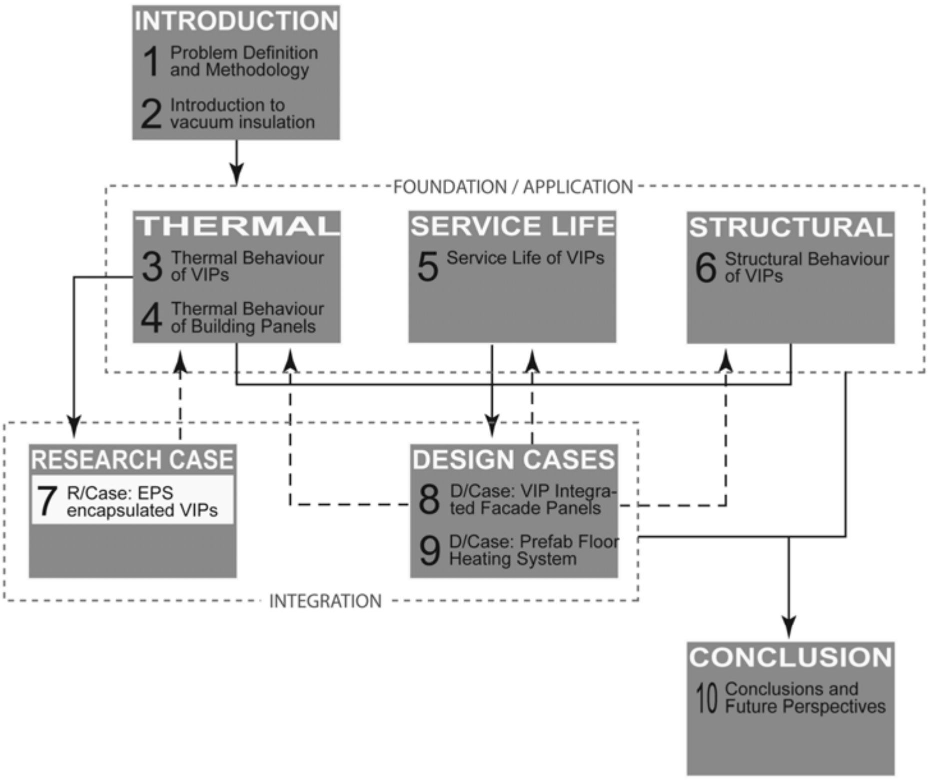
INTRODUCTION
1 Problem Definition and Methodology
2 Introduction to vacuum insulation
FOUNDATION / APPLICATION
THERMAL
3 Thermal Behaviour of VIPs
4 Thermal Behaviour of Building Panels
SERVICE LIFE
5 Service Life of VIPs
STRUCTURAL
6 Structural Behaviour of VIPs
RESEARCH CASE
7 R/Case: EPS encapsulated VIPs
DESIGN CASES
8 D/Case: VIP Integrated Facade Panels
9 D/Case: Prefab Floor Heating System
INTEGRATION
CONCLUSION
10 Conclusions and Future Perspectives

7

R/ Case: EPS encapsulated VIPs

Research Case Study into the effects of incorporating a VIP into an EPS insulation board on overall thermal performance

Very often for reasons of protection, reduced dimensional tolerances or ease of installation, a vacuum insulation panel is integrated into an EPS insulation board. Such boards however have a disadvantage that an additional thermal bridge is created along the panel's perimeter due to a strip of EPS. Commissioned by industry therefore, a parameter study into the effects of adding a VIP to an EPS insulation board on thermal performance has been executed. In this study several tools for calculating the overall thermal performance of such a component have been used: numerical simulation software, the analytical models presented in chapters 3 and 4 and international standards. The effect of multiple parameters was investigated: thermal conductivity of the VIP core, thickness of barrier envelope, VIP thickness, thickness of EPS layers and width of EPS strips along the component's perimeter.

Section 7.1 starts with an introduction into existing EPS encapsulated VIPs, into the type of panel studied in this chapter and the boundary conditions for this study. In section 7.2 then a 3D numerical analysis is performed. These analyses result in the observation that a local maximum in thermal performance exists at a certain thickness of the VIP inside the component. In section 7.3 this phenomenon is studied in more detail two-dimensionally using numerical simulation software and analytical models. After these analyses, an analytical model presented in chapter 3 is used to proof the existence of the aforementioned phenomenon.

7.1 INTRODUCTION

7.1.1 Encapsulated VIPs

Due to the very thin barrier laminate foil-VIPs are very fragile; besides, a VIP is a prefabricated component having high dimensional tolerances ranging from +2 to -5 mm in length and width and from +1 to -1 mm in thickness (Va-Q-tec AG, 2008)[1]; moreover, due to its prefabricated nature, a VIP can not be cut or shaped on site without losing performance. Therefore vacuum insulation panels are sometimes integrated into an additional insulation board or protected by an additional material. First it is important to clearly define these encapsulated VIPs. They are prefabricated high performance insulation components consisting of a foil-VIP core (core material and barrier envelope), enclosed in and rigidly connected to a material of lesser insulation quality. In practise two types can be distinguished presented in Figure 7.1: EPS or PU encapsulated VIPs in which EPS or PU foam encloses a VIP on all sides (top, bottom and perimeter); and fleece, rubber or polymeric foam covered VIPs in which a protective material covers a VIP on one or either surface (top and/or bottom).

Several manufactures already produce or use both of the aforementioned types of encapsulated VIPs. The first type with PU foam for example was used by Variotec (Stölzel, 2003) as core for high performance spandrel and door panels as can be seen in Figure 7.2[2]. Moreover, in a demonstration project for a Passivhaus in

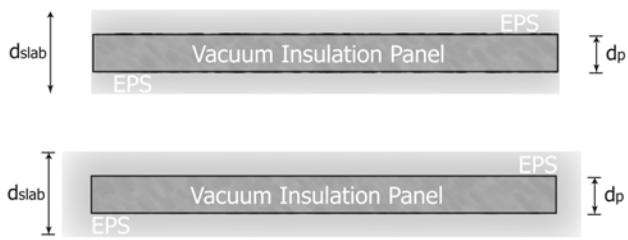

Figure 7.1

Schematic representation of an EPS encased VIP (top) and an EPS encapsulated VIP (bottom).

[1] Dimensional tolerances stated by Variotec (2007) are -2 to +3 mm for length and width and +2 mm for thickness. Porextherm (2005) specifies tolerances of +1 to -2 mm for sizes from 0 to 500 mm, +1 to -4 mm for sizes from 500 to 1000 mm and +1 to -6 for sizes larger than 1000 mm. The tolerance for panel thickness is specified as +1 to -1 mm from 0 to 20 mm, +1 to -2 mm from 20 to 30 mm and +1 to -3 mm for panels thicker than 30 mm.

[2] These panels are however no longer mentioned in the booklet *Veni Vici VIP* by Variotec (2007). Instead the booklet mentions sandwich elements (Qasa-light and Qasa-sandwich) with either 0.3 mm thick aluminium or 4 mm thick high density (500 kg·m^{-3}) massive PU face sheets. These panels should however be considered as 'regular' building panels.

Figure 7.2

Vacupur - PU encapsulated VIP inside a spandrel panel (Stölzel, 2003).

Bersenbrück EPS encapsulated VIPs were applied for insulating massive façade walls (Zwerger and Klein, 2005a; Zwerger and Klein, 2005b; Platzer et al., 2005). To reduce thermal bridges due to the EPS edge strips, an additional layer of 80 mm EPS was added to the wall, so that an effective *U*-value of 0.147 was achieved with a total thickness of the insulation layer of 140 mm of which 20 mm VIP. Zwerger and Klein (2005a) argues that this additional layer of insulation can be omitted if EPS only covers the top and bottom surface of a VIP and not the perimeter as a result reducing thermal edge effects. With such a system, we obtain the second type of encapsulated VIP. In the framework of an exhibition for the construction industry in Trier, Germany, 12 row houses by Lamberty/Schmitz & Hoffmann Architects were insulated with these EPS covered VIPs. Also manufacturers, like Va- Q-tec AG (Va-Q-VIP B) and Porextherm (Vacupor NT-B2, Vacupor RP and Vacupor PS), have brought VIP products on the market with added protective materials on both sides of the panel. Two of them have been technically approved by the German Institute for Building Technology (DIBt Z-23.11-1662 and DIBt Z-23.11-1658).

Some researchers did also small-scale studies into the effects of applying an additional insulation layer to a vacuum insulation panel. In their study for reducing the thermal bridge effect due to stainless steel barriers around VIPs by creating so-called serpentine edges, Thorsell and Källebrink (2005) and Thorsell (2006a; 2006b) also investigated the effect of an additional insulation layer on the linear thermal transmittance of VIP edges. As can be seen from Figure 7.3, they found that the linear thermal transmittance of a VIP edge decreases for decreasing boundary heat transfer coefficient[3], i.e. for increasing insulation layer thickness[4]. This analysis was performed for a 30 mm thick VIP ($\lambda_c = 5.0 \cdot 10^{-3}$ W·m^{-1}·K^{-1}) with a stainless steel

[3] This was called coefficient of surface heat transfer in the work of Thorsell.

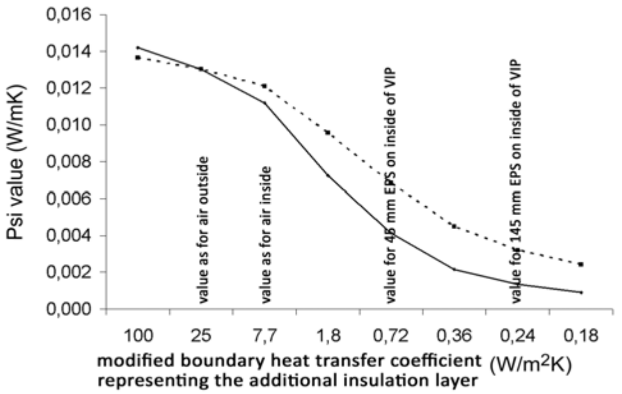

Figure 7.3

Effect of modified boundary heat transfer coefficient, representing the adjoining insulation layers, on the linear thermal transmittance of a 30 mm thick VIP with a stainless steel barrier and a serpentine edge configuration (Thorsell and Källebrink, 2005).

Continuous line: insulation added to one side of the VIP; Broken line: insulation added to both sides of the VIP.

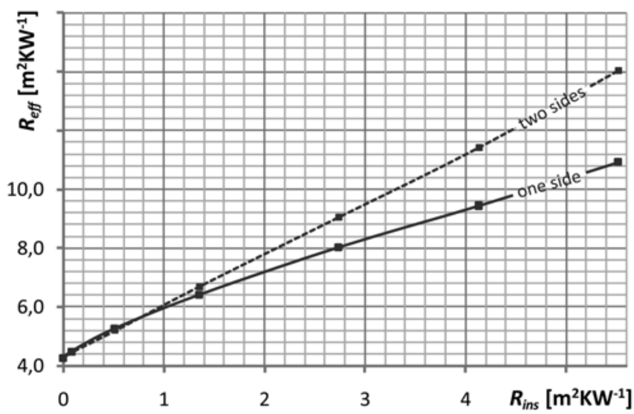

Figure 7.4

Effect of adjoining insulation layers on the effective thermal resistance of a 30 mm thick VIP with a stainless steel barrier and a serpentine edge configuration recalculated from Thorsell and Källebrink (2005).

barrier envelope (λ_f = 15 W·m^{-1}·K^{-1}) with a serpentine edge. The results however will be similar if the panel would not have such an edge. These linear thermal transmittance results are used to calculate the overall thermal resistance including boundary resistances, R_{eff} [m^2·K·W^{-1}], to show the effect of adding insulation layers on one or both sides of a VIP. The results are presented in Figure 7.4. As can be seen, the overall thermal performance of the encapsulated VIPs studied increases if the thermal resistance of the insulation layer increases.

---

[4] An insulation layer adjoining a VIP has a certain thickness, d_{ins}, and thermal conductivity, λ_{ins}. These two properties can combine in a thermal resistance as d_{ins} / λ_{ins}. Along the surface of all materials exposed to air a boundary heat transfer coefficient exists, which is the reciprocal value of a boundary heat transfer resistance. As a simplification, both resistances can be superposed to form a total resistance between the VIP and the surrounding air. This total resistance then can be considered as a modified boundary heat transfer resistance. It is important to note here that in this simplification some information concerning the influence of insulation thickness especially near thermal bridges gets lost.

Not only Thorsell and Källebrink studied the influence of adjoining insulation layers, also Ghazi Wakili et al. (2005) and Willems et al. (2005) studied did. Ghazi Wakili et al. (2005) researched a VIP with a thickness of 20 or 30 mm, with a metallised barrier and a thermal conductivity, λ_c, of $8.0 \cdot 10^{-3}$ W·m^{-1}·K^{-1}, which is the common 25 years prediction value, encapsulated by 10 mm material with variable thermal conductivity on all sides. Willems et al. (2005) studied EPS encapsulated VIPs incorporating VIPs with a thickness of 10 to 40 mm, with a metallised barrier and a thermal conductivity, λ_c, of $8.0 \cdot 10^{-3}$ W·m^{-1}·K^{-1} encapsulated by EPS of variable thickness. Both reached similar conclusions as Thorsell and Källebrink (2005).

As an empirical study finally, Nussbaumer et al. (2006) studied the application of an EPS encapsulated VIP attached to a concrete wall among others using a guarded hot box apparatus. They showed that such components with 40 mm VIP could improve the thermal performance of a concrete wall with 95% and that in accordance with previously mentioned studies the protective EPS layers reduce the thermal edge effect of the high barrier laminate along the VIP's perimeter. These results make a more in-depth study of such EPS encapsulated VIPs very interesting.

Table 7.1 *– Parameters used for modelling and simulating an EPS encapsulated VIP.*

parameter	symbol	value	unit
thickness of VIP	d_p	10/20/30/40/50	mm
thickness of slab	d_{slab}	100	mm
thickness of aluminium layer in laminate	t_f	40	μm
total laminate thickness	$t_{f;tot}$	$= t_f + 50 = 90$	μm
thickness of alu. in laminate near edge [a]	t_e	$= t_f / \varphi = 40/0.67 = 60$	μm
total laminate thickness near edge	$t_{e;tot}$	$= t_{f;tot} / \varphi = 135$	μm
length of EPS slab	l	1000	mm
width of EPS slab	w	1000	mm
VIP to VIP distance	a_{mid}	50	mm
VIP to edge distance 1	$a_{edge;1}$	25/50	mm
VIP to edge distance 2	$a_{edge;2}$	25/50	mm
length of VIP	$= 1000 - 2a_{edge;1} = 950$ or 900		mm
width of VIP	$= 500 - a_{edge;2} - a_{mid}/2 = 450$ or 425		mm
chamfer length of corners	b	50	mm
thermal conductivity VIP core	λ_c	$4.0/6.0/8.0 \cdot 10^{-3}$	W·m^{-1}·K^{-1}
thermal conductivity laminate	λ_f	160	W·m^{-1}·K^{-1}
thermal conductivity Polystyrene	λ_{EPS}	$36 \cdot 10^{-3}$	W·m^{-1}·K^{-1}
temperature 1	T_i	293	K
temperature 2	T_e	273	K
boundary heat transfer coefficient	α_i	7.8	W·m^{-2}·K^{-1}
boundary heat transfer coefficient	α_e	25	W·m^{-2}·K^{-1}

[a] φ is explained in subsection 3.3.4 on page 79. Half of the laminate along the edge is 90 μm and half of it 3x90 μm. A small part of the seam is assumed to protrude along the surface of the VIP. $\varphi = 0.67$ was therefore chosen representing a seam in-between types b and c (page 78).

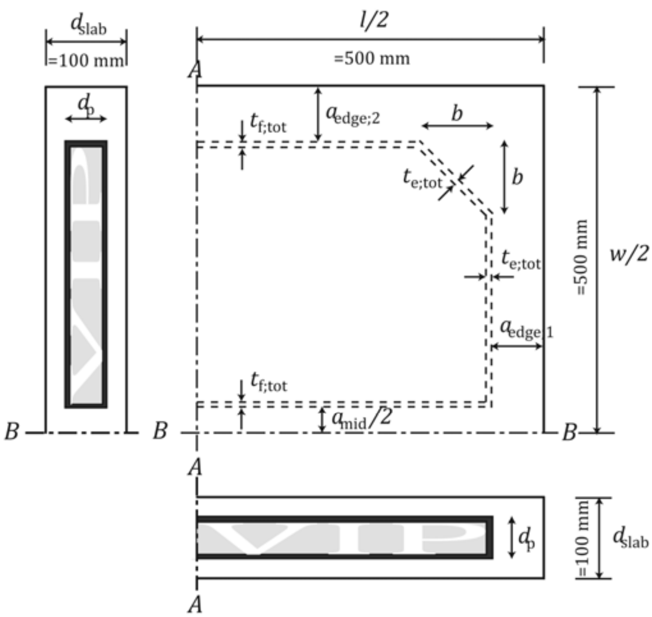

Figure 7.5

Schematic representation of a quarter of an EPS encapsulated VIP.

7.1.2 Background of case-study

Commissioned by the industry, a parameter study has been executed into the thermal improvement of EPS insulation boards by integrating VIPs. It was executed for panels with a fixed size of 1x1 m^2 and fixed thickness of 100 mm[5]. Such an element with fixed outer dimensions was filled with two identical VIPs having variable thickness and size. The dimensions and geometry of this component are presented in Figure 7.5 and Table 7.1. Only a quarter of an EPS encapsulated VIP was simulated to reduce computation time and to still have sufficient accuracy despite the limitations of the software (32K nodes). Within this parameter study, the influence of three parameters on the effective thermal resistance was studied:

- The thickness of the VIPs, d_p: 0, 10, 20, 30, 40, 50, 60, 75, 90, 95 and 99 mm;
- The thermal conductivity of the VIP core, λ_c: $4.0\cdot10^{-3}$, $6.0\cdot10^{-3}$ and $8.0\cdot10^{-3}$ $W\cdot m^{-1}\cdot K^{-1}$;
- The width of the EPS edge, $a_{edge,1}$ and $a_{edge,2}$: 25 and 50 mm.

[5] The type and size of the panel was specified by a manufacturer. This specification included the outer dimensions of the EPS insulation board, the shape of the VIPs, the existence and size of EPS at the edges, and the choice for an aluminium foil laminate with an aluminium layer of 40 μm to safeguard the service life at all cost.

To study these variations systematically, numerical simulations using the ANSYS for three-dimensional and Trisco for two-dimensional models were run. One result of such an analysis is the heat flow through the element from the warm side of the panel towards the cold side, Q [W]. This heat flow can be used to determine the average or effective thermal resistance of the plate, $R_{c;\mathrm{eff}}$ [$m^2 \cdot K \cdot W^{-1}$] as[6]

$$R_{c;eff} = \frac{S \cdot \Delta T}{Q} - \frac{1}{\alpha_i} - \frac{1}{\alpha_e} \qquad (7.1),$$

in which S is the surface area of the EPS encapsulated VIP (=$0.5w \cdot 0.5l$ =0.25 m^2 for 3D simulations). Using this R-value as a measure of overall thermal performance, performance improvement by adding a VIP to an EPS insulation board can now be studied. An EPS insulation board with a thickness of 100 mm is used as reference having a thermal resistance, $R_{c;0}$, of 2.778 $m^2 \cdot K \cdot W^{-1}$. In the 3D parameter study the barrier laminate consisted of a 40 μm thick aluminium foil (with a thickness of 60 μm along the panel's edge)[3]. In the 2D study the thickness of this barrier varied.

7.2 3D Parameter Study

The results of the numerical simulations according to the method and 3D model described in the previous section are presented in Table 7.2 in form of a thermal resistance ratio being the calculated effective thermal resistance divided by the thermal resistance of a 100 mm thick EPS insulation board. This resistance ratio reflects the improvement of the thermal performance of the EPS insulation board by adding a vacuum insulation panel. Moreover, Figure 7.6 presents a subset of the results graphically: the effective thermal resistance of an EPS encapsulated VIP with $a_{\mathrm{edge},1}$=25 mm and $a_{\mathrm{edge},2}$=50 mm.

As can be seen, the thermal performance of an EPS encapsulated VIP decreases with increasing thermal conductivity of the VIP core. This is not surprising since an increase of λ_c conduces to an increased heat flux through the central area of the component. For an EPS encapsulated VIP with a total thickness of 100 mm, with a 20 mm thick VIP and with EPS of 25 mm along its edge, for instance, the effective thermal resistance is 3.71 $m^2 \cdot K \cdot W^{-1}$ if $\lambda_c = 4.0 \cdot 10^{-3}$ $W \cdot m^{-1} \cdot K^{-1}$ and 3.33 $m^2 \cdot K \cdot W^{-1}$ if $\lambda_c = 8.0 \cdot 10^{-3}$ $W \cdot m^{-1} \cdot K^{-1}$.

---

[6] It is important to note that all thermal resistances specified in this chapter from section 7.2 onwards are resistances of the material only, thus without boundary resistances of the interface between material and air.

Table 7.2 *– Results of the parameter study of an EPS encapsulated VIP using ANSYS numerical simulation software: thermal resistance ratio, $R_{c;eff}$ / $R_{c;0}$ [-].*

		$a_{edge;2}$ [mm]	25		50	
λ_c [Wm^{-1}K^{-1}]	d_p [mm]	$a_{edge;1}$ [mm]	25	50	25	50
$4.0\cdot10^{-3}$	10		1.27	1.24	1.24	1.22
	20		1.34	1.30	1.31	1.27
	30		**1.35**	**1.31**	**1.32**	**1.28**
	40		1.34	1.29	1.31	1.27
	50		1.32	1.27	1.28	1.24
$6.0\cdot10^{-3}$	10		1.19	1.17	1.18	1.16
	20		1.26	1.23	1.23	1.21
	30		**1.27**	**1.24**	**1.25**	**1.22**
	40		1.27	1.23	1.24	1.21
	50		1.25	1.21	1.22	1.18
$8.0\cdot10^{-3}$	10		1.14	1.13	1.13	1.12
	20		1.20	1.18	1.18	1.16
	30		**1.21**	**1.19**	**1.19**	**1.17**
	40		1.21	1.18	1.19	1.16
	50		1.19	1.16	1.17	1.14

Moreover, the overall thermal performance of an EPS encapsulated VIP decreases with increasing width of the EPS strips along its edge which is to be expected too since the thermal conductivity of EPS is higher than of evacuated fumed silica. The wider the EPS edge strips thus, the worse the thermal bridge and as a result the worse the component's overall thermal performance. In illustration, for an EPS encapsulated VIP with a total thickness of 100 mm, with a 20 mm thick VIP and with $\lambda_c = 4.0\cdot10^{-3}$ W·m^{-1}·K^{-1}, the effective thermal resistance was found to be 3.71 m^2·K·W^{-1} if the EPS edge strips are 25 mm and 3.53 m^2·K·W^{-1} if these strips are 50 mm.

Besides, as already discernible from Table 7.2 but more clearly visible from Figure 7.6, a maximum in effective thermal performance exists for a certain VIP thickness. For all the EPS encapsulated VIPs studied three-dimensionally, this maximum lies near a VIP thickness of 30 mm. Contrary to expectation thus the thermal performance does not improve beyond a certain thickness of the VIP despite that the thermal performance of the central area, i.e. not considering thermal bridges, does increase proportional to VIP thickness. The cause for the existence of such a maximum in thermal performance must therefore be related to thermal edge effects caused by the use of aluminium. In the next section this phenomenon is studied in detail and explained using two-dimensional numerical and analytical models.

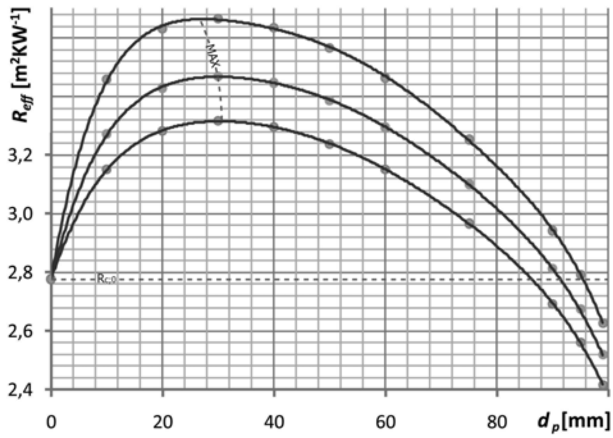

Figure 7.6

Effective thermal performance of an EPS encapsulated VIP with a 40 μm aluminium barrier envelope (AF:40).

$a_{edge,1}$=25 mm;
$a_{edge,2}$=50 mm;

top: λ_c=4.0·10⁻³ W·m⁻¹·K⁻¹;
middle: λ_c=6.0·10⁻³W·m⁻¹·K⁻¹;
bottom: λ_c=8.0·10⁻³ W·m⁻¹·K⁻¹.

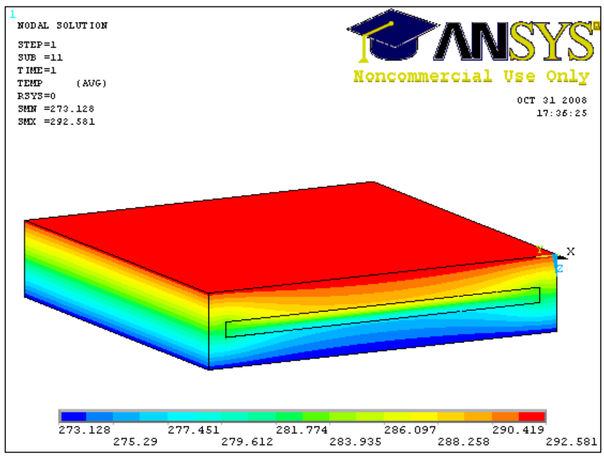

Figure 7.7a

Temperature distribution through the cross-section A-A of an EPS encapsulated VIP with a 40 μm aluminium barrier envelope (AF:40).

$a_{edge,1}$ = 25 mm;
$a_{edge,2}$ = 50 mm;
λ_c = 4.0·10⁻³W·m⁻¹·K⁻¹;
α_1 = 7.8 W·m⁻¹·K⁻¹;
α_2 = 25 W·m⁻¹·K⁻¹;
T_1 = 293 K;
T_2 = 273 K.

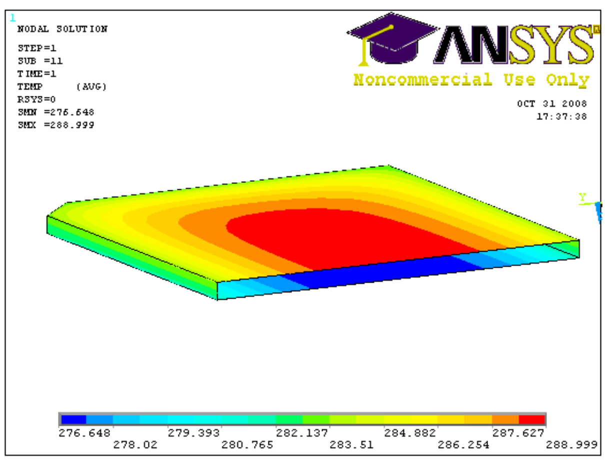

Figure 7.7b

Temperature distribution at the interface between the 40 μm aluminium barrier envelope (AF:40) and EPS.

$a_{edge,1}$ = 25 mm;
$a_{edge,2}$ = 50 mm;
λ_c = 4.0·10⁻ W·m⁻¹·K⁻¹;
α_1 = 7.8 W·m⁻¹·K⁻¹;
α_2 = 25 W·m⁻¹·K⁻¹;
T_1 = 293 K;
T_2 = 273 K.

A last interesting and important observation related to the previous phenomenon is that the thermal performance of an EPS encapsulated VIP with very thick VIP (beyond 85 resp. 95 mm depending on the thermal conductivity of the core material) drops even below the performance of a 100 mm thick EPS board. For an EPS encapsulated VIP with a total thickness of 100 mm, with $\lambda_c = 4.0 \cdot 10^{-3}$ W·m^{-1}·K^{-1} and with EPS strips of 25 mm along its edge, e.g., the effective thermal resistance is 2.78 m^2·K·W^{-1} if no VIP is present and 2.63 m^2·K·W^{-1} if a VIP of 99 mm is inserted. So, a very thick vacuum insulation panel inside an EPS mantle does not automatically imply an improved thermal performance relative to an equally thick EPS insulation board.

7.3 2D Analysis of Phenomenon of Maximum in Thermal Performance

The phenomenon that a maximum in thermal performance occurs for an EPS encapsulated VIP at a certain thickness of this VIP inside is studied in more detail in this section using a two-dimensional model with only one thermal bridge at one edge of a component. It is studied numerically using the software tool TRISCO and analytically both using the model for calculating the linear thermal transmittance presented previously in this chapter and the calculation procedure described in ISO 6946:2007 (2007). The numerical simulations are according to the method of section 4.2 and equation (7.1) while the analytical results are obtained according to the model of section 4.3.1 and equation (4.3).

The 2D model consists of a VIP (core and barrier envelope) integrated into an EPS board. The EPS layers on top and below the VIP are of equal thickness (=(0.1-d_p)/2). The total thickness of the EPS encapsulated VIP component, the width of the component's central area and the width of the EPS edge strip are kept constant at 100 mm, 500 mm and 25 mm respectively. The thickness of the VIP within the component, d_p, is varied from 1 to 99 mm while the thickness of the aluminium foil in the barrier laminate, t_f, is varied from 0 to 6 to 10 to 20 to 40 μm. The thermal conductivity of the VIP core and the boundary heat transfer coefficients are kept constant at $4.0 \cdot 10^{-3}$ W·m^{-1}·K^{-1}, 7.8 W·m^{-2}·K^{-1}and 25 W·m^{-2}·K^{-1}. As a result of this configuration only one linear thermal bridge consisting of both the aluminium layer and the EPS edge strip is studied.

Figure 7.8[7] gives a graphic overview of the results of the effective thermal resistance calculation as function of VIP thickness. The figure summarises three

[7] The numbers accompanying the markers and continuous lines represent the thickness of the aluminium foil based barrier envelope, t_f.

Figure 7.8

Effective thermal resistance of an EPS encapsulated VIP (2D model) as function of VIP thickness d_p (abscissa) and foil thickness t_f (different lines).

markers: numerical results;
continuous lines: analyt. model
dotted lines: ISO 6946;
dashed line: no thermal bridge;

$\lambda_c = 4.0 \cdot 10^{-3}$ W·m^{-1}·K^{-1};
$\lambda_f = 160$ W·m^{-1}·K^{-1};
α_1=7.8m^2·K·W^{-1}; α_2=25m^2·K·W^{-1}.

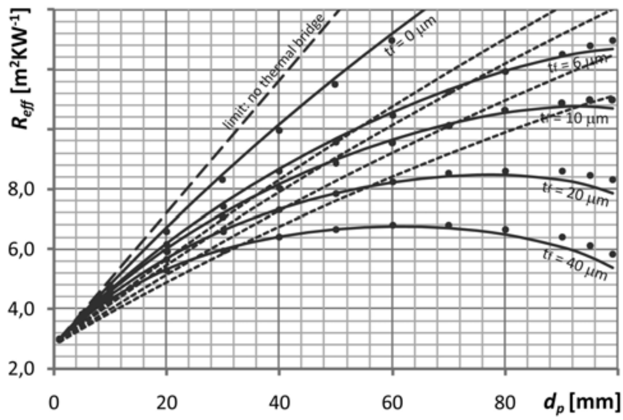

Figure 7.9

Effective thermal resistance as function of VIP thickness of a VIP with an EPS edge strip of 25 mm and no EPS top and bottom layers.

a1.) with modified boundary heat transfer coefficients [W·m^{-2}·K^{-1}] on both sides (broken lines);
a2.) with boundary heat transfer coefficients common for air inside and outside (broken line);
b.) the corresponding EPS encapsulated VIP (continuous line).

$\lambda_c = 4.0 \cdot 10^{-3}$ W·m^{-1}·K^{-1};
$\lambda_f = 160$ W·m^{-1}·K^{-1};
$t_f = 40$ µm.

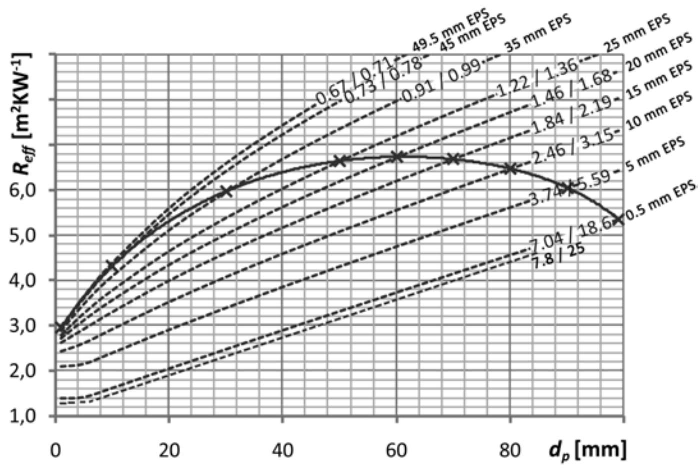

Figure 7.10

Schematic drawing of the 2D calculation model of an EPS encapsulated VIP with (top) and without (bottom) EPS layers on top and at the bottom of the VIP. The top drawing corresponds to Figure 7.8 while the bottom drawing corresponds to Figure 7.9.

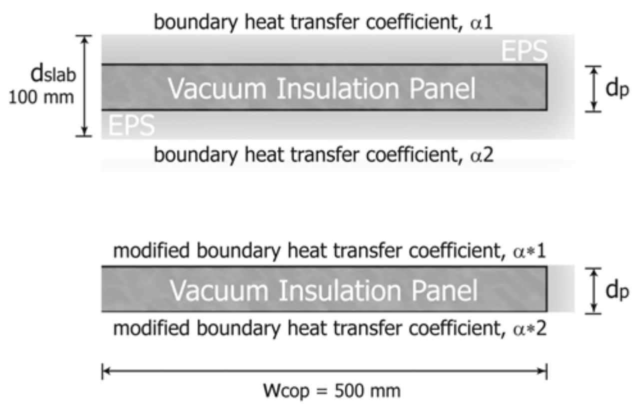

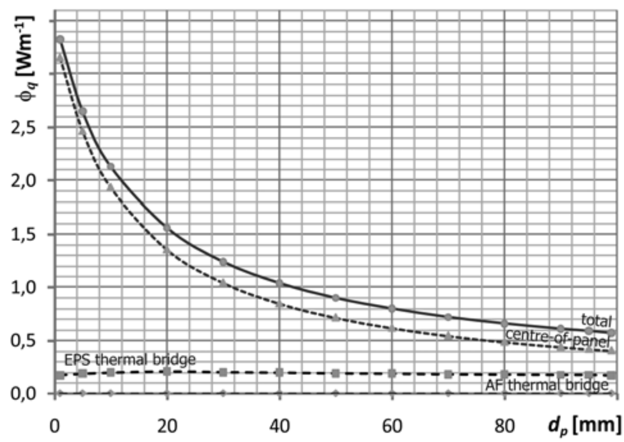

Figure 7.11a

Decomposition of the heat flows through all elements of the EPS encapsulated VIP component (2D model) as function of VIP thickness.

t_f = 0 μm alu.; *d_{slab} = 100 mm; a_{edge} = 25 mm; w_{cop} = 500 mm; $\lambda_c = 4.0 \cdot 10^{-3}\ W \cdot m^{-1} \cdot K^{-1}$; $\lambda_f = 160\ W \cdot m^{-1} \cdot K^{-1}$; $\varphi = 0.67$; $\alpha_1 = 7.8 m^2 \cdot K \cdot W^{-1}$; $\alpha_2 = 25 m^2 \cdot K \cdot W^{-1}$.*

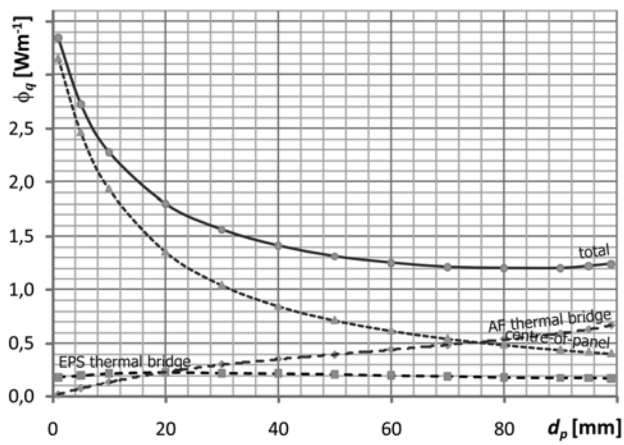

Figure 7.11b

Decomposition of the heat flows through all elements of the EPS encapsulated VIP component (2D model) as function of VIP thickness.

t_f = 20 μm alu.; *d_{slab} = 100 mm; a_{edge} = 25 mm; w_{cop} = 500 mm; $\lambda_c = 4.0 \cdot 10^{-3}\ W \cdot m^{-1} \cdot K^{-1}$; $\lambda_f = 160\ W \cdot m^{-1} \cdot K^{-1}$; $\varphi = 0.67$; $\alpha_1 = 7.8 m^2 \cdot K \cdot W^{-1}$; $\alpha_2 = 25 m^2 \cdot K \cdot W^{-1}$.*

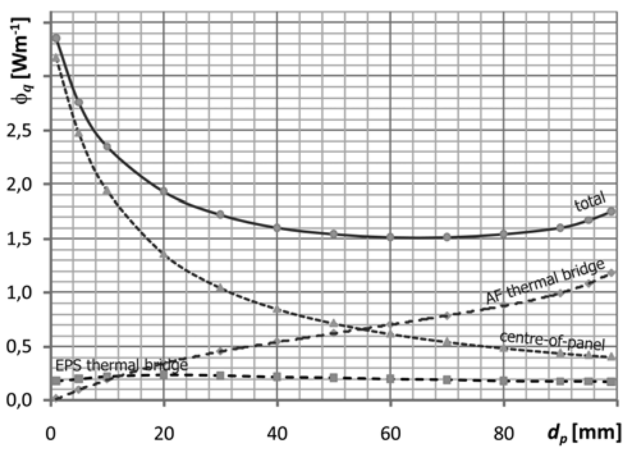

Figure 7.11c

Decomposition of the heat flows through all elements of the EPS encapsulated VIP component (2D model) as function of VIP thickness.

t_f = 40 μm alu.; *d_{slab} = 100 mm; a_{edge} = 25 mm; w_{cop} = 500 mm; $\lambda_c = 4.0 \cdot 10^{-3}\ W \cdot m^{-1} \cdot K^{-1}$; $\lambda_f = 160\ W \cdot m^{-1} \cdot K^{-1}$; $\varphi = 0.67$; $\alpha_1 = 7.8 m^2 \cdot K \cdot W^{-1}$; $\alpha_2 = 25 m^2 \cdot K \cdot W^{-1}$.*

ways of calculating the effective thermal resistance. First, the markers represent numerical calculations using Trisco. The overall thermal resistance is then obtained using eq. 7.1. Second, the continuous lines represent analytical computations with the advanced model for calculating thermal edge effects in building components as presented in section 4.3.1 and using equation 4.3. Third, the dotted lines represent analytical calculations according to international standard ISO 6946:2007 (2007).

In this Figure 7.8, the limiting case (dashed line) represents a component without thermal bridge caused by either the foil or the EPS strip, i.e. only the central area of the EPS encapsulated VIP component. Since no thermal bridge is present, the thermal resistance of this configuration is a linear function of VIP thickness and forms the maximum achievable thermal resistance of such a component. Due to a thermal bridge (either EPS strip or EPS strip + barrier laminate) the thermal resistance of practical EPS encapsulated VIPs deviates from and is lower than the thermal resistance of the limiting component without thermal bridge. The difference between the broken line representing the limiting case and the continuous line representing the component with a barrier envelope with 0 μm aluminium[8] shows the influence of the 25 mm wide EPS strip along the component's edge, while the difference between the continuous lines representing a component with a barrier envelope with a certain aluminium thickness t_f and the component with 0 μm aluminium indicates the influence of this specific barrier laminate. From this Figure 7.8 it expectedly becomes clear that the thicker the aluminium layer, the larger the difference in thermal resistance between the limiting case and the component with thermal bridge.

Another observation from this same figure is that below a certain thickness of the aluminium layer, no local maximum value in thermal resistance at a certain VIP thickness exists. For the EPS encapsulated VIP studied two-dimensionally, this aluminium thickness lies near 10 μm. So, within the range of EPS encapsulated VIPs studied in this section, components with an aluminium layer thickness beyond 10 μm do have a local maximum in thermal performance at a certain VIP thickness while other components do not. This indicates that the barrier envelope at the component's edge is (partially) causing this phenomenon.

A final interesting observation from Figure 7.8 is that the difference between the effective thermal resistance calculated numerically and the effective thermal resistance determined with the analytical model from section 4.3.1 is very small. Only for large VIP thickness a small deviation occurs. However, the results from the thermal bridge models from ISO 6946:2007 (2007) differ significantly from both aforementioned models. This clearly indicates that the models from the standard are only valid for weak thermal bridges.

---

[8] The line for t_f = 0 μm is hardly visible; it overlaps with the corresponding continuous line.

Moreover, Figure 7.9 indicates the responsibility of the thickness of the EPS layer on top and at the bottom of the panel, represented by the modified boundary heat transfer coefficient[9]. The broken lines in this figure present R_{eff} as function of VIP thickness of a VIP with 40 μm aluminium barrier layer, an EPS edge strip of 25 mm but no EPS top and bottom layers, or in other words it presents the effective thermal resistance of a VIP with an EPS strip at its side and subjected to varying boundary conditions (Figure 7.10 bottom). Broken lines for several boundary conditions are plotted[10]. As we can see from these lines, the effective thermal resistance of these components always increases with increasing VIP thickness; no local maximum in overall thermal performance exists, even for laminates with more than 10 μm aluminium[11].

The broken lines in this same figure are chosen in such a way that they represent the following VIP thickness in the corresponding EPS encapsulated VIP from the top most line to the bottom line: 1, 10, 30, 50, 60, 70, 80, 90, 99 mm. The crossing of these broken lines with vertical lines through these corresponding VIP thicknesses, produces the values of R_{eff} of a corresponding EPS encapsulated VIP with a barrier of 40 μm aluminium. The line through these crossings is plotted in Figure 7.9 too as a continuous line. As can be seen from this continuous line, a local maximum in thermal performance at a certain VIP thickness now arises indicating that variation in modified boundary heat transfer coefficients is in any case partly responsible for the phenomenon.

---

[9] Since the outer dimensions of the EPS encapsulated VIP are fixed, the thickness of the EPS top and bottom layer decreases with increasing VIP thickness. This in turn implies that the combined resistance of the boundary layer between EPS and air and of the EPS top or bottom layer decreases as well with increasing VIP thickness. As a consequence, the modified boundary heat transfer coefficient, α^*, decreases with increasing VIP thickness. This coefficient can be computed using equation (3.20) from chapter 3.

[10] These coefficients are chosen in such a way that they represent the combination of a 'regular' boundary heat transfer coefficient (7.8 $m^2 \cdot K \cdot W^{-1}$ and 25 $m^2 \cdot K \cdot W^{-1}$ on either side) and a certain EPS thickness according to equation (3.20) from chapter 3. The combination of 0.73 / 0.78 $m^2 \cdot K \cdot W^{-1}$ corresponds to 45 mm EPS on either side; 1.46 / 1.68 $m^2 \cdot K \cdot W^{-1}$ to 20 mm EPS on either side; and 2.46 / 3.15 $m^2 \cdot K \cdot W^{-1}$ to 10 mm EPS on either side.

[11] Figure 7.9 also shows a curvature of the lines at small VIP thickness and linearity at higher thickness. This behaviour results from a decreased importance of the thermal bridge on the overall thermal performance for these specific panels as the thickness of the panel increases. In case of VIPs with large thermal bridges (thick metal based barrier laminates) Figure 3.7 in chapter 3 showed that the linear thermal transmittance decreases with increasing panel thickness within the thickness range of practical importance and provided that the boundary heat transfer coefficients are constant. So, at small panel thickness in this figure, the effect of the thermal bridge is still visible by the curvature in the line. At higher panel thickness, though, the linear thermal transmittance has become insignificant as a result of which only the effect of the central area is visible as a linear relation between thermal resistance and panel thickness.

Figure 7.12

Temperature profiles through an EPS encapsulated VIP with one linear thermal bridge. (upper half as symmetric)

$t_f = 40\ \mu m$; $d_{slab} = 100$ mm; $a_{edge} = 25$ mm; $w_{cop} = 500$ mm; $\lambda_c = 4.0{\cdot}10^{-3}\ W{\cdot}m^{-1}{\cdot}K^{-1}$; $\lambda_f = 160\ W{\cdot}m^{-1}{\cdot}K^{-1}$; $\varphi = 0.667$; $\alpha_1=7.8m^2{\cdot}K{\cdot}W^{-1}$; $\alpha_2=25m^2{\cdot}K{\cdot}W^{-1}$;

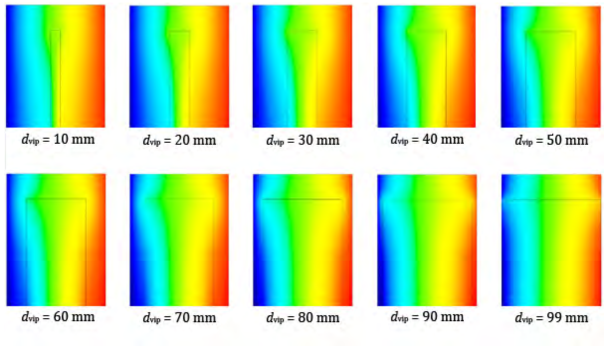

Figure 7.13a

Plot of the derivative of $\phi_q/\Delta T$ to VIP thickness as function of VIP thickness of an EPS encapsulated VIP.

Numbers along the lines are the thickness of the barrier laminate, t_f, in μm.

$d_{slab} = 100$ mm; $a_{edge} = 25$ mm; $w_{cop} = 500$ mm; $\lambda_c = 4.0{\cdot}10^{-3}\ W{\cdot}m^{-1}{\cdot}K^{-1}$; $\lambda_f = 160\ W{\cdot}m^{-1}{\cdot}K^{-1}$; $\varphi = 0.667$; $\alpha_1=7.8m^2{\cdot}K{\cdot}W^{-1}$; $\alpha_2=25m^2{\cdot}K{\cdot}W^{-1}$.

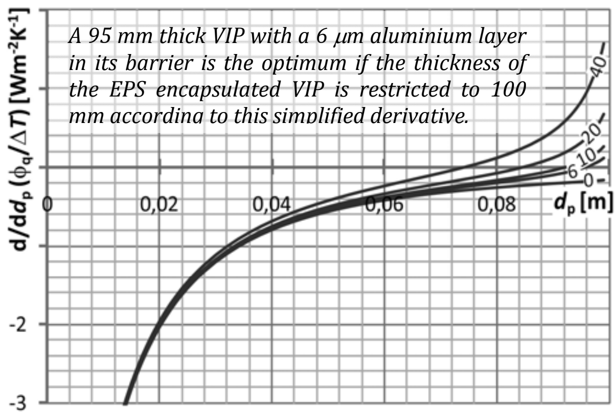

Figure 7.13b

Plot of the derivative of $\phi_q/\Delta T$ to VIP thickness as function of VIP thickness of an EPS encapsulated VIP.

Numbers along the lines are the thermal conductivity of the VIP core, λ_c, in $W{\cdot}m^{-1}{\cdot}K^{-1}$.

$t_f = 40\ \mu m$; $d_{slab} = 100$ mm; $a_{edge} = 25$ mm; $w_{cop} = 500$ mm; $\lambda_f = 160\ W{\cdot}m^{-1}{\cdot}K^{-1}$; $\varphi = 0.667$; $\alpha_1=7.8m^2{\cdot}K{\cdot}W^{-1}$; $\alpha_2=25m^2{\cdot}K{\cdot}W^{-1}$.

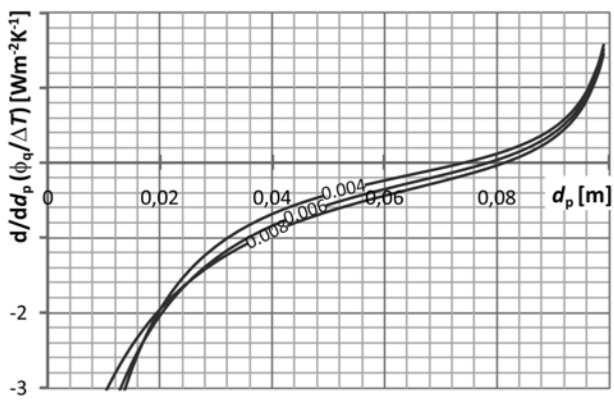

A decomposition[12] of the heat flows through the elements of the EPS encapsulated VIP, as presented in Figure 7.11, also shows the influence of the aluminium barrier and its thickness on effective thermal performance. As can be seen from a comparison of these three figures, the heat flows through the central area of the component and the EPS edge strip are more-or-less the same for a component with an aluminium foil of 0 μm, 20 μm and 40 μm. However, the heat flow through the barrier laminate in the thermal bridge increases for increasing aluminium thickness, as can be expected since the conductance of a thicker foil is higher. More interestingly, the heat flow through the laminate at the component's edge increases for increasing VIP thickness, contrary to what is expected based on chapter 3, and it increases stronger if the aluminium layer inside the laminate is thicker. The extent of this increase can only be explained by the influence of the thinning of the EPS top and bottom layer, i.e. the increase of the modified boundary heat transfer coefficient. The combined effect of a decrease in heat flow through the central area because of increased VIP thickness and an increase in heat flow through the aluminium-based barrier laminate for increasing VIP thickness now results in the coming into existence of a local minimum in heat flow or a local maximum in thermal performance. It also explains why such a maximum in performance does not exist for all laminate thicknesses.

7.4 SUBSTANTIATION OF EXISTENCE OF MAXIMUM IN THERMAL PERFORMANCE

The existence of a maximum in thermal performance at a certain VIP thickness can be mathematically shown using the analytical models developed and presented in chapters 3 and 4. This substantiation can be provided by developing a model for calculating the total heat flow through an EPS encapsulated VIP, by subsequently taking the derivative of this formula to the thickness of the VIP inside and by finally equating this derivative to zero. If there is a VIP thickness, d_p, for which this derivative equals zero than the phenomenon exists and the maximum thermal performance can be found at this thickness.

---

[12] The heat flow through the centre-of-panel area is obtained by multiplying the area of the centre-of-panel region with the temperature difference over the component (20 K) and by dividing this product by the 1D thermal resistance of the central area of the component; the heat flow through the EPS strip at the component's edge is determined by the difference in numerically calculated heat flow through an EPS encapsulated VIP without barrier envelope at the component's edge and the heat flow through the central area of the component; the heat flow through the barrier envelope at the component's edge finally is calculated from the difference between numerically computed heat flow through an EPS encapsulated VIP with and without a barrier envelope along the component's edge.

The total heat flow through an EPS encapsulated VIP can be subdivided into a heat flow through the central area of the panel in which thermal bridge effects are neglected and a heat flow through the thermal bridge along the edge of a component including barrier laminate and EPS strip. In the 2D case studied in this section, the first can be calculated from $U_{cop}\cdot A_{cop}\cdot \Delta T$, while the latter can be obtained from $\psi_{thermalbridge}\cdot \Delta T$. Since however the models for calculating the ψ-value of a building component (section 4.3) or of a VIP with non-zero thermal conductivity (chapter 3) are too complex to easily compute a derivative, the simplified model for $\psi_{vip,edge,0}$ from chapter 3 is used.

In appendix A71, the model for the total heat flow through an EPS encapsulated VIP and its derivative are presented. This derivative is plot against VIP thickness in Figure 7.13 for several EPS encapsulated VIPs. As can be seen, for most components this derivative indeed crosses the abscissa proving the existence of a maximum in thermal performance at a certain thickness of the VIP inside the component. Moreover, the thinner the aluminium layer in the barrier laminate, the thicker the VIP can get to obtain this local maximum which is in accordance with Figure 7.8. According to this figure, however, an EPS encapsulated VIP with a barrier laminate thickness of 6 μm should not exhibit a local maximum in thermal performance while according to Figure 7.13a it should. These differences result from the simplifying assumption made to develop the analytical heat flow model. The numerical model in this respect should be taken as the correct reference.

7.5 CONCLUSIONS AND SUMMARY

As we have seen, the thermal performance of an EPS insulation slab of 1x1x0.1 m^3 can be improved by including vacuum insulation panels. As a result a so-called EPS encapsulated VIP emerges. If a strip of 25 or 50 mm EPS along the panel's perimeter and a strip of 50 mm EPS between both VIPs are considered, the system's thermal performance can be improved with approximately 35% at maximum with 30 mm thick VIPs. Concerning this improvement, it is important to bear in mind that the thermal conductivity of the core equals $4\cdot 10^{-3}$ $W\cdot m^{-1}\cdot K^{-1}$ and more importantly that the envelope consists of a 40 μm aluminium foil. If more common metallised films or thinner aluminium foil laminates are used as envelope, a higher performance increase can be obtained. As can be expected, this performance increase reduces if the EPS strips widen or the thermal conductivity of the core increases.

Besides, it was shown for an EPS encapsulated VIP component with 2D-simulations that a local maximum in thermal performance exists at a certain VIP thickness. This phenomenon was numerically also seen in a more complex three-dimensional subcomponent. It can be explained from a decomposition of heat flows through the separate elements of such a component: a.) the heat flow through the centre-of-panel area decreases since the thermal resistance of this region increases directly proportional to the thickness of the VIP; b.) the heat flow through the EPS edge strip remains constant; c.) the heat flow through the aluminium barrier of the laminate increases with increasing VIP thickness– the higher the product of laminate thickness and thermal conductivity, the more rapid the increase. The combined effect of these heat flows results in the occurrence or otherwise of a local maximum in thermal performance at a specific VIP thickness.

Two parameters can be held responsible for this occurrence: the product of the aluminium thickness inside the laminate and thermal conductivity of this aluminium on the one hand and the adjoining layer, which thermal conductivity and thickness can be simplified for calculations into a single parameter, the modified boundary heat transfer coefficient on the other hand. As seen during the analysis, the phenomenon does not occur if the modified boundary heat transfer coefficients are constant, or similarly if the thickness of the EPS top and bottom layer is constant[13]. If this variability in boundary heat transfer does exist, than the product of laminate thickness and thermal conductivity as a second criterion determines whether or not a local maximum in thermal performance exists. If this product is small then the decrease of the heat flow through the centre-of-panel area for increasing VIP thickness is always more rapid than the increase of the heat flow through the barrier laminate within the thermal bridge for increasing VIP thickness; no maximum in thermal performance then exists. If this product is high, then a maximum does exist.

A final interesting observation from this chapter is that the difference between the effective thermal resistances calculated numerically and analytically using the equations from section 4.3.1 is very small. However, the results from the thermal bridge models from ISO 6946:2007 (2007) differ significantly from both aforementioned models. This clearly indicates that the models from the standard are only valid for weak thermal bridges.

[13] But then of course the preset condition of this chapter from section 7.1.2 onwards, i.e. a constant total thickness of 100 mm, is no longer fixed.

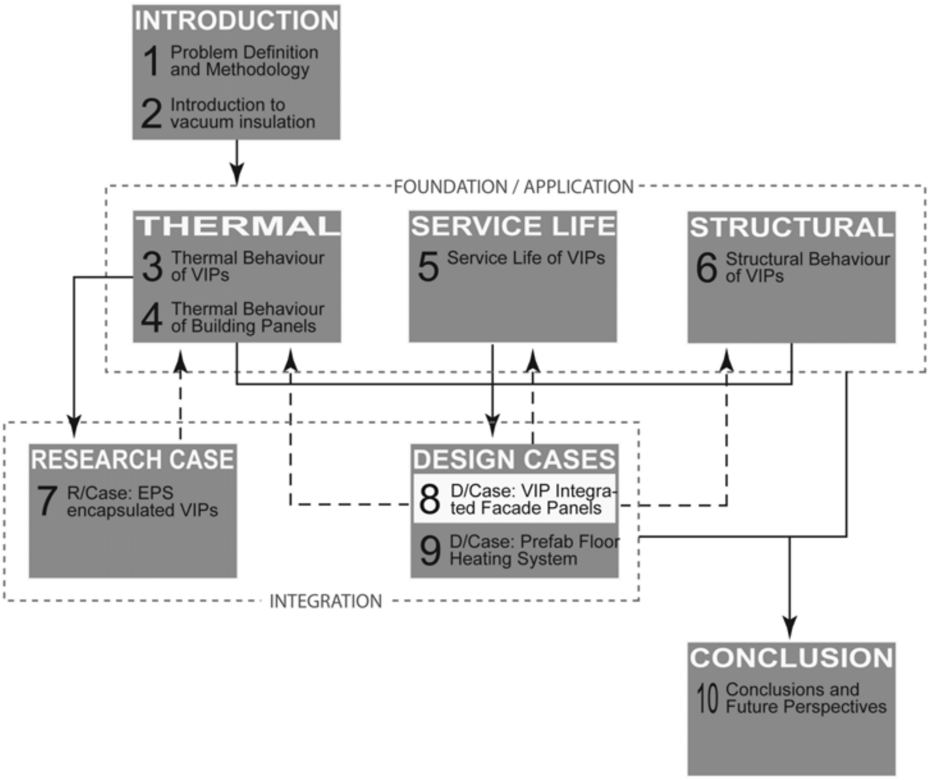
INTRODUCTION
1 Problem Definition and Methodology
2 Introduction to vacuum insulation
FOUNDATION / APPLICATION
THERMAL
3 Thermal Behaviour of VIPs
4 Thermal Behaviour of Building Panels
SERVICE LIFE
5 Service Life of VIPs
STRUCTURAL
6 Structural Behaviour of VIPs
RESEARCH CASE
7 R/Case: EPS encapsulated VIPs
DESIGN CASES
8 D/Case: VIP Integrated Facade Panels
9 D/Case: Prefab Floor Heating System
INTEGRATION
CONCLUSION
10 Conclusions and Future Perspectives

D/CASE VIP INTEGRATED FAÇADE PANELS 8

DESIGN CASE STUDY: PRINCIPAL DESIGNS OF HIGH THERMAL PERFORMANCE, SLIM, PREFABRICATED FAÇADE COMPONENTS

After being used in refrigerators and transport containers for quite some time, vacuum insulation panels (VIPs) have recently been introduced to the building sector. Over the last decade, several buildings have been erected primarily in Switzerland and Germany acting as demonstration projects for the use of VIPs in buildings. However, in most projects this high performance insulation material replaces conventional thermal insulators, as a consequence of which the potential of vacuum insulation is not exploited to its full extent. The objective of this chapter therefore is to show how the properties of VIPs can be exploited in actual façade designs.

This chapter therefore starts with a brief overview of some of the demonstration projects in section 8.1. Subsequent to this introduction, requirements will be formulated for new types of VIP integrated façade designs. Based upon these requirements and the principal relations among them, section 8.2 typologically introduces a range of VIP integrated façade panels including critical thoughts regarding their fitness for the building industry, thermal behaviour and structural performance. From this overview, two panel types will be discussed in more detail: the sandwich panel and the edge spacer panel. Based upon previous discussions then, three designs of VIP integrated façade components will be presented and evaluated in sections 8.4, 8.5 and 8.6: the sandwich component, the membrane component and the encasing component. These design examples demonstrate the potential of VIPs for architectural constructions. With the proliferation and wide-spread application of VIPs in façade constructions, the energy performance of buildings in their occupational phase can be reduced considerably. In this respect, vacuum insulation panels can thus contribute to a more sustainable society.

The façade components designed in this chapter have abbreviated names that are based on the following principles: First, one or two capitals give the type of panel (S for sandwich component, M for a component using a membrane alone, MS for a component using a membrane and stiffening elements between VIPs (for the remainder identical to M-panel), and E for components having an encasing on either side of the VIP. Second, behind a hyphen the name of the most striking material is given. This can either be the face sheet or the wooden encasing.

8.1 INTRODUCTION

8.1.1 Introduction

Application of vacuum insulation panels in buildings is still limited due to the novelty of the material to building practitioners and due to the care required for adequate and safe use. If integrated properly into building constructions, the potential of VIPs can be very high, though. Simmler et al. (2005) even estimate that, if the entire existing non-insulated building stock of the European Union is insulated with 2 cm of vacuum insulation, the requirements of the Kyoto-protocol (UNFCCC, 1997) for the European Union are easily met. With the proliferation and wide-spread application of VIPs in façade constructions, the energy performance of buildings in their occupational phase can be lowered considerably. In this respect, vacuum insulation panels can thus contribute to reducing greenhouse gases.

In this chapter several façade panels including details and mounting system will be designed and evaluated on their thermal and structural performance and service life. Using these designed examples it will be shown that indeed a high thermal performance with limited construction thickness is possible. By showing these examples hopefully architects and engineers are challenged to come up with more examples which will be applied and evaluated in practise. Before these façade designs are presented, first several demonstration projects in which VIPs have been applied and some existing VIP integrated façade systems will be discussed. Moreover, the criteria which need to be fulfilled by these systems need to be set, too.

8.1.2 Demonstration buildings and project-independent building products with VIPs

Originally vacuum insulation panels have been developed for consumer goods and transport boxes. Required long service lives for buildings and the fragility of the product, however, among others impeded architectural applications. Yet, over the last decade, several buildings have been erected in Europe in which VIPs have been applied. In most of these buildings, the original core material of the VIP, open-porous polymer foam, was replaced by fumed silica, outperforming polymer foams on service life by many years. In this same period some manufacturers have also integrated VIPs in some of their products. More information on these demonstration buildings and products with VIPs can be found in appendix A82, in which also two tables are included presenting an overview of products and demonstration buildings with references to additional literature.

8.2 VIPs in Building Panels

8.2.1 Requirements on VIP integrated building panels

For the application of VIPs in buildings two approaches exist: on-site application and integration in prefabricated components. While with respect to the first approach a certain body of knowledge and experience has been obtained through research conducted in the framework of the IEA ECBCS Annex 39 (Binz et al., 2005), the second approach has not yet been systematically investigated until now.

If applied in buildings, vacuum insulation panels are subjected to legal requirements, in most cases heavier than the requirements coming from traditional VIP applications, like refrigerators. Based on the European Construction Products Directive (European Council, 1988), seven product-related technical requirements on building products in general and thus VIPs in specific can be distinguished[1]:

a) structural requirements (mechanical resistance and stability)
b) fire protection requirements (safety in case of fire)
c) requirements regarding hygiene, health and environment
d) application safety and fitness for use (safety in use)
e) acoustical requirements (protection against noise)
f) thermal requirements (energy economy and beat retention)
g) service life requirements and/or possibility of being repaired

Only the structural and thermal behaviour of VIP integrated panels and their service life will be dealt with in subsequent sections since these are strongly interrelated and are most interesting from a design perspective[2]. Table 8.1 presents an overview of the most important requirements on VIP integrated building panels, both sandwiches and edge spacer constructions. Most requirements are taken from the Dutch Building Code (VROM, 2001) and its accompanying standards (NEN or EN standards and product guidelines).

---

[1] Service life is not explicitly mentioned in annex 1 on essential requirements of this directive but follows from the sentence: "such requirements must, subject to normal maintenance, be satisfied for an economically reasonable working life" (European Council, 1988, annex 1).

[2] With respect to fire safety, it is important to mention that fumed silica is inherently fire safe. The barrier envelope containing polymers, however, negatively influences a VIP's fire behaviour. Fire spread along the surface of the laminate is quite rapid, while at the same time a loss of vacuum due to a damaged laminate significantly reduces the Young's modulus of the core. The exact fire behaviour however strongly depends on the context in which the panel is applied and will therefore not be elaborated in this chapter.

Service life requirements

The thermal conductivity of the core material of a VIP significantly depends on the gas pressure and the amount of water absorbed as explained in chapter 5. Since this gas pressure and water content slowly but gradually increase over time, the thermal conductivity of a VIP will increase too. This increase is called thermal conductivity ageing. The actual service life of a prefabricated component incorporating a VIP mainly depends on this thermal conductivity ageing of the VIP inside. This thermal ageing then determines the service life of the product[3]. The service life demands on a VIP (the required or desired t_{sl}) depend on the application, as explained in section 5.1.1. The service life of façade panels for office buildings was explained to be ranging from 20 to 30 years while the service life of residential houses is considered to be somewhere between 50 and 100 years for contemporary buildings.

Thermal requirements

The thermal requirements on a VIP component consist on the one hand of restrictions with regard to a maximum thermal transmittance to minimize thermal losses and on the other hand of a criterion for a minimum inside surface temperature to avoid condensation.

For the first requirement, two construction properties are important: the central thermal transmittance, U_{cop} [$W{\cdot}m^{-2}{\cdot}K^{-1}$], and the linear thermal transmittance of the edge, ψ_{edge} [$W{\cdot}m^{-1}{\cdot}K^{-1}$]. As explained in Chapters 3 and 4, together with panel geometry and size both properties combine into a single property describing the thermal performance of such a panel as a whole, U_{eff} [$W{\cdot}m^{-2}{\cdot}K^{-1}$]. The Dutch Building Code (VROM, 2001) at this moment specifies a required thermal resistance, R_c-value[4], of 2.5 $m^2{\cdot}K{\cdot}W^{-1}$ for the opaque parts of a façade[5], i.e. U = 0.37 $W{\cdot}m^{-2}{\cdot}K^{-1}$. Such thermal requirements, however, are minimum requirements. If, e.g., passivhauses are designed, an average U-value of 0.15 $W{\cdot}m^{-2}{\cdot}K^{-1}$ is common (Graf, 2003).

For the second requirement, an estimation of the inner surface temperature at the major thermal bridge is needed. This surface temperature is also influenced by aforementioned central and linear thermal transmittances.

---

[3] As thermal conductivity limit for the service life, $8.0{\cdot}10^{-3}$ $W{\cdot}m^{-1}{\cdot}K^{-1}$ is used in this chapter. Service life definition from chapter 5 is used throughout this chapter.

[4] Contrary to U-values, thermal resistances 'of the construction layers', or R_c-values, as specified in the Dutch building code, do not include boundary resistances.

[5] If building panels however are placed inside a framework, like a curtain wall façade, additional thermal bridges due to the mullions need to be considered as well. This requirement should therefore be considered as the effective thermal resistance of the entire façade.

Table 8.1 – *Overview of most important requirements on opaque VIP integrated façades.*

requirement	indicator	criterion	Standards and Codes
statics / safety	strength stiffness stability integrity	S(F_d, M_d, GE_d)⩽R(F_d, M_d, GE_d) S(F_d, M_d, GE_d)⩽R(F_d, M_d, GE_d) S(F_d, M_d, GE_d)⩽R(F_d, M_d, GE_d) sufficient integrity safety in case of failure	BB artt. 2, 111, 174 / NEN 6702 TGB / VMRG kwaliteitseisen en adviezen 1993 / BRL 2701 / NEN 2608
fire safety	flammability smoke density [m^{-1}] fire spread/resistance [min]	self extinguishing class 1 or 2 ⩽ 10 > 30	BB artt. 12t/m16, 116t/m118, 174, 185, 231t/m233, 236, 256t/m258, 261 / NEN 6061, 6063, 6065, 6066, 6082
hygiene, health and environment	Eco99/m², UBP97/m² Hazardous materials mold growth water penetration with Δp	<1500, <35000 no formaldehyde, cadmium, asbestos and cfc no mold growth no penetration	BB artt. 26, 27, 33, 71, 121, 122, 127, 151, 197, 198, 204, 228, 268 / NEN 2686, 2778, 3660
acoustics	airborne sound reduction for rail or road traffic, $G_{A;k}$ [dB(A)]	> noise exposure – 33 (houses: 'verblijfsgebied') > noise exposure – 35 (houses: 'verblijfsruimte') > noise exp. – 40 (offices) > 20	BB artt. 3.1, 3.2, 120, 194, 241 / NEN 5077
energy	U_{eff} [W m^{-2} K^{-1}]	< 0.4 (requirement by law) < 0.15 (Passivhaus)	BB artt. 70, 150, 227 / NEN 1068
service life	service life, t_{sl} [years]	> 20/30 (façades), > 50/70 (buildings) And/or possibility of being repaired or replaced	
aesthetics	displacements, δ [m] flatness, diag. [mm·m^{-1}]	< 1/200 * span (mullions) < 1/200 * span / < 10 mm (single pane glazing) < 1/360 * span / < 8 mm (double pane glazing) < 5	NEN 6702 / SR 1990 / BRL 2701 / NEN 2608 / NEN 3660

Structural requirements

The structural boundary conditions have an important effect on the requirements that must be met by a VIP. For instance, structural requirements regarding flexion only apply to VIPs used in sandwich panels. In practically all other construction systems, a VIP does not have to bear flexural loads. The component in total (façade or door panel), however, does have to meet structural requirements, but the panel facings and edge spacer construction fulfil these.

From a structural point of view, two types of requirements can be distinguished: ultimate limit state requirements (safety) and service limit state requirements (aesthetics and practicality). The ultimate limit state requirements comprise of both sufficient strength of the component and safety in case of damage, i.e. a panel should not fall out of its frame. The serviceability limit state requirements comprise sufficient stiffness of the panel and sufficient flatness.

Moreover, two types of external loads need special consideration. First, winds loads are the primary loads acting on façade panels. The extent of these loads depends on several factors, among which are the impact pressure which depends on place on Earth (geographic location and height above the ground), the building's size and orientation towards prevailing wind direction. Since it is economically not viable to dimension façade elements according to hardly ever occurring extreme weather conditions, VMRG-kwaliteitseisen en adviezen 2009 (2008) and BRL 2701 (2003) state that for horizontal displacements of posts and beams and of glass panes, a pressure of 0.75 times the maximum impact pressure, p_w [$N \cdot m^{-2}$], should be used for checking the static structural behaviour of the façade (Renckens, 1996). For Dutch conditions, the highest impact pressure equals 2.07 kPa on a façade on a building located in the coastal area at an altitude above 150 m. Second, thermal loads need to be considered as well. As a result of insolation, large temperature differences might occur across a façade. These temperature differences may lead to thermal expansion/contraction and additional deflection. Moreover, if thermal movement is restricted additional stresses are introduced.

8.2.2 Interrelationships among requirements

Based upon the previously presented set of requirements, it is possible to investigate the (inter)relationships between these requirements for prefabricated building components, resulting in the scheme presented in Figure 8.1. In this scheme some additional material, geometrical or environmental properties (black boxes) are added to clarify non-direct relationships. As seen, several relationships among properties and requirements exist, two of which will be discussed in more detail.

First, there exists an important relation between the thermal performance of a VIP-incorporated building component on the one hand and its structural performance on the other hand. Whether this relationship is mainly determined by the properties of the VIP itself, or by a spacer at the component's edge, primarily depends on its structural behaviour, i.e. does it structurally act as a sandwich or as an 'edge-spacer' construction, e.g. double-glazing. In these spacer constructions, structural behaviour is completely determined by a combined action of this spacer and the outside facing. As a consequence, both the facing and the spacer need to be dimensioned accordingly, in most cases resulting in high thermal losses at the panel's edge. Proper detailing and materials selection can on the one hand minimize this thermal bridge significantly, but also influence the structural performance of the component. For sandwiches with a VIP core, though, no structural spacer is needed, on the one hand resulting in the possibility of reducing thermal bridging, but on the other hand imposing additional structural requirements on the VIP itself. Both examples indicate the significant interaction between thermal and structural performance.

Second, the relationship between thermal performance and VIP service life is important. The service life of a vacuum insulation panel is typically defined as the elapsed time from the moment of manufacturing until the moment the thermal conductivity of the core material, λ_c, has increased to some critical value, λ_{cr}. As seen in previous chapters, the thermal conductivity of the core is not a constant value but is subject to ageing. Since the thermal performance of a VIP façade component or a VIP integrated building construction primarily depends on the centre-of-panel thermal conductivity combined with a geometry-based multiple of the linear thermal transmittance of the component edge, the application of an arbitrary value for λ_{cr} as a maximum allowable centre-of-panel thermal conductivity indirectly influences the service life of a VIP integrated building component. In general, however, beside this functional service life, which is for VIP based on physical processes, an economic and an aesthetic service life can be defined as well, which are related to maintenance and appearance respectively.

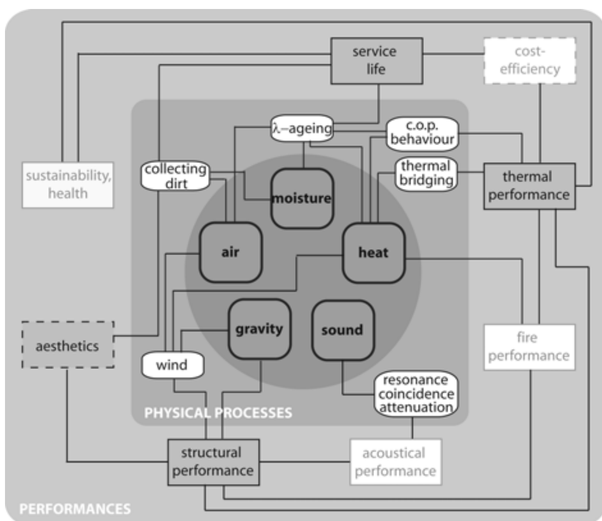

Figure 8.1

Relationships between different requirements for VIP incorporated building panels. Regarding performances, the white boxes denote performances that are not studied explicitly in this chapter, while the performances in the gray boxes are. Continuous and broken lines in these cases represent physical performances and customer's desires respectively.

8.2.3 Classification of VIP integrated building panels

Before designs of VIP integrated building panels are made, they are first classified into several main groups. If one now looks deeper into their construction, different construction types can be distinguished. These differences arise from differences in the number of layers on one level and structural action on a sublevel. Figure 8.2 shows a scheme in which façade panels are classified into four types.

Two types are of special interest for integrating VIPs: the edge spacer construction and the sandwich panel. Since VIPs are very fragile and prone to damage by puncture of the barrier, the VIP preferably needs to be protected throughout all phases of the construction process. Triple layer constructions (Figure 8.2) in that respect inherently have these protective properties, as a result of which they are preferred to two layer constructions. Both the edge spacer construction and the sandwich construction will be investigated more thoroughly in this chapter.

Phenomenologically both the edge spacer and the sandwich panel consist of a face sheet on either side of the panel, a core made of VIP and a closure along the panel's perimeter. In case of an edge spacer panel, this closure should be a structural spacer; in case of a sandwich panel, it can just be a simple protective tape or profile. The function of the structural spacer is mechanical while the function of the tape or weak profile is protective. This protective function can be twofold: preventing the VIP inside from damage and safeguarding the integrity of a panel in case of such damage to the VIP or to the bond between face sheets and core.

As a result, the difference between both panel types lies in a difference in structural behaviour. While a sandwich panel allows shear forces to be transmitted from the face sheets to the core owing to a structural adhesion between both, an edge spacer panel does not. Due to a lack of such a structural connection, a

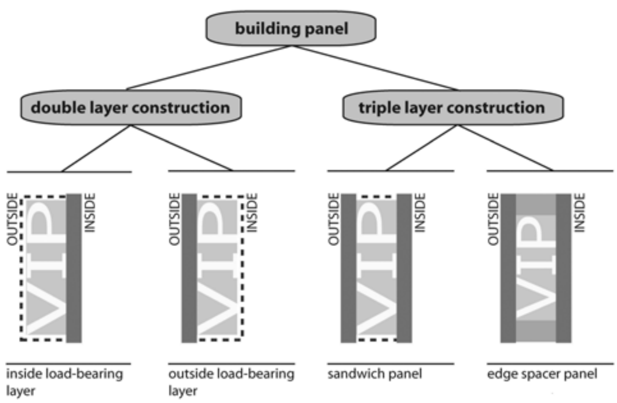

Figure 8.2

Typological classification of building/façade panels based upon the number of layers and the type of structural action.

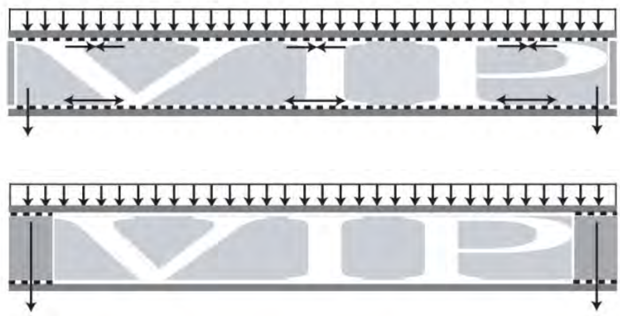

Figure 8.3

Structural action of a sandwich component (a) and an 'edge-spacer' component (b). (→←: pressure; ←→: tension). Force arrows not scaled.

structural spacer along the perimeter of a spacer panel is required to transmit forces towards the main load bearing structure. In these panels, insulation material is just inserted into the cavity as an inlay. In general, the high bending stiffness of a sandwich panel arises from co-operation of all layers while the (lower) bending stiffness of spacer panels results from individual action of each layer. Figure 8.3 schematically illustrates this difference.

8.3 SANDWICH PANELS VERSUS EDGE SPACER PANELS

8.3.1 Thermal Behaviour

As explained previously, spacer panels need a relatively strong edge profile to connect the exterior to the interior face sheet and to the load bearing structure. Sandwich panels on the other hand only require a thin tape or a small sectional profile to protect the edge of the VIP against puncture and to safeguard the system from hazardous situations if the vacuum inside the VIP fails. In chapter 4 some spacers were used for testing an advanced analytical model for calculating the linear thermal transmittance due to these spacers. From this chapter, we already saw that a non-metallic tape outperformed all other spacers regarding thermal performance.

Using the linear thermal transmittance values computed in chapter 4, the effective *U*-value can be plotted against panel size for square façade panels with 2 1.5 mm thick aluminium face sheets, with a 40 mm thick VIP as core and with variable spacers. The results are presented in Figure 8.4a. As can bee seen, of the three panels plotted, solely a panel with a non-metallic tape thermally performs according to Passivhaus standard, at least for panels bigger than approximately 0.8x0.8 m^2. For such panels, Figure 8.4b shows that at least 40 mm VIP is required to obtain a performance according to this standard, at least for the first years of usage.

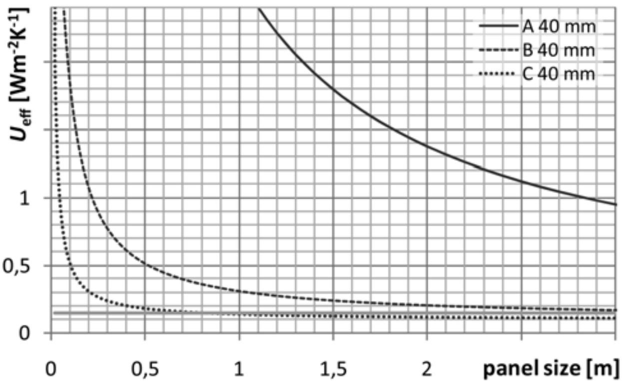

Figure 8.4a

Effective U-value of three square façade panels as function of panel size with the following specifications

face sheets: 2x 1.5 mm alu.
film: 3 layer metallised;
$\lambda_c = 4.0 \cdot 10^{-3}$ W·m^{-1}·K^{-1};
d_c = 40 mm;
α_i=7.8 W·m^{-2}·K^{-1}; α_e=25 W·m^{-2}·K^{-1}.

A: alu. double-glazing spacer;
B: thermoplastic spacer;
C: non-metallic tape.

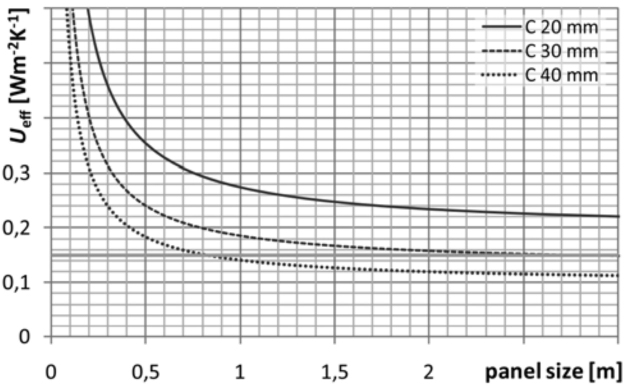

Figure 8.4b

Effective U-value of three square façade panels as function of panel size with the following specifications

face sheets: 2x 1.5 mm alu.
spacer: non-metallic tape;
film: 3 layer metallised;
$\lambda_c = 4.0 \cdot 10^{-3}$ W·m^{-1}·K^{-1};
d_c = 20 / 30 / 40 mm.
α_i=7.8 W·m^{-2}·K^{-1}; α_e=25 W·m^{-2}·K^{-1}.

Panels with an aluminium double-glazing spacer, an optimised thermoplastic spacer and a folded edge spacer (Figure 4.5a in chapter 4) can only achieve Passivhaus standard with VIPs thicker than 40 mm. From a thermal perspective, panels having a reinforced non-metallic tape as edge, i.e. sandwich panels, are therefore preferred to other panels. As a case-study therefore first a VIP integrated sandwich was designed which will be further elaborated in section 8.4.

8.3.2 Structural Behaviour

Depending on the size of a component and the width of the spacer, the structural behaviour of an edge spacer construction can be considered as a plate supported by a frame along its perimeter. The connection between plate and frame is either schematised as a hinge if the size of the edge is small relative to the dimension of the panel or as a rigid connection if the size of the edge is large relative to the dimension of the panel. Since however in practice spacers are small relative to the size of the building panel, the first would be the best representation for this type of panel. A disadvantage of such a construction is that wind loads are to a large extent 'absorbed' by the outermost facing. Due to the core material some of this load is transmitted to the core material and then to the inner facing. The combination of face sheets and core however does not structurally co-operate but acts as separately loaded plates, as a consequence resulting in considerable thickness of the facings.

Since the facings are adhered to the core material in a sandwich construction, a combined flexural action occurs (sandwich behaviour). The panel therefore does not act as the sum of three layers, but exhibits synergy between all layers. The facings are primarily responsible for taking up a bending moment, while the core material is responsible for taking up shear forces. The deflection of a sandwich panel is therefore smaller than the deflection of an edge spacer construction under the same load provided that the materials and dimensions are the same. For such sandwich behaviour a good bond[6] between face sheets and barrier film on the one hand and between laminate and VIP core on the other hand is required.

Table 8.2 *– Overview of indicative results on flexural tests on sandwich panels with a VIP core (150x350 mm²) and either 4 mm mdf or 4 mm glass face sheets.*

	$(EI)_s$ measured [N·m²][a]	$(EI)_s$ theoretical [N·m²][b]	$\sigma_{s;uts}$ measured [MPa][c,d]
mdf facings VIP, intact	15	$4.6 \cdot 10^2$	4.3 ± 0.6
mdf facings VIP, vented	6.7	Not calculated due to unpredictable sliding of laminate over core	3.9 ± 0.5
glass facings VIP, intact	$2.1 \cdot 10^2$	$1.3 \cdot 10^4$	4.1 ± 1.6

[a] It is important to note that, although 8 identical panels were tested for obtaining each result (duplication tests; 4 panels for 3-point testing and 4 panels for 4-point testing), these results should be considered indicative only since the testing machine available (100 kN Instron tensile tester) in fact was too inaccurate for testing VIP integrated sandwiches. Moreover, it is outside the scope of this dissertation to do a full-scale and in-depth study into the flexural behaviour of VIP integrated panels.

[b] These values are calculated from the properties of VIPs (chapter 6) and equation (8.1) (mdf: E = 2.5 GPa (tension/compr.); ν=0.21; glass: E = 70 GPa; ν=0.24; VIP: E = 38.5 MPa; ν=0.4).

[c] $\sigma_{s;uts}$ is the ultimate flexural strength of the sandwich panel defined as the normal stress at which one of the face sheets fails.

[d] Specified uncertainties are for a 95% reliability interval.

---

[6] According to Musgrave (2009), this adhesive should be a thermoset adhesive since a thermoplast would creep over time.

To obtain a first impression of the quality of the aforementioned bond, three-point and four-point flexion tests on sandwich panels according to ASTM C393 (1992) have been conducted[7]. These panels were made of a 20 mm thick VIP with face sheets of either 4 mm thick mdf or glass sheets. The results of these tests are presented in Table 8.2. Since the experiments resulted in the clear notion that shear in the adhesive between VIP and facing strongly influences the results, this table presents both the measured and the theoretical flexural stiffness, $(EI)_s$ [N·m²].

In general and not considering shear effects in the adhesive layer, the flexural stiffness of a symmetrical sandwich panel/beam is defined as

$$(EI)_s = E_f \frac{w_p (d_p^3 - d_c^3)}{12(1-\nu_f^2)} + E_c \frac{w_p d_c^3}{12(1-\nu_c^2)} \tag{8.1},$$

in which E_f [Pa] is the Young's modulus of the face sheets, E_c [Pa] is the Young's modulus of the core, w_p [m] is the width of the sandwich panel, d_p [m] is the total thickness of the panel, d_c [m] is the thickness of the core, ν_c [-] is the Poisson's ratio of the core and ν_f [-] is the Poisson's ratio of the face sheets. According to ASTM C393 (1992), the shear stiffness of a perfect sandwich panel can be obtained from

$$(GA)_s = G_c \frac{(d_p + d_c)^2 w_p}{4 d_c} \tag{8.2},$$

with G_c [Pa] the shear modulus of the core.

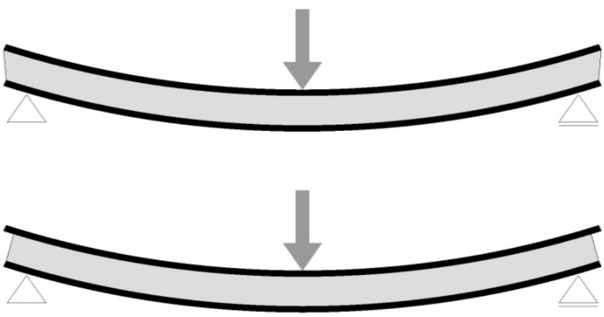

Figure 8.5

Bending of a sandwich panel without sliding of top face sheet (top) and with sliding of top face sheet (bottom). The latter represents the behaviour observed.

[7] The adhesive used to fix the face sheets onto the vacuum insulation is a polyurethane based glue. All panels had an overhang at both ends of 25 mm and the distance between the load points of the four-point bending apparatus was150 mm for the 150x350 mm² panels. The radius of the load points and the supports was 10 mm. The vacuum insulation panels consist of a fumed silica core with a laminated metallized polymer high barrier film.

Figure 8.6

VIP integrated sandwich panel with a VIP core of 150x750x20 mm³ and 2 4 mm thick mdf face sheets glued using a Polyurethane adhesive after a three-point flexion test. Sliding of top face sheet is clearly visible.

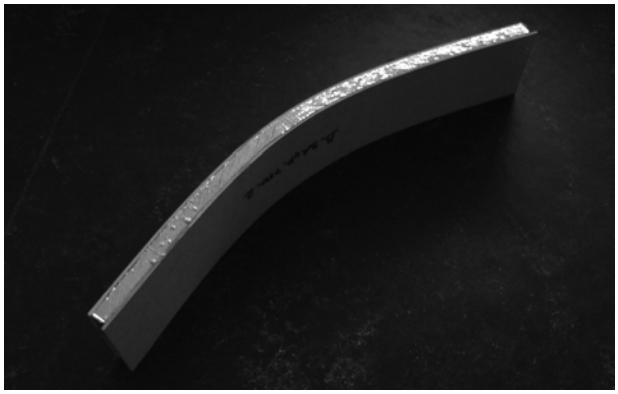

As indicated by Table 8.2, the values of the measured flexural stiffness significantly differ from the 'theoretical' ones based on (measured) properties of VIPs (chapter 6 and equation (8.1)). This discrepancy is primarily caused by shear in the adhesive layer between face sheet and VIP. Due to this viscous adhesive layer, the total sandwich deflection not only results from shear in the core and bending in the core and facing, but also from shear in the adhesive layer (and between barrier and core), resulting in significantly larger deformations than theoretically predicted[8]. This theoretical flexural stiffness is thus only valid if no shear deformation in the adhesive layer occurs (Figure 8.5 top) and not if sheer occurs in this layer (Figure 8.5 bottom). As can be seen from Figure 8.6, it was found that the upper facing shifted about 5 mm on both sides from the core material for an intact VIP with mdf face sheets and 2 mm for a damaged VIP with mdf face sheets, resulting in a 'strain' in this adhesive layer of 2 x 5 mm / 350 mm = 2.9% and 2 x 2 mm / 350 mm = 1.1% respectively, implying that shear between face sheets and VIP plays an important role in reducing the theoretical flexural stiffness of a sandwich panel[9]. This is also substantiated by calculations of the bending stiffness of the VIP core itself, based on its measured Young's modulus and a panel width of 150 mm[10]: intact VIP 20 mm

[8] It must however be noted the vacuum insulation panels used for these tests had a metallised film based laminate with an outer layer of PET and were glued onto glass or mdf face sheets. For many practical applications steel or aluminium face sheets might be of more interest. These have not been tested. No conclusions can thus be drawn regarding the bond between VIP barrier and such facing materials.

[9] Concerning VIP integrated sandwich panels with glass face sheets, sliding was hard to detect since the deflections and deformations were much smaller. Moreover, sliding did not occur between bottom face sheet and VIP.

[10] In case no structural bond between VIP and face sheets is available, the total flexural stiffness of the system can be obtained by adding the individual stiffness of each layer. For panels with a VIP core and 2 4 mm thick mdf face sheets, approximately 4 N·m² for the

thick $(EI)_{vip}$ = 4.6 N·m²; damaged VIP 20 mm thick $(EI)_{vip}$ = 2.5 N·m². Since this flexural stiffness of the VIP itself is only slightly smaller than the measured sandwich panel flexural stiffness (Table 8.2), it can be concluded that the behaviour of these tested panels is far from ideal, resulting in panels that are not suitable for façades. So, more research has to be conducted into the optimisation of adhesive-VIP and adhesive-facing interfaces which is outside the scope of this study[11].

It is finally important to realise that this sliding both occurs between face sheet and VIP barrier laminate and between barrier laminate and VIP core. The values presented previously combine both effects in a single value. Sliding of the barrier laminate relative to the VIP core is however an inherent property of a vacuum insulation panel if connected to a face sheet and does thus always occur, as a result of which perfect sandwich behaviour is never achievable.

8.4 VIP INTEGRATED SANDWICH PANEL (S-AL/STEEL PANEL)

8.4.1 General description

Although preliminary flexion tests on VIP integrated sandwich panels and tensile strength and peel strength tests on the interface between face sheet and VIP barrier showed that a good bond between VIP and face sheets is difficult to obtain, still a VIP integrated sandwich panel was designed. More research into these adhesives and surface treatments might result in a bond sufficiently strong. And as observed before, sandwich panels have a high potential for creating very thin façade panels with very high thermal performance. In this section therefore, a sandwich façade panel design will be discussed and analysed. The type of adhesive and its properties will be left out of the discussion.

The VIP integrated sandwich component consists of the following elements and materials (Figure 8.7a): a 40 mm thick vacuum insulation panel with a fumed silica core and a metallised barrier envelope with three metallisation layers, named Lam.1 or MF3 in previous chapters; a 1.5 mm thick aluminium or steel face sheet on the panel's exterior side, a 1.0 mm thick aluminium or steel face sheet on the panel's interior side[12]; Spaceloft™ aerogel insulation blankets at the panel's sides (3 mm)

---

influence of these face sheets needs to be added to the values presented here. And for 2 4 mm glass sheets approximately 110 N·m².

[11] Information on tests with adhesives for VIP integrated sandwich panels is in appendix A83.

[12] The properties discussed in this section are mainly based on aluminium facings.

and in the junction between two adjoining panels (6+9 mm); a reinforced non-metallic tape connecting both face sheets as safeguard in case of VIP failure; rubber gaskets and sealing materials; 2 or 3 mm thick aluminium or steel grips.

The face sheets are structurally adhered to the VIP resulting in a façade panel with a nominal thickness of only 43 mm[13]. As will be discussed in the section on expected structural behaviour, the span and thus size of such a component is limited due to its slimness. Moreover, the size of a standard VIP with a fumed silica core is limited to 1000x1200 mm^2 which may limit the size of the sandwich component[14,15]. The sandwich components are therefore placed in a grid of 900 mm by 1200 mm or of 1800 mm by 1200 mm if two VIPs are inserted in one component. Such a grid corresponds to regular grid dimensions in the architectural practice. A detailed section through the junction between two components is presented in Figure 8.7a. To give an impression that also double-glazing can be integrated, Figure 8.7b presents a section through a joint with a frame for double-glazing[16].

Since VIPs currently have large dimensional production tolerances[17], space needs to be available in the junction area to accommodate these. These production tolerances are drawn in Figure 8.7a as a broken line along the VIP's perimeter (inside and outside). Production tolerances in panel thickness are about +1/-1 mm[17] resulting in small difference in thickness of the entire component and thus small difference between components. These differences are too small to observe. Production tolerances in length and width are bigger and need special consideration.

---

[13] According to Maysenholder (2008), adding a sheet of 1 mm rubber on either side of the panel between VIP and face sheet may strongly improve acoustic performance.

[14] The size of a film-based VIP is limited primarily due to production limitations, such as the size of the vacuum chamber. In Europe currently two manufacturers have a technical approval for applying one of their VIPs in building projects in Germany: Va-Q-tec AG (Va-Q-vip B) (DIBt Z-23.11.1658, 2007) and Porextherm Dämmstoffe GmbH (Vacupor NT B2) (DIBt Z-23.11.1662, 2007). Va-Q-vip B has a maximum size of 1000x1200 mm^2, a minimum size of 300x400 mm^2 and a thickness between 10 and 40 mm. Vacupor NT(-B2) has a maximum standard size of 1000x1200 mm^2 , a minimum standard size of 250x600 mm^2 and a standard thickness between 10 and 30 mm. The maximum size Porextherm can deliver is 1000x2200x50 mm^3.

[15] In some cases more than one VIP can be integrated into a sandwich component.

[16] It is important to note that this frame for integrating double-glazing into the façade system was not investigated thoroughly (structurally and thermally) and designed accordingly. The drawing is therefore just meant as an indication that it can be done.

[17] Current production tolerances of typical VIPs are: Va-Q-vip: length tolerances of +2/-4 mm for panels from 1 to 500 mm, +2/-5mm for panels from 501 to 1000 mm and +3/-6mm for panels from 1001 to 1200 mm; thickness tolerance of +1/-1 mm (Va-Q-tec AG, 2008). Vacupor NT: length tolerances of +1/-2 mm for panels from 1 to 500 mm, +1/-4mm for panels from 501 to 1000 mm and +1/-6mm for panels from 1001 to 1200 mm; thickness tolerances of +1/-1 mm for panels from 1 to 20 mm, +1/-2mm for panels from 21 to 30 mm and +1/-3mm for panels from 31 to 50 mm (Porextherm Dämmstoffe GmbH, 2009).

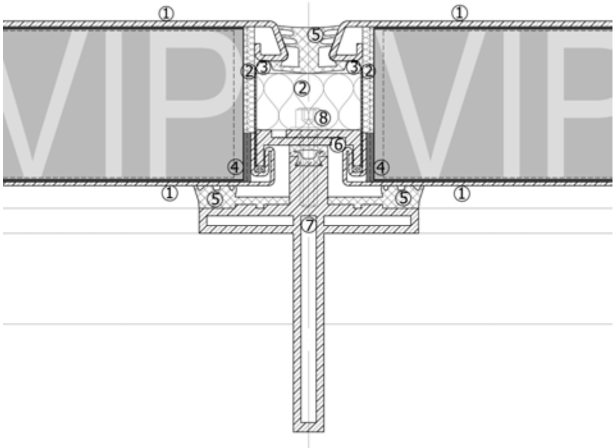

Figure 8.7a

Detailed horizontal section through the junction of two S-al sandwich components. Scale: 1/2.

1.) aluminium face sheets;
2.) Spaceloft™ insulation;
3.) non-metallic tape;
4.) (PU-based) adhesive;
5.) rubber seals and gaskets;
6.) mounting system;
7.) aluminium mullion;
8.) M5x20 socket screw.

Note: S-al stands for a VIP integrated sandwich panel with aluminium face sheets as opposed to S-steel which contains steel face sheets.

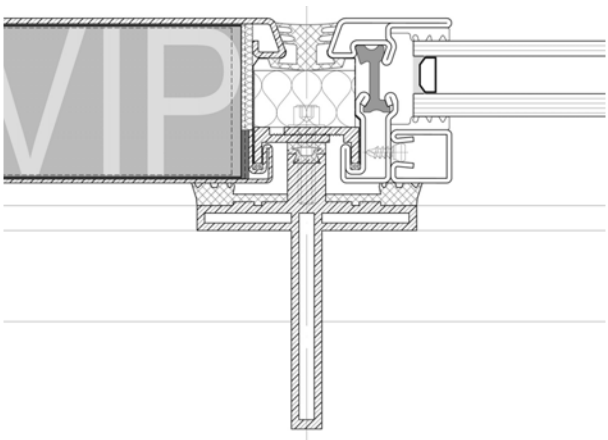

Figure 8.7b

Indicative horizontal section through the junction of an S-al sandwich component and a double-glazing frame. Scale: 1/2.

In case of VIP integrated sandwich panels, they can be accommodated in the thickness of the adhesive between inside face sheet and VIP at the panel's side and in the thickness of the Spaceloft™ insulation layer at this same side. If due to too large VIPs the thickness of the Spaceloft™ layer becomes less than 3 mm, a strip of, Compriband needs to be used in stead.

The face sheet at the panel's interior side is profiled in such a way that the grips can hook into this profiled edge. Space for adjusting the position of the façade components relative to each other and to the post-and-beam system is also available and accommodated by the system of grips: within a junction area each component can move from nominal position 3.5 mm to the right (or top) and 3.5 mm to the left (or bottom), in total thus 7 mm. It is expected that this suffices since the posts and beams can be positioned as well.

Figure 8.8a

The corner of the face sheet at the panel's exterior; left: artist impression; right: cutting pattern in flat metal sheet to produce this corner of the exterior face sheet.

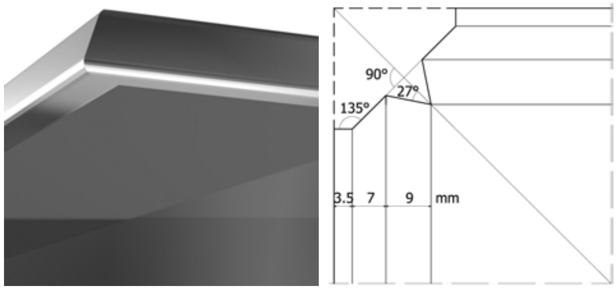

Figure 8.8b

Artist impression of the corner of an S-al sandwich component.

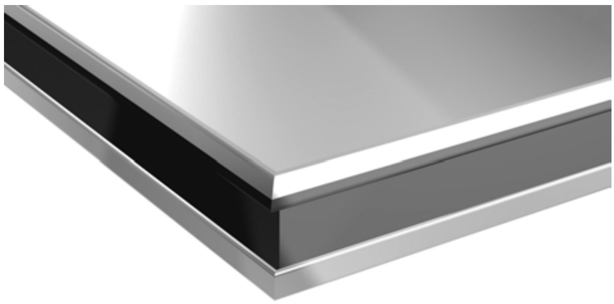

Producing an S-al panel, first the face sheets are prepared. From a sheet of metal some material needs to be cut away from its corners (Figure 8.8a). Then the edge of this sheet can be folded several times to obtain the profiled edge required. Finally, the corners need to be welded to obtain a closed shell. After preparing the face sheets, these sheets are glued onto the VIP and pressed together while the adhesive cures. Afterwards, the aerogel insulation blanket and reinforced non-metallic tape are added to the system finalizing the production process. It is important that the components are kept in factory for several weeks after production to assure that no damage of the VIP occurred during manufacture.

The air tightness between two adjoining components is maintained by a rubber seal between both exterior face sheets and by rubber gaskets between the post-and-beam system and the interior face sheet. Water tightness is primarily arranged by the aforementioned rubber seal between both exterior face sheets. Water penetrating this seal is blocked by pressure equalisation in the innermost cavity within this seal where it can either be transported to a vertical joint or if already in this joint drip downwards.

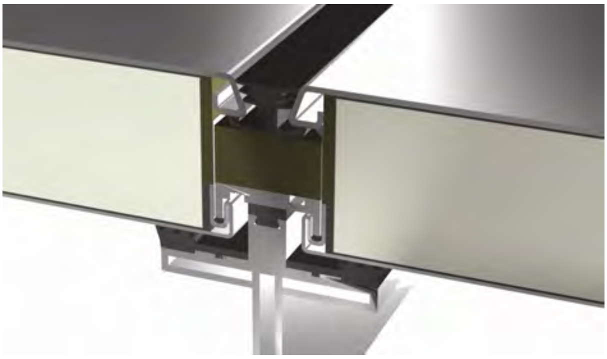

Figure 8.9

Rendering of the joint between two S-al components.

8.4.2 Expected thermal behaviour

The joints between two components and between two VIPs within a large component (1200x1800 mm^2) have been thermally simulated for both a thermal conductivity of the VIP core, λ_c, of $4.0 \cdot 10^{-3}$ W·m^{-1}·K^{-1} (initial condition) and $8.0 \cdot 10^{-3}$ W·m^{-1}·K^{-1} (end-of-life condition). The methodology for these simulations has already been explained in chapter 4[18].

A 40 mm thick VIP was chosen for this and other components to be presented in the next sections since 30 mm is insufficient to obtain Passivhaus standard with components of practical sizes (Figure 8.4b), since this thickness can be delivered by most manufacturers without changing their production facilities and since a component as thin as possible is desired. Figure 8.10 presents an image of the temperature field through the joint between two components while Table 8.3 (several pages later) summarises the calculated ψ-values of both this junction and of the connection of two VIPs within a large component. Between brackets, the end-of-life values are given. Based upon these linear thermal transmittance values and the dimensions of the component, the overall U_{eff}-value of an S-al component can be calculated. For a component of 900x1200 mm^2, this value becomes 0.163 W·m^{-2}·K^{-1} at initial conditions and 0.184 W·m^{-2}·K^{-1} (south façade) after 25 years. For a component of 1800x1200 mm^2, these values become 0.146 W·m^{-2}·K^{-1} and 0.168 W·m^{-2}·K^{-1} respectively. These values show that the small VIP integrated sandwich component does not meet the requirement of Passivhaus standard while the large component at initial conditions does.

---

[18] The central area of the component is defined by the outer dimensions of the VIP inside. It is important to realise that this linear thermal transmittance in all cases represents half the linear thermal transmittance of the entire joint. Moreover, in accordance with chapter 4 section 4.2, this linear thermal transmittance includes both centre-of-panel-edge-interactions and the total edge heat flow according to linear thermal transmittance definition (c) (Fig. 4.1).

Figure 8.10

Temperature field in the joint between two S-al components.

$T_i = 20^{o}C$ (red); $T_e = 0^{o}C$ (blue); $\alpha_i = 7.8\ W \cdot m^{-1} \cdot K^{-1}$; $\alpha_e = 25\ W \cdot m^{-1} \cdot K^{-1}$; $\varphi = 0.75$; $\lambda_c = 4.0 \cdot 10^{-3}\ W \cdot m^{-1} \cdot K^{-1}$; $\lambda_{film} = 0.54\ W \cdot m^{-1} \cdot K^{-1}$; $\lambda_{alu} = 225\ W \cdot m^{-1} \cdot K^{-1}$; $\lambda_{glue} = 0.28\ W \cdot m^{-1} \cdot K^{-1}$; $\lambda_{rubber} = 0.32\ W \cdot m^{-1} \cdot K^{-1}$; $\lambda_{tape} = 0.3\ W \cdot m^{-1} \cdot K^{-1}$; $\lambda_{aerogel} = 13.5 \cdot 10^{-3}\ W \cdot m^{-1} \cdot K^{-1}$; Air gaps according to NEN1068:2001 (2001). Heat flow line increment: 0.03 W.

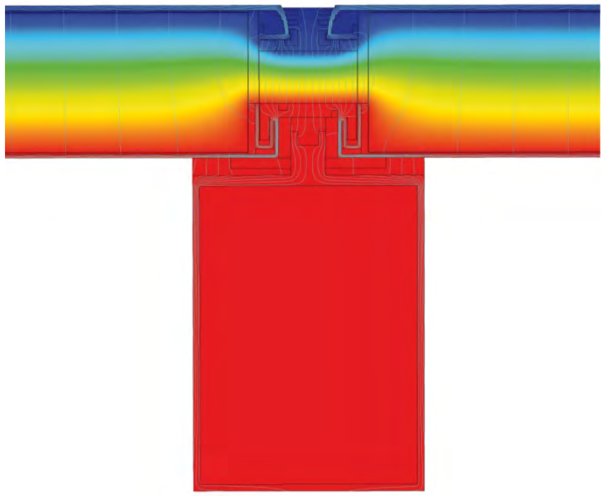

8.4.3 Expected service life

The service life of the VIPs inside the component has been estimated too. The calculation procedure for obtaining this estimate is explained in the interlude on page 236. These service life predictions have been performed for façade components oriented on a south, north and west façade. Figures 8.11 and 8.12 present the temperature of the VIP's barrier laminate on the cold and warm side of a south-oriented component with aluminium or steel facings respectively[19]. Moreover, Table 8.3 summarises the computed service life influencing factors and VIP service lives.

As can be observed, the service life of these panels under practical conditions is higher than the service life of an identical panel under laboratory conditions, i.e. f_{sl}[20]

[19] In these simulations, the solar heat absorption coefficient of anodised aluminium and coated steel were used, 0.45 and 0.85. Although this coefficient strongly depends on colour, most values in practice will lie between both aforementioned values, as a result of which they form an upper and lower boundary. Moreover, as boundary heat transfer coefficient a value of 15 $W \cdot m^{-2} \cdot K^{-1}$ is used. This value approximately corresponds to a wind speed of 1 $m \cdot s^{-1}$. On annual average the boundary heat transfer coefficient in the Netherlands is often considered to be 25 $W \cdot m^{-2} \cdot K^{-1}$, a value which is also used in standards (NEN-EN-ISO 10077-1, 2004). However, for the prediction of the service life of a VIP it is better to use more extreme than average conditions, i.e. low wind speed, since an estimate on the safe side is then obtained. A value of 15 $W \cdot m^{-2} \cdot K^{-1}$ would correspond to such low wind speed conditions (Leijendeckers et al., 1997). As a final remark, it must again be stressed that the influence of rh on the permeance of the VIP's barrier is not considered. The service life estimate is no longer on the safe side.

[20] In agreement with section 5.3.2, f_{sl} is the ratio of the VIP's actual service life in application, t_{sl}, and its service life determined in a laboratory at 23°C and 50% rh, t_{lab}. It must be stressed that for determining t_{sl} and t_{lab} identical panels of identical dimensions are used. Differences between t_{sl} and t_{lab} thus result from differences in climatic conditions.

is larger than 1. These high values primarily result from the assumption that no water vapour and dry gas intake occurs through the barrier envelope at those places where it is connected via an adhesive to a face sheet, from a lower annual Arrhenius average temperature of the laminate in practise relative to lab conditions and from the omission of the effect of relative humidity on the permeance of the laminate. Especially this latter effect results in an overestimation of real service life values (see also footnote 31 for getting an indication of this influence).

Moreover, the service life of a VIP inside a component with steel face sheets is somewhat lower than that of a VIP inside a component with aluminium face sheets. In case of a south orientation this difference is between 15% and 20%. It results from a higher Arrhenius average temperature of the barrier due to a higher solar heat absorption coefficient used in the simulations for steel relative to aluminium. But also VIPs inside these components easily fulfil the requirement on service life (λ_{cr} = 8.0 W·m^{-1}·K^{-1} no thermal bridging) set to at least 30 years for a façade.

It must finally be noted that the service life of a VIP in a sandwich panel is difficult to estimate since the effect of an adhesive on the properties of the barrier envelope is unknown. Moreover, the face sheet directly adhered to a VIP was considered to act as an additional barrier thus increasing the service life. The extent to which this occurs is unknown. The values presented here therefore are indicative.

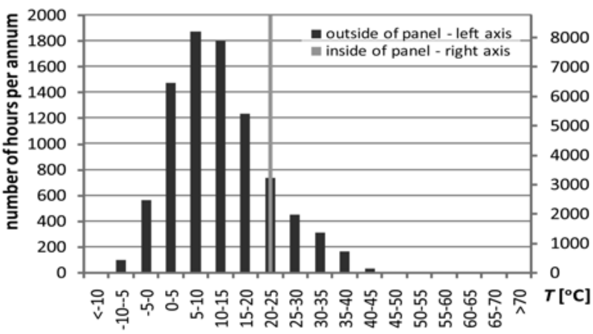

Figure 8.11

Histogram of the number of hourly temperatures per annum of the VIP barrier laminate on the inside (light grey) and outside (dark grey) of a sandwich component with aluminium face sheets (S-al panel) and south orientation. Note: wind speed used for determining heat transfer from and towards surrounding air is 1 m·s^{-1}. When there is no wind, temperatures even get higher. Since such low wind speeds do not occur regularly, the effect on calculations will be small.

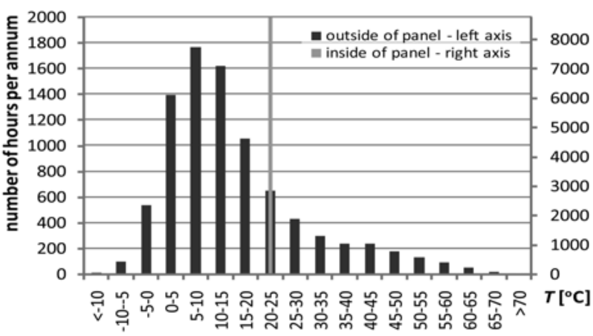

Figure 8.12

Histogram of the number of hourly temperatures per annum of the VIP barrier laminate on the inside (light grey) and outside (dark grey) of a sandwich component with steel face sheets (S-steel panel) and south orientation for a location in the Netherlands.

The service life of the vacuum insulation panels inside the S-al component and other components can be estimated if the environmental conditions around the VIP are known. Relevant parameters in this respect are the temperature of the barrier laminate, the relative humidity and the partial water vapour pressure directly in front of the barrier laminate. Because of the relation between temperature, relative humidity and partial water vapour pressure via the water vapour saturation pressure, only two parameters need to be calculated, one of which is the temperature.

If these parameters are known, the service life can be predicted using the method discussed in chapter 5 sections 5.2 and 5.3 using service life influencing factors for including dynamic effects in the computations. According to this method, the environmental parameters need to be known as function of position over the surface of a VIP and as function of time. For ease of computation, first the arithmetic averages of the temperature over the VIP surface at the cold side, over its surface at the warm side and over the VIP's edges are calculated from a steady-state numerical simulation using Trisco. Then for each surface, the ratio $e = (T_i - T_e)/(T_i - T_{f;i;av})$ is calculated. In this ratio, T_i [K] is the temperature of the space behind the façade (=22°C), T_e [K] is the temperature of the air outside the building and $T_{f;iav}$ [K] is the Arrhenius average temperature of the surface (Simmler and Brunner, 2005). The model for simulating the hourly values of temperature, relative humidity and partial water vapour pressure, can then be reduced to three semi steady-state one-dimensional systems in which the temperature of each surface of the barrier laminate is estimated as $T_{f;i;av} = (T_e(t) + (e-1)\cdot T_i) / e$ for each time step. Using test reference climate data from 1995 from De Bilt (NL), hourly temperatures for each surface of the VIP are then calculated which can be used as basis for calculating $f_{w;T+\phi}$ and $f_{g;T+\phi}$.The sol-air-temperature, which both includes outside temperature and solar irradiation, is used for T_e. This latter temperature heavily depends on outdoor wind conditions while the solar absorption coefficient strongly depends on the colour and texture of the surface of the outer face sheet. Among others for these reasons predicted service life values should be considered indicative only.

For calculating the relative humidity and partial water vapour pressure directly surrounding the VIP, it is assumed that a façade system is never completely closed from outside air. In practice there will always be some air exchange between a cavity inside these façade components and the air outside by for example a small hole used for water drainage. For each time step, the relative humidity and partial water vapour pressure can now be calculated as follows: a change in temperature in the cavity results in a change of volume of the air in this cavity; this volume change is compensated by air exchange with the air surrounding the component – either air intake if the volume decreases or air outlet if the volume increases; if air is entering the cavity an amount of water vapour is taken along which can be calculated based on the change in volume, the outside temperature (thus saturation concentration) and the outside relative humidity; if air is leaving the cavity an amount of water vapour is leaving the cavity as well calculated from the concentration of water vapour in the cavity air; from the resulting water vapour concentration in the cavity and the air temperature in this cavity, the relative humidity and water vapour pressure can be computed; in a similar fashion a change in external barometric pressure can result in an air flow towards or from the cavity, assumed that pressure equalisation occurs; a 1% change in barometric pressure yields a 1% change in cavity air volume.

In case of a sandwich panel in which a face sheet is structurally adhered to the VIP barrier laminate, it is assumed that this adhesive and face sheet act as a perfect barrier to water vapour and gas permeation, as a result of which these VIP surfaces no longer participate in the process of gas pressure and water content increase in the VIP core.

Due to a membrane on four sides enveloping a wooden membrane panel, no air exchange between the cavities along the faces of the VIPs inside their environment is assumed. Moreover, Accoya wood in contact with the air inside aforementioned cavities absorbs and desorbs moisture. For calculating the relative humidity inside these cavities therefore a different approach is used. This approach is explained in appendix 81.

From these temperature, relative humidity and partial water vapour pressure values, in principal all service life influencing factors can be calculated according to the equations presented in section 5.3 and from these factors and material data presented in chapter 5 the service life can iteratively be computed. However, due to lack of knowledge on the influence of relative humidity on the permeability of a metallised barrier laminate $a_{w;\phi}$ and $a_{g;\phi}$ cannot be determined and therefore $f_{w;\phi}$ and $f_{g;\phi}$ are calculated solely based on temperature effects and not on relative humidity effects. Since in general the relative humidity in the air cavities surrounding a VIP within a building component is higher than 50%, which is the reference laboratory condition, the predicted service lives are higher than if relative humidity effects are considered.

8.4.4 Expected structural behaviour

As explained in a previous section, perfect sandwich behaviour is not likely to occur in case of a VIP integrated sandwich panel. Within the framework of this study, a good structural bond between mdf, a resin bounded composite cladding panel and glass face sheets on the one hand and a VIP barrier laminate on the other hand could not be established experimentally. Besides, sliding of the barrier laminate over the VIP core might occur because shear stresses in the interface between laminate and core might exceed friction if the load on the panel exceeds a certain value. From a structural perspective therefore more research into the connection of face sheet to barrier laminate and barrier laminate to core needs to be conducted.

If it is however assumed that perfect sandwich behaviour does occur and that loads are transferred in one direction as in a beam, which is likely to occur for façade panels with high aspect ratio, then the flexural stiffness of a panel of 1 m wide according to equation (8.1) equals $84\cdot10^3$ N·m² for an S-al panel and $245\cdot10^3$ N·m² for an S-steel panel. If however no structural bond between face sheets and VIP exists, this stiffness reduces to 198 N·m² and 252 N·m² for aforementioned panels respectively. This latter value is significantly lower than the first value. The actual

Table 8.3 *– Overview of the thermal behaviour of VIP integrated sandwich panels with either aluminium or steel face sheets and the service life of the VIPs inside.*

	Sandwich panel (S-al panel)			Sandwich panel (S-al panel)			Sandwich panel (S-steel panel)		
Size [mm^2]	900x1200			1800x1200			900x1200		
VIPs [mm^3]	1 pc. of 866x1166x40			2 pcs. of 883x1166x40			1 pc. of 866x1166x40		
mass [kg]	18			36			33		
d_p [mm]	43 (nominal)			43 (nominal)			43 (nominal)		
Thermal [g]									
$\psi_{edge;junction;1}$ [$W\cdot m^{-1}\cdot K^{-1}$][e]	0.0189 (0.0189)			0.0189 (0.0189)			0.0184 (0.0184)		
$\psi_{edge;junction;2}$ [$W\cdot m^{-1}\cdot K^{-1}$][e]	0.0189 (0.0189)			0.0189 (0.0189)			0.0184 (0.0184)		
$\psi_{edge;stiffener}$ [$W\cdot m^{-1}\cdot K^{-1}$][e]	-			0.0013 (0.0010)[f]			-		
U_{eff} initial [$W\cdot m^{-2}\cdot K^{-1}$]	0.163			0.146			0.161		
U_{eff} at 25 yrs [$W\cdot m^{-2}\cdot K^{-1}$]	0.183 (N) - 0.184 (S)			0.168			0.182 (N) - 0.184 (S)		
U_{eff} end of life [$W\cdot m^{-2}\cdot K^{-1}$]	0.251			0.236			0.250		
Service life									
	North	*South*	*West*	*North*	*South*	*West*	*North*	*South*	*West*
$f_{w;T+\phi}$ [-][a,b,d]	0.62	0.68	0.66	0.62	0.68	0.66	0.65	0.81	0.75
$f_{w;p}$ [-] [d]	0.85	0.85	0.87	0.85	0.85	0.87	0.86	0.85	0.88
$f_{g;T+\phi}$ [-] [a,b,d]	0.60	0.67	0.64	0.60	0.67	0.64	0.64	0.81	0.75
$f_{g;p}$ [-] [d]	1.00	1.00	1.00	1.00	1.00	1.00	1.00	1.00	1.00
t_{sl} [yr] [a,b,d,h]	306	276	285	306	276	285	287	229	243
f_{sl} [-] [a,b,d,h]	2.76	2.48	2.57	2.76	2.48	2.57	2.59	2.06	2.19
$\bar{T}_{e;arith.}$ [^oC]^c	10.6	12.2	11.5	10.6	12.2	11.5	11.6	14.8	13.3
$\bar{T}_{e;arrh.}$ [^oC]^c	15.9	17.3	16.6	15.9	17.3	16.6	14.3	19.9	18.9

[a] The effect of relative humidity on the water vapour and gas transmission rate of the barrier envelope is neglected in the calculation of $f_{w;T+\phi}$ and $f_{g;T+\phi}$. Since the annual average relative humidity surrounding the VIP is higher than the reference laboratory condition of 50% r.h. at a temperature of 23°C, the service life values presented in this table are higher than if r.h.-effects are considered. [b] Absorption coefficient anodised aluminium and coated steel are 0.45 and 0.85 respectively (vd Linden, 2000), T_i = 22°C, α_e = 15 $W\cdot m^{-2}\cdot K^{-1}$ (wind speed ± 1 $m\cdot s^{-1}$), α_i = 7.8 $W\cdot m^{-2}\cdot K^{-1}$, outside conditions according to weather data from De Bilt and Wageningen in 1995(NL), no nocturnal long-wave radiation. [c] These temperatures are calculated as annual temperatures of the entire VIP thus including both surfaces and its perimeter. For calculating the Arrhenius average temperature, an activation energy of 50 $kJ\cdot mol^{-1}$ is used. [d] For determining the service life influencing factors and the service life of VIPs within S-al and S-steel components, perfect gas and water vapour tightness of the combination of barrier envelope, adhesive and face sheet is assumed. Water vapour and dry gases solely permeate the barrier through the panel's edge. It must be stressed that in practise some water vapour and gas will permeate through these layers. The predicted values here are

thus overestimated values. Besides, the service life measured in a laboratory does include gas and water intake through the surface of a VIP as a result of which f_{sl}, the service life factor (section 5.3.2), is larger than unity even for panels with a steel face sheet on a south orientation. [e] The linear thermal transmittance values presented in this table always solely represent one half a junction. [f] This linear thermal transmittance is only present in a sandwich panel of 1200x1800 mm^2 and represents the thermal bridge due the barrier films between 2 adjoining VIPs. [g] The values between brackets are end-of-life values. [h] λ_{cr} = 8.0 W·m^{-1}·K^{-1} for the core, thus thermal bridge effects not considered in the prediction.

structural behaviour of the sandwich component will be in-between both limit conditions. In case a wind load of 2.3 kN·m^{-2} including safety factors acts on a façade component that transmits this load one-dimensionally to its supports and that has a span of 1.2 m and a maximum deflection of 0.002 times its span, the required flexural stiffness would be 26·10^3 N·m^2. This requirement can easily be met if perfect sandwich behaviour occurs but may be to stringent if such behaviour is unavailable.

8.4.5 Evaluation

As we have seen in the previous sections, a VIP integrated sandwich panel would create a very thin façade system at the same time having high thermal performance. Moreover, even if the assumption that no water vapour and dry gas permeates through the surfaces of the barrier directly attached to the face sheets does not hold, a long service life may be obtained. Besides, a façade system made of these VIP integrated sandwiches thermally outperforms a system made of sheet-VIPs (VISs) since the high conducting materials penetrating the thermal barrier in case of S-al/steel panels (VIP barrier and non-metallic tape; sum of $\lambda_i \cdot t_i$ =0.22·10^{-3} W·K^{-1} per junction) conduct less heat than in case of a sheet-VIP (thin stainless steel edge membrane; $\lambda \cdot t$ =9.7·10^{-3} W·K^{-1} per junction; Figure 4.5b in chapter 4). Also, the thermal quality of the VIP can be checked on-site after installation using thermography since an increased temperature in front of a defective panel will be detectible due to the weakness of the thermal bridge despite the use of highly conducting metal sheets[21]. However, if a broken VIP is detected, the entire component needs to be demounted and replaced; the VIP itself cannot be replaced easily. This bond also inhibits recycling. Moreover, during this study a good bond between face sheets and laminate could not be established.

[21] Simulations with a temperature difference of 20^{o}C from inside to outside showed that the maximum temperature difference between the outer face sheet of an intact and of a broken component is about 1.4^{o}C. This difference is easily detected. Besides, internal pressure sensors inside a VIP able to transmit data via radio frequencies might also be used (Caps et al., 2008).

To check whether the predicted service lives of VIPs inside E- and M-components are within a plausible range, the service life prediction of a VIP of 0.5x0.5x0.02 m^3 installed as roof terrace insulation by Simmler and Brunner (2005) is used as reference. Based on actual measurements they predicted a service life of 31.6 years for $\lambda_{cr} = 8 \cdot 10^{-3}$ $W \cdot m^{-1} \cdot K^{-1}$. This value applies to very small panels and needs to be recalculated for panels with a size of 1.0x1.2x0.04 m^3.

Simmler and Brunner (2005) measured a pressure increase of 2.1 mbar/yr. This pressure increase is among others determined by the volume of the vacuum insulation panels, its surface area and circumference. Using the area and perimeter related permeance values from Table 5.1b, it can be calculated that the gas transmission rate through the entire barrier envelope of the larger panel is about 2.4 times the transmission rate through the smaller panel. Moreover, the volume of the larger panel is 9.6 times the volume of the smaller panel. So, under the same environmental conditions the pressure increase rate of the large panel should be 2.1x2.4/9.6=0.53 mbar/yr.

They also calculated a time constant for water content increase, τ_w, of 35.6 yr. This time constant is also among others determined by the volume of the VIPs, its surface area and circumference. Again using the area and perimeter related permeance values from Table 5.1b, the water vapour transmission rate through the entire barrier envelope of the larger panel can be calculated to be about 3.5 times the transmission rate through the envelope of the small panel. As a result, the time constant for a panel of 1.0x1.2x0.04 m^3 under the same environmental conditions becomes 35.6/3.5x9.6=98.8 yr.

From these values, a service life of 104 years of a VIP of 1.0x1.2x0.04 m^3 with a fumed silica core and metallised barrier is calculated according to the methodology and conditions described by Simmler and Brunner (2005). This value is significantly lower than the service life calculated for VIPs inside components in this chapter. This has several causes: 1.) in-situ measurements versus calculations based upon simulations and lab values; 2.) different Arrhenius average temperatures; 3.) not considering relative humidity effects on the permeability of the barrier; 4.) low solar heat absorption coefficient of aluminium (a=0.45); 5.) in case of S-panels, the assumption that the glue is perfectly vapour and gas tight. The third and fifth effects are most important (p.250).

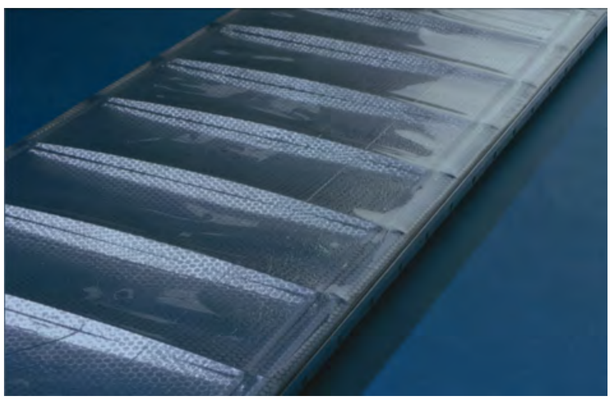

Figure 8.13

Mock-up of temporary VIP integrated thermal insulation lamella (cremers, 2006).

8.5 VIP INTEGRATED MEMBRANE PANEL (M-WOOD PANEL)

8.5.1 General description

One of the disadvantages of sandwich components is that, due to a structural bond between face sheets and VIP, its recycling potential is inhibited. A new façade panel is therefore designed in which the use of adhesives and sealants is limited to a far extent. Moreover, in accordance with cradle-to-cradle ideology, the component should be designed in such a way that materials can be separated from each other after being disposed of. As a result, biological materials can be returned into the biosphere while technical materials can be re-used in the technosphere (McDonough and Braungart, 2002). These façade panels are named VIP integrated panels with a membrane and a wooden frame, or in short membrane panels, or M-wood panels.

As part of his doctoral research, Jan Cremers designed a system of lamellae for temporary thermal insulation (Cremers, 2006). Such a system using a membrane for creating structural rigidity allowed for a thermally optimised 'edge' because of small contact points between two lamellae. One lamella consists of a VIP, a polycarbonate framework encapsulating the VIP and a membrane wrapped around this framework, as can be seen from Figure 8.13. If designed properly such a system limits the amount of 'highly' conducting materials penetrating the thermal barrier to the VIP barrier and this membrane. This membrane should be pre-stressed to combine the VIP and the encasing into a single component and to increase the stiffness of the system[22]. This idea of an encasing enveloped by a pre-stressed membrane is in this chapter taken as a reference for designing the M-wood panel; it is modified for a façade system since the requirements regarding size, structural behaviour and air and water tightness are much stronger for façade systems.

The membrane components designed in this chapter consist of the following materials: a 40 mm thick VIP with a fumed silica core and a metallised barrier envelope with three metallisation layers; a membrane of translucent bio-polymer[23]

---

[22] As a membrane ETFE foil was used introducing a certain amount of transparency and architectural expression. For more stringent requirements regarding stiffness and strength, a PTFE coated fabric of glass or aramide fibres can be used (Buitink Technology, 2009). Both types of membranes can be recycled (downcycled), for example using Texyloop® technology (SAS/Texyloop, 2009), or maybe even re-used.

[23] No exact specification of this bio-polymer will be given here since many developments into improving the quality of these materials are currently on-going. For reducing the amount of

(±0.5 mm thick); a framework[24] or encasing made of Accoya™ wood; Spaceloft™ aerogel insulation blankets at the panel's sides (6+9 mm) and inside the stiffeners (6 mm); a compression bond between wooden encasing and VIP for accommodating dimensional tolerances and protection; a stainless steel element for pre-stressing the membrane; silica gel as drying agent inside the component's outer cavity; and mechanical fasteners (socket screws, regular screws, bolds and L-shaped metal plates for increasing the rigidity of corners). Detailed sections of this membrane component are presented in Figure 8.14. Figure 8.15 presents a section through a joint with a frame for double-glazing[16]. With on both sides of the VIP a cavity of 22 mm, the total thickness of the entire component becomes approximately 85 mm[25].

In production, first the wooden encasings are prepared. From rectangular wooden sections (32x50 or 32x75 mm^2), the required shapes are made. These are then attached to each other forming a framework. Since such a rectangular framework lacks rigidity of its own - the corners are pinned connections - 2 mm thick steel L-shaped plates are added at the corners to connect different sections to one another using regular screws, as can be seen from Figure 8.16. Moreover, a pattern of skew wooden sections is added to this framework as bracings. They are connected to the framework as shown in Figure 8.17. Moreover, if the membrane

---

water vapour penetrating this barrier and thus the amount of silica gel needed in the cavity however it might need a SiO_x coating. This is also true if ETFE foil is used.

[24] Since part of the encasing needed to be at the side of a VIP for keeping these panels in place, a material with a thermal conductivity as low as possible had to be selected. Metals fail this criterion. Moreover, since the encasing, especially the stiffeners, contributes significantly to the stiffness of a component (subsection 8.5.4), a material with a Young's modulus as high as possible was needed. Most polymers fail this criterion. Materials having both low thermal conductivity and high flexural modulus are fibre reinforced polymers and wood. Several fibre reinforced polymers were studied, like carbon filled polyamide (PA 30% PAN carbon fibre) having a Young's modulus of 19.3 to 20.7 GPa and a thermal conductivity of 0.594 to 0.618 $W \cdot m^{-1} \cdot K^{-1}$ (Granta Design, 2008), biodegradable polymers and Duralin fibre reinforced polypropylene (Stamboulis et al., 2000). Except for carbon filled PA or glass fibre reinforced polymers, these polymers however lacked sufficient stiffness (Tserki et al., 2006; Yu et al., 2006; Riedel and Nickel, 1999; Liu et al., 2007; Kim et al., 2006; Nauta et al., 2001). Moreover, reinforced polymers have recycling difficulties. As a consequence, Accoya® wood was selected as the material of choice (Titan Wood, 2008). More information is in Appendix A84.

[25] The final configuration is practically symmetrical, except for small details. Symmetry was chosen for several reasons. First, for facilitating the connection between component and load-bearing structure, i.e. post-and-beam system, the side facing the interior of the building needs to be flat. Second, for machining wood easily, a certain thickness and volume of this wood is required. Third, due to the previous requirement, the dimensions of the wooden encasing were already large enough for safely transmitting wind loads to the load-bearing system. Therefore no additional material and thus no asymmetry were required. Fourth, a component as thin as possible was desired. As a result, the membrane is no longer curved or segmented, like a cable-stayed beam, but flat. It does therefore hardly partake in structural action, except for transmitting wind loads towards the wooden encasing. The membrane has thus mainly become a protective shield for the VIP and a means of architectural expression.

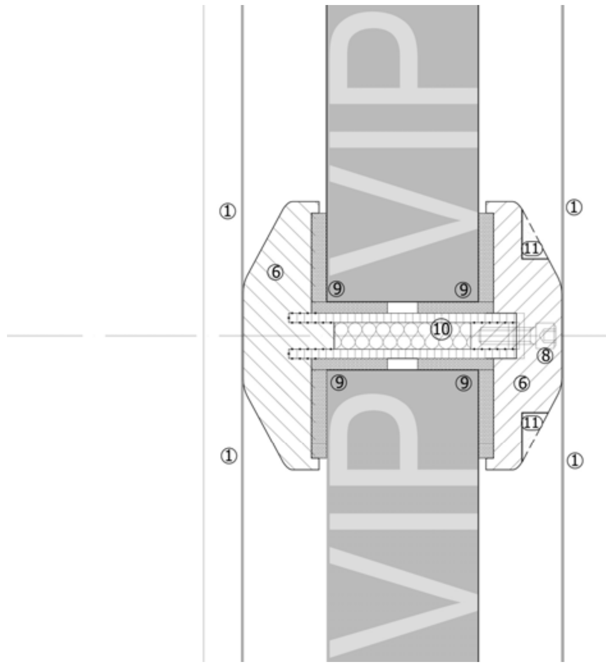

Figure 8.14a

Detailed vertical section through a stiffener inside an M-wood membrane component. Scale: 1/2.

1.) membrane;
2.) Spaceloft™ insulation;
3.) stainless steel element for pre-stressing the membrane;
4.) 2 mm thick aluminium cover plate on top of 3 mm thick alu. closing section;
5.) rubber seals or hairy weather-strips ;
6.) wooden encasing;
7.) wooden mullion and connecting system;
8.) mechanical fasteners;
9.) Compression band, like Illmod eco;
10.) 'sandwich' made of 3 mm plywood and 6 mm Spaceloft™;
11.) drying agent: silica gel.

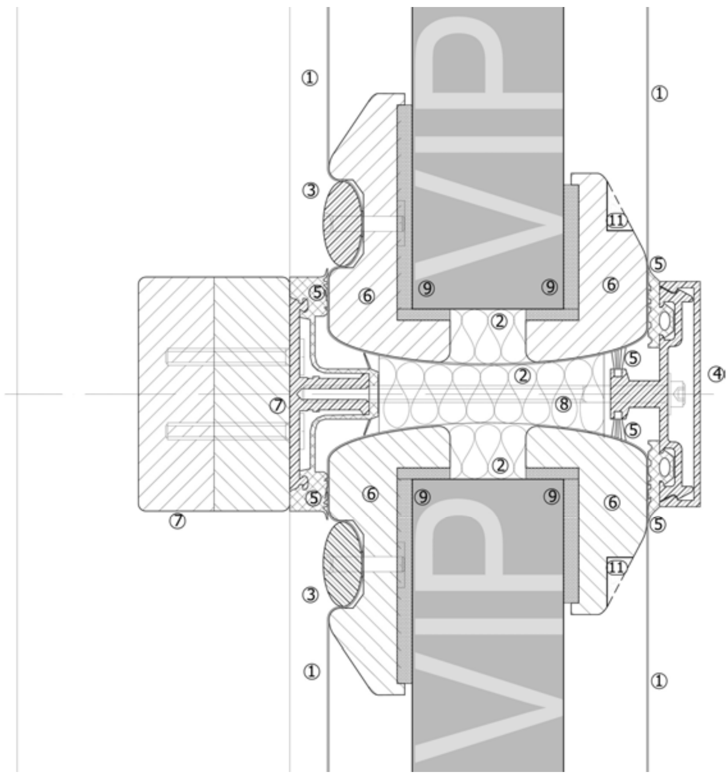

Figure 8.14b

Detailed vertical section through a junction between two M-wood membrane components. Scale: 1/2.

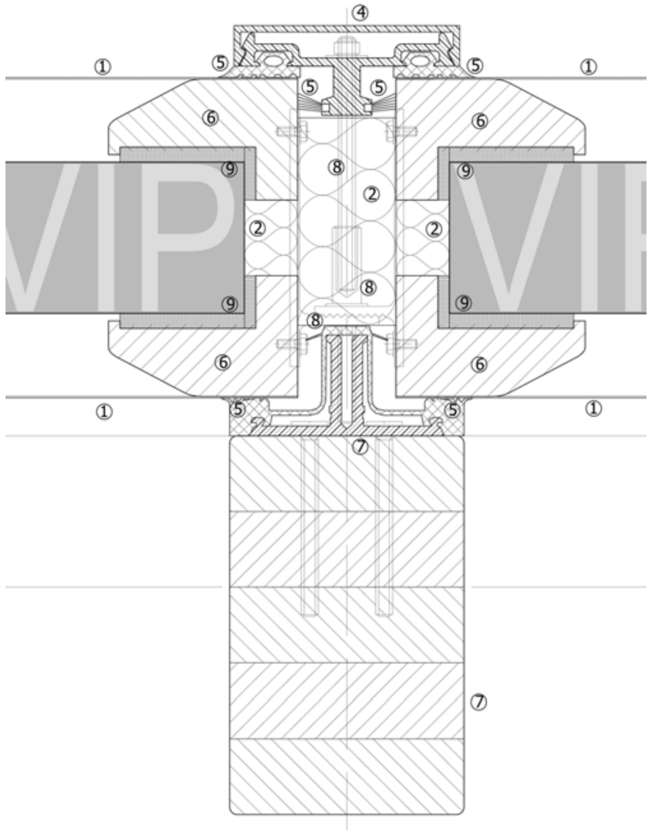

Figure 8.14c

Detailed horizontal section through a load-bearing junction between two M-wood membrane components. Scale: 1/2.

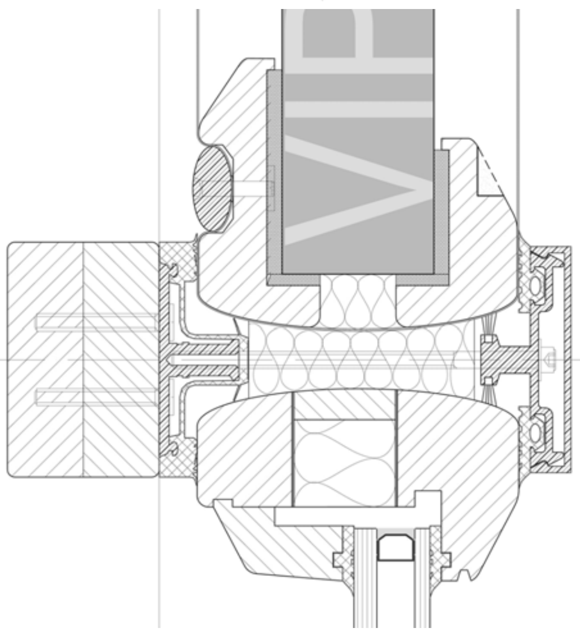

Figure 8.15

Indicative vertical section through the junction of an M-wood membrane component and a double-glazing frame. Scale: 1/2.

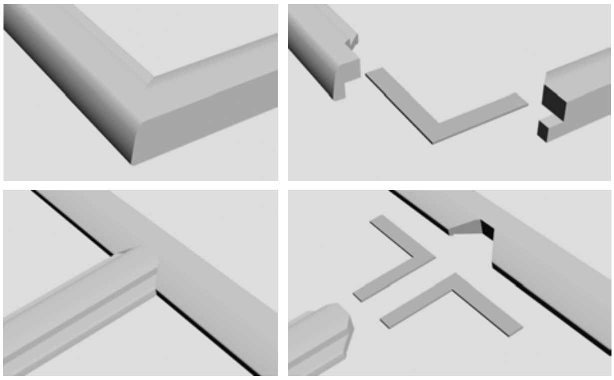

Figure 8.16

Renderings of connections between wooden sections using metal L-shape for improving rigidity of corner.

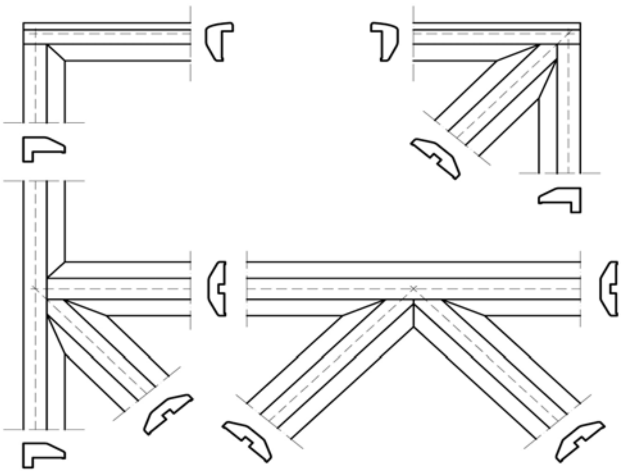

Figure 8.17

Top view of connections between all types of wooden sections.

has a certain amount of transparency, this framework with bracings can be used for architectural expression. Several configurations are then possible, examples of which are presented in Figure 8.18[26]. To these wooden encasings a compression band, like Illmod Eco, is attached at the appropriate positions. After positioning the VIPs inside the encasing at the component's interior side and Spaceloft™ insulation to fill the gaps in the junction area, the exterior encasing is placed on top of these elements and connected with M5 socket screws to the interior face sheet and by

[26] If the membrane lacks transparency, then the entire encasing can be simplified to a plate of OSB or plywood of approximately 10 to 15 mm thick. This would reduce the labour-intensiveness of these components significantly. Like the transparent version presented in the text, however, this version will have relatively low bending stiffness unless a very high pre-stress and curved plates are used. Regarding such opaque components, the encasing components presented in section 8.6 will be more practical and more suitable for façades.

Figure 8.18

Potential configurations of bracings within wooden framework, together forming a wooden encasing.

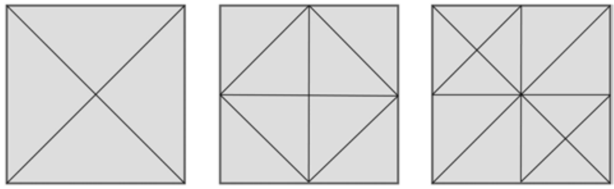

steel grips, which are also used for connecting the component to a post-and-beam system[27], as can be seen from Figure 8.14c. Finally, the membrane is wrapped around this system and pre-stressed using an elliptical stainless steel element. It is important that the components are kept in factory for several weeks for quality assurance using a pressure-sensitive sensor and RFID chip (Caps et al., 2008).

As will be discussed in the section on expected structural behaviour, the stiffening elements are primarily responsible for giving the component sufficient stiffness thus determining the maximum span of the component. Since they span in one direction, the size of the other direction can be chosen with less limitations[28]. For this component standard sizes of 900x1800 mm^2, 1200x1800 mm^2 and 1200x3600 mm^2 are therefore chosen, corresponding to regular grid dimensions in the architectural practice. The entire component is fixed to this post-and-beam system using steel grips that are screwed onto the wooden encasing. The properties of these three panels are presented in Table 8.4.

To accommodate the large dimensional tolerances of VIPs both in thickness and length, which are drawn as a broken line along the VIP's perimeter (inside and outside) in Figure 8.14a and b, a compression band, like Illbrück illmod eco, between

[27] During the design stage it was decided to separate the load-bearing post-and-beam system from the membrane component. As might be seen from Figure 8.14c, the wooden section at the warm side of the component can be modified and enlarged so as to immediately act as a load-bearing element spanning between two floors. Such a system would reduce the amount of labour on site. Still, it was decided for multiple reasons to separate both elements. First, the problem of accommodating large dimensional tolerances from concrete floors is now transferred to the post-and-beam system for which standard systems already exist. Second, façade components can now be made in standard sizes without the need for variability in dimensions resulting from different load cases. And third, the connection between both wooden encasings should have been made more sturdy as a result of which deteriorating the thermal performance of the component. As a result from this separation, however, the wooden encasings are no longer rigid by themselves and need additional bracings.

[28] As limitations can be mentioned size constraints imposed by the size of vacuum insulation panels, size limitations because of transport and handling, and constraints by the use of architectural grids. Moreover, as will be shown in the section on thermal performance, a minimum size might be imposed on the component by thermal performance requirements.

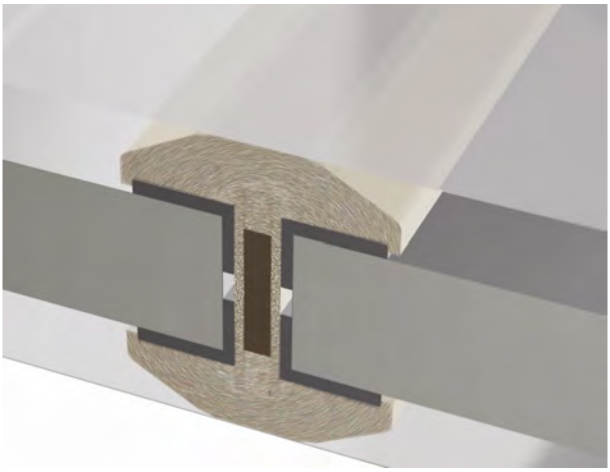

Figure 8.19a

Rendering of the joint between two MS-wood components.

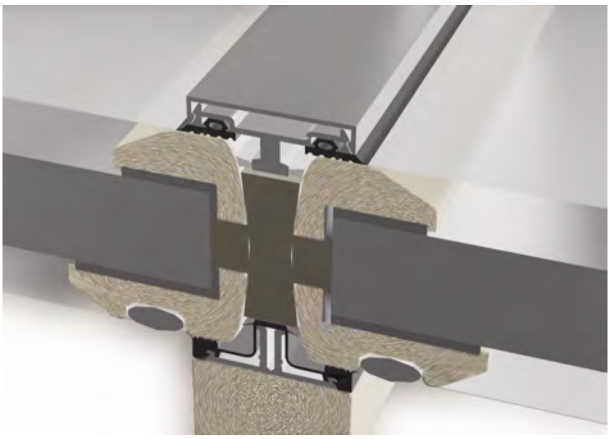

Figure 8.19b

Rendering of a stiffening element inside an MS-wood component.

the VIP and the wooden encasing is used. Since this can easily be compressed and stretched, the gap between VIP and encasing is always closed. It also separates the metal L-shapes for increasing the rigidity of corner from the VIP thus reducing damage risk. Inside the component between two VIPs and along the component's circumference, Spaceloft™ insulation is added to improve the thermal performance of these junctions. This insulation material is slightly compressible and can thus also accommodate dimensional tolerances if necessary.

The grips along two sides of the component's perimeter connect the component to a mullion, i.e. the bearing system. The actual connection is made by mechanical fasteners. Space for adjusting the position of the façade components relative to each other and relative to the post-and-beam system is available and accommodated by this system of grips: within a junction area each component can move from nominal position 5 mm to the right (or top) and 5 mm to the left (or bottom), in total thus 10 mm using slotted holes. It is expected that this suffices since the posts and beams can be positioned as well.

Air and water tightness between two components, finally, is achieved by rubber gaskets on both sides of the component and hairy weather-strips inside the cover section. Water penetrating the outer seal of a horizontal junction is captured behind the seal where pressure equalisation can occur and water droplets can be transported towards a vertical junction. Water penetrating a vertical junction is captured in a similar way and transported by gravity downwards. Since the relative humidity inside the outermost cavity of the component often reaches 100%[29] if no desiccant measures are taken according to simulations for predicting the VIP's service life, silica gel is added into this cavity as drying agent[30].

8.5.2 Expected thermal behaviour

The joints between two components and between two VIPs within a component (stiffening elements) have been thermally simulated using Trisco as computational tool for both a thermal conductivity of the VIP core, λ_c, of $4.0 \cdot 10^{-3}$ W·m^{-1}·K^{-1} (initial condition) and $8.0 \cdot 10^{-3}$ W·m^{-1}·K^{-1} (end-of-life condition). The methodology for calculating the linear thermal transmittance of these joints has already been explained in chapter 4[18]. Again a 40 mm thick VIP was chosen for these M-components for the same reasons as explained previously for S-components.

Figure 8.20 presents images of the temperature field through two joints between components and the joint between two VIPs inside a component while Table 8.4 summarises the calculated ψ-values of all junctions. Between brackets, the end-of-life values are given. Based upon these linear thermal transmittance values and the dimensions of the component, the overall U_{eff}-value of an M-wood panel can be estimated. For a component of 1200x1800 mm^2 for example, this value becomes 0.136 W·m^{-2}·K^{-1} at initial conditions, 0.166 W·m^{-2}·K^{-1} after 25 years on a south orientation and 0.212 W·m^{-2}·K^{-1} at the end of its life after 142 years when the arbitrary criterion of $\lambda_{cr} = 8.0 \cdot 10^{-3}$ W·m^{-1}·K^{-1} has been reached. Figure 8.21 finally presents the effective U-value of a component as function of width and panel length. As can be seen, only small components do not meet the requirement set by Passivhaus standard at initial conditions.

---

[29] One of the boundary conditions for these simulations is a starting condition, i.e. the condition under which the component is produced, of 23°C and 50% r.h.

[30] The calculations on expected service life do not include the effect of such a desiccant.

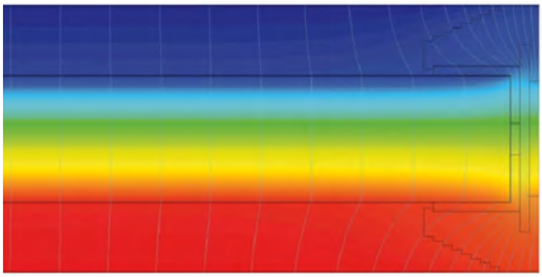

Figure 8.20a

Temperature field in the joint between two VIPs inside an MS-wood component.

$T_i = 20^oC$ (red); $T_e = 0^oC$ (blue);
$\alpha_i = 7.8\ W{\cdot}m^{-1}{\cdot}K^{-1}$;
$\alpha_e = 25\ W{\cdot}m^{-1}{\cdot}K^{-1}$; $\varphi = 0.75$;
$\lambda_c = 4.0{\cdot}10^{-3}\ W{\cdot}m^{-1}{\cdot}K^{-1}$;
$\lambda_{film} = 0.54\ W{\cdot}m^{-1}{\cdot}K^{-1}$;
$\lambda_{wood} = 0.19\ W{\cdot}m^{-1}{\cdot}K^{-1}$;
$\lambda_{membrane} = 0.5\ W{\cdot}m^{-1}{\cdot}K^{-1}$;
$\lambda_{thermobond} = 0.05\ W{\cdot}m^{-1}{\cdot}K^{-1}$;
$\lambda_{steel} = 16.2\ W{\cdot}m^{-1}{\cdot}K^{-1}$;
$\lambda_{aerogel} = 13.5{\cdot}10^{-3}\ W{\cdot}m^{-1}{\cdot}K^{-1}$;
$\lambda_{alu} = 225\ W{\cdot}m^{-1}{\cdot}K^{-1}$;
$\lambda_{rubber} = 0.32\ W{\cdot}m^{-1}{\cdot}K^{-1}$;

Air gaps according to NEN1068:2001 (2001). Heat flow line increment: 0.03 W.

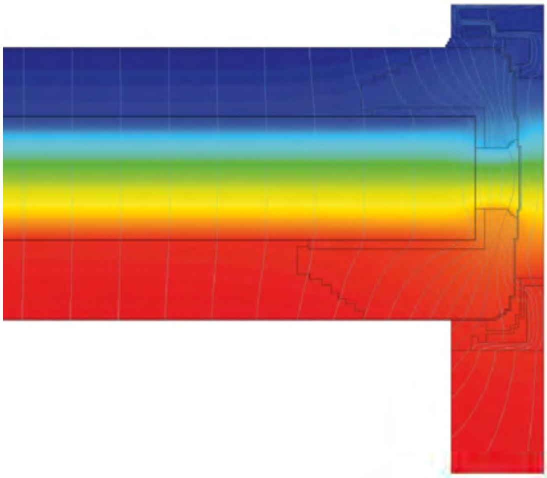

Figure 8.20b

Temperature field in the horizontal joint between two MS-wood components.

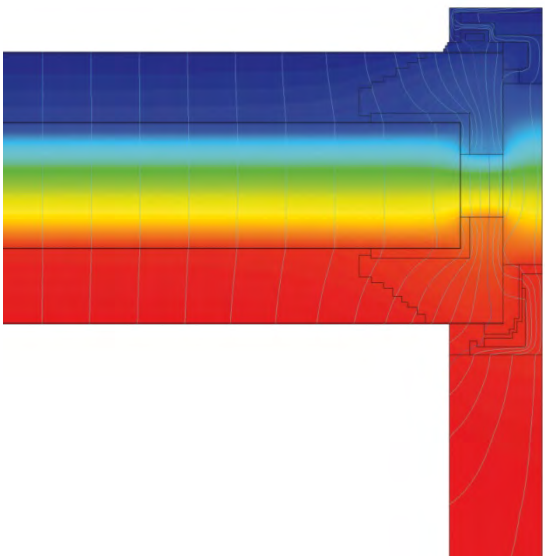

Figure 8.20c

Temperature field in the vertical joint between two MS-wood components.

Figure 8.21

Effective U-value of an MS-wood membrane component. The numbers along the lines denote the width [m] of a panel. Broken lines represent end-of-life values while continuous lines represent initial values. Conditions and thermal conductivity values used are specified in Figure 8.20.

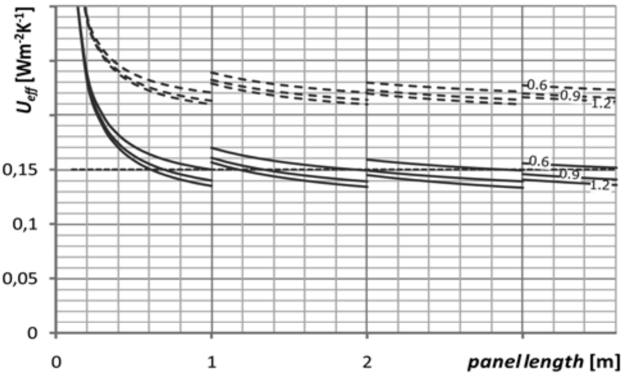

8.5.3 Expected service life

The service life of VIPs inside the component has been estimated by the calculation procedure described in the first interlude on page 236 and appendix A81. The air in the air cavities along both faces of the VIP is in contact with wood having the capability of absorbing and desorbing water. This effect, for which a calculation model is presented in appendix A81, is accounted for in the service life predictions. Service lives have again been predicted for façade components oriented on a south, north and west façade. Figures 8.22 and 8.23present the temperature of the barrier laminate on the cold and warm side of a south-oriented vacuum insulation panel and the relative humidity of the air in the corresponding cavities. Moreover, Table 8.4 summarises the general results regarding service life influencing factors and service life.

As can be observed from these service life values, the service life of these panels under practical conditions is between 130 and 180 years which is higher than the service life of an identical panel under laboratory conditions, i.e. the service life factor f_{sl} is larger than 1. These relatively high values for the service life primarily result from a lower Arrhenius annual average temperature of the barrier laminate in the tested conditions relative to laboratory conditions and from the omission of the effect of relative humidity on the permeance of the barrier laminate.

Moreover, it is important to observe that due to the omission of the effect of relative humidity on the permeance of the barrier laminate, service life predictions are too high. Brunner (2004) shows that at 80% relative humidity and 23°C the water content increase rate through a metallised barrier (MF3) around a VIP of

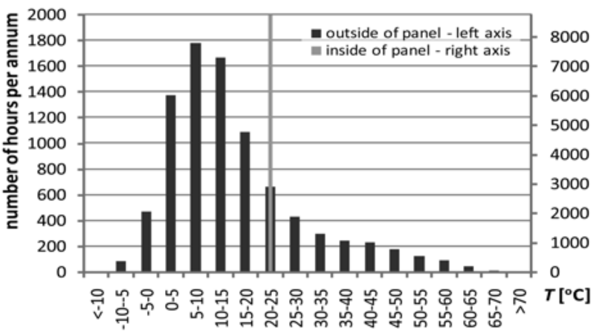

Figure 8.22

Histogram of the number of hourly temperatures per annum of the VIP barrier laminate on the inside (light grey) and outside (dark grey) of an M-component with south orientation for a location in the Netherlands.

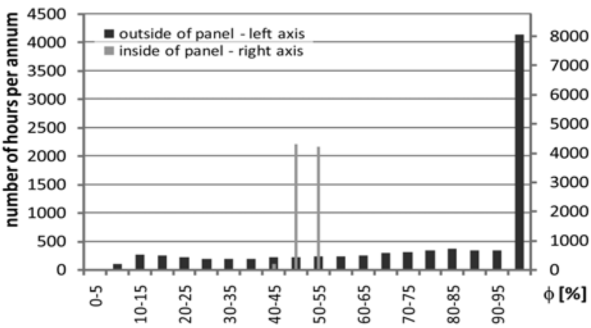

Figure 8.23

Histogram of the number of hourly relative humidity values per annum around the VIP barrier laminate on the inside (light grey) and outside (dark grey) of an M-component with with south orientation for a location in the Netherlands. Annual arithmetic average r.h. external cavity 75%, internal cavity 50%.

0.25x0.25x0.02 m^3 is about 2 times this increase rate at 50% r.h. and 23°C. He also shows that this increase factor decreases for increasing panel dimension. The effect however can still be significant[31]. Regarding the effect of relative humidity on gas pressure increase rate, this factor is 1.7 for the same panel (Brunner, 2004). After a certain time span, which is very often before the end of life if a VIP is blessed with high age, water vapour inside the core material (and also water content via the sorption isotherm of the core) practically[32] reaches equilibrium with its

[31] As a thought experiment to get an idea of the influence of relative humidity on service life of a VIP inside an M-wood component of 1200x3600 mm^2 on a south orientation and to compare the resulting expected service life with a case monitored in practise (Simmler and Brunner, 2005), $f_{w;T+\phi}$ is multiplied arbitrarily by 1.8 and , $f_{g;T+\phi}$ by 1.5. As a consequence, the service life reduces from 142 to 92 years (f_{sl} from 1.30 to 0.84). This value is close to the value found by Simmler and Brunner (2005) extrapolated to a panel size of 1000x1200x40 mm^3 as presented in the interlude near section 8.4.5.

[32] The word 'practically' is used here since in practice no steady-state conditions are present as a result of which the water vapour inside the core follows these fluctuating conditions with a certain time lag and amplitude dampening.

surroundings. If such equilibrium is achieved before the end-of-life, water vapor and water content hardly influence the service life any longer.

Figure 8.23 finally shows that condensation is highly likely to occur on the inner surface of the membrane on the cold side of the component during many hours a year in a Dutch climate[33]. For preventing moisture problems inside this cavity, perforated metal encasings containing silica gel as drying agent are inserted into parts of the wooden encasing. The influence of silica gel on the relative humidity of air inside the cavities has not been investigated further. If the amount of silica gel is sufficient, risk of condensation is assumed to be reduced since the cavity now is similar to a cavity of double-glazing.

8.5.4 Expected structural behaviour

As explained previously, the structural action of these membrane components mainly derives from the wooden encasings encompassing the VIPs, or in particular from the 'beams' between two VIPs inside such a component. Analogous to steel wide flange I-sections, these wooden beams consist of two flanges of Accoya® wood and a web of two 3 mm thick plywood. As can be seen from Figure 8.14a, in between the two plywood sheets of the web, Spaceloft™ aerogel insulation is added. If required for strength and stiffness, this Spaceloft™ can be replaced by Styrofoam or Polyurethane foam insulation creating a small sandwich component as web. The overall thermal performance of the component then however slightly decreases. The flange on the warm side of the panel is glued onto the web while the flange on the cold side is connected using socket screws, as a result of which the outer encasing can be removed from panel for replacing broken VIPs.

Since these wooden beams span in one direction from mullion to mullion, their structural capacity is either limited by strength or by stiffness. Since the ratio of beam height to span is 1 to 15, the beam's stiffness will be the limiting factor. According to Dutch standards (NEN6760:2008), the representative flexural modulus of a softwood with a specific mass between 450 and 550 $kg \cdot m^{-3}$ is 16000 MPa (class C50). The resulting bending stiffness of this beam then becomes $36 \cdot 10^3$ $N \cdot m^2$. Since these beams carry a load equal to the wind pressure on the exterior surface of the

---

[33] For the simulation initial conditions of 23°C and 50% r.h. were taken.

Table 8.4 – *Overview of the thermal behaviour of VIP integrated membrane panels and the service life of the VIPs inside.*

	Membrane panel (M-wood panel)			Membrane panel (M-wood panel)			Membrane panel (M-wood panel)		
Size [mm^2]	900x1800			1200x1800			1200x3600		
VIPs [mm^3]	2 pcs. 873x880x40			2 pcs. 880x1173x40			4 pcs. 880x1173x40		
mass [kg]	26			35			66		
d_p [mm]	85			85			85		
Thermal [e]									
$\psi_{edge;junction;1}$ [$W \cdot m^{-1} \cdot K^{-1}$][d]	0.0129 (0.0124)			0.0129 (0.0124)			0.0129 (0.0124)		
$\psi_{edge;junction;2}$ [$W \cdot m^{-1} \cdot K^{-1}$][d]	0.0149 (0.0144)			0.0149 (0.0144)			0.0149 (0.0144)		
$\psi_{edge;stiffener}$ [$W \cdot m^{-1} \cdot K^{-1}$][d]	0.0119 (0.0114)			0.0119 (0.0114)			0.0119 (0.0114)		
U_{eff} initial [$W \cdot m^{-2} \cdot K^{-1}$]	0.141			0.136			0.136		
U_{eff} at 25 yrs [$W \cdot m^{-2} \cdot K^{-1}$]	0.169 (N) – 0.171 (S)			0.163 (N) – 0.166 (S)			0.163 (N) – 0.166 (S)		
U_{eff} end of life [$W \cdot m^{-2} \cdot K^{-1}$]	0.216			0.212			0.212		
Service life									
	North	*South*	*West*	*North*	*South*	*West*	*North*	*South*	*West*
$f_{w;T+\phi}$ [-][a,b]	0.86	0.92	0.90	0.87	0.93	0.91	0.87	0.93	0.91
$f_{w;p}$ [-]	0.85	0.86	0.86	0.85	0.86	0.86	0.85	0.86	0.86
$f_{g;T+\phi}$ [-] [a,b]	0.66	0.85	0.78	0.66	0.85	0.78	0.66	0.85	0.78
$f_{g;p}$ [-]	1.00	1.00	1.00	1.00	1.00	1.00	1.00	1.00	1.00
t_{sl} [yr] [a,b,f]	161	129	139	179	142	153	179	142	153
f_{sl} [-] [a,b,f]	1.62	1.30	1.39	1.63	1.30	1.40	1.63	1.30	1.40
$\bar{T}_{e;arith.}$ [^oC][c]	12.0	15.2	13.7	12.0	15.2	13.7	12.0	15.2	13.7
$\bar{T}_{e;arrh.}$ [^oC][c]	17.0	20.7	19.4	17.0	20.7	19.4	17.0	20.7	19.4

[a] The effect of relative humidity on the water vapour and gas transmission rate of the barrier envelope is neglected in the calculation of $f_{w;T+\phi}$ and $f_{g;T+\phi}$. Since the annual average relative humidity surrounding the VIP is higher than the laboratory condition of 50% r.h. at a temperature of 23°C, the service life values presented in this table are higher than if r.h.-effects are considered. [b] Absorption coefficient of membrane is taken as 0.92 (solar transmission coefficient assumed 0), T_i = 22°C, α_e = 15 $W \cdot m^{-2} \cdot K^{-1}$ (wind speed ± 1 $m \cdot s^{-1}$), outside conditions according to weather data from De Bilt and Wageningen in 1995(NL), no nocturnal long-wave radiation. [c] These temperatures are calculated as annual temperatures of the entire VIP thus including both surfaces and its perimeter. For calculating the Arrhenius average temperature, an activation energy of 50 $kJ \cdot mol^{-1}$ is used. [d] The linear thermal transmittance values presented in this table always solely represent one half a junction. [e] The values between brackets are end-of-life values. [f] λ_{cr} = 8.0 $W \cdot m^{-1} \cdot K^{-1}$ for the core, thus thermal bridge effects not considered in the prediction.

panel multiplied by the distance between two beams, which equals[34] 2.1 $kN \cdot m^{-1}$, and since the maximum deflection of these beams is limited to 0.002 times its span, which corresponds to 2.4 mm, a flexural stiffness of $24 \cdot 10^3$ $N \cdot m^2$ is required. The beams thus fulfil this requirement regarding bending stiffness.[35]

The membrane around the entire component solely acts as element for transmitting wind loads towards beams and for pressing the encasings onto the VIP as a result of which a rigid panel emerges. They do not further significantly partake in structural action. Moreover, as explained earlier, the corners between wooden members of the encasing are made more rigid by steel L-shaped corner plates while the entire frame is braced by additional wooden elements increasing the rigidity of the component in in-plane direction.

8.5.5 Evaluation

As we have seen in the previous sections, a VIP integrated membrane panel would create a façade panel with high thermal performance. Although almost twice as thick as sandwich panels, membrane panels can still be considered slim. Moreover, the membrane component does not have the disadvantages of recycling difficulties and adhesion problems of the sandwich component; all materials, except if a polymeric foam is used inside beam elements, can easily be separated. Moreover, a transparent membrane, which can be used if this membrane does not have to take up too high loads, allows for architectural expression of the wooden encasing including bracings.

Besides, if a broken VIP is detected, the entire component can be demounted and re-opened, so that a new intact VIP can be installed; the quality of these VIPs can be checked on-site several years after installation of the components onto a façade using a thermographic camera since the cavity between membrane and VIP is not ventilated and since the thermal conductance of the membrane is low.

---

[34] The maximum wind pressure in the Netherlands is 2.07 $kN \cdot m^{-2}$ on a façade of a building located in the coastal region at an altitude higher than 150 m. According to Renckens (1996) this load should be multiplied by 0.75 for checking the static structural behavior of façade components. For variable loads Dutch standards (TGB1990) state that this load should be multiplied by a safety factor of 1.5 for offices. Width a maximum distance between the stiffening elements of 0.9 m, the equally distributed load on these elements thus becomes: 2.07x0.75x1.5x0.9=2.1 $kN \cdot m^{-1}$.

[35] It must be observed that creep of these wooden beams is not considered. Since the membrane panels are placed in vertical façades, no permanent load causing flexion acts on the beams, except maybe loads resulting from imperfect alignment. These loads however are small. Wind loads acting on the façade panels are variable loads and as a result not considered in calculations concerning creep.

However, production of a VIP integrated membrane component is labour-intensive. Moreover, the membrane and so the entire component is very fragile as a result of which the suitability for the building industry is limited unless personnel is specifically educated in handling these components. Therefore a final façade component will be presented in the next section more robust and suitable for the building industry.

8.6 VIP INTEGRATED PANEL WITH METAL ENCASING (E-AL/STEEL PANEL)

8.6.1 General description

It was discussed previously that a good bond between face sheets and VIP barrier laminate in case of VIP integrated sandwich panels is difficult to achieve, that such a bond inhibits recycling and that membrane based façade panels are very fragile and therefore less suitable for use in buildings. This section therefore presents a third and last façade system combining some of the principles of the previously discussed systems. These façade panels are dubbed VIP integrated panels with a metal encasing of either aluminium or steel, or in short encasing panels, or E-panels.

These encasing components (Figure 8.24a stiffener and 8.24b junction between two components) consist of the following elements and materials: a 40 mm thick vacuum insulation panel with a fumed silica core and a metallised barrier envelope with three metallisation layers (61 μm HDPE, and three times 12 μm metallised PET); a 2 mm thick aluminium or steel face sheet on the panel's exterior side, a 1.5 mm thick aluminium or steel face sheet on the panel's interior side including stiffening and connecting elements welded onto these sheets[36]; if desired or needed a phase change material[37] encapsulated in a 0.5 mm thick stainless steel casing, protected on one side by a 2 mm thick foamed film and placed in the cavity between VIP and interior face sheet to increase the thermal inertia of the room immediately behind

---

[36] The properties discussed in this section are based on aluminium face sheets unless specified otherwise.

[37] A polyethylene glycol 600 based phase change material can for instance be chosen since it is readily available on the market, has a phase change temperature in an optimal range for application in buildings and is relatively inexpensive. Moreover, Ahmad et al. (2006) showed that a combination of this type of PCM with vacuum insulation could significantly reduce peak temperatures in a test cell compared to a similar test cell configuration without PCM. Although they found these promising results with a layer of 25 mm PCM, numerical simulations showed that 10 mm PCM would also have an important positive effect on the interior climate.

the façade[38]; Spaceloft™ insulation at the panel's sides (3 times 6 mm along two sides and 1 time 6 mm on the other sides) and inside the stiffeners (2 times 6 mm); a reinforced non-metallic tape connecting both face sheets as safeguard in case of VIP failure; and a sealant.

The face sheets are structurally connected to one another by mechanically fastening the stiffening elements with M5x45 socket screws, by connectors in the junction area using M5x55 socket screws and as a safeguard by a reinforced non-metallic tape along the component's perimeter. This composition results in a nominal thickness of the component of 62 mm, which is thicker than the S-panel (Figure 8.7) but more slender than the M-panel (Figure 8.14). If a PCM is used than an asymmetrical panel configuration is obtained since the thickness of the outer cavity is determined by the structural constraints, i.e. stiffness required of the stiffening elements, while the thickness of the inner cavity is determined by the thickness of the PCM.

As will be discussed in the section on expected structural behaviour, the stiffening elements increase the stiffness of the face sheets thus determining the maximum span of the component. Since they span in one direction, the size of other direction can be chosen with less limitations. Limitations have already been mentioned in section 8.5.1. For this component a standard size of 1200x1800 mm^2 and of 1200x3600 mm^2 is therefore chosen, corresponding to regular grid dimensions in the architectural practice. The properties of these two panels are presented in Table 8.5. A detailed section through the junction between two components and through a stiffening element is presented in Figures 8.24a and b. To give an impression that also double-glazing can be integrated into the system, Figure 8.25 presents a section through a joint with a frame for double-glazing[16].

The stiffening elements along the component's perimeter, i.e. the grips, are designed in such a way that they can act as connecting system for coupling the component to a post-and-beam bearing system. The actual connection is made by mechanical fasteners. The grips and the thickness of the panel need to be manufactured with relatively high accuracy; in thickness the position of the grips may not vary more than about 1 mm, or otherwise two components cannot hook into each other at their edges. Space for adjusting the position of the façade

[38] If the building already has high thermal mass from floors and walls, the phase change material can also be omitted reducing the thickness of the cavity from 12 mm to 6 mm. The 2 mm thick foamed film is used both for protecting the VIP's barrier against damage by small particles and dust grains lying on the PCM encasing and for accommodating dimensional tolerances of the VIP (and PCM).

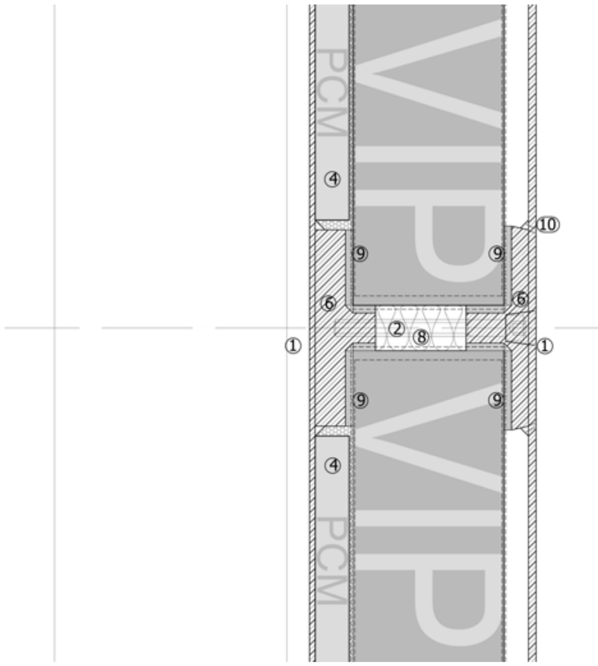

Figure 8.24a

Detailed vertical section through a stiffener inside an E-al encasing component. Scale: 1/2.

1.) aluminium face sheets;
2.) Spaceloft™ insulation;
3.) non-metallic tape;
4.) PCM (paraffin based) wrapped in stainless steel and protective fleece;
5.) sealant;
6.) aluminium strips welded onto face sheets;
7.) aluminium mullion;
8.) M5x45/55 socket screw;
9.) Compression band, like Illmod eco;
10.) water drainage.

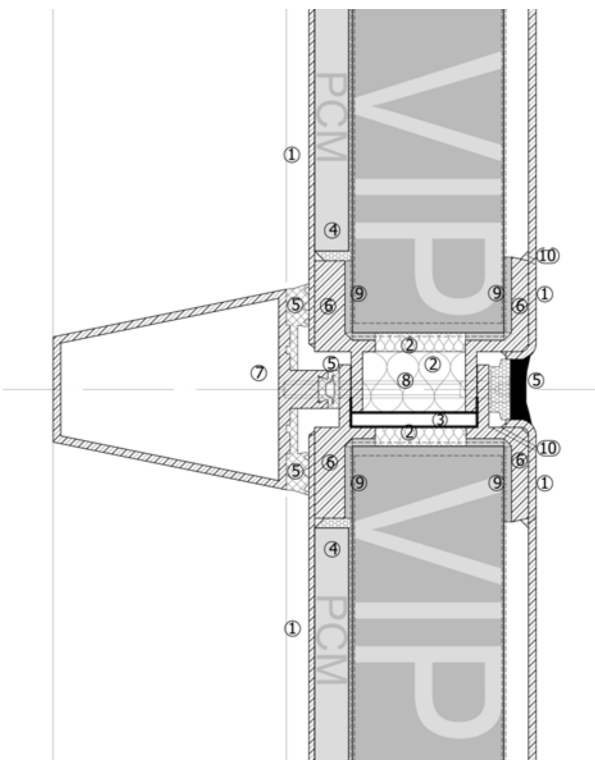

Figure 8.24b

Detailed vertical section through a junction between two E-al encasing components. Scale: 1/2.

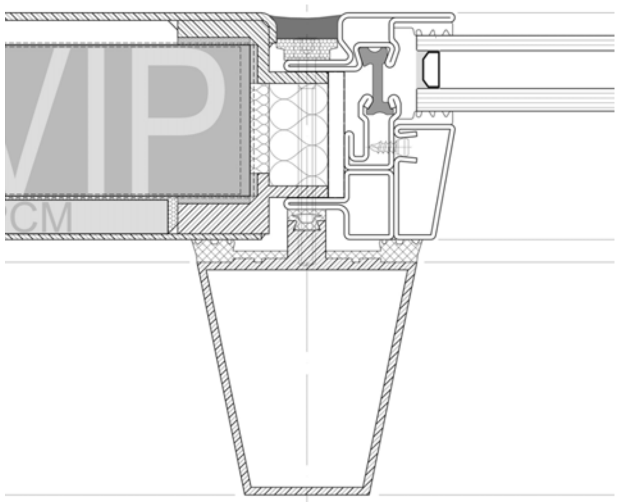

Figure 8.25

Indicative horizontal section through the junction of an E-al component and a double-glazing frame. Scale: 1/2.

components relative to each other and relative to the post-and-beam system is also available and accommodated by the system of grips: within a junction area each component can move from nominal position 4 mm to the right (or top) and 4 mm to the left (or bottom), in total thus 8 mm using slotted holes. It is expected that this suffices since the posts and beams can be positioned as well.

During production of an E-panel, first the metal encasings are prepared. From a sheet of metal, first some material (square pattern) needs to be cut away from the corners of the face sheet on the component's outside. Then the edge of this sheet can be folded and its corners welded. Next, the stiffening elements, cut to the right size and angle, are welded to both face sheets obtaining two metal encasings (Figure 8.26a/b and 8.27a/b) to which compriband[39] is attached at the appropriate positions. After positioning the PCM, the protective foam film, the VIPs and Spaceloft™ insulation to fill the gaps between two VIPs, the exterior encasing is placed on top of these elements and connected with M5 socket screws to the interior face sheet. Finally, Spaceloft™ insulation and afterwards a non-metallic tape are placed along the system's perimeter finalizing the production process of these components.

[39] As explained in section 8.5.1, this compriband is used for protecting the VIP barrier from the metal encasing and for accommodating dimensional tolerances of the vacuum insulation panels inside.

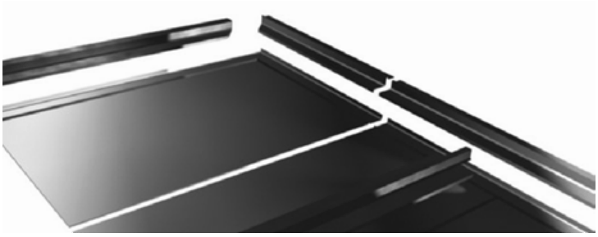

Figure 8.26a

Rendering of the inside of the face sheet on the panel's exterior side with stiffening elements before welding.

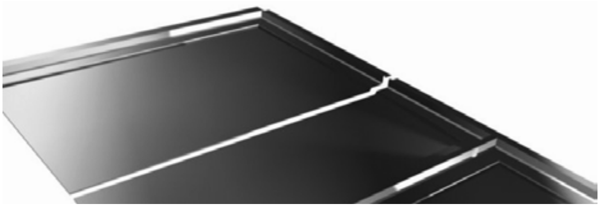

Figure 8.26b

Rendering of the inside of the face sheet on the panel's exterior side with stiffening elements after welding.

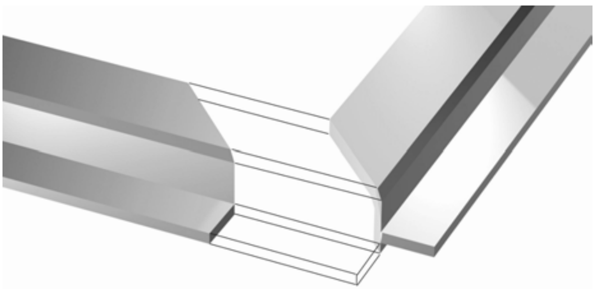

Figure 8.27a

Corner solution of the connecting profiles/stiffening elements along the component's perimeter.

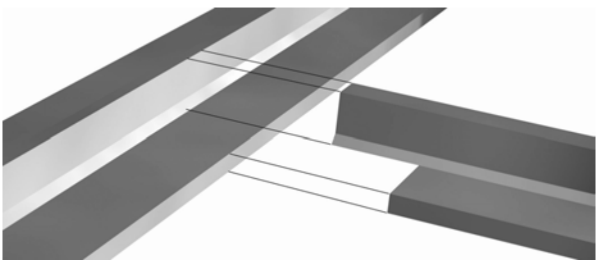

Figure 8.27b

Connection of the stiffening elements to the connecting profiles along the component's perimeter.

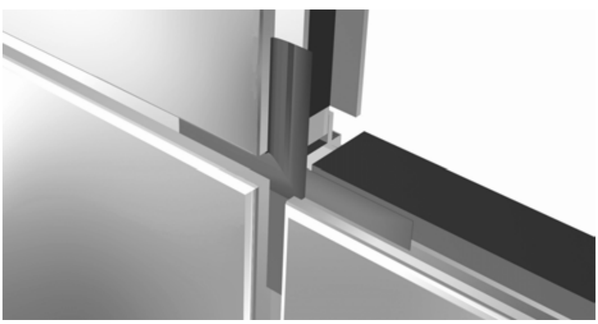

Figure 8.28

Junction between four façade components. One component is left out of the rendering. Dpc foil for making this junction water tight behind the sealant.

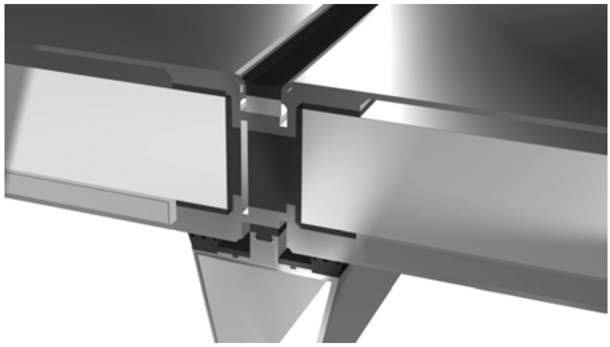

Figure 8.29a

Rendering of the joint between two E-al components.

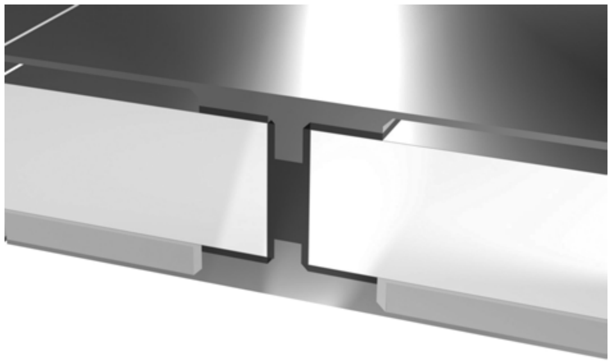

Figure 8.29b

Rendering of a stiffening element inside an E-al component.

Air tightness between two adjoining components is maintained by rubber gaskets between the post-and-beam system and the interior face sheet. If necessary, additional rubber seals or compriband can be added along the sides of the grips at the interior side of the component. Water tightness is primarily arranged by a sealant between both exterior face sheets. Water penetrating this seal is blocked by the metal grips behind this seal and can be drained through small openings in the exterior face sheet, as can be seen from Figure 8.24a/b (number 10). Leakage through the seal of a vertical joint can drip downwards through this joint by means of gravity and accompanied over a junction of four components by a strip of dpc foil which is a PP or PE based water tight foil, as pictured in Figure 8.28. If due to a 100%[40] relative humidity inside the outermost cavity of the component condensation occurs at the coldest surface, small holes in face sheet allow this condensate to leave the cavity, as shown in Figure 8.24a/b (number 10).

[40] One of the boundary conditions for these simulations is a starting condition, i.e. the condition under which the component is produced, of 23^{o}C and 50% r.h.

8.6.2 Expected thermal behaviour

The joints between two components and between two VIPs within a component have been thermally simulated for both a thermal conductivity of the VIP core, λ_c, of $4.0\cdot10^{-3}$ W·m^{-1}·K^{-1} (initial condition) and $8.0\cdot10^{-3}$ W·m^{-1}·K^{-1} (end-of-life condition). The methodology for calculating the linear thermal transmittance of these joints has already been explained in chapter 4[18]. Again a 40 mm thick VIP was chosen for these E-components for the same reasons as explained previously with S-components.

Figures 8.31a and b present images of the temperature field through the joint between two components and the joint between two VIPs inside a component while Table 8.5 summarises the calculated ψ-values of both junctions. Between brackets, the end-of-life values are given. Based upon these values and the dimensions of the component, the overall U_{eff}-value of an E-al component can be calculated. For a component of 1200x1800 mm^2, this value becomes 0.146 W·m^{-2}·K^{-1} at initial conditions and 0.177 W·m^{-2}·K^{-1} after 25 years on a south orientation. For a component of 1200x3600 mm^2, these values become 0.140 W·m^{-2}·K^{-1} and 0.171 W·m^{-2}·K^{-1} respectively. These values show that both VIP integrated encasing components meet the requirement of the Passivhaus standard based on initial values. After 50 years of use, only slightly higher values are reasonable since the service life of a panel is estimated to be 150 years or more. Figure 8.30 finally presents the effective U-value of a panel as function of width and panel length. As can be seen, only small components never meet this requirement.

8.6.3 Expected service life

The service life of the vacuum insulation panels inside the component has been estimated by the same calculation procedure as described in the interlude on page 236. Contrary to VIP integrated sandwich panels, water vapour and dry gas permeation does occur through the large faces of the VIP inside the component. Service lives have again been predicted for façade components oriented on a south, north and west (or east) façade. Figures 8.32 and 8.33 present the annual temperature distribution of the barrier laminate on the cold and warm side of a south-oriented vacuum insulation panel and of the relative humidity of the air in the corresponding cavities. Moreover, Table 8.5 summarises the general results regarding service life influencing factors and service life.

As can be observed from these service life values, the service life of these panels under practical conditions is again higher than the service life of an identical panel under laboratory conditions, i.e. the service life factor f_{sl} is larger than 1. These relatively high values for the service life primarily result from a lower Arrhenius annual average temperature of the barrier laminate in the application conditions

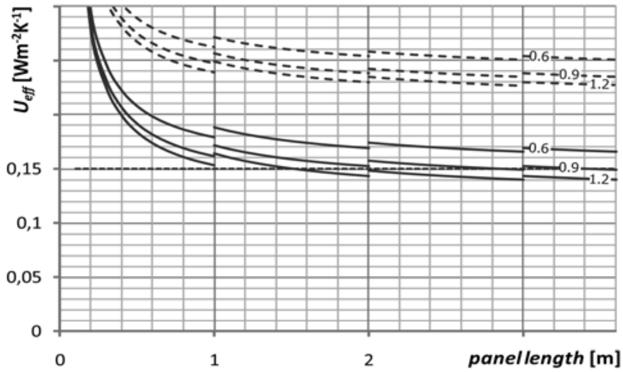

Figure 8.30

Effective U-value of an aluminium based encasing panel. The numbers along the lines denote the width [m] of a panel. Broken lines represent end-of-life values while continuous lines represent initial values. Conditions and thermal conductivity values used are specified in Figure 8.31.

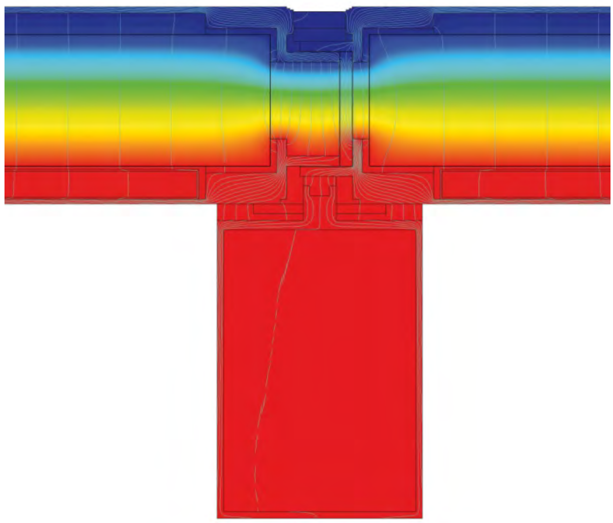

Figure 8.31a

Temperature field in the joint between two E-al components. Alternative mullion.

$T_i = 20^{o}C$ *(red);* $T_e = 0^{o}C$ *(blue);*
$\alpha_i = 7.8\ W{\cdot}m^{-1}{\cdot}K^{-1}$;
$\alpha_e = 25\ W{\cdot}m^{-1}{\cdot}K^{-1}$; $\varphi = 0.75$;
$\lambda_c = 4.0{\cdot}10^{-3}\ W{\cdot}m^{-1}{\cdot}K^{-1}$;
$\lambda_{film} = 0.54\ W{\cdot}m^{-1}{\cdot}K^{-1}$;
$\lambda_{alu} = 225\ W{\cdot}m^{-1}{\cdot}K^{-1}$;
$\lambda_{steel} = 16.2\ W{\cdot}m^{-1}{\cdot}K^{-1}$;
$\lambda_{thermobond} = 0.05\ W{\cdot}m^{-1}{\cdot}K^{-1}$;
$\lambda_{tape} = 0.3\ W{\cdot}m^{-1}{\cdot}K^{-1}$;
$\lambda_{aerogel} = 13.5{\cdot}10^{-3}\ W{\cdot}m^{-1}{\cdot}K^{-1}$;
$\lambda_{pcm} = 0.2\ W{\cdot}m^{-1}{\cdot}K^{-1}$;
$\lambda_{rubber} = 0.32\ W{\cdot}m^{-1}{\cdot}K^{-1}$;
Air gaps according to NEN1068:2001 (2001). Heat flow line increment: 0.03 W.

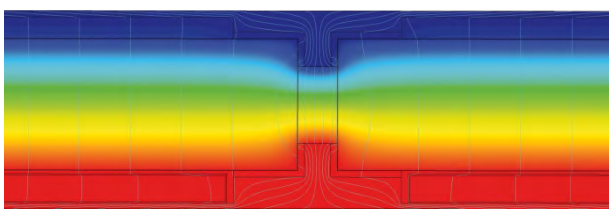

Figure 8.31b

Temperature field in the stiffening elements inside an E-al component.

***Table 8.5** – Overview of the thermal behaviour of VIP integrated metal encasing panels with either aluminium or steel face sheets and the service life of the VIPs inside.*

	PANEL WITH ALUMINIUM ENCASING (E-AL PANEL)			PANEL WITH ALUMINIUM ENCASING (E-AL PANEL)			PANEL WITH STEEL ENCASING (E-ST PANEL)		
Size [mm^2]	1200x1800 mm^2			1200x3600 mm^2			1200x3600 mm^2		
VIPs [mm^3]	2 pc. of 879x1170x40 mm^3			4 pc. of 879x1170x40 mm^3			4 pc. of 879x1170x40 mm^3		
mass [kg]	76			145			260[g]		
d_p [mm]	62			62			62		
THERMAL [e]									
$\psi_{edge;junction;1}$ [$W{\cdot}m^{-1}{\cdot}K^{-1}$][d]	0.0175 (0.0177)			0.0175 (0.0177)			0.0172 (0.0174)		
$\psi_{edge;junction;2}$ [$W{\cdot}m^{-1}{\cdot}K^{-1}$][d]	0.0175 (0.0177)			0.0175 (0.0177)			0.0172 (0.0174)		
$\psi_{edge;stiffener}$ [$W{\cdot}m^{-1}{\cdot}K^{-1}$][d]	0.0060 (0.0062)			0.0060 (0.0062)			0.0056 (0.0058)		
U_{eff} initial [$W{\cdot}m^{-2}{\cdot}K^{-1}$]	0.146			0.140			0.139		
U_{eff} at 25 yrs [$W{\cdot}m^{-2}{\cdot}K^{-1}$]	0.176 (N) – 0.177 (S)			0.171			0.170 (N) – 0.171 (S)		
U_{eff} end of life [$W{\cdot}m^{-2}{\cdot}K^{-1}$]	0.232			0.227			0.226		
SERVICE LIFE									
	North	*South*	*West*	*North*	*South*	*West*	*North*	*South*	*West*
$f_{w;T+\phi}$ [-][a,b]	0.88	0.90	0.89	0.88	0.90	0.89	0.89	0.93	091
$f_{w;p}$ [-]	0.86	0.85	0.87	0.86	0.85	0.87	0.86	0.85	0.88
$f_{g;T+\phi}$ [-][a,b]	0.67	0.72	0.70	0.67	0.72	0.70	0.70	0.82	0.77
$f_{g;p}$ [-]	1.00	1.00	1.00	1.00	1.00	1.00	1.00	1.00	1.00
t_{sl} [yr][a,b,f]	177	168	169	177	168	169	171	150	154
f_{sl} [-][a,b,f]	1.59	1.51	1.52	1.59	1.51	1.52	1.53	1.35	1.39
$\bar{T}_{e;arith.}$ [^oC][c]	10.7	12.3	11.6	10.7	12.3	11.6	11.7	14.7	13.3
$\bar{T}_{e;arrh.}$ [^oC][c]	17.1	18.1	17.8	17.1	18.1	17.8	17.8	20.8	19.2

[a] The effect of relative humidity on the water vapour and gas transmission rate of the barrier envelope is neglected in the calculation of $f_{w;T+\phi}$ and $f_{g;T+\phi}$. Since the annual average relative humidity surrounding the VIP is higher than the reference laboratory condition of 50% r.h. at a temperature of 23°C, the service life values presented in this table are higher than if r.h.-effects are considered. [b] Absorption coefficient of anodised aluminium and coated steel are 0.45 and 0.85 resp. (vd Linden, 2000), T_i = 22°C, α_e = 15 $W{\cdot}m^{-2}{\cdot}K^{-1}$ (wind speed ± 1 $m{\cdot}s^{-1}$), outside conditions according to weather data from De Bilt and Wageningen 1995(NL), no nocturnal long-wave radiation. [c] These temperatures are calculated as annual temperatures of the entire VIP thus including both surfaces and its perimeter. For calculating the Arrhenius average temperature, an activation energy of 50 $kJ{\cdot}mol^{-1}$ is used. [d] The linear thermal transmittance values presented in this table always solely represent one half a junction. [e] The values between brackets are end-of-life values. [f] λ_{cr} = 8.0 $W{\cdot}m^{-1}{\cdot}K^{-1}$ for the core, thus no thermal bridge effects in the prediction. [g] The mass of these components was estimated based upon the same volume of stainless steel compared to aluminium. Since optimisation might lead to the use of less aluminium, this is an upper limit.

relative to laboratory conditions and from the omission of the effect of relative humidity on the permeance of the barrier laminate (interlude on p. 240 and footnote 30). As can be seen, all VIPs easily fulfil the requirement on service life of 30 years.

Interestingly, the service life of VIPs inside E-components is significantly smaller than that of VIPs inside S-components. The reduction in service life can be as large as approximately 42% if a VIP in an S-al panel is compared to one in an E-al panel. Clearly, this difference results from the assumed absence of water vapour and dry gas permeation through the faces of the VIP laminate inside an S-panel. Despite the high uncertainty in the service life prediction of a VIP inside a sandwich component due to lack of knowledge of the influence of an adhesive on the properties of the barrier laminate, it is based on these results highly likely that this difference in service life does exist.

Figure 8.33 finally shows that condensation is highly likely to occur on the inner surface of the exterior face sheet during many hours a year in a Dutch climate (initial conditions of 23°C and 50% r.h.). This condensate needs to be drained out of this cavity by small holes in the face sheet. Lowering the temperature and relative humidity during production would only reduce the amount of condensation during the first weeks or maybe months after production.

Figure 8.32

Histogram of the number of hourly temperatures per annum of the VIP barrier laminate on the inside (light grey) and outside (dark grey) of a component with aluminium encasing (E-al panel) and south orientation for a location in the Netherlands.

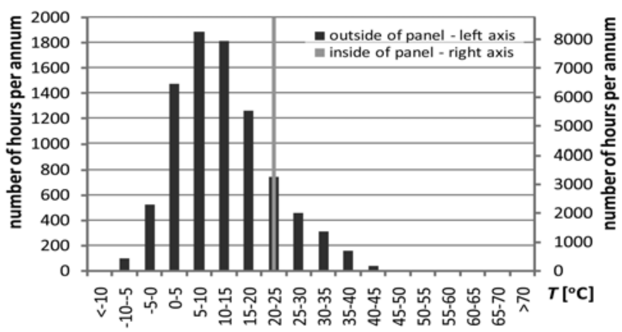

Figure 8.33

Histogram of the number of hourly relative humidity values per annum around the VIP barrier laminate on the inside (light grey) and outside (dark grey) of a component with aluminium encasing (E-al panel) and south orientation for a location in the Netherlands. Annual arithmetic average r.h. external cavity 77%, internal cavity 52%.

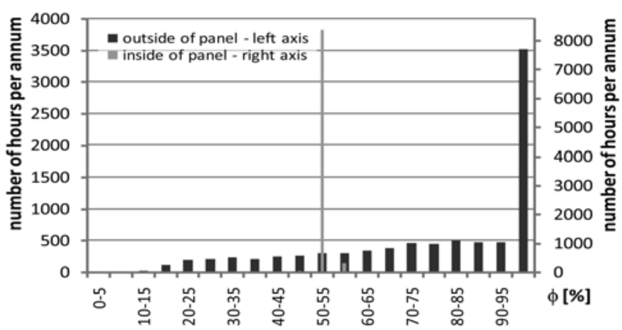

8.6.4 *Expected structural behaviour*

As explained previously, the stiffening elements - both at the component's perimeter and in its central area - increase the stiffness of the face sheets thus influencing the system's maximum span. Especially for panels with a high aspect ratio, i.e. its length is multiple times its width, these stiffening elements can be considered to act as 'beams' in co-operation with the face sheets. Under such conditions these stiffeners at the panel's central area span in one direction between two members of the post-and-beam system and carry a load equal to the wind pressure on the exterior surface of the panel multiplied by the distance between two stiffening elements. This load then equals 2.1 $kN{\cdot}m^{-1}$.[34] In case a maximum deflection of 0.002 times its span is allowed, corresponding to 2.4 mm, a flexural stiffness of $24{\cdot}10^3$ $N{\cdot}m^2$ is required.

The bending stiffness of the stiffening element in the central area of the panel equals $6.8{\cdot}10^2$ $N{\cdot}m^2$ in case of E-al components and $2.1{\cdot}10^3$ $N{\cdot}m^2$ in case of E-steel components if it would work on its own[41,42]. In practise, however, one stiffening element would never act solitarily; wind loads are partly transmitted via VIP flexion from one encasing to the other and partly via the mechanical connection between adjoining stiffening elements, i.e. an element from the exterior and one from the interior encasing. Since these adjoining stiffening elements are connected with mechanical fasteners and pressed onto the VIP creating a certain friction-based connection between stiffening element and VIP, both adjoining stiffening elements and part of the VIP co-operate in transferring loads to the post-and-beam system, as can be seen from Figure 8.34. Neglecting the influence of the VIP and assuming perfect co-operation, the bending stiffness of this composite system[40] approximately becomes $59{\cdot}10^3$ $N{\cdot}m^2$ for an E-al panel and $1.8{\cdot}10^5$ $N{\cdot}m^2$ for an E-steel panel, with which the requirement regarding structural stiffness is met. It must finally be observed that for smaller panels also two-dimensional load distribution occurs and that loads are partly also transmitted via bending of the VIP inside the component, both improving the performance of the component; and that the connection between both adjoining stiffening elements is never perfect, decreasing the performance of the component. If however sufficient mechanical fasteners are used, it is expected that its performance will never decrease to below the required flexural stiffness.

---

[41] For calculating the stiffness of the stiffeners,$(EI)_{stiff}$, the face sheet directly on top of the stiffening element is considered to co-operate under the assumption that its structural contribution to the stiffness of the stiffening elements stops beyond the width of the stiffener.

[42] As can be seen from Figure 8.24a, each stiffening element in the central area of the components is geometrically made up of two squares. The square between the VIPs has a width of 8 mm and a height of 12 mm; the other square has a width of 56 mm and a height of 6.5 mm (including face sheet). The neutral plane through this section lies at 3.86 mm measured from the exterior side of the face sheet. The bending stiffness of this section can now be calculated using the stiffness of each square and Steiner's rule.

Figure 8.34

Schematic representation of the structural action in a stiffening element at the central area of a VIP integrated component with a metal encasing: E-component.

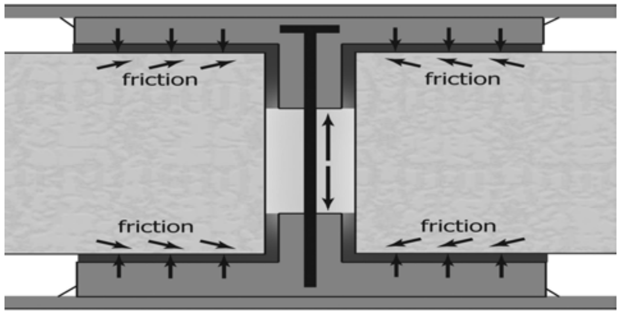

8.6.5 Evaluation

As we have seen, a VIP integrated encasing panel would create a thin façade system at the same time having a high thermal performance. Regarding both thickness and thermal performance, such an E-component performs in between a sandwich component and a membrane component. Moreover, the encasing component does not have the disadvantages of recycling difficulties and adhesion problems of the sandwich component and the fragility of the membrane component. This system thus combines the best of both systems. And if a broken VIP is detected, the entire component can be demounted and opened, so that a new intact VIP can be installed. Moreover, as for both previously presented façade systems, the thermal quality of the VIP can be checked on-site after installation using a thermography (footnote 21). Checking a VIP inside this component after installation using a Va-Q-check sensor or RFID technology, however, would require the component to be demounted. In any case, VIP integrated encasing panels would be a robust solution for integrating vacuum insulation panels in façade components suitable for the building practise.

8.7 Final Remarks and Conclusions Concerning Façade Systems

8.7.1 Final remarks

Evaluating all three previously discussed façade components, the most promising system for actual application in buildings might currently be the VIP integrated component with aluminium encasings[43]. Compared to a sandwich component and a

[43] The previous observation that E-panels currently are most interesting for the application of VIPs in façade systems is not surprising since it more-or-less results from the design process(es). Thermal simulations showed that sandwich panels have a high potential for creating thermally highly façade panels due to the absence of a strong edge spacer. As a result,

membrane component, this system combines the best of these components[44] and solves several issues those components still have: contrary to a sandwich component, the encasing component is demountable and recyclable; contrary to a membrane component, it is labour-extensive and robust. Moreover, since the appearance of these components does not deviate from current façade systems, acceptance by the building industry will be high. As a consequence, wide-spread application is possible resulting in a considerable improvement of current curtain-wall façades on their energy performance, as can also be seen from Figure 8.35.

However, some final remarks must be made regarding aforementioned façade systems. First, since no structural experiments or simulations have been conducted with the façade components, their exact structural behaviour is unknown. Such experiments or simulations might result in additional changes in the designs. Second, the specifics of details might depend on the production capabilities of a manufacturer. As a result, if the façade components presented in this chapter are further engineered in co-operation with a manufacturer, several modifications might be needed for optimising the components in relation with production processes. Third, the influence of production and maintenance costs has not been considered explicitly during the design process. Such considerations might require the components to be simplified. These façade component designs should therefore be considered as principal designs solely and not as ready-for-market products.

8.7.2 Conclusions

Two relations were found to be of special importance when designing VIP integrated façade components.

First, between thermal performance and structural performance. Whether this relation is mainly determined by the behaviour of the VIP itself, or by the spacer of the component, primarily depends on its mechanical behaviour, i.e. does it act as a

---

the S-panel was conceived and designed. However, due to lack of proven reliability of the adhesive layer between face sheets and VIP barrier laminate and due to this adhesive's inability to separate both materials from each other after disposal, a new approach was needed. One such approach was found in the design of d a system of lamellae for temporary thermal insulation by Cremers (2006). Cremers showed that with the combination of two polymeric encasings and a membrane VIP integrated lamellae could be designed having high thermal performance. This idea was adopted and modified to design the M-panels. However, due to the system's high fragility and low structural rigidity and stiffness, again a new approach was needed. For the third and last façade design, the basic ideas from both aforementioned systems were taken as starting conditions to conceive a system that combines the best of both worlds: the use of rigid metal sheets from the S-panel and the use of a double system of encasings from the M-panel. These basic ideas finally resulted in the E-panel.

[44] Concerning overall thermal performance and service life of the VIPs inside, all components designed perform similar. Differences are small.

Figure 8.35

Categorisation of VIP integrated façade panels on their thermal performance, their complexity/ fragility and their usability for practise (S-panel is sandwich panel; E-al panel is a VIP integrated encasing panel; M-panel is membrane panel with wooden encasing; cavity-filled panel 1 is a panel with 40 mm VIP, a 6 and a 4 mm glass sheet and an aluminium spacer; cavity-filled panel 2 is identical to panel 1 but with a thermoplastic spacer. (upper dots denote initial performance, lower dots performance at end of life).

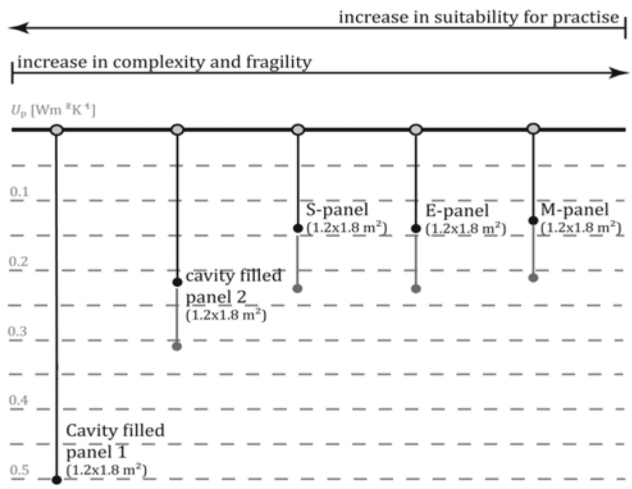

sandwich construction or as an 'edge-spacer' construction. For edge-spacer constructions, a strong and stiff structural spacer is needed resulting in large thermal edge effects. For sandwich constructions with a VIP core, however, no structural spacer is required, on the one hand potentially improving its overall thermal performance, but on the other hand imposing additional structural requirements on the VIP itself.

Second, between thermal performance and VIP service life. As seen in previous chapters, the thermal conductivity of the core is not a constant value but is subjected to ageing. Since the thermal performance of a VIP integrated façade component primarily depends on this central thermal conductivity combined with a geometry-based multiple of the linear thermal transmittance of the component edge, the application of an arbitrary value for a maximum allowable thermal conductivity directly influences the service life of a VIP integrated into a building component.

Existing VIP integrated façade panels are principally of the edge-spacer type lacking high thermal performance. These panels resemble a double-glazing system in which the air cavity is filled with a VIP and for which the spacer along its edge is thermally improved. But even with these improved spacers, thermal 'leakage' along the perimeter renders the high thermal performance of a VIP inappropriate. A 1.2x1.8 m^2 façade panel with an improved thermoplastic spacer, a sheet of 4 mm float glass, a sheet of 6 mm float glass and a 40 mm thick VIP with a metallised barrier laminate positioned inside the panel's cavity, for instance, still has an effective *U*-value of 0.21 W·m^{-2}·K^{-1}, which is more than twice its centre-of-panel value of 0.10 W·m^{-2}·K^{-1}.

VIP integrated sandwich components not requiring a structural spacer, have improved thermal performance since a thin reinforced non-metallic tape suffices to protect the VIP inside the component and to prevent the panel from collapsing in case of VIP failure. If, for example, the spacer of aforementioned façade panel is replaced by such a tape, then the overall *U*-value reduces from 0.21 $W \cdot m^{-2} \cdot K^{-1}$ to 0.11 $W \cdot m^{-2} \cdot K^{-1}$. However, the structural performance of a sandwich component entirely depends on the quality of the bond between face sheets and VIP barrier. Such a high quality bond could not be realised within the framework of this study due to too much shear in the adhesive layer between face sheet and VIP and due to sliding of the VIP's barrier laminate over its core. It is important to realise that, even if a perfect bond might be established, this latter effect is an inherent property of a VIP connected to a face sheet and does thus always occur. Although not studied within the framework of this dissertation, this sliding may also deteriorate the barrier quality of the envelope at the panel's sides, as a consequence reducing its service life. VIPs should therefore be applied in structural sandwiches with the highest care.

As we have seen in this chapter, the potential of applying VIPs in façades of buildings can be very high, though. With a thickness of the insulation layer of only 40 mm and a thickness of an entire façade component between 43 mm and 85 mm, Passivhaus standard for the thermal quality of the façade can be achieved at initial conditions, i.e. U_{eff}<0.15 $W \cdot m^{-2} \cdot K^{-1}$. Assuming approximately that 50 years is one third of the VIP's service life and that its thermal conductivity approximately increases directly proportional to time, the overall *U*-value of the façade panels from tables 8.3, 8.4 and 8.5 will be between 0.16 and 0.20 $W \cdot m^{-2} \cdot K^{-1}$ after 50 years.

However, actual application does involve solving several technical hurdles. In the case of structural sandwiches, a good bond between face sheets and VIP barrier laminate needs to be obtained[45]. In the case of edge spacer panels, the spacer needs to be thermally and structurally optimised. With the presented principal designs of three façade components, systems have been developed that combine high thermal performance, structural soundness, limited thickness and aesthetical satisfaction. With the wide-spread application of VIPs in façades, the energy performance of buildings during their lifetime can be improved considerably. In this respect, vacuum insulation panels can thus contribute to a more sustainable society.

[45] It must however be noted that tests have been performed using VIPs with a metallised film laminate (outer layer of PET) and glass, a resin bounded composite cladding panel or mdf face sheets. For many practical applications however steel or aluminium facings might be of more interest. These have not been tested as a result of which no conclusions can be drawn regarding the bond between VIP barrier and such facings. A weakness between laminate and core exists as well resulting in inherent sliding between both in case of flexural loading.

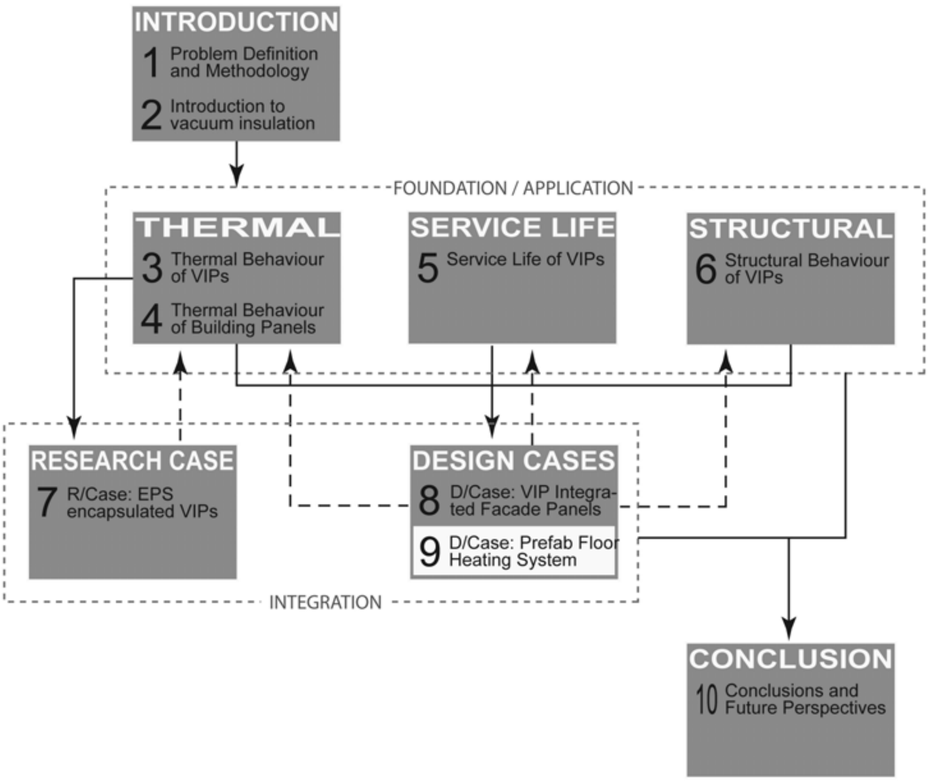
INTRODUCTION
1 Problem Definition and Methodology
2 Introduction to vacuum insulation
FOUNDATION / APPLICATION
THERMAL
3 Thermal Behaviour of VIPs
4 Thermal Behaviour of Building Panels
SERVICE LIFE
5 Service Life of VIPs
STRUCTURAL
6 Structural Behaviour of VIPs
RESEARCH CASE
7 R/Case: EPS encapsulated VIPs
DESIGN CASES
8 D/Case: VIP Integrated Facade Panels
9 D/Case: Prefab Floor Heating System
INTEGRATION
CONCLUSION
10 Conclusions and Future Perspectives

D/CASE VIP INTEGRATED FLOOR HEATING SYSTEM 9

DESIGN CASE STUDY: PRINCIPAL DESIGNS OF A HIGH PERFORMANCE, THIN, DRY, PREFABRICATED FLOOR HEATING AND COOLING SYSTEM

Since energy standards are likely to become more stringent in the future paving the way for the implementation of sustainable and renewable energy sources in the built environment, low temperature heating and high temperature cooling systems are likely to become the dominant heating and cooling system for dwellings. Especially for refurbishment and when thermal de-coupling between spaces is required, the desire for a thin but high performance thermal insulation layer below a floor heating system may be an incentive for the use of vacuum insulation panels. Having discussed the application and integration of these panels in façade systems in the previous chapter, this chapter discusses their use as insulation layer below a floor heating and cooling system, or in particular the water foil carpet system. This water foil carpet system is the result of a collaborative research and development project involving Well Design, BouwhulpGroep, Cauberg-Huygen raadgevend ingenieurs, Metz Consult and Delft University of Technology.

This chapter starts with a brief overview of some existing floor heating systems and projects in which VIPs have been applied on top of a construction floor. Subsequent to this introduction, service and legal requirements on vacuum insulation panels below a floor heating and cooling systems will be formulated and studied in section 9.2. Section 9.3 then introduces and briefly describes some aspects of the water foil carpet floor heating and cooling system. One performance variant of this system involves the use of vacuum insulation panels as thermal insulation layer. Aspects related to thermal performance, service life and structure-borne sound insulation will finally be elaborated upon in section 9.4 showing the possibilities of applying VIPs in combination with surface heating and cooling systems.

9.1 INTRODUCTION

9.1.1 Introduction

In recent years, VIPs have been applied ever more increasingly in buildings. In these mainly demonstration buildings, one part of a building seems to have particularly grown into a potentially successful area for the application of VIPs: roof terraces and access balconies. The advantages of VIPs over conventional thermal insulators here are clear: the distance in height between the floor on the inside of the building and on the roof terrace diminishes making access to the building from the terrace or balcony easier (Binz et al., 2005). Similar to roof terrace insulation, insulation on top of a floor might prove another interesting application area, especially in refurbished buildings. Since a thin insulation layer reduces the need for changes on interior walls and facades (door posts, doors, etc.) or even on the height of the room, these cost-savings can be used as an argument in favour of VIPs. As will be discussed in section 9.1.3, several buildings have already been refurbished using VIPs on top of the floor.

Several years ago, a collaborative R&D project under the auspices of SenterNovem was initiated[1]. This project aimed at developing a thin, prefabricated, dry, high performance floor heating and cooling system particularly for dwellings[2]. The main requirements on this system were that it can be used in newly erected and refurbished buildings, that it can both heat and cool, that it is thin and can easily be installed. Because of the desire for reduced thickness, VIPs were initially selected as a solution for the insulation layer. Since such a system uses relatively low temperatures for heating and high temperatures for cooling, primary energy can be saved. Moreover, it facilitates the use of sustainable energy sources in buildings.

Although in the end VIPs have not been integrated in this floor heating and cooling system because of cost and fragility issues, several remarks on their use with this system will be made. A short discussion on thermal performance, acoustics and service life will be presented as well. Using this example, it will be shown that a high performance floor heating and cooling system with limited construction thickness is attainable. Because the project during which this floor heating and cooling system is developed is subjected to secrecy and because this dissertation deals with VIPs and not surface heating system, the system itself will not be discussed in detail.

---

[1] In this collaborative research and development project, several partners closely co-operate: Well Design, BouwhulpGroep, Cauberg-Huygen, Metz Consult and TU Delft.

[2] In the year 2006, a similar project undertaken by Tobler AG and dr. Eicher+Pauli AG was initiated in Switzerland. The outcome of this project however is still unknown to author.

9.1.2 *Existing floor heating and cooling systems*

Multiple floor heating systems are currently available on the market[3]. Four of these systems, typologically representing a large part of the systems available, will be discussed briefly: system A, system B, system C and a traditional wet system. A fifth system, not available on the market will be discussed as well: an improved dry system[4]. Information about these systems is obtained from Roth Werke GmbH (2007), Clina Heiz- und Kühlelemente GmbH (2007), Willems and Kraan (2003), and publication ISSO 49 (ISSO, 2002). A general overview of their configuration and some of their properties is presented in Figure 9.1 and Table 9.1.

In general these systems consist of an insulation layer of 30 to 40 mm which fulfils both an acoustic and a thermal function. In the dry systems, this insulation layer may also be used for including ducts for transporting the heating or cooling medium, i.e. water. In so-called wet systems, this ductwork is positioned in the screed on top of this insulation layer. However, the improved dry system consists of both an insulation layer and an additional 35 mm thick wood wool cement board which includes slots for positioning this ductwork.

In wet systems, the screed either consists of a sand-cement based or a gypsum based fluid, which generally hardens in a period of several days. In case of dry systems, though, the screed consists of gypsum fibre boards or wood based materials on top of which someone can immediately walk.

Besides this insulation layer and screed, dry systems often additionally have a profiled metal plate in contact with the tubing for improving the heat distribution along the surface of the floor. This heat deflector is unnecessary for wet systems since the screed fulfils this task.

The advantages of a dry system over a wet system are (Linthorst, 2007, Roijen, 2004): quicker installation; demountable; low mass; allowance for less installed volume per day; reduced thermal mass of screed and thus reduced response time. Disadvantages however are (Linthorst, 2007): size and weight of panels are limited due to handling; the large number of panels results in increased handling; good logistics are important; high risk of leaking connections; reduced structure-borne sound insulation; because of flat panels, floors need to be levelled and cleaned.

---

[3] Since one of the requirements on the floor system is that it can both heat and cool, electrical floor heating systems are not considered in this chapter.

[4] This floor heating system was termed improved dry system by Willems and Kraan (2003) since it uses no screed of sand-cement or anhydrite thus being a dry system and since it is acoustically improved, especially in the lower frequency range, compared to a regular dry system owing to an increased thickness of the cavity between 'screed' and construction floor.

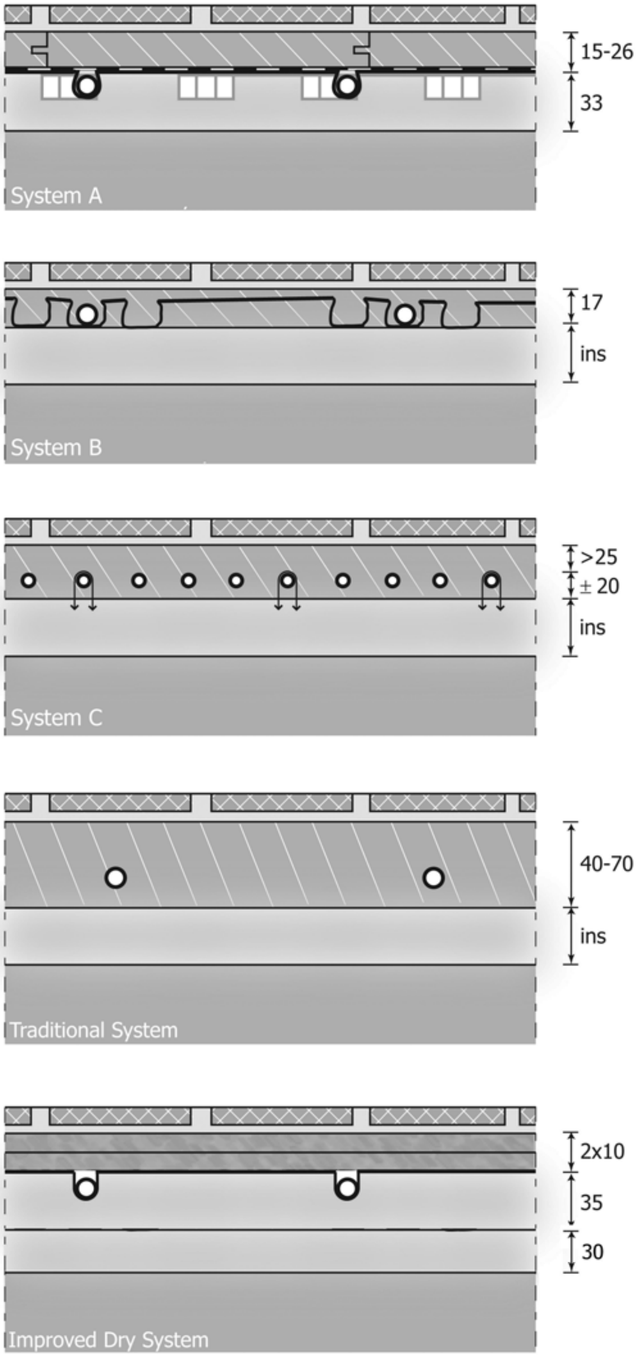

Figure 9.1

Schematic cross-sections through several floor heating systems currently on the market, except for the improved dry system.

Dimensions in millimetres.

System A: 33 mm PS, metal heat deflector, 15 to 26 mm screed.

System B: 30 to 40 mm insulation, 17 mm sand-cement based screed with a polyester formwork for positioning ducts.

System C: 30 to 40 mm insulation, 40 to 50 mm sand-cement based screed (or other type of screed) with capillary tube mats.

Traditional system: 30 to 40 mm insulation, 40 to 70 mm sand-cement based screed with tubing system.

Improved dry system: 30 to 40 mm insulation, 50 mm wood wool cement board, including slots for ducts, metal heat deflector, 2x10 mm gypsum fibre board.

***Table 9.1** – Selection of properties of several types of floor heating system.*

property	System A	System B	System C	traditional	improved drysystem
system type	dry	wet	wet	wet	dry
mass of screed [$kg \cdot m^{-2}$]	21-35	37	80-100	100-170	24
thickness of screed [mm]	15-26	17	40-50	40-70	20
total thickness [mm]	48-59	47-57	70-90	70-110	100
tube diameter [mm]	14	14	4.3	17	17
distance between tubes [m]	0.1-0.3	0.1-0.3	0.03	0.1-0.3	0.1-0.3

9.1.3 Floors and roof terraces insulated with VIPs

Many roof terraces and floors in Germany and Switzerland have already been insulated using VIPs. As explained earlier, the main advantage of insulating these floors and terraces with VIPs is the resulting limited construction thickness. If for example a flat roof terrace is insulated using VIPs in stead of PU foam insulation board, the difference in vertical position of the top surface of the floor between the inside of the building and the terrace can be reduced by several centimetres. By using VIPs thus an unpleasantly high step can be avoided. Moreover, in case of energetic improvement of buildings, like the renovation of a historic court house in Schaffhausen, the use of VIPs as floor insulation might avoid costly modifications to doors and door posts (Binz et al., 2005).

However, the use of VIPs on top of floors may also have disadvantages:

- VIPs are only feasible if available construction height is limited;
- Exact laying plans and parts lists are required prior to installation;
- Irregularities along the perimeter of a floor, like ducts and columns, need to be dealt with as a consequence often resulting in the use of conventional thermal insulator materials in these areas;
- Surface irregularities on top of the floor need to be removed or levelled before the panels can be laid;
- On-site application of VIPs increases the risk of damage during installation;
- Replacing damaged VIPs may involve destroying a large part of the screed resulting in high cost.

Notwithstanding these drawbacks many roof terraces and floors have already been insulated using VIPs[5]. One of these projects will briefly be described below: a sun-space in Germany.

[5] A non-exhaustive overview of projects in which VIPs have been applied is in appendix A83.

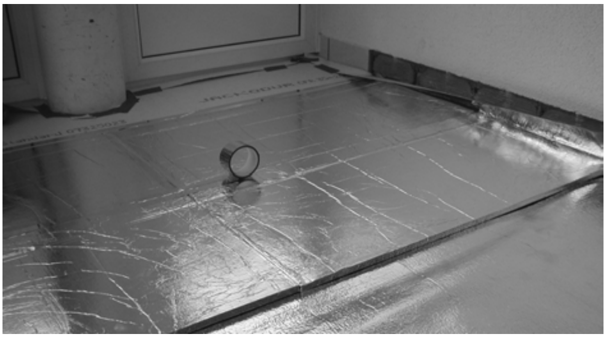

Figure 9.2a

Sun-space, Germany: the vacuum insulation panels are laid on top of protective polyethylene foam. Then the joints between VIPs are sealed using an aluminium-foil based tape and the room's perimeter is insulated with conventional material. (photo by R. Caps).

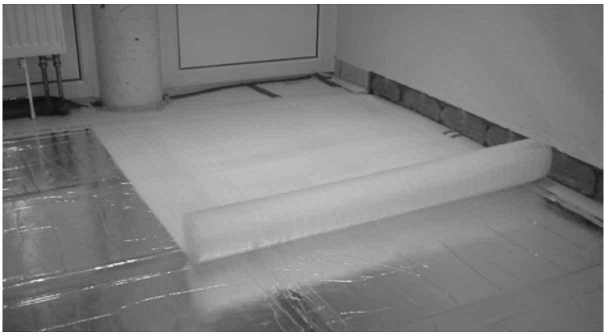

Figure 9.2b

Sun-space, Germany: on top of the VIPs, 3 mm thick polyethylene foam is added for protection. (photo by R. Caps).

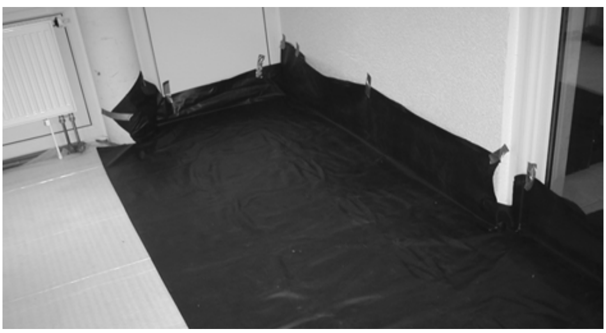

Figure 9.2c

Sun-space, Germany: the protective foam is covered by a 0.2 mm thick watertight PE film which prevents water from leaking from the anhydrite screed towards the VIPs. (photo by R. Caps).

SUN-SPACE IN GERMANY

Very often rooms that were originally conceived as sun-space are added to the living area of a dwelling. This implies that the sun-space, originally outside the heated zone of this dwelling, becomes part of this heated zone. As a result, this space should meet more stringent thermal requirements. Because the floor of this sun-space lacked good thermal insulation, it had to be thermally upgraded. Floors of sun-spaces however almost always lie at the same height as the floor of the adjacent room, irrevocably resulting in a step between both floors if one is insulated. The height of this step can be reduced using VIPs in stead of conventional insulators on top of the floor or can be prevented using under-floor insulation. However, in this particular project installing insulation below the floor was hardly possible, in any case not feasible. As a result, the planners decided to use VIPs on top of the floor.

After the removal of the original tile floor, the floor was first cleaned and covered by a 3 mm thick layer of polyethylene foam. This protective layer levels the concrete floor, prevents damage to the VIPs from dust, grain particles and surface irregularities and protects the insulation against moisture from below[6]. On top of this protective layer VIPs were laid, connected to each other by an aluminium-foil based tape and flanked by conventional insulators along the room's perimeter. Then, this package is again covered by 3 mm thick protective foam and a 0.2 mm thick layer of watertight polyethylene film forming the underlying strata for 25 mm to 55 mm gypsum based screed. Especially at places where VIPs are loaded, protective layers are required to prevent accidental damage. However, due to the sheer amount of materials laid on to the floor in subsequent order, the process is highly labour-intensive. Moreover, the boundary strip of conventional thermal insulation material along the room's perimeter forms a weakness in the thermal barrier of the floor.

9.2 VIPs and Floor Heating Systems: requirements

9.2.1 Future developments influencing floor heating systems

In Western Europe, currently several interesting developments strongly influencing the way we dwell and build, are ongoing. In the framework of a SenterNovem funded research project into sustainable project development based upon "sustainable building, refurbishing and dwelling beyond the year 2015", BouwhulpGroup studied these developments in detail (Persoon, 2008).

Besides the ageing of the population and the continuing separation between dwelling and health care, this study observes trends towards more individuality, more emphasis on experience and larger physiological differences between people. These changes in society require that new buildings are adaptable to changing user patterns and that comfort for these users is provided tailored to individual needs.

[6] Especially for roof terrace and access balcony insulation, an additional water tight film is placed below this thin PE foam or Ethafoam layer as an additional water barrier.

Moreover, this study clearly shows that refurbishment of existing buildings becomes more and more important within the years to come. As a result, occupants at the same time owners become the most important clients commissioning construction projects. This development coincides with a growing tendency towards more prefabrication in the construction sector resulting in an increased role of manufacturers. Both developments are likely to change the position and role of the players in the construction sector.

These developments impose the following requirements on building systems that provide comfort to the occupants of a building (Persoon, 2008): The system

- should respond quickly and must be individually controlled;
- should be able to deliver a base quality and several additional levels of quality in accordance with the desires of the individual client[7];
- should be applicable in both newly erected and retrofitted buildings
- should be installed as a complete dry system by one professional with in total two or three work steps, reducing time of installation and failure costs;
- should be competitive with existing systems.

If this system is then applied in existing buildings, the following additional prerequisites are imposed onto the system (Persoon, 2008): The system

- should have the ability to be used in co-operation with existing comfort systems;
- should be suitable for application on existing wooden and concrete floors;
- should be modular or adaptable in size;
- should fit a dry refurbishment method;
- should not impose restrictions on the craftsmanship of an installer.

9.2.2 *Requirements on vacuum insulation panels*

In general, the primary functions of an insulation layer below a floor heating and cooling system on top of the construction floor are thermal and acoustic insulation.

Thermal insulation below a floor heating and cooling system is always required for reducing heat losses towards the space or ground below the floor[8] and for improving the responsiveness of the system. It is now important to distinguish

[7] The base quality of a floor heating and cooling system is providing sufficient comfort regarding heating and cooling. Additional levels of quality could be increased thermal resistance or acoustic performance.

[8] The energy flowing from the heating system to the space below the floor or from the space below to the cooling system reduces the system's efficiency. For a similar reason, insulation material is added along the perimeter of the room to separate the screed from the walls.

between two situations: the floor separates between the interior of a building and outdoor air or the soil and the floor separates between spaces within a building. In the first case, the Dutch Building Code (VROM, 2001) requires a thermal resistance of the construction, R_c, of 2.5 $m^2 \cdot K \cdot W^{-1}$. In the latter case, no requirement is specified by Dutch or European Codes. However, for improving the efficiency of the heating and cooling system, for improving the controllability of this system and for assuring thermal de-coupling of the system from the space below, a thermal resistance of the insulation layer and construction floor of 1.5 to 2.0 $m^2 \cdot K \cdot W^{-1}$ should be realised (Roijen, 2004). Preliminary standard NEN-EN 1264-4ontw (2007) specifies a thermal resistance of the insulation layer below the floor heating and cooling system varying from 0.75 to 2.0 $m^2 \cdot K \cdot W^{-1}$ depending on the temperature conditions below the floor. If the space below the floor is heated, this standard prescribes a minimum thermal resistance of the insulation layer of 0.75 $m^2 \cdot K \cdot W^{-1}$. [9]

Acoustic insulation is principally required if the floor separates two dwellings or rooms of a different proprietor. Requirements on such floors are both specified for air-borne sound and for structure-borne sound. In these cases, the characteristic sound insulation indexes for air-borne and structure-borne sound, $I_{lu;k}$ and I_{co}, calculated according to NEN 5077 (2008) should be higher than 0 dB and +5 dB respectively. In the Netherlands, however, these minimum requirements are very often tightened in private contracts between proprietor and contractor with approximately 10 dB. Floors separating two spaces within one dwelling need to fulfil less stringent requirements: $I_{lu;k}$ and I_{co} should both be higher than -20 dB.

Concerning structural requirements, solely limit state requirements on the insulation layer are relevant. Since this insulation layer forms an intermediary between the screed onto which loads act and the structural floor, the insulation need to be able to transfer these loads without causing internal damage to its own structure and without too much compression. According to Dutch standards (NEN6702:2007), the main loads acting on a floor are represented by an equally distributed surface load, the value of which varies between 1.75 $kN \cdot m^{-2}$ for housing to more than 5.0 $kN \cdot m^{-2}$ for industrial buildings and libraries. Since however a pressure load of approximately 100 $kN \cdot m^{-2}$ acts on the core of an evacuated VIP, the additional surface load can easily be transferred. Moreover, Va-Q-tec AG (2008) states that the maximum allowable pressure load on a Va-Q-vip is 150 $kN \cdot m^{-2}$. Besides surface loads point loads need to be carefully considered. Such point loads might puncture the barrier and decrease the panel's service life. According to Dutch standards (NEN6702:2007), these point loads vary from 3 to more than 10 kN. To prevent accidental damage, VIPs should thus be covered by a load-spreading plate.

[9] Since this values is lower than the value for thermal de-coupling found by Roijen (2004), an R-value of 1.5 $m^2 \cdot K \cdot W^{-1}$ is chosen for thermal de-coupling of two heated spaces.

Table 9.2 *– Overview of most important (legal) requirements on VIPs integrated into a floor heating and cooling system (partly taken from Roijen (2004)).*

Require - ment	Floor between interior of building and ground or outside	Floor between different dwellings or owners	Floor between different spaces within one dwelling	Dutch Standards and Codes
statics / safety	Equally distributed surface loads between 1.75 and 5.0 kNm^{-2}; Careful with point loads	Equally distributed surface loads between 1.75 and 5.0 kNm^{-2}; Careful with point loads	Equally distributed surface loads between 1.75 and 5.0 kNm^{-2}; Careful with point loads	BB2003 §2.1.1, NEN 6702 TGB
fire safety	No requirements	fire spread resistance ≥ 60 min. (dwelling in condominium)	No requirements provided that rooms are located in 1 compartment	BB2003 §2.14.1, NEN 6068
acoustics	No requirements	Characteristic air-borne sound transmission index, $I_{lu;k} \geq 0$ dB; Characteristic structure-borne sound transmission index, $I_{co} \geq +5$ dB; Private: $I_{co} \geq +15$ dB	Characteristic air-borne sound transmission index, $I_{lu;k} \geq -20$ dB; Characteristic structure-borne sound transmission index, $I_{co} \geq -20$ dB;	BB2003 dep. 3.3 and 3.5, NEN 5077
energy	$R_c \geq 2.5$ m^2KW^{-1} Sust.build.: $R_c \geq$ 3.0 m^2KW^{-1} Requirements concerning EPC and f-factor	$R_{ins} \geq 0.75$ m^2KW^{-1} Thermal de-coupling: $R_{ins+floor}$ ≥ 1.5 m^2KW^{-1}	$R_{ins} \geq 0.75$ m^2KW^{-1} Thermal de-coupling: $R_{ins+floor}$ ≥ 1.5 m^2KW^{-1}	BB2003 dep. 3.7, 5.1 and 5.3, NEN-EN 1264-4, NEN 2778
service life	service life, t_{SL} >20 to 30 years	service life, t_{SL} >20 to 30 years	service life, t_{SL} >20 to 30 years	

The flatness and roughness of the structural floor should be considered too. According to Roijen (2004) two requirements are relevant: First, flatness over a distance of approximately 1 to 2 m; this unevenness gives rise to an increased risk of the occurrence of gaps between VIP and structural floor either damaging the panels or causing acoustic discomfort. Second, surface roughness over a small distance; such surface irregularities might locally inflict high point loads and puncture the barrier.

Figure 9.3

Relationships between different requirements on VIPs used as thermal/acoustic insulation below floor heating and cooling systems. Regarding performances, the white boxes denote performances that are not studied explicitly in this chapter, while the performances in the gray boxes are. Continuous and broken lines in these cases represent physical performances and customer's desires respectively.

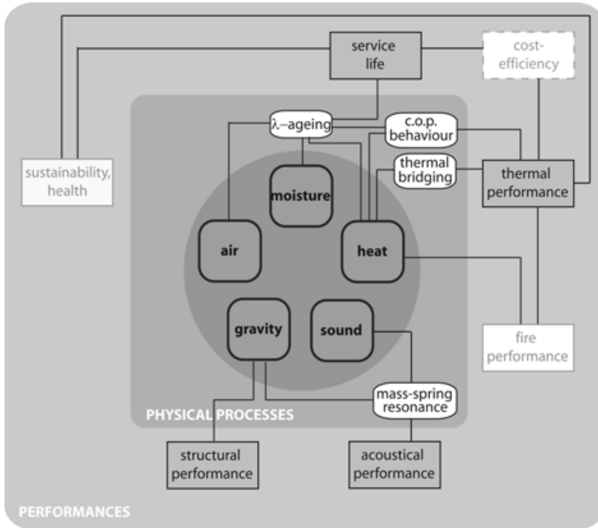

9.2.3 Interrelationships among requirements

Based upon the previously presented set of requirements, it is possible to investigate the (inter)relationships between these requirements on VIPs used as thermal or acoustic insulation below a floor heating and cooling system. This results in the scheme presented in Figure 9.3. As can be seen, several relationships among properties and requirements exist, two of which are especially important in case of insulation below a floating screed.

First, there exists an important relationship between the thermal performance of a VIP as thermal insulator on the one hand and its service life on the other hand via the physical process of thermal conductivity ageing. This relationship has already been discussed thoroughly in the previous chapter on VIP integrated façade components and will therefore not be discussed here.

Second, the relationship between structural behaviour and acoustics, especially structure-borne sound insulation, needs to be considered. The frequency at which resonance of this mass-spring system, i.e. the floating screed and the insulation layer, occurs depends on the mass of this screed and the dynamic stiffness of the insulation layer. This dynamic stiffness depends on the dynamic Young's modulus and the thickness. This dynamic Young's modulus is a material property which relates to the static Young's modulus. And this static Young's modulus in turn influences the structural behaviour, i.e. the compression, of the insulation layer.

9.2.4 (Thermal) mass of screeds

An important distinction concerning both the thermal and acoustic performance of a floor heating and cooling system relates to the specific (thermal) mass of the screed on top of the insulation layer. A high specific thermal mass of the screed in general results in a slowly responding system.

Publication ISSO 49 (ISSO, 2002) in general distinguishes between two types of thermal mass: high thermal mass and low thermal mass. Floor heating systems with high thermal mass are considered to have a response time of more than 2 hours while systems with low thermal mass have a response time below 2 hours. Practically speaking, a wet floor heating system without thermal insulation has a very high thermal mass, a wet floor heating system with floating screed has medium to high thermal mass, while an insulated dry system has low thermal mass.

Moreover, a high mass of the screed also influences the structure-borne sound insulation performance of a floor heating system as will be shown in section 9.4. The higher the mass of this screed on top of an insulation layer acting as an acoustic spring, the lower the resonance frequency of this mass-spring system. This frequency should preferably be below 80 Hz to avoid acoustic nuisances (Drolenga and Willems, 2005). In combination with this mass of the screed, the dynamic stiffness of the insulation layer is important. According to Drolenga and Willems (2005), it should be chosen between 5 and 20 $MN \cdot m^{-3}$ measured according to NEN-ISO 9052-1 (1992) or a similar standard.

9.3 PRINCIPAL DESIGN OF FLOOR HEATING AND COOLING SYSTEM

9.3.1 Brief

Since this high performance, slim, dry, prefabricated floor heating and cooling system is developed in the framework of a SenterNovem subsidised collaborative research and development project with several commercial partners, exact details of the system cannot be presented for reasons of confidentiality. The system itself is therefore omitted from the discussion.

Based upon a study of existing floor heating systems, of the improved dry system, of future developments in housing preferences, the following brief was formulated for this heating and cooling system. In addition to requirements from the European Construction Products Directive (European Council, 1988) and requirements elaborated upon in the previous sections, this system should (Linthorst, 2007):

- have a price of at most 30 €·m^{-2} including installation;
- be in accordance with plug&play philosophy;
- have system boundaries at the top of the construction floor and at the bottom of the carpet;
- be able to both heat and cool;
- be in accordance with IFD (industrial, flexible and demountable) philosophy.

This latter requirement for instance implies that the floor heating and cooling system needs to be prefabricated preferably in large quantities, needs to have a high and constant quality and needs to be intelligent, standardised, transformable, demountable, re-usable and sustainable.

9.3.2 Ideation: Water Foil Carpet and Advanced VIP

Based upon the aforementioned requirements, several ideas and concepts were formulated. One of the leading ideas within this ideation seemed to be the integration of as many functions as possible in one layer in stead of the traditional separation of functions. Such a strategy of integration might reduce the number of work steps and increase the suitability for prefabrication. This ideation resulted in five concepts: water foil carpet, boxed cast-floor, Parabeam panels, foldable all-in-one panels and advanced VIP. The first type was chosen for further development since it was evaluated as having an acceptable price and good development potential, can be manufactured using existing and cheap production technologies, is simple to handle on the construction site, can be quickly and easily installed and demounted, and has a good temperature diffusion. This system will however not be discussed because of a pledge of secrecy. The advanced VIP however is very interesting from a perspective of the use of vacuum insulation panels and will be discussed here in a bit more detail.

The advanced VIP system was conceived as a functional integration of both heating and cooling layer, thermal and acoustic insulation using vacuum insulation panels. If separate ducts are used, the position of these can be on top of the insulation layer, inside the core of a vacuum insulation panel, or in slots made in the VIP. The first and last types are presented Figure 9.4. Since the second system would require these ducts to penetrate the barrier envelope of the VIP, this system would have increased risk of short service life. As a result, this type of integration does not consider the properties of VIPs thoughtfully. The first system, although hardly requiring further research and development since it uses existing products, still requires many work steps. The last system therefore seems to be very promising for creating a high performance, prefabricated, dry, floor heating and cooling system.

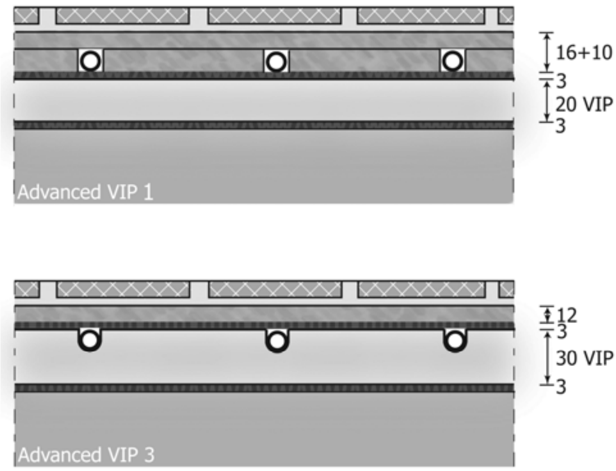

Figure 9.4

Schematic cross-sections through two VIP integrated floor heating systems. Dimensions in millimetres.

Advanced VIP 1: 3 mm Ethafoam protective layer, 20 mm VIP, 3 mm Ethafoam protective layer, 2 layers of gypsum fibre board in which ducts are integrated.

Advanced VIP 3: 3 mm Ethafoam protective layer, 30 mm VIP in which ducts are integrated, 3 mm Ethafoam protective layer, 12 mm gypsum fibre board.

If now the barrier film at the top of the panel, i.e. the barrier in contact with the ducts, is made of an aluminium-foil based laminate[10], a long service life can be achieved despite high temperatures while at the same time heat can be evenly distributed over the surface of the floor using this aluminium layer. To prevent however large thermal bridges along the panel's perimeter, the barrier at the panel's bottom needs to be made of a metallised-film based laminate thus producing a combi-laminate (chapter 3). Moreover, such a system could be produced as components with a size of for example 600x1200 mm^3 and with connectors for easily coupling the ducts of each component allowing rapid installation.

However, the large number of couplings would increase the risk of leakage. Besides, production methods for producing VIPs with slots for ducts along their surface need to be developed still, preferably methods for customised production. Moreover, VIPs are very fragile and currently expensive as a result of which it was decided not to investigate these advanced VIP components any further; the high cost of VIPs would just render the system uncompetitive compared to alternatives[11]. During the project it was also decided that the thermal and acoustic layer should be separated from the heating layer. This would allow the system to be customisable with respect to its performances (comfort, acoustics and energy use). VIPs have thus no longer been considered as part of the research and development project.

---

[10] with a relatively thick aluminium foil of for instance 15 or 20 μm.

[11] Although costs and revenues should be integrally considered, manufacturers and contractors still mainly solely look at the investment cost of a floor heating system. As a result, high thermal performance or limited thickness is generally not considered in cost calculations.

9.3.3 *Three performance variants of the Water Foil Carpet*

Based upon the previously described requirement of having a component delivering base quality that can be upgraded to fulfil more stringent requirements regarding thermal and acoustic performance, several variants have been conceived having different performance. The base variant solely consists of the water foil carpet system with no thermal or acoustic insulation and with a 12 mm thick Fermacell covering. This base variant solely provides or extracts heat, is cheapest and thinnest but does not have any additional quality. It can for instance be used on top of the second floor in single-family houses where no or hardly any requirements are set regarding acoustics or thermal de-coupling, or on top of an already insulated first floor in single-family housing.

If a floor however separates between two dwellings, acoustics and thermal de-coupling do become important, as seen from Table 9.2. Then a material between the water foil carpet and the construction floor needs to be added. This can for example be 50 mm acoustic rock wool or 18 mm Spaceloft™ insulation blankets. With both materials the *R*-value of the insulation layer becomes about 1.3 $m^2 \cdot K \cdot W^{-1}$, which together with the construction floor[12] should practically suffice in guaranteeing thermal de-coupling. From an acoustic perspective, both sub-variants are expected to perform in a similar way. The main difference between them then is their thickness and cost: using 50 mm rock wool provides a cheap solution however with the penalty of a thick floor; using 18 mm Spaceloft™ provides a very thin solution however with the penalty of high cost. The specific conditions of application might favor the one over the other.

In case a high thermal performance of the insulation layer below the floor heating and cooling system is required, then the third variant might provide a high performance solution. 20 mm vacuum insulation panels protected by 3 mm Ethafoam on both sides are used as thermal insulation. If also acoustic requirements are in place, then the 12 mm thick Fermacell board on top of the water foil carpet can be replaced by a 20 mm thick covering increasing the mass of this screed and thus reducing the frequency at which resonance occurs. The thermal resistance of the insulation layer approximately is 4.6 $m^2 \cdot K \cdot W^{-1}$ while the total thickness of the floor heating system including insulation is no more than 50 mm. This variant therefore combines high thermal performance with limited construction height however with the penalty of very high cost, as can be seen from Table 9.3. The properties of the VIPs in this variant will be discussed in more detail in section 9.4.

---

[12] A 200 mm thick reinforced concrete construction floor increases this resistance with approximately 0.12 $m^2 \cdot K \cdot W^{-1}$. Moreover, the boundary heat exchange coefficient at the bottom of the floor would also add 1/5.6=0.18 $m^2 \cdot K \cdot W^{-1}$ to this resistance.

Table 9.3 – Performance variants of water foil carpet.

property	variant 1: base quality	variant 2.1: thermal de-coupling and acoustics	variant 2.2: thermal de-coupling and acoustics	variant 3: high thermal performance
insulation layer	-	acoustic rock wool - 50 mm	Spaceloft™ - 18 mm	VIP - 20 mm
screed	12 mm Fermacell	20 mm Fermacell	20 mm Fermacell	12 mm Fermacell
total thickness [mm]	24	82	50	50
R_{ins} [$m^2 \cdot K \cdot W^{-1}$]	0	1.3	1.3	4.6[a]
mass of screed [$kg \cdot m^{-2}$]	15	25	25	15
dyn. stiffness of insulation [$MN \cdot m^{-3}$][b]	-	6 - 26	n/a	9 - 19
indicative cost of insulation [$€ \cdot m^{-2}$][c]	0	15 - 20	40 - 50	100 - 120

[a] The VIPs consist of a fumed silica core, a 3-layered metallised film on the cold side of the panel and a 25 μm thick stainless steel foil based laminate on the warm side. The ψ-value of the edge of this panel is $4.3 \cdot 10^{-3}$ $W \cdot m^{-1} \cdot K^{-1}$. The R-value of this panel is calculated for a panel size of 600x1200 mm^2 and 2 additional layers of 3 mm Ethafoam.

[b] Values of the dynamic stiffness are obtained from Drolenga and Willems (2005): for rock wool s'_t varies between 0.3/thickness and 1.3/thickness. The dynamic Young's modulus of Spaceloft™ is unknown but expected to be similar to that of mineral fibre insulation. Values of VIPs are discussed in section 9.4.

[c] These values are estimated from data obtained from manufacturers.

9.4 VIPs as Thermal Insulation Layer

9.4.1 *General remarks*

To protect the VIPs below the water foil carpet against water from a leaking floor heating system and against damage, a thin layer of watertight film and a protective layer of for instance 3 mm thick polymer foam need to be inserted between both components. As explained earlier, also between the construction floor and the vacuum insulation panels a protective layer is required. In stead of separately installing these protective layers on site, vacuum insulation panels having such layers installed in factory can be used as well. Using these latter panels reduces the number of work steps on site and thus labour cost.

Since the application of VIPs as thermal insulator below a floor heating and cooling system principally is the same as the use of these panels on roof terraces or entrance balconies, a large body of knowledge on how to apply these panels has already become available (Binz et al., 2005). This knowledge for example is available through VIP manufacturers and contractors. A thorough discussion will therefore be omitted here. It suffices to say that exact laying plans and parts lists are required since vacuum insulation panels cannot be shaped on site and since such planning may avoid the use of conventional material next to walls; that the structural behaviour of VIPs under compression poses no problems; that surface irregularities on top of the construction floor need to be removed or levelled before the panels can be laid; that these panels need to be installed carefully to reduce the risk of damage.

9.4.2 *Thermal behaviour and service life*

It is important to realise that the environmental boundary conditions under which vacuum insulation panels below a floor heating (and cooling) system have to operate deviate significantly from the boundary conditions in facades. For estimating the service life of these panels, here solely the conditions below a floor heating system are considered since they are most severe regarding service life; at high temperature, moisture and dry gas uptake by a VIP is much higher than at low temperature represented by the Arrhenius function. In this study 40°C is taken as the average temperature of the water in the floor heating system for as long as the system is operating while 22°C is used as long as the system is out of use. For reasons of simplicity it is assumed that the system is in use for half a year each year. A one-dimensional analysis of the temperature profile through a concrete floor with floor heating and VIPs then results in a boundary temperature of approximately 22°C on the other side of the panel[13]. The relative humidity is kept constant at 50%.

For three types of vacuum insulation panel, i.e. one with a fumed silica core and a 8 μm thick aluminium foil based laminate, one with a fumed silica core and a three layer metallised film based laminate and one with a fumed silica core and a combination of a 8 μm thick aluminium foil based laminate on the warm side and a three layer metallised film based laminate on the cold side, the linear thermal transmittance and resulting effective thermal conductivity as function of ratio l_p/S_p has been calculated and displayed in Figure 9.5a. As can be seen and as already known from chapter 3, the effective thermal conductivity is always highest for a VIP with a metal foil based barrier laminate and lowest for a VIP with a metallised film based laminate provided that the thermal conductivity of the core material is equal. Interestingly, the thermal performance of a VIP with a combined barrier envelope almost equals that of a VIP with a metallised film based barrier envelope.

---

[13] The floor consists of the following layers from bottom to top: 200 mm reinforced concrete, 3 mm Ethafoam, 20 mm VIP, 3 mm Ethafoam, 0.2 mm watertight film, water foil carpet, 12 mm Fermacell, 6 mm parquet. The temperature of the space below the floor is 21°C.

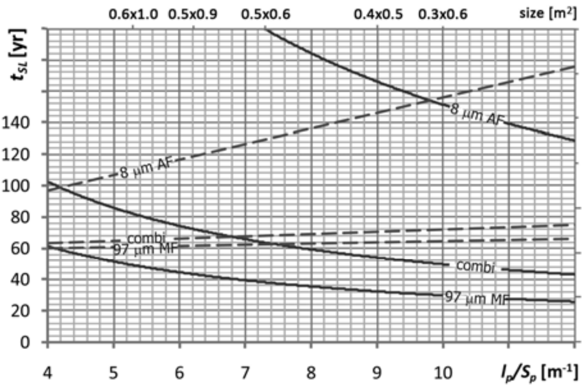

Figure 9.5a

Thermal performance and service life of three types of vacuum insulation panel (with an 8 μm aluminium foil based laminate, a three layer metallised film based laminate and a combination of both) as function of l_p/S_p. Thermal bridging is not considered in service life prediction. Continuous lines represent service life while broken lines represent effective thermal conductivity.

T_1 = 40°C / 22°C; T_2 = 22°C; RH=50%; φ=0.75; $\lambda_{c;o}$=0.004 $W{\cdot}m^{-1}{\cdot}K^{-1}$.

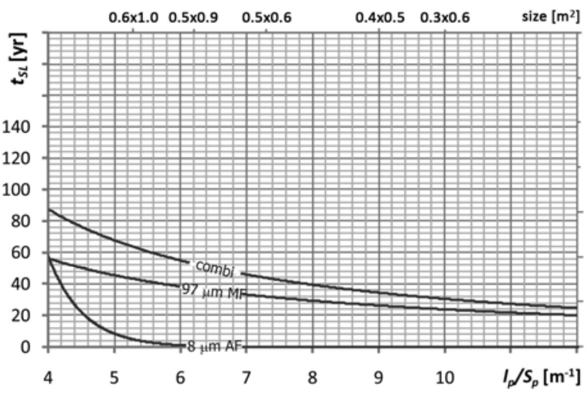

Figure 9.5b

Service life of three types of vacuum insulation panel (with an 8 μm aluminium foil based laminate, a three layer metallised film based laminate and a combination of both) as function of l_p/S_p. Thermal bridge effects are considered in service life prediction.

Moreover, the service life of aforementioned panels has been estimated too. Service lives in which thermal bridge effects are not considered are presented in Figure 9.5a6 by the continuous lines and service lives in which thermal edge effects are considered are presented in Figure 9.5b[14]. As can be seen from Figure 9.5a and as

[14] In case thermal edge effects are not considered in service life predictions, this service life is calculated based upon an initial thermal conductivity of the core material of $4.2{\cdot}10^{-3}$ $W{\cdot}m^{-1}{\cdot}K^{-1}$ and a final end of life thermal conductivity of the core material of $8.0{\cdot}10^{-3}$ $W{\cdot}m^{-1}{\cdot}K^{-1}$. In case thermal edge effects are considered in service life predictions, this service life is computed based upon an initial thermal conductivity of the core material of $4.2{\cdot}10^{-3}$ $W{\cdot}m^{-1}{\cdot}K^{-1}$ and a final end of life effective thermal conductivity of the entire panel of $8.0{\cdot}10^{-3}$ $W{\cdot}m^{-1}{\cdot}K^{-1}$. In these computations, vacuum insulation panels are treated as separate entities not thermally connected to other materials.

already known from chapter 5, the service life of panels with an aluminium foil based laminate is longest if thermal bridge effects are not included in the service life prediction. And again a VIP with a combined barrier laminate performs in-between a panel with aluminium foil based laminate and a panel with a metallised film based laminate.

If however thermal bridging is included in the predictions, the situation completely changes. Now, VIPs with a combined barrier laminate perform best concerning service life. This can easily be explained because the thermal bridge effect due to aluminium foil based barrier laminates is so strong that for small panels with a ratio l_p/S_p higher than approximately 6 m^{-1} even at initial conditions the panel's effective thermal conductivity already exceeds the end-of-life criterion of $8.0 \cdot 10^{-3}$ $W \cdot m^{-1} \cdot K^{-1}$; and that for these panels with a smaller ratio this edge effect still is very big[15].

Based upon both thermal considerations and service life predictions, a combined barrier laminate of a metal foil based laminate on the warm side and metallised film based laminate on the cold side is therefore the preferred choice for VIPs used below a floor heating system[16,17]. For these panels, the service life, in which thermal edge effects are included, can be higher than 30 years provided that the ratio l_p/S_p is smaller than approximately 10 m^{-1} and the panel's thickness is 20 mm, or in other

---

[15] It is however important to realise that in these calculations VIPs are treated as separate entities not thermally connected to other materials. As we have seen in chapter 4, the materials surrounding a VIP influence the value of the linear thermal transmittance resulting. This implies that the conclusion that VIPs with a combined laminate perform best may not always be true. However, the linear thermal transmittance of the edge of a VIP is more strongly influenced if materials with high thermal conductivity are used on top or below the VIP than if materials with low thermal conductivity are used. Since the VIPs are protected on either side by a 3 mm thick ethafoam layer, the conclusion is highly plausible.

[16] The aluminium foil based laminate in this analysis can be replaced by a 25 mm thick stainless steel foil based laminate as well. Although no data regarding permeances of this laminate are available, it is expected that it performs similarly to an aluminium foil based laminate concerning service life.

[17] An alternative to the use of 20 mm thick VIPs with a combined barrier laminate is the use of two layers of 10 mm thick VIPs with an aluminium foil based barrier laminate positioned in such a way seams do not overlap. These panels have relatively high service life, although slightly shorter than similar 20 mm thick panels, and due to their shifted positioning good thermal performance as well. For an insulation layer of 40 mm VIP with a 7 μm aluminium foil based barrier laminate, the linear thermal transmittance due to this envelope reduces from $2.2 \cdot 10^{-2}$ $W \cdot m^{-1} \cdot K^{-1}$ for a one-layered configuration to $9.5 \cdot 10^{-3}$ $W \cdot m^{-1} \cdot K^{-1}$ for a shifted two-layered configuration ($\lambda_c = 4.0 \cdot 10^{-3}$ $W \cdot m^{-1} \cdot K^{-1}$; φ=1) (van Went, 2002). The thermal bridge effect thus reduces by a factor 2.3. Despite these thermal advantages, however, such multiple insulation layers would increase the number of work steps on the construction site and thus the labour cost significantly. As a result, this double layered configuration is not advocated.

words the panel's width and length are bigger than 0.4 m in case of square panels. If thermal bridging is not considered in the service life prediction, the service life of these panels is higher than 30 years provided that l_p/S_p is smaller than approximately 14 m^{-1} and the panel's thickness is 20 mm, or in other words the panel's width and length are bigger than 0.29 m in case of square panels.

9.4.3 Acoustics

In the framework of this collaborative research and development project into an integrated, prefabricated, dry floor heating component, several measurements to determine some acoustic properties of vacuum insulation panels have been performed. The most relevant acoustic properties of the insulation layer below a floating screed are its dynamic stiffness, s'_t [$MN \cdot m^{-3}$], and as appropriate its sound absorption coefficient, α [-].

The dynamic stiffness of VIP samples of 200x200x20 mm^3 consisting of a fumed silica core and a 3-layer metallised film based envelope have been measured using equipment from TNO Delft according to standard NEN-ISO 9052-1:1992 (1992)[18]. Intact VIPs, vented VIPs, fumed silica cores, and fumed silica cores wrapped in a fleece of glass fibres have been subjected to this testing procedure[19]. Two masses have been used for the measurements: a plate of 7.7 kg (193 $kg \cdot m^{-2}$) and one of 0.784 kg (20 $kg \cdot m^{-2}$)[20]. The results of these tests are tabularised in Table 9.4.

According to Drolenga and Willems (2005), an improvement of the structure-borne sound insulation index, I_{co}, by about 8 dB is possible for an insulation layer with a stiffness of 14.0 $MN \cdot m^{-3}$ and a mass of the floating screed of 20 $kg \cdot m^{-2}$. It is therefore expected that this improvement is achievable with VIPs as thermal insulator below the water foil carpet floor heating system and a 20 mm thick Fermacell screed fulfilling legal requirements on a floor separating between different dwellings or spaces of different proprietor. To obtain a higher improvement either a thicker vacuum insulation panel, an additional layer of a wood wool magnesite board, or a screed with higher mass needs to be applied.

---

[18] It is important to note that due to the composite nature of a VIP, these measured values cannot directly be generalised to obtain values for panels of other dimensions. Size effects have not been studied due to the limited capabilities of the testing procedure and equipment.

[19] For each variation 6 to 12 duplication tests have been conducted.

[20] The mass of these plates on top of the samples is relevant because it relates to the mass of the floating screed on top of this insulation in practise. Together with the dynamic stiffness it determines the frequency at which resonance occurs and thus influences the practical structure-borne sound insulation index. A wet sand-cement based screed typically has a mass of 85 to 125 $kg \cdot m^{-2}$ while a screed of dry plate material typically has a mass of 20 to 25 $kg \cdot m^{-2}$.

Table 9.4 *– Results of dynamic stiffness measurements on VIPs (200x200x20 mm³).*

type of sample	mass [kg·m^{-2}]	s'_t [MN·m^{-3}]	E_{dyn} [MPa]
intact vacuum insulation panel	193	12.5 ± 1.4	0.25 ± 0.03
intact vacuum insulation panel	20	14.0 ± 4.7	0.28 ± 0.09
vented vacuum insulation panel	193	14.6 ± 1.2	0.29 ± 0.02
vented vacuum insulation panel	20	12.8 ± 1.3	0.26 ± 0.03
fumed silica core (no vacuum)	193	24.2 ± 1.9	0.48 ± 0.04
fumed silica core (no vacuum)	20	34.4 ± 3.4	0.69 ± 0.07
fumed silica core + fleece (no vacuum)	193	16.0 ± 3.1	0.32 ± 0.06
fumed silica core + fleece (no vacuum)	20	21.0 ± 4.2	0.42 ± 0.08

NB: Values are given for a 95% reliability interval.

The average dynamic stiffness in MN·m^{-3} of a VIP of 200x200x20 mm^3 with a low-weight screed can be obtained from $0.28/d_p$ with d_p in meter. As a comparison, the dynamic stiffness of a plate of acoustic glass fibre or rock wool board equals $0.15/d_p$ to $0.25/d_p$ and $0.30/d_p$ to $1.30/d_p$ respectively (Drolenga and Willems, 2005). A 20 mm thick vacuum insulation panel (200x200 mm^2) acoustically thus performs better than a rock wool board but worse than a glass fibre board. With *m*' the mass of the screed [kg·m^{-2}], the frequency at which resonance occurs can now be calculated from these values as (NEN-ISO 9052-1:1992)

$$f_r = \frac{1}{2\pi}\sqrt{\frac{s'_t}{m'}} \tag{9.1}$$

Not only has the dynamic stiffness been measured, but also the sound absorption coefficient, α, of intact VIPs. This coefficient has been measured in third octave bands according to NEN-EN-ISO 354:2003 (2003) in a reverberation chamber at Cauberg-Huygen. Figure 9.6 presents the results of these measurements. As can be seen clearly, three phenomena are superposed to form the final absorption coefficient: friction of air inside pores, resonance of the barrier (mass) onto the core (spring), and a reduction of porous absorption due to shielding at low frequencies.

Absorption in porous materials occurs because a vibrating air layer inside the pores of these materials via friction dissipates energy reducing the amount of energy in the sound wave. Characteristic for this type of absorption is that it mainly occurs at higher frequencies and as a result increases from low to high frequency. Especially important for such absorption is the specific flow resistance of this material. Fumed silica has a high flow resistance due to its very fine pore structure.

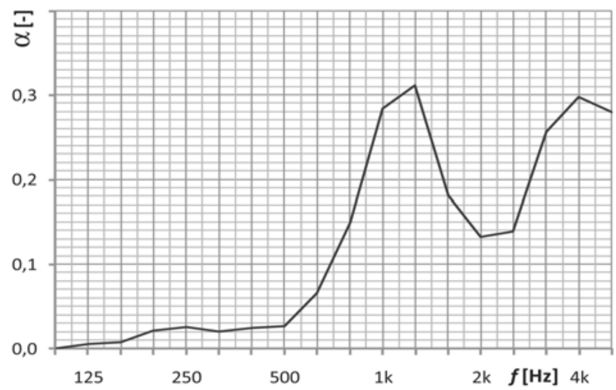

Figure 9.6

Sound absorption coefficient of 20 mm thick vacuum insulation panels as function of frequency. Multiple panel sizes have been measured simultaneously: 8 panels of 597x997 mm², 4 panels of 493x597 mm² and 4 panels of 453x597 mm². Volume of reverberation chamber 211 m³; air temperature 18°C; relative humidity: 40%.

As a result, a large fraction of the sound wave hitting this material is reflected at the material's surface and does not enter the material where it can dissipate its energy. The sound absorption coefficient of a vacuum insulation panel with a fumed silica core therefore is limited to 0.3 at most, as can be seen from Figure 9.6.

In case of sound absorption in porous materials, a second phenomenon plays an important role as well: shielding of the material's pores by a layer of paint or a film. Below a certain frequency, f_{film} [Hz], a film or layer of paint will induce a reduction of sound absorption since it inhibits the access of a sound wave to the porous material. This frequency can be estimated from (Cauberg et al., 2001)

$$f_{film} = \frac{\rho_{air} c_{air}}{2\pi \rho_f t_f} \qquad (9.2).$$

In this equation, $\rho_f t_f$ [kg·m^{-2}] is the mass of the laminate and $\rho_{air} c_{air}$ [kg·m^{-2}·s^{-1}] the specific acoustic impedance of air. For standard three-layer metallised laminates with a mass of 0.106 kg·m^{-2}, this boundary frequency is 616 Hz.

The third phenomenon is resonance of the laminate (mass) onto the core (spring). This resonance peak approximately lies between 1000 and 1250 Hz. It occurs because the envelope and core act as a mass-spring system and in this way result in increased absorption during resonance. The frequency where this occurs can be estimated by the following equation (Cauberg et al., 2001)

$$f_r = \frac{1}{2\pi} \sqrt{\frac{s'_t}{\left(m' + 0.6\sqrt{ab}\right)}} \qquad (9.3),$$

with a [m] and b [m] the length and width of the panel. Using the smallest dimensions of panels tested, this frequency is estimated near 921 Hz which is slightly below the resonance peak observed.

9.5 CONCLUSIONS CONCERNING VIPS APPLIED BELOW FLOOR HEATING

The use of vacuum insulation panels as thermal insulator on top of a floor might have several advantages over conventional thermal insulators, among which are a reduced step between inside floor and roof terrace and the avoiding of modifications to doors and door posts. However, several possible drawbacks might limit their use: VIPs are very expensive and therefore only feasible if available construction height is limited; exact laying plans and parts lists are required prior to installation; irregularities along the perimeter of a floor, like ducts and columns, need to be dealt with as a consequence often resulting in the use of conventional thermal insulator materials in these areas; surface irregularities on top of the floor need to be removed or levelled before the panels can be laid; on-site application of VIPs increases the risk of damage during installation as a result of which integration into prefabricated components is the preferred solution; replacing damaged VIPs may involve destroying a large part of the screed[21].

Both these advantages and disadvantages also hold for VIPs applied on top of a construction floor below a floor heating system. Mainly because of high investment cost and high risk of damage during installation, vacuum insulation panels were not advocated as insulation layer below the water foil carpet floor heating and cooling system. Since however future developments, like increased attention for refurbishment, higher energetic requirements on buildings, improved thermal de-coupling between rooms and individual comfort demands, steer developments towards high performance, easily installed and at the same time thin floor heating and cooling systems, vacuum insulation panels may have high potential in the (near) future. But then either investment costs need to decrease or practitioners in the building industry need to start using integral and life cycle costing methods.

If VIPs are to be used below a floating screed, two relationships were found of practical importance. First, there exists an important relationship between the thermal performance of a VIP as thermal insulator on the one hand and its service life on the other hand via the physical process of thermal conductivity ageing.

---

[21] Concerning the insulation layer below a floor heating system, in many situations aerogel insulation blanket have more favourable intrinsic and extrinsic properties than vacuum insulation panels. They can hardly be damaged, have no inherent thermal bridges, are flexible, can be shaped and sized on site, are less expensive and exhibit no thermal conductivity ageing. Drawbacks however are that these insulation blankets are still limited to a thickness of 6 and 9 mm, as a result of which multiple layers are needed. Such multiple layers result in more work steps on site and higher labour cost. Besides, due to a lower thermal conductivity, a thicker insulation layer might be needed compared to VIPs.

Second, the relationship between structural behaviour and acoustics - especially structure-borne sound insulation - via the static and dynamic Young's modulus is relevant. These two examples again show how important it is to make an integral design for building systems in which vacuum insulation panels are to be applied.

Since the water in a floor heating system in operation has a temperature significantly above laboratory conditions[22], the service life of the vacuum insulation panels below such a system might be a concern. If however the barrier envelope is conceived as a combination of a metal foil based laminate on the warm side and a metallised film based laminate on the cold side, both a high thermal performance and high service life[23] can be achieved. For a vacuum insulation panel of 0.5x0.6x0.02 m^3 with a fumed silica core and such a combined barrier envelope, for instance, a service life of approximately 46 years or 64 years was calculated if either thermal edge effects are or are not considered in the calculation scheme. This value meets the requirement of 30 years set in advance. The effective thermal conductivity of such a panel would approximately be $4.7 \cdot 10^{-3}$ $W \cdot m^{-1} \cdot K^{-1}$.

Moreover, from a structure-borne sound insulation perspective, vacuum insulation panels might also be able to fulfill legal demands. Having a dynamic stiffness of[24] 14.0 ± 4.7 $MN \cdot m^{-3}$, 20 mm thick vacuum insulation panels can improve the structure-borne sound insulation index by +8 dB or more provided that the mass of the floating screed is higher than 20 $kg \cdot m^{-2}$ (Drolenga and Willems, 2005). A 20 mm thick small vacuum insulation panel acoustically thus performs better than a rock wool board but worse than a glass fibre board of the same thickness. Its sound absorption coefficient however is rather limited and almost never exceeds 0.3.

---

[22] The water temperature of the water foil carpet was determined to be between 45°C near the entry point and 35°C near the exit point.

[23] Even if temperature effects are considered in service life predictions, a high enough service life can be achieved using this barrier envelope.

[24] Value was measured for panels of 200x200x20 mm^3 with a fumed silica core, a three-layer metallised barrier envelope and a screed of 20 $kg \cdot m^{-2}$.

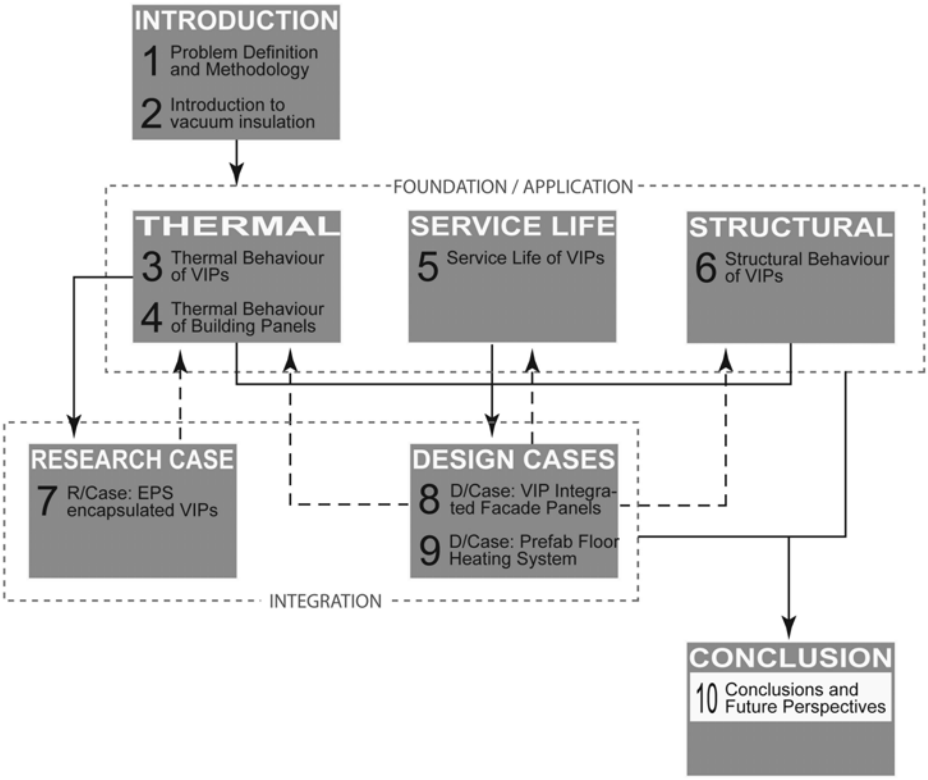
INTRODUCTION
1 Problem Definition and Methodology
2 Introduction to vacuum insulation
FOUNDATION / APPLICATION
THERMAL
3 Thermal Behaviour of VIPs
4 Thermal Behaviour of Building Panels
SERVICE LIFE
5 Service Life of VIPs
STRUCTURAL
6 Structural Behaviour of VIPs
RESEARCH CASE
7 R/Case: EPS encapsulated VIPs
DESIGN CASES
8 D/Case: VIP Integrated Facade Panels
9 D/Case: Prefab Floor Heating System
INTEGRATION
CONCLUSION
10 Conclusions and Future Perspectives

CONCLUSIONS AND RECOMMENDATIONS 10

10.1 Answer to and Reflection on Research Questions

10.1.1 Key questions 1 and 2: Foundation and Application

In chapter 1 on methodology the main research question of this study was divided into three key research questions. The first and second of these key questions related to the domain of foundation and application and were formulated as

How and to what extent influence thermal, hygrothermal and structural factors the overall performance of vacuum insulation panels and how can these factors be modelled with sufficient accuracy for design purposes on the level of a vacuum insulation panel?

How and to what extent influence thermal, hygrothermal, structural factors the overall performance of VIP integrated building components and constructions and how can these factors be modelled with sufficient accuracy for design purposes on the level of VIP integrated building components?

Both key research questions are divided into three aspects, i.e. thermal, hygrothermal and structural aspects, and in fact contain two questions. The first relates to the influence of certain factors on the performance of VIPs and VIP integrated components whereas the latter relates to models or schemes for calculating their performance. Each of these aspects will be treated separately.

An important feature of vacuum insulation panels are thermal bridge effects, either caused by the laminate which entirely envelopes the core, by spacers in building components, or by other structural elements. The first and second are linear thermal bridges and can be represented by a linear thermal transmittance which reflects the additional heat flow through this thermal bridge per unit area and per unit temperature difference. As a result, the higher this linear thermal transmittance, the worse the overall thermal performance of a VIP or a building component is.

The linear thermal transmittance caused by a metallised film based laminate around a VIP with a thickness beyond 20 mm can be estimated with sufficient accuracy for design and engineering purposes from the product of the thermal conductivity and thickness of this envelope at the panel's edge divided by the thickness of the core, $\lambda_f t_f / d_p$. Thermal edge effects occurring in vacuum insulation panels with a thickness of more than 20 mm and enveloped by a metal foil based laminate can be estimated using the linear thermal transmittance equation presented in this dissertation for a VIP with λ_c =0 W·m^{-1}·K^{-1}. For computations required in the early stages of a design and development process, these simplified equations are sufficiently accurate. If higher accuracy is required, if the thickness of a VIP is less than 20 mm or if VIPs are integrated into building components, more advanced models should be used. These models were derived in chapters 3 and 4.

From these models we can learn that the overall thermal performance of VIPs or building components, i.e. the thermal performance in which thermal edge effects are accounted for, primarily depends on the thermal conductivity and thickness of the core, the ratio of panel circumference to surface area, l_p/S_p, and the linear thermal transmittance resulting from the thermal bridge. For VIPs, this linear thermal transmittance again is influenced by the thermal conductivity and thickness of the core, the (weighted average) thermal conductivity and thickness of the barrier envelope on either side and the type and configuration of seams and adjoining air gaps. Similar parameters influence the linear thermal transmittance of the edge of building components with spacers: thickness and thermal conductivity of the core, thermal conductivity and thickness of the face sheets, the width of the edge zone and the thermal conductance of this edge.

In general, the overall thermal performance increases for decreasing ratio of panel circumference to surface area, i.e. for increasing panel size, for decreasing thermal conductivity and thickness of the envelope – or combination of envelope and face sheets -, for decreasing thermal conductivity of the core and for decreasing width and thermal conductance of the laminate or spacer at the perimeter. The reasons for this are that less heat is collected and transferred to the edge by the face sheets or barrier laminate if their thickness and thermal conductivity decrease while also less heat is transferred through the thermal bridge if this becomes smaller or less conducting relative to the centre-of-panel region.

The influence of panel thickness on overall thermal performance is more complicated. In general, the linear thermal transmittance first increases to a maximum value and then decreases again to zero if panel thickness increases. This peak value mostly lies in the range of VIPs used in practise. Panel thickness however also influences the thermal performance of the centre-of-panel area. Here, increased thickness results in increased thermal resistance. The combined effect thus determines the influence of panel thickness on overall thermal performance.

In general, for VIPs with a barrier envelope of a metallised film based laminate and in any case practical dimensions, the effect of a change in panel thickness on the overall thermal transmittance is stronger than the effect of a change in perimeter to surface area ratio. For VIPs with a barrier envelope of a 6 to 10 μm thick aluminium foil based laminate and practical dimensions, however, the effect of a division into half of the ratio l_p/S_p on overall thermal performance has a similar extent as a doubling of the panel's thickness. In case of building components with strong edge effects and practical dimensions, a change in panel size has a stronger effect on overall thermal performance than a change in the thickness of the VIP inside this component. Since VIPs are mostly integrated into building constructions, an increase in panel size is in most cases preferred to an increase in panel thickness. This is in accordance with the most promising feature of VIPs: limited thickness. Currently, however, the maximum size of a VIP is limited by production capabilities, i.e. the size of the vacuum chamber. Larger vacuum chambers might therefore be a sensible solution for achieving even higher thermal performance than currently possible.

Moreover, from simulations on several building components it became clear that it is very difficult to achieve 'passivhaus standard' with building panels with a VIP core thinner than 40 mm, even at the beginning of service life. This result implies that, if such high standards are desired, then sandwich panels, not needing a strong edge profile, are the preferred choice from a thermal perspective.

Another important feature of VIPs is their finite service life. It is important to realise, though, that after expiry of this service life no sudden damage occurs to the panel; it is just that slowly but gradually the thermal conductivity of its core increases due to ingress of water vapour and dry atmospheric gases and that a certain value of this thermal conductivity is said to indicate the end of life. Most researchers and manufacturers in Europe use $8.0 \cdot 10^{-3}$ $W \cdot m^{-1} \cdot K^{-1}$ as critical value for this thermal conductivity. Starting from a thermal conductivity of $4.0 \cdot 10^{-3}$ $W \cdot m^{-1} \cdot K^{-1}$, this means that the service life expires if this thermal conductivity doubles, or in other words if the thermal resistance – not considering thermal edge effects – is reduced by half. The effective thermal conductivity of the entire VIP or building component instead of the thermal conductivity of the core can also be used as terminating criterion.

In chapter 5, the aspects of service life of VIPs and building components was studied. Based upon existing literature, models for estimating this ageing effect were presented and modified to include semi-dynamic boundary conditions using so-called service life influencing factors. Moreover, since these models are rather complex, two approximation models, one for estimating the service life of VIPs with a fumed silica core and one for VIPs with polymeric foam based core with desiccant, were derived and presented, as well. These models are especially suitable for use in the design and engineering phase. By comparing the first models to more advanced ones, it was shown that differences between both are acceptably small.

If the service life of a VIP is defined using a criterion for the effective thermal conductivity, thermal bridge effects should be considered when VIP service lives are computed. As can be expected, the effect of thermal shunting on the service life is smallest for large panels and panels having a small linear thermal transmittance, i.e. VIPs with a MF3 barrier. The service life of a small VIP with a metal-based barrier envelope, however, may significantly be reduced due to a strong thermal bridge effect; a reduction with more than 50% is quite normal for such panels. If thermal shunting ís included and if the criterion for the effective thermal conductivity of a vacuum insulation panel inside a building component is set at $8.0 \cdot 10^{-3}$ W·m^{-1}·K^{-1}, a building panel with facings for which $\lambda_{f;j}\, t_{f;j} \geq 0.3$ W·K^{-1} combined with either an aluminium double-glazing spacer, a folded edge spacer or an optimised thermoplastic spacer even is never suitable for application in buildings since the thermal conductivity of the core at initial conditions added with an increase factor representing the thermal bridge effect is already higher than the thermal conductivity criterion, except for large panels with sizes beyond practical limits.

In general, the service life of a VIP is principally determined by the properties of the core, the presence and effectiveness of getters and desiccants, the initial vacuum and water content, degassing of the core and the laminate, the envelope's permeance for atmospheric gases and water vapour, the quality of the seam, the panel's dimensions and the environmental conditions regarding temperature, relative humidity, partial water vapour pressure and air pressure. Since, the first five factors can hardly be influenced by architects and building engineers, especially the last two are interesting from the perspective of construction design.

Since permeation of water vapour and dry atmospheric gases occurs both through the flat surfaces and the seam of a VIP, its dimensions and ratio of perimeter to surface area l_p/S_p strongly influence the service life. Since aluminium foil based envelopes in their flat surfaces are almost impermeable to atmospheric gases, these size effects are stronger for these envelopes than for metallised film based envelopes. Moreover, the time constants for atmospheric gases and for water are both directly proportional to panel volume, as a consequence of which the service life is also directly proportional to panel thickness. In general, thus, the larger the ratio l_p/S_p and the thicker the panel, the higher its service life is.

The most important temperature effect is the dependency of the water vapour and gas transmission rate through the barrier envelope on temperature: the higher the temperature is, the higher the transmission rates are. The most important relative humidity effect is the dependency of the water vapour and to a lesser extent gas transmission rate through the barrier envelope on relative humidity. The exact physical mechanisms involved in this dependency are still insufficiently clear for complex multilayered films. The partial water vapour and air pressure surrounding a VIP, finally, increase the driving potential for water vapour and dry gas permeation and thus also influence the service life.

Due to the integration of these VIPs into a building construction, however, the environmental conditions surrounding the VIP may change from constant (laboratory) conditions to real-life fluctuating conditions. If a VIP is applied in a façade component that is used in a temperate Western-European climate, the conditions regarding temperature in general are such that the service life of this panel in application is higher than the service life of an identical panel under standard laboratory conditions (23°C and 50% RH). These relatively high values for the service life primarily result from a lower Arrhenius annual average temperature of the barrier laminate in these practical conditions relative to laboratory conditions and from the omission of relative humidity effects in the computations. This latter effect can however have a strong influence on service life. If a VIP however is used in-situ below a floor heating system, then the temperature on one side of this panel may be as high as 45°C when the system is in operation while the other side more-or-less remains between 20°C to 25°C. Due to this very high temperature on one side of the panel, its service life in general lies below the value it would have under the aforementioned laboratory conditions. In these two examples thermal edge effects are not considered in the service life computation scheme.

A third important feature of VIPs applied structurally is their flexural behaviour. A VIP is a composite system and must therefore be regarded as such. From a structural perspective, it is analogous to reinforced pre-stressed concrete: the core then resembles concrete, the barrier envelope the reinforcement and the atmospheric pressure a pre-stress in the core. Using this analogy, the entire flexural behaviour of a VIP with a fumed silica core and a metallised film based barrier can be modelled. The transitions between separate stages in its flexural behaviour then are: buckling of the top laminate, physical failure, yield of the lower laminate, crack formation in the tension zone of the core, up-setting in the compression zone of the core and finally structural failure. Although structural failure is the final stage in the failure process, physical failure, i.e. the formation of (micro-)cracks in the barrier envelope, strongly influences the panel's service life. Moreover, we have seen that the Young's modulus of a vented VIP is much smaller than of an intact VIP. For reasons of safety therefore, either the transition of physical failure or the behaviour of a vented VIP should be taken as limit state, the choice of which depending on which of the two poses the highest restrictions.

Models for estimating an effective equivalent Young's modulus were derived, too. Considering its cross-sectional geometry and assuming a perfect interface between the barrier laminate and the core, the Young's modulus of a VIP composite system can be modelled as an equivalent Young's modulus, which considers the composite nature of a VIP, or as an equivalent effective Young's modulus, which also includes shear effects. It is important to realise that both moduli are not material properties but depend on the material properties of the constituents of the composite, the cross-sectional geometry and, in case of the effective equivalent modulus, also on the type of loading, load-to-support distance and span.

These models readily clarify that if the ratio of panel thickness to span decreases shear effects become less pronounced, as a result of which the panel's effective equivalent Young's modulus increases. Moreover, the fact that the flexion modulus of the core is several orders of magnitude smaller than the Young's modulus of typical barrier envelopes in tension and compression, a decrease in panel thickness also results in an increase in equivalent Young's modulus. It must however be noted that the bending stiffness, i.e. the product of effective equivalent Young's modulus and area moment of inertia, of a VIP does increase with increasing panel thickness due to the third power of thickness in the area moment of inertia.

Moreover, experimental flexion tests on both intact and vented VIPs showed that the equivalent effective Young's modulus considerably reduces when a VIP is damaged. For a panel under four-point bending with a thickness of 20 mm, a width of 120 mm, a span of 200 mm and a load-to-support distance of 40 mm, the Young's modulus, in which shear effects are considered, approximately reduces by 50% after venting. The exact reduction of this modulus depends on panel geometry (height and width of the core and thickness of the barrier) and - if shear effects are included - on context (type of loading). The reduction in Young's modulus is caused by the structural inactivity of the barrier envelope in the compression zone in case a VIP is vented. Protective measures therefore need to be in place to prevent a panel from collapsing if vented.

Overview of approximate influence of d_c and ratio l_p / S_p on properties of VIPs with practical sizes and under typical environmental conditions.

d_c (or d_p) x 2 →	ψ-value	x ½ (MF barrier, d_p>20 mm)	(eq. 3.17)
		> x ½ but < x 1 (AF barrier)	(eq. 3.15)
	U_{eff}	x ½ (MF barrier, d_p>20 mm)	(eq. 3.9/17)
		> x ½ but < x 1 (AF barrier)	(eq. 3.9/15)
	t_{sl}	x 2	(eq. 5.33)
	E_{eq}	x 2^3 (for thin panels: < x 2^3)	(eq. 6.2)
l_p / S_p x 2 →	ψ–value	unaffected	
	$\Delta U_{thermal\ bridge}$	x 2	(eq. 3.9)
	U_{eff}	U_{cop} + 2x $\Delta U_{thermal\ bridge}$	(eq. 3.9)
	t_{sl}	x 0.58 (MF3 barrier at 20°C)	(eq. 5.33)
		x 0.55 (AF:8 barrier at 20°C)	(eq. 5.33)
	E_{eq}	hardly affected	

10.1.2 Key question 3: Integration

In chapter 1 on methodology the main research question of this study was divided into three key research questions. The third of these key questions related to the domain of integration and was formulated as

> *How, taking into account their specific properties and behaviour, can vacuum insulation panels be integrated successfully into building components and constructions?*

In this dissertation a floor heating system, an EPS encapsulated VIP and prefabricated façade components were used to investigate the integration of VIPs into building constructions and to test the models and methods developed.

Concerning the models developed, they on the one hand complement existing data but more importantly they clearly explicate the relations between parameters influencing the performance of VIPs. Contrary to numerical tools, which are black boxes, such explicit relations facilitate design and engineering processes in a way that they show us in advance what will happen if a certain parameter is changed. Thus without needing to perform actual computations, designers and engineers are able to improve their engineered designs and create optimised products.

The case studies in this dissertation showed that the approximation model for calculating thermal bridge effects due to VIP barrier envelopes, the approximation model for calculating the service life of vacuum insulation panels with a core of fumed silica, and the model for estimating the Young's modulus of a VIP are sufficiently accurate and easy to handle as a result usable in a design process. The advanced model for calculating thermal edge effects occurring in building components, the advanced service life prediction model and the structural model for calculating the curvature and moment capacity of a vacuum insulation panel under flexural load, however, are too complex to be used in form of equations during the initial design phase of building components. If included in a spreadsheet or graphically displayed, however, they are very usable both in the design and in the engineering phase of building components and systems.

It is however important to note that the models for estimating thermal edge effects have difficulties coping with building components in which the spacer or other element at the component's edge continues to beyond the edge region. For such components it is difficult to define a thermal conductance of this edge. As a result, the façade components in chapter 8 had to be thermally simulated using numerical software tools and could not be simplified to be used in the analytical models. Moreover, since these models in general were not derived to include the junction and the connection between two components, like a post-and-beam system, many systems in practise still need to be simulated numerically.

It is also important to note that, if vacuum insulation panels are applied in most practical situations, the environmental conditions surrounding them fluctuate. As a consequence, service life influencing factors are needed to include these fluctuations into service life predictions. These service life influencing factors can best be included in the advanced service life prediction model. This advanced model, although complex, should therefore be used if more accurate results are required.

To protect vacuum insulation panels against incidental damage during transportation, storage and handling on site, they should preferably be integrated in prefabricated building components. If integrated into such components, a strong relation between structural behaviour and thermal performance may be present. Depending on the type of component, i.e. an edge spacer component or a sandwich component, the structural performance of the system is mainly determined by either the outer face sheet in combination with the spacer along the component's edge or the combined action of face sheets and VIP core. In the first case, a strong spacer is required to connect both face sheets and to transmit external loads towards a secondary load-bearing structure, very often leading to high thermal edge effects. In the second case, however, no structural edge is required, on the one hand resulting in the possibility of improving the overall thermal performance of the panel, but on the other hand imposing additional structural requirements on the VIP itself.

In the case of structural sandwiches, a good, strong and stiff bond between face sheets and VIP barrier laminate needs to be obtained. If a perfect bond can be established, panels consisting of a 40 mm thick core of vacuum insulation panel and two 1 or 2 mm thick high stiffness face sheets are able to withstand wind loads occurring in the Netherlands. However, such a high quality bond could not be established within the framework of this study because of two effects: too much shear in the adhesive layer between face sheet and the VIP's barrier envelope and sliding of this barrier laminate over the core material. It is important to realise that this latter effect is an inherent property of a vacuum insulation panel connected to a face sheet. Vacuum insulation panels should therefore only be applied in sandwich components subjected to flexion with the highest care. Notwithstanding these issues, VIP integrated sandwich components have the highest potential for creating thin high performance façade components.

Since the application of VIPs in sandwich components still involves solving several technical hurdles, since the risk of damage to the envelope is imminent in these components and since vacuum insulation panels glued onto face sheets cannot easily be separated after disposal, edge spacer components might, at least temporarily, be the preferred choice. Since however these components have a high risk of large heat losses through their perimeter, their edge needs to be thermally optimised. The principal designs of two such façade components presented in this dissertation showed that the potential of applying vacuum insulation panels in façades can be very high. With a thickness of the insulation layer of only 40 mm and a thickness of an entire component between 43 mm and 85 mm, a U_{eff}-value less than 0.15 $W \cdot m^{-2} \cdot K^{-1}$ can be achieved at initial conditions. Even after 25 years, U_{eff} of these panels can be less than 0.18 $W \cdot m^{-2} \cdot K^{-1}$.

Since vacuum insulation panels are very fragile and subjected to thermal conductivity ageing, the possibility of replacing them can improve their application potential. If VIPs are integrated into building components, like those designed in the framework of this dissertation, VIPs can be replaced by exchanging entire components, or if the components themselves are entirely demountable by solely exchanging VIPs. Defective VIP integrated façade components can be replaced by new components. The connection between a façade component and a secondary load-bearing system, though, must allow for such replacements. In case vacuum insulation panels are applied below a floor heating system or a floating screed, they can hardly be replaced if a sand-cement based or anhydrite screed is used or if a traditional tube-based floor heating system is used; destruction of this screed or de-coupling of the ducts then is needed. Vacuum insulation panels can only be easily replaced if a dry screed is used in combination with a modular floor heating system.

If for protection a vacuum insulation panel is incorporated in an EPS insulation board, a so-called EPS encapsulated VIP or an EPS covered VIP comes into existence. If such an EPS insulation board has a fixed thickness, a maximum in thermal performance may occur at a certain thickness of the VIP inside. This phenomenon was both observed in complex three-dimensional and in two-dimensional studies into EPS encapsulated VIPs with an envelope containing an aluminium layer thicker than 10 μm and having a core thermal conductivity of $4.0 \cdot 10^{-3}$ $W \cdot m^{-1} \cdot K^{-1}$. It is therefore not always best to increase the thickness of a vacuum insulation panel as much as possible. If however the total thickness of a component is not fixed but increases correspondingly with increasing thickness of the vacuum insulation panel inside, such a maximum in thermal performance does not occur. In these cases, an increased thickness of a vacuum insulation panel results in an increased thermal performance.

10.2 Final Conclusions

As we have seen in this dissertation, it is clear that vacuum insulation panels can be applied successfully in building constructions. It is however important that such integration is performed meticulously. Based upon this doctoral study, the following guidelines and considerations for applying vacuum insulation panels in building constructions can be derived in addition to remarks already made in the previous sections and to guidelines already specified by Binz et al. (2005).

Since VIPs might be invisibly damaged during integration in prefabricated components or during transport, storage or on-site installation, an increased thermal conductivity ageing might occur. As a result, the panel's thermal conductivity criterion might be reached decades before its service life was expected to be expired. As already known from previous research (Binz et al., 2005) – but too important to omit here - VIPs should be applied in building constructions in such a way that their quality can be checked on-site either via infrared thermography or RFID sensors and that broken panels can easily be replaced or repaired.

Moreover, since the effect of liquid water on the ageing behaviour of vacuum insulation panels is still unknown, long lasting surface condensation on top of their surface should be avoided. In case of non-airtight components, such condensation might be prevented by introducing a surface which is colder than the vacuum insulation panel and thus acts as a surface onto which condensation occurs first; or by facilitating the drainage of condensed water out of the component. In the VIP integrated component with metal encasing (E-panel) designed in chapter 8, for instance, both ways of reducing liquid water exposure are in place.

Large dimensional tolerances of vacuum insulation panels, especially in length and width, should be accounted for in a design that integrates these panels. This can be achieved by reserving sufficient space between vacuum insulation panels and surrounding materials and by subsequent filling of these spaces with a material that has low thermal conductivity and is compressible (and expandable). Using such materials assures that gaps are always closed and that convective heat flows from one side of the panel to the other are blocked. Such convective thermal shortcuts might otherwise render the high thermal quality of the VIP inadequate.

Prefabrication is preferred to on-site application. Since vacuum insulation panels are very fragile, integration into prefabricated components reduces the risk of damage during transport, storage, handling and installation. Moreover, conditioned environmental conditions in a factory may reduce the amount of water (vapour) captured inside a building component.

10.3 Recommendations for Subsequent Studies

All research projects into the application of vacuum insulation panels in buildings and building services - including this doctoral research - generated a large body of knowledge. Still, however, many aspects need to be investigated either more thoroughly or completely from scratch. The following studies can be recommended:

- Research into the effect of relative humidity (or the combined effect of *RH* and *T*) on the permeance of dry atmospheric gases and water vapour through VIP barriers. It is important that this research is performed on complete vacuum insulation panels of several sizes (and for several barrier laminates). The area-related and seal-related permeance can then be separated from each other enabling the completion of service life prediction models.

- Not only are the exact influence of relative humidity on the permeance of multi-layered laminates and their permeation mechanisms hardly understood, also the effect of an adhesive and the effect of structural bending on the service life of a vacuum insulation panel are unclear. These effects might be important for knowing the long-term behaviour of vacuum insulation panels in structural applications, like sandwich components.

- Since we have seen in this thesis that VIP integrated sandwich components are very promising candidates for obtaining very slim but at the same time high performance façade components, more studies need to be conducted into the adhesion of face sheets onto the barrier envelope of vacuum insulation panels. New glues and/or surface treatments, like UV/Ozone treatments, might help creating a good bond between both elements. Moreover, the long-term stability of such bonds and creep-effects need to be included in these studies as well to get more information on the reliability of such components.

- Besides, the VIP integrated façade components designed in the framework of this doctoral study should be prototyped and improved based upon knowledge obtained through these mock-ups. The actual building of a prototype very often brings to light the bottlenecks concerning the production, assembly and installation of the built components. These bottlenecks can then be technically improved before they are taken into manufacture.

- If vacuum insulation panels are applied structurally, as in case of VIP integrated sandwich components, the structural behaviour of intact and vented vacuum insulation panels should be known in advance. In this dissertation, preliminary studies into this behaviour have been conducted. More studies, especially into the observed effect of partial buckling of the top barrier envelope and into possible size-dependent properties of fumed silica are needed - like concrete, the strength of fumed silica might depend on the height of the tested specimen. Moreover, additional four-point flexion tests on VIP samples of several sizes might additionally test the failure model and E-model.

- Research into the improvement of envelopes. For application in buildings it is important that long service lives are guaranteed while at the same time high thermal performance is needed. Since aluminium foil based barrier laminates result in a high service life with the penalty of high thermal bridging and metallised film based laminates result in low thermal bridging with the penalty of relatively low service life, new (multi-layered) barrier laminates based upon low conducting materials with low permeability might be interesting especially for harsh, high temperature environments. Future developments into SiO_x deposited films or nano-technology might prove interesting.
- Moreover, since vacuum insulation panels are very expensive compared to conventional thermal insulators and since a large portion of these expenses go into the production of fumed silica, new high performance but cheap(er) core materials are needed for large-scale adoption of vacuum insulation panels by the building industry. These materials however need to be of similar quality as fumed silica.
- Besides, cost models for estimating life cycle costs of vacuum insulation panels are needed. These models should include investment, installation, maintenance and demolition costs and revenues either resulting from reduced energy costs or from increased rental income. Such models may help making a more honest comparison of vacuum insulation panels to conventional thermal insulators in feasibility studies.
- Finally, more thermal and hygrothermal studies from a practical perspective into the use of vacuum insulation panels in common constructions and their details are needed. These studies should also address the influence of design and construction errors on overall performance.
- Last but not least, more studies involving long-term monitoring of vacuum insulation panels in actual applications might increase our knowledge on the long-term behaviour of vacuum insulation panels regarding their thermal performance, service life and if applicable their structural behaviour.

OUTLOOK

PAST, PRESENT AND FUTURE

O

OUTLOOK

As an advocate of light-weight structures and 4D design[1], Richard Buckminster Fuller, born in Massachusetts in 1895, developed several technology-based solutions for solving the problems of his time. In 1929, for instance, he presented his well-know Dymaxion House, a single-family house constructed from lightweight materials in which the rooms are radially organised in a hexagonal plan and suspended from a central mast. This house was conceived as a temporary, movable space not fixed to a specific location. Other designs he made and constructed were the Dymaxion Car (1933), emergency shelters, the Dymaxion Map of the World (1946) and the Wichita House.

At the end of the 1940s, geodesic domes had caught the attention of Buckminster Fuller. Such domes were able to create the largest spans without intermediate supporting systems. In 1950 his first full-sized geodesic dome was constructed in Montreal. In the years to follow, he developed and constructed many more domes around the world and perfected their detailing as a result speeding-up the construction process. This development culminated in 1960 in the proposal of a double layer tensegrity dome with a 2 mile diameter over midtown Manhattan. According to his personal calculations, this dome would pay-off within 10 years solely by saving on snow removal costs. Moreover, among others due to a reduced surface area exposed to the elements, a reduction of more than 90% in energy use for heating and cooling can be achieved, Buckminster Fuller stated (Buckminster Fuller, 1968). Although it is questionable whether such reductions really are achievable, the idea seems interesting. Continuing this line of thought one could image that the glazed panels used to for this dome are made of evacuated glazing as a result improving the thermal resistance of this shell.

Figure 0.1

Artist impression of Richard Buckminster Fuller's dome over midtown Manhattan, New York. (Buckminster Fuller, 1968)

[1] 4D design not only includes the three dimensions of space but also the time component.

Entirely at the other end of the spectrum is the idea of providing comfort to an individual in a highly localised small space. If taken to the extreme such local comfort could be provided by creating a very small conditioned cocoon or halo around a person. As audio spotlight technology[2] does for sound, this comfort halo would create a micro-environment around a person tailored to personal needs and desires. As a result, only this small conditioned bubble needs to be environmentally controlled. For harsh and very extreme environments such cocoons in fact already exist in the form of spacesuits and biosuits, like the spacesuit designed by MIT professor of aeronautics, astronautics and engineering systems Dava J. Newman presented in Figure O.2 (Trafton, 2007). One might however argue that such biosuits are only practical and sensible for extreme conditions as outer space and on other planets. In our own well-tempered environments on Earth, we would rather do without pressurized helmets; those would highly limit social interaction.

Both aforementioned ideas currently seem to be far-fetched and maybe even undesirable. Moreover, among others due to the conservative nature of the building industry, it is still more practical to consider energy performance on the level of buildings (and on the level of urban neighborhoods for energy delivery systems).

Figure O.2

Spacesuit designed by a team of MIT specialists led by prof. Dava J. Newman. (image by Donna Coveney - web.mit.edu/newsoffice/2007/biosuit-0716.html)

[2] Audio spotlight technology is a technology which provides sound in a highly localised position by creating "a very narrow beam of sound from a small acoustic source, by generating only ultrasound" (Holosonic Research Labs, 2009; Pompei, 1999).

From a perspective of high thermal performance, a skin around a building completely evacuated might seem and interesting solution; as with a thermos bottle no thermal bridges would exist except where doors penetrate this barrier. With such a building enclosure an extremely tight heat barrier can be created[3].

However, since on most places on Earth the external climate exhibits seasonal and diurnal fluctuations, it might be more important to focus our future research efforts on materials or constructions with variable thermal (and hygrothermal) properties in stead of on further reducing the thermal conductivity of materials or constructions to extremely low values. With such dynamic materials[4], the thermal resistance of the building skin can be high in winter to trap heat inside but low in summer to get rid of excess heat. Baetens (2009) and Jelle et al. (2009) theoretically presents some possibilities of how materials with either improved thermal properties or variable properties might be conceived. Using such materials and constructions might be more beneficial to reducing primary energy consumption of buildings than using high performance materials with constant properties.

Besides having variable properties, new materials or constructions should be robust as well. One of the main problems currently with film-based vacuum insulation panels is their fragility. The thermal conductivity of its core of fumed silica increases from approximately $4.0 \cdot 10^{-3}$ $W \cdot m^{-1} \cdot K^{-1}$ to $20 \cdot 10^{-3}$ $W \cdot m^{-1} \cdot K^{-1}$ when a VIP gets vented. As a consequence, their thermal performance deteriorates with a factor 5, not considering thermal bridge effects. It is thus imperative that new materials combine the good thermal properties of vacuum insulation panels with robustness. If for instance nanotechnology is able to develop rigid, open-celled, low-density, porous insulation materials with very fine pores (smaller than about 10 nm in diameter), evacuation is no longer required for obtaining high thermal performance at ambient pressure (Baetens, 2009; Jelle et al., 2009). Such materials then are robust, can be processed on site and are not plagued by inherent thermal bridges since no barrier is needed. Hence, these improved thermal insulation materials are handled and applied in a similar way as conventional thermal insulation materials. Due to the conservative nature of the building industry, this fact alone makes large-scale adoption of these materials more easily than the adoption of fragile evacuated insulations.

---

[3] It is important that such a barrier is fool proof and robust. Leaks in this barrier, which would immediately render the construction useless, need to be prevented at all cost, or measures to monitor the performance combined with methods to repair broken barriers must be developed.

[4] These dynamic materials should not be confused with a concept known as dynamic insulation, or dynamic wall heat recovery. This concept consists of an open-porous, insulated wall through which external (ventilation) air is led driven by a pressure potential over this wall. In case of a counter flow system, the wall exchanges heat with this ventilation air as a result reducing the apparent thermal transmittance of the wall.

Moreover, future high performance thermal insulation materials should be relatively cheap as well. Since most practitioners in the buildings industry and their clients still primarily use investment cost as the main financial criterion, expensive vacuum insulation panels will not easily proliferate through the building sector. Currently, a square meter of vacuum insulation panel still costs over 100 Euros while a square meter of mineral fibre insulation board costs a fraction of this value. Vacuum insulation panels are just too expensive to be easily accepted by the building industry. As a result, future investigations should also consider this cost aspect; new core materials which are cheap and have a fine pore structure are therefore needed (Mukhopadyaya et al., 2008; 2009).

However, a strategy for reducing greenhouse gas emissions and for improving sustainability solely based on technology-driven solutions may however not be easily adopted by the building industry unless enforced by law and international treaties since the building industry is conservative, practitioners in the building sector have many conflicting interests, and many people do not see the urge for immediate measures regarding sustainability and energy reduction. Such more stringent laws and building codes will irrevocably stimulate the wide-spread adoption of vacuum insulation panels by practitioners in the building industry and steer research efforts into the development of more robust, high thermal performance insulation materials and variable performance insulation materials. As a result of these developments, the implementation of sustainable energy sources in the built environment is facilitated creating a more healthy and sustainable environment for people to live and work in.

REFERENCES

R

R1 BIBLIOGRAPHY

Abley, I. (2007), "Immediate prospects for vacuum insulation in the British site built housing sector", presented at *the 8th International Vacuum Insulation Symposium*, ZAE-Bayern/UniWue, Würzburg, September 18-19, 2007.

Achtziger, J. (1960), "Wärmeleitfähigkeitsmessungen an Isolierstoffen mit dem Plattengerät bei tiefen Temperaturen", *Kältetechnik* 12 (12): 372-375.

Ahmad, M., A. Bontemps, H. Sallée and D. Quenard (2006), "Thermal testing and numerical simulation of a prototype cell using light wallboards coupling vacuum insulation panels and phase change material", *Energy and Buildings* 38 (6): 673-681.

Akker, H.E.A. van den and R.F. Mudde (1998), *Fysische Transportverschijnselen I*, Delft University Press, second edition, Delft, 282 pages, ISBN: 90 407 1204 2.

Arnold, B. (2007), "Anwendungen von VIP im Bauwesen – Umfangreiche Erfahrungen aus Anwendungen in der Schweiz", In: Heinemann, U. (ed.), *Proceedings of the third professional conference VIP-BAU*, ZAE-Bayern / Universität Würzburg, Würzburg, September 20, 2007, pp. 75-90.

Araki, K, D. Kamoto and S. Matsuoka (2009), "Optimization about Multilayer Laminated Film and Getter Device Materials of Vacuum Insulation Panel for Using at High Temperature", *Journal of Materials Processing Technology* 209(1): 271-282.

Arrhenius, S.A. (1889), "Über die Reaktionsgeschwindigkeit bei der Inversion von Rohzucker durch Säuren", *Zeitschrift für Physikalische Chemie* 4: 226-248

Ashby, M.F. (2005), *Materials Selection in Mechanical Design*, third edition, Elsevier Butterworth-Heinemann, Oxford, 603 pages, ISBN: 0 7506 6168 2.

Aspen Aerogels Inc. (2007), *Ultra thin Spaceloft insulation*, brochure, Aspen Aerogels Inc., Northborough.

ASTM C 297 (1992), "Standard Test Method for Tensile Strength of Flat Sandwich Constructions in Flatwise Plane", In: Annual Book of Standards vol. 15.03, American Society for Testing and Materials International.

ASTM C 393 (1992), "Standard Test Method for Flexural Properties of Flat Sandwich Constructions", In: Annual Book of Standards vol. 15.03, American Society for Testing and Materials International.

ASTM C 1484 (2001), "Standard Specification for Vacuum Insulation Panels", American Society for Testing and Materials International.

ASTM E 345 (1993), "Standard Test Methods of Tension Testing of Metallic Foil", American Society for Testing and Materials International.

Aysen, A. (2002), *Soil Mechanics: Basic Concepts and Engineering Applications*, Balkema, Lisse, 459 pages.

Ball, R.D., I.G. Simpson and S. Pang (2001), "Measurement, modeling and prediction of equilibrium moisture content in Pinus radiata heartwood and sapwood", *Holz als Roh- und Werkstoff* 59 (6): 457-462.

Baetens, R. (2009), *Properties, Requirements and Possibilities for Highly Thermal Insulating Materials and Solutions in Buildings – State-of-the-Art and Beyond*, MSc-thesis, Faculty of Architecture, Catholic University of Leuven, Leuven, 177 pages.

Beck, A., M. Binder and O. Frank (2009), "Dynamic simulation of VIP moisture and heat transport", In: R. Ogden and M. Overend (eds.), Proceedings of the *9th International Vacuum Insulation Symposium*, High thermal performance and more space from thin insulations, Oxford Brookes University / University of Cambridge, London, September 17-18, 2009, p. 1-9.

Beck, A. and O. Frank (2005), "Auswirkungen von Wärmebrücken beim Einsatz hocheffizienter Vakuumisolationspaneelen am Bau", In: G.-W. Mainka, U. Heinemann, M. Wollensak & K. Riesner (eds.), *Proceedings of the second professional conference VakuumIsolationsPaneele – Evakuierte Dämmungen im Bauwesen – Erfahrungen aus der Praxis*, ZAE-Bayern / Projektträger Jülich / Universität Rostock / Hochschule Wismar, Wismar, June 16-17, 2005, pp. U1-U10.

Beck, A., O. Frank and M. Binder (2007a), "Wärmebrücken – die planerische Herausforderung beim Einsatz von Vakuum-Wärmedämmelementen", In: Heinemann, U. (ed.), *Proceedings of the third professional conference VIP-BAU*, ZAE-Bayern / Universität Würzburg, Würzburg, September 20, 2007, pp. 61-74.

Beck, A., O. Frank and M. Binder (2007b), "Influence of water content on the thermal conductivity of vacuum insulation panels with fumed silica kernels", In: A. Beck et al. (eds.), *Proceedings of the 8th International Vacuum Insulation Symposium*, ZAE-Bayern/UniWue, Würzburg, September 18-19, 2007, pp. 1-9.

Bendergast, P. and B. Malone (1999), "Characterization and Commercialization of INSTILL Vacuum Insulation Core", *Vuoto scienza et tecnologia* 28 (1-2): 77-82.

Bindel, D. (2005), "Erfahrungen aus der handwerklichen Verarbeitung von VIP in der Sanierung", In: G.-W. Mainka, U. Heinemann, M. Wollensak & K. Riesner (Eds.), *Proceedings of the second professional conference VakuumIsolationsPaneele – Evakuierte Dämmungen im Bauwesen – Erfahrungen aus der Praxis*, ZAE-Bayern / Projektträger Jülich / Universität Rostock / Hochschule Wismar, Wismar, June 16-17, 2005, pp. G1-G5.

Bindel, D. (2007), "VIP in der Sanierung, Chance auf Fördermittel – VIP im CO_2-Gebäudesanierungsprogramm der KFW", In: Heinemann, U. (ed.), *Proceedings of the third professional conference VIP-BAU*, ZAE-Bayern / Universität Würzburg, Würzburg, September 20, 2007, pp. 117-126.

Binz, A. (2003). "Europe's Energy Stars", *Home Energy* 2003 (Sept./Oct.): 28-29.

Binz, A., et al. (2002), "Vakuum-Dämmung im Baubereich", *proceedings of the 12th Swiss status-seminar Energie- und Umweltforschung im Bauwesen*, ETH Zürich, Zürich, September 12-13, 2002, pp. 113-122.

Binz, A. A. Moosmann, G. Steinke, U. Schonhardt, F. Fregnan, H. Simmler, S. Brunner, K. Ghazi, R. Bundi, U. Heinemann, H. Schwab, J.J.M. Cauberg, M.J. Tenpierik, G.A. Johannesson, T.I. Thorsell, M. Erb and B. Nussbaumer (2005), *Vacuum Insulation in the Building Sector. Systems and Applications. Subtask B,* IEA ECBCS Annex 39 HiPTI, 111 pages.

Binz, A and G. Steinke (2005), "Applications of Vacuum Insulation in the Building Sector", In: M. Zimmermann (ed.), *Proceedings of the 7th International Vacuum Insulation Symposium*, EMPA, Dübendorf, September 28-29, 2005, pp. 43-48.

Binz, A and G. Steinke (2006), "Vacuum Insulation Panels in the Building Sector", In: … (eds.), Proceedings of the *4th European Conference on Energy Performance and Indoor Climate in Buildings*, ENTPE, Lyon, November 20-22, 2006, p. 1-6.

Boermans, Th. And C. Petersdorff (2008), *U-values for better energy performance of buildings*, report for Eurima, Ecofys GmbH, Köln, [online], available: http://www.eurima.org/

Boyce, W.E. and R.C. DiPrima (1997), *Elementary Differential Equations and Boundary Value Problems*, John Wiley and Sons Inc, New York, 749 pages.

Brendeng, E (1978), "Predicting Conductance of LNG-Tank Insulation", Report of the DKV-meeting 5: 69-80.

BRL 2701 (2003), "Nationale beoordelingsrichtlijn voor het KOMO Attest(-met-productcertificaat) voor metalen gevelelementen", SKG – Stichting Kwaliteit Gevelbouw.

BRL 4103-1 (preliminary) (2000), "Nationale beoordelingsrichtlijn voor het KOMO Attest(-met-productcertificaat) voor sandwichpanelen - deel 1: algemene eisen", BDA-INTRON / SKG – Stichting Kwaliteit Gevelbouw.

Brodt, K.H. (1995), *Thermal Insulations: Cfc-Alternatives and Vacuum Insulation*, PhD-thesis, Delft University of Technology, Delft, 173 pages.

Brodt, K.H. and G.C.J. Bart (1994), "Performance of sealed evacuated panels as thermal insulation", *International Journal of Refrigeration* 17 (4): 257-262.

Brunner, S. (2004), "Aging at accelerating conditions", Presentation given at the IEA Annex 39 meeting in Ottawa, April 29, 2004.

Brunner, S., Ph. Gasser, H. Simmler and K. Ghazi Wakili (2006), "Investigation of aluminium-coated polymer laminates by focused ion beam etching", *Surface and Coatings Technology* 200 (20-21): 5908-5914.

Brunner, S. and H. Simmler (2003), "Service Life Prediction for Vacuum Insulation Panels (VIP)", In: *Proceedings of International Conference on Solar Energy Use in Buildings (CISBAT)*, EPFL, Lausanne, October 8, 2003, pp. 1-6.

Brunner S. and H. Simmler (2005a), "Aging and Service Life of VIP in Buildings", In: M. Zimmermann (ed.), *Proceedings of the 7th International Vacuum Insulation Symposium*, EMPA, Dübendorf, September 28-29, 2005, pp. 15-22.

Brunner S. and H. Simmler (2005b), "Monitoring of VIP in Building Applications", In: M. Zimmermann (ed.), *Proceedings of the 7th International Vacuum Insulation Symposium*, EMPA, Dübendorf, September 28-29, 2005, pp. 35-42.

Brunner, S. and H. Simmler (2007), "In situ Performance Assessment and Service Life of Vacuum Insulation Panels (VIP) in Buildings", In: A. Beck et al. (eds.), *Proceedings of the 8th International Vacuum Insulation Symposium*, ZAE-Bayern/UniWue, Würzburg, September 18-19, 2007, pp. 1-8.

Brunner, S. and H. Simmler (2008), "In situ performance assessment of vacuum insulation panels in a flat roof construction", *Vacuum* 82 (7): 700-707.

Brunner, S., P.J. Tharian, H. Simmler, K. Ghazi Wakili (2008), "Focused ion beam (FIB) etching to investigate aluminium-coated polymer laminates subjected to heat and moisture loads", *Surface and Coatings Technology* 202 (24): 6054-6063.

Buckminster Fuller, R. (1968), "Why Not Roofs over our Cities?", *Think* 1968 (1-2): 8-11.

Buitink Technology (2009), Buitink Technology – Advanced Lightweight Structures, Duiven, accessed January 26, 2009, <http://www.buitinkzeilmakerij.nl/>.

Bundi, R. (2003), "Vakuumisolierte Paneele. Forschung und Entwicklung im Fassadenbau", *Fassade* 2003 (3): 19-22.

Bundi, R., Th. Nussbaumer, Ch. Tanner and H. Mühlebach (2005), "Meβtechnische und rechnerische Untersuchungen an einer mit Vakuum-Isolations-Paneele gedämmten Holztür", *Bauphysik* 27 (1): 21-27.

Burch D., J.W. Martin and M.R. van Landingham (2002), "Computer Analysis of a Polymer Coating Exposed to Field Weather

Conditions", *Journal of Coatings Technology* 74 (924): 75-86.

Burger, T. and J. Fricke (1998), "Aerogels: Production, Modification and Applications", *Ber. Bunsenges. Phys. Chem*. 102 (11): 1–6.

Büttner, D., C. Stark, M. Keller & J. Fricke (2005), "Fast Method to Check the Thermal Performance of Metal-Covered VIP", In: M. Zimmermann (ed.), Proceedings of the 7th *International Vacuum Insulation Symposium*, EMPA, Dübendorf, September 28-29, 2005, p. 67-76.

Büttner, D., C. Stark, D. Kraus and M.H. Keller (2005), "Messverfahren zur Qualitätskontrolle bei Vakuumisolationspaneelen", In: G.-W. Mainka, U. Heinemann, M. Wollensak and K. Riesner (eds.), Proceedings of the second professional conference *VakuumIsolationsPaneele – Evakuierte Dämmungen im Bauwesen – Erfahrungen aus der Praxis*, ZAE-Bayern / Projektträger Jülich / Universität Rostock / Hochschule Wismar, Wismar, June 16-17, 2005, pp. Y1-Y9.

Cabot Corporation (2003), *What is a NagogelR Aerogel?*, Brochure, Cabot Corporation, Billerica.

Callister, W.D. Jr. (2000), *Materials Science and Engineering. An Introduction*, John Wiley and Sons Inc, New York, 871 pages.

Caps, R. (2003), "Maβnahmen zur Qualitätssicherung von Vakuumdämmplatten", In: Proceedings of the first professional conference *VakuumIsolationsPaneele – Evakuierte Dämmungen im Bauwesen*, ZAE-Bayern / Projektträger Jülich / Universität Rostock / Hochschule Wismar, Rostock-Warnemünde July 10–11, 2003, pp. R1-R11.

Caps, R. (2005a), "Monitoring Gas Pressure in Vacuum Insulation Panels", In: M. Zimmermann (ed.), *Proceedings of the 7th International Vacuum Insulation Symposium*, EMPA, Dübendorf, September 28-29, 2005, pp. 57-66.

Caps, R. (2005b), "Kann der langfristige Anstieg der Wärmeleitfähigkeit in VIPs wesentlich verringert werden?", In: G.-W. Mainka, U. Heinemann, M. Wollensak & K. Riesner (Eds.), *Proceedings of the second professional conference VakuumIsolationsPaneele – Evakuierte Dämmungen im Bauwesen – Erfahrungen aus der Praxis*, ZAE-Bayern / Projektträger Jülich / Universität Rostock / Hochschule Wismar, Wismar, June 16-17, 2005, pp. C1-C8.

Caps, R. (2006), "Vacuum Insulation Panels for Buildings and Technical Applications", In: … (eds.), Proceedings of the *4th European Conference on Energy Performance and Indoor Climate in Buildings*, ENTPE/INIVE EENG/IEA ECBCS, Lyon, November 20-22, 2006, p. 1-6.

Caps, R., H. Beyrichen, D. Kraus and S. Weismann (2008), "Quality control of vacuum insulation panels: Methods of measuring gas pressure", *Vacuum* 82 (7): 691-699.

Caps, R. and J. Fricke (2000), "Thermal Conductivity of Opacified Powder Filler Materials for Vacuum Insulations", *International Journal of Thermophysics* 21 (2): 445-452.

Caps, R., U. Heinemann, M. Ehrmanntraut and J. Fricke (1999), "Evacuated Insulation Panels Filled with Pyrogenic Silica Powders: Properties and Applications", In: *Proceedings of the 15th European Conference on Thermophysical Properties*, ZAE-Bayern, Würzburg, September 5-9, 1999, pp. 815-820.

Caps, R., U. Heinemann, M. Ehrmanntraut and J. Fricke (2001), "Evacuated Insulation Panels Filled with Pyrogenic Silica Powders: Properties and Applications", *High Temperatures - High Pressures* 33 (2): 151-156.

Caps R., J. Hetfleisch, Th. Rettelbach and J. Fricke (1995), "Thermal Conductivity of Spun Glass Fibers as Filler Material for

Vacuum Insulations", In: K.E. Wilkes, R.B. Dinwiddie and R.S. Graves (eds.), *Thermal Conductivity 23 - Proceedings of the 23rd International Thermal Conductivity Conference,* Nashville, October 29 – November 1, 1995, Technomic Publishing Company Inc., Lancaster, pp. 373-382.

Carmi, Y. (2007), "Ultra High Barrier VIP Laminates – New Solutions for Tougher Requirements", presented at *the 8th International Vacuum Insulation Symposium*, ZAE-Bayern/UniWue, Würzburg, September 18-19, 2007.

Carslaw, H.S. and J. Jaeger (1959), *Conduction of Heat in Solids*, Clarendon Press, Oxford, 510 pages, ISBN: 0-19-853303-9.

Cauberg, J.J.M. (2000), *lecture notes CT4220 Bouwfysica 2*, Publication bureau Civil Engineering, TUDelft, Delft.

Cauberg, J.J.M. (2002), "Vacuümisolatiepanelen - mogelijkheden voor de bouw" *Bouwfysica,* 12 (1): 4-8.

Cauberg, J.J.M., A.C. van der Linden and E.H. van den Ham (2001), *lecture notes CT3220 Bouwfysica 1*, Publication bureau Civil Engineering, TUDelft, Delft.

Cauberg, J.J.M., M.J. Tenpierik, H.F.E. Beyrichen, R.H.J. Looman, J. van Malsen and W.H. van der Spoel (2006), *Thermo-mechanical Properties of Metallised Barrier Films*, Final report for EU/Craft VACI - WP10: Assessment of Sealing, TU Delft, Delft (projectnr.: COOP-CT-2003-508026), pp. 1-94.

Cauberg, J.J.M., M.J. Tenpierik, H.F.E. Beyrichen, R.H.J. Looman, J. van Malsen and W.H. van der Spoel (2006), *Operational Heat Transfer and Ageing Process of Vacuum Insulated Panels at Cryogenic and Low Temperatures*, Final report for EU/Craft VACI - WP20: Operational Heat Transfer and Ageing Process , TU Delft, Delft (projectnr.: COOP-CT-2003-508026), pp. 1-63.

du Cauzé de Nazelle, G.R.M. (1995), *Thermal Conductivity Ageing of Rigid Closed Cell Polyurethane Foams.,* PhD-thesis, Faculty of Applied Physics, TUDelft, Delft, 327 pages, ISBN: 90-9007962-9.

Cheetham, A.K., G. Férey and Th. Loiseau (1999), "Open-Framework Inorganic Materials", *Angewandte Chemie Int. Ed.* 38 (22): 3268-3292.

Clina Heiz- und Kühlelemente GmbH (2007), *Capillary Tube Systems – The ideal radiant heating and cooling system for solar power systems and heat pumps: flat, fast, comfortable, efficient, environmentally friendly, and long lasting*, Brochure, Clina Heiz- und Kühlelemente GmbH, Berlin.

Clinton, J. (2002), "Thermal resistance and polyiso insulation", *Professional Roofing* magazine, February 2002, [online], available at: http://www.professionalroofing.net/archives/past/feb02/polyisofeature.asp [October 12, 2009].

Collins, R.E. and T.M. Simko (1998), "Current Status of the Science and Technology of Vacuum Glazing", *Solar Energy* 62 (3): 189-213.

Coquard, R and D. Quenard (2007), "Modeling of Heat Transfer in Nanoporous Silica - Influence of Moisture", In: A. Beck et al. (eds.), *Proceedings of the 8th International Vacuum Insulation Symposium*, ZAE-Bayern/UniWue, Würzburg, September 18-19, 2007, pp. 1-13.

Cunnington, G. R. Jr. and C.L. Tien (1978), "Heat Transfer in the Presence of a Gas", *Thermal Conductivity* 15: 325-333.

Cremers, J. (2005a), "Typology of Applications for Opaque and Translucent VIP in the Building Envelope and their Potential for Temporary Thermal Insulation", In: M. Zimmermann (ed.), *Proceedings of the 7th International Vacuum Insulation Symposium*, EMPA, Dübendorf, September 28-29, 2005, pp. 189-196.

Cremers, J. (2005b), ”Systematisierung architektonischer Anwendungsmöglichkeiten von Vakuum-Dämmsystemen im Bereich der Gebäudehülle”, In: G.-W. Mainka, U. Heinemann, M. Wollensak & K. Riesner (Eds.), *Proceedings of the second professional conference VakuumIsolationsPaneele – Evakuierte Dämmungen im Bauwesen – Erfahrungen aus der Praxis*, ZAE-Bayern / Projektträger Jülich / Universität Rostock / Hochschule Wismar, Wismar, June 16-17, 2005, pp. P1-P11.

Cremers, J. (2006a), “Schlank und hochgedämmt – Vakuum-Dämmsystem in nichttragenden Aussenwandsystemen”, *Fassade 2006* (2): 19-23.

Cremers, J. (2006b), “Vakuum-Dämmsysteme – Einsatzmöglichkeiten in Fassadenelementen“, *Deutsches Architektenblatt* 2006 (11): 65 – 68.

Cremers, J. (2006c), *Einsatzmöglichkeiten von Vakuum-Dämmsystemen im Bereich der Gebäudehülle*, Ph.D.-thesis, Technische Universität München, München, 248 pages.

Damani, M., U. Vogt and Th. Graule (2001), “Preliminary Study on High Performance Thermal Insulation Materials with Gastight Porosity”, In: *Proceedings of the IEA International Conference and Workshop High Performance Thermal Insulations (HiPTI) – Vacuum Insulated Products (VIP),* EMPA, Dübendorf, January 22-24, 2001, pp. 95-98.

Davies, J.M. (2001), *Lightweight Sandwich Construction*, Blackwell Science Ltd, Oxford/London/Edinburgh/Malden/Carlton /Delavigne, 370 pages.

Davis, M.E. (2002), “Ordered porous materials for emerging applications”, *Nature* 417 (6891): 813-821.

Degen K.G., S. Rossetto, R. Caps, J. Fricke (1994), “Evacuated Multilayer Foil Insulations – Minimization of Heat Transfer”, In T.W. Tong (ed.), *Thermal Conductivity 22 - Proceedings of the 22nd International Thermal Conductivity Conference,* Arizona, November 1 – November7, 1993, Technomic Publishing Company Inc., Lancaster, pp. 401-412.

Delichatsios, M., B. Paroz and A. Bhargava (2003), “Flammability properties for charring materials”, *Fire Safety Journal* 38 (3): 219-228.

Despond, S., E. Espuche and A. Domard (2001), “Water Sorption and Permeation in Chitosan Films: Relation Between Gas Permeability and Relative Humidity”, *Journal of Polymer Science Part B – Polymer Physics* 39 (24): 3114-3127.

DIBt Z-23.11.1658 (2007), “Vakuum-Wärmedämmplatten aus Kieselsäure "va-Q-vip"”, algemeine bauaufzichtliche Zulassung (abZ), Deutsches Institut für Bautechnik.

DIBt Z-23.11.1662 (2007), “Vakuum-Wärmedämmplatten aus Kieselsäure "Vacupor NT-B2"”, algemeine bauaufzichtliche Zulassung (abZ), Deutsches Institut für Bautechnik.

Diefenbach, N. And M. Groβklos (2007), ”Development of Prefabricated Floor-to-Ceiling Insulation Elements with Integrated VIPs”, presented at *the 8th International Vacuum Insulation Symposium*, ZAE-Bayern/UniWue, Würzburg, September 18-19, 2007.

Disch, R. (2007), “VIP als Element der Plusenergie-Bauweise – Das Beispiel des Sonnenschiffs in Freiburg“, In: Heinemann, U. (ed.), *Proceedings of the third professional conference VIP-BAU*, ZAE-Bayern / Universität Würzburg, Würzburg, September 20, 2007, pp. 127-136.

Dow Chemical (2004), “Optimizing vacuum insulation performance using INSTILL Vacuum Insulation Core - A design guide for fabricators and OEMs*”*, Dow Chemical Company, [online], available: http://www.dow.com/, [March 1, 2004].

Dow Chemical (2004), “Physical and Performance Properties. INSTILL HT.

Vacuum Insulation Core”, Dow Chemical Company, [online], available: http://www.dow.com/, [March 1, 2004].

Dreyer, J. and A. Korjenic (2005), “Investigation of the Hygrical-Thermal Suitability of Vacuum Insulation Boards for Refurbishment of Viennese “Gründerzeit”-Buildings”, In: M. Zimmermann (ed.), *Proceedings of the 7th International Vacuum Insulation Symposium*, EMPA, Dübendorf, September 28-29, 2005, pp. 139-144.

Drolenga, J.C. and E.M.M. Willems (2005), *Zwevende dekvloeren in de woningbouw*, Stichting BouwResearch, Rotterdam, 48 pages.

Duijvestein, C.A.J. (1989), “An ecological approach to building”, In: W. Riedijk, J. Boes, W. Ravesteijn (eds.), *Appropriate technology in industrialized countries*, Delft University Press, Delft, 372 pages.

DuPont Teijin Films (2004), “Mylar Polyester Film. Introduction to Mylar Polyester Films”, Product information, [online], available: http://www.tijin.co.jp/, [March 5, 2004].

DuPont Teijin Films (2004), “Mylar 200 SBL 300”, Product information, [online], available: http://www.tijin.co.jp/, [March 5, 2004].

Earthtrends (2008), “Earthtrends Data Tables: Energy Consumption by Sector2005”, data table, [online], available: http://earthtrends.wri.org/pdf_library/data_tables/ene3_2005.pdf, [Octobre 20, 2008].

Eberhardt, H.-F. (2005), ”Vom Pulver zur Paneele – Wie entsteht ein VIP?”, In: G.-W. Mainka, U. Heinemann, M. Wollensak and K. Riesner (eds.), *Proceedings of the second professional conference VakuumIsolationsPaneele – Evakuierte Dämmungen im Bauwesen – Erfahrungen aus der Praxis*, ZAE-Bayern / Projektträger Jülich / Universität Rostock / Hochschule Wismar, Wismar, June 16-17, 2005, pp. B1-B9.

Eberhardt, H.-F. (2007), ”Vacuum Insulation Panels (VIP) in energy efficient cooling appliances for improving the environment of our children’s world”, In: A. Beck et al. (eds.), *Proceedings of the 8th International Vacuum Insulation Symposium*, ZAE-Bayern/UniWue, Würzburg, September 18-19, 2007, pp. 1-9.

Eberlein, J. (2007), “Wärmebrückenkompendium: VIP und „In Isothermen Veritas““, In: Heinemann, U. (ed.), *Proceedings of the third professional conference VIP-BAU*, ZAE-Bayern / Universität Würzburg, Würzburg, September 20, 2007, pp. 51-60.

Ebert, A. (2003), “VIP in der Anwendung mit beheizten Innenflächen.”, In: *Proceedings of the first professional conference VakuumIsolationsPaneele – Evakuierte Dämmungen im Bauwesen*, ZAE-Bayern / Projektträger Jülich / Universität Rostock / Hochschule Wismar, Rostock-Warnemünde July 10–11, 2003, pp. H1-H11.

Ebert, A. (2005), ”Heizen und Dämmen – moderne Technik zieht sich an”, In: G.-W. Mainka, U. Heinemann, M. Wollensak & K. Riesner (Eds.), *Proceedings of the second professional conference VakuumIsolationsPaneele – Evakuierte Dämmungen im Bauwesen – Erfahrungen aus der Praxis*, ZAE-Bayern / Projektträger Jülich / Universität Rostock / Hochschule Wismar, Wismar, June 16-17, 2005, pp. L1-L4.

Eekhout, A.C.J.M. (1997), *POPO. Proces organisatie voor productontwikkeling*, Delft University Press, Delft, 164 pages.

Eicher, H, M. Erb and A. Binz (2000), *Hochleistungswärmedämmung HLWD,* Final report, Dr. Eicher+Pauli AG and Institut für Energie Fachhochschule beider Basel, Basel, 36 pages.

Eicher, H. (2001), “The role of High Performance Insulation in energy efficiency”, M. Zimmermann (ed.), Proceedings of the International Conference and Workshop *High Performance Thermal Insulations*

(HiPTI) – Vacuum Insulated Products (VIP), January 22-24, 2001, EMPA, Dübendorf, pp. 9-12.

Elastogran GmbH - BASF (2005), *Thermal Conductivity Versus Pressure Inside Open Cell PU Foams*, fact sheet, Elastogran GmbH – BASF, Lemförde.

Erb, M. (2001), “VIP’s for Buildings – Research and Development”, In: M. Zimmermann (ed.), Proceedings of the International Conference and Workshop *High Performance Thermal Insulations (HiPTI) – Vacuum Insulated Products (VIP),* January 22-24, 2001, EMPA Dübendorf, pp. 71-80.

Erb, M. (2003), “IEA Annex 39 – High Performance Thermal Insulation”, In: Proceedings of the first professional conference *VakuumIsolationsPaneele – Evakuierte Dämmungen im Bauwesen*, ZAE-Bayern / Projektträger Jülich / Universität Rostock / Hochschule Wismar, Rostock-Warnemünde July 10–11, 2003, pp. L1-L10.

Erb, M (2005), “IEA/ECBCS – Annex 39 High Performance Thermal Insulation”, In: M. Zimmermann (ed.), *Proceedings of the 7th International Vacuum Insulation Symposium*, EMPA, Dübendorf, September 28-29, 2005, pp. 49-56.

Erb, M. and H. Simmler (2008), *Vakuumdämmung im Baubereich – Deklaration und Auslegung*, Report for the Bundesamt für Energie, date November 30, 2008, 12 pages.

Erbenich, G. (2003b), “Anwendungen von VIP im Bauwesen”, In: *Proceedings of the first professional conference VakuumIsolationsPaneele – Evakuierte Dämmungen im Bauwesen*, ZAE-Bayern / Projektträger Jülich / Universität Rostock / Hochschule Wismar, Rostock-Warnemünde July 10–11, 2003, pp. N1-N9.

Erbenich, G. (2009), “How to identify a high quality VIP – Methods and techniques to guarantee high quality in production and application, In: R. Ogden and M. Overend (eds.), Proceedings of the *9th International Vacuum Insulation Symposium*, High thermal performance and more space from thin insulations, Oxford Brookes University / University of Cambrigde, London, September 17-18, 2009, p. 1-10.

European Council (1988), *The Construction Products Directive*, Council Directive 89/106/EC, Strasbourg, December 21, 1988.

European Parliament and Council (2002), *Directive on the Energy Performance of Buildings*, Council Directive 2002/91/EC, December 16, 2002.

European Union (2006), *Action Plan for Energy Efficiency (2007-12)*, COM(2006) 545, [online], available: http://europa.eu/scadplus/leg/en/lvb/l27064.htm, [May 16, 2007].

European Union (2007), *Strategy on climate change: the way ahead for 2020 and beyond*, COM(2007) 2, [online], available: http://europa.eu/scadplus/leg/en/lvb/l28188.htm, [March 3, 2007].

Ewing, L. (2005), *History and Uses of Polyurethane Foam,* [online], available: http://members.aol.com/profchm/ewing.html, [September 15, 2005].

Faherty, K.F. and Th.G. Williamson (1999), *Wood Engineering and Construction Handbook*, 3rd edition, McGraw-Hill Inc., New York, 871 pages.

Fanney, A.H., Ch.A. Saunders and S.D. Hill (1994), “Test Procedures for Advanced Insulation Panels”, In: … (eds.), *Proceedings of the International CFC and Halon Alternatives Conference*, Washington DC , Octobre 24-26, 1995 , p. 149-161.

Fay, R. M. (1991), “Fiber Glass for Use in Evacuated Thermal Insulations”, *Journal of Thermal Insulation* 14 (1): 195 – 210.

Fine, H.A. (1989), “Advanced Evacuated Thermal Insulations: The State of the Art”, *Journal of Thermal Insulation* 12 (1): 183 – 208.

Fechner, O. (2007), “Die algemeine bauaufsichtliche Zulassung am Beispiel des VIP-Elementes“, In: Heinemann, U. (ed.), *Proceedings of the third professional conference VIP-BAU*, ZAE-Bayern / Universität Würzburg, Würzburg, September 20, 2007, pp. 101-116.

Feinst, W. (2001), “Existing and future applications for advanced low energy buildings, especially passive houses”, In: M. Zimmermann and H. Bertschinger (eds.), *Proceedings of the IEA International Conference and Workshop High Performance Thermal Insulations (HiPTI) – Vacuum Insulated Products (VIP),* January 22-24, 2001, EMPA Dübendorf, pp. 63-70.

Feldman, D. (2001), “Polymer Barrier Films”, *Journal of Polymers and the Environment* 9 (2): 49-55.

Feng, A., B.J. McCoy, Z.A. Munir and D.E. Cagliostro (1996), “Water Adsorption and Desorption Kinetics on Silica Insulation”, *Journal of Colloid and Interface Science* 180 (1): 276-284.

Ferle, A. (2005), ”Praxistaugliche Hochleistungswärmedämmsysteme in der Sanierung”, In: G.-W. Mainka, U. Heinemann, M. Wollensak & K. Riesner (Eds.), *Proceedings of the second professional conference VakuumIsolationsPaneele – Evakuierte Dämmungen im Bauwesen – Erfahrungen aus der Praxis*, ZAE-Bayern / Projektträger Jülich / Universität Rostock / Hochschule Wismar, Wismar, June 16-17, 2005, pp. I1-I4.

Fesmire, J.E. (2006), “Aerogel insulation systems for space launch applications”, *Cryogenics* 46 (2-3): 111-117.

Forstner, M. (2007), “VIP-basierte Problemlösungen in der Sanierung“, In: Heinemann, U. (ed.), *Proceedings of the third professional conference VIP-BAU*, ZAE-Bayern / Universität Würzburg, Würzburg, September 20, 2007, pp. 21-31.

Fricke, J. (2001), “Physical Aspects of Heat Transfer and the Development of Thermal Insulations”, In: Proceedings of the IEA International Conference and Workshop *High Performance Thermal Insulations (HiPTI) – Vacuum Insulated Products (VIP)*, EMPA, Dübendorf, January 22-24, 2001, pp. 13-21.

Fricke, J. (2005), “From Dewars to VIPs – One Century of Progress in Vacuum Insulation Technology”, In: M. Zimmerman (ed.), Proceedings of the *7th International Vacuum Insulation Symposium*, EMPA, Dübendorf, September 28-29, 2005, pp. 5-14.

Fricke, J., U. Heinemann and H.P. Ebert (2008), “Vacuum insulation panels – From research to market“, *Vacuum* 82 (7): 680-690.

Fricke, J., H. Schwab and U. Heinemann (2006), “Vacuum Insulation Panels – Exciting Thermal Properties and Most Challenging Applications”, *International Journal of Thermophysics* 27 (4): 1123–1139.

Friese, K.R. (2007), “Insulation System with Foil covered Vacuum-Elements for Operational Plants under Cryogenic Conditions”, presented at *the 8th International Vacuum Insulation Symposium*, ZAE-Bayern/UniWue, Würzburg, September 18-19, 2007.

Galbraith, G.H. and R.C. McLean (1990), “Interstitial Condensation and the Vapor Permeability of Building Materials,” *Energy and Buildings* 14 (3): 193-196.

Galbraith, G.H., R.C. McLean and J.S. Guo (1998), “Moisture permeability data presented as a mathematical relationship”, *Building Research and Information* 26 (3): 157-168.

Garnier, G., D. Quenard, B. Yrieix, M. Chauvois, L. Flandin and Y. Bréchet (2007), “Optimization, design, and durability of vacuum insulation panels”, In: A. Beck et al. (eds.), *Proceedings of the 8th International Vacuum Insulation Symposium*, ZAE-

Bayern/UniWue, Würzburg, September 18-19, 2007, pp. 1-8.

Geisler, M., J. Wachtel, F. Hemberger, T. Schultz, S. Vidi and H.-P. Ebert (2007), “Trilobal Polyimide Fibre Insulation for Cryogenic Applications”, In: A. Beck et al. (eds.), *Proceedings of the 8th International Vacuum Insulation Symposium*, ZAE-Bayern/UniWue, Würzburg, September 18-19, 2007, pp. 1-10.

Gellert, R. (2003), “Bauaufsichtliche Anforderungen an Dämmstoffe am Beispiel von Vakuumdämmplatten”, In: *Proceedings of the first professional conference VakuumIsolationsPaneele – Evakuierte Dämmungen im Bauwesen*, ZAE-Bayern / Projektträger Jülich / Universität Rostock / Hochschule Wismar, Rostock-Warnemünde Juli 10–11, 2003, pp. S1-S24.

Gellert, R., W. Albrecht & Ch. Sprengard (2005), ”Einflussfaktoren auf die bauphysikalischen Eigenschaften von VIPs: vom Labormesswert zum anwendungsbezogenen Bemessungswert”, In: G.-W. Mainka, U. Heinemann, M. Wollensak & K. Riesner (Eds.), *Proceedings of the second professional conference VakuumIsolationsPaneele – Evakuierte Dämmungen im Bauwesen – Erfahrungen aus der Praxis*, ZAE-Bayern / Projektträger Jülich / Universität Rostock / Hochschule Wismar, Wismar, June 16-17, 2005, pp. T1-T8.

Gere, J.M. and S.P. Timoshenko (1999), *Mechanics of Materials*, fourth SI Edition, Stanley Thornes Ltd., Cheltenham, 913 pages.

Ghazi Wakili, K. (2008), “The world energy crisis – Part 2: Some more vacuum-based solutions” [Editorial], *Vacuum* 82 (7): 679.

Ghazi Wakili, K., R. Bundi and B. Binder (2004), “Effective Thermal Conductivity of Vacuum Insulation panels”, *Building Research and Information* 32 (4): 293-299.

Ghazi Wakili, K., T. Nussbaumer and R. Bundi (2005), “Thermal Performance of VIP Assemblies in Building Constructions”, In: M. Zimmerman (ed.), *Proceedings of the 7th International Vacuum Insulation Symposium*, EMPA, Dübendorf, September 28-29, 2005, pp. 131-138.

Gilbo, C.F. (1985), “Thermal Conductivity Measurement using a Thin-Heater Apparatus”, *Journal of Building Physics* 9 (2): 92-101

Glicksman, L.R. (1991), “Two-Dimensional Heat Transfer Effects on Vacuum and Reflective Insulations”, *Journal of Thermal Insulation* 14 (4): 281 – 294.

Graf, A. (2003), *Neue Passivhäuser: 24 Beispiele für den Energiestandard der Zukunft Deutschland-Österreich-Schweiz*, Callwey, München, 127 pages.

Granta Design (2008), *CES Edupack 2008*, software tool for material’s selection.

Green, M.A. (1998), “Heat Transfer Through a Multilayer Insulation System as a Function of Pressure in the Cryostat Vacuum Space”, *Advances in Cryogenic Engineering*, vol. 43B, Plenum Press, New York, pp. 1313-1318.

Gregorio, P. di (2003), “VIP: formulas and rules for designers and final users”, In: *Proceedings of the Xth European Conference on Technological Innovations in Air Conditioning and Refrigeration Industry*, Politechnico di Milano, Milan, June 27-28, 2003, [online], Available:http://www.centrogalileo.it/noavoPA/Articoli%20tecnici/INGLESE%20CONVEGNO/SAES%20GETTERS%20inglese.doc [2006, August 1].

Griffith, B. and D. Arasteh (1995), “Advanced insulations for refrigerators/freezers: the potential for new shell designs incorporating polymer barrier construction”, *Energy and Buildings* 22 (3): 219-231.

Grobe, C. (2005), ”Einsatz von VIPs zur kostengünstigen Problemlösung”, In: G.-W. Mainka, U. Heinemann, M. Wollensak & K. Riesner (Eds.), *Proceedings of the second* *professional conference VakuumIsolationsPaneele – Evakuierte Dämmungen im Bauwesen – Erfahrungen aus der Praxis*, ZAE-Bayern / Projektträger Jülich / Universität Rostock / Hochschule Wismar, Wismar, June 16-17, 2005, pp. S1-S9.

Groβklos, M. (2005), ”Energetische Sanierung von Fassaden mit Groβformatigen, vorgefertigten Dämmelementen”, In: G.-W. Mainka, U. Heinemann, M. Wollensak & K. Riesner (Eds.), *Proceedings of the second professional conference VakuumIsolationsPaneele – Evakuierte Dämmungen im Bauwesen – Erfahrungen aus der Praxis*, ZAE-Bayern / Projektträger Jülich / Universität Rostock / Hochschule Wismar, Wismar, June 16-17, 2005, pp. J1-J7.

Grynning, S., R. Baetens, B.P. Jelle, A. Gustavsen, S. Uvsløkk and V. Meløysund (2009), *Vakuumsisolasjonspaneler for bruk I bygingner – Egenskaper, krav og muligheter*, project report nr. 31, Sintef Building and Infrastructure, Oslo.

Grynning, S., B.P. Jelle, S. Uvsløkk, R. Baetens, V. Meløysund and A. Gustavsen (2009), “Comparison of laboratory investigations and numerical simulations of vacuum insulation panels in various wall structure arrangements”, In: R. Ogden and M. Overend (eds.), Proceedings of the *9th International Vacuum Insulation Symposium*, High thermal performance and more space from thin insulations, Oxford Brookes University / University of Cambridge, London, September 17-18, 2009, p. 1-10.

Gudmundsson, K. (2009), “A parametric study of a metal sandwich VIP”, In: R. Ogden and M. Overend (eds.), Proceedings of the *9th International Vacuum Insulation Symposium*, High thermal performance and more space from thin insulations, Oxford Brookes University / University of Cambridge, London, September 17-18, 2009, p. 1-10.

Guevara-Arauza, J.C., E.M. Yahia, L. Cedeno and L.M.M. Tijskens (2006), ”Modeling the Effects of Temperature and Relative Humidity on Gas Exchange of Prickly Pear Cactus (Opuntia spp.) Stems”, *LWT Food Science and Technology* 39 (7): 796-805.

Güttler, K., H. Weinläder and H.-P. Ebert (2007), ”Influence of Spacer Systems on Heat Transfer in Evacuated Glazing”, In: A. Beck et al. (eds.), *Proceedings of the 8th International Vacuum Insulation Symposium*, ZAE-Bayern/UniWue, Würzburg, September 18-19, 2007, pp. 1-9.

Hagentoft, C.-E. (2001), *Introduction to Building Physics*, first edition, Studentlitteratur AB, Lund, 422 pages.

Hale, W.R., K.K. Dohrer, M.R. Tant and I.D. Sand (2001), “Diffusion model for water vapor transmission through microporous polyethylene/$CaCO_3$ films”, *Colloids and Surfaces A: Physicochemical and Engineering Aspects* 187-188: 483-491.

Hameetman, P. (2005), *Toolkit duurzame woningbouw – voor ontwikkelaars, gemeenten en ontwerpers*, Aeneas, Boxtel, 205 pages.

Hangleiter, M. (2005), ”Systematisiertes Bauen mit Vakuumgedämmten Betonfertigteilen”, In: G.-W. Mainka, U. Heinemann, M. Wollensak & K. Riesner (Eds.), *Proceedings of the second professional conference VakuumIsolationsPaneele – Evakuierte Dämmungen im Bauwesen – Erfahrungen aus der Praxis*, ZAE-Bayern / Projektträger Jülich / Universität Rostock / Hochschule Wismar, Wismar, June 16-17, 2005, pp. V1-V7.

Hangleiter, M. and S. Weismann (2006), "Systematisiertes Bauen mit vakuumgedämmten Betonfertigteilen“, *Bauphysik* 28 (3): 192-197.

Hanika, M. (2004), *Zur Permeation durch aluminiumbedampfte Polypropylen- und Polyethylenterephtalatfolien*, Dissertation, Technische Universität München.

Hanita Coatings (2004), “High Barrier Laminate for Vacuum Insulation Panels”, Hanita Coatings, [online], available: http://www.hanitacoatings.com, [January 8, 2004].

Hasselaar, B.L.H. (2004), *Vernieuwbare Isolatie als Duurzaam Alternatief. Een onderzoek naar de prestaties van vernieuwbare isolatiematerialen*, MSc-thesis, Faculty of Architecture, Delft University of Technology, Delft, 133 pages.

Heinemann, U. (2003), “Evakuierte Isolationen im Überblick”, In: *Proceedings of the first professional conference VakuumIsolationsPaneele – Evakuierte Dämmungen im Bauwesen*, ZAE-Bayern / Projektträger Jülich / Universität Rostock / Hochschule Wismar, Rostock-Warnemünde, Juli 10–11, 2003, pp. A1-A24.

Heinemann, U. (2005a), “Influence of Water on the Total Heat Transfer in ‘Evacuated’ Insulations”, In: M. Zimmerman (ed.), *Proceedings of the 7th International Vacuum Insulation Symposium*, EMPA, Dübendorf, September 28-29, 2005, pp. 23-34.

Heinemann, U. (2005b), ”Wesen, Potentiale und Besonderheiten von Vakuumisolationspaneelen”, In: G.-W. Mainka, U. Heinemann, M. Wollensak & K. Riesner (Eds.), *Proceedings of the second professional conference VakuumIsolationsPaneele – Evakuierte Dämmungen im Bauwesen – Erfahrungen aus der Praxis*, ZAE-Bayern / Projektträger Jülich / Universität Rostock / Hochschule Wismar, Wismar, June 16-17, 2005, pp. A1-A10.

Heinemann, U. (2007), “Vakuumisolationspaneele – Potentiale und Besonderheiten“, In: Heinemann, U. (ed.), *Proceedings of the third professional conference VIP-BAU*, ZAE-Bayern / Universität Würzburg, Würzburg, September 20, 2007, pp. 9-19.

Heinemann, U. (2008), “Influence of Water on the Total Heat Transfer in ‘Evacuated‘ Insulations“, *International Journal of Thermophysics* 29 (2): 735-749.

Heinemann, U., R. Caps, J. Fricke (1999), “Characterization and Optimization of Filler Materials for vacuum Super Insulations”, *Vuoto scienza et tecnologia* 28 (1-2): 43-46.

Hertz, H. (1882), “Über die Berürung fester elastischer Körper”, *Journal für die Reine und Angewandte Mathematik* 92: 156-171.

HEV Schweiz (2009), “Paritätische Lebensdauertabelle”, Hauseigentümerverband Schweiz, [online], available: http://www.hev-schweiz.ch/vermieten-verwalten/lebensdauertabelle/, [October 9, 2009].

Hinnells, M. (2008), “Technologies to achieve demand reduction and microgeneration in buildings”, *Energy Policy* 36 (12): 4427-4433.

van't Hoff, J. H. (1884), *Études de Dynamique Chimique*, F. Muller, Amsterdam, 215 pages.

Hofmann, A. (2006), “The thermal conductivity of cryogenic insulation materials and its temperature dependence”, *Cryogenics* 46 (11): 815-824.

Hokoi, S. and M.K. Kumaran (1993), “Experimental and Analytical Investigations of Simultaneous Heat and Moisture Transport through Glass Fiber Insulation”, *Journal of Thermal Insulation and Building Envelopes* 16 (3): 263-292.

Holosonic Research Labs, Inc. (2009), “Audio Spotlight”, [online], accessed June 5, 2009, < http://www.holosonics.com/>.

Hoogendoorn, P. (2001), “Development of vacuum insulation panel with stainless steel envelope”, In: M. Zimmermann (ed.), Proceedings of the International Conference and Workshop *High Performance Thermal Insulations (HiPTI) – Vacuum Insulated Products (VIP),* January 22-24, 2001, EMPA Dübendorf, pp. 107-113.

Holman, J.P. (1997), *Heat Transfer*, McGraw-Hill Inc., New York, eight edition, 696 pages.

Hostler, S.R., A.R. Abramson, M.D. Gawryla, S.A. Bandi and D.A. Schiraldi (2008), "Thermal conductivity of clay-based aerogel", *International Journal of Heeat and Mass Transfer* 52 (3-4): 665-669.

Hottel, H.C. and A.F. Sarofilm (1967), *Radiative Transfer*, McGraw-Hill, New York, 520 pages.

Hüsing, N and U. Schubert (1998), "Aerogels – Airy Materials: Chemistry, Structure, and Properties", *Angewandte Chemie Int. Ed.* 37 (1-2): 22-45.

IRC NRC (2004), "Canadian Building Digest. CBD-168. Rigid Thermosetting Plastic Foams", Institute for Research in Construction (IRC) National Research Council Canada (NRC), [online], available: http://irc.nrc-cnrc.gc.ca/, [October 16, 2004].

ISO 6946:2007 (2007), "Building components and building elements - Thermal resistance and thermal transmittance - Calculation method", International Standardization Organization.

ISO 10077-2:2003 (2003), "Thermal Performance of Windows, Doors and Shutters – Calculation of Thermal Transmittance – Part 2: Numerical Method for Frames", International Standardization Organization.

ISSO 49 (2002), *vloerverwarming / wandverwarming en vloer- en wandkoeling*, Instituut voor Studie en Stimulering van Onderzoek op het gebied van gebouwinstallaties.

Jacobsen, M.Z. (1999), *Fundamentals of Atmospheric Modelling*, Cambridge University Press, Cambridge, 828 pages.

Jacobsen, S. (2003), "Hochbarrierefolie für Vakuum-Isolationspaneele – eine Übersicht", In: *Proceedings of the first professional conference VakuumIsolationsPaneele – Evakuierte Dämmungen im Bauwesen*, ZAE-Bayern / Projektträger Jülich / Universität Rostock / Hochschule Wismar, Rostock-Warnemünde, July 10–11, 2003, pp. D1-D7.

Jelle, B.P., A. Gustavsen and R. Baetens (2009), "Beyond vacuum insulation panels – How may it be achieved", In: R. Ogden and M. Overend (eds.), Proceedings of the *9th International Vacuum Insulation Symposium*, High thermal performance and more space from thin insulations, Oxford Brookes University / University of Cambridge, London, September 17-18, 2009, p. 1-10.

Jensen, K.I. and J.M. Schultz (2007), "Transparent aerogel Windows – results from an EU FP5 project", In: A. Beck et al. (eds.), *Proceedings of the 8th International Vacuum Insulation Symposium*, ZAE-Bayern/UniWue, Würzburg, September 18-19, 2007, pp. 1-8.

Jong, T.M. de and D.J.M. van der Voordt (2002), *Ways to study and research: urban, technical and architectural design*, Delft University Press Science, Delft, 554 pages.

Jordi, M. (2006), "Development of a low energy house with vacuum insulation", In: … … (eds.), *Proceedings of the 4th European Conference on Energy Performance and Indoor Climate in Buildings*, ENTPE, Lyon, November 20-22, 2006, p. 1-6.

Kaczmarek, D. (2005a), "Barrier Films for Vacuum Insulation Panels (VIP)", In: M. Zimmermann (ed.), *Proceedings of the 7th International Vacuum Insulation Symposium*, EMPA, Dübendorf, September 28-29, 2005, pp. 91-97.

Kaczmarek, D. (2005b), "Barrierefolien für Vakuum-Isolationspaneele im Bauwesen", In: G.-W. Mainka, U. Heinemann, M. Wollensak & K. Riesner (Eds.), *Proceedings of the second professional conference VakuumIsolationsPaneele – Evakuierte Dämmungen im Bauwesen – Erfahrungen aus der Praxis*, ZAE-Bayern / Projektträger Jülich / Universität Rostock / Hochschule Wismar, Wismar, June 16-17, 2005, pp. D1-D7.

“Kaefer Group promotes vacuum insulation for LNG installations”, *LNG journal,* May 2006, pp.44-46.

Kaganer, M.G. (1969), *Thermal Insulation in Cryogenic Engineering*, IPST, Jerusalem, 220 pages.

Kalkman, A.J. (2008), “Passiefhuizen in de seriematige woningbouw”, *Bouwfysica* 19 (3): 14-17.

Kamke, F.A. (2006), “Densified Radiata Pine for Structural Composites”, *Maderas Ciencia y tecnología* 8 (2): 83-92.

Kämpfen, B. (2003), “A New Synthesis of Architecture and Energy“, *Home Energy* 2003 (Sept./Oct.): 24-27.

Kenard, E.H. (1938), *Kinetic Theory of Gases*, McGraw-Hill Book Company Inc, New York, 483 pages.

Kerspe, J.H. (2007), ”Newly Designed Vacuum-Insulation for Big Pipes and Pipelines”, In: A. Beck et al. (eds.), *Proceedings of the 8th International Vacuum Insulation Symposium*, ZAE-Bayern/UniWue, Würzburg, September 18-19, 2007, pp. 1-13.

Keitzl, Ch. (2003), “Einsatzbeispiele und Perspektiven: Mechanisch belastbare Vakuum-Dämmelemente im Bauwesen”, In: *Proceedings of the first professional conference VakuumIsolationsPaneele – Evakuierte Dämmungen im Bauwesen*, ZAE-Bayern / Projektträger Jülich / Universität Rostock / Hochschule Wismar, Rostock-Warnemünde July 10–11, 2003, pp. Q1-Q12.

Kim, S.W., S.H. Lee, J.S. Kang and K.H. Kang (2006), “Thermal Conductivity of Thermoplastics Reinforced with Natural Fibres”, *International Journal of Thermophysics* 27 (6): 1873-1881.

Kistler, S.S. (1932), “Coherent Expanded-Aerogels”, *J. of Physical Chemistry* 36 (1): 52-62.

Kistler, S.S. (1935), “The Relation between Heat Conductivity and Structure in Silica Aerogel”, *J. of Physical Chemistry* 39 (1): 79-85.

Knudsen, M.H.C. (1934), *The Kinetic Theory of Gases*, Methuen, London, 64 pages.

Kollár, L.P. and G.S. Springer (2003), *Mechanics of Composite Structures*, Cambridge University Press, Cambridge, 480 pages.

Koschade, R (2000), *Die Sandwichbauweise*, Verlag für Architektur und Technische Wissenschaften GmbH Ernst & Sohn, Berlin, 387 pages.

Koschenz, M. And B. Lehmann (2000), *Thermoaktieve Bauteilsysteme*, EMPA, Dübendorf.

Kraus, D., D. Büttner, U. Heinemann and J. Fricke (2005), “Non-destructive Method to Determine the Water Vapour Pressure in Vacuum Insulation Panels (VIP)”, In: M. Zimmermann (ed.), *Proceedings of the 7th International Vacuum Insulation Symposium*, EMPA, Dübendorf, September 28-29, 2005, pp. 77-84.

Krauter, M. (2007), “Praxiserfahrung eines geschulten Fachbetriebes – Einsatz bauaufsichtlich zugelassener Vakuumdämmplatten“, In: Heinemann, U. (ed.), *Proceedings of the third professional conference VIP-BAU*, ZAE-Bayern / Universität Würzburg, Würzburg, September 20, 2007, pp. 33-41.

Kücükpinar, E., H. Güçlü, A. Soysal and F. Özkadi (2001), ”Experimental and theoretical evaluation methods of vacuum level change inside various types of vacuum insulation panels”, In: *Proceedings of the fourth Vacuum Insulation Association Symposium*, VIA, Rome, May 23-24, 2001.

Kundu, P.P. and S. Choe (2003), “Transport of Moist Air Through Microporous Polyolefin Films”, *Journal of Macromolecular Science C - Polymer Reviews* 43 (2): 143-186.

Lahsasni, S., M. Kouhila, M. Mahrouz and N. Kechaou (2002), “Experimental study and modelling of adsorption and desorption isotherms of prickly pear peel (Opuntia ficus indica)", *Journal of Food Engineering* 55 (3): 201 –207.

Lahsasni, S., M. Kouhila, M. Mahrouz and M. Fliyou (2003), "Moisture adsorption-desorption isotherms of prickly pear cladode (Opuntia ficus indica) at different temperatures", *Energy Conversion and Management* 44 (6): 923 –936.

Lahsasni, S., M. Kouhila and M. Mahrouz (2004), "Adsorption-desorption isotherms and heat of sorption of prickly pear fruit (Opuntia ficus indica)", *Energy Conversion and Management* 45 (2): 249 –261.

Lallich, S., F. Enguehard and D. Baillis (2007), "Radiative properties of silica nanoporous matrices", In: A. Beck et al. (eds.), *Proceedings of the 8th International Vacuum Insulation Symposium*, ZAE-Bayern/UniWue, Würzburg, September 18-19, 2007, pp. 1-7.

Langowski, H.-C. (1998), "Barriereeigenschaften von Folien, Schichten und Verbunden", In: IVV (ed.), *Verpackungen aus Kunststofffolien. Neue Entwicklungen und Anwendungsfelder*, Proceedings of the FachPack 98 Symposium, Octobre 15, 1998, IVV, Freising, pp. ...

Langowski, H.-C. (2005), "Stofftransport durch polymere und anorganische Schichten", *Vakuum in Forschung und Praxis* 17 (1): 6-13.

Lay, D.C. (1997), *Linear Algebra and its Applications*, Addison-Wesley Publishing Company, Reading, 486 pages.

Leijendeckers, P.H.H., J.B. Fortuijn, F. van Herwijnen and H. Leegwater (1997), *Polytechnisch Zakboekje*, 48th edition, Koninklijke PBNA, Arnhem.

Lenz, K., Ph.L. Leistner, K. Sedlbauer and N. König (2005), "Vakuumisolationspaneele aus hygrothermischer und akustischer Sicht", In: G.-W. Mainka, U. Heinemann, M. Wollensak & K. Riesner (Eds.), *Proceedings of the second professional conference VakuumIsolationsPaneele – Evakuierte Dämmungen im Bauwesen – Erfahrungen aus der Praxis*, ZAE-Bayern / Projektträger Jülich / Universität Rostock / Hochschule Wismar, Wismar, June 16-17, 2005, pp. E1-E13.

Levebre, G. (2001), "Ceramis® Packaging material for VIP" In: M. Zimmermann and H. Bertschinger (eds.), *Proceedings of the IEA International Conference and Workshop High Performance Thermal Insulations (HiPTI) – Vacuum Insulated Products (VIP),* January 22-24, 2001, EMPA Dübendorf, pp. 37-46.

Lichtblau, F. and N. Jendges (2005), "VIP in der Architektur: Zwei ganzheitliche Prototypen Bestand/Neubau aus Sicht der Planer", In: G.-W. Mainka, U. Heinemann, M. Wollensak & K. Riesner (Eds.), *Proceedings of the second professional conference VakuumIsolationsPaneele – Evakuierte Dämmungen im Bauwesen – Erfahrungen aus der Praxis*, ZAE-Bayern / Projektträger Jülich / Universität Rostock / Hochschule Wismar, Wismar, June 16-17, 2005, pp. Q1-Q10.

Lichtenberg, J. (2002), *Ontwikkelen van Projectongebonden Bouwproducten.*, PhD-thesis, Delft University of Technology, Delft.

Linden, A.C. van der (2000), *Bouwfysica*, fifth edition, SMD educatieve uitgevers / Waltman, Leiden, 283 pages.

Linthorst, P. (2007), *Zwevende dekvloer met LTV en HTK – Samenvatting Ontwikkelingsfase 1*, Intermediate report for SenterNovem, WellDesign, Utrecht, [unpublished], pp. 1-22.

Liu, H., J. Li and Y. Hu (1999), "A transport model for sorption and desorption of penetrants in glassy polymer membrane", *Fluid Phase Equilibria* 158–160 (1): 1035–1044.

Liu, Q., T. Stuart, M. Hughes, H.S.S. Sharma and G. Lyons (2007), "Structural biocomposites from flax – Part II: The use of PEG and PVA as interfacial compatibilising agents", *Composites: Part A: applied science and manufacturing* 38 (5): 1403-1413.

Londry, F.A. and A.J. Slavin (1991), “Effective Thermal Conductivity of a Packed Bed of Hollow Zirconia Microspheres under Vacuum and under 100 kPa of Argon”, *Journal of the American Ceramics Society* 74 (12): 3118-3125.

Lubbinge, P. (2004), *Testen vacuüm panelen*, Laboratory report 545, Paramelt, Heerhugowaard.

Luib, M. (2005), ”Produkte und Systeme mit VIPs – Verbundelemente für vorgehängte Fassaden”, In: G.-W. Mainka, U. Heinemann, M. Wollensak & K. Riesner (Eds.), *Proceedings of the second professional conference VakuumIsolationsPaneele – Evakuierte Dämmungen im Bauwesen – Erfahrungen aus der Praxis*, ZAE-Bayern / Projektträger Jülich / Universität Rostock / Hochschule Wismar, Wismar, June 16-17, 2005, pp. K1-K9.

Lysen, E.H. (1996), "Trias Energica: Solar Energy Strategies for Developing Countries", In: … (eds.), Proceedings of the *Eurosun Conference*, Freiburg, September 16-19, 1996, pp. 1-6.

Malsen, J. van, M.J. Tenpierik, R.H.J. Looman and J.J.M. Cauberg (2008), “Heat seal strength of barrier films used in vacuum insulation panels at room temperature and at -130^{o}C”, *J. of Plastic Film and Sheeting* 24 (1): 35-52.

Mainka, G.-W. (2003), “VIP ohne inneres Stützgerüst am Beispiel von VI-Gläsern”, In: *Proceedings of the first professional conference VakuumIsolationsPaneele – Evakuierte Dämmungen im Bauwesen*, ZAE-Bayern / Projektträger Jülich / Universität Rostock / Hochschule Wismar, Rostock-Warnemünde July 10–11, 2003, pp. F1-F8.

Manini, P. (1997), “The Combogetter as a Key Component in the Vacuum Insulated Panels (VIPs) Technology”, *Vuoto* XXVI (2): 45-48.

Manini, P. (1999), “Vacuum issues in Vacuum Insulated Panels Technology and the role of the Getter”, *Vuoto* XXVIII (1-2): 39-42.

Manini, P, E. Rizzi, G. Pastore and P. Gregorio (2003), “Engineering Insulation. Advances in VIP Design for Super Insulation of Domestic Appliances”, *Appliance Magazine* 2003 (6), [online], Available: http://www.appliancemagazine.com/ [2004, October 27].

Manz, H., S. Brunner and L. Wullschleger (2006), ”Triple vacuum glazing: Heat transfer and basic mechanical design constraints”, *Solar Energy* 80 (12): 1632-1642.

Marais, S., Y. Hirata, D. Langevin, C. Chappey, T.Q. Nguyen and M. Metayer (2002), “Permeation and Sorption of Water and Gases through EVA Copolymers Films”, *Materials Research Innovations* 6 (2): 79-88.

Materna, R. (2001), “VIP’s for advanced retrofit solutions for buildings”, In: M. Zimmermann and H. Bertschinger (eds.), *Proceedings of the IEA International Conference and Workshop High Performance Thermal Insulations (HiPTI) – Vacuum Insulated Products (VIP),* January 22-24, 2001, EMPA Dübendorf, pp. 55-62.

Maysenhölder, W. (2008a), “Sound Transmission Loss of Vacuum Insulation Panels”, In: … (eds.), Proceedings of *Acoustics’08*, ASA/EAA/SFA, Paris, June 29-July 4, 2008, pp. 1-6.

Maysenhölder, W. (2008b), “Schalldämmung mit Vakuumisolationspaneelen: Messung und rechnerische Modellierung”, *Bauphysik* 30 (6): 366-372.

McAdams, W.H. (1954), *Heat Transmission,* 3rd ed., McGraw-Hill, New York, 532 pages.

McDonough, W. (1992), “The Hannover Principles – Design for Sustainability”, Prepared for EXPO 2000 The World’s Fair in Hannover Germany, [online], Available: http://www.mcdonough.com/ [2008, February 21].

McDonough, W. and M. Braungart (2002), *Cradle to Cradle. Remaking the Way We Make*

Things, North Point Press, New York, 193 pages.

Metz, R. (2008), *Geprefabriceerde Geïntegreerde Elementen voor Grootschalige LTV Toepassing – Report 02 – Period May 2007 till December 2007*, Intermediate report for SenterNovem, Metz Consult, Hilversum, [unpublished], pp. 1-6.

Miesbauer, O., M. Schmidt and H.-C. Langowski (2008), "Stofftransport durch Schichtsysteme aus Polymeren und dünnen anorganischen Schichten", *Vakuum in Forschung und Praxis* 20 (6): 32-40.

Mikhal'chenko, R. S., A. G. Gerzhin, V. T. Arkhipov and N. P. Pershin (1964), "Effective thermal conductivity of multilayer vacuum insulation as a function of its thickness", *Journal of Engineering Physics and Thermophysics* 15 (3): 887-889.

Mil'man, S.B. and M.G. Kaganer (1975), "Study of radiative heat transfer in vacuum-powder insulation by infrared spectroscopy", *Inzhenerno-Fizicheskii Zhurnal* 29 (1):40-45.

Möller, K., Th. Gevert and A. Holmström (2001), "Examination of a low density polyethylene (LDPE) film after 15 years of service as an air and water vapour barrier", *Polymer Degradation and Stability* 73 (1): 69-74.

Mooi, R. (2009), "Isolerende houten kozijnen en drielaags glas – Voorzichtig debuut op de Nederlandse markt", *NBD Magazine* 2009 (6-7): 20-23.

Moonen, F. (2001), *Ontwerp van een geïndustrialiseerde funderingswijze*, PhD-thesis, Eindhoven University of Technology, Eindhoven.

Morel, B., L. Autissier and D. Autissier (2007), "Modifications of a pyrogenic silica exposed to moist air", In: A. Beck et al. (eds.), *Proceedings of the 8th International Vacuum Insulation Symposium*, ZAE-Bayern/UniWue, Würzburg, September 18-19, 2007, pp. 1-8.

Morel, B., L. Autissier, D. Autissier, D. Lemordant, B. Yrieix and D. Quenard (2009), "Pyrogenic silica ageing under humid atmosphere", *Powder Technology* 190 (1-2): 225-229

Mourik, P. van and J. van Dam (2001), *Materiaalkunde voor ontwerpers en constructeurs*, Delft University Press, Delft, 420 pages.

Muir, A. and M. Overend (2009), "A parametric feasibility study on active vacuum insulation panels for buildings", In: R. Ogden and M. Overend (eds.), Proceedings of the *9th International Vacuum Insulation Symposium*, High thermal performance and more space from thin insulations, Oxford Brookes University / University of Cambridge, London, September 17-18, 2009, p. 1-10.

Mukhopadhyaya, P (2004), "High-performance insulation materials", *Solplan Review* 118 (9): 16-17.

Mukhopadhyaya, P, K. Kumaran, J. Lackey, N. Normandin & D. van Reenen (2005), "Methods for evaluating long-term changes in thermal resistance of vacuum insulation panels.", In: … (eds.), Proceedings of the *10th Canadian Conference on Building Science and Technology*, Ottawa, May 12-13, 2005, pp. 169-181.

Mukhopadhyaya, P, K. Kumaran, N. Normandin, D. van Reenen and J. Lackey (2008), "High-Performance Vacuum Insulation Panel: Development of Alternative Core Materials", *Journal of cold regions engineering* 22 (4): 103-123.

Mukhopadhyaya, P, K. Kumaran, N. Normandin and D. van Reenen (2009), "Fibre-powder composite as core material for vacuum insulation panel", In: R. Ogden and M. Overend (eds.), Proceedings of the *9th International Vacuum Insulation Symposium*, High thermal performance and more space from thin insulations, Oxford Brookes University / University of Cambridge, London, September 17-18, 2009, p. 1-9.

Musgrave, D.S. (2005), "Finite Element Analysis Used to Model VIP Barrier Film Performance", In: M. Zimmermann (ed.), *Proceedings of the 7th International Vacuum Insulation Symposium*, EMPA, Dübendorf, September 28-29, 2005, pp. 99-104.

Musgrave, D.S. (2007), "Finite Element Analysis of Bending Barrier Films", In: A. Beck et al. (eds.), *Proceedings of the 8th International Vacuum Insulation Symposium*, ZAE-Bayern/UniWue, Würzburg, September 18-19, 2007, pp. 1-7.

Musgrave, D.S. (2009), "Structural vacuum insulation panels", In: R. Ogden and M. Overend (eds.), Proceedings of the *9th International Vacuum Insulation Symposium*, High thermal performance and more space from thin insulations, Oxford Brookes University / University of Cambridge, London, September 17-18, 2009, p. 1-8.

NAHB research centre (2002), *Accelerating the Adoption of Vacuum Insulation Technology in Home Construction, Renovation, and Remodeling*, NAHB research centre Inc., Upper Malboro, 52 pages.

Napp, V., R. Caps, H.-P. Ebert and J. Fricke (1999), "Optimization of the thermal radiation extinction of silicon carbide in a silica powder matrix", *Journal of Thermal Analysis and Calorimetry* 56 (1): 77-85.

Nauta, J.P., J.P. Overbeek, J. Braam, H. Bos, R. Brouwer, G. Pott, D. van Rooijen, J. Visser, B. van Voorn (2001), *Lichtgewicht transportmiddelen op basis van hernieuwbare grondstoffen*, Report, ATO / Focwa / Ceres / Wientjes / ECN / TUDelft / Kiem, Amsterdam.

Nemanič, V. (1995), "Vacuum Insulating Panel", *Vacuum* 46 (8-10): 839-842.

NEN-EN-ISO 354:2003 (2003), "Acoustics – Measurement of sound absorption in a reverberation room", Nederlands Normalisatie Instituut.

NEN 1068:2001 (2001), "Thermische isolatie van gebouwen – Rekenmethoden", Nederlands Normalisatie Instituut.

NEN 1068:2001/A2 (2004), "Thermische isolatie van gebouwen – Rekenmethoden - Wijzigingsblad", Nederlands Normalisatie Instituut.

NEN-EN 1264-2:2008 (2008), "Water based surface embedded heating and cooling systems – Part 2: Floor heating – Prove methods for the determination of the thermal output using calculation and test methods", Nederlands Normalisatie Instituut.

NEN-EN 1264-4ontw:2007 (2007), "Water based surface heating and cooling systems – Part 4: Installation", Nederlands Normalisatie Instituut.

NEN 5077+C1:2008 (2008), "Noise control in buildings – Determination methods for performances concerning airborne sound insulation of facades, airborne sound insulation, impact sound insulation, sound levels caused by technical services and reverberant time", Nederlands Normalisatie Instituut.

NEN 6702:2007 (2007), "Technical principles for building structures – TGB 1990 – Loadings and deformations", Nederlands Normalisatie Instituut.

NEN-ISO 6707-1:2004 (2004), "Building and civil engineering – Vocabulary – Part 1: General terms", Nederlands Normalisatie Instituut.

NEN 6760:2008 (2008), "Technische grondslagen voor bouwconstructies – TGB1990 – Timber structures – Basic requirements and determination methods", Nederlands Normalisatie Instituut.

NEN-EN-ISO 7730:1996 (1996), "Gematigde thermische binnenomstandigheden – Bepaling van de PMV- en de PPD-waarde en specificatie van de voorwaarden", Nederlands Normalisatie Instituut.

NEN-ISO 9052-1:1992 (1992), “Acoustics – Determination of dynamic stiffness – Part 1: Materials used under floating floors in dwellings”, Nederlands Normalisatie Instituut.

NEN-EN-ISO 10077-1:2004 (2004), “Thermische eigenschappen van ramen, deuren en luiken – Berekening van de warmtedoorgangscoëfficiënt – Deel 1: Algemeen”, Nederlands Normalisatie Instituut.

NEN-EN-ISO 10211:2008 (2008), “Thermal bridges in building construction – Heat flows and surface temperatures – Detailed calculations”, Nederlands Normalisatie Instituut.

NEN-EN 12667:2001 (2001), “Thermal performance of building materials and products – Determination of thermal resistance by means of guarded hot plate and heat flow meter methods – Products of high and medium thermal resistance”, Nederlands Normalisatie Instituut.

NEN-EN 13162:2009 (2009), “Thermal insulation products for buildings – Factory made mineral wool (MW) products – Specification”, Nederlands Normalisatie Instituut.

NEN-EN 13171:2009 (2009), “Thermal insulation products for buildings – Factory made wood fibre (WF) products – Specification”, Nederlands Normalisatie Instituut.

NEN-EN-ISO 13790:2008 (2008), “Energy performance of buildings – Calculation of energy use for space heating and cooling”, Nederlands Normalisatie Instituut.

NEN-EN 13947:2000 (2000), “Thermische eigenschappen van vliesgevels – Berekening van de warmtegeleiding – Vereenvoudigde methode”, Nederlands Normalisatie Instituut.

NEN-ISO 15686-2:2001 (2001), “Buildings and constructed assets – Service life planning – Part 2: Service life prediction procedure”, Nederlands Normalisatie Instituut.

NF T 56 101 (1976), “Alveolar products made with elastomer or polymer: compression test of rigid material”, Association Francaise de Normalisation.

NF T 56 102 (1976), “Alveolar products made with elastomer or polymer: flexion test of rigid material”, Association Francaise de Normalisation.

Noller, K., C. Stramm, S. Amberg-Schwab, U. Weber, S. Günther and N. Schiller (2007), ”New POLO concepts to manufacture VIP barrier film laminates based on hybrid barrier layers”, presented at *the 8th International Vacuum Insulation Symposium*, ZAE-Bayern/UniWue, Würzburg, September 18-19, 2007.

Novem (2000), *Energiebewust ontwerpen van nieuwbouwwoningen. Vademecum*, second edition, Novem and Boom, Sittard/Delft, 206 pages.

Nowara, E. (2005), ”Tempsafe elements – Vakuum-Wärmedämmelemente mit Stahldeckschichten”, In: G.-W. Mainka, U. Heinemann, M. Wollensak & K. Riesner (Eds.), *Proceedings of the second professional conference VakuumIsolationsPaneele – Evakuierte Dämmungen im Bauwesen – Erfahrungen aus der Praxis*, ZAE-Bayern / Projektträger Jülich / Universität Rostock / Hochschule Wismar, Wismar, June 16-17, 2005, pp. F1-F15.

NPR 2068:2002 (2002), “Thermische isolatie van gebouwen – Vereenvoudigde rekenmethoden”, Nederlands Normalisatie Instituut.

Nussbaumer, T., R. Bundi, Ch. Tanner and H. Muehlebach (2005), “Thermal Analysis of a wooden door system with integrated vacuum insulation panels”, *Energy and Buildings* 37 (11): 1107-1113.

Nussbaumer, T., K. Ghazi Wakili and Ch. Tanner (2006), “Experimental and numerical investigation of the thermal performance of a protected vacuum-insulation system applied to a concrete wall", *Applied Energy* 83 (8): 841-855.

Oesterle, E., R.-D. Lieb, M. Lutz and W. Heusler (2001), *Double-Skin Facades. Integrated Planning. Building Physics, Construction, Aerophysics, Air-Conditioning, Economic Viability*, Prestel, München, 207 pages.

Ogden, R. and Ch. Kendrick (2005), "VIP Cladding Panels for Buildings: Applications and Conceptual Solutions", In: M. Zimmermann (ed.), *Proceedings of the 7th International Vacuum Insulation Symposium*, EMPA, Dübendorf, September 28-29, 2005, pp. 153-160.

Omer, S.A., S.B. Riffat and G. Qiu (2007), "Thermal insulations for hot water cylinders: a review and a conceptual evaluation", *Buildings Serv. Eng. Res. Technol.* 28 (3): 275-293.

Papaefthimiou, S., G. Leftheriotis, P. Yianoulis, T.J. Hyde, P.C. Eames, Y. Fang, P.-Y. Pennarun and P. Jannasch (2006), "Development of electrochromic evacuated advanced glazing", *Energy and Buildings* 38 (12): 1455 – 1467.

Persoon, J. (2008), "Overwegingen bij het beoordelen van componenten voor vloerverwarming", note written in the framework of the Senter-Novem research project 'Geprefabriceerde geïntegreerde elementen voor grootschalige LTV toepassing', [unpublished], pp. 1-4.

Phillip, B.L. and T.J. Shepodd (2000), "Versatile new polymers based getters", In: *Proceedings of the third Conference of the Vacuum Insulation Association,* VIA, Vancouver, June 7 – 8, 2000, pp. 1-17.

Physibel (2002), *TRISCO Manual of Version 10.0 w*, Physibel, Maldegem, 65 pages.

Platzer, W. (2007a), "Numerical Simulation of Vapour and Gas Transport into a VIP panel", In: A. Beck et al. (eds.), *Proceedings of the 8th International Vacuum Insulation Symposium*, ZAE-Bayern/UniWue, Würzburg, September 18-19, 2007, pp. 1-10.

Platzer, W. (2007b), "Optimisation and testing of an VIP Exterior Thermal Insulation Composite System (ETICS)", In: A. Beck et al. (eds.), *Proceedings of the 8th International Vacuum Insulation Symposium*, ZAE-Bayern/UniWue, Würzburg, September 18-19, 2007, pp. 1-8.

Platzer, W., C. Stramm, S. Amberg-Schwab and M. Köhl (2005), "Development of Innovative Insulation Systems on the Basis of Vacuum Insulation Panels", In: M. Zimmermann (ed.), *Proceedings of the 7th International Vacuum Insulation Symposium*, EMPA, Dübendorf, September 28-29, 2005, pp. 105-112.

Pompei, F.J. (1999), "The Use of Airborne Ultrasonics for Generating Audible Sound Beams", *Journal of the Audio Engineering Society* 47 (9): 726-731.

Pool, M. (2005), "VIP Architektur – Gestaltungsmöglichkeiten und Wirtschaflichkeit", In: G.-W. Mainka, U. Heinemann, M. Wollensak & K. Riesner (Eds.), *Proceedings of the second professional conference VakuumIsolationsPaneele – Evakuierte Dämmungen im Bauwesen – Erfahrungen aus der Praxis*, ZAE-Bayern / Projektträger Jülich / Universität Rostock / Hochschule Wismar, Wismar, June 16-17, 2005, pp. R1-R9.

Pool, M. (2009), "Insulation of a mixed use building with 7 storeys in Munich with VIP", In: R. Ogden and M. Overend (eds.), Proceedings of the *9th International Vacuum Insulation Symposium*, High thermal performance and more space from thin insulations, Oxford Brookes University / University of Cambridge, London, September 17-18, 2009, p. 1-9.

Porextherm (2004), "Vakuum Isolations Paneelen Technologie", Porextherm, [online], available: http://www.porextherm.com/, [February 16, 2004].

Porextherm (2004), "Auswahl von Barrierematerialien, Porextherm, [online], available: http://www.porextherm.com/, [February 16, 2004].

Porextherm (2005), "Vacupor® – Vakuum Isolation Paneele. Technisches Datenblatt", Porextherm, [online], available: http://www.porextherm.com/, [April 23, 2005].

Porextherm (2009), "Vacupor® NT. Technisches Datenblatt", Porextherm, [online], available: http://www.porextherm.de/, [March 24, 2009].

Porextherm (2009), "Vacupor® NT-B2. Technisches Datenblatt", Porextherm, [online], available: http://www.porextherm.de/, [March 24, 2009].

Porextherm (2009), "Vacupor® RP. Technisches Datenblatt", Porextherm, [online], available: http://www.porextherm.de/, [March 24, 2009].

Porextherm (2009), "Vacupor® PS. Technisches Datenblatt", Porextherm, [online], available: http://www.porextherm.de/, [March 24, 2009].

Porextherm (2009), "Vacupor® FP. Technisches Datenblatt", Porextherm, [online], available: http://www.porextherm.de/, [March 24, 2009].

Porta, P. della (1996), "Gas problem and gettering in sealed-off vacuum devices", *Vacuum* 47 (6-8): 771-777.

Quenard, D. and H. Sallée (2004), *Silica Based Core Materials for Vacuum Insulation Panels*, Draft report for task A of IEA Annex 39 HiPTI, Centre Scientifique et technique du Bâtiment Etablissement de Grenoble Division Caractérisation Physique des Matériaux, [unpublished].

Quenard, D. and H. Sallée (2005), "From VIP's to Building Facades: Three Levels of Thermal Bridges", In: M. Zimmerman (ed.), *Proceedings of the 7th International Vacuum Insulation Symposium*, EMPA, Dübendorf, September 28-29, 2005, pp. 113-120.

Rädecke, E. (2005), "Vakuumisolationen im Flachdach – hohe Wärmedämmung und geringe Aufbauhöhe – kein Widerspruch – Problemlösung am Beispiel von Terrassenaufbauten", In: G.-W. Mainka, U. Heinemann, M. Wollensak & K. Riesner (Eds.), *Proceedings of the second professional conference VakuumIsolationsPaneele – Evakuierte Dämmungen im Bauwesen – Erfahrungen aus der Praxis*, ZAE-Bayern / Projektträger Jülich / Universität Rostock / Hochschule Wismar, Wismar, June 16-17, 2005, pp. X1-X9.

Raicu, A. and K. Noller (2003), "Entwicklung innovativer Wärmedämmsysteme mit VIP für Anwendungen im Bauwesen", In: Proceedings of the first professional conference *VakuumIsolationsPaneele – Evakuierte Dämmungen im Bauwesen*, ZAE-Bayern / Projektträger Jülich / Universität Rostock / Hochschule Wismar, Rostock-Warnemünde Juli 10–11, 2003, pp. J1-J5.

Randel, P. (2001), "Vacuum Insulation Panel with fumed silica", *Proceedings of the IEA International Conference and Workshop High Performance Thermal Insulations (HiPTI) – Vacuum Insulated Products (VIP),* January 22-24, 2001, EMPA Dübendorf, pp. 27-32.

Randel, P. (2003), "Nanoporöse Dämmstoffe auf Basis Fumed Silica", In: *Proceedings of the first professional conference VakuumIsolationsPaneele – Evakuierte Dämmungen im Bauwesen*, ZAE-Bayern / Projektträger Jülich / Universität Rostock / Hochschule Wismar, Rostock-Warnemünde Juli 10–11, 2003, pp. C1-C4.

Rath, D. (1989), *Wärmetransport in evakuierten Dämmsystemen*, PhD-thesis, Universität Dortmund, Dortmund, 119 pages.

Reim, M., W. Körner, J. Manara, S. Korder, M. Arduini-Schuster, H.-P. Ebert and J. Fricke (2005), “Silica aerogel granulate material for thermal insulation and daylighting”, *Solar Energy* 79 (2): 131-139.

Reisacher, H. (2003). “VIP – Stand der Technik.”, In: Proceedings of the first professional conference *VakuumIsolationsPaneele – Evakuierte Dämmungen im Bauwesen*, ZAE-Bayern / Projektträger Jülich / Universität Rostock / Hochschule Wismar, Rostock-Warnemünde Juli 10–11, 2003, pp. B1-B7.

Renckens, J.L.M. (1996), *Gevels & Architectuur. Facades in glas en aluminium*, Vereniging Metalen Ramen en Gevelbranche (VMRG), Nieuwegein, 255 pages.

Rentas, F.J., V.W. Macdonald, D.M. Houchens, P.J. Hmel and Th.J. Reid (2004), “New insulation technology provides next-generation containers for “iceless” and lightweight transport of RBCs at 1 to 10^{o}C in extreme temperatures for over 78 hours”, *Transfusion* 44 (2): 210-216.

Riedel, U. and J. Nickel (1999), ”Natural fibre-reinforced biopolymers as construction materials – new discoveries”, *Die Angewandte Makromolekulare Chemie* 272 (1): 34-40.

Rigacci, A. (1997), *Elaboration d’aérogels de silice monolithique et étude des relations entre leur structure et leur conductivité thermique*, Ph.D.-thesis, Ecole nationale supérieure des mines de Paris, Sophia Antipolis, Paris, 388 pages.

Roderick, K., B. Glover and D. Smith (2005), “Applications of Vacuum Insulation Panels in Extreme Environments”, In: M. Zimmermann (ed.), *Proceedings of the 7th International Vacuum Insulation Symposium*, EMPA, Dübendorf, September 28-29, 2005, p. 85-90.

Rogatzki, P. (2009), “The Hanson EcoHouse™ and Hanson QuickBuild™ walling system”, In: R. Ogden and M. Overend (eds.), Proceedings of the *9th International Vacuum Insulation Symposium*, High thermal performance and more space from thin insulations, Oxford Brookes University / University of Cambridge, London, September 17-18, 2009, p. 1-8.

Roijen, E.J.A. (2004), *Toepassingsmogelijkheden van Vacuüm Isolatie Panelen bij LTV vloer- en wandverwarmingssystemen in woningen*, Final report for SenterNovem, CHRI, Maastricht (projectnr.: 1034-03-11-05-010), pp. 1-41.

Roijen, E.J.A., R. Roijakkers and M.J. Tenpierik (2006), *Toepassingsmogelijkheden vacuümisolatiepanelen in gebouwinstallaties*, Final report for SenterNovem, TUDelft and CHRI, Delft (projectnr.: 1034-03-11-05-015), pp. 1-66.

Roth Werke GmbH (2007), *Flächen-Heiz- und Kühlsysteme – Systemlösungen für alle Anwendungsbereiche*, Brochure, Roth Werke GmbH, Dautphetal.

Rowe, R.K., S. Rimal and H. Sangam (2009), “Ageing of HDPE geomembrane exposed to air, water and leachate at different temperatures”, *Geotextiles and Geomembranes* 27 (2):137-151.

Rusek, S.J. (2009), “Gen3 Long Life High Performance Vacuum Insulation Panel for Construction Applications”, In: R. Ogden and M. Overend (eds.), Proceedings of the *9th International Vacuum Insulation Symposium*, High thermal performance and more space from thin insulations, Oxford Brookes University / University of Cambridge, London, September 17-18, 2009, p. 1-8.

Sangwook S. and B.P. Rice (2003), “Sandwich construction with carbon foam core materials”, *Journal of Composite Materials* 37 (15): 1319-1336.

SAS / Texyloop (2009), Texyloop®, Saint-Jean de Soudain, accessed April 9, 2009, <http://www.texyloop.com/>.

Saurel, R., A. Pajonk and J. Andrieu (2004), “Modelling of French Emmental cheese water activity during salting and ripening periods”, *Journal of Food Engineering* 63 (2): 163–170.

Schalkoort, T.A.J. and P.G. Luscuere (1996), *Klimaatinstallaties – integratie van gebouw en installaties*, Faculty of Architecture, TU Delft, Delft.

Schankland, I.R. (1989), “Measurements of Gas Diffusion in closed-cell Foams. Insulating Materials. Testing and Applications”, In: D.L. McElroy and J.F. Kimpflen (eds.), ASTM/STP/1030, Philadelphia, pp. 174-188.

Scheers, P.C.M. (2001), *Lecture notes High Rise Buildings. Finishing Constructions*, publicatieburo Civil Engineering, TUDelft, Delft.

Schittich, Ch., G. Staib, D. Balkow, M. Schuler and W. Sobek (1999), *Glass Construction Manual*, Birkhäuser Publishers Edition Detail, München, 328 pages.

Schmidheiny, S. (1992), *Changing Course: A Global Business Perspective on Development and the Environment*, MIT Press, Cambridge, 400 pages.

Schneider, N. (2003), “Anwendungen Nanoporöser Dämmstoffe im Bauwesen.”, In: *Proceedings of the first professional conference VakuumIsolationsPaneele – Evakuierte Dämmungen im Bauwesen*, ZAE-Bayern / Projektträger Jülich / Universität Rostock / Hochschule Wismar, Rostock-Warnemünde July 10–11, 2003, pp. M1-M4.

Schönhardt, U. (2003), *Oekobilanz eines Vakuum-Isolations-Panels (VIP),* Report, Fachhochschule Nordwestschweiz (FHNW), Institut für Energie, Basel, 68 pages.

Schultz, J.M. and K.I. Jensen (2008), ”Evacuated aerogel glazings”, *Vauum* 82 (7): 723-729.

Schupp, H.B. (2003), “VIP im Mauerwerksbau”, In: *Proceedings of the first professional conference VakuumIsolationsPaneele – Evakuierte Dämmungen im Bauwesen*, ZAE-Bayern / Projektträger Jülich / Universität Rostock / Hochschule Wismar, Rostock-Warnemünde July 10–11, 2003, pp. O1-O8.

Schwab, H. (2003), “VIP unter baupraktischen Bedingungen, Erfahrungen aus dem Projekt: Vakuumdämmungen für Gebäude”, In: *Proceedings of the first professional conference VakuumIsolationsPaneele – Evakuierte Dämmungen im Bauwesen*, ZAE-Bayern / Projektträger Jülich / Universität Rostock / Hochschule Wismar, Rostock-Warnemünde July 10–11, 2003, pp. I1-I20.

Schwab, H. (2004), *Vakuumisolationspaneele – Gas- und Feuchteeintrag sowie Feuchte- und Wärmetransport*, Ph.D.-thesis, Julius-Maximilians-Universität Würzburg, Würzburg, 86 pages.

Schwab, H., U. Heinemann, A. Beck, H.-P. Ebert and J. Fricke (2005a), “Dependence of Thermal Conductivity on Water Content in Vacuum Insulation Panels with Fumed Silica Kernels”, *J. of Thermal Env. and Bldg. Sci.* 28 (4): 319-326.

Schwab, H., U. Heinemann, A. Beck, H.-P. Ebert and J. Fricke (2005b), “Permeation of Different Gases Through Foils used as Envelopes for Vacuum Insulation Panels”, *J. of Thermal Env. and Bldg. Sci.* 28 (4): 293-317.

Schwab, H., U. Heinemann, A. Beck, H.-P. Ebert and J. Fricke (2005c), “Prediction of Service Life for Vacuum Insulation Panels with Fumed Silica Kernel and Foil Cover”, *J. of Thermal Env. and Bldg. Sci.* 28 (4): 357-374.

Schwab, H., U. Heinemann, J. Wachtel, H.-P. Ebert and J. Fricke (2005d), “Predictions for the Increase in Pressure and Water Content of Vacuum Insulation Panels (VIPs) Integrated into Building Constructions using Model Calculations”, *J. of Thermal Env. and Bldg. Sci.* 28 (4): 327-344.

Schwab, H., C. Stark, J. Wachtel, H.-P. Ebert and J. Fricke (2005e), “Thermal Bridges in Vacuum-Insulated Building Facades”, *J. of Thermal Env. and Bldg. Sci.* 28 (4): 345-355.

Schwab, H., J. Wachtel, H. Scheuerpflug, C. Stark, U. Heinemann, H.-P. Ebert and J. Fricke (2003), *Entwicklung und Anwendung von evakuierten höchsteffizienten Dämmungen für Gebäude (Vakuumdämmung für Gebäude)*, Final report ZAE 2 – 1203 – 21 (2003), ZAE-Bayern, Würzburg.

Scurlock, R.G. and B. Saull (1976), “Development of Multilayer Insulations with Thermal Conductivities Below 0.1 μW/cm K”, *Cryogenics* 16 (5): 303-311.

Simko, T.M., A.C. Fischer-Cripps and R.E. Collins (1998), “Temperature-induced stresses in vacuum glazing: Modelling and Experimental Validation”, *Solar Energy* 63 (1): 1-21.

Simmler, H. (2001), “Measurements of Physical Properties of VIP”, In: M. Zimmermann and H. Bertschinger (eds.), *Proceedings of the IEA International Conference and Workshop High Performance Thermal Insulations (HiPTI) – Vacuum Insulated Products (VIP),* January 22-24, 2001, EMPA Dübendorf, pp. 47-53.

Simmler, H. and S. Brunner (2004), “Kann die Lebensdauer von Vakuumisolationssystemen vorausgesagt werden?”, Statusseminar 2004, [online], Available: http://www.vip-bau.ch/ [2004, December 12].

Simmler, H. (2005), ”High Performance Thermal Insulations: Aktivitäten und Ergebnisse des IEA Annex 39”, In: G.-W. Mainka, U. Heinemann, M. Wollensak & K. Riesner (eds.), *Proceedings of the second professional conference VakuumIsolationsPaneele – Evakuierte Dämmungen im Bauwesen – Erfahrungen aus der Praxis*, ZAE-Bayern / Projektträger Jülich / Universität Rostock / Hochschule Wismar, Wismar, June 16-17, 2005, pp. O1-O13.

Simmler, H. and S. Brunner (2005), “Vacuum insulation panels for building application. Basic properties, aging mechanisms and service life”, *Energy and Buildings* 37 (11): 1122-1131.

Simmler, H. and S. Brunner (2006), “Thermal Properties and service life of vacuum insulation panels (VIP)”, In: *Proceedings of the 4th European Conference on Energy Performance and Indoor Climate in Buildings*, ENTPE, Lyon, November 20-22, 2006, p. 1-6.

Simmler, H., S. Brunner, U. Heinemann, H. Schwab, K. Kumaran, Ph. Mukhopadhyaya, D. Quénard, H. Sallée, K. Noller, E. Kücükpinar-Niarchos, C. Stramm, M.J. Tenpierik, J.J.M. Cauberg and M. Erb (2005), *Vacuum Insulation Panels. Study on VIP-components and Panels for Service Life Prediction of VIP in Building Applications. Subtask A,* IEA ECBCS Annex 39 HiPTI, 153 pages.

Skottke, T. and W. Willems (2009), “A concept of a new high efficient insulation material: Glass coated vacuum sandwich elements”, In: N.T. Bayazit, G. Manioğlu, G.K. Oral and Z. Yilmaz (eds.), *Energy Efficiency and New Approaches – Proceedings of the 4th International Building Physics Conference*, ITU, Istanbul, 15-18 June 2009, pp. 119-126.

Smith, D., L. Warren, K. Roderick, J. Hoffman, R. Perkes and Q. Shrimpton (2005), “Controlled Temperature Packaging Using On-Demand Cooling from Active Vacuum Insulation Panels”, In: M. Zimmermann (ed.), *Proceedings of the 7th International Vacuum Insulation Symposium*, EMPA, Dübendorf, September 28-29, 2005, pp. 183-188.

Smoluchowski, M. (1898), “Über den Temperatursprung bei der Wärmeleitung von Gasen”, *Sitzungsbericht of the Akademie der Wissenschaft (Wiener Berichte 107)*, Wien.

Spoel, W.H. van der (2004), *Prestatiebeheersing van lage-temperatuur vloer- en wandverwarming als woningkoelsysteem*, Final report for

SenterNovem, TUDelft, Delft, (project nr. 0220-01-01-19-1202), p 1-90.

Stamboulis A, C.A. Baillie, S.K. Garkhail, H.G.H. van Melick and T.Peijs (2000), "Environmental durability of flax fibres and their composites based on pp matrix", *Applied Composite Materials* 7(5-6): 273-294.

Stölzel, Ch. (2003), "VIP-gedämmte Auβen-, Spezial- und Funktionstüren sowie Sandwichelemente für den Holzhausbau.", In: *Proceedings of the first professional conference VakuumIsolationsPaneele – Evakuierte Dämmungen im Bauwesen*, ZAE-Bayern / Projektträger Jülich / Universität Rostock / Hochschule Wismar, Rostock-Warnemünde July 10–11, 2003, pp. G1-G13.

Stölzel, Ch. (2005), "Entwicklung von vakuumgedämmten Verbundfertigteilen im Passivhausstandard in einem Prototypen", In: G.-W. Mainka, U. Heinemann, M. Wollensak & K. Riesner (Eds.), *Proceedings of the second professional conference VakuumIsolationsPaneele – Evakuierte Dämmungen im Bauwesen – Erfahrungen aus der Praxis*, ZAE-Bayern / Projektträger Jülich / Universität Rostock / Hochschule Wismar, Wismar, June 16-17, 2005, pp. W1-W7.

Stölzel, Ch. (2007), "Vom VIP zum handlingsicheren Bauteil", In: U. Heinemann (ed.), *Proceedings of the third professional conference VIP-BAU*, ZAE-Bayern / Universität Würzburg, Würzburg, September 20, 2007, pp. 91-100.

Stovall, T.K. and A. Brzenzinski (2002), "Vacuum Insulation Round Robin to Compare Different Methods of Determining Effective Vacuum Insulation Panel Thermal Resistance", In: A.O. Desjarlais and R.R. Zarr (eds.), *Insulation Materials: Testing and Applications*, 4th volume, STP 1426, American Society for Testing and Materials (ASTM), West Conshohocken, PA.

Takegoshi, E, Y. Hirasawa and S. Imura (1985), "Heat Transport of Powder as the Subject of Cryogenic insulation", Second report of Heat Conduction under Vacuum, *Bulletin of JSME* 28 (244): 2352-2359.

Tao, W.-H., C.-C. Chang and J.-Y. Lin (2000), "An Energy-Efficiency Performance Study of Vacuum Insulation Panels", *J. of Cellular Plastics* 36 (6): 441-449.

Teniers, C. (2009), "How laminates with Eval™ EVOH film improve the performance of VIPs", In: R. Ogden and M. Overend (eds.), Proceedings of the *9th International Vacuum Insulation Symposium*, High thermal performance and more space from thin insulations, Oxford Brookes University / University of Cambridge, London, September 17-18, 2009, p. 1-9.

Teniers, C. and D. Houssier (2007), "Aluminium metallised bi-oriented EVOH film for vacuum insulation applications", In: A. Beck et al. (eds.), *Proceedings of the 8th International Vacuum Insulation Symposium*, ZAE-Bayern/UniWue, Würzburg, September 18-19, 2007, pp. 1-7.

Thomas, G.B. Jr. and R.L. Finney (1996), *Calculus*, Addison-Wesley Publishing Company, Reading, 1139 pages.

Thorsell, T.I. and I. Källebrink (2005), "Edge loss minimization in vacuum insulation panels", In: G. Jóhannesson (ed.), *Proceedings of the 7th Nordic Building Physics Symposium*, IBRI / KTH, Reykjavik, June 13-15, 2005, pp. 945-952.

Thorsell, T.I. (2006a), *Vacuum insulation in buildings – Means to prolong service life*, Licentiate Thesis, Royal Institute of Technology (KTH), Stockholm, 43 pages.

Thorsell, T.I. (2006b), "Edge loss minimization in vacuum insulation panels.", In: Fazio, Ge, Rao and Desmarais (eds.), *Research in Building Physics and Building Engineering*, Taylor and Francis Group, London, UK, pp. 251-256.

ThyssenKrupp tempsafe GmbH (2003), "Tempsafe® floor – Technische Daten", brochure, [online], Available: http://www.tempsafe.de/, [2003, May 11].

Timmerhaus, K.D. (2007), "Insulation Progress since the Mid-1950s", In: Timmerhaus, K.D. and R.P. Reed, *Cryogenic Engineering, International Cryogenic Monograph Series Part 3*, Springer, New York, pp. 120-133.

Titan Wood Ltd (2008), "Accoya® - The strength within", brochure, [online], Available: http://titanwood.com/, [January 26, 2009].

Trafton, A. (2007), "One giant leap for space fashion: MIT team designs sleek, skintight spacesuit", *MIT news* July 16, 2007.

Tseng, P.C. and H.S. Chu (2009), "The effects of PE additive on the performance of polystyrene vacuum insulation panels", *International Journal of Heat and Mass Transfer* 52 (13-14): 3084-3090.

Tserki, V., P. Matzinos and C. Panayiotou (2006), "Novel biodegradable composites based on treated lignocellulosic waste flour as filler Part II: Development of biodegradable composites using treated and compatibilized waste flour", *Composites: Part A: applied science and manufacturing* 37 (9): 1231-1238.

United Nations Framework Convention on Climate Change (1992), *Convention of Rio de Janeiro*, Rio de Janeiro, 32 pages.

United Nations Framework Convention on Climate Change (1997), *Kyoto Protocol*, Kyoto, 23 pages.

Variotec (2007), *Veni Vici VIP – Planen Bauen Sanieren mit VIP + Qasa - den hocheffizienten und raumsparenden Wärmebrückenkillern*, Variotec, Neumarkt, 64 pages.

Va-Q-tec AG (2002), "Einsatz von Vakuumdämmplatten als Bodenisolierung in einem Wintergarten", [online], Available: http://www.va-q-tec.de/, [2004, December 17].

Va-Q-tec AG (2008), Va-Q-tec AG, Würzburg, accessed January 29, 2008, <http://www.vaqtec.de/>.

Verhoeven, A.C. (1990), *Bouwfysica 1*, Delft University press, Delft, 128 pages.

VIP-Bau (2003), "Vakuüm-dämmsysteme für den Baubereich - Information zur Vakuumdämmung im Baubereich und dem Angebot des Projektes vip-bau.ch", brochure, [online], Available: http://www.vip-bau.ch/, [2004, February 21].

VMRG – Vereniging Metalen Ramen en Gevelbranche (2008), *VMRG-kwaliteitseisen en Adviezen® 2009*, Vereniging Metalen Ramen en Gevelbranche, Nieuwegein.

VROM - Dutch Ministry of Housing, Spatial Planning and Environment (2001), *Bouwbesluit Stb. 2001, 410*, Den Haag, August 7, 2001.

Wacker-Ceramics GmbH (2003), "WDS® Mikroporöse Dämmstoffe – Effiziente Wärmeisolierung ist nur noch eine Frage von Millimetern", brochure, [online], Available: http://www.wacker.com/, [2003, September 21].

Wang, X, N. Walliman, R. Ogden and C. Kendrick (2007), "VIP and their applications in buildings: a review", *Construction Materials* 160 (4): 145-153.

Weber, R. (2001), "Flexible Pipes with High Performance Thermal Insulation", In: *Proceedings of the IEA International Conference and Workshop High Performance Thermal Insulations (HiPTI) – Vacuum Insulated Products (VIP),* January 22-24, 2001, EMPA Dübendorf, pp. 99-100.

Weinläder, H., H.-P. Ebert and J. Fricke (2005), "VIG – Vacuum Insulation Glass", In: M. Zimmermann (ed.), *Proceedings of the 7th International Vacuum Insulation Symposium*, EMPA, Dübendorf, September 28-29, 2005, pp. 197-204.

Went, K. van (2002), *Vacuüm isolatie panelen*, MSc-thesis, Faculty of Civil Engineering and

Geosciences, Delft University of Technology, Delft, 200 pages.

Wessling, F.C., M.D. Moser and J.M. Blackwood (2004), “Subtle Issues in the Measurement of the Thermal Conductivity of Vacuum Insulation Panels”, *Journal of Heat Transfer* 126 (2): 155-160.

Wieleba, R. (2007), “Fuβbodensanierung mit VIP und dem dünnsten, selbsttragenden Fuβbodenheizungssystem“, In: Heinemann, U. (ed.), *Proceedings of the third professional conference VIP-BAU*, ZAE-Bayern / Universität Würzburg, Würzburg, September 20, 2007, pp. 43-50.

Wilde, P. de (2004), *Computational Support for the Selection of Energy Saving Building Components*, PhD-thesis, Delft University of Technology, DUP, Delft, 220 pages.

Willems, W.M. (2003a), “Zur Dauerhaftigkeit ausgewählter Vakuum-Dämmsysteme”, In: *Proceedings of the first professional conference VakuumIsolationsPaneele – Evakuierte Dämmungen im Bauwesen*, ZAE-Bayern / Projektträger Jülich / Universität Rostock / Hochschule Wismar, Rostock-Warnemünde July 10–11, 2003, pp. P1-P14.

Willems, W.M. (2003b), “Vakuumtechnik im Bauwesen. Lecture notes“, Fakultät für Bauingenieurwesen Ruhr-Universität Bochum, [online], available: http://www.ruhr-uni-bochum.de/, [March 2, 2003].

Willems, E.M.M. and A.A. Kraan (2003), *Industrieel te vervaardigen zwevende dekvloeren met LTV en hoogwaardige akoestische kwaliteit*, Final report for SenterNovem, CHRI, Rotterdam, pp. 1-36.

Willems, W.M. and K. Schild (2005), “The Next Generation of Insulating Materials: Vacuum Insulation”, In: G. Jóhannesson (ed.), *Proceedings of the 7th Nordic Building Physics Symposium*, IBRI / KTH, Reykjavik, June 13-15, 2005, pp. 920-927.

Willems, W. and K. Schild (2006), “The use of Vacuum Insulated Sandwiches (VIS) in building constructions”, In:, *Proceedings of the 4th European Conference on Energy Performance and Indoor Climate in Buildings*, ENTPE, Lyon, November 20-22, 2006, p. 1-6.

Willems, W. and K. Schild (2008), "Where to use vacuum insulation … and where not!", In: C. Rode (eds), Proceedings of the 8th *Symposium on Building Physics in the Nordic Countries*, DTU/SBi/IDA, Copenhagen, June 16-18, 2008, pp. 1165-1172.

Willems, W.M., K. Schild and G. Hellinger (2005), “Numerical Investigation on Thermal Bridge Effects in Vacuum Insulating Elements”, In: M. Zimmermann (ed.), *Proceedings of the 7th International Vacuum Insulation Symposium*, EMPA, Dübendorf, September 28-29, 2005, pp. 145-152.

Wilson, C.F., T.M. Simko and R.E. Collins (1998), “Heat conduction through the support pillars in vacuum glazing”, *Solar Energy* 63 (6): 393-406.

Winkler, H. (2005), ”Gebäudesanierung mit VIP am Beispiel der Kita Plappersnut”, In: G.-W. Mainka, U. Heinemann, M. Wollensak & K. Riesner (Eds.), *Proceedings of the second professional conference VakuumIsolationsPaneele – Evakuierte Dämmungen im Bauwesen – Erfahrungen aus der Praxis*, ZAE-Bayern / Projektträger Jülich / Universität Rostock / Hochschule Wismar, Wismar, June 16-17, 2005, pp. H1-H9.

Winkler, H. and G.-W. Mainka (2003), “Einfluss von Wärmebrückenwirkungen bei VIP-Konstruktionen”, In: *Proceedings of the first professional conference VakuumIsolationsPaneele – Evakuierte Dämmungen im Bauwesen*, ZAE-Bayern / Projektträger Jülich / Universität Rostock / Hochschule Wismar, Rostock-Warnemünde July 10–11, 2003, pp. E1-E8.

Winkler, H. and G.-W. Mainka (2005), “Development and First Experiences of a Prefabricated VIP-Sandwich-Element for Fast and Secure Application on Building Surfaces”, In: M. Zimmermann (ed.), *Proceedings of the 7th International Vacuum Insulation Symposium*, EMPA, Dübendorf, September 28-29, 2005, pp. 121-130.

Wipak (2008), "Vacuum Insulation Panels – New film meets building regulations", *Wipak E-zine* (2008) 1, accessed February 4, 2008, <http://www.wipak.com/magazine/108article2.html>.

Wollensack, M. (2003), "Energetische Sanierung mit VIP", In: Proceedings of the first professional conference *VakuumIsolationsPaneele – Evakuierte Dämmungen im Bauwesen*, ZAE-Bayern / Projektträger Jülich / Universität Rostock / Hochschule Wismar, Rostock-Warnemünde July 10–11, 2003, pp. K1-K6.

Wong, Ch.-M., Sh.-J. Tsai, Ch.-H. Ying and M.-L. Hung (2006), "Effect of Low Density Polyethylene on Polystyrene Foams", *Journal of Cellular Plastics* 42 (2): 153-163.

Woods, G. (1990), *The ICI Polyurethane Book*, 2nd edition, John Wiley & Sons, New York, 364 pages.

Yamada, M. (2005), "Development on New Vacuum Insulation Panel, "Chip-Vacua"", In: M. Zimmermann (ed.), *Proceedings of the 7th International Vacuum Insulation Symposium*, EMPA, Dübendorf, September 28-29, 2005, pp. 181-182.

Yan, Y. (2006), *Vacuum insulation panels*, MSc-thesis, Faculty of Civil Engineering and Geosciences, Delft University of Technology, Delft, 110 pages.

Yeganeh, M. (2007), "A vacuum thermal insulation structurally stiffened by air pressure", In: A. Beck et al. (eds.), *Proceedings of the 8th International Vacuum Insulation Symposium*, ZAE-Bayern/UniWue, Würzburg, September 18-19, 2007, pp. 1-8.

Yoon, I.S. and T.-H. Song (2009), "Development of a multiple layer vacuum insulation chip", *International Journal of Heat and Mass Transfer* 52 (5-6): 1276-1283.

Yu, L., K. Dean and L.Li (2006), "Polymer blends and composites from renewable resources", *Progress in polymer science* 31 (6): 576-602.

Zehender, H. (1964), "Einfluss der freien Konvektion auf die Wärmeleitfähigkeit einer leichten Mineralfasermatte bei tiefen Temperaturen", *Kaltetechnik* 16 (10): 308-311.

Zhao, S., B. Zhang and X. He (2009), "Temperature and pressure dependent effective thermal conductivity of fibrous insulation", *International Journal of Thermal Sciences* 48 (2): 440-448.

Zhang, Z.M., I.J. Britt and M.A. Tung (2001), "Permeation of Oxygen and Water Vapor through EVOH Films as Influenced by Relative Humidity", *Journal of Applied Polymer Science* 82 (8): 1866-1872.

Zhang, Z.M. (2007), *Nano/Microscale Heat Transfer*, McGraw-Hill Professional, New York, 479 pages.

Zhitomirskii, I.S., A.M. Kislov & V.G. Romanenko (1976), "Nonstationary problem of heat transfer in laminar-vacuum insulation", *Inzhenerno-Fizicheskii Zhurnal* 32 (5): 806-813.

Zwerger, M. and H. Klein (2005a), "Integration of VIP's into External Wall Insulation System", In: M. Zimmermann (ed.), *Proceedings of the 7th International Vacuum Insulation Symposium*, EMPA, Dübendorf, September 28-29, 2005, pp. 173-180.

Zwerger, M. and H. Klein (2005b), "Integration von VIPs in Wärmedämm-Verbundsysteme", In: G.-W. Mainka, U. Heinemann, M. Wollensak and K. Riesner (eds.), *Proceedings of the second professional conference VakuumIsolationsPaneele – Evakuierte Dämmungen im Bauwesen – Erfahrungen aus der Praxis*, ZAE-Bayern / Universität Rostock / Hochschule Wismar, Wismar, June 16-17, 2005, pp. N1-N7.

R2 List of Publications by Author Related to VIPs

2005

Binz, A., A. Moosmann, G. Steinke, U. Schonhardt, F. Fregnan, H. Simmler, S. Brunner, K. Ghazi, R. Bundi, U. Heinemann, H. Schwab, J.J.M. Cauberg, M.J. Tenpierik, G.A. Johannesson, T.I. Thorsell, M. Erb and B. Nussbaumer (2005), *Vacuum Insulation in the Building Sector. Systems and Applications. Subtask B,* IEA ECBCS Annex 39 HiPTI, 111 pages.

Cauberg, J.J.M. and M.J. Tenpierik (2005), "4.1 Vacuumisolatiepanelen en andere noviteiten", In: D.W. Dicke and E.M. Haas (eds.), *Praktijkhandboek Duurzaam Bouwen*, Weka Publishers, Amsterdam, pp. 4.1 VAC 1-20.

Cauberg, J.J.M. and M.J. Tenpierik (2005). "From VIP to Building Panel", In: M. Zimmermann (ed.), Proceedings of the *7th International Vacuum Insulation Symposium*, EMPA, Dübendorf, September 28-29, 2005, p. 161-172.

Simmler, H., S. Brunner, U. Heinemann, H. Schwab, K. Kumaran, Ph. Mukhopadhyaya, D. Quénard, H. Sallée, K. Noller, E. Kücükpinar-Niarchos, C. Stramm, M.J. Tenpierik, J.J.M. Cauberg and M. Erb (2005), *Vacuum Insulation Panels. Study on VIP-components and Panels for Service Life Prediction of VIP in Building Applications. Subtask A,* IEA ECBCS Annex 39 HiPTI, 153 pages.

Tenpierik, M.J. and J.J.M. Cauberg (2005), "Vacuum Insulation Panels in Building Facades: Moisture and Temperature Conditions during Insolation", In: G.A. Jóhannesson (ed.), Proceedings of the 7th *symposium on building physics in the Nordic countries*, IBRI / KTH, Reykjavik, June 13-15, 2005, pp. 937-944.

Also published in: Cauberg, J.J.M. and M.J. Tenpierik (2005), "Vacuum Insulation Panels in Building Facades: Moisture and Temperature Conditions during Insolation", *Nordic Journal of Building Physics,* special section for the 7th symposium on Building Physics in the Nordic Countries 2005, pp. 1 - 8.

2006

Cauberg, J.J.M., M.J. Tenpierik, H.F.E. Beyrichen, R.H.J. Looman, J. van Malsen and W.H. van der Spoel (2006), *Thermo-mechanical Properties of Metallised Barrier Films*, Final report for EU/Craft VACI - WP10: Assessment of Sealing, TU Delft, Delft (projectnr.: COOP-CT-2003-508026), pp. 1-94.

Cauberg, J.J.M., M.J. Tenpierik, H.F.E. Beyrichen, R.H.J. Looman, J. van Malsen and W.H. van der Spoel (2006), *Operational Heat Transfer and Ageing Process of Vacuum Insulated Panels at Cryogenic and Low Temperatures*, Final report for EU/Craft VACI - WP20: Operational Heat Transfer and Ageing Process , TU Delft, Delft (projectnr.: COOP-CT-2003-508026), pp. 1-63.

Roijen, E.J.A., R. Roijakkers and M.J. Tenpierik (2006), *Toepassingsmogelijkheden vacuümisolatiepanelen in gebouwinstallaties*, Final report for SenterNovem, TUDelft and CHRI, Delft (projectnr.: 1034-03-11-05-015), pp. 1-66.

Tenpierik, M.J. (2006). *Vacuum Insulation Panels Applied in Building Panels*, Final report for SenterNovem, TUDelft, Delft (projectnr.: 0130-01-03-02-001), pp. 1-56.

Tenpierik, M.J. and J.J.M. Cauberg (2006), "Vacuum Insulation Panel: Friend or Foe?", In: R. Compagnon, P. Haefeli and W. Weber (eds.), Proceedings of the 23rd international conference on *Passive and Low Energy*

Architecture, PLEA / Hesso / Unige, Genève, September 6-8, 2006, pp. I-535-540.

Tenpierik, M.J., R.H.J. Looman and J.J.M. Cauberg (2006), "Vacuümisolatie voor cryogene toepassing", *Koude & Luchtbehandeling* 99 (6): 32-35.

2007

Cauberg, J.J.M. and M.J. Tenpierik (2007), "Sound Reduction of Vacuum Insulation Based Sandwich Panels", In: A. Beck et al. (eds.), *Proceedings of the 8th International Vacuum Insulation Symposium*, ZAE-Bayern/UniWue, Würzburg, September 18-19, 2007, pp. 1-8.

Cauberg, J.J.M. and M.J. Tenpierik (2007), "Sound Reduction of Vacuum Insulation Based Building Panels", In: A. Lara (ed.), *Proceedings of the 19th international congress on acoustics*, ICA/SEA/IA, Madrid, September 2-7, 2007, pp. 1-6.

Tenpierik, M.J. and J.J.M. Cauberg (2007), "Analytical Models for Calculating Thermal Bridge Effects Caused by Thin High Barrier Envelopes around Vacuum Insulation Panels", *Journal of Building Physics* 30 (3): 185-215.

Tenpierik, M.J. and J.J.M. Cauberg (2007), "VIP Integrated Facade Designs: The Advantage of Combining High Thermal Performance with Limited Construction Thickness", In: S.K. Wittkopf and Tan B.K. (eds.), *Proceedings of the 24th international conference on passive and low energy architecture*, PLEA/NUS/RBP, Singapore, September 22-24, 2007, pp. 303-310.

Tenpierik, M.J., J.J.M. Cauberg and T.I. Thorsell (2007), "Integrating vacuum insulation panels in building constructions: an integral perspective", *Construction Innovation* 7 (1): 38-53.

Tenpierik, M.J., J. van Malsen, R.H.J. Looman and J.J.M. Cauberg (2007), "Thermo-Mechanical Behaviour of Barrier Laminates and Heat Seals", In: A. Beck et al. (eds.), *Proceedings of the 8th International Vacuum Insulation Symposium*, ZAE-Bayern/UniWue, Würzburg, September 18-19, 2007, pp. 1-8.

Tenpierik, M.J., W.H. van der Spoel and J.J.M. Cauberg (2007), "Analytical Models for Predicting Thermal Bridge Effects due to VIP Barrier Envelopes", In: A. Beck et al. (eds.), *Proceedings of the 8th International Vacuum Insulation Symposium*, ZAE-Bayern/UniWue, Würzburg, September 18-19, 2007, pp. 1-10.

Tenpierik, M.J., W.H. van der Spoel and J.J.M. Cauberg (2007), "Simplified Analytical Models for Service Life Prediction of a Vacuum Insulation Panel", In: A. Beck et al. (eds.), *Proceedings of the 8th International Vacuum Insulation Symposium*, ZAE-Bayern/UniWue, Würzburg, September 18-19, 2007, pp. 1-8.

2008

Malsen, J. van, M.J. Tenpierik, R.H.J. Looman and J.J.M. Cauberg (2008), "Heat seal strength of barrier films used in vacuum insulation panels at room temperature and at -130^{o}C", *J. of Plastic Film and Sheeting* 24 (1): 35-52.

Tenpierik, M.J., W.H. van der Spoel and J.J.M. Cauberg (2008), "Analytical Model for Predicting Thermal Bridge Effects due to Vacuum Insulation Panel Barrier Envelopes", *Bauphysik* 30 (1): 38-45.

Tenpierik, M.J., W.H. van der Spoel and J.J.M. Cauberg (2008), "An Analytical Model for Calculating Thermal Bridge Effects in High Performance Building Enclosure", *J. of Building Physics* 31 (4): 361-387.

Tenpierik, M.J., W.H. van der Spoel and J.J.M. Cauberg (2008), "Analytical Model for Computing Thermal Bridge Effects in High Performance Building Panels", In: C. Rode (eds), Proceedings of the 8th *Symposium on Building Physics in the Nordic Countries*, DTU/SBi/IDA, Copenhagen, June 16-18, 2008, pp. 9-16.

Also published in: Tenpierik, M.J., W.H. van der Spoel and J.J.M. Cauberg (2008), "Analytical Model for Computing Thermal Bridge Effects in High Performance Building Panels", *Nordic Journal of Building Physics,* special section for the 8th symposium on Building Physics in the Nordic Countries 2008, pp. 1 - 8.

Timmeren, A van, J. Kristinsson, R.M.J. Bokel, B.L.H. Hasselaar, A.K. Lassen, A.C. van der Linden, R.H.J. Looman, W.H. van der Spoel and M.J. Tenpierik (2008). "Climate integrated design of building skins", In: Knaack and Klein (eds.), *The future envelope 2: architecture - climate skin*, Delft, Delft University of Technology, pp. 57-66.

2009 and beyond

Baetens, R., B.P. Jelle, J.V. Thue, M.J. Tenpierik, S. Grynning, S. Uvsløkk and A. Gustavsen (in press), "Vacuum Insulation Panels (VIPs) for Building Applications: A Review", *Energy and Buildings* …

Tenpierik, M.J. and J.J.M. Cauberg (submitted), "Thermal Optimization of EPS encapsulated VIPs", *Building Research and Information* …

Tenpierik, M.J., J.J.M. Cauberg and W.H. van der Spoel (2009), "EPS encapsulated VIPs: A Thermal Performance Study", In: R. Ogden and M. Overend (eds.), Proceedings of the *9th International Vacuum Insulation Symposium*, High thermal performance and more space from thin insulations, Oxford Brookes University / University of Cambridge, London, September 17-18, 2009, pp. 1-10.

Tenpierik, M.J., A. van Timmeren, W.H. van der Spoel and J.J.M. Cauberg (2009), Vacuum Insulation panels and Architecture: Cradle-to-Cradle Façade Systems", In: A.A.J.F. van den Dobbelsteen et al. (eds.), *Proceedings of the 3rd CIB conference on smart and sustainable build environments*, TUDelft/CIB, Delft, June 15-19, 2009, pp. 1-8.

R3 CURRICULUM VITAE

Martinus Johannes Tenpierik was born on 11 June 1979 in De Bilt in the Netherlands. He studied at Delft University of Technology in the Netherlands from which he graduated with honours in both Architecture and Building Technology in 2003. Because of his graduation project, he obtained an honorary membership of the association for renewable insulation materials in the Netherlands ('vereniging voor vernieuwbare isolatiematerialen'). During his studies he participated in several organisations related to Delft University of Technology (student member of the advisory committee on education of the faculty of Architecture; board member of student association BouT).

In 2004 he started working as a research fellow at both the faculties of Civil Engineering and Architecture in Delft, resulting in the initiation in 2005 of a PhD research project aimed at studying the applicability of vacuum insulation panels in building constructions from a building physical, structural and architectural perspective. In 2006, his work was awarded the second prize for best poster on the symposium 'Integral Design of Structures'. In the framework of his PhD studies, he has published many papers in conference proceedings and in international scientific journals and has actively participated in several national and international research projects (EU/Craft - VACI: Vacuum Insulation for the Cooling Industry; IEA ECBCS - Annex 39 HiPTI: High Performance Thermal Insulation for buildings and building systems; SenterNovem EOS – Toepassingsmogelijkheden van vacuümisolatiepanelen in gebouwinstallaties; SenterNovem SMT – Vacuümisolatiepanelen geïntegreerd in bouwpanelen; SenterNovem EOS – Geprefabriceerde geïntegreerde elementen voor grootschalige LTV toepassing).

Besides his PhD studies, he also worked as a freelance architect for Architectuurstudio M.J. Tenpierik designing small-scale single-family houses and housing extensions.

SYMBOLS

S

SYMBOLS

ROMAN SYMBOLS AND ABBREVIATIONS

a	m	height of window opening
a	-	service life function
a	m	distance between load points
a_m	$W \cdot m^{-1} \cdot K^{-1}$	proportionality factor for obtaining wet thermal conductivity of a VIP
A	m^2	cross-sectional area
A	m^{-2}	parameter in linear thermal transm. formula
b	m	width
b	m	chamfer length
B	m^{-2}	parameter in linear thermal transm. formula
c	$m^3 \cdot kg^{-1}$ or $kg \cdot kg^{-1}$	capacity of getter and desiccant
c_{buc}	-	partial buckling coefficient
c_i	$g \cdot m^{-3}$	moisture production
c_{oj}	K	temperature of face sheet or barrier film in undisturbed area
C_p	$J \cdot kg^{-1} \cdot K^{-1}$	specific heat with constant pressure
c_V	$J \cdot kg^{-1} \cdot K^{-1}$	specific heat with constant volume
C	m^{-4}	parameter in linear thermal transm. formula
C_t	$€ \cdot m^{-2} \cdot yr^{-1}$	annual rent
d	m	thickness
d	m	diameter
D	m^{-4}	parameter in linear thermal transm. formula
e	$m^2 \cdot kg^{-1}$	mass specific extinction coefficient
e	$W \cdot m^{-1} \cdot K^{-1}$	parameter in linear thermal transm. formula
E	m^{-1}	extinction coefficient
E	-	eigenvector
E	$N \cdot m^{-2}$	Young's modulus
E-panel		VIP integrated panel with a metal encasing
E_a	$J \cdot mol^{-1}$	activation energy for permeation
Eco99	Milli-pt$\cdot m^{-2}$	environmental impact indicator
f	Hz	frequency
f	-	service life factor
f	$N \cdot m^{-2}$	stress (material property)
F	N	force
G	$N \cdot m^{-2}$	shear modulus
$G_{A;k}$	dB	air-borne sound reduction
h	m	height
HDT	^oC or K	heat deflection temperature
HSS	$N \cdot mm^{-1}$	heat seal strength

i	-	interest rate
I	m^4	area moment of inertia
I_{co}	dB(A)	structure-borne sound insulation index
I_{lu}	dB(A)	air-borne sound insulation index
K	$W \cdot m^{-1} \cdot K^{-1}$	thermal conductance of an edge
K_A	$€ \cdot m^{-2}$	cost of insulation material per square meter
$K_{R;spec}$	$€ \cdot W \cdot m^{-4} \cdot K^{-1}$	specific thermal insulation cost
K_V	$€ \cdot m^{-3}$	cost of insulation material per cubic meter
l^{2D}	m	simulated panel length
l_e	m	length of building plan including facades
l_i	m	length of building plan excluding facades
l_p	m	perimeter length or circumference
L	m	length
M	$kg \cdot mol^{-1}$	molar mass
M	$N \cdot m$	bending moment
M-panel		VIP integrated panel with a membrane envelope
m	kg	mass
m'	$kg \cdot m^{-2}$	mass per square meter
mfp	m	mean free path
n	-	number of stories of building
n	-	index of refraction
N	m^{-1}	parameter in linear thermal transm. formula
N	N	normal force
N_2TR	$cm^3 \cdot m^{-2} \cdot day^{-1} \cdot bar^{-1}$	nitrogen transmission rate
O_2TR	$cm^3 \cdot m^{-2} \cdot day^{-1} \cdot bar^{-1}$	oxygen transmission rate
p	Pa, mbar	pressure
$p_{1/2}$	Pa, mbar	typical gas pressure at which one half of the gas conductivity $\lambda_{g;0}$ has developed
P	$W \cdot m^{-2}$	power
q	$W \cdot m^{-2}$	heat flux
Q	W	heat flow
Q	$m^3(STP) \cdot m^{-2} \cdot s^{-1} \cdot Pa^{-1}$	
	$kg \cdot m^{-2} \cdot s^{-1} \cdot Pa^{-1}$	permeance
r	m	radius
r	$m^2 \cdot K \cdot W^{-1}$	thermal boundary resistance
R	$m^2 \cdot K \cdot W^{-1}$	thermal resistance
R_w	dB	sound attenuation
RH	%	relative humidity
s	m	width of a light beam
s'_t	$MN \cdot m^{-3}$	dynamic stiffness
S	m^2	surface area
S-panel		VIP integrated sandwich component
S_a	$m^2 \cdot kg^{-1}$	specific area
t	sec, min, yr	time
t	m	small thickness

$t'_{ac80,w,0,d}$	days	the number of days for which the relative humidity near the coldest point on the surface of a floor with floor cooling is higher than 80%
t_{sl}	yr	service life
T	^oC, K	temperature
u	$kg \cdot kg^{-1}$	water content
U	$W \cdot m^{-2} \cdot K^{-1}$	thermal transmittance
UBP97	$pt \cdot m^{-2}$	environmental impact indicator
v	$m^2 \cdot s^{-1}$	kinetic viscosity
V	m^3	volume
VST	^oC, K	vicat softening temperature
w	m	width (of spacer or edge region)
w_e	m	width of building plan including facades
w_i	m	width of building plan excluding facades
WVTR	$g \cdot m^{-2} \cdot day^{-1}(\cdot bar^{-1})$	water vapour transmission rate
x	m	mathematical position or distance
y	m	mathematical position or distance
z_0	m	distance from the top of the core material to the neutral plane of the entire cross-section of the damaged VIP

DIMENSIONLESS NUMBERS

Gr^*	-	modified Grasshoff number
Kn	-	Knudsen number
n	-	F_{buc} / N_d
Pr	-	Prandtl number
Ra^*	-	modified Rayleigh number
ξ	-	ratio $(\lambda_{film} t_{film}) / (\lambda_{facing} t_{facing})$
φ	-	ratio $\lambda_f t_f / \lambda'_f t'_f$

PHYSICAL CONSTANTS

d_c	$3.53 \cdot 10^{-10}$ m	collision diameter of air molecules
g	$9.81\ m \cdot s^{-2}$	specific gravity
k_B	$1.38 \cdot 10\text{-}23\ J \cdot K^{-1}$	Boltzmann constant
k_w	$2.898 \cdot 10^{-3}\ m \cdot K$	Wien's constant
N_A	$6.02 \cdot 10^{23}\ mol^{-1}$	Avogadro constant
R	$8.31\ J \cdot kg^{-1} \cdot K^{-1}$	universal gas constant
γ	1.4	ratio of specific heat at constant pressure and the specific heat at constant volume for air at STP
σ	$5.67 \cdot 10^{-8}\ W \cdot m^{-2} \cdot K^{-4}$	Stefan-Bolzmann constant

GREEK SYMBOLS

α	$W{\cdot}m^{-2}{\cdot}K^{-1}$	boundary heat transfer coefficient
α	-	sound absorption coefficient
α_k	-	accommodation coefficient
β	K^{-1}	thermal expansion coefficient
γ	rad	angle of incidence of light beam
δ	-	small change in ….
δ	m	average distance between the surfaces of two spheres for powder insulation or an equivalent average void diameter for foamed or fibre-based insulation materials
δ	$kg{\cdot}m^{-1}{\cdot}s^{-1}{\cdot}Pa^{-1}$	permeability
δ	m	displacement
ε	-	porosity
ε	-	strain
ζ	-	dimensionless variable used for computing the thermal performance of floor heating
η	-	dimensionless variable used for computing the thermal performance of floor heating
λ	$W{\cdot}m^{-1}{\cdot}K^{-1}$	thermal conductivity
λ	m^{-1}	eigenvalue
κ	m^{-1}	curvature
ν	-	Poisson's ratio
ξ	m^{-2}	load and span factor
ρ	$kg{\cdot}m^{-3}$	density or specific mass
σ	$N{\cdot}m^{-2}$	stress
τ	S, yr	time constant
ϕ	-	relative humidity
ϕ_q	$W{\cdot}m^{-1}$	heat flow per meter
$\phi\hat{}'_{w,0,d}$	%	the relative humidity near the coldest point on the floor surface of a floor with floor cooling
χ	$W{\cdot}K^{-1}$	corner thermal transmittance
X	-	dimensional variable in gas conduction equation
ψ	$W{\cdot}m^{-1}{\cdot}K^{-1}$	linear thermal transmittance

SUBSCRIPTS

0	initial state
0	unrestricted state
0	without thermal bridge
airgap	air gap
al	aluminium
av	average
b	floor finish
buc	buckling
c	core
c	concerning entire construction
c	compression
cool	concerning cooling
cop	centre-of-panel
corner	concerning the panel's corner
critical	critical
c;ups	upsetting of core material
d	design
dam	concerning a damaged VIP
des	desiccant
dry	concerning a dry state
e	concerning the panel's edge
e	external or exterior
edge	concerning the panel's edge
eff	effective
eps	expanded polystyrene
eq	equivalent
evac	in evacuated state
f	face sheets and/or barrier film
f	fibre
facing	face sheet
fail	structural failure
film	barrier envelope
g	gas
get	getter
gr	solid grains
heat	concerning heating
i	internal or interior
ins	insulation
k	area-related
kobru	thermal bridge
kr	related to the space below a floor
L	length-related
lab	concerning laboratory conditions
lim	limit
m	melt
p	panel
p	particle
p	pressure related
phys	physical failure
pl	plasticity state
pol	polymer or polyester
r	radiation
r	resonance
rup	rupture
s	solid (skeleton)
s	related to corner temperature
sat	saturation
span	span
steel	steel
storey	storey
surface	concerning a floor's surface
T	temperature related
tot	total
u	ultimate
vip	concerning a VIP
vl	screed
w	water
wv	water vapour
y	yield
ϕ	relative humidity related
'	concerning a property per square meter
'	concerning a property regarding the panel's edge

APPENDIXES TO CHAPTER 2

A

(pressed) fumed silica powder board - Wacker WDS®/HDK® or Degussa Aerosil®

Meso-porous silicates are minerals for which the main chemical building blocks are silicon surrounded by electronegative ligands. In many minerals, these ligands are oxygen atoms, very often co-ordinated tetrahedrally with the silicon atom centred. Silicates are the most predominant minerals within the Earth's crust, with quartz at a number one position. Natural silicates are the basic ingredients for many technical materials, like cement, glass and porcelain (Eberhardt, 2005). As potential core material, two types of silicate are of importance: precipitated silica and pyrogenic or fumed silica. The first can be produced at lower cost than the latter but has coarser pores (a factor 3) as a result of which it is less suitable for VIPs[1] (Cremers, 2006c).

In the 1940s, pyrogenic or fumed silica became available at low costs, as a consequence of which it replaced aerogels in many applications. In 1942 Harry Kloepfer at Degussa Corp first invented this type of nano-structured silica-based material (Fricke et al., 2008). By burning an organic precursor at 1200 ^{o}C (high-temperature hydrolysis and condensation), he obtained a silica powder, sold under the name Aerosil® (Fricke, 2005; Eberhardt, 2005). The production process (flame process) is according to the following chemical reaction: $SiCl_4 + 2\ H_2 + O_2 \rightarrow SiO_2 + 4\ HCl$. During this process silica-aggregates of about 10 to 100 μm in size are formed, which contain at their surfaces isolated reactive silanol-groups (SiOH-groups). These groups can bind different gases and thus act as getters prolonging the life span of a VIP (Randel 2003). Before the silica particles are pressed into boards, glass fibres and opacifiers, like 10 to 20 %mass silicon carbide (Napp et al., 1999), are added for increased integrity and reduced radiative heat transfer. Before the panel is finally evacuated and the laminate sealed, the fumed silica board should be heated to about 110^{o}C to remove all water (vapour).

The disadvantage of the original Aerosil® for VIP application is that the powder particles need to be retained during the process of evacuation. For vacuum insulation panels therefore compressed powder boards are therefore used, like Wacker WDS. Wacker WDS is highly dispersed fumed silica (Hoch-disperse Kieselsäure), containing SiO_2 (65%), ferric oxide (about 30%) and TiO_2 as IR-absorber or silicon carbide as opacifier (Wacker, 2003). Like all silica-based insulator materials it can be used as a high-temperature insulator (up to 1000 ^{0}C) as well as a low-temperature insulator (down to -190 ^{0}C). For a vacuum insulated panel

[1] As explained in chapter 3, the smaller the pore size, the less stringent the requirements on the vacuum needed to obtain high thermal performance. Therefore a core material with very small pores, preferably within the nanometer range, is advocated.

this means that the service temperature range is determined by the properties of the foil alone. WDS has a relatively high density of 140 to 340 kg/m^3, is non-toxic and non-flammable (Wacker, 2003).

WDS, from Wacker Chemie GmbH, is highly dispersed fumed silica containing SiO_2 (80%), and TiO_2 or silicon carbide (15%) as opacifier[2] (Wacker, 2003). Like all silica-based insulator materials, it can both be used as a high-temperature (up to 1000°C) and a low-temperature insulator (down to -190 °C). The low thermal conductivity at high temperatures is due to the small contact points between the different SiO_2-particles and the small void sizes that reduce gas conduction. WDS has a relatively high density of 120 to 340 kg·m^{-3}, is non-toxic, non-flammable and produces hardly any dust during production (Wacker, 2003). Disadvantages of the fumed silica boards are their high price and their sensitivity to moisture.

Aerogel – Cabot Nanogel®

Aerogels are meso-porous insulator materials, produced from water glass. Their small pore size, which on average can be between 20 and 150 nm (Hüsing and Schubert, 1998), is favourable for application in VIPs. Moreover, their thermal stability makes aerogels excellent high-temperature insulators, up to a temperature of 800°C. Other interesting properties of aerogel are its sound absorbance[3], hydrophobity, UV-stability, recyclability, non-flammability and light transmittance provided that no opacifier is added[4]. A disadvantage, though, is its brittleness. This reduces the application of aerogels to situations where no tensile or small compressive forces act on the insulation material. Despite some disadvantages aerogels are promising insulator materials. Aerogels based on silica, alumina or ferric oxides all have similar properties.

The original production process of aerogels was quite difficult and therefore expensive due to the so-called supercritical drying process (Cabot, 2003). If the gel is dried in air, the surface tension of the evaporating liquids compress the delicate structure of the lattice and free hydroxyl-groups cement the shrunken gel together, leaving a hard glassy substance, the volume of which is reduced to some percent of its original volume. To tackle this problem, Kistler (Kistler, 1932) developed a

[2] In general, the following substances might be used as opacifier: carbon black, titanium oxide, iron oxide and silicon carbide (Cremers, 2005).

[3] Bulk Nanogel® has similar sound absorbing characteristics to mineral fibre insulation (Cabot, 2003).

[4] Cabot (Cabot, 2003) states that the light transmittance through Nanogel® is more than 80% per cm. Cremers (Cremers, 2005) explains that aerogels come in three forms: as powder, as granules, and as a monolith. Only the granular and monolithic forms are to some extent translucent.

technique to dry the gel without collapsing the structure. This technique is called supercritical drying. He used the phenomenon that above a certain critical temperature and pressure a fluid becomes supercritical, thus loosing its surface tension. So, without surface tension the tenuous structure of the drying gel is not affected. However, the costly process, the required safety precautions and the expensive raw material hindered a large-scale commercial production.

In the 1990s, another production method was developed at the University of New Mexico using the process of silation to modify the internal surface structure of the hydrogel (Fesmire, 2006). After the production of the hydrogel ,a silating agent ($HOSi(CH_3)_3$) is added to the substance. The hydroxyl-part of the silating agent reacts with the six hydroxyl-groups of the hydrogel ($SiO_2(OH)_6$) molecules. The structure formed in this way keeps the internal structure of the gel intact during the drying process. As a consequence, lower temperatures and pressures can be applied. Nowadays, the following chemical reaction (wet chemical sol-gel process) is used to produce aerogels: $Na_2SiO_3 + 2\ HCl + n\ H_2O \rightarrow SiO_2 \cdot H_2O + 2\ NaCl + m\ H_2O$. The conditions for this polymerization process, such as temperature, pH-value, time and silicate concentration, define the exact properties. To give the aerogel sufficient strength, fibre glass is often mixed with the gel. Opacifiers, like Carbon Black, may also be added to suppress radiation heat transfer. (Cabot, 2003).

Low density rigid PU-foam – Elastogran Elastocool® or ICI/Huntsman Vacpac®

Polyurethane foam normally comes as a closed-cell polymer foam with a density higher than 28 $kg \cdot m^{-3}$ to maintain its stiffness and lower than 50 $kg \cdot m^{-3}$ to have a low overall thermal conductivity (Brodt, 1995). Its effectiveness as a thermal insulant depends mainly on the presence of a gas phase within the closed cells with a lower thermal conductivity than air[5]. This so-called blowing agent is a remnant of the production process and permeates very slowly out of the foam, thus creating a long life span of the product. In the production process the chemically inert blowing agent is mixed very quickly with the basic polymer ingredients. The polymerization reaction that then occurs is exothermic and can be described with the following reaction (most common way of manufacturing PU):

$$OH\text{-}R\text{-}OH + \text{diisocyanate} + H_2O + BA \rightarrow \text{Polyurethane} + CO_2 + BA$$

During this reaction the blowing agents vaporize and expand in volume. Together with the presence of CO_2-gas this leads to a gas-filled void structure, resulting in a porosity of up to 97% (Ewing, 2005). Another advantage of the presence of a

[5] The thermal conductivity of a CFC-11 filled polyurethane foam insulation board of 35 mm can be as low as $17 \cdot 10^{-3}\ W \cdot m^{-1} \cdot K^{-1}$ directly after production and increases to about $35 \cdot 10^{-3}\ W \cdot m^{-1} \cdot K^{-1}$ after several decades (Brodt, 1995).

blowing agent during production is its ability to take up heat, which lowers the foam reaction temperature. This is important because the permeation of CO_2 out of the foam depends on temperature; the higher the temperature, the higher the permeation rate. So, with lower reaction temperatures, the CO_2 will be present in the voids at least until the moment that the foam has reached sufficient strength to withstand external pressure on its own. This will take approximately 1 minute from blending (Woods, 1990).

If the Polyurethane foam is to be applied as filler for vacuum insulation panels, the cell structure must be opened and preferably the pore size minimized. Besides, the strength and stiffness must be sufficient to withstand an external pressure of 1 bar. Opening the cells of the foam is a very delicate procedure, because none of the cells may be left closed. The gases present in the still closed cell would otherwise permeate through the foam, raising the gas pressure and thus the thermal conductivity in the entire foam.

A disadvantage of open-celled Polyurethane foam is its sensitivity to pressure increases at relatively low gas pressure already (Simmler et al., 2005; Fricke et al., 2006). A pressure rise from 0.1 mbar to 1 mbar leads to an increase of the thermal conductivity by about 90% (from about $8.5 \cdot 10^{-3}$ to $16 \cdot 10^{-3}$ $W \cdot m^{-1} \cdot K^{-1}$), compared to an increase of only 2% (from $3.6 \cdot 10^{-3}$ to $3.7 \cdot 10^{-3}$ $W \cdot m^{-1} \cdot K^{-1}$) for fumed silica (Elastogran, 2005; Caps et al., 2001). This makes Polyurethane foam less fit for VIPs. Potential applications are those areas where weight is critical. Another disadvantage is the limited thermal stability; the service temperature has an upper limit of 105°C (IRC NRC, 2004). This makes Polyurethane unqualified for high temperature applications. Moreover, the material cannot (yet) be recycled.

Extruded Polystyrene foam – Dow Instill®

Extruded Polystyrene foam, like PU foam, normally is a closed cell polymeric foam. So to be effective as a core material for vacuum insulation panels the cell structure must be opened to make evacuation of the pores possible. Such a micro cellular open cell variant is INSTILL, once produced by the Dow Chemical Company but no longer available. XPS-foams have several advantages and disadvantages.

A first disadvantage is that, like with all materials with coarse pores, the thermal conductivity is at the 0.1 mbar to 100 mbar pressure range very sensitive to changes in internal gas pressure, although its performance is slightly better than that of open cell rigid Polyurethane foam[6] (Dow Chemical, 2004). A second

[6] According to Tseng and Chu (2009), adding about 2% polyethylene (PE) to XPS foam may improve the thermal performance of this insulation material. In their studies they were able to reduce the thermal conductivity of a vacuum insulation panel filled with this improved XPS

disadvantage is outgassing. Since it is very difficult to manufacture polymeric foams with 100% open cells, outgassing might cause a severe problem for application in VIPs if the foam is not stored and dried before application (Cremers, 2006c). Another disadvantage all polymer foams have in common is the limited thermal stability; the upper service temperature limits at 88 ^{0}C (Dow Chemical, 2004), which is even lower that the maximum allowable temperature of PU-foam.

Advantages however are its low mass density, its low production cost and the ease of its handling making the material a good candidate for those situations where mass is more important than thermal conductivity or ageing properties. The material can also be recycled. Moreover, INSTILL is an inert non-hygroscopic core material. This has the advantage that the material, when stored under normal circumstances, needs no pre-conditioning (drying) before it can be used in a vacuum insulation panel. This reduces production cost and time and creates the possibility of producing the VIP elsewhere. A manufacturer, however, can decide to dry the material before it is used, which reduces the evacuation time. Evacuation times generally vary from 2 to 3 minutes for small panels (Dow Chemical, 2004). This so-called pump down time, though, depends very much on the evacuation procedure, the equipment and the panel size. Besides, it can be shaped easily for example with a hot wire or hand saw with minimal dusting.

Fibre glass insulation – Johns Manville

Fibre glass blankets might be used as VIP core materials, as well. These boards consist of heat treated, pressed and oriented glass fibres (Fay, 1991; Zhao et al., 2009). Fibre orientation is an important issue when applying these blankets as a VIP core. The fibres having a relatively high thermal conductivity easily transfer heat from one side of the panel to the other if oriented in a direction perpendicular to its surface. As a consequence, the fibres need to be oriented in in-plane direction causing anisotropy regarding thermal conductivity. At very low gas pressure, the thermal conductivity of fibre glass insulation blankets in a direction perpendicular to its surface can be as low as $1.5 \cdot 10^{-3}$ $W \cdot m^{-1} \cdot K^{-1}$ at room temperature. The requirement for fibre orientation also makes these insulation blankets relatively expensive (Cremers, 2006c). Another disadvantage of fibre glass blankets is their lack of mechanical stiffness causing large shrinkage when evacuated and outgassing of the binder resin (Fay, 1991). Fibre glass insulation therefore is only practicable for VIPs that have a stiff encasing of its own, like sheet-VIPs.

---

foam from $6.5 \cdot 10^{-3}$ $W \cdot m^{-1} \cdot K^{-1}$ to $4.4 \cdot 10^{-3}$ $W \cdot m^{-1} \cdot K^{-1}$ which is almost as good as fumed silica based VIPs.

Metal foil laminates

Metals can be considered among the materials with the lowest permeability to water vapour and atmospheric gases. From a certain thickness onwards, metals can be considered as completely gastight. Two types of metal foil laminates are currently in use for VIPs: the aluminium foil laminates (AF) and the stainless steel foil laminates (SSF). AF laminates mainly consist of an aluminium layer of 5 to 12 μm, with on one side a protective polymeric top layer, e.g. PA, PE or PET, which protects the aluminium from being punctured by small particles, inhibits corrosion and strengthens the film, and on the other side a sealing layer, e.g. PE or PET, which gives the foil the ability of being sealed. Sometimes an additional barrier layer is added to the configuration. The different layers are kept together by means of an adhesive. A stainless steel foil usually has a thickness of 25 μm to 50 μm.

In these laminates, the main barrier layer is the aluminium or stainless steel foil. This is a highly effective barrier against vapour and gas permeation with an oxygen transmission rate below what is currently detectable: $5 \cdot 10^{-3}$ $cm^3 \cdot cm \cdot m^{-2} \cdot day^{-1} \cdot bar^{-1}$ (Reisacher, 2003). Moreover, its barrier properties are hardly affected by environmental conditions as well (temperature, relative humidity and mechanical stresses). The great disadvantage of these layers, though, is their high thermal conductivity (λ_{Al} = 160 to 225 $W \cdot m^{-1} \cdot K^{-1}$ and λ_{steel} = 15 to 25 $W \cdot m^{-1} \cdot K^{-1}$). Together with the thickness required for the barrier function, this leads to a large amount of heat being transferred via the edges of the VIP. Minimizing the thickness of the aluminium or steel layer is not always possible. Below a certain thickness of the layer, especially below about 6 μm for aluminium foils, so-called pinholes occur in the material layer. These microscopic defects, which are a remnant of the rolling process, form small channels through the barrier and increase the permeability of the foil considerably.

One way to minimize thermal bridge effects is reducing the thickness of the aluminium layer at the edges to zero and replace it here with a less conducting material. This way the aluminium layer only covers the large facings perpendicular to the main heat flow. The overall gas tightness of the panel only decreases moderately, whereas the thermal properties of the panel significantly improve (Brodt, 1995).

Metal deposition films / metallised film laminates

To reduce the thermal edge effect of metal foil laminates, the thickness of the metal layer in these films must be minimized. But in very thin metal films so-called pinholes increase the permeability considerably. A solution to this problem is depositing thin metal or metal oxide layers on a carrier film. One technique to accomplish this is called vacuum deposition. Metal deposition layers often have a thickness approximately varying from 30 to 100 nm while aluminium oxide or silicon oxide deposition layers only have a thickness of about 10 nm. These deposition layers thus are considerably thinner than the aluminium foil used in metal foil laminates (Eicher et al., 2000). Metallised film laminates thus combine relatively good barrier and good thermal properties[7]. However, due to thinner metal or oxide layers the barrier quality of these laminates is less than that of metal foil laminates but better than that of laminated polymer films. Typical values for the oxygen and water vapour transmission rate are below $1 \cdot 10^{-2}$ $cm^3 \cdot m^{-2} \cdot day^{-1} \cdot bar^{-1}$ at 23^oC and 0.1 $g \cdot m^{-2} \cdot day^{-1} \cdot bar^{-1}$ at 38^oC and 90% RH respectively (Reisacher, 2003).

Typical metallised laminates consist of two or three aluminium, aluminium oxide or silicon oxide layers deposited on multiple polymer substrates[8], e.g. PET, PP, PE or PA. Besides these metallised polymer layers, a sealing layer of PE or PET is added too. Since many of these polymers are transparent or at least translucent, the appearance of the laminate is dominated by the deposition layer: silvery for aluminium or aluminium oxide and transparent or translucent for silicon oxide. 'Metallised' film laminates with silicon carbide depositions combined with translucent aerogel thus open up new perspectives for highly efficient translucent insulation. Disadvantages of metallised film laminates (MF) are their sensitivity to cracking due to flexion, their moderate tearing strength, risk of delaminating and their properties being strongly influenced by environmental conditions.

Laminated polymer films

Because single polymer layers would not fulfil all of the requirements for a high barrier envelope, several polymers are laminated together using PU adhesive or co-extruded to form a composite polymeric laminate. Three basic layer functions, which are also present in the aforementioned barrier laminates, can be identified from the inside tot the outside: sealing layer, barrier layer and protective layer. The sealing

---

[7] Oxide deposition layers, like silicon oxide, even have a lower thermal conductivity than metal deposition layers. The thermal conductivity of a metal deposition layer is about 200 $W \cdot m^{-1} \cdot K^{-1}$ (Ghazi Wikili et al., 2004) while that of a silicon oxide deposition layer is approximately 0.8 $W \cdot m^{-1} \cdot K^{-1}$ (Cremers, 2005).

[8] Although aluminium oxide and silicon oxide are no metals, in this dissertation polymers on which one of these layers are deposited are still called metallised films.

and protective layers regularly consist of one material each. The barrier layer on the other hand can be constructed from multiple films. Figure A22.1 presents an overview of transmission rates of some materials and Table A22.1 shows the effect of laminating on oxygen transmission rate.

The permeability of most of the polymeric barrier films is rather high, relative to metal foil laminates and metal deposition films; typically the oxygen and water vapour transmission rates are hardly below $1 \cdot 10^{-2}$ $cm^3 \cdot m^{-2} \cdot day^{-1} \cdot bar^{-1}$ at 23°C and 0.1 $g \cdot m^{-2} \cdot day^{-1} \cdot bar^{-1}$ at 38°C and 90% RH respectively (Reisacher, 2003). Moreover barrier properties are highly dependent on the environmental conditions under which the foil must operate. High temperatures and high relative humidity increase the permeability enormously. Lifetimes of VIPs with laminated polymer films are thus rather low. But nonetheless they can be used for those applications where product lifetimes are low. In these cases the low thermal conductivity of polymers - and thus the absence of any thermal edge effect - can be exploited. Recent developments, though, have improved the barrier properties of laminated polymer films considerably. One of these improved films is the so-called Mylar® film (DuPont Teijin Films, 2004). This film was especially designed for vacuum insulation panel applications.

Table A22.1 – *Oxygen transmission rate of some polymer laminates (DuPont Teijin Films, 2004)*

Barrier laminate	O_2TR [$cm^3 \cdot m^{-2} \cdot day^{-1} \cdot bar^{-1}$]
PET	138
PET + PVDC	7.65
PET + PVDC + deposited metal	0.15

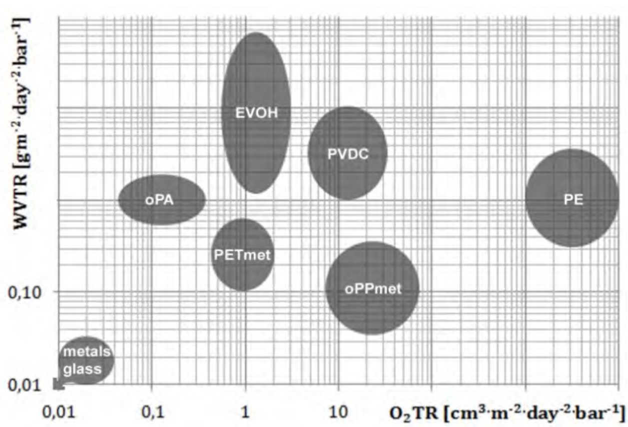

Figure A22.1

Oxygen and water vapour transmission rates of several polymers and metallised polymers according to Levebre (2001).

A23 Other Materials and Devices Applied in VIPs

Besides the components mentioned in section 2.5, i.e. core material, barrier envelope and getters/desiccants, several other components might be present in vacuum insulation technology: spacers, evacuation valves and metering aids.

Spacers are used in vacuum insulating glass to maintain a distance between the two sheets or in VIPs with a core which lacks sufficient stiffness to resist a 1 bar pressure difference. In case of vacuum insulating glass, these spacers are cylindrical or spherical support pillars made of ceramics, like alumina, or metals, like stainless steel or Inconel 718 (a nickel based alloy) (Wilson et al., 1998). Their size varies between 0.25 to 0.50 mm in diameter and 0.1 to 0.2 mm in height (Simko et al., 1998). A result of all types of spacers is an increased heat flow though the panel thus decreasing its thermal performance.

Evacuation valves are typically used in vacuum insulation with thick envelopes: Vacuum insulation glass and sheet-VIPs. They were used in the first generation of film-VIPs too but caused many problems with gas tightness (Cremers, 2006c). Using evacuation valves changes the VIP's production process: In stead of first evacuating the core and then sealing the envelope in a vacuum chamber, the complete envelope is closed first under normal atmospheric conditions and then evacuated through the evacuation valve. The valve is then closed using a Viton ring (ThyssenKrupp tempsafe, 2003). A disadvantage of an evacuation valve is that it is a potential weak spot in the barrier envelope, especially in case of film-VIPs. An important advantage however is the ability to repair and re-evacuate a panel when it is vented. Moreover, the size of the panel is no longer limited to the size of the vacuum chamber.

Metering aids are materials or devices that are added to a VIP in order to be able to quantitatively measure or qualitatively indicate the thermal quality of the panel. Determining the quality of a VIP is important for both quality assurance of panels leaving the factory and for determining damaged panels after installation on site. Several methods of determining the quality exist. Most of them are based on estimating the gas pressure inside the core material[9] (Caps et al., 2008). Some of these methods, like the foil lift-off method[10] and IR-thermography[11] do not require

[9] It is not possible to determine the exact thermal performance of a VIP core by solely measuring the gas pressure. As will be explained in Chapter 3 and 5, liquid water absorbed by this core also influences its thermal conductivity (Simmler et al., 2005; Schwab et al., 2005). Determination of the water content is therefore important as well. Measuring the gas pressure however does give a good indication of whether a VIP is still intact or not.

[10] The foil lift-off method is based on the principle that the thin barrier envelope of a VIP will lift off if the pressure surrounding the VIP is below the pressure inside the VIP. A VIP is therefore placed in a small chamber in which the air pressure can be lowered to very small

material or devices added to the VIP while other methods, like the spinning rotor gauge method[12], the Va-Q-check® method[13], the Vac-Intact® method[14] and the method using RFID-tags[15] do. A complete overview of measuring devices is presented in Cremers (2006c), Simmler et al. (2005) and Caps et al. (2008).

---

values. Then the air pressure in this chamber is slowly reduced while at the same time the position of the surface of the envelope is monitored by a laser. The pressure at which the envelope starts to lift off then equals the pressure in the core (Caps et al., 2008; Eberhardt, 2005; 2009; Simmler, 2001). A disadvantage of this method is that it may damage a panel.

[11] Infrared thermography uses the principle that all matter having a temperature above 0 K emits radiation and that the wavelength at which it emits the most energy depends on temperature according to Wien's law. For a temperature typical for the built environment this peak is within the infrared wavelength range, from 780 nm to 400 μm. Besides, the emissivity of the surface material also has a big influence on the IR-image. Vented VIPs can be distinguished from intact VIPs since they have a higher surface temperature on the outside. This method however only works if the panels are not installed in a back-ventilated façade or a façade with thick highly conducting layers around the VIP (Binz et al., 2005).

[12] The spinning rotor gauge method uses the principle that the friction between a rotating steel ball and the residual gas inside the VIP core depends on the gas pressure of this gas. The deceleration of the rotating ball, suspended in a magnetic field and made to rotate by a fluctuating magnetic field, is measured. The relative decrease in spinning frequency is a measure of the gas pressure of the residual gas (Caps et al., 2008).

[13] The Va-Q-check® method, developed by Va-Q-tec AG, uses a 0.2 mm thick fibre fleece and a 0.5 mm thick metal plate both with a diameter of 30 mm and installed into a VIP directly below the barrier envelope. An external sensor head, which is heated to about 70°C, is then pressed onto the barrier envelope on top of the fleece. The heat of the sensor head then flows through the barrier laminate and the fleece into the metal plate, which acts as a heat sink. After a few seconds a steady-state condition is obtained. Since this measurement time is short, the heat sink does not significantly change its temperature thus allowing an estimation of the thermal resistance of both the fleece and barrier laminate by measuring the heat flow with a meter integrated into the measurement head. These thermal resistances are then used to determine the thermal conductivity of the fleece from which in turn the internal gas pressure is estimated. Several types of fleece material are available, the choice for which depends on the required sensitivity within a certain pressure interval (Caps et al., 2008; Caps, 2005; Eberhardt, 2009).

[14] The Vac-Intact® method, developed by Tuscarora Inc. of the ISC group, uses a spring which is put into a cylindrical gap in the VIP core. If the VIP is evacuated, a 1 bar pressure difference will act over the spring as a result compressing it. This is visible as a dent in the surface of the VIP. If the VIP however is vented, the spring is not compressed creating a bubble on the VIP surface. This method is only able to distinguish vented from intact VIPs (Cremers, 2005).

[15] This method uses so-called radio frequency identification tags to transmit data from this RFID-tag, or a sensor connected to it, to a remote reader. Va-Q-tec AG (Caps et al., 2008) developed a pressure-sensitive device based on RFID techniques. As long as the internal gas pressure is below 600 mbar, this device transmits a signal to a passive RFID-tag which in turn transmits its signal to an external reader at a distance of several tens of centimeters. If the VIP is vented, the device does not transmit a signal (Caps et al., 2008). This method is thus able to distinguish between intact and vented VIPs. The advantage is that the method does not require a device to visibly see or make direct contact with the surface of the VIP.

A24 GETTERS AND DESICCANTS

A getter is a 'device' which physically absorbs or chemically binds gases up to its saturation point; a desiccant is a substance which physically binds water molecules up to its saturation point. These substances are thus able to remove gas and water molecules from the core's pores. During the service lifetime of a VIP the gas pressure in its core will increase steadily. Directly after production the rate at which this pressure increases may be higher than a few weeks afterwards due to possible outgassing of the core and the barrier. This degradation of the internal vacuum can be alleviated or at least postponed by adding getters and desiccants to the inside of the panel. Another advantage of these devices is that the initial pressure of the vacuum does not have to be as low as without getter or desiccant, because some of the residual gases are captured and taken from the vacuum.

Gases that have the most profound influence on the quality of the vacuum are water vapour (H_2O), oxygen (O_2) and nitrogen (N_2), because of the relative abundance of these gases in our atmosphere. The effect of other gases present in air (CO_2, CO, Ar) is more-or-less negligible. N_2, O_2 and CO_2 may be gettered by Barium or Lithium. Some getters are specifically designed to capture one specific gas. However, most getters used in VIPs are designed as combo-getter (Manini, 1997; Manini, 1999). Several materials can be used as desiccant. The most common is calcium oxide (CaO). Alternative vapour-absorbers are molecular sieve, silica gel, clay or calcium sulfate ($CaSO_4$). Calcium- or Cobalt- and Barium oxide can be used as well. Table A24.1 presents some qualitative information about different desiccants. The amount of getter or desiccant and the exact type are determined by the type of core, the type of barrier, the panel size and the required service life.

***Table A24.1** – Properties of desiccant material (van Went, 2002).*

Property	Molecular sieve	Silica gel	Clay	Calcium oxide
Low RH capacity	outstanding	insufficient	moderate	outstanding
Adsorption rate	very high	high	high	slow
Capacity at 25°C / 40% RH	high	high	moderate	high
High temperature capacity	outstanding	insufficient	insufficient	high

Table A24.2 – *Gettering capacity of SAES Getters Combogetter® (Model 5M1040) (Manini, 1999)*

Gas	**Capacity [mbar·l]**
Air	5.3
CO / CO_2	8
H_2	93
H_2O	800
Blowing agents (Cyclopentane and R141b)	1.3

Appendixes to Chapter 3 A

A31 DERIVATION OF THERMAL BRIDGE EQUATION FOR λ_C = 0 W·M^{-1}·K^{-1}

The thermal bridge due to the continuous high barrier laminate enveloping a VIP can be schematically represented as in Figure A31.1. For the derivation of the approximation model the following are assumed:

- The length of the vacuum insulation panel is infinite. At a defined distance x and y from the origin, the temperature of the foil at surface i, therefore, equals the surrounding air temperature, T_i. At that point the influence of the thermal bridge on the temperature of the laminate has diminished.
- The boundary heat transmission coefficient α_i is constant across the surface of layer i and the temperature within the barrier laminate T_j (j=x or j=y) is constant over the cross-section through this laminate.
- Additional radiative heat transfer processes that are not covered by the heat transmission boundary coefficients, α_i, are not considered.
- No lateral heat exchange between different VIPs in the panel edge region occurs.
- The thermal conductivity of the core material, λ_c, equals 0 W·m^{-1}·K^{-1}.

Based on these assumptions, the following differential equations can be derived for the temperature distribution in the laminate (Cauberg, 2000):

$$\frac{d^2T_x}{dx^2} = N_1^2(T_x - T_1) \qquad \text{(A31.1a)},$$

$$\frac{d^2T_y}{dy^2} = N_2^2(T_y - T_2) \qquad \text{(A31.1b)},$$

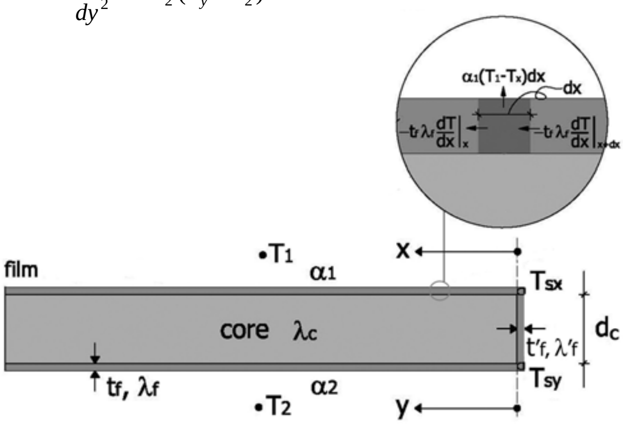

Figure A31.1

Schematic representation of the thermal bridge arising from the thin film high barrier envelope around a vacuum insulation panel with N_j defined as:

$$N_j = \sqrt{\frac{\alpha_i}{t_f \lambda_f}} \qquad \text{(A31.2).}$$

In these equations and in the figure, α_i [W·m^{-2}·K^{-1}] is the heat transmission coefficient at boundary surface 1 or 2 respectively, d_p [m] is the thickness of the core of the vacuum insulation panel [m], t_f [m] is the thickness of the foil, λ_f [W·m^{-1}·K^{-1}] is the thermal conductivity of the foil, λ_c [W·m^{-1}·K^{-1}] is the thermal conductivity of the core, T_i [K] is the air temperature on side1 or 2 respectively, T_x [K] is the temperature of the barrier laminate in x-direction corresponding to side 1 and T_y [K] is the temperature of the laminate in y-direction corresponding to side 2.

The solutions for the temperature T_x and T_y based on Equation (A31.1a) and (A31.1b) and the boundary conditions according to Figure A31.1 are:

$$T_x = T_1 + (T_{sx} - T_1)\frac{e^{N_1(L_1-x)} - e^{-N_1(L_1-x)}}{e^{N_1L_1} - e^{-N_1L_1}} \qquad \text{(A31.3a),}$$

$$T_y = T_2 + (T_{sy} - T_2)\frac{e^{N_2(L_2-y)} - e^{-N_2(L_2-y)}}{e^{N_2L_2} - e^{-N_2L_2}} \qquad \text{(A31.3b).}$$

L_1 and L_2 [m] are the distances from x=0 and y=0 to the points where the effect of the thermal bridge on the laminate (surface) temperature has become insignificant and T_sx and T_sy [K] are the temperatures of the laminate at the corner of the panel on side 1 and 2 respectively. Equations (A31.3a) and (A31.3b) can be rearranged to:

$$T_x = T_1 + (T_{sx} - T_1)\left(\frac{e^{+N_1L_1}e^{-N_1x} - e^{-N_1L_1}e^{+N_1x}}{e^{N_1L_1} - e^{-N_1L_1}}\right) \qquad \text{(A31.4a),}$$

$$T_y = T_2 + (T_{sy} - T_2)\left(\frac{e^{+N_2L_2}e^{-N_2y} - e^{-N_2L_2}e^{+N_2y}}{e^{N_2L_2} - e^{-N_2L_2}}\right) \qquad \text{(A31.4b).}$$

Under the conditions given in Figure A31.1, the heat flow, ϕ_q [W·m^{-1}], at x=0 must satisfy the following condition:

$$\phi_q = -t_f \lambda_f \frac{dT_y}{dy} = -t_f^{'} \lambda_f^{'} \frac{(T_{sy} - T_{sx})}{d_p} \qquad \text{(A31.5a),}$$

with t'_f [m] the thickness of the laminate at the edge (including seam) and λ'_f [W·m^{-1}·K^{-1}] the thermal conductivity of the laminate at this edge. This equation can be rewritten as:

$$-t_f \lambda_f \frac{dT_y}{dy} = -K(T_{sy} - T_{sx}) \quad \text{(A31.5b)},$$

with $K = \lambda'_f t'_f / d_p$, of which the reciprocal value is the resistance between x=0 and y=0. If Equations (A31.4a) and (A31.4b) are differentiated and multiplied with $-t_f\lambda_f$, the following equations are obtained:

$$-t_f \lambda_f \frac{dT_y}{dy} = +t_f \lambda_f N_2 (T_{sy} - T_2) \left[\frac{e^{N_2(L_2-y)} + e^{-N_2(L_2-y)}}{e^{N_2L_2} - e^{-N_2L_2}} \right] = -K(T_{sy} - T_{sx}) \quad \text{(A31.6a)},$$

$$+t_f \lambda_f \frac{dT_x}{dx} = -t_f \lambda_f N_1 (T_{sx} - T_1) \left[\frac{e^{N_1(L_1-x)} + e^{-N_1(L_1-x)}}{e^{N_1L_1} - e^{-N_1L_1}} \right] = -K(T_{sy} - T_{sx}) \quad \text{(A31.6b)}.$$

For $y \rightarrow 0$ the middle term of Equation (A31.6a) becomes:

$$\lim_{y \to 0} t_f \lambda_f N_2 (T_{sy} - T_2) \left[\frac{e^{N_2(L_2-y)} + e^{-N_2(L_2-y)}}{e^{N_2L_2} - e^{-N_2L_2}} \right] = t_f \lambda_f N_2 (T_{sy} - T_2) \left[\frac{e^{N_2L_2} + e^{-N_2L_2}}{e^{N_2L_2} - e^{-N_2L_2}} \right]$$

(A31.7).

Under the assumption that $N_2L_2 >> 0$, and thus that $e^{-N_2L_2} \approx 0$ Equation (A31.7) can be simplified to:

$$t_f \lambda_f N_2 (T_{sy} - T_2) \left[\frac{e^{N_2L_2} + e^{-N_2L_2}}{e^{N_2L_2} - e^{-N_2L_2}} \right] = t_f \lambda_f N_2 (T_{sy} - T_2) \quad \text{(A31.8)}.$$

Combining Equations (A31.8) and (A31.6a) yields:

$$t_f \lambda_f N_2 (T_{sy} - T_2) = -K(T_{sy} - T_{sx}) \quad \text{(A31.9a)}.$$

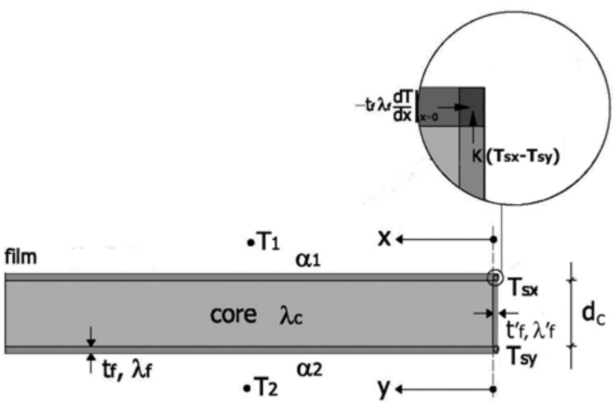

Figure A31.2

Schematic representation of the heat balance in the barrier envelope at the corner of a vacuum insulation panel

The same analysis for the *x*-direction results in:

$$t_f \lambda_f N_1 (T_{sx} - T_1) = +K(T_{sy} - T_{sx}) \quad \text{(A31.9b).}$$

By equating (A31.9a) and (A31.9b), T_{sy} and T_{sx} can be expressed as follows:

$$T_{sy} = \frac{t_f \lambda_f N_2 (t_f \lambda_f N_1 + K) T_2 + t_f \lambda_f N_1 K T_1}{\left[(t_f \lambda_f N_2 + K)(t_f \lambda_f N_1 + K) - K^2\right]} \quad \text{(A31.10a),}$$

$$T_{sx} = \frac{t_f \lambda_f N_1 (t_f \lambda_f N_2 + K) T_1 + t_f \lambda_f N_2 K T_2}{\left[(t_f \lambda_f N_2 + K)(t_f \lambda_f N_1 + K) - K^2\right]} \quad \text{(A31.10b).}$$

The heat flow through the high barrier laminate at the panel edge, i.e. the thermal bridge, can now be calculated as:

$$\phi_q = t_f^{'} \lambda_f^{'} \frac{(T_{sy} - T_{sx})}{d_p} = K(T_{sy} - T_{sx}) \quad \text{(A31.11).}$$

Combining Equations (A31.10a), (A31.10b) and (A31.11) leads after some rearranging to

$$\phi_q = \frac{1}{\dfrac{1}{K} + \dfrac{1}{N_1 t_f \lambda_f} + \dfrac{1}{N_2 t_f \lambda_f}} (T_1 - T_2) \quad \text{(A31.12),}$$

from which the linear thermal transmittance, $\psi_{vip,edge,0}$ [W·m-1·K-1], can be obtained by dividing Equation (A31.12) by the temperature difference ($T_1 - T_2$):

$$\psi_{vip,edge,0} = \frac{1}{\dfrac{1}{K} + \dfrac{1}{N_1 t_f \lambda_f} + \dfrac{1}{N_2 t_f \lambda_f}} \quad \text{(A31.13).}$$

After substitution of the proper equations for K, N_1 and N_2 into (A31.13), after some rearrangements, Equation (A31.13) becomes:

$$\psi_{vip,edge,0} = \frac{1}{\dfrac{d_p}{t_f^{'} \lambda_f^{'}} + \dfrac{1}{\sqrt{\alpha_1 t_f \lambda_f}} + \dfrac{1}{\sqrt{\alpha_2 t_f \lambda_f}}} \quad \text{(A31.14).}$$

A32 Derivation of General VIP Edge Thermal Bridge Equation

The thermal bridge due to the continuous high barrier laminate enveloping a VIP can be schematically represented as in Figure A32.1. As can be seen from the figure, an additional heat flow through the core material is considered for the derivation of this general model. The assumptions used for this model are the same as the assumptions for the specific model derived for zero core material thermal conductivity. An exception to these assumptions however is that the thermal conductivity of the core material does no longer need to equal 0 W·m^{-1}·K^{-1}.

Based on these assumptions, the following steady-state heat balance equation can be formulated for the x-direction (Figure A32.1):

$$t_f \lambda_f \left.\frac{dT_x}{dx}\right|_x - t_f \lambda_f \left.\frac{dT_x}{dx}\right|_{x+dx} - \alpha_1 (T_1 - T_x)dx + \frac{\lambda_c}{d_p}(T_x - T_y)dx = 0 \qquad \text{(A32.1).}$$

In this equation, α_i [W·m^{-2}·K^{-1}] is the heat transmission coefficient at boundary surface 1 or 2 respectively, d_p [m] is the thickness of the core of the vacuum insulation panel [m], t_f [m] is the thickness of the foil, λ_f [W·m^{-1}·K^{-1}] is the thermal conductivity of the foil, λ_c [W·m^{-1}·K^{-1}] is the thermal conductivity of the core, T_i [K] is the air temperature on side 1 or 2 respectively, T_x [K] is the temperature of the barrier laminate in x-direction corresponding to side 1 and T_y [K] is the temperature of the barrier laminate in y-direction corresponding to side 2.

Dividing Equation (A32.1) by dx, taking the limit for $dx \rightarrow 0$ and assuming that t_f and λ_f are constant over x, results after some reformulation in

$$\frac{d^2 T_x}{dx^2} - \left(\frac{\alpha_1}{t_f \lambda_f} + \frac{\lambda_c}{t_f \lambda_f d_p} \right) \cdot T_x = -\frac{\alpha_1}{t_f \lambda_f} T_1 - \frac{\lambda_c}{t_f \lambda_f d_p} T_y \qquad \text{(A32.2),}$$

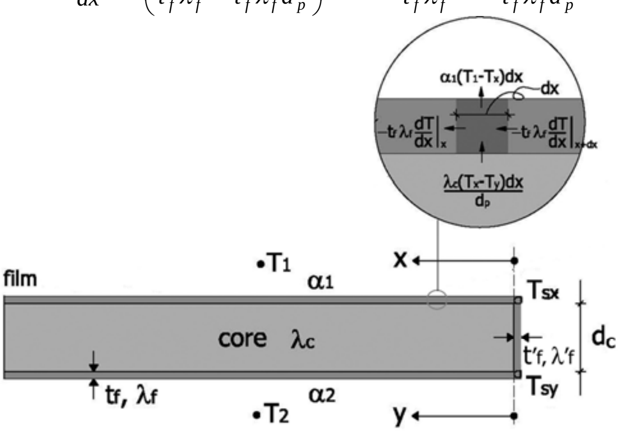

Figure A32.1

Schematic representation of the thermal bridge arising from the thin film high barrier envelope around a vacuum insulation panel or in

$$\frac{d^2T_x}{dx^2} - N_1^2 T_x + BT_y = -A_1 T_1 \qquad \text{(A32.3a).}$$

For the y-direction a similar non-homogeneous second-order differential equation for the temperature distribution in the high barrier laminate can be derived:

$$\frac{d^2T_y}{dy^2} - N_2^2 \cdot T_y + BT_x = -A_2 T_2 \qquad \text{(A32.3b),}$$

in which N_i, A_i and B are defined as

$$N_i = \sqrt{\frac{\alpha_i}{t_f \lambda_f} + \frac{\lambda_c}{t_f \lambda_f d_p}} \qquad \text{(A32.3c),}$$

$$A_i = \frac{\alpha_i}{t_f \lambda_f} \qquad \text{(A32.3d),}$$

$$B = \frac{\lambda_c}{t_f \lambda_f d_p} \qquad \text{(A32.3e),}$$

with i = 1 or 2.

Equations (A32.3a) and (A32.3b) form a non-homogeneous system of second-order linear differential equations that can be written as the following matrix equation

$$\begin{bmatrix} T_x'' \\ T_y'' \end{bmatrix} - \begin{bmatrix} N_1^2 & -B \\ -B & N_2^2 \end{bmatrix} \cdot \begin{bmatrix} T_x \\ T_y \end{bmatrix} = \begin{bmatrix} -A_1 T_1 \\ -A_2 T_2 \end{bmatrix} \qquad \text{(A32.4),}$$

which has as a general solution

$$\overline{T} = c_1 \overline{E}_1 e^{\lambda_1 x} + c_2 \overline{E}_2 e^{\lambda_2 x} + c_3 \overline{E}_3 e^{\lambda_1 x} + c_4 \overline{E}_4 e^{\lambda_2 x} + \overline{c}_0 \qquad \text{(A32.5).}$$

In this solution λ_1, λ_2, λ_3, λ_4 are the eigenvalues of the square matrix, while the vectors $\overline{E}$ are the eigenvectors of the system. From these equations, the eigenvalues, eigenvectors and vector $\overline{c}_0$ can be calculated as

$$\lambda_{1,2,3,4} = \pm \sqrt{\frac{(N_1^2 + N_2^2) \pm \sqrt{(N_1^2 - N_2^2)^2 + 4B^2}}{2}} \qquad \text{(A32.6),}$$

$$\overline{E}_i = \begin{bmatrix} \dfrac{1}{B} \\ \overline{N_2^2 - \lambda_i^2} \end{bmatrix} \qquad (A32.7),$$

$$\overline{c}_0 = -\begin{bmatrix} \dfrac{A_1 N_2^2 T_1 + BA_2 T_2}{B^2 - N_1^2 N_2^2} \\ \dfrac{A_2 N_1^2 T_2 + BA_1 T_1}{B^2 - N_1^2 N_2^2} \end{bmatrix} \qquad (A32.8).$$

The constants c_1 to c_4 are constants depending on the boundary conditions of the system of equations, which can be stated as

$$\begin{bmatrix} T_x \\ T_y \end{bmatrix} = \begin{bmatrix} T_1^* \\ T_2^* \end{bmatrix} \qquad \text{for } x = y = L \qquad (A32.9a),$$

$$\begin{bmatrix} T_x \\ T_y \end{bmatrix} = \begin{bmatrix} T_{sx} \\ T_{sy} \end{bmatrix} \qquad \text{for } x = y = 0 \qquad (A32.9b).$$

In these boundary conditions, L is the distance from x=0 and y=0 to the points where the effect of the thermal bridge on the surface temperature has become insignificant, T_1* and T_2* are the temperatures of the laminate at distance L_i from the thermal bridge at side one and two respectively and T_{sx} and T_{sy} the temperatures of the laminate at x=0 and y=0. T_1* and T_2* are determined from a one-dimensional temperature calculation through the ideal cross-section without thermal bridge effects. The constants c_1 to c_4 are now found from substituting the boundary conditions in Equation (A32.5), resulting in

$$\begin{bmatrix} c_1 \\ c_2 \\ c_3 \\ c_4 \end{bmatrix} = \begin{bmatrix} a - d + bf - beg + cg - f + eg - g \\ d - bf + beg - cg \\ f - eg \\ g \end{bmatrix} \qquad (A32.10),$$

in which the parameters a to g are defined as

$$a = T_{sx} - c_{0x} \qquad (A32.11a),$$

$$b = \frac{\left(\lambda_3^2 - \lambda_1^2\right)}{\left(\lambda_2^2 - \lambda_1^2\right)} \cdot \frac{\left(N_2^2 - \lambda_2^2\right)}{\left(N_2^2 - \lambda_3^2\right)} = 0 \qquad (A32.11b),$$

$$c = \frac{\left(\lambda_4^2 - \lambda_1^2\right)}{\left(\lambda_2^2 - \lambda_1^2\right)} \cdot \frac{\left(N_2^2 - \lambda_2^2\right)}{\left(N_2^2 - \lambda_4^2\right)} = 1 \qquad (A32.11c),$$

$$d=\frac{\left(\left(T_{sy}-c_{0y}\right)-\left(T_{sx}-c_{0x}\right)\cdot\frac{B}{N_2^2-\lambda_1^2}\right)}{\left(\frac{B}{N_2^2-\lambda_2^2}-\frac{B}{N_2^2-\lambda_1^2}\right)} \quad \text{(A32.11d),}$$

$$e=\frac{\left(e^{\lambda_4 L}-e^{\lambda_1 L}\right)-\left(e^{\lambda_2 L}-e^{\lambda_1 L}\right)}{\left(e^{\lambda_3 L}-e^{\lambda_1 L}\right)} \quad \text{(A32.11e),}$$

$$f=\frac{\left(T_1^*-c_{0x}\right)-\left(T_{sx}-c_{0x}\right)e^{\lambda_1 L}-d\cdot\left(e^{\lambda_2 L}-e^{\lambda_1 L}\right)}{\left(e^{\lambda_3 L}-e^{\lambda_1 L}\right)} \quad \text{(A32.11f),}$$

$$g=\frac{h}{i} \quad \text{(A32.11g),}$$

$$h=\left(T_2^*-c_{0y}\right)-\left(T_{sx}-c_{0x}\right)\frac{B}{N_2^2-\lambda_1^2}e^{\lambda_1 L}-d\cdot\left(\frac{B}{N_2^2-\lambda_2^2}e^{\lambda_2 L}-\frac{B}{N_2^2-\lambda_1^2}e^{\lambda_1 L}\right)$$
$$-f\cdot\left(\frac{B}{N_2^2-\lambda_3^2}e^{\lambda_3 L}-\frac{B}{N_2^2-\lambda_1^2}e^{\lambda_1 L}\right)$$

(A32.11h),

$$i=\frac{B}{N_2^2-\lambda_4^2}e^{\lambda_4 L}-\frac{B}{N_2^2-\lambda_2^2}e^{\lambda_2 L}-e\cdot\left(\frac{B}{N_2^2-\lambda_3^2}e^{\lambda_3 L}-\frac{B}{N_2^2-\lambda_1^2}e^{\lambda_1 L}\right) \quad \text{(A32.11i).}$$

If the limit for $L \rightarrow \infty$ is taken, Equation (A32.10) reduces to

$$\lim_{L\to\infty}\begin{bmatrix}c_1\\c_2\\c_3\\c_4\end{bmatrix}=\lim_{L\to\infty}\begin{bmatrix}a-d+bf-beg+cg-f+eg-g\\d-bf+beg-cg\\f-eg\\g\end{bmatrix}=\begin{bmatrix}a-d\\d\\0\\0\end{bmatrix} \quad \text{(A32.12),}$$

Under the conditions given in Figure A32.1, the heat flow, $\phi_{q;edge}$ [W·m^{-1}], at x=0 must satisfy the following condition:

$$\phi_{q;edge}=-t_f\lambda_f\frac{dT_x}{dx}=-t'_f\lambda'_f\frac{(T_{sx}-T_{sy})}{d_p} \quad \text{(A32.13a),}$$

with t'_f [m] the thickness of the laminate at the edge, λ'_f [W·m^{1}·K^{-1}] the thermal conductivity of the foil at the edge, T_{sx} [K] the temperature of the barrier foil at x = 0 and T_{sy} [K] the temperature of the barrier foil / film at y = 0. Equation (A32.13a) can be written as:

$$-t_f \lambda_f \frac{dT_x}{dx} = -K(T_{sx} - T_{sy}) \qquad \text{(A32.13b)},$$

with $K = \lambda'_f t'_f / d_p$, of which the reciprocal value is the resistance between x=0 and y=0. If Equation (A32.5) is differentiated and multiplied with $t_f \lambda_f$ and if the value zero for c_3 and c_4 is substituted, the following equation is obtained:

$$-t_f \lambda_f \frac{dT_x}{dx} = -t_f \lambda_f c_1 \lambda_1 \overline{E}_{1x} e^{\lambda_1 x} - t_f \lambda_f c_2 \lambda_2 \overline{E}_{2x} e^{\lambda_2 x} \qquad \text{(A32.14)}.$$

For $x \rightarrow 0$ the left side of Equation (A32.14) becomes:

$$\lim_{x \downarrow 0} \left[-t_f \lambda_f \frac{dT_x}{dx} \right] = -t_f \lambda_f c_1 \lambda_1 \overline{E}_{1x} - t_f \lambda_f c_2 \lambda_2 \overline{E}_{2x} \qquad \text{(A32.15)}.$$

For the y-direction a similar equation can be derived, resulting in the following set of equations:

$$-t_f \lambda_f c_1 \lambda_1 - t_f \lambda_f c_2 \lambda_2 = -K(T_{sx} - T_{sy}) \quad \text{for } x=0 \qquad \text{(A32.16a)},$$

$$-t_f \lambda_f c_1 \lambda_1 \frac{B}{N_2^2 - \lambda_1^2} - t_f \lambda_f c_2 \lambda_2 \frac{B}{N_2^2 - \lambda_2^2} = +K(T_{sx} - T_{sy}) \quad \text{for } y=0 \qquad \text{(A32.16b)}.$$

Simultaneously solving this system of equations results in the following solutions for T_{sx} and T_{sy}:

$$T_{sx} = \frac{\left[e_4(K + a_2) + e_1(K - e_3)\right] c_{0x} - \left[e_3(K + e_2) + e_2(K - e_3)\right] c_{0y}}{(K - e_3)(K + e_1) - (K + e_2)(K - e_4)} \qquad \text{(A32.17a)},$$

$$T_{sy} = \frac{\left[e_4(K + e_1) + e_1(K - e_4)\right] c_{0x} - \left[e_3(K + e_1) + e_2(K - e_4)\right] c_{0y}}{(K - e_3)(K + e_1) - (K + e_2)(K - e_4)} \qquad \text{(A32.17b)},$$

in which

$$e_1 = -\frac{\left(t_f \lambda_f \lambda_1 - t_f \lambda_f \lambda_2\right)}{\left(\frac{B}{N_2^2 - \lambda_2^2}\right) - \left(\frac{B}{N_2^2 - \lambda_1^2}\right)} \qquad \text{(A32.18a)},$$

$$e_2 = \left[\frac{\left(t_f \lambda_f \lambda_1 \left(\dfrac{B}{N_2^2 - \lambda_1^2} \right) - t_f \lambda_f \lambda_2 \left(\dfrac{B}{N_2^2 - \lambda_2^2} \right) \right)}{\left(\left(\dfrac{B}{N_2^2 - \lambda_2^2} \right) - \left(\dfrac{B}{N_2^2 - \lambda_1^2} \right) \right)} \right] \qquad \text{(A32.18b),}$$

$$e_3 = \frac{\left(t_f \lambda_f \lambda_1 - t_f \lambda_f \lambda_2 \right)}{\left(\dfrac{B}{N_2^2 - \lambda_2^2} \right) - \left(\dfrac{B}{N_2^2 - \lambda_1^2} \right)} = -a_1 \qquad \text{(A32.18c),}$$

$$e_4 = \left[\frac{\left(t_f \lambda_f \lambda_1 \left(\dfrac{B}{N_2^2 - \lambda_2^2} \right) - t_f \lambda_f \lambda_2 \left(\dfrac{B}{N_2^2 - \lambda_1^2} \right) \right)}{\left(\left(\dfrac{B}{N_2^2 - \lambda_2^2} \right) - \left(\dfrac{B}{N_2^2 - \lambda_1^2} \right) \right)} \right] \qquad \text{(A32.18d).}$$

Because of non-zero thermal conductivity of the core material, not all heat is transferred through the thermal bridge and thus the general definition for the linear thermal transmittance must be applied to the vacuum insulation panel, which is

$$\psi_{vip,edge} = \frac{\phi_q - \phi_{q;0}}{\Delta T} \qquad \text{(A32.19),}$$

with ϕ_q [W·m^{-1}] the total heat flow through the vacuum insulation panel, including thermal bridge and $\phi_{q;0}$ [W·m^{-1}] the total heat flow through the vacuum insulation panel in the case no thermal bridge existed (Figure A32.2).

The total heat flow through a VIP without thermal bridge can be calculated as

$$\phi_{q;0} = \int_0^{L_1} q_0 dx = \int_0^{L_1} \alpha_1 (T_1 - T_x) dx = \alpha_1 (T_1 - T_1^*) \cdot L_1 \qquad \text{(A32.20).}$$

Figure A32.2

Schematic representation of the heat flows through an undisturbed panel and a panel with a thermal bridge arising from the thin film high barrier envelope of a vacuum insulation panel

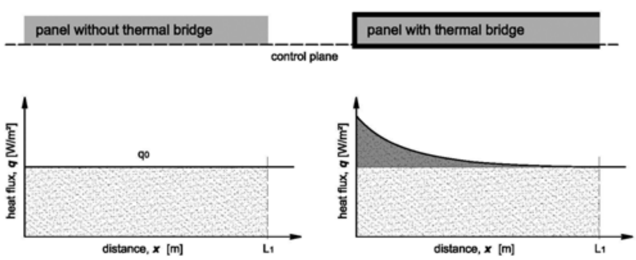

In this equation L_1 [m] is the length of the panel. For the heat flow through the panel with thermal bridge, a similar equation can be derived

$$\phi_q = \int_0^{L_1} q \cdot dx = \int_0^{L_1} \alpha_1 (T_1 - T_x) dx = \alpha_1 (T_1 - \overline{T}_x) \cdot L_1 \qquad \text{(A32.21)},$$

in which $\overline{T}_x$ [K] is the average laminate temperature in x-direction, defined as

$$\overline{T}_x = \frac{1}{L_1} \int_0^{L_1} T_x dx \qquad \text{(A32.22)},$$

resulting in

$$\overline{T}_x = \frac{c_1}{\lambda_1 L_1}\left(e^{\lambda_1 L_1} - 1\right) + \frac{c_2}{\lambda_2 L_1}\left(e^{\lambda_2 L_1} - 1\right) + \frac{c_3}{\lambda_3 L_1}\left(e^{\lambda_3 L_1} - 1\right) + \frac{c_4}{\lambda_4 L_1}\left(e^{\lambda_4 L_1} - 1\right) + c_{0x}$$

(A32.23).

Equation (A32.23) is valid under the assumption that $L < L_1$ (or in words: the distance from the thermal bridge ($x = 0$) to the position at which the effect of the thermal bridge is negligible should be smaller than the length of the panel). Moreover, the coefficients c_1 to c_4 are to be taken from Equation (A32.10) and not from (A32.12), thus without letting $L \rightarrow \infty$. The additional heat flow due to the thermal bridge can now be calculated from Equations (A32.20) and (A32.21) as

$$\phi_q - \phi_{q;0} = \alpha_1 L_1 \cdot (T_1^* - \overline{T}_x) \qquad \text{(A32.24)}.$$

Since T_1^* equals c_{0x}, Equation (A32.24) can be written as

$$\phi_q - \phi_{q;0} = -\alpha_1 \cdot \left[\frac{c_1}{\lambda_1}\left(e^{\lambda_1 L_1} - 1\right) + \frac{c_2}{\lambda_2}\left(e^{\lambda_2 L_1} - 1\right) + \frac{c_3}{\lambda_3}\left(e^{\lambda_3 L_1} - 1\right) + \frac{c_4}{\lambda_4}\left(e^{\lambda_4 L_1} - 1\right)\right] \qquad \text{(A32.25)}.$$

If now the limit is taken for $L \rightarrow \infty$, this equation simplifies to

$$\lim_{L \to \infty}\left(\phi_q - \phi_{q;0}\right) = \alpha_1 \cdot \left[\frac{a-d}{\lambda_1} + \frac{d}{\lambda_2}\right] \qquad \text{(A32.26)},$$

resulting finally in the following equation for the linear thermal transmittance of a VIP edge

$$\psi_{vip,edge} = \frac{\phi_q - \phi_{q;0}}{\Delta T} = \frac{\alpha_1}{(T_1 - T_2)} \cdot \left[\frac{a-d}{\lambda_1} + \frac{d}{\lambda_2}\right] \qquad \text{(A32.27)},$$

which equals

$$\psi_{vip,edge} = \frac{\alpha_1}{(T_1 - T_2)} \cdot \left[\frac{(T_{sy} - c_{0y})(\lambda_1 - \lambda_2) + (T_{sx} - c_{0x}) \left(\frac{B\lambda_2 (N_2^2 - \lambda_1^2) - B\lambda_1 (N_2^2 - \lambda_2^2)}{(N_2^2 - \lambda_1^2)(N_2^2 - \lambda_2^2)} \right)}{\left(\frac{B\lambda_1 \lambda_2 (\lambda_2^2 - \lambda_1^2)}{(N_2^2 - \lambda_1^2)(N_2^2 - \lambda_2^2)} \right)} \right]$$

(A32.28).

Combining Equations (A32.17a), (A32.17b) and (A32.28) results, after rearranging, in

$$\psi_{vip,edge} = \frac{\alpha_1 (c_{0x} - c_{0y})}{(T_1 - T_2)} \cdot \left[\frac{(a_1 K + a_4 K) \cdot (\lambda_1 - \lambda_2) + (a_2 K + a_3 K) \left(\frac{B\lambda_2 (N_2^2 - \lambda_1^2) - B\lambda_1 (N_2^2 - \lambda_2^2)}{(N_2^2 - \lambda_1^2)(N_2^2 - \lambda_2^2)} \right)}{\left[(K + a_1)(K - a_3) - (K + a_2)(K - a_4) \right] \left(\frac{B\lambda_1 \lambda_2 (\lambda_2^2 - \lambda_1^2)}{(N_2^2 - \lambda_1^2)(N_2^2 - \lambda_2^2)} \right)} \right]$$

(A32.29),

With help of Equations (A32.3c), (A32.3d), (A32.3e), (A32.18a) to (A32.18d) and (A32.29), the final equation for the linear thermal transmittance of the edge of a vacuum insulation panel is obtained:

$$\psi_{vip,edge} = \frac{1}{1 + \frac{\lambda_c}{\alpha_1 d_p} + \frac{\lambda_c}{\alpha_2 d_p}} \cdot \left[\frac{\alpha_1 (N_2^2 - B)}{\frac{t_f \lambda_f}{K} \left(N_1^2 N_2^2 - B^2 \right) - \lambda_1 \sqrt{N_1^2 N_2^2 - B^2} \left(1 + \frac{2B}{\sqrt{D}} \right) - \lambda_2 \sqrt{N_1^2 N_2^2 - B^2} \left(1 - \frac{2B}{\sqrt{D}} \right)} \right]$$

(A32.30),

in which *D* is the discriminator of the second square root of the eigenvalues, or

$$D = \left(N_1^2 - N_2^2 \right)^2 + 4B^2 \qquad \text{(A32.31).}$$

If now finally the limit for $\lambda_c \rightarrow 0$ is taken for Equation (A32.30), the equation for zero core thermal conductivity arises:

$$\lim_{\lambda_c \downarrow 0} \psi_{vip,edge} = \frac{1}{\frac{d_p}{t_f^{'} \lambda_f^{'}} + \frac{1}{\sqrt{\alpha_1 t_f \lambda_f}} + \frac{1}{\sqrt{\alpha_2 t_f \lambda_f}}} = \psi_{vip,edge,0} \qquad \text{(A32.32).}$$

For a VIP with a combined barrier envelope, e.g. a combination of an aluminium foil on one side and a metallised film on the other side, the linear thermal transmittance can be computed analytically as

$$\psi_{vip;edge} = \frac{\alpha_1 \left\{ \frac{\lambda_{f1} t_{f1}}{\sqrt{D}} D - \frac{\lambda_{f2} t_{f2}}{\sqrt{D}} \left[B_1 \left(N_2^2 + N_1^2 \right) + 2\sqrt{C}(B_2 - B_1) + N_2^2 \frac{\left(N_2^2 - N_1^2 \right)^2}{B_1} + B_2 \left(3N_2^2 - N_1^2 \right) \right] \right\}}{1 + \frac{\lambda_c}{d_p \alpha_1} + \frac{\lambda_c}{d_p \alpha_2}}$$

$$\Bigg/ \left\{ + \lambda_1 \sqrt{C} \left[\lambda_{f1} t_{f1} \left(1 + \frac{N_2^2 - N_1^2 + \sqrt{D}}{2B_1} \right) + \lambda_{f2} t_{f2} \left(1 - \frac{N_2^2 - N_1^2 - \sqrt{D}}{2B_1} \right) \right] \right.$$

$$- \lambda_2 \sqrt{C} \left[\lambda_{f1} t_{f1} \left(1 + \frac{N_2^2 - N_1^2 - \sqrt{D}}{2B_1} \right) + \lambda_{f2} t_{f2} \left(1 - \frac{N_2^2 - N_1^2 + \sqrt{D}}{2B_1} \right) \right]$$

$$\left. + \frac{\lambda_{f1} t_{f1} \lambda_{f2} t_{f2} \sqrt{C}}{K\sqrt{D}} \left[(B_1 - B_2)\left(N_1^2 + N_2^2 \right) - \frac{\left(N_2^2 - N_1^2 \right)^2}{B_1} \sqrt{C} - 2(B_1 + B_2)\sqrt{C} \right] \right\}$$

(A33.1).

In this equation $t_{f;j}$ and $\lambda_{f;j}$ are the thickness and thermal conductivity of the laminate on side 1 (corresponding to α_1) and side 2 (corresponding to α_2) respectively. Moreover, the following parameters are defined slightly differently from the equation presented in section 3.3:

$$N_j = \sqrt{\frac{\alpha_i}{t_{f;j}\lambda_{f;j}} + \frac{\lambda_c}{t_{f;j}\lambda_{f;j}d_p}} \quad \text{(A33.2),}$$

$$B_j = \frac{\lambda_c}{t_{f;j}\lambda_{f;j}d_p} \quad \text{(A33.3),}$$

$$\lambda_1 = -\sqrt{\frac{(N_1^2 + N_2^2) - \sqrt{(N_1^2 - N_2^2)^2 + 4B_1B_2}}{2}} \quad \text{(A33.4),}$$

$$\lambda_2 = -\sqrt{\frac{(N_1^2 + N_2^2) + \sqrt{(N_1^2 - N_2^2)^2 + 4B_1B_2}}{2}} \quad \text{(A33.5),}$$

$$C = N_1^2 N_2^2 - B_1 B_2 \qquad \text{(A33.6),}$$

$$D = \left(N_1^2 - N_2^2\right)^2 + 4B_1 B_2 \qquad \text{(A33.7).}$$

Finally, the thermal conductance of the edge, *K* [W·m^{-1}·K^{-1}] needs to be defined. It can be obtained from a thermal resistance network analysis. In general it was defined as

$$K = \frac{\lambda_f^{'} t_f^{'}}{d_p} \qquad \text{(A33.8).}$$

If both films continue over the edge of the panel until half the panel thickness, *K* is defined as

$$K = \frac{2\lambda_{f;1} t_{f;1} \lambda_{f;2} t_{f;2}}{\left(\lambda_{f;1} t_{f;1} + \lambda_{f;2} t_{f;2}\right) d_p} \qquad \text{(A33.9).}$$

A34 Thermal Conductivity of Porous Media

A34.1 Solid skeleton thermal conductivity

On a macroscopic level the conductive heat flux can be modelled according to Fourier's law, which states proportionality between heat flux and temperature gradient:

$$\vec{q}_s = -\lambda_s \cdot \nabla T \qquad \text{(A34.1).}$$

The thermal conductivity, λ_s, in this equation is a material constant, which varies amongst others with temperature of the material; the higher the temperature, the better heat is conducted and thus the higher the thermal conductivity. It is a property that can vary with direction, which is especially important for fibre-based core materials. Because, however, in practical applications of VIPs heat primarily flows in a direction normal to the panel surface, only this direction is considered.

To be able to understand the solid skeleton thermal conductivity, the microstructure of a material needs to be considered. From a microscopic point of view, the material structure needs to be considered as well. Kinetic transport theory shows that on a microscopic level two different ways of heat conduction exist, the dominance of which depends on material structure: heat transfer by electrons or by phonons.

In high thermal conductivity materials, like metals, the first heat transfer mechanism dominates. These materials consist of a crystal structure in which a cloud of free valence electrons, the so-called Cottrell cloud, binds positive ion cores together. These free electrons are not bonded to any particular ion core and can thus move freely through the material. During such a movement an electron transports energy in the form of internal energy (and kinetic energy) from one place to another. It moves at very high speeds, but is scattered and slowed down by collisions with large atoms and crystal imperfections. Due to this high speed, the rate of heat transfer by means of electrons is high.

In materials with lower heat conductivity, i.e. thermal insulators, the second mechanism is more important because of absence of many free electrons. Atoms in these materials are not bounded by free electrons but mainly by covalence or mutual electron pairs. The atoms in these structures vibrate, the magnitude of which depends on temperature. During these vibrations collisions with other vibrating atoms occur and kinetic energy is transferred from the atom with high kinetic energy to the atom with less kinetic energy. This process of lateral collisions is often described with the theoretical concept of phonons. The speed of a phonon in a

Figure A34.1

Possible paths for heat flow in a powder-based material

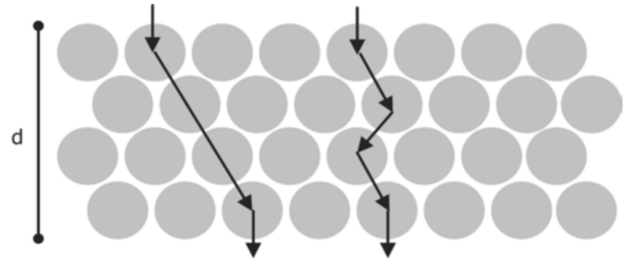

material equals the speed of a sound wave through this material, which is much slower than the speed of an electron. Due to this low rate of heat transfer, the thermal conductivity of insulator materials is significantly lower than the conductivity of conductor materials. Phonons are, like electrons, scattered and decelerated by discontinuities. Since electrons and phonons are both scattered at grain boundaries and by material defects, amorphous and chemically polluted materials are preferred as thermal insulator.

It is very difficult to derive theoretical relationships for the solid thermal conductivity of porous media, except for powder-based materials, like fumed silica. For these materials Brodt (1995) explains that two factors influence their thermal conductivity. First, the path that heat needs to 'travel' is not a straight line from one side of the panel to another, as can be seen from Figure A34.1. Owing to the stacking of spheres, point-like contacts between the different particles exist, as a result of which deviations in the heat flow path from a straight line occur. This implies that the term representing a distance in Fourier's equation, dx, increases significantly, consequently reducing the heat flux, q. Second, the thermal resistance against heat flow through the solid skeleton of powder-based materials is principally based upon the resistances of the point-like contacts between different spheres. This resistance is much higher than the resistance of the granular material itself, as a result reducing the heat flux, or effective solid conductivity, as well.

For the thermal resistance of these point contacts, the radius of the grains is important. According to Hertz (1882), the radius of the point-like contact between two spheres, r [m], under a force, F [N], can be described as

$$r = \left[\frac{3}{4} \cdot \frac{1-\nu^2}{E} \cdot r_{gr} \cdot F \right]^{1/3} \qquad \text{(A34.2).}$$

In this equation ν [-] is the Poisson's ratio, E [Pa] the Young's modulus and r_{gr} [m] the (original) radius of the sphere. According to Brodt (1995), this contact radius can be correlated to the thermal resistance of this contact bridge, R [$K \cdot W^{-1}$] described by

$$R = \frac{1}{2\lambda_{gr} r} \qquad \text{(A34.3)},$$

with λ_{gr} [$W \cdot m^{-1} \cdot K^{-1}$] the thermal conductivity of the solid material grains. Brodt (1995) shows that for a powder material with an average particle size of approximately 1 μm, a thermal conductivity of the solid material of 1.5 $W \cdot m^{-1} \cdot K^{-1}$, a porosity of 0.95, a Poisson's ratio of 0.16 and a Young's modulus of $70 \cdot 10^9$ Pa (aerosil), this equation yields a thermal resistance of $6.2 \cdot 10^6$ $K \cdot W^{-1}$.

The total thermal resistance of a powder material, R_{tot} [$m \cdot K \cdot W^{-1}$], can now be calculated by multiplying this contact resistance with a (geometrical) factor N_s/N_A, taking into account the number and distribution of spheres:

$$R_{tot} = R\frac{N_s}{N_A} \qquad \text{(A34.4)}.$$

In this equation N_s is the number of spheres per unit length and N_A the number of spheres per unit area. From this total thermal resistance the solid thermal conduction can finally be calculated from

$$\lambda_s = \frac{1}{R_{tot}} \qquad \text{(A34.5)}.$$

Two important dependencies for the solid thermal conductivity, not explicitly clear from the aforementioned formulae, need to be discussed: its dependency on temperature and its dependency on density.

For the dependency of solid thermal conductivity on temperature many empirical relations are known. Caps et al. (2001), for example, found that the solid conductivity of pyrogenic silica powders is proportional to the thermal conductivity of silica glass:

$$\lambda_s = A\,[-8.5 \cdot 10^{-15}\,T^4 + 2.1 \cdot 10^{-11}\,T^3 - 1.95 \cdot 10^{-8}\,T^2 + 8.83 \cdot 10^{-6}\,T] \qquad \text{(A34.6)},$$

in which A is a proportionality parameter depending on porosity, ε, and in which T is the Kelvin temperature. Caps and Fricke (2000) also found a relationship between the solid conductivity and the highest applied load during pressing fumed silica boards. As a second example perlite powder can be mentioned, a material for which Takegoshi et al. (1985) suggested that

$$\lambda_s = 0.0244 \cdot T^{0.667} \qquad \text{(A34.7).}$$

For the dependency of solid thermal conductivity on density, ρ [kg·m^{-3}], the following general relationship is valid (Fricke, 2001; Fricke et al., 2006)

$$\lambda_s \sim \rho^{\alpha} \qquad \text{(A34.8).}$$

For foams, the power constant, α, is almost 1, while for aerosil, fumed silica and aerogel, it is approximately 1.5 to 2.

Experimental determination of this solid conductivity can be performed by measuring the thermal conductivity at different temperatures and at very low pressure. In this low-pressure region, gas conduction can be neglected as will be explained in the next section. Because the radiative conductivity linearly depends on the mean temperature raised to the third power, extrapolating the acquired data to a temperature of 0 K yields the conductivity of the solid matrix. It must however be noted that this procedure only works as long as the solid thermal conductivity and the radiative extinction do not strongly depend on temperature (Fricke et al., 2008).

A34.2 Gas conduction thermal conductivity

While the mechanism of gas conduction is principally the same as of solid conduction through a thermal insulator, differences arise due to the absence of a rigid structure for gases. As a result, the average distance between individual molecules is significantly larger than in a solid phase. Collisions therefore are likely to occur less often. Hence, the thermal conductivity of a gas, λ_g [W·m^{-1}·K^{-1}], is less than that of a solid material grain, λ_{gr}.

From kinetic gas theory several theoretical relationships for the unrestricted[16] gas thermal conductivity, $\lambda_{g;0}$, have been derived. For ideal one-atomic gases, for example, this unrestricted gas conductivity is directly proportional to the square root of mean gas temperature[17], T, (Rath, 1989)

---

[16] Unrestricted means that the gas is not limited in its movement by boundaries or other obstacles.

[17] Van den Akker and Mudde (1998) argue that the above-mentioned analysis bases on a simplified model for the behaviour of molecules, in which the assumption is made that molecules are hard and elastic spheres. They discuss that a more realistic and complex analysis of the behaviour of gas molecules shows that $\lambda_{g;0} \sim T^{0.7\ a\ 0.75}$, provided that pressure and temperature are within normal values.

$$\lambda_{g;0} = \frac{k_B}{d_c^2}\sqrt{\frac{k_B N_A T}{\pi^3 M}} \qquad \text{(A34.9a).}$$

In this equation k_B is the Boltzmann constant (k_B = 1.38·10^{-23} J·K^{-1}), d_c [m] the collision diameter, N_A the Avogadro constant (N_A = 6.02·10^{23} mol^{-1}) and M [kg·mol^{-1}] the molar mass. For more-atomic ideal gases this relationship becomes (Rath, 1989)

$$\lambda_{g;0} = \frac{5}{16}\frac{R}{M}\frac{1}{d_c^2}\sqrt{\frac{MRT}{\pi N_A^2}}\left(\frac{c_V}{MR}+\frac{9}{4}\right) \qquad \text{(A34.9b),}$$

in which R is the universal gas constant (R = 8.31 J·kg^{-1}·K^{-1}) and c_V [J·kg^{-1}·K^{-1}] the specific heat with constant volume. This gas thermal conductivity, $\lambda_{g;0}$ is independent of gas pressure. Rath (1989) explains that the number of molecules, and thus the number of collisions, is directly proportional to pressure, while the mean free path of these molecules[18], and thus the amount of energy transferred per collision, is inversely proportional to this pressure. Consequently, both effects cancel each other out.

Since many gases not completely exhibit theoretically predicted behaviour, several linear equations for the unrestricted gas conductivity, in most cases only valid for small temperature ranges, exist (Brodt, 1995). Rath (1989) for example gives an equation for air at intervals around standard temperature and pressure:

$$\lambda_{g;0} = 2.454\cdot 10^{-2} + 7.861\cdot 10^{-5}\cdot (T-273)^{0.983} \qquad \text{(A34.9c).}$$

For air at atmospheric pressure and at 10 °C, this equation yields for $\lambda_{g;0}$ approximately 25.3·10^{-3} W·m^{-1}·K^{-1}. These theoretical and empirical relationships, however, are only applicable to ideal situations in which molecules are not restrained and are perfect.

If, however, a gas is placed between two parallel flat plates with an intermediate distance δ [m], which is in the same order of magnitude as the mean free path of the gas molecules, the molecules near the edges are restrained in their movement (Smoluchowski effect (Smoluchowski, 1898)) and almost all collisions are between gas molecule and boundary which are highly elastic. As a result, the gas thermal conductivity reduces. In such situations the gas conductivity, λ_g, does depend on pressure and can, according to McAdams (1954), be expressed as

---

18 The mean free path of a gas is the average distance a molecule traverses before it collides with another gas molecule.

$$\lambda_g = \frac{\lambda_{g;0}}{1 + \frac{2X \cdot mfp}{\delta}} \quad \text{(A34.10)},$$

provided that no convection occurs[19].

For the gas thermal conductivity, this equation shows that besides the unrestricted gas thermal conductivity three parameters are of importance: a dimensionless variable X, the mean free path of the considered gas, mfp [m] and the distance between the boundaries, δ [m].

This mean free path of the unrestricted molecules is the average distance a gas molecule travels between two collisions, being a function of gas pressure, p_g [Pa]. This pressure dependency can easily be explained by looking at the number of gas molecules per unit volume at different pressures. The lower the pressure, the fewer molecules per unit volume and thus the larger the distance travelled between collisions. The mean free path can be expressed as (Simmler et al., 2005)

$$mfp = \frac{k_B \cdot T}{\sqrt{2} \cdot \pi d_c^2 p_g} = c\frac{T}{p_g} \quad \text{(A34.11)},$$

with T the absolute temperature and d_c the collision diameter of the molecule (for nitrogen $3.53 \cdot 10^{-10}$ m at ambient pressure and 298 K). The proportionality constant in the second part of equation (A34.11), c, differs for each type of gas. For air[20], for example, this constant equals $2.49 \cdot 10^{-5}$ m·Pa·K^{-1}, at ambient pressure resulting in a mean free path of $7 \cdot 10^{-8}$ m and at a pressure of 1 mbar in a value of $7 \cdot 10^{-5}$ m.

According to Kennard (1938), the dimensionless variable, X, can be calculated as

$$X = \frac{9\gamma - 5}{2\gamma + 2} \cdot \frac{2 - \alpha_k}{\alpha_k} = \frac{2\gamma}{\gamma + 1} \cdot \frac{2 - \alpha_k}{\alpha_k} \cdot \frac{1}{\Pr} \quad \text{(A34.12)},$$

[19] In the original equation, the second term in the denominator is multiplied by the square root of a temperature ratio as $\lambda_g = \lambda_{g;0} / \left(1 + \frac{2X \cdot mfp}{\delta}\sqrt{\frac{T_{m,FM}}{T_{m,DF}}}\right)$ (Zhang, 2007). In this equation, $T_{m,FM}$ [K] and $T_{m,DF}$ [K] are the effective mean temperatures of the gas inside the pores in a collisional or free molecular regime respectively. They can be calculated from the temperatures of the surfaces between which heat transfer through the gas phase phenomenologically occurs (Zhang, 2007). In case the temperature difference between these surfaces is small, the temperature ratio in aforementioned equation becomes unity.

[20] To calculate the constant for air, the properties of nitrogen are used.

in which γ is the ratio of specific heat at constant pressure and the specific heat at constant volume ($\gamma = c_p/c_v = c_p/(c_p-R)$=1.4 for air), α_k [21]an accommodation coefficient (between 0.87 and 1.0 for the combination of air and most materials used in engineering (Zhang, 2007) and 0.96 for water vapour (Jacobsen, 1999)) and *Pr* the dimensionless Prandtl-number, which is for air at ambient pressure and 25°C approximately 0.7.

Although Equation (A34.10) is only valid for a gas between two parallel plates, it can be used to estimate the gas conductivity in a void of a micro porous thermal insulating material. The distance, δ, in that case is not the distance between two parallel plates, but an average distance between the surfaces of two spheres for powder insulation or an equivalent average void diameter for foamed or fibre-based insulation materials. This average distance, or mean chord distance, is a function of mean particle diameter, d_p, or mean fibre diameter, d_f, and of porosity, ε. For a spherular silica based core material, it can be estimated as (Rath, 1989)

$$\delta = \frac{2\varepsilon \overline{d}_p}{3(1-\varepsilon)} \qquad \text{(A34.14a)},$$

or as (Simmler et al., 2005)

$$\delta = \frac{\varepsilon}{\rho S_a} \qquad \text{(A34.14b)}.$$

In this equation S_a [m^2·kg^{-1}] is the specific area of the core material.

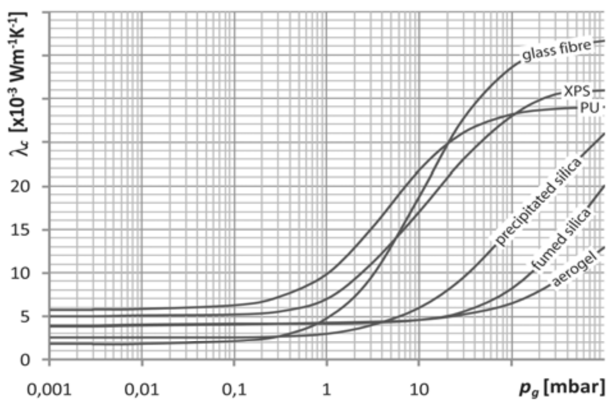

Figure A34.2

Effective thermal conductivity of different potential VIP core materials as function of internal gas pressure. Based on Cabot (2003) and Simmler et al. (2005).

[21] The accommodation coefficient describes incomplete energy transfer from a gas molecule to the pore wall during a collision (Kennard, 1938).

Combining Equations (A34.10) to (A34.14), we can now rewrite equation (A34.10) to

$$\lambda_g = \frac{\lambda_{g;0}}{1 + C\dfrac{T}{\delta \cdot p_g}} \qquad \text{(A34.16)},$$

clearly showing that four properties are relevant in developing vacuum insulation: the type of gas (first gas property), the gas pressure (second gas property), the temperature (environmental property), and an equivalent pore diameter (insulation material property). In this equation *C* is a constant, which depends on the type of gas and on the core material via *X*. In literature about vacuum insulation panels, often a slightly different form of Eq. (A34.16) is used (Caps et al., 2001). This equation expresses the gas conductivity amongst others as a function of pore gas pressure, p_g, and a typical gas pressure at which one half of the gas conductivity $\lambda_{g;0}$ has developed, $p_{1/2}$

$$\lambda_g = \frac{\lambda_{g;0}}{1 + \dfrac{p_{1/2}}{p_g}} \qquad \text{(A34.17)}.$$

From both equations (A34.16) and (A34.17), we can learn that, if the gas pressure is reduced, gas conductivity will be reduced as well. In chapter 6 on service life predictions, values for $\lambda_{g;0}$ and $p_{1/2}$ will be given for some material-gas-combinations.

Equations that describe the thermal conductivity of the gas at high gas pressure where the gas was considered to be unrestricted can be derived from kinetic gas theory. Similarly, an equation for the thermal conductivity at very low gas pressure can be derived (Kaganer, 1969). This thermal conductivity is often referred to as the molecular thermal conductivity (Schwab, 2004) and given by

$$\lambda_{g,molecular} = \frac{\gamma + 1}{\gamma - 1} \cdot \frac{\alpha_k}{2 - \alpha_k} \cdot \sqrt{\frac{R}{8\pi M T}}\, p_g \delta \qquad \text{(A34.18)}.$$

As can be seen, the thermal conductivity at low gas pressure is directly proportional to this pressure.

To determine now the contribution of gas conduction to the overall thermal conductivity of the entire material, one must find a relationship for the gas conductivity of a packed bed. Cunnington (1978) developed a semi-empirical relationship that expresses thermal gas conductivity through such a packed bed, $\lambda_{g;calc}$, as a function of the parallel plates gas conductivity, λ_g, expressed as

$$\lambda_{g;calc} = \lambda_g \left[5.8 \frac{(1-\varepsilon)^2}{1-\lambda_g/\lambda_{gr}} \left[\frac{1}{1-\lambda_g/\lambda_{gr}} \ln \frac{\lambda_{gr}}{\lambda_g} - \frac{3-\lambda_g/\lambda_{gr}}{2} \right] + 1 \right] \quad \text{(A34.19).}$$

For most core materials used in vacuum insulation panels, the porosity, ε, is very high ($\varepsilon > 0.8$), as a consequence of which the quadratic term in this equation becomes negligible. As a result, Equation (A34.19) simplifies to

$$\lambda_{g;calc} \approx \lambda_g \quad \text{(A34.20),}$$

in which gas-solid interactions are neglected.

Based upon the basic physics of gas conduction through porous insulator materials, a description of the effect of reducing gas pressure in vacuum insulation panels can be presented. Figure A34.2 demonstrates how for different potential VIP core materials the thermal conductivity is reduced due to a reduction of internal gas pressure. As can be seen, three different pressure regions can be distinguished: low pressure region, intermediate pressure region and high pressure region.

In the low pressure region, a plateau exists for which gas conduction is practically non-existent, as a result of which reducing gas pressure does not have any further effect. This occurs if the so-called Knudsen-number has become much larger than 1. This Knudsen-number is defined as the ratio of the mean free path of the gas molecules to the equivalent void size (Knudsen, 1911):

$$Kn = \frac{mfp}{\delta} \quad \text{(A34.21).}$$

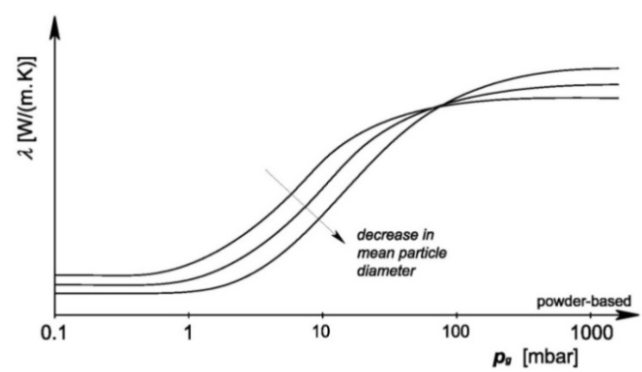

Figure A34.3

Effect of pore size or mean particle diameter on effective thermal (gas) conductivity as a function of internal gas pressure for a powder based material, based upon Rath (1989).

Figure A34.4

Effect of pore size or mean fibre diameter on effective thermal (gas) conductivity as a function of internal gas pressure for a fibre based material, based upon Rath (1989)

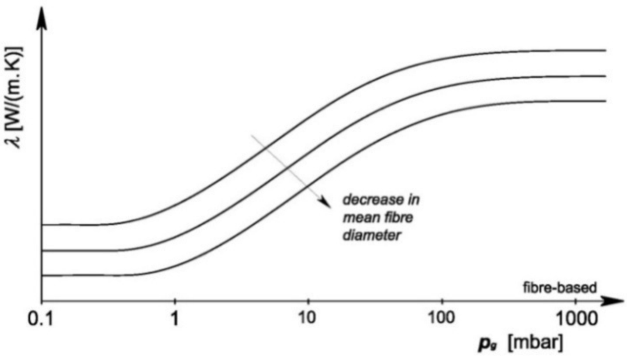

In this low pressure region, the mean free path of the gas molecules is much larger than the size of the voids in which the gas in trapped. This implies that collisions between gas molecules hardly occur. In the remaining collisions between gas molecules and the void surrounding solid material, which are almost completely elastic, hardly any energy is transferred.

In the high pressure region, i.e. if the Knudsen-number is much less than 1, a second plateau exists at which changes in gas pressure hardly influence gas conduction inside the material pores as well. Here, the mean free path is less than the void size and lateral collisions between molecules are dominant. The gas conductivity in this region takes on a constant value, which equals the unrestricted gas thermal conductivity, $\lambda_{g;0}$.

In the intermediate range, finally, where $Kn \approx 1$, the transition between high thermal gas conductivity and practically zero gas conductivity occurs. In this intermediate region, changes in gas pressure strongly affect gas conductivity.

Since in the definition of the Knudsen-number the mean free path, *mfp*, and the void size, expressed by δ, are present, both factors can influence the gas thermal conductivity. Reducing this void size has a similar effect as reducing the internal gas pressure. For vacuum insulation technology, therefore, materials with small pore sizes and a pressure reduced to below the Knudsen region should be taken. Figure A34.3 and Figure A34.4 show the effect of void size on gas conduction. As can be seen, reducing void size shifts the steep increase in the graph to the right and reduces the thermal conductivity at low pressure, both of which are favourable for vacuum insulation fills. At pressures near ambient, however, the thermal conductivity for powder-based core materials is raised somewhat, while it decreases for fibre-based materials (Rath, 1989).

A34.3 Gas convection thermal conductivity

Several researchers showed that in general (free) convection may be neglected in porous media with very low internal pore gas pressure. Achtziger (1960) and Zehender (1964), for example, demonstrated that at low temperatures this convection in vacuum insulation panels may be neglected, while Rath (1989) argued that free convection may be neglected in most porous vacuum insulation core materials as well, except for very light-weight fibre-based core materials (ρ < 50 kg·m^{-3}).

This free convection in open porous media can be neglected, if the following condition for a modified Rayleigh number, Ra^*, is satisfied (Brendeng, 1978)

$$Ra^* < 4\pi^2 \quad \text{(A34.22).}$$

This modified Rayleigh number can be calculated from the intrinsic permeability coefficient of the material, δ_0 [m^2]:

$$Ra^* = Gr^* \Pr = \frac{g \cdot \beta \cdot \Delta T \cdot L \cdot \delta_0 \cdot \rho \cdot c_p}{\nu \cdot \lambda} \quad \text{(A34.23),}$$

in which Gr^* is a modified Grasshoff number, Pr is the Prandtl number, g is the specific gravity (g = 9.81 m·s^{-2}), β [K^{-1}] the thermal expansion coefficient, L [m] some dimensional property, ρ [kg·m^{-3}] the density, c_p [J·kg^{-1}·K^{-1}] the specific heat with constant pressure, ν [m^2·s^{-1}] the kinetic viscosity and λ [W·m^{-1}·K^{-1}] the thermal conductivity of the gas.

A34.4 Radiative thermal conductivity

While conduction and convection need a medium (solid, liquid or gas) to transport energy, and can thus be eliminated by removing this medium, radiation does not, thus being present in a vacuum as well. Radiation is energy transfer by means of electromagnetic waves. The amount of heat transferred through radiation significantly depends on temperature. Every object with a temperature above 0 K radiates energy, represented by photons. The higher the temperature of a body, the more it radiates. The wavelength at with most radiation is emitted, $\hat{\lambda}$, depends on temperature according to Wien's law as

$$\hat{\lambda} \cdot T = k_w \quad \text{(A34.24).}$$

The constant, k_w, in this equation is called Wien's constant and equals 2.898·10^{-3} m·K.

If now the mean free path of the radiative photons is much smaller than the thickness of the insulating material (material is optically dense), if this mean free path does not depend on wavelength, and if the temperature differences are small, radiation through a porous material can be regarded as a diffusion process, which can be modelled according to Fourier's law (Hottel, 1967) as

$$q_r = -\lambda_r \frac{dT}{dx} \qquad \text{(A34.25).}$$

The radiation conductivity, λ_r [W·m^{-1}·K^{-1}], in this equation is expressed as (Caps and Fricke, 2000; Hostler et al., 2008; Reim et al., 2005; Hottel, 1967)

$$\lambda_r = \frac{16n^2\sigma\overline{T}_r^3}{3E(T_r)} \qquad \text{(A34.26),}$$

with n the index of refraction of the insulating material ($n^2 \approx 1.1$ for low density fumed silica (Napp et al., 1999)), σ the Stefan-Bolzmann constant, which equals $5.67 \cdot 10^{-8}$ W·m^{-2}·K^{-4}, $\overline{T}$ the mean temperature and and $E(T_r)$ [m^{-1}] the extinction coefficient, which is the product of density, ρ [kg·m^{-3}], and mass specific extinction coefficient, $e(T)$ [m^2·kg^{-1}]. If however the optical thickness of the material is low, the radiative thermal conductivity becomes dependent on panel thickness, d_p [m], and might be described by (Caps et al., 1995)

$$\lambda_r = \frac{16n^2\sigma\overline{T}_r^3}{3E(T_r) + 4/d_p} \qquad \text{(A34.27).}$$

The mean temperature in Equation (A34.27) is calculated as the Rosseland's average temperature inside the insulation material as (Mil'man and Kaganer, 1975)

$$\overline{T}_r^3 = \frac{\left(T_1^2 + T_2^2\right)\left(T_1 + T_2\right)}{4} \qquad \text{(A34.28).}$$

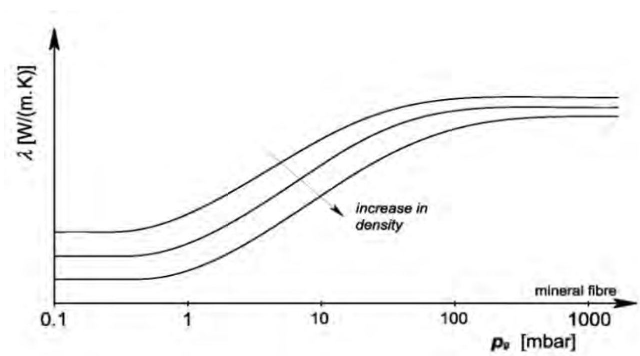

Figure A34.5

Effect of density on overall thermal conductivity for a fibre-based insulation material, based upon Rath (1989).

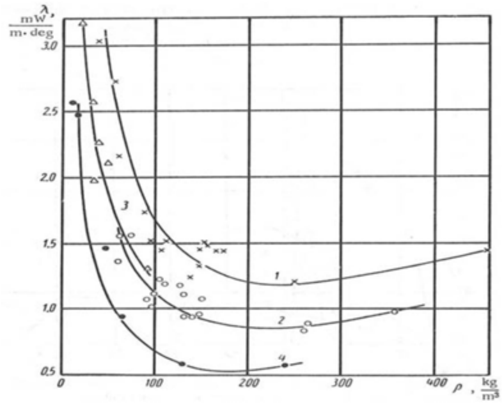

Figure A34.6

Thermal conductivity of evacuated aerogel (1), perlite (2), mipora (3) and glass wool (4) as function of density. Boundary temperatures were 293 K and 90 K. (Kaganer, 1969).

Based on the previous discussion, three methods of reducing the thermal radiation through a meso-porous VIP core material can be distinguished:

- Increasing density, thus reducing average void size, as shown in Figure A34.5. Kaganer showed that the radiative thermal conductivity is inversely proportional to density and that the solid thermal conductivity is directly proportional to density (Kaganer, 1969). He thus stated that the thermal conductivity of an evacuated porous medium is determined from:

  $$\lambda_{evac} = c_1 / \rho + c_2 \rho \qquad \text{(A34.29)},$$

  with c_1 and c_2 constants. Figure A34.6 demonstrates the effect of density on solid conduction and radiation for several evacuated materials. As can be seen, an optimum density exists for which the total thermal conductivity is minimal;

- Adding opacifiers, infrared absorbers or infrared blockers (carbon black, iron oxide or silicon carbide). These added materials more-or-less influence the specific extinction coefficient. This also implies that the constant c_1 in equation (A34.29) decreases if e increases, as a result of which the minimum in λ_{evac} will lie at lower density;

- Adding aluminium powder with a small particle diameter to a powder-based core material during production, also influencing the specific extinction coefficient (Rath, 1989). Adding aluminium powder only works, if the particle diameter of the aluminium powder is much smaller than the average particle diameter of the core material itself. A disadvantage is that for vacuum insulation panels, core materials with very small pore sizes are favoured, which consequently leads to the requirement of very fine aluminium powder with its risk of dust explosions.

Figure A35a

Comparison of numerical data (markers) to analytical model (continuous lines) of the linear thermal transmittance as function of panel thickness for a VIP with an AF barrier with different foil thicknesses

$\lambda_f = 225\ W\cdot m^{-1}\cdot K^{-1}$;
$\lambda_c = 2\cdot 10^{-3}\ W\cdot m^{-1}\cdot K^{-1}$;
$\varphi = 1$;
$\alpha_1 = 7.8\ m^2\cdot K\cdot W^{-1}$;
$\alpha_2 = 25\ m^2\cdot K\cdot W^{-1}$.

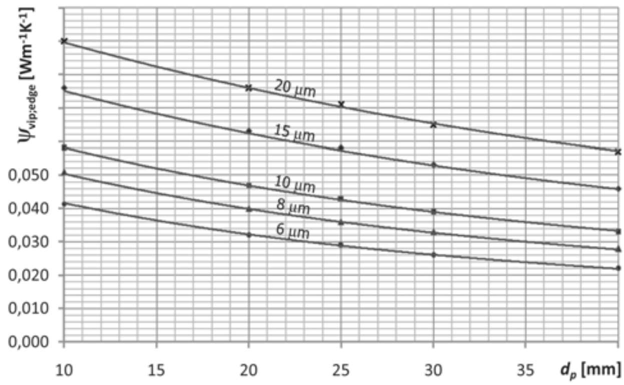

Figure A35b

Comparison of numerical data (markers) to analytical model (continuous lines) of the linear thermal transmittance as function of panel thickness for a VIP with an AF barrier with different foil thicknesses

$\lambda_f = 225\ W\cdot m^{-1}\cdot K^{-1}$;
$\lambda_c = 4\cdot 10^{-3}\ W\cdot m^{-1}\cdot K^{-1}$;
$\varphi = 1$;
$\alpha_1 = 7.8\ m^2\cdot K\cdot W^{-1}$;
$\alpha_2 = 25\ m^2\cdot K\cdot W^{-1}$.

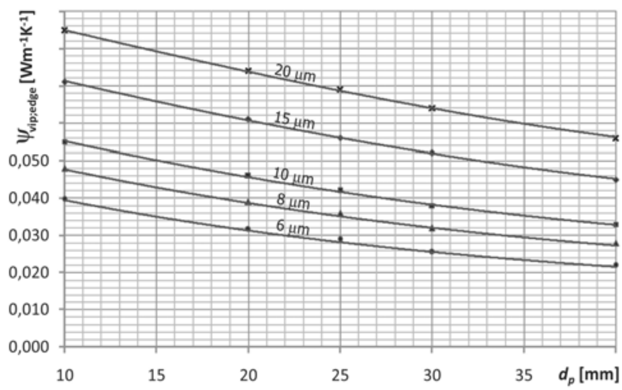

Figure A35c

Comparison of numerical data (markers) to analytical model (continuous lines) of the linear thermal transmittance as function of panel thickness for a VIP with an AF barrier with different foil thicknesses

$\lambda_f = 225\ W\cdot m^{-1}\cdot K^{-1}$;
$\lambda_c = 6\cdot 10^{-3}\ W\cdot m^{-1}\cdot K^{-1}$;
$\varphi = 1$;
$\alpha_1 = 7.8\ m^2\cdot K\cdot W^{-1}$;
$\alpha_2 = 25\ m^2\cdot K\cdot W^{-1}$.

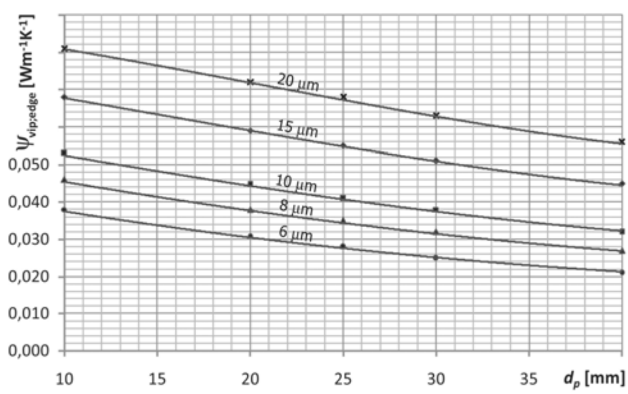

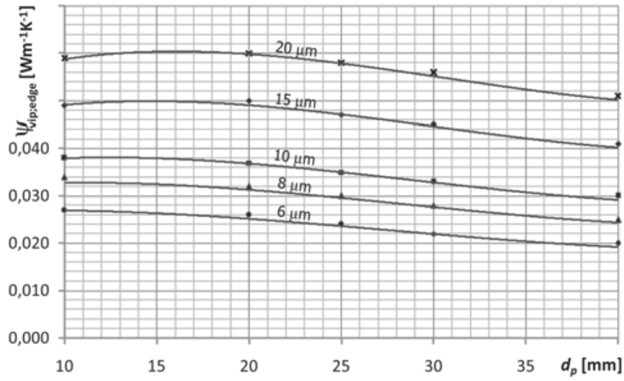

Figure A35d

Comparison of numerical data (markers) to analytical model (continuous lines) of the linear thermal transmittance as function of panel thickness for a VIP with an AF barrier with different foil thicknesses

λ_f = 225 W·m-1·K-1;
λ_c = 20·10-3 W·m-1·K-1;
φ = 1;
α_1 = 7.8 m2·K·W-1;
α_2 = 25 m2·K·W-1.

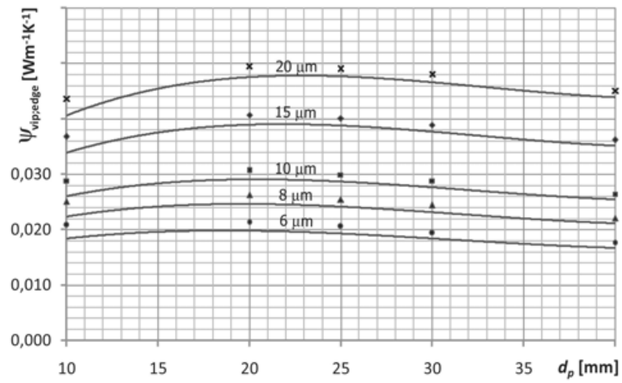

Figure A35e

Comparison of numerical data (markers) to analytical model (continuous lines) of the linear thermal transmittance as function of panel thickness for a VIP with an AF barrier with different foil thicknesses

λ_f = 225 W·m-1·K-1;
λ_c = 40·10-3 W·m-1·K-1;
φ = 1;
α_1 = 7.8 m2·K·W-1;
α_2 = 25 m2·K·W-1.

Figure A36a

Comparison of numerical data (markers) to analytical model (continuous lines) of the linear thermal transmittance as function of panel thickness for a VIP with a SSF barrier with different foil thicknesses

$\lambda_f = 25\ W\cdot m^{-1}\cdot K^{-1}$;
$\lambda_c = 2\cdot 10^{-3}\ W\cdot m^{-1}\cdot K^{-1}$;
$\varphi = 1$;
$\alpha_1 = 7.8\ m^2\cdot K\cdot W^{-1}$;
$\alpha_2 = 25\ m^2\cdot K\cdot W^{-1}$.

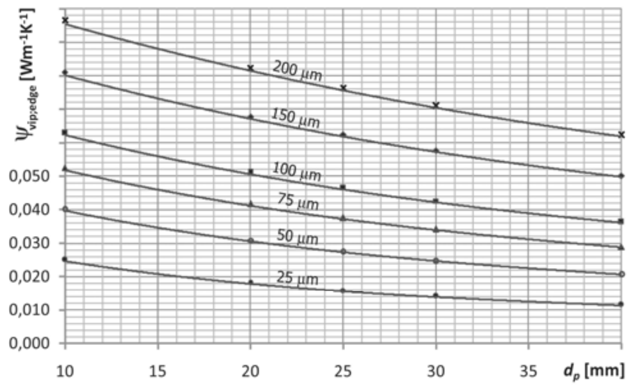

Figure A36b

Comparison of numerical data (markers) to analytical model (continuous lines) of the linear thermal transmittance as function of panel thickness for a VIP with a SSF barrier with different foil thicknesses

$\lambda_f = 25\ W\cdot m^{-1}\cdot K^{-1}$;
$\lambda_c = 4\cdot 10^{-3}\ W\cdot m^{-1}\cdot K^{-1}$;
$\varphi = 1$;
$\alpha_1 = 7.8\ m^2\cdot K\cdot W^{-1}$;
$\alpha_2 = 25\ m^2\cdot K\cdot W^{-1}$.

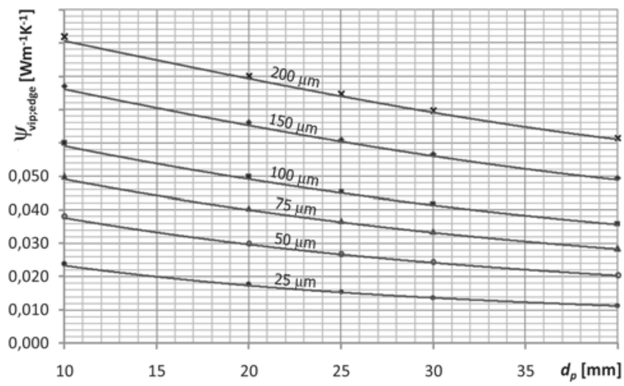

Figure A36c

Comparison of numerical data (markers) to analytical model (continuous lines) of the linear thermal transmittance as function of panel thickness for a VIP with a SSF barrier with different foil thicknesses

$\lambda_f = 25\ W\cdot m^{-1}\cdot K^{-1}$;
$\lambda_c = 6\cdot 10^{-3}\ W\cdot m^{-1}\cdot K^{-1}$;
$\varphi = 1$;
$\alpha_1 = 7.8\ m^2\cdot K\cdot W^{-1}$;
$\alpha_2 = 25\ m^2\cdot K\cdot W^{-1}$.

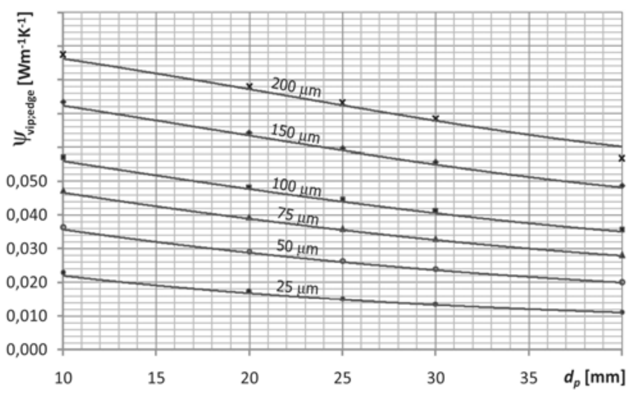

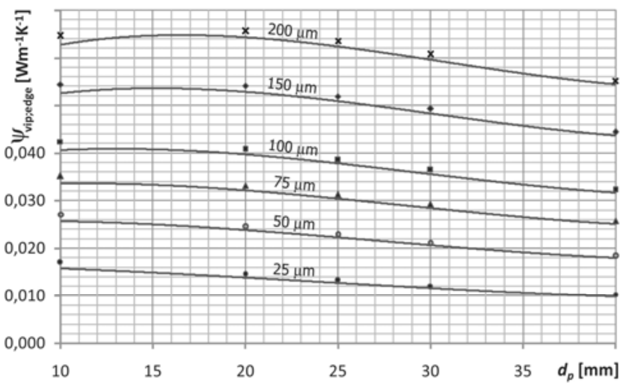

Figure A36d

Comparison of numerical data (markers) to analytical model (continuous lines) of the linear thermal transmittance as function of panel thickness for a VIP with a SSF barrier with different foil thicknesses

$\lambda_f = 25\ W{\cdot}m^{-1}{\cdot}K^{-1}$;
$\lambda_c = 20{\cdot}10^{-3}\ W{\cdot}m^{-1}{\cdot}K^{-1}$;
$\varphi = 1$;
$\alpha_1 = 7.8\ m^2{\cdot}K{\cdot}W^{-1}$;
$\alpha_2 = 25\ m^2{\cdot}K{\cdot}W^{-1}$.

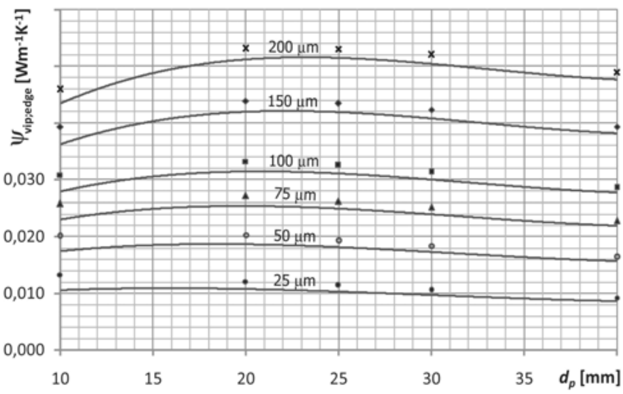

Figure A36e

Comparison of numerical data (markers) to analytical model (continuous lines) of the linear thermal transmittance as function of panel thickness for a VIP with a SSF barrier with different foil thicknesses

$\lambda_f = 25\ W{\cdot}m^{-1}{\cdot}K^{-1}$;
$\lambda_c = 40{\cdot}10^{-3}\ W{\cdot}m^{-1}{\cdot}K^{-1}$;
$\varphi = 1$;
$\alpha_1 = 7.8\ m^2{\cdot}K{\cdot}W^{-1}$;
$\alpha_2 = 25\ m^2{\cdot}K{\cdot}W^{-1}$.

Figure A37a

Comparison of numerical data (markers) to analytical model (continuous lines) of the linear thermal transmittance as function of panel thickness for a VIP with a MF barrier with different film thicknesses

film: MF;
$\lambda_c = 2 \cdot 10^{-3}\ W \cdot m^{-1} \cdot K^{-1}$;
$\varphi = 1$;
$\alpha_1 = 7.8\ m^2 \cdot K \cdot W^{-1}$;
$\alpha_2 = 25\ m^2 \cdot K \cdot W^{-1}$.

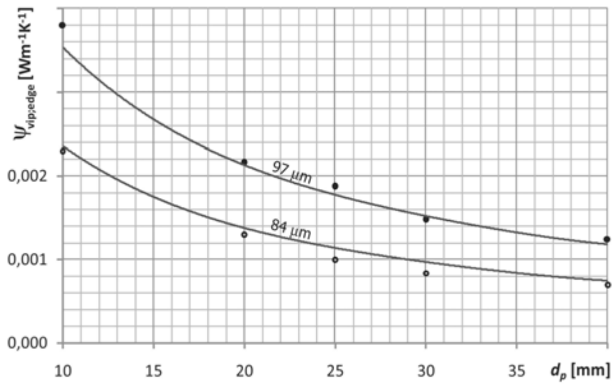

Figure A37b

Comparison of numerical data (markers) to analytical model (continuous lines) of the linear thermal transmittance as function of panel thickness for a VIP with a MF barrier with different film thicknesses

film: MF;
$\lambda_c = 4 \cdot 10^{-3}\ W \cdot m^{-1} \cdot K^{-1}$;
$\varphi = 1$;
$\alpha_1 = 7.8\ m^2 \cdot K \cdot W^{-1}$;
$\alpha_2 = 25\ m^2 \cdot K \cdot W^{-1}$.

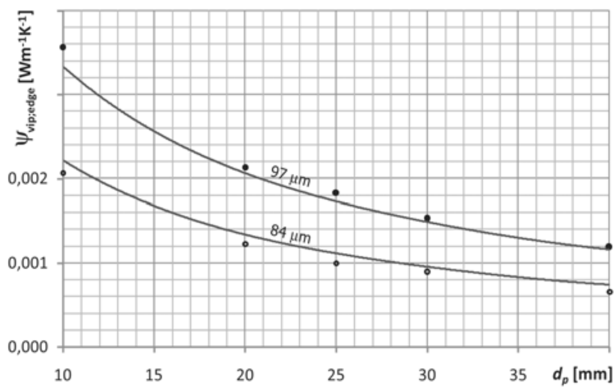

Figure A37c

Comparison of numerical data (markers) to analytical model (continuous lines) of the linear thermal transmittance as function of panel thickness for a VIP with a MF barrier with different film thicknesses

film: MF;
$\lambda_c = 6 \cdot 10^{-3}\ W \cdot m^{-1} \cdot K^{-1}$;
$\varphi = 1$;
$\alpha_1 = 7.8\ m^2 \cdot K \cdot W^{-1}$;
$\alpha_2 = 25\ m^2 \cdot K \cdot W^{-1}$.

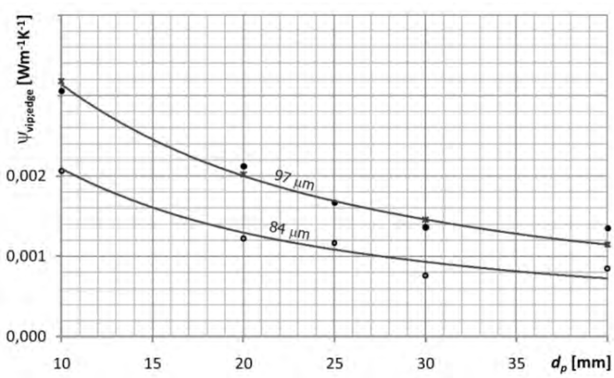

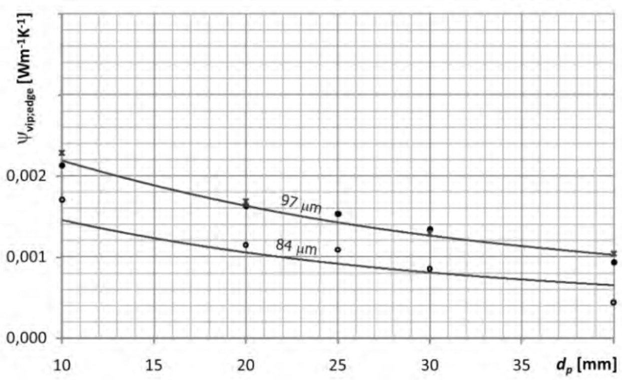

Figure A37d

Comparison of numerical data (markers) to analytical model (continuous lines) of the linear thermal transmittance as function of panel thickness for a VIP with a MF barrier with different film thicknesses

film: MF;
$\lambda_c = 20 \cdot 10^{-3}\ W \cdot m^{-1} \cdot K^{-1}$;
$\varphi = 1$;
$\alpha_1 = 7.8\ m^2 \cdot K \cdot W^{-1}$;
$\alpha_2 = 25\ m^2 \cdot K \cdot W^{-1}$.

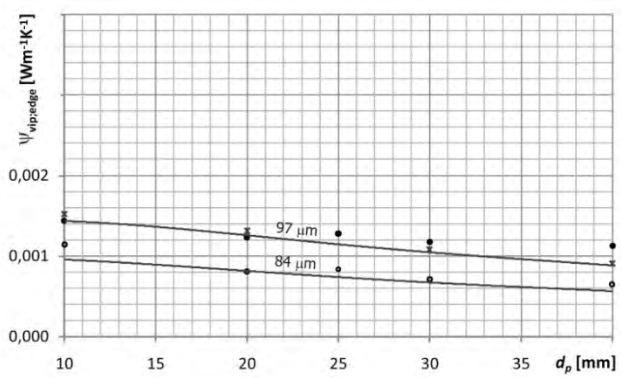

Figure A37e

Comparison of numerical data (markers) to analytical model (continuous lines) of the linear thermal transmittance as function of panel thickness for a VIP with a MF barrier with different film thicknesses

film: MF;
$\lambda_c = 40 \cdot 10^{-3}\ W \cdot m^{-1} \cdot K^{-1}$;
$\varphi = 1$;
$\alpha_1 = 7.8\ m^2 \cdot K \cdot W^{-1}$;
$\alpha_2 = 25\ m^2 \cdot K \cdot W^{-1}$.

Having given a theoretical discussion in chapter 3 and having presented an analytical model to determine the value of the linear thermal transmittance with relatively high accuracy, it is now interesting to investigate the effects of typical high barrier envelopes on the overall thermal performance of vacuum insulation panels, indicated by their effective thermal transmittance, U_{eff}, or effective thermal conductivity, λ_{eff}, and to compare them with alternative thermal insulators.

For this investigation the following high barrier envelopes have been selected as typical: a 6 μm and 8 μm thick aluminium foil laminate, a 25 μm and 50 μm thick stainless steel foil laminate, a 97 μm three-layer metallized film and a combined envelope of a 8 μm thick aluminium foil laminate on the warm side of the panel and a 97 μm three-layer metallized film on the cold side of the panel. Aluminium foil laminates originally used in the packaging industry had a thickness of 10 μm or more. Due to improvements in foil production technology, it is nowadays possible to produce pinhole free[22] 6 μm thick aluminium foils (Reisacher, 2003). Due to the high linear thermal transmittance caused by this aluminium foil, a foil as thin as possible should be applied, as a consequence of which a 6 μm and 8 μm thick foil laminate are selected. Similar considerations apply to the selection of a stainless steel barrier envelope. Due to their high thermal conductivity, they should be as thin as possible. Standard thickness of stainless steel foils, however, is bigger than that of aluminium foils. A stainless steel foil of 25 or 50 μm is currently at the edge of production technology and thus selected for analysis. With respect to metallized films, however, gas and water vapour barrier properties are the dominating factor in selecting an appropriate envelope. Since the water vapour and gas permeance of these films is higher than the permeance of equivalent metal foils, a sufficient number of metallization layers are required to maintain the core material in an evacuated state for a period as long as required for building applications, as will be explained in Chapter 5. Nowadays, three-layer metallized films are therefore widely used as barrier for vacuum insulation panels. Finally, a combined envelope with a thin aluminium foil laminate and a metallized film is selected since it is a new concept for obtaining both high thermal performance and long service life, even for small panels (Caps, 2003).

---

[22] Pinholes are microscopic defects in a thin metal foil (or polymer film) caused by the rolling process. They reduce the resistance to gas and water vapour penetration considerably. In fact, pin holes are the only paths through which gases penetrate thin metal foils.

Based on the model presented in the previous sections, the U_{eff}-value and λ_{eff}-value of a VIP can be plotted as function of panel thickness and ratio of perimeter to surface area for selected barrier envelopes. These plots are presented in Figure A38.1 presenting the U_{eff}-value of a VIP with λ_c = 0.004 W·m^{-1}·K^{-1}, in Figure A38.2 presenting the U_{eff}-value of a VIP with λ_c = 0.008 W·m^{-1}·K^{-1} and in Figure A38.3 presenting the λ_{eff}-value of a VIP with λ_c = 0.004 W·m^{-1}·K^{-1}. As can be seen, the overall thermal performance of a VIP with a metal-based barrier envelope strongly depends on the size and aspect ratio of the panel. A vacuum insulation panel with a core material thermal conductivity of 0.004 W·m^{-1}·K^{-1}, a 6 μm aluminium foil laminate, a thickness of 20 mm and a ratio φ of 0.67 (Figure A38.1a), for instance, has an effective thermal conductance of 0.38 W·m^{-2}·K^{-1} for l_p / S_p = 5 m^{-1} and of 0.57 W·m^{-1}·K^{-1} for l_p / S_p = 10 m^{-1}.[23] The thermal bridge effect is thus considerable and non-negligible for these panels. For metallized films but also for the combined envelope, however, the overall thermal performance only moderately depends on this perimeter to surface area ratio. The lines denoting equal thermal performance are almost horizontal in the U_{eff}-value plots. This implies that the effect of the edge on the overall thermal performance is small. From the λ_{eff}-plots similar conclusions can be drawn.

---

[23] A perimeter to surface area ratio of 5 m^{-1} corresponds to a panel of 0.6x1.2 m^2 and a ratio of 10 m^{-1} corresponds to a panel of 0.3x0.6 m^2.

Figure A38.1a

Surface plot of the effective U-value of a VIP as function of panel thickness, d_p [m], and perimeter to surface area ratio, l_p/S_p [m^{-1}]. Values along the lines denote the U_{eff}-value [$W \cdot m^{-2} \cdot K^{-1}$].

Barrier: AF 6 μm
$\lambda_f = 225\ W \cdot m^{-1} \cdot K^{-1}$;
$t_f = 6\ \mu m$; $\lambda_c = 4 \cdot 10^{-3}\ W \cdot m^{-1} \cdot K^{-1}$;
$\varphi = 0.67$; $\alpha_1 = 7.8\ m^2 \cdot K \cdot W^{-1}$;
$\alpha_2 = 25\ m^2 \cdot K \cdot W^{-1}$;

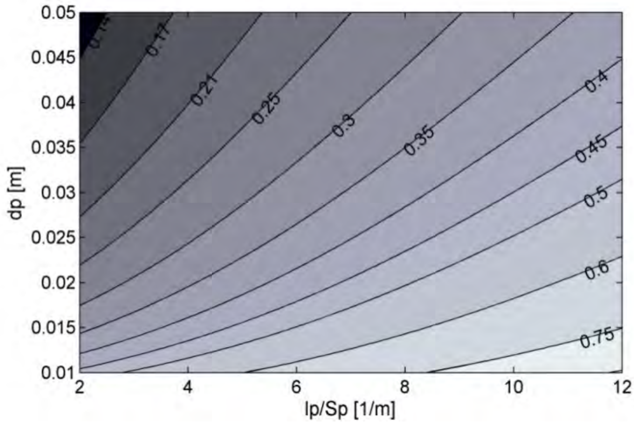

Figure A38.1b

Surface plot of the effective U-value of a VIP as function of panel thickness, d_p [m], and perimeter to surface area ratio, l_p/S_p [m^{-1}]. Values along the lines denote the U_{eff}-value [$W \cdot m^{-2} \cdot K^{-1}$].

Barrier: AF 8 μm
$\lambda_f = 225\ W \cdot m^{-1} \cdot K^{-1}$;
$t_f = 8\ \mu m$; $\lambda_c = 4 \cdot 10^{-3}\ W \cdot m^{-1} \cdot K^{-1}$;
$\varphi = 0.67$; $\alpha_1 = 7.8\ m^2 \cdot K \cdot W^{-1}$;
$\alpha_2 = 25\ m^2 \cdot K \cdot W^{-1}$;

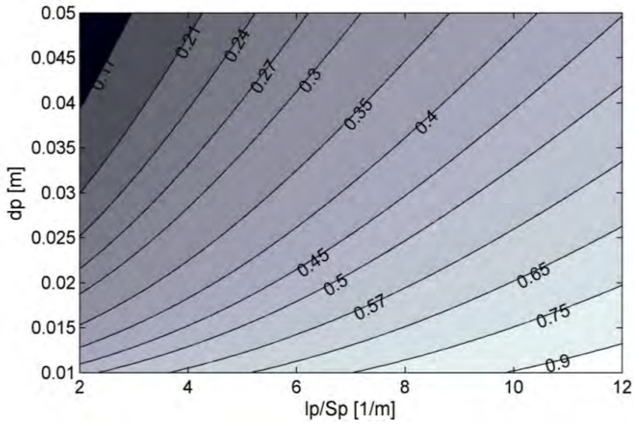

Figure A38.1c

Surface plot of the effective U-value of a VIP as function of panel thickness, d_p [m], and perimeter to surface area ratio, l_p/S_p [m^{-1}]. Values along the lines denote the U_{eff}-value [$W \cdot m^{-2} \cdot K^{-1}$].

Barrier: SSF 25 μm
$\lambda_f = 25\ W \cdot m^{-1} \cdot K^{-1}$;
$t_f = 25\ \mu m$;
$\lambda_c = 4 \cdot 10^{-3}\ W \cdot m^{-1} \cdot K^{-1}$;
$\varphi = 0.67$; $\alpha_1 = 7.8\ m^2 \cdot K \cdot W^{-1}$;
$\alpha_2 = 25\ m^2 \cdot K \cdot W^{-1}$;

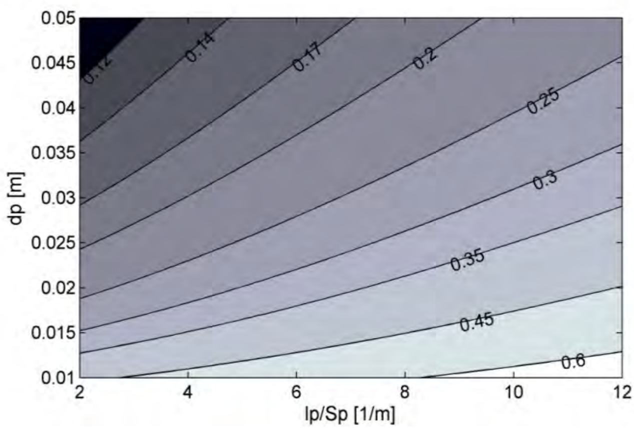

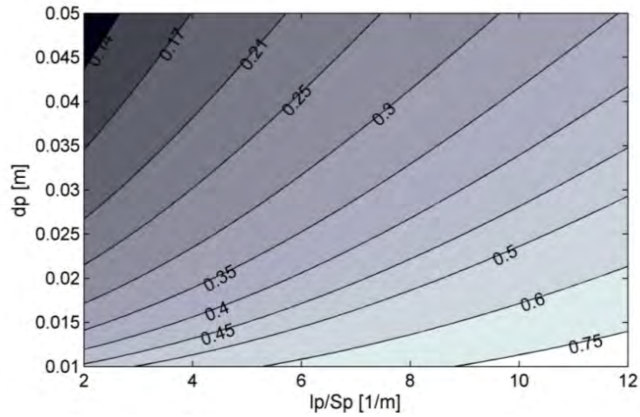

Figure A38.1d

Surface plot of the effective U-value of a VIP as function of panel thickness, d_p [m], and perimeter to surface area ratio, l_p/S_p [m^{-1}]. Values along the lines denote the U_{eff}-value [$W \cdot m^{-2} \cdot K^{-1}$].

Barrier: SSF 50 μm
$\lambda_f = 25\ W \cdot m^{-1} \cdot K^{-1}$;
$t_f = 50 \mu m$;
$\lambda_c = 4 \cdot 10^{-3}\ W \cdot m^{-1} \cdot K^{-1}$;
$\varphi = 0.67$; $\alpha_1 = 7.8\ m^2 \cdot K \cdot W^{-1}$;
$\alpha_2 = 25\ m^2 \cdot K \cdot W^{-1}$;

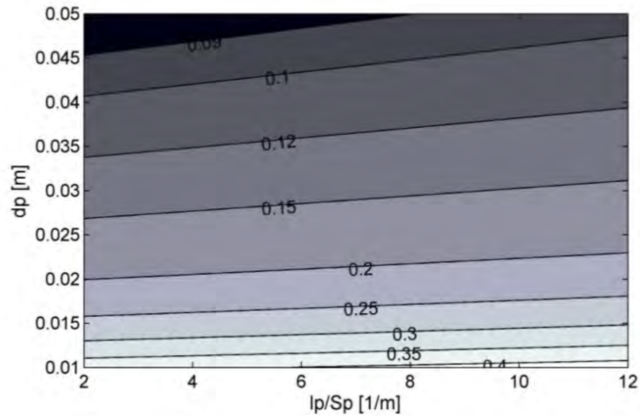

Figure A38.1e

Surface plot of the effective U-value of a VIP as function of panel thickness, d_p [m], and perimeter to surface area ratio, l_p/S_p [m^{-1}]. Values along the lines denote the U_{eff}-value [$W \cdot m^{-2} \cdot K^{-1}$].

Barrier: MF3
$\lambda_f = 0.54\ W \cdot m^{-1} \cdot K^{-1}$;
$t_f = 97 \mu m$;
$\lambda_c = 4 \cdot 10^{-3}\ W \cdot m^{-1} \cdot K^{-1}$;
$\varphi = 0.67$; $\alpha_1 = 7.8\ m^2 \cdot K \cdot W^{-1}$;
$\alpha_2 = 25\ m^2 \cdot K \cdot W^{-1}$;

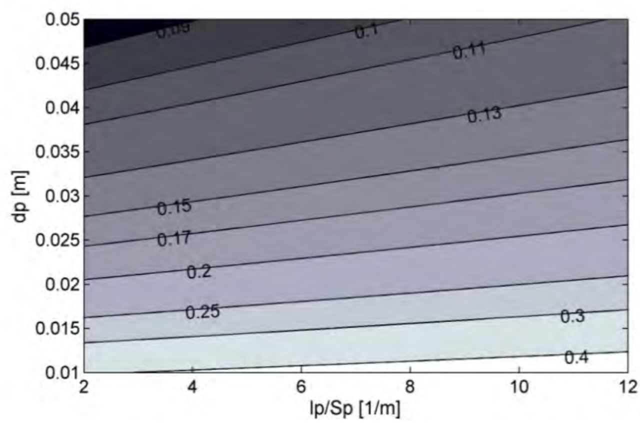

Figure A38.1f

Surface plot of the effective U-value of a VIP as function of panel thickness, d_p [m], and perimeter to surface area ratio, l_p/S_p [m^{-1}]. Values along the lines denote the U_{eff}-value [$W \cdot m^{-2} \cdot K^{-1}$].

Barrier: combination
MF3 on cold side
AF 8 μm on warm side
$\lambda_c = 4 \cdot 10^{-3}\ W \cdot m^{-1} \cdot K^{-1}$;
$\varphi = 0.67$; $\alpha_1 = 7.8\ m^2 \cdot K \cdot W^{-1}$;
$\alpha_2 = 25\ m^2 \cdot K \cdot W^{-1}$;

Figure A38.2a

Surface plot of the effective U-value of a VIP as function of panel thickness, d_p [m], and perimeter to surface area ratio, l_p/S_p [m^{-1}]. Values along the lines denote the U_{eff}-value [$W{\cdot}m^{-2}{\cdot}K^{-1}$].

Barrier: AF 6 μm
λ_f = 225 $W{\cdot}m^{-1}{\cdot}K^{-1}$;
t_f = 6 μm; $\lambda_c = 8{\cdot}10^{-3}$ $W{\cdot}m^{-1}{\cdot}K^{-1}$;
φ = 0.67; α_1 = 7.8 $m^2{\cdot}K{\cdot}W^{-1}$;
α_2 = 25 $m^2{\cdot}K{\cdot}W^{-1}$;

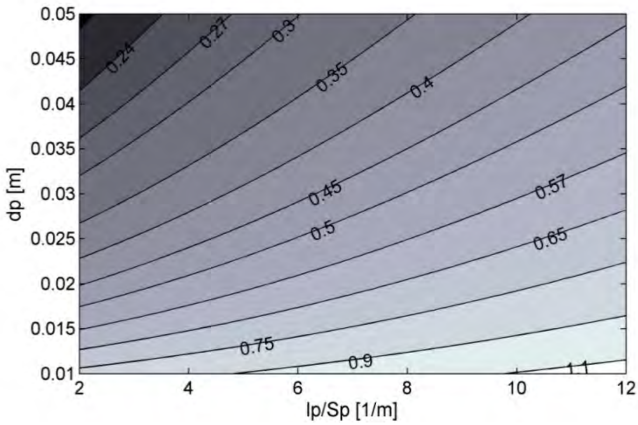

Figure A38.2b

Surface plot of the effective U-value of a VIP as function of panel thickness, d_p [m], and perimeter to surface area ratio, l_p/S_p [m^{-1}]. Values along the lines denote the U_{eff}-value [$W{\cdot}m^{-2}{\cdot}K^{-1}$].

Barrier: AF 8 μm
λ_f = 225 $W{\cdot}m^{-1}{\cdot}K^{-1}$;
t_f = 8 μm; $\lambda_c = 8{\cdot}10^{-3}$ $W{\cdot}m^{-1}{\cdot}K^{-1}$;
φ = 0.67; α_1 = 7.8 $m^2{\cdot}K{\cdot}W^{-1}$;
α_2 = 25 $m^2{\cdot}K{\cdot}W^{-1}$;

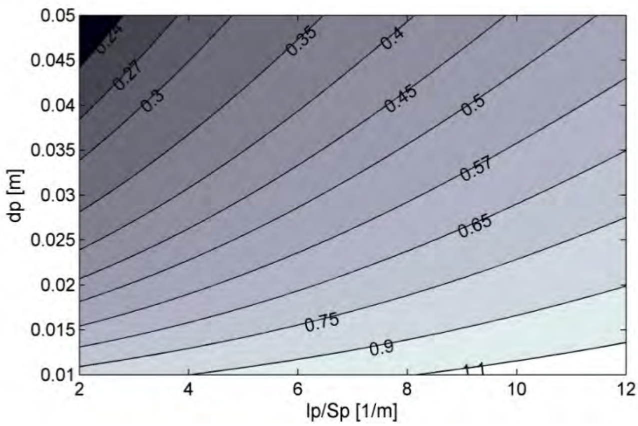

Figure A38.2c

Surface plot of the effective U-value of a VIP as function of panel thickness, d_p [m], and perimeter to surface area ratio, l_p/S_p [m^{-1}]. Values along the lines denote the U_{eff}-value [$W{\cdot}m^{-2}{\cdot}K^{-1}$].

Barrier: SSF 25 μm
λ_f = 25 $W{\cdot}m^{-1}{\cdot}K^{-1}$;
t_f = 25 μm;
$\lambda_c = 8{\cdot}10^{-3}$ $W{\cdot}m^{-1}{\cdot}K^{-1}$;
φ = 0.67; α_1 = 7.8 $m^2{\cdot}K{\cdot}W^{-1}$;
α_2 = 25 $m^2{\cdot}K{\cdot}W^{-1}$;

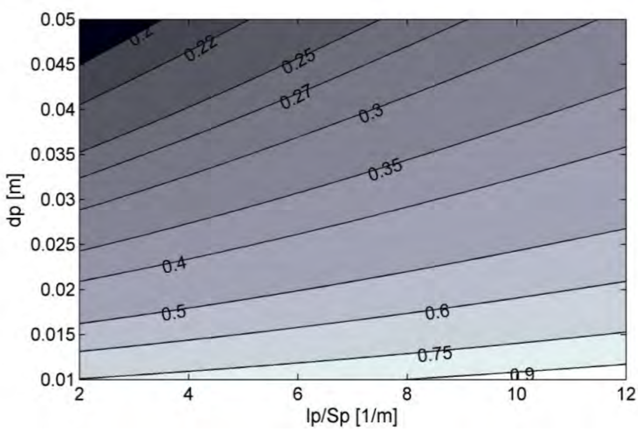

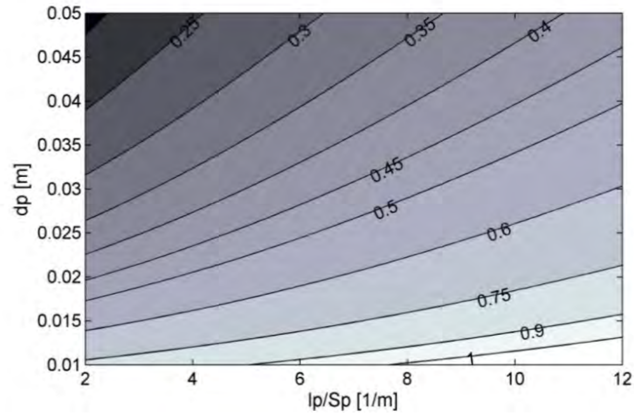

Figure A38.2d

Surface plot of the effective U-value of a VIP as function of panel thickness, d_p [m], and perimeter to surface area ratio, l_p/S_p [m^{-1}]. Values along the lines denote the U_{eff}-value [$W \cdot m^{-2} \cdot K^{-1}$].

Barrier: SSF 50 μm
$\lambda_f = 25\ W \cdot m^{-1} \cdot K^{-1}$;
$t_f = 50 \mu m$;
$\lambda_c = 8 \cdot 10^{-3}\ W \cdot m^{-1} \cdot K^{-1}$;
$\varphi = 0.67$; $\alpha_1 = 7.8\ m^2 \cdot K \cdot W^{-1}$;
$\alpha_2 = 25\ m^2 \cdot K \cdot W^{-1}$;

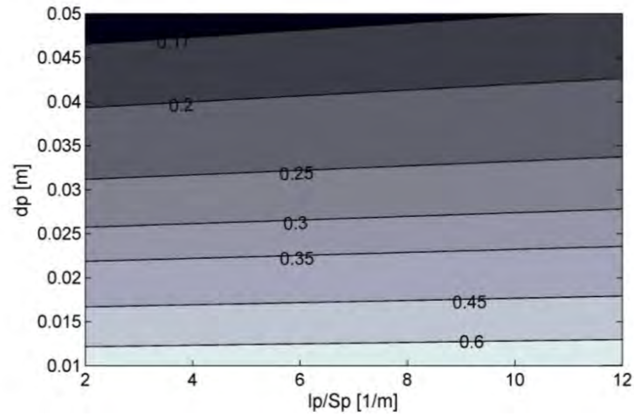

Figure A38.2e

Surface plot of the effective U-value of a VIP as function of panel thickness, d_p [m], and perimeter to surface area ratio, l_p/S_p [m^{-1}]. Values along the lines denote the U_{eff}-value [$W \cdot m^{-2} \cdot K^{-1}$].

Barrier: MF3
$\lambda_f = 0.54\ W \cdot m^{-1} \cdot K^{-1}$;
$t_f = 97 \mu m$;
$\lambda_c = 8 \cdot 10^{-3}\ W \cdot m^{-1} \cdot K^{-1}$;
$\varphi = 0.67$; $\alpha_1 = 7.8\ m^2 \cdot K \cdot W^{-1}$;
$\alpha_2 = 25\ m^2 \cdot K \cdot W^{-1}$;

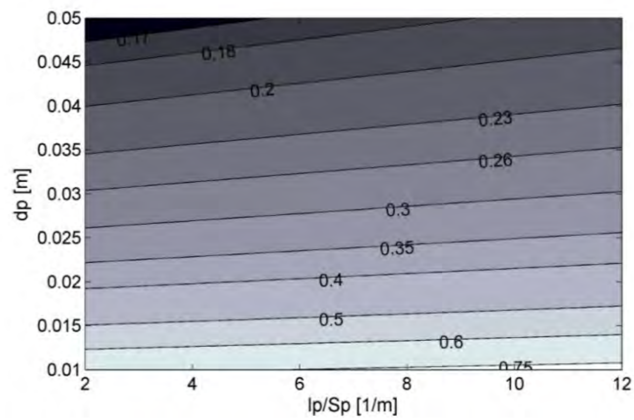

Figure A38.2f

Surface plot of the effective U-value of a VIP as function of panel thickness, d_p [m], and perimeter to surface area ratio, l_p/S_p [m^{-1}]. Values along the lines denote the U_{eff}-value [$W \cdot m^{-2} \cdot K^{-1}$].

Barrier: combination
MF3 on cold side
AF 8 μm on warm side
$\lambda_c = 8 \cdot 10^{-3}\ W \cdot m^{-1} \cdot K^{-1}$;
$\varphi = 0.67$; $\alpha_1 = 7.8\ m^2 \cdot K \cdot W^{-1}$;
$\alpha_2 = 25\ m^2 \cdot K \cdot W^{-1}$;

Figure 38.3a

Surface plot of the effective thermal conductivity of a VIP as function of panel thickness, d_p [m], and perimeter to surface area ratio, l_p/S_p [m^{-1}]. Values along the lines denote the λ_{eff}-value [mW·m^{-1}·K^{-1}].

Barrier: AF 6 μm
λ_f = 225 W·m^{-1}·K^{-1};
t_f = 6 μm; λ_c = 4·10^{-3} W·m^{-1}·K^{-1};
φ = 0.67; α_1 = 7.8 m^2·K·W^{-1};
α_2 = 25 m^2·K·W^{-1};

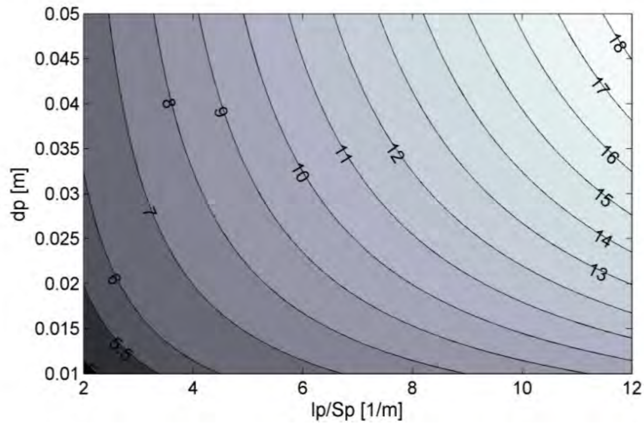

Figure 38.3b

Surface plot of the effective thermal conductivity of a VIP as function of panel thickness, d_p [m], and perimeter to surface area ratio, l_p/S_p [m^{-1}]. Values along the lines denote the λ_{eff}-value [mW·m^{-1}·K^{-1}].

Barrier: AF 8 μm
λ_f = 225 W·m^{-1}·K^{-1};
t_f = 8 μm; λ_c = 4·10^{-3} W·m^{-1}·K^{-1};
φ = 0.67; α_1 = 7.8 m^2·K·W^{-1};
α_2 = 25 m^2·K·W^{-1};

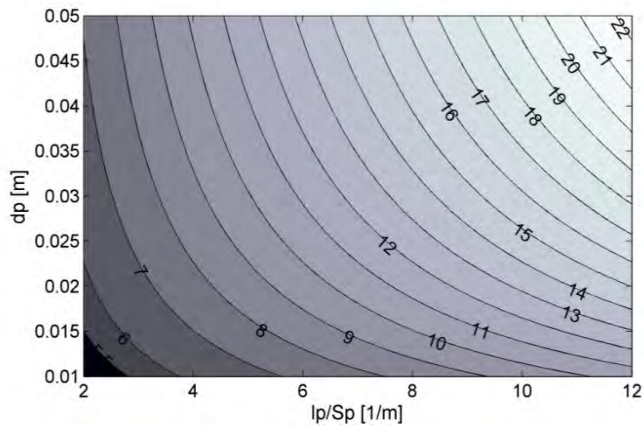

Figure 38.3c

Surface plot of the effective thermal conductivity of a VIP as function of panel thickness, d_p [m], and perimeter to surface area ratio, l_p/S_p [m^{-1}]. Values along the lines denote the λ_{eff}-value [mW·m^{-1}·K^{-1}].

Barrier: SSF 25 μm
λ_f = 25 W·m^{-1}·K^{-1};
t_f = 25 μm;
λ_c = 4·10^{-3} W·m^{-1}·K^{-1};
φ = 0.67; α_1 = 7.8 m^2·K·W^{-1};
α_2 = 25 m^2·K·W^{-1};

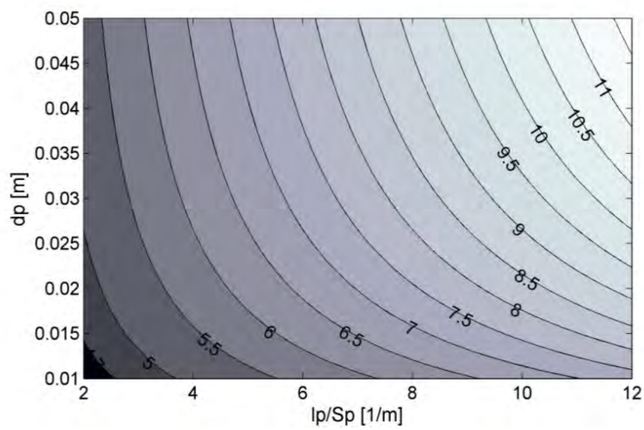

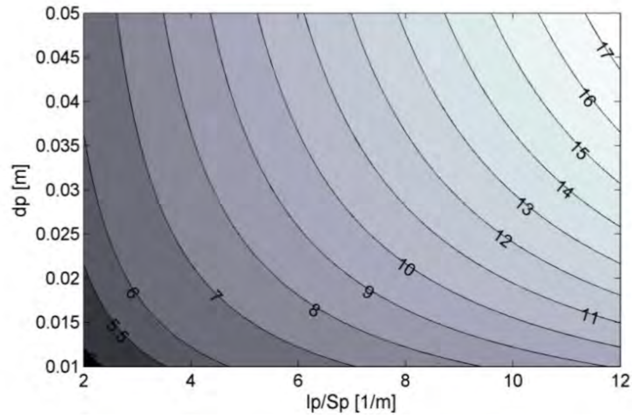

Figure 38.3d

Surface plot of the effective thermal conductivity of a VIP as function of panel thickness, d_p [m], and perimeter to surface area ratio, l_p/S_p [m^{-1}]. Values along the lines denote the λ_{eff}-value [mW·m^{-1}·K^{-1}].

Barrier: SSF 50 μm
λ_f = 25 W·m^{-1}·K^{-1};
t_f = 50μm;
λ_c = 4·10^{-3} W·m^{-1}·K^{-1};
φ = 0.67; α_1 = 7.8 m^2·K·W^{-1};
α_2 = 25 m^2·K·W^{-1};

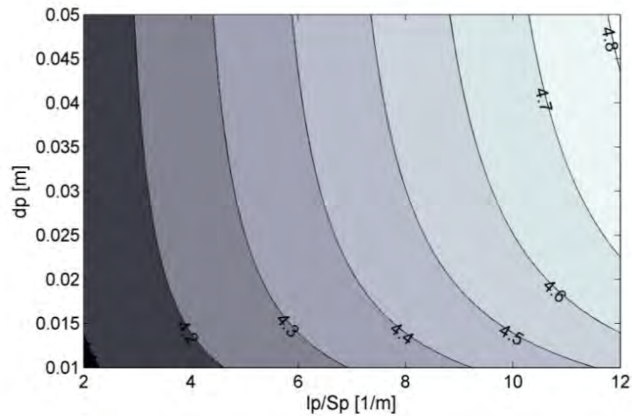

Figure 38.3e

Surface plot of the effective thermal conductivity of a VIP as function of panel thickness, d_p [m], and perimeter to surface area ratio, l_p/S_p [m^{-1}]. Values along the lines denote the λ_{eff}-value [mW·m^{-1}·K^{-1}].

Barrier: MF3
λ_f = 0.54 W·m^{-1}·K^{-1};
t_f = 97μm;
λ_c = 4·10^{-3} W·m^{-1}·K^{-1};
φ = 0.67; α_1 = 7.8 m^2·K·W^{-1};
α_2 = 25 m^2·K·W^{-1};

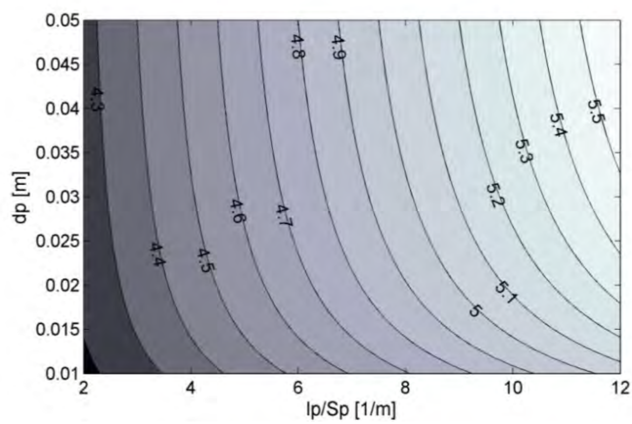

Figure 38.3f

Surface plot of the effective thermal conductivity of a VIP as function of panel thickness, d_p [m], and perimeter to surface area ratio, l_p/S_p [m^{-1}]. Values along the lines denote the λ_{eff}-value [mW·m^{-1}·K^{-1}].

Barrier: combination
MF3 on cold side
AF 8 μm on warm side
λ_c = 4·10^{-3} W·m^{-1}·K^{-1};
φ = 0.67; α_1 = 7.8 m^2·K·W^{-1};
α_2 = 25 m^2·K·W^{-1};

Table A39.1 - *Overview of numerically computed linear thermal transmittances [W·m^{-1}·K^{-1}]*

λ_c [W·m^{-1}·K^{-1}]	λ_l [W·m^{-1}·K^{-1}]	aluminium foil 225					stainless steel foil 25						metallized film 0.39	metallized film 0.54
	d_p [mm] \ t_l [µm]	6	8	10	15	20	25	50	75	100	150	200	84	97
0.002	10	0.041	0.051	0.058	0.076	0.090	0.025	0.040	0.053	0.063	0.081	0.097	0.002	0.004
	20	0.032	0.040	0.047	0.063	0.076	0.018	0.031	0.042	0.051	0.068	0.082	0.001	0.002
	25	0.029	0.036	0.043	0.058	0.071	0.016	0.028	0.038	0.047	0.062	0.076	0.001	0.002
	30	0.026	0.033	0.039	0.053	0.065	0.014	0.025	0.034	0.043	0.058	0.071	0.001	0.001
	40	0.022	0.028	0.033	0.046	0.057	0.012	0.021	0.029	0.036	0.050	0.062	0.001	0.001
0.004	10	0.040	0.048	0.055	0.071	0.085	0.024	0.038	0.050	0.060	0.077	0.092	0.002	0.004
	20	0.032	0.039	0.046	0.061	0.074	0.018	0.030	0.041	0.050	0.066	0.080	0.001	0.002
	25	0.029	0.036	0.042	0.056	0.069	0.016	0.027	0.037	0.046	0.061	0.075	0.001	0.002
	30	0.026	0.032	0.038	0.052	0.064	0.014	0.024	0.034	0.042	0.057	0.070	0.001	0.002
	40	0.022	0.028	0.033	0.045	0.056	0.011	0.021	0.029	0.036	0.050	0.062	0.001	0.001
0.006	10	0.038	0.046	0.053	0.068	0.081	0.023	0.036	0.047	0.057	0.073	0.088	0.002	0.003
	20	0.031	0.038	0.045	0.059	0.072	0.017	0.029	0.039	0.048	0.064	0.078	0.001	0.002
	25	0.028	0.035	0.041	0.055	0.068	0.015	0.026	0.036	0.045	0.060	0.073	0.001	0.002
	30	0.025	0.032	0.038	0.051	0.063	0.014	0.024	0.033	0.041	0.056	0.069	0.001	0.001
	40	0.021	0.027	0.032	0.045	0.056	0.011	0.020	0.028	0.036	0.049	0.057	0.001	0.001
0.020	10	0.027	0.034	0.038	0.049	0.059	0.017	0.027	0.035	0.042	0.054	0.065	0.002	0.002
	20	0.026	0.032	0.037	0.050	0.060	0.015	0.025	0.033	0.041	0.054	0.066	0.001	0.002
	25	0.024	0.030	0.035	0.047	0.058	0.013	0.023	0.031	0.039	0.052	0.064	0.001	0.002
	30	0.022	0.028	0.033	0.045	0.056	0.012	0.021	0.029	0.037	0.049	0.061	0.001	0.001
	40	0.020	0.025	0.030	0.041	0.051	0.010	0.019	0.026	0.032	0.044	0.055	0.000	0.001
0.040	10	0.021	0.025	0.029	0.037	0.044	0.013	0.020	0.026	0.031	0.039	0.046	0.001	0.001
	20	0.021	0.026	0.031	0.041	0.050	0.012	0.020	0.027	0.033	0.044	0.053	0.001	0.001
	25	0.021	0.025	0.030	0.040	0.049	0.011	0.019	0.026	0.033	0.043	0.053	0.001	0.001
	30	0.019	0.024	0.029	0.039	0.048	0.011	0.018	0.025	0.031	0.042	0.052	0.001	0.001
	40	0.018	0.022	0.026	0.036	0.045	0.009	0.017	0.023	0.029	0.039	0.049	0.001	0.001

APPENDIXES TO CHAPTER 4 A

A41 DERIVATION OF THERMAL BRIDGE EQUATION FOR BUILDING PANELS

The thermal bridge due to the continuous high barrier laminate enveloping a VIP can be represented schematically as in Figure A41.1. This scheme is in principal also valid for the development of the governing differential equations for component edge thermal bridges. For the derivation of the model the following are assumed:

- The length of the (VIP integrated) building panel is infinite. At a defined distance x and y from the origin, the temperature profile over de thickness of the panel, therefore, equals the undisturbed steady-state one-dimensional temperature profile. At that point the influence of the thermal bridge on the temperature of the facing has diminished.
- The boundary heat transmission coefficient α_j is constant across the surface of layer j and the facing temperature $T_{f;j}$ is constant in the cross-section through the facing.
- Additional radiative heat transfer processes that are not covered by the heat transmission boundary coefficients, α_j, are not considered.
- No lateral heat exchange between different panels in the edge region occurs.

Based on these assumptions, the following steady-state heat balance equation can be formulated for the x-direction (Figure A41.1) through the facings (including laminates):

$$t_{f1}\lambda_{f1}\left.\frac{dT_x}{dx}\right|_x - t_{f1}\lambda_{f1}\left.\frac{dT_x}{dx}\right|_{x+dx} - \alpha_1(T_1 - T_x)dx + \frac{\lambda_c}{d_c}(T_x - T_y)dx = 0 \qquad \text{(A41.1).}$$

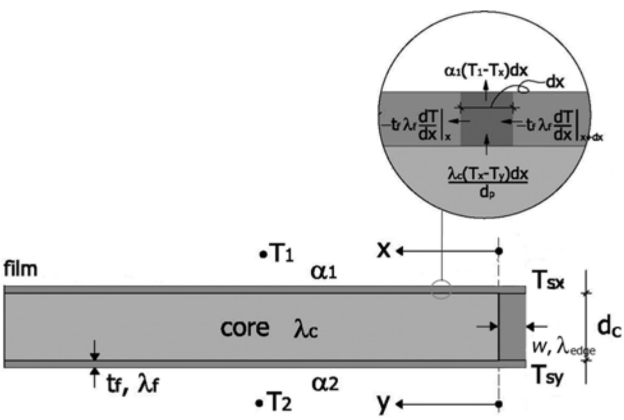

Figure A41.1

Schematic representation of the thermal bridge arising from the thin film high barrier envelope of a vacuum insulation panel.

In this equation α_j[W·m^{-2}·K^{-1}] is the heat transmission coefficient at boundary surface 1 or 2 respectively, d_c [m] is the thickness of the vacuum insulation panel or the insulated core of the panel, t_{fj} [m] is the thickness of the laminate and facing on side 1 (interior) or 2 (exterior), λ_{fj} [W·m^{-1}·K^{-1}] is the effective thermal conductivity of the laminate and facing on side 1 (interior) or 2 (exterior), λ_c [W·m^{-1}·K^{-1}] is the thermal conductivity of the VIP core or insulation core, T_j [K] is the air temperature on side 1 (interior) or 2 (exterior), T_x [K] is the temperature of the barrier laminate in x-direction (in the facing on side 1) and T_y [K] is the temperature of the barrier laminate in y-direction (in the facing on side 2).

Dividing Equation (A41.1) by dx, taking the limit for $dx \rightarrow 0$ and assuming that t_{f1} and λ_{f1} are constant over x, results in

$$\frac{d^2T_x}{dx^2} - \left(\frac{\alpha_1}{t_{f1}\lambda_{f1}} + \frac{\lambda_c}{t_{f1}\lambda_{f1}d_c}\right)\cdot T_x = -\frac{\alpha_1}{t_{f1}\lambda_{f1}}T_1 - \frac{\lambda_c}{t_{f1}\lambda_{f1}d_c}T_y \quad \text{(A41.2),}$$

or in

$$\frac{d^2T_x}{dx^2} - N_1^2T_x + B_1T_y = -A_1T_1 \quad \text{(A41.3a).}$$

For the y-direction (other side of the panel) a similar non-homogeneous second-order differential equation for the temperature distribution in the facing and high barrier laminate can be derived:

$$\frac{d^2T_y}{dy^2} - N_2^2 \cdot T_y + B_2T_x = -A_2T_2 \quad \text{(A41.3b),}$$

in which N_j, A_j and B_j are defined as (with j = 1 or 2)

$$N_j = \sqrt{\frac{\alpha_j}{t_{f;j}\lambda_{f;j}} + \frac{\lambda_c}{t_{f;j}\lambda_{f;j}d_c}} \quad \text{(A41.3c),}$$

$$A_j = \frac{\alpha_j}{t_{f;j}\lambda_{f;j}} \quad \text{(A41.3d),}$$

$$B_j = \frac{\lambda_c}{t_{f;j}\lambda_{f;j}d_c} \quad \text{(A41.3e),}$$

Equations (A41.3a) and (A41.3b) form a non-homogeneous system of second-order linear differential equations that can be written as the following matrix equation

$$\begin{bmatrix} T_x'' \\ T_y'' \end{bmatrix} - \begin{bmatrix} N_1^2 & -B_1 \\ -B_2 & N_2^2 \end{bmatrix} \cdot \begin{bmatrix} T_x \\ T_y \end{bmatrix} = \begin{bmatrix} -A_1 T_1 \\ -A_2 T_2 \end{bmatrix} \quad \text{(A41.4),}$$

which has as general solution

$$\overline{T} = c_1 \overline{E}_1 e^{\lambda_1 x} + c_2 \overline{E}_2 e^{\lambda_2 x} + c_3 \overline{E}_3 e^{-\lambda_3 x} + c_4 \overline{E}_4 e^{-\lambda_4 x} + \overline{c}_0 \quad \text{(A41.5).}$$

In this solution λ_1, λ_2, λ_3, λ_4 are the eigenvalues of the square matrix, while the vectors $\overline{E}$ are the eigenvectors of the system. From these equations, the eigenvalues, eigenvectors and vector $\overline{c}_0$ can be calculated as

$$\lambda_{1,2,3,4} = \pm \sqrt{\frac{(N_1^2 + N_2^2) \pm \sqrt{(N_1^2 - N_2^2)^2 + 4B_1B_2}}{2}} \quad \text{(A41.6),}$$

$$\overline{E}_i = \begin{bmatrix} 1 \\ \dfrac{B_2}{N_2^2 - \lambda_i^2} \end{bmatrix} \quad \text{(A41.7),}$$

$$\overline{c}_0 = -\begin{bmatrix} \dfrac{A_1 N_2^2 T_1 + B_1 A_2 T_2}{B_1 B_2 - N_1^2 N_2^2} \\ \dfrac{A_2 N_1^2 T_2 + B_2 A_1 T_1}{B_1 B_2 - N_1^2 N_2^2} \end{bmatrix} \quad \text{(A41.8).}$$

The constants c_1 to c_4 are constants depending on the boundary conditions of the system of equations, which can be stated as

$$\begin{bmatrix} T_x \\ T_y \end{bmatrix} = \begin{bmatrix} T_1^* \\ T_2^* \end{bmatrix} \quad \text{for } x = y = L \quad \text{(A41.9a),}$$

$$\begin{bmatrix} T_x \\ T_y \end{bmatrix} = \begin{bmatrix} T_{sx} \\ T_{sy} \end{bmatrix} \quad \text{for } x = y = 0 \quad \text{(A41.9b).}$$

In these boundary conditions, L is the distance from x=0 and y=0 to the points where the effect of the thermal bridge on the facing temperature has become insignificant, T_1* and T_2* the temperatures of the facing at distance L_i from the thermal bridge at side one and two respectively and T_{sx} and T_{sy} the temperatures of the facing at x=0 and y=0. T_1* and T_2* can be calculated from a one-dimensional temperature calculation through the ideal cross-section without thermal bridge effects. The constants c_1 to c_4 can now be found from substituting the boundary conditions in equation (A41.5), resulting in

$$\begin{bmatrix} c_1 \\ c_2 \\ c_3 \\ c_4 \end{bmatrix} = \begin{bmatrix} a - d + bf - beg + cg - f + eg - g \\ d - bf + beg - cg \\ f - eg \\ g \end{bmatrix} \tag{A41.10}$$,

in which the parameters a t/m g are defined as

$$a = T_{sx} - c_{0x} \tag{A41.11a}$$,

$$b = \frac{\left(\lambda_3^2 - \lambda_1^2\right)}{\left(\lambda_2^2 - \lambda_1^2\right)} \cdot \frac{\left(N_2^2 - \lambda_2^2\right)}{\left(N_2^2 - \lambda_3^2\right)} = 0 \tag{A41.11b}$$,

$$c = \frac{\left(\lambda_4^2 - \lambda_1^2\right)}{\left(\lambda_2^2 - \lambda_1^2\right)} \cdot \frac{\left(N_2^2 - \lambda_2^2\right)}{\left(N_2^2 - \lambda_4^2\right)} = 1 \tag{A41.11c}$$,

$$d = \frac{\left(\left(T_{sy} - c_{0y}\right) - \left(T_{sx} - c_{0x}\right) \cdot \dfrac{B_2}{N_2^2 - \lambda_1^2}\right)}{\left(\dfrac{B_2}{N_2^2 - \lambda_2^2} - \dfrac{B_2}{N_2^2 - \lambda_1^2}\right)} \tag{A41.11d}$$,

$$e = \frac{\left(e^{\lambda_4 L} - e^{\lambda_1 L}\right) - \left(e^{\lambda_2 L} - e^{\lambda_1 L}\right)}{\left(e^{\lambda_3 L} - e^{\lambda_1 L}\right)} \tag{A41.11e}$$,

$$f = \frac{\left(T_1^* - c_{0x}\right) - \left(T_{sx} - c_{0x}\right) e^{\lambda_1 L} - d \cdot \left(e^{\lambda_2 L} - e^{\lambda_1 L}\right)}{\left(e^{\lambda_3 L} - e^{\lambda_1 L}\right)} \tag{A41.11f}$$,

$$g = \frac{h}{i} \tag{A41.11g}$$,

$$\begin{aligned} h = {} & \left(T_2^* - c_{0y}\right) - \left(T_{sx} - c_{0x}\right) \frac{B_2}{N_2^2 - \lambda_1^2} e^{\lambda_1 L} - d \cdot \left(\frac{B_2}{N_2^2 - \lambda_2^2} e^{\lambda_2 L} - \frac{B_2}{N_2^2 - \lambda_1^2} e^{\lambda_1 L}\right) \\ & - f \cdot \left(\frac{B_2}{N_2^2 - \lambda_3^2} e^{\lambda_3 L} - \frac{B_2}{N_2^2 - \lambda_1^2} e^{\lambda_1 L}\right) \end{aligned} \tag{A41.11h}$$,

$$i = \frac{B_2}{N_2^2 - \lambda_4^2} e^{\lambda_4 L} - \frac{B_2}{N_2^2 - \lambda_2^2} e^{\lambda_2 L} - e \cdot \left(\frac{B_2}{N_2^2 - \lambda_3^2} e^{\lambda_3 L} - \frac{B_2}{N_2^2 - \lambda_1^2} e^{\lambda_1 L}\right) \tag{A41.11i}$$.

If the limit for $L \rightarrow \infty$ is taken, equation (A41.10) reduces to

$$\lim_{L\to\infty}\begin{bmatrix}c_1\\c_2\\c_3\\c_4\end{bmatrix}=\lim_{L\to\infty}\begin{bmatrix}a-d+bf-beg+cg-f+eg-g\\d-bf+beg-cg\\f-eg\\g\end{bmatrix}=\begin{bmatrix}a-d\\d\\0\\0\end{bmatrix} \qquad \text{(A41.12)},$$

Under the conditions given in Figure A41.1, the heat flow, $\phi_{q;edge}$ [W·m-1], at x=0 must satisfy the following condition:

$$\phi_{q;edge}=-t_{f1}\lambda_{f1}\frac{dT_x}{dx}=-K(T_{sx}-T_{sy}) \qquad \text{(A41.13)},$$

with K [W·m1·K-1]the thermal conductance of the edge which combines among others the width of the edge, w [m], the effective thermal conductivity of the edge, λ_{edge} [W·m1·K-1][24], and the thickness of the VIP, d_c [m]. T_{sx} [K] is the temperature of the barrier facing (and laminate) at x = 0 and T_{sy} [K] the temperature of the barrier facing (and laminate) at y = 0.

If equation (A41.5) is differentiated and multiplied with $t_f\lambda_f$ and if the value zero for c_3 and c_4 is substituted, the following equation is obtained:

$$-t_{f1}\lambda_{f1}\frac{dT_x}{dx}=-t_{f1}\lambda_{f1}c_1\lambda_1\overline{E}_{1x}e^{\lambda_1 x}-t_{f1}\lambda_{f1}c_2\lambda_2\overline{E}_{2x}e^{\lambda_2 x} \qquad \text{(A41.14)}.$$

For $x \rightarrow 0$ the left side of equation (A41.14) becomes:

$$\lim_{x\downarrow 0}\left[-t_{f1}\lambda_{f1}\frac{dT_x}{dx}\right]=-t_{f1}\lambda_{f1}c_1\lambda_1\overline{E}_{1x}-t_{f1}\lambda_{f1}c_2\lambda_2\overline{E}_{2x} \qquad \text{(A41.15)}.$$

For the y-direction a similar equation can be derived, resulting in the following set of equations:

$$-t_{f1}\lambda_{f1}c_1\lambda_1-t_{f1}\lambda_{f1}c_2\lambda_2=-K(T_{sx}-T_{sy}) \qquad \text{for } x=0 \qquad \text{(A41.16a)},$$

$$-t_{f2}\lambda_{f2}c_1\lambda_1\frac{B_2}{N_2^2-\lambda_1^2}-t_{f2}\lambda_{f2}c_2\lambda_2\frac{B_2}{N_2^2-\lambda_2^2}=+K(T_{sx}-T_{sy}) \qquad \text{for } y=0 \qquad \text{(A41.16b)}.$$

[24] The effective thermal conductivity of the panel's edge is defined as the ratio of thickness, d_c, and its thermal resistance, R_{edge}. This thermal resistance can be estimated from a thermal resistance network representation of this edge.

If, however, the thickness of the edge (the thermal bridge) increases, like for building component edge spacers, the heat flow from and to the surrounding air over the width of this edge, w [m], is no longer insignificant and must thus be added, which is demonstrated in Figure A41.2, yielding

$$-t_{f1}\lambda_{f1}c_1\lambda_1 - t_{f1}\lambda_{f1}c_2\lambda_2 + K(T_{sx} - T_{sy}) - \alpha_1 w(T_1 - T_{sx}) = 0$$

for x=0 (A41.16c),

$$-t_{f2}\lambda_{f2}c_1\lambda_1 \frac{B_2}{N_2^2 - \lambda_1^2} - t_{f2}\lambda_{f2}c_2\lambda_2 \frac{B_2}{N_2^2 - \lambda_2^2} - K(T_{sx} - T_{sy}) + \alpha_2 w(T_2 - T_{sy}) = 0$$

for y=0 (A41.16d).

Solving this system of equations results in the following solutions for T_{sx} and T_{sy}:

$$T_{sx} = \frac{[e_4(K+e_2) + e_1(K-e_3) + e_4\alpha_2 w]c_{0x} - [e_3(K+e_2) + e_2(K-e_3) + e_3\alpha_2 w]c_{0y}}{(K-e_3)(K+e_1) - (K+\alpha_2 w + e_2)(K+\alpha_1 w - e_4)}$$
$$- \frac{(K-e_3)\alpha_2 w T_2 + [(K+e_2)\alpha_1 w + \alpha_1\alpha_2 w^2]T_1}{(K-e_3)(K+e_1) - (K+\alpha_2 w + e_2)(K+\alpha_1 w - e_4)}$$

(A41.17a),

$$T_{sy} = \frac{[e_4(K+e_1) + e_1(K-e_4) + e_1\alpha_1 w]c_{0x} - [e_3(K+e_1) + e_2(K-e_4) + e_2\alpha_1 w]c_{0y}}{(K-e_3)(K+e_1) - (K+\alpha_2 w + e_2)(K+\alpha_1 w - e_4)}$$
$$- \frac{(K+e_1)\alpha_1 w T_1 + [(K-e_4)\alpha_2 w + \alpha_1\alpha_2 w^2]T_2}{(K-e_3)(K+e_1) - (K+\alpha_2 w + e_2)(K+\alpha_1 w - e_4)}$$

(A41.17b),

in which

$$e_1 = +\frac{B_1(\lambda_1 - \lambda_2)}{\sqrt{D}}\lambda_{f2}t_{f2} \quad \text{(A41.18a)},$$

$$e_2 = -\frac{2B_1B_2}{\sqrt{D}}\left(\frac{\lambda_1}{N_2^2 - N_1^2 + \sqrt{D}} - \frac{\lambda_2}{N_2^2 - N_1^2 - \sqrt{D}}\right)\lambda_{f2}t_{f2} \quad \text{(A41.18b)},$$

$$e_3 = -\frac{B_1(\lambda_1 - \lambda_2)}{\sqrt{D}}\lambda_{f1}t_{f1} \quad \text{(A41.18c)},$$

$$e_4 = -\frac{2B_1B_2}{\sqrt{D}}\left(\frac{\lambda_1}{N_2^2 - N_1^2 - \sqrt{D}} - \frac{\lambda_2}{N_2^2 - N_1^2 + \sqrt{D}}\right)\lambda_{f1}t_{f1} \quad \text{(A41.18d)}.$$

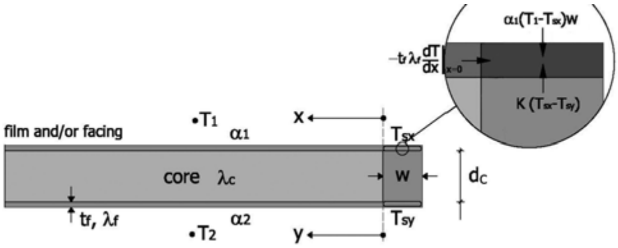

Figure A41.2

Energy balance at the edge of a building panel taking into consideration the width of this edge.

The heat flow through the edge, or the thermal bridge, can now be calculated as:

$$\phi_{q;edge} = K(T_{sx} - T_{sy}) \qquad \text{(A41.19),}$$

For a vacuum insulation panel with zero thermal conductivity all heat transfers though this edge from one side to the other side, resulting in the following definition for the linear thermal transmittance

$$\psi_{edge}^{(c)} = \frac{\phi_{q;edge}}{(T_1 - T_2)} \qquad \text{(A41.20).}$$

Because the equation desired is for non-zero thermal conductivity, the general definition for the linear thermal transmittance must be applied, which is

$$\psi_{edge}^{(c)} = \frac{\phi_{q;total} - \phi_{q;0}}{\Delta T} \qquad \text{(A41.21),}$$

with $\phi_{q;total}$ [W·m^{-1}] the total heat flow through the VIP incorporated component, including thermal bridge and $\phi_{q;0}$ [W·m^{-1}] the total heat flow through this component in case there is no thermal bridge, as shown in Figure A41.3.

The total heat flow through a component without thermal bridge under steady-state conditions can now be calculated as

$$\phi_{q;0} == \alpha_1 (T_1 - T_1^*) \cdot L_1 \qquad \text{(A41.22).}$$

In this equation L_1 [m] is the length of the panel. For the heat flow through the panel with thermal bridge, a similar equation can be derived

$$\phi_{q;total} = q_{edge} w + \int_0^{L_1} q \cdot dx = \alpha_1 (T_1 - T_{sx}) w + \int_0^{L_1} \alpha_1 (T_1 - T_x) dx = \alpha_1 \left[(T_1 - T_{sx}) w + (T_1 - \overline{T}_x) L_1 \right]$$

(A41.23),

Figure A41.3

Idealised representation of the heat flows through an undisturbed panel and a panel with a thermal bridge arising from an edge spacer.

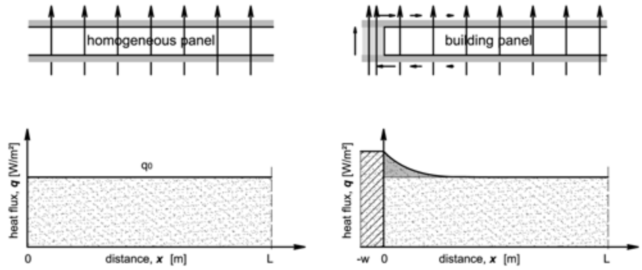

in which q_{edge} [W·m⁻²] and q [W·m⁻²] are the heat fluxes through the edge and the centre-of-panel region respectively and $\overline{T}_x$ [K] is the average facing surface temperature in x-direction, defined as

$$\overline{T}_x = \frac{1}{L_1}\int_0^{L_1} T_x dx \qquad \text{(A41.24)},$$

resulting in

$$\overline{T}_x = \frac{c_1}{\lambda_1 L_1}\left(e^{\lambda_1 L_1}-1\right)+\frac{c_2}{\lambda_2 L_1}\left(e^{\lambda_2 L_1}-1\right)+\frac{c_3}{\lambda_3 L_1}\left(e^{\lambda_3 L_1}-1\right)+\frac{c_4}{\lambda_4 L_1}\left(e^{\lambda_4 L_1}-1\right)+c_{0x}$$

(A41.25).

Equation (A41.25) is valid under the assumption that $L < L_1$ (or in words: the distance from the cold bridge ($x = 0$) to the position at which the effect of the thermal bridge is negligible should be smaller than the length of the panel). Moreover, the coefficients c_1 to c_4 are to be taken from equation (A41.10) and not from (A41.12), thus without letting $L \rightarrow \infty$. The additional heat flow due to the thermal bridge can now be calculated from equations (A41.24) and (A41.25) as

$$\phi_{q;total} - \phi_{q;0} = \alpha_1 w \cdot (T_1 - T_{sx}) + \alpha_1 L_1 \cdot (T_1^* - \overline{T}_x) \qquad \text{(A41.26)}.$$

Since T_1^* equals c_{0x}, equation (A41.26) can be written as

$$\phi_{q;total} - \phi_{q;0} = \alpha_1 \cdot \left[w \cdot (T_1 - T_{sx}) - \frac{c_1}{\lambda_1}\left(e^{\lambda_1 L_1}-1\right) - \frac{c_2}{\lambda_2}\left(e^{\lambda_2 L_1}-1\right) - \frac{c_3}{\lambda_3}\left(e^{\lambda_3 L_1}-1\right) - \frac{c_4}{\lambda_4}\left(e^{\lambda_4 L_1}-1\right)\right]$$

(A41.27).

If now the limit is taken for $L \rightarrow \infty$, this equation simplifies to

$$\lim_{L\to\infty}\left(\phi_{q;total} - \phi_{q;0}\right) = \alpha_1 \cdot \left[w \cdot (T_1 - T_{sx}) + \frac{a-d}{\lambda_1} + \frac{d}{\lambda_2} \right] \qquad \text{(A41.28),}$$

resulting finally in the following equation for the linear thermal transmittance

$$\psi_{edge}^{(c)} = \frac{\phi_{q;total} - \phi_{q;0}}{\Delta T} = \frac{\alpha_1}{(T_1 - T_2)} \cdot \left[w \cdot (T_1 - T_{sx}) + \frac{a-d}{\lambda_1} + \frac{d}{\lambda_2} \right] \qquad \text{(A41.29),}$$

which equals

$$\psi_{edge}^{(c)} = \frac{\alpha_1}{(T_1 - T_2)} \cdot \left[w \cdot (T_1 - T_{sx}) + \frac{(T_{sy} - c_{0y})(\lambda_1 - \lambda_2) + (T_{sx} - c_{0x})\left(\frac{B_2 \lambda_2}{(N_2^2 - \lambda_2^2)} - \frac{B_2 \lambda_1}{(N_2^2 - \lambda_1^2)} \right)}{\left(\frac{B_2}{(N_2^2 - \lambda_2^2)} - \frac{B_2}{(N_2^2 - \lambda_1^2)} \right) \lambda_1 \lambda_2} \right] \qquad \text{(A41.30),}$$

or

$$\psi_{edge}^{(c)} = \frac{\alpha_1}{(T_1 - T_2)} \cdot \left[w \cdot (T_1 - T_{sx}) - \frac{B_1 (T_{sy} - c_{0y})(\lambda_1 - \lambda_2) + B_1 B_2 (T_{sx} - c_{0x}) \left(\frac{\lambda_2}{(N_2^2 - \lambda_2^2)} - \frac{\lambda_1}{(N_2^2 - \lambda_1^2)} \right)}{\sqrt{CD}} \right] \qquad \text{(A41.31).}$$

In this equation C and D are calculation parameters defined as

$$C = N_1^2 N_2^2 - B_1 B_2 \qquad \text{(A41.32a),}$$

$$D = \left(N_1^2 - N_2^2\right)^2 + 4 B_1 B_2 \qquad \text{(A41.32b),}$$

Combining equations (A41.8), (A41.17), (A41.18) and (A41.31) results, after several algebraic exercises, in

$$
\begin{aligned}
\frac{\psi_{edge}}{\alpha_1} = {} & \lambda_{f1} t_{f1} \frac{A_2 B_1 K w}{2\sqrt{D} C G}\left[(N_1^2 + N_2^2)(\lambda_1 - \lambda_2) + \sqrt{D}(\lambda_1 + \lambda_2)\right] \\
& - \lambda_{f1} t_{f1} \frac{A_1 B_1}{\sqrt{C^3} G}\left[\alpha_2 w B_2 - K A_2\right] \\
& + \lambda_{f1} t_{f1} \frac{\alpha_2 w^2 B_1}{2\sqrt{D} C G}\left[A_2 (N_2^2 - N_1^2)(\lambda_1 - \lambda_2) + A_2 \sqrt{D}(\lambda_1 + \lambda_2)\right. \\
& \left. - 2 A_1 B_2 (\lambda_1 - \lambda_2)\right] \\
& - \lambda_{f2} t_{f2} \frac{A_2 K w}{2\sqrt{D} C G}\left[N_1^2 (N_2^2 - N_1^2)(\lambda_1 - \lambda_2) - 2 B_1^2 (\lambda_1 - \lambda_2)\right. \\
& \left. - N_1^2 \sqrt{D}(\lambda_1 + \lambda_2)\right] \\
& - \lambda_{f2} t_{f2} \frac{A_2}{D\sqrt{C^3} G}\left[K A_1 - \alpha_1 w B_1\right]\left[N_2^2 (N_2^2 - N_1^2)^2 + B_1 B_2 (3N_2^2 - N_1^2)\right. \\
& \left. + 2\sqrt{C}(B_1 B_2 - B_1^2) + B_1^2 (N_1^2 + N_2^2)\right] \\
& + \lambda_{f1} t_{f1} \lambda_{f2} t_{f2} \frac{A_2 B_1 w}{4 D C G}\left[((N_2^2 - N_1^2)^2 + 4B_1^2)\left(N_1^2 + N_2^2 - 2\sqrt{C}\right)\right. \\
& \left. - D\left(N_1^2 + N_2^2 + 2\sqrt{C}\right)\right] - \frac{K \alpha_2 w^2}{G} \\
& + K \alpha_2 w A_1 (A_1 B_2 - A_2 B_2 - A_2^2) \frac{(\lambda_1 - \lambda_2)}{\sqrt{D}\sqrt{C^3} G} \\
& - \alpha_1 \alpha_2 w^2 B_1 (A_1 B_2 - A_2 N_2^2) \frac{(\lambda_1 - \lambda_2)}{\sqrt{D}\sqrt{C^3} G} \\
& - (K A_1 - \alpha_1 w B_1) \alpha_2 w A_2 \left(N_1^2 + N_2^2 - \sqrt{D} - 2\sqrt{C}\right) \frac{\lambda_2}{2\sqrt{D}\sqrt{C^3} G}
\end{aligned}
$$

(A41.33),

with

$$
\begin{aligned}
G = {} & \left[\left(\lambda_{f1} t_{f1} (K + \alpha_2 w) - \lambda_{f2} t_{f2} (K + \alpha_1 w)\right) \frac{(N_2^2 - N_1^2)}{2\sqrt{D}} + \frac{B_1 K}{\sqrt{D}}\left(\lambda_{f1} t_{f1} + \lambda_{f2} t_{f2}\right)\right](\lambda_1 \\
& - \lambda_2) + \left[\frac{\left(\lambda_{f1} t_{f1} (K + \alpha_2 w) + \lambda_{f2} t_{f2} (K + \alpha_1 w)\right)}{2}\right](\lambda_1 + \lambda_2) \\
& + \frac{\lambda_{f1} t_{f1} \lambda_{f2} t_{f2}}{D}\left[(N_1^2 + N_2^2) B_1 (B_1 - B_2) - 2 B_1 (B_1 + B_2)\sqrt{C}\right. \\
& \left. - (N_2^2 - N_1^2)^2 \sqrt{C}\right] - K w (\alpha_1 + \alpha_2) - \alpha_1 \alpha_2 w^2
\end{aligned}
$$

(A41.34).

From the last two equations, it can be seen that the linear thermal transmittance is independent of the temperature difference over the building panel.

A42 Derivation of Equation for the Effective Width of Facings

At the edge of a building panel, heat transferring through the thermal bridge is deflected towards the high-conducting face sheets at the transition between edge spacer and facing. As a consequence, heat flow paths are prolonged thus changing the thermal conductance of the edge. The 'regular' resistance of the edge is therefore corrected by adding an additional width, the effective width, w_{eff} [m], as explained in Chapter 4. This effective width is defined as the distance from the edge of the building panel to the point at which the lateral heat flow in the high barrier film equals the perpendicular heat flow through the facing and boundary layer, as shown in Figure A42.1, or in mathematical terms as:

$$\phi_{q;\,film} = \phi_{q;\,facing} \qquad \text{(A42.1).}$$

The heat flow in the high barrier film (on side 1) can be obtained from Fourier's law of heat transfer[25]:

$$\phi_{q;\,film;1} = \frac{\lambda_{film;1} t_{film;1}}{w_{eff;x1}} \left[T_{sx} - T_{fx}(w_{eff}) \right] \qquad \text{(A42.2a).}$$

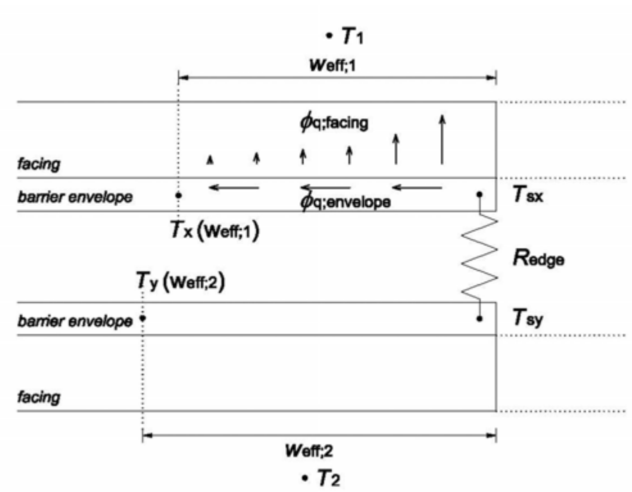

Figure A42.1

Schematic representation of a building panel edge including a definition of the facing effective width.

[25] An explanation of the symbols used is found in Appendix 41 and in Figure A42.1.

The heat flow through the face sheet (on side 1) in a direction perpendicular to its surface is obtained from integrating the heat flux through this surface from the corner to w_{eff}:

$$\phi_{q;\,facing;1} = \int_0^{w_{eff;x1}} q_x dx = \int_0^{w_{eff;x1}} \frac{T_{fx}(x) - T_1}{\dfrac{t_{facing;1}}{\lambda_{facing;1}} + \dfrac{1}{\alpha_1}} dx = \frac{w_{eff;x1}}{\dfrac{t_{facing;1}}{\lambda_{facing;1}} + \dfrac{1}{\alpha_1}} \left(\overline{T}_{fx} - T_1\right) \qquad \text{(A42.3).}$$

After substituting equations (A42.2) and (A42.3) in equation (A42.1), an equation for w_{eff} can be obtained:

$$w_{eff;x1} = \sqrt{\frac{T_{sx} - T_{fx}(w_{eff;x1})}{\overline{T}_{fx} - T_1} \lambda_{film;1} t_{film;1} \left(\frac{t_{facing;1}}{\lambda_{facing;1}} + \frac{1}{\alpha_1} \right)} \qquad \text{(A42.4),}$$

which can be written in a more general form as

$$w_{eff;ij} = \sqrt{\frac{T_{si} - T_{fi}(w_{eff;ij})}{\overline{T}_{fi} - T_j} \lambda_{film;j} t_{film;j} \left(\frac{t_{facing;j}}{\lambda_{facing;j}} + \frac{1}{\alpha_j} \right)} \qquad \text{(A42.5).}$$

In case the temperature of the barrier laminate decreases linearly with x from T_{si} at the component's corner to c_{oi} at w_{eff}, the temperature ratio in the previous equation equals approximately 2.

The geometry of the spacers can be found on page 102 and their designation on 104.

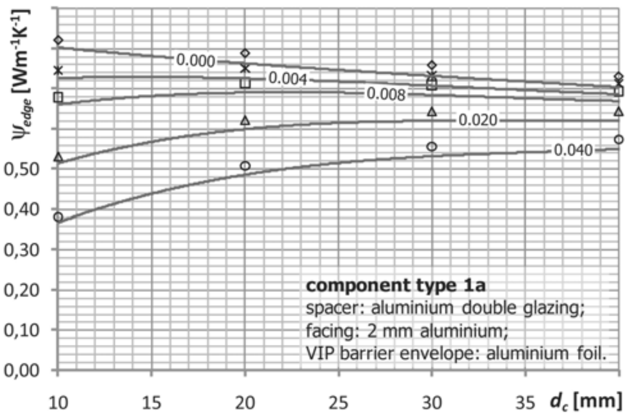

Figure A43.1a

Comparison of numerical (markers) to analytical (lines) data of the linear thermal transmittance as function of panel thickness for a VIP integrated building panel.

Spacer: alu. double-glazing;
Face sheets: 2 mm aluminium;
VIP barrier: aluminium foil;
$\varphi = 0.67$;
$\alpha_1 = 7.8\ m^2 \cdot K \cdot W^{-1}$;
$\alpha_2 = 25\ m^2 \cdot K \cdot W^{-1}$.

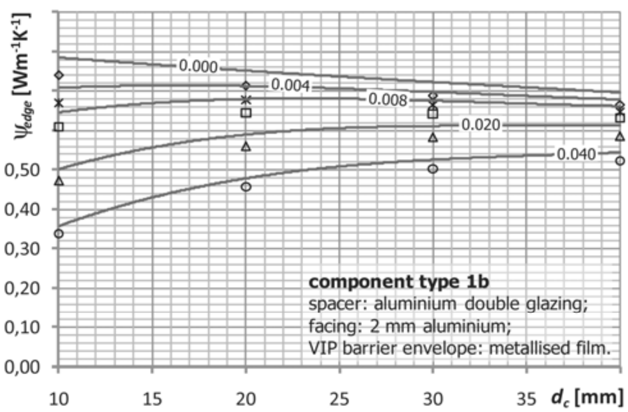

Figure A43.1b

Comparison of numerical (markers) to analytical (lines) data of the linear thermal transmittance as function of panel thickness for a VIP integrated building panel.

Spacer: alu. double-glazing;
Face sheets: 2 mm aluminium;
VIP barrier: metallised film;
$\varphi = 0.67$;
$\alpha_1 = 7.8\ m^2 \cdot K \cdot W^{-1}$;
$\alpha_2 = 25\ m^2 \cdot K \cdot W^{-1}$.

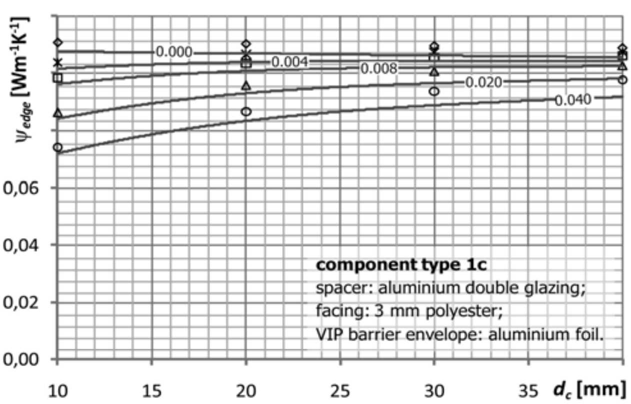

Figure A43.1c

Comparison of numerical (markers) to analytical (lines) data of the linear thermal transmittance as function of panel thickness for a VIP integrated building panel.

Spacer: alu. double-glazing;
Face sheets: 3 mm polyester;
VIP barrier: aluminium foil;
$\varphi = 0.67$;
$\alpha_1 = 7.8\ m^2 \cdot K \cdot W^{-1}$;
$\alpha_2 = 25\ m^2 \cdot K \cdot W^{-1}$.

Figure A43.1d

Comparison of numerical (markers) to analytical (lines) data of the linear thermal transmittance as function of panel thickness for a VIP integrated building panel.

Spacer: alu. double-glazing;
Face sheets: 3 mm polyester;
VIP barrier: metallised film;
φ = 0.67;
α_1 = 7.8 $m^2 \cdot K \cdot W^{-1}$;
α_2 = 25 $m^2 \cdot K \cdot W^{-1}$.

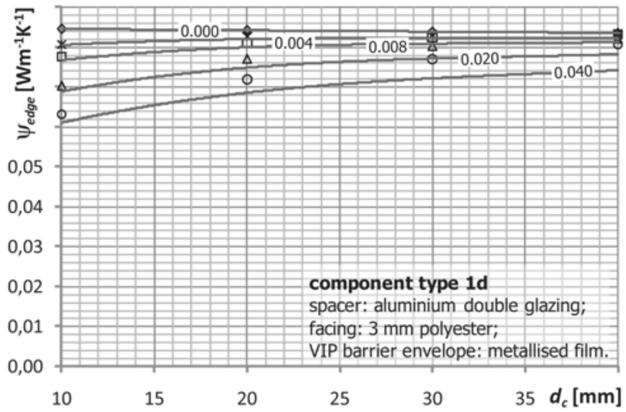

Figure A43.1e

Comparison of numerical (markers) to analytical (lines) data of the linear thermal transmittance as function of panel thickness for a VIP integrated building panel.

Spacer: alu. double-glazing;
Face sheets: 1.5 mm steel;
VIP barrier: aluminium foil;
φ = 0.67;
α_1 = 7.8 $m^2 \cdot K \cdot W^{-1}$;
α_2 = 25 $m^2 \cdot K \cdot W^{-1}$.

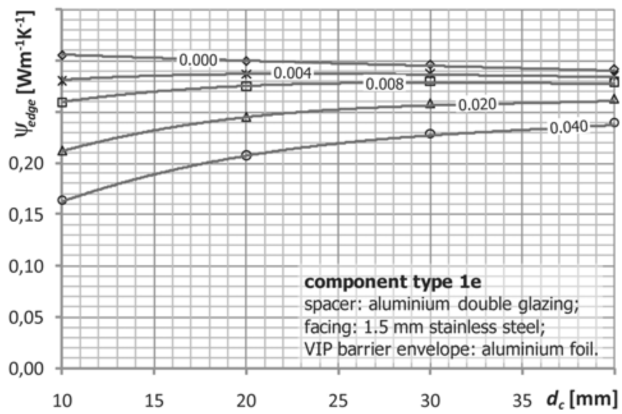

Figure A43.1f

Comparison of numerical (markers) to analytical (lines) data of the linear thermal transmittance as function of panel thickness for a VIP integrated building panel.

Spacer: alu. double-glazing;
Face sheets: 1.5 mm steel;
VIP barrier: metallised film;
φ = 0.67;
α_1 = 7.8 $m^2 \cdot K \cdot W^{-1}$;
α_2 = 25 $m^2 \cdot K \cdot W^{-1}$.

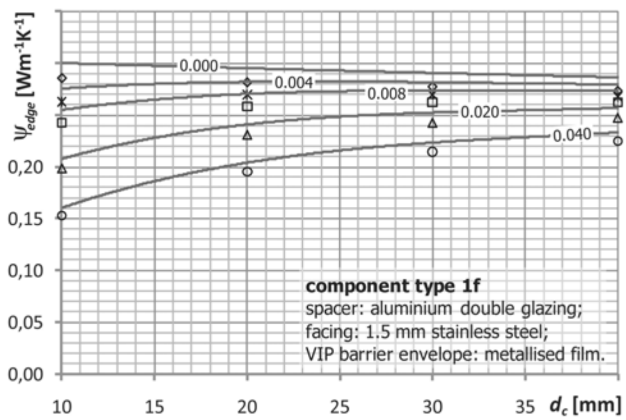

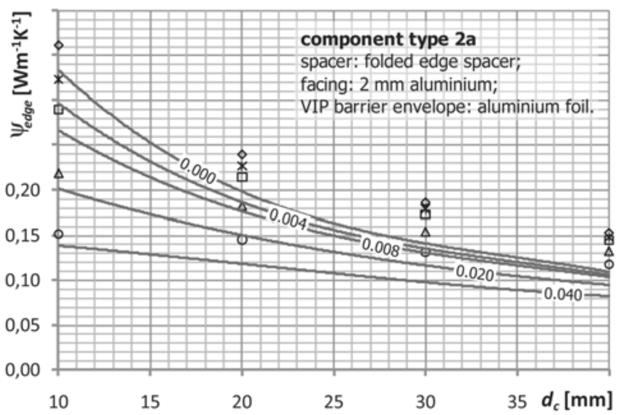

Figure A43.2a

Comparison of numerical (markers) to analytical (lines) data of the linear thermal transmittance as function of panel thickness for a VIP integrated building panel.

Spacer: folded edge spacer;
Face sheets: 2 mm aluminium;
VIP barrier: aluminium foil;
$\varphi = 0.67$;
$\alpha_1 = 7.8\ m^2 \cdot K \cdot W^{-1}$;
$\alpha_2 = 25\ m^2 \cdot K \cdot W^{-1}$.

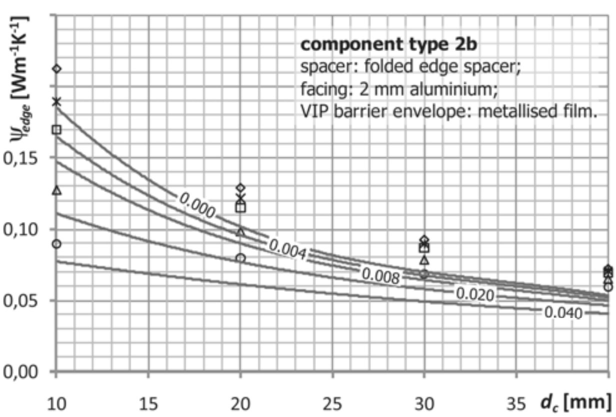

Figure A43.2b

Comparison of numerical (markers) to analytical (lines) data of the linear thermal transmittance as function of panel thickness for a VIP integrated building panel.

Spacer: folded edge spacer;
Face sheets: 2 mm aluminium;
VIP barrier: metallised film;
$\varphi = 0.67$;
$\alpha_1 = 7.8\ m^2 \cdot K \cdot W^{-1}$;
$\alpha_2 = 25\ m^2 \cdot K \cdot W^{-1}$.

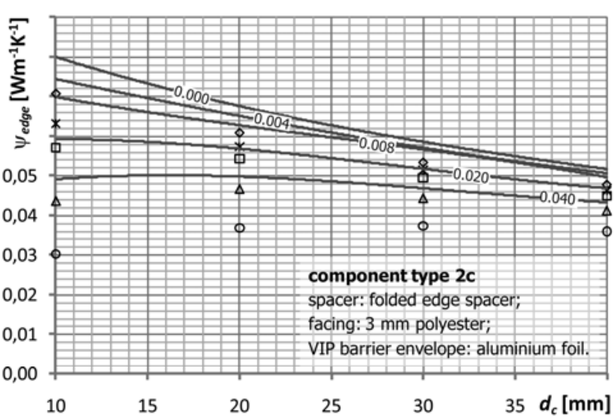

Figure A43.2c

Comparison of numerical (markers) to analytical (lines) data of the linear thermal transmittance as function of panel thickness for a VIP integrated building panel.

Spacer: folded edge spacer;
Face sheets: 3 mm polyester;
VIP barrier: aluminium foil;
$\varphi = 0.67$;
$\alpha_1 = 7.8\ m^2 \cdot K \cdot W^{-1}$;
$\alpha_2 = 25\ m^2 \cdot K \cdot W^{-1}$.

Figure A43.2d

Comparison of numerical (markers) to analytical (lines) data of the linear thermal transmittance as function of panel thickness for a VIP integrated building panel.

Spacer: folded edge spacer;
Face sheets: 3 mm polyester;
VIP barrier: metallised film;
$\varphi = 0.67$;
$\alpha_1 = 7.8\ m^2 \cdot K \cdot W^{-1}$;
$\alpha_2 = 25\ m^2 \cdot K \cdot W^{-1}$.

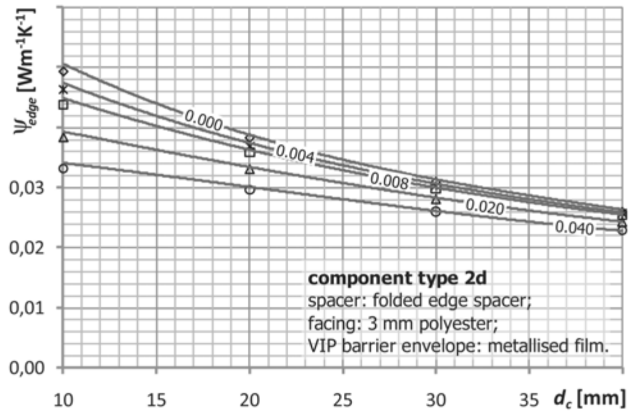

Figure A43.3a

Comparison of numerical (markers) to analytical (lines) data of the linear thermal transmittance as function of panel thickness for a VIP integrated building panel.

Spacer: non-metallic tape;
Face sheets: 2 mm aluminium;
VIP barrier: aluminium foil;
$\varphi = 0.67$;
$\alpha_1 = 7.8\ m^2 \cdot K \cdot W^{-1}$;
$\alpha_2 = 25\ m^2 \cdot K \cdot W^{-1}$.

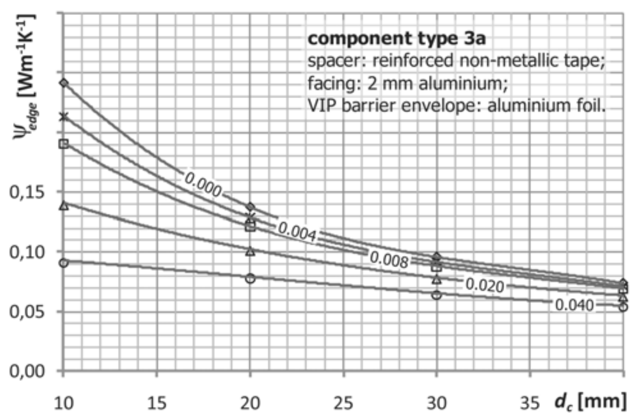

Figure A43.3b

Comparison of numerical (markers) to analytical (lines) data of the linear thermal transmittance as function of panel thickness for a VIP integrated building panel.

Spacer: non-metallic tape;
Face sheets: 2 mm aluminium;
VIP barrier: metallised film;
$\varphi = 0.67$;
$\alpha_1 = 7.8\ m^2 \cdot K \cdot W^{-1}$;
$\alpha_2 = 25\ m^2 \cdot K \cdot W^{-1}$.

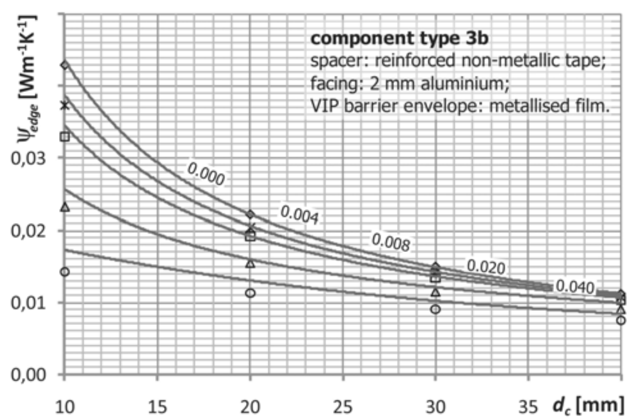

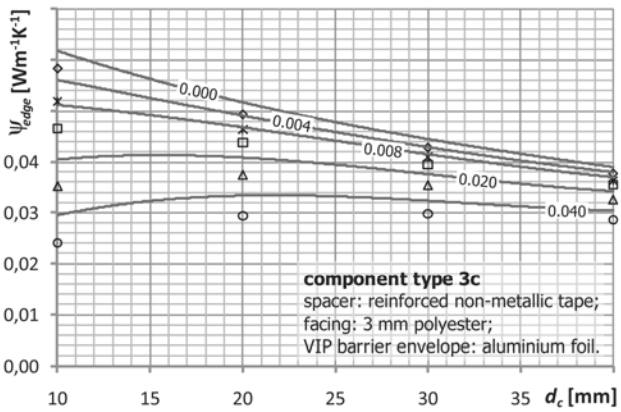

Figure A43.3c

Comparison of numerical (markers) to analytical (lines) data of the linear thermal transmittance as function of panel thickness for a VIP integrated building panel.

Spacer: non-metallic tape;
Face sheets: 3 mm polyester;
VIP barrier: aluminium foil;
$\varphi = 0.67$;
$\alpha_1 = 7.8\ m^2 \cdot K \cdot W^{-1}$;
$\alpha_2 = 25\ m^2 \cdot K \cdot W^{-1}$.

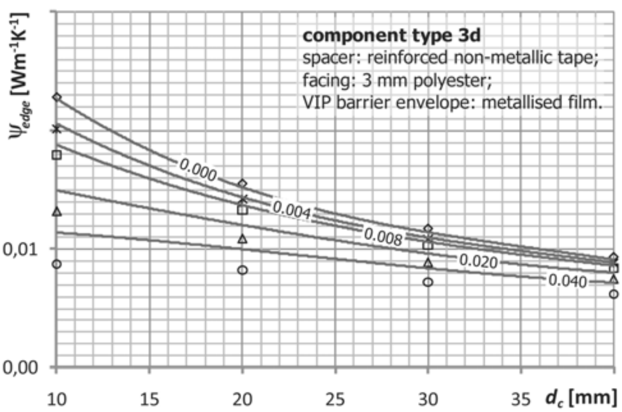

Figure A43.3d

Comparison of numerical (markers) to analytical (lines) data of the linear thermal transmittance as function of panel thickness for a VIP integrated building panel.

Spacer: non-metallic tape;
Face sheets: 3 mm polyester;
VIP barrier: metallised film;
$\varphi = 0.67$;
$\alpha_1 = 7.8\ m^2 \cdot K \cdot W^{-1}$;
$\alpha_2 = 25\ m^2 \cdot K \cdot W^{-1}$.

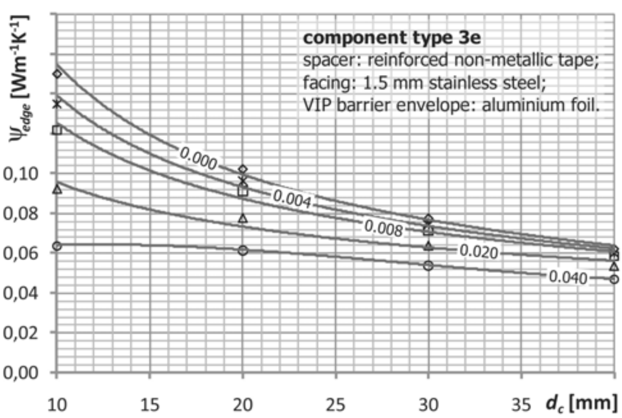

Figure A43.3e

Comparison of numerical (markers) to analytical (lines) data of the linear thermal transmittance as function of panel thickness for a VIP integrated building panel.

Spacer: non-metallic tape;
Face sheets: 1.5 mm steel;
VIP barrier: aluminium foil;
$\varphi = 0.67$;
$\alpha_1 = 7.8\ m^2 \cdot K \cdot W^{-1}$;
$\alpha_2 = 25\ m^2 \cdot K \cdot W^{-1}$.

Figure A43.3f

Comparison of numerical (markers) to analytical (lines) data of the linear thermal transmittance as function of panel thickness for a VIP integrated building panel.

Spacer: non-metallic tape;
Face sheets: 1.5 mm steel;
VIP barrier: metallised film;
φ = 0.67;
α_1 = 7.8 $m^2{\cdot}K{\cdot}W^{-1}$;
α_2 = 25 $m^2{\cdot}K{\cdot}W^{-1}$.

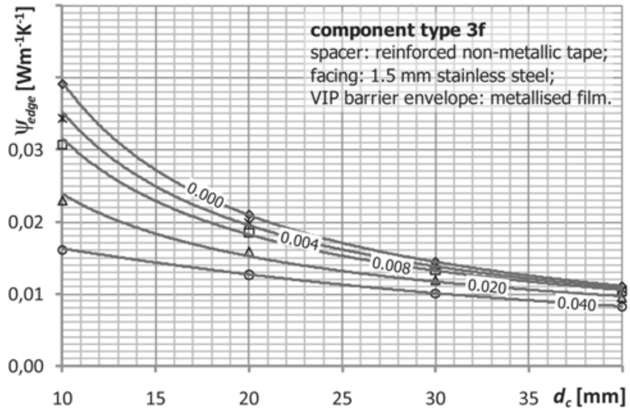

Figure A43.4a

Comparison of numerical (markers) to analytical (lines) data of the linear thermal transmittance as function of panel thickness for a VIP integrated building panel.

Spacer: thermoplastic spacer;
Face sheets: 2 mm aluminium;
VIP barrier: aluminium foil;
φ = 0.67;
α_1 = 7.8 $m^2{\cdot}K{\cdot}W^{-1}$;
α_2 = 25 $m^2{\cdot}K{\cdot}W^{-1}$.

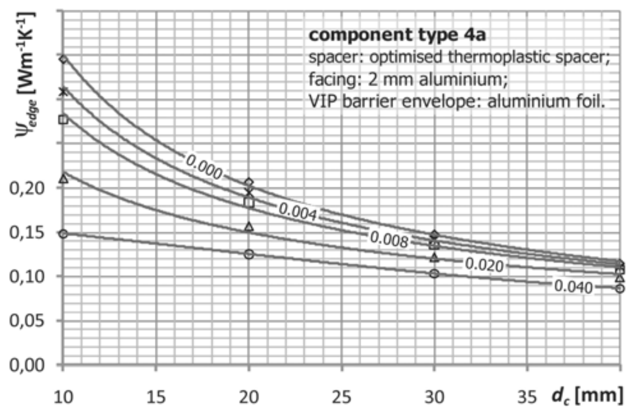

Figure A43.4b

Comparison of numerical (markers) to analytical (lines) data of the linear thermal transmittance as function of panel thickness for a VIP integrated building panel.

Spacer: thermoplastic spacer;
Face sheets: 2 mm aluminium;
VIP barrier: metallised film;
φ = 0.67;
α_1 = 7.8 $m^2{\cdot}K{\cdot}W^{-1}$;
α_2 = 25 $m^2{\cdot}K{\cdot}W^{-1}$.

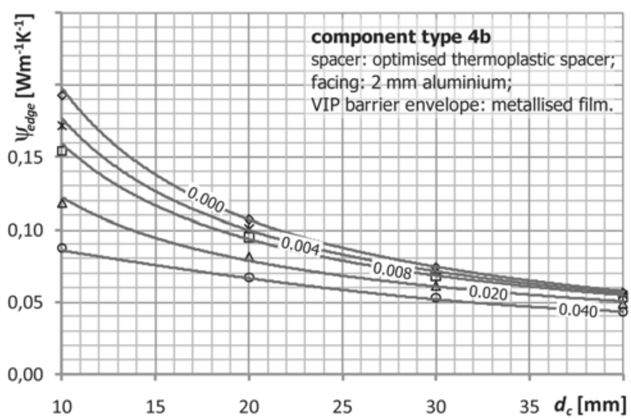

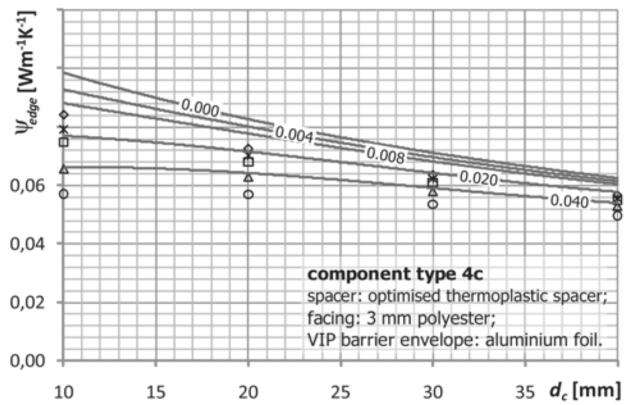

Figure A43.4c

Comparison of numerical (markers) to analytical (lines) data of the linear thermal transmittance as function of panel thickness for a VIP integrated building panel.

Spacer: thermoplastic spacer;
Face sheets: 3 mm polyester;
VIP barrier: aluminium foil;
φ = 0.67;
α_1 = 7.8 $m^2 \cdot K \cdot W^{-1}$;
α_2 = 25 $m^2 \cdot K \cdot W^{-1}$.

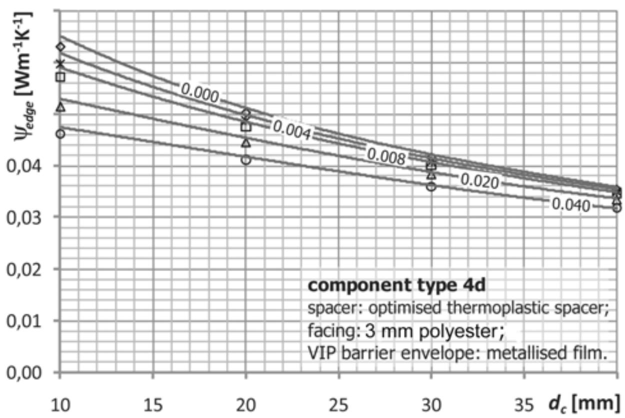

Figure A43.4d

Comparison of numerical (markers) to analytical (lines) data of the linear thermal transmittance as function of panel thickness for a VIP integrated building panel.

Spacer: thermoplastic spacer;
Face sheets: 3 mm polyester;
VIP barrier: metallised film;
φ = 0.67;
α_1 = 7.8 $m^2 \cdot K \cdot W^{-1}$;
α_2 = 25 $m^2 \cdot K \cdot W^{-1}$.

While in the main text of chapter 4, subsection 4.3.3, equation (4.5) was tested for symmetrical building panels, i.e. building panels that have identical face sheets on both sides, in this appendix the equation is tested for ten asymmetrical panels. For reasons of comparison, only panels with an aluminium double-glazing spacer were used for which numerical data was available through research by van Went (2002). The thickness of the VIP varies from 16 to 24 mm and the facings are either made of aluminium (2, 3 or 4 mm) or of glass (6 or 8 mm). Table A44.1 presents the results of the simulations for all tested panel variants. From a comparison of the numerical to the analytical data, it can be observed that also for asymmetrical building panels the difference between the analytically predicted values and the numerical data is small with a maximum deviation found of about 7.5%.

Table A44.1a *- Comparison of numerical to analytical data for the linear thermal transmittance of several asymmetrical building panels ($\lambda_c = 4.0 \cdot 10^{-3}$ W·m⁻¹·K⁻¹).*

nr.	1		2		3		4		5	
facing 1	aluminium		aluminium		aluminium		aluminium		aluminium	
$t_{facing;1}$ [mm]	2		2		2		2		3	
d_c [mm]	16		18		16		18		20	
facing 2	glass		aluminium		glass		glass		aluminium	
$t_{facing2}$ [mm]	6		4		8		6		3	
barrier	AF[a]	MF[b]	AF	MF	AF	MF	AF	MF	AF	MF
t_{film} [μm]	6	97	6	97	6	97	6	97	6	97
spacer	alu. double-glazing		alu. double-galzing		alu. double-galzing		alu. double-galzing		alu. double-galzing	
λ_{edge} [W·m⁻¹·K⁻¹]	4.91	4.38	5.33	4.79	4.91	4.38	5.33	4.79	5.73	5.17
ψ_{num} [W·m⁻¹·K⁻¹]	0.37	0.32	0.84	0.74	0.38	0.33	0.37	0.32	0.90	0.78
ψ_{ana} [W·m⁻¹·K⁻¹]	0.34	0.31	0.79	0.77	0.35	0.30	0.35	0.31	0.84	0.82
deviation [%]	-6.5	-4.6	-5.6	4.2	-6.1	-7.1	-5.1	-4.1	-7.0	4.5

[a] AF stands for aluminium foil laminate.
[b] MF stands for metallised film laminate.

Table A44.1b *- Comparison of numerical to analytical data for the linear thermal transmittance of several asymmetrical building panels (λ_c = 4.0·10^-3^ W·m^-1^·K^-1^.)*

nr.	6		7		8		9		10	
facing 1	aluminium		aluminium		aluminium		aluminium		aluminium	
$t_{facing;1}$ [mm]	2		2		2		2		2	
d_c [mm]	18		20		24		20		24	
facing 2	glass		glass		aluminium		glass		glass	
$t_{facing2}$ [mm]	8		6		2		8		6	
barrier	AF	MF	AF	MF	AF	MF	AF	MF	AF	MF
t_{film} [μm]	6	97	6	97	6	97	6	97	6	97
spacer	alu. double-glazing		alu. double-galzing		alu. double-galzing		alu. double-galzing		alu. double-galzing	
λ_{edge} [W·m^-1^·K^-1^]	5.33	4.79	5.73	5.17	6.46	5.88	5.73	5.17	6.46	5.88
ψ_{num} [W·m^-1^·K^-1^]	0.38	0.33	0.37	0.32	0.77	0.68	0.38	0.33	0.37	0.32
ψ_{ana} [W·m^-1^·K^-1^]	0.35	0.31	0.35	0.31	0.73	0.71	0.35	0.31	0.35	0.31
deviation [%]	-6.8	-7.6	-5.1	-3.8	-5.5	4.4	-6.8	-7.3	-5.1	-3.8

Figure A45.1a

Comparison of numerical (markers) to analytical (lines) data of the linear thermal transmittance as function of panel thickness for a sheet-based VIP. The numbers accompanying the lines denote the thickness [mm] of facing 1 and 2 respectively.

$\lambda_c = 0\ W{\cdot}m^{-1}{\cdot}K^{-1}$;
$\alpha_1 = 7.8\ m^2{\cdot}K{\cdot}W^{-1}$;
$\alpha_2 = 25\ m^2{\cdot}K{\cdot}W^{-1}$.

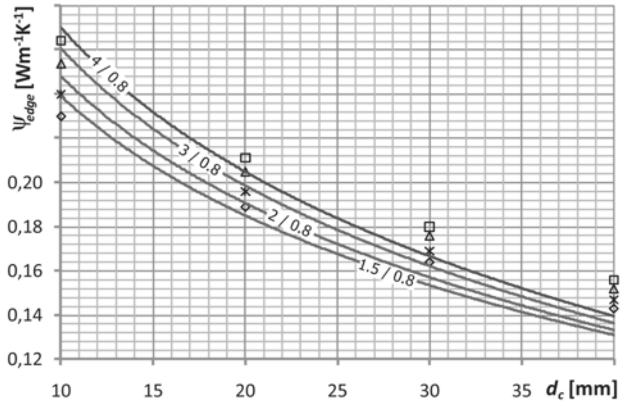

Figure A45.1b

Comparison of numerical (markers) to analytical (lines) data of the linear thermal transmittance as function of panel thickness for a sheet-based VIP. The numbers accompanying the lines denote the thickness [mm] of facing 1 and 2 respectively.

$\lambda_c = 4.0{\cdot}10^{-3}\ W{\cdot}m^{-1}{\cdot}K^{-1}$;
$\alpha_1 = 7.8\ m^2{\cdot}K{\cdot}W^{-1}$;
$\alpha_2 = 25\ m^2{\cdot}K{\cdot}W^{-1}$.

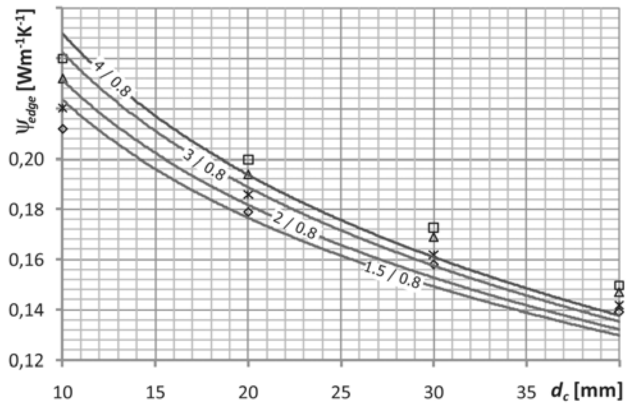

Figure A45.1c

Comparison of numerical (markers) to analytical (lines) data of the linear thermal transmittance as function of panel thickness for a sheet-based VIP. The numbers accompanying the lines denote the thickness [mm] of facing 1 and 2 respectively.

$\lambda_c = 8.0{\cdot}10^{-3}\ W{\cdot}m^{-1}{\cdot}K^{-1}$;
$\alpha_1 = 7.8\ m^2{\cdot}K{\cdot}W^{-1}$;
$\alpha_2 = 25\ m^2{\cdot}K{\cdot}W^{-1}$.

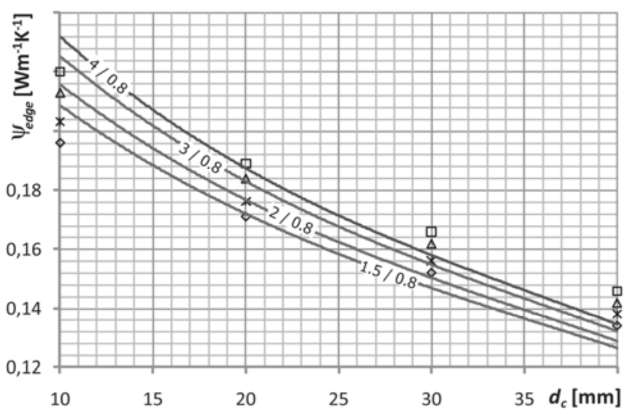

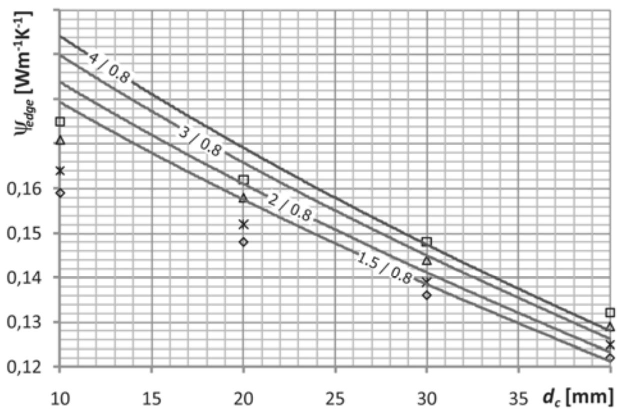

Figure A45.1d

Comparison of numerical (markers) to analytical (lines) data of the linear thermal transmittance as function of panel thickness for a sheet-based VIP. The numbers accompanying the lines denote the thickness [mm] of facing 1 and 2 respectively.

λ_c = 20·10^{-3} W·m^{-1}·K^{-1};
α_1 = 7.8 m^2·K·W^{-1};
α_2 = 25 m^2·K·W^{-1}.

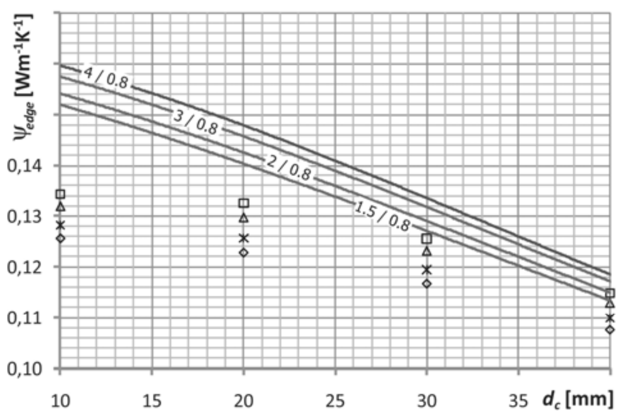

Figure A45.1e

Comparison of numerical (markers) to analytical (lines) data of the linear thermal transmittance as function of panel thickness for a sheet-based VIP. The numbers accompanying the lines denote the thickness [mm] of facing 1 and 2 respectively.

λ_c = 40·10^{-3} W·m^{-1}·K^{-1};
α_1 = 7.8 m^2·K·W^{-1};
α_2 = 25 m^2·K·W^{-1}.

A46 Air Gaps between Adjacent VIPs: A tabular comparison of numerical and Analytical Data Using the Advanced Model

***Table A46.1** – Comparison of the linear thermal transmittance of a VIP with an air gap between two adjacent panels calculated both using the advanced analytical model and numerical simulation software. Barrier envelope: AF:10 / 50 μm HDPE-10 μm AL-40 μm PET / λ_{eq}=20.3 W·m⁻¹·K⁻¹. Numerical data from Schild and Willems (2007)*

d_p [mm]	λ_c [W/mK]	gap width 1 mm numerical	gap width 1 mm analytical	gap width 2.5 mm numerical	gap width 2.5 mm analytical	gap width 5 mm numerical	gap width 5 mm analytical
10	0	0.0612	0.0617	0.0657	0.0669	0.0733	0.0757
	$4.0\cdot10^{-3}$	0.0554	0.0558	0.0600	0.0611	0.0675	0.0700
	$8.0\cdot10^{-3}$	0.0505	0.0509	0.0551	0.0563	0.0626	0.0652
	$20\cdot10^{-3}$	0.0397	0.0399	0.0442	0.0454	0.0519	0.0546
	$40\cdot10^{-3}$	0.0288	0.0289	0.0334	0.0347	0.0413	0.0442
20	0	0.0477	0.0478	0.0513	0.0518	0.0578	0.0586
	$4.0\cdot10^{-3}$	0.0451	0.0453	0.0490	0.0494	0.0555	0.0562
	$8.0\cdot10^{-3}$	0.0430	0.0431	0.0469	0.0471	0.0534	0.0540
	$20\cdot10^{-3}$	0.0375	0.0373	0.0413	0.0415	0.0478	0.0485
	$40\cdot10^{-3}$	0.0305	0.0303	0.0345	0.0347	0.0412	0.0419
30	0	0.0392	0.0392	0.0427	0.0428	0.0485	0.0488
	$4.0\cdot10^{-3}$	0.0378	0.0378	0.0413	0.0414	0.0473	0.0474
	$8.0\cdot10^{-3}$	0.0366	0.0365	0.0401	0.0401	0.0460	0.0461
	$20\cdot10^{-3}$	0.0333	0.0330	0.0368	0.0366	0.0426	0.0427
	$40\cdot10^{-3}$	0.0287	0.0283	0.0322	0.0320	0.0382	0.0382
40	0	0.0333	0.0335	0.0368	0.0368	0.0425	0.0426
	$4.0\cdot10^{-3}$	0.0325	0.0325	0.0358	0.0359	0.0417	0.0417
	$8.0\cdot10^{-3}$	0.0318	0.0317	0.0351	0.0350	0.0408	0.0408
	$20\cdot10^{-3}$	0.0294	0.0292	0.0329	0.0326	0.0386	0.0384
	$40\cdot10^{-3}$	0.0263	0.0259	0.0296	0.0293	0.0355	0.0351

***Table A46.2** – Comparison of the linear thermal transmittance of a VIP with an air gap between two adjacent panels calculated both using the advanced analytical model and numerical simulation software. Barrier envelope: AF:6 / 50 μm HDPE-6 μm AL-25 μm PET / λ_{eq}=15.1 $W{\cdot}m^{-1}{\cdot}K^{-1}$.*

d_p [mm]	λ_c [W/mK]	gap width 1 mm		gap width 2.5 mm		gap width 5 mm	
		numerical	analytical	numerical	analytical	numerical	analytical
10	0	0.0447	0.0450	0.0490	0.0498	0.0567	0.0580
	$4.0{\cdot}10^{-3}$	0.0405	0.0407	0.0449	0.0456	0.0525	0.0539
	$8.0{\cdot}10^{-3}$	0.0370	0.0372	0.0413	0.0421	0.0490	0.0504
	$20{\cdot}10^{-3}$	0.0292	0.0292	0.0335	0.0343	0.0412	0.0429
	$40{\cdot}10^{-3}$	0.0213	0.0214	0.0259	0.0268	0.0336	0.0356
20	0	0.0335	0.0336	0.0372	0.0374	0.0435	0.0439
	$4.0{\cdot}10^{-3}$	0.0318	0.0318	0.0355	0.0356	0.0418	0.0422
	$8.0{\cdot}10^{-3}$	0.0304	0.0303	0.0340	0.0341	0.0404	0.0406
	$20{\cdot}10^{-3}$	0.0265	0.0263	0.0301	0.0302	0.0366	0.0368
	$40{\cdot}10^{-3}$	0.0217	0.0214	0.0255	0.0255	0.0320	0.0323
30	0	0.0270	0.0271	0.0305	0.0305	0.0363	0.0364
	$4.0{\cdot}10^{-3}$	0.0261	0.0261	0.0296	0.0296	0.0354	0.0355
	$8.0{\cdot}10^{-3}$	0.0253	0.0252	0.0286	0.0286	0.0346	0.0346
	$20{\cdot}10^{-3}$	0.0229	0.0228	0.0264	0.0263	0.0323	0.0322
	$40{\cdot}10^{-3}$	0.0200	0.0196	0.0234	0.0231	0.0292	0.0291
40	0	0.0228	0.0229	0.0262	0.0262	0.0320	0.0320
	$4.0{\cdot}10^{-3}$	0.0223	0.0222	0.0257	0.0256	0.0313	0.0314
	$8.0{\cdot}10^{-3}$	0.0218	0.0216	0.0251	0.0250	0.0308	0.0308
	$20{\cdot}10^{-3}$	0.0203	0.0200	0.0236	0.0234	0.0293	0.0291
	$40{\cdot}10^{-3}$	0.0181	0.0177	0.0215	0.0211	0.0271	0.0268

***Table A46.3 –** Comparison of the linear thermal transmittance of a VIP with an air gap between two adjacent panels calculated both using the advanced analytical model and numerical simulation software. Barrier envelope: MF3 / 3x 12 μm alPET -61 μm HDPE / λ_{eq}=0.54 W·m^{-1}·K^{-1}.*

		gap width 1 mm		gap width 2.5 mm		gap width 5 mm	
d_p [mm]	λ_c [W/mK]	numerical	analytical	numerical	analytical	numerical	analytical
10	0	0.0065	0.0067	0.0102	0.0110	0.0184	0.0189
	$4.0 \cdot 10^{-3}$	0.0060	0.0062	0.0102	0.0104	0.0179	0.0182
	$8.0 \cdot 10^{-3}$	0.0056	0.0058	0.0098	0.0100	0.0175	0.0177
	$20 \cdot 10^{-3}$	0.0047	0.0049	0.0089	0.0091	0.0164	0.0167
	$40 \cdot 10^{-3}$	0.0036	0.0043	0.0076	0.0084	0.0153	0.0160
20	0	0.0460	0.0048	0.0083	0.0086	0.0150	0.0152
	$4.0 \cdot 10^{-3}$	0.0450	0.0046	0.0083	0.0084	0.0148	0.0149
	$8.0 \cdot 10^{-3}$	0.0044	0.0044	0.0082	0.0081	0.0147	0.0147
	$20 \cdot 10^{-3}$	0.0040	0.0040	0.0076	0.0077	0.0141	0.0141
	$40 \cdot 10^{-3}$	0.0035	0.0036	0.0070	0.0072	0.0134	0.0136
30	0	0.0039	0.0041	0.0075	0.0078	0.0136	0.0138
	$4.0 \cdot 10^{-3}$	0.0039	0.0040	0.0076	0.0076	0.0136	0.0137
	$8.0 \cdot 10^{-3}$	0.0040	0.0039	0.0076	0.0075	0.0136	0.0135
	$20 \cdot 10^{-3}$	0.0036	0.0036	0.0073	0.0072	0.0133	0.0131
	$40 \cdot 10^{-3}$	0.0032	0.0033	0.0067	0.0068	0.0127	0.0127
40	0	0.0037	0.0038	0.0073	0.0074	0.0132	0.0133
	$4.0 \cdot 10^{-3}$	0.0037	0.0037	0.0073	0.0073	0.0132	0.0132
	$8.0 \cdot 10^{-3}$	0.0036	0.0037	0.0073	0.0072	0.0131	0.0131
	$20 \cdot 10^{-3}$	0.0036	0.0035	0.0071	0.0070	0.0131	0.0128
	$40 \cdot 10^{-3}$	0.0031	0.0032	0.0068	0.0066	0.0126	0.0124

A47 Thermal Performance Plots of VIP Integrated Building Panels

The geometry of the spacers can be found on p. 102 and their designations on p. 104.

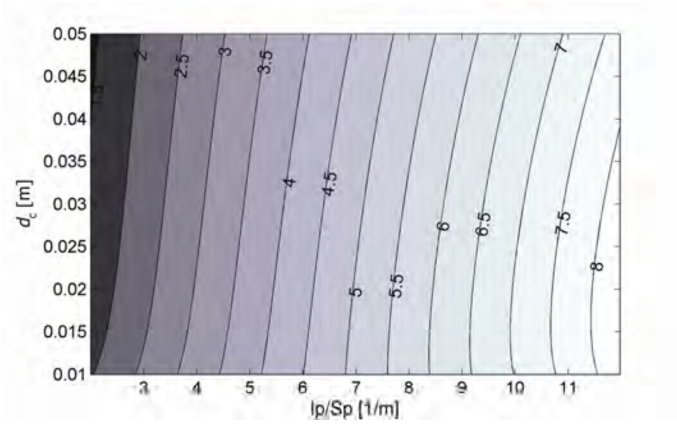

Figure A47.1a

Plot of the U_{eff}-value of a VIP-integrated building panel as function of thickness, d_c [m], and perimeter to surface area ratio, l_p/S_p [m^{-1}]. Values along the lines denote U_{eff} [$W{\cdot}m^{-2}{\cdot}K^{-1}$].

Spacer: alu. double-glazing;
Face sheets: 2 mm aluminium;
VIP barrier: metallised film;
$\lambda_c = 4.0{\cdot}10^{-3}$ $W{\cdot}m^{-1}{\cdot}K^{-1}$;
$\alpha_1 = 7.8$ $m^2{\cdot}K{\cdot}W^{-1}$;
$\alpha_2 = 25$ $m^2{\cdot}K{\cdot}W^{-1}$;

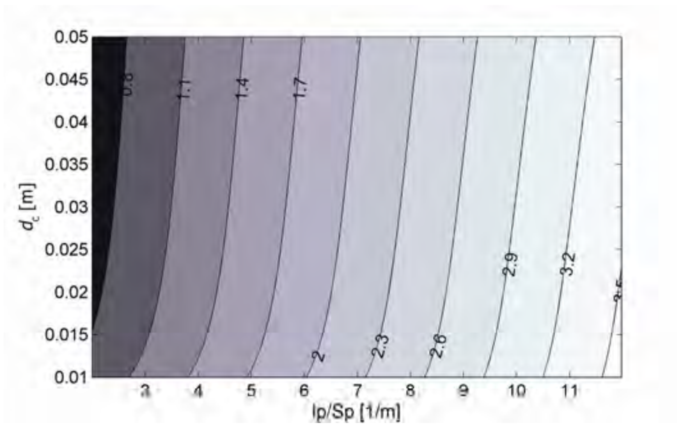

Figure A47.1b

Plot of the U_{eff}-value of a VIP-integrated building panel as function of thickness, d_c [m], and perimeter to surface area ratio, l_p/S_p [m^{-1}]. Values along the lines denote U_{eff} [$W{\cdot}m^{-2}{\cdot}K^{-1}$].

Spacer: alu. double-glazing;
Face sheets: 1.5 mm steel;
VIP barrier: metallised film;
$\lambda_c = 4.0{\cdot}10^{-3}$ $W{\cdot}m^{-1}{\cdot}K^{-1}$;
$\alpha_1 = 7.8$ $m^2{\cdot}K{\cdot}W^{-1}$;
$\alpha_2 = 25$ $m^2{\cdot}K{\cdot}W^{-1}$;

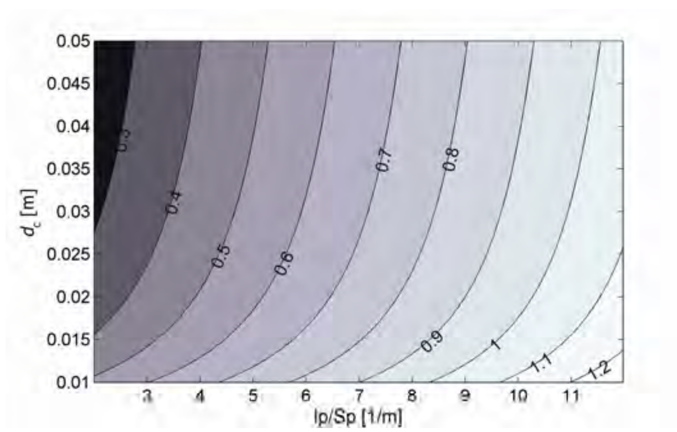

Figure A47.1c

Plot of the U_{eff}-value of a VIP-integrated building panel as function of thickness, d_c [m], and perimeter to surface area ratio, l_p/S_p [m^{-1}]. Values along the lines denote U_{eff} [$W{\cdot}m^{-2}{\cdot}K^{-1}$].

Spacer: alu. double-glazing;
Face sheets: 3 mm polyester;
VIP barrier: metallised film;
$\lambda_c = 4.0{\cdot}10^{-3}$ $W{\cdot}m^{-1}{\cdot}K^{-1}$;
$\alpha_1 = 7.8$ $m^2{\cdot}K{\cdot}W^{-1}$;
$\alpha_2 = 25$ $m^2{\cdot}K{\cdot}W^{-1}$;

Figure A47.2a

Plot of the U_{eff}-value of a VIP-integrated building panel as function of thickness, d_c [m], and perimeter to surface area ratio, l_p/S_p [m^{-1}]. Values along the lines denote U_{eff} [$W \cdot m^{-2} \cdot K^{-1}$].

Spacer: folded edge spacer;
Face sheets: 2 mm aluminium;
VIP barrier: metallised film;
$\lambda_c = 4.0 \cdot 10^{-3}\ W \cdot m^{-1} \cdot K^{-1}$;
$\alpha_1 = 7.8\ m^2 \cdot K \cdot W^{-1}$;
$\alpha_2 = 25\ m^2 \cdot K \cdot W^{-1}$;

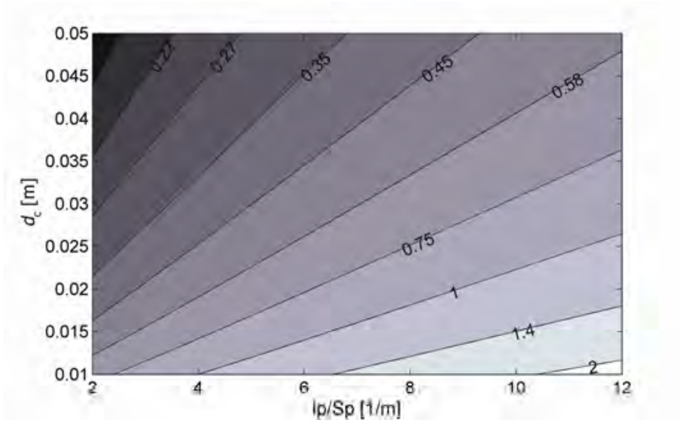

Figure A47.2b

Plot of the U_{eff}-value of a VIP-integrated building panel as function of thickness, d_c [m], and perimeter to surface area ratio, l_p/S_p [m^{-1}]. Values along the lines denote U_{eff} [$W \cdot m^{-2} \cdot K^{-1}$].

Spacer: folded edge spacer;
Face sheets: 3 mm polyester;
VIP barrier: metallised film;
$\lambda_c = 4.0 \cdot 10^{-3}\ W \cdot m^{-1} \cdot K^{-1}$;
$\alpha_1 = 7.8\ m^2 \cdot K \cdot W^{-1}$;
$\alpha_2 = 25\ m^2 \cdot K \cdot W^{-1}$;

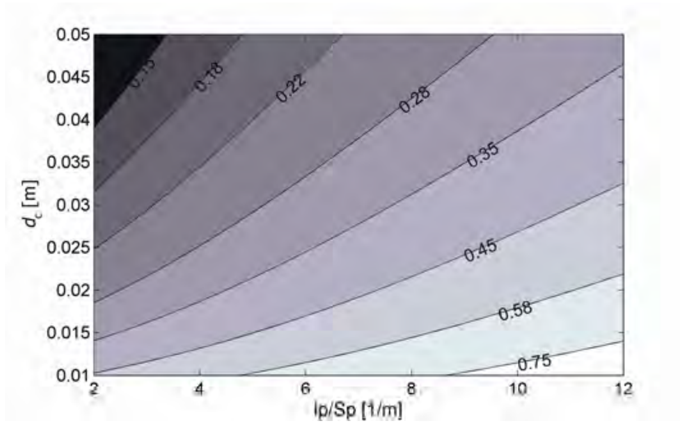

Figure A47.3a

Plot of the U_{eff}-value of a VIP-integrated building panel as function of thickness, d_c [m], and perimeter to surface area ratio, l_p/S_p [m^{-1}]. Values along the lines denote U_{eff} [$W \cdot m^{-2} \cdot K^{-1}$].

Spacer: non-metallic tape;
Face sheets: 2 mm aluminium;
VIP barrier: metallised film;
$\lambda_c = 4.0 \cdot 10^{-3}\ W \cdot m^{-1} \cdot K^{-1}$;
$\alpha_1 = 7.8\ m^2 \cdot K \cdot W^{-1}$;
$\alpha_2 = 25\ m^2 \cdot K \cdot W^{-1}$;

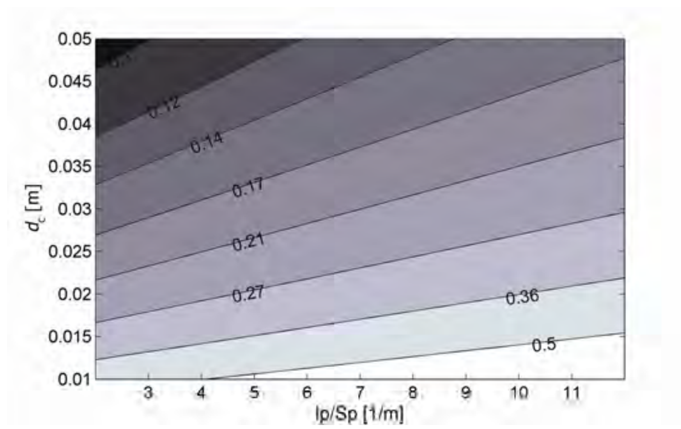

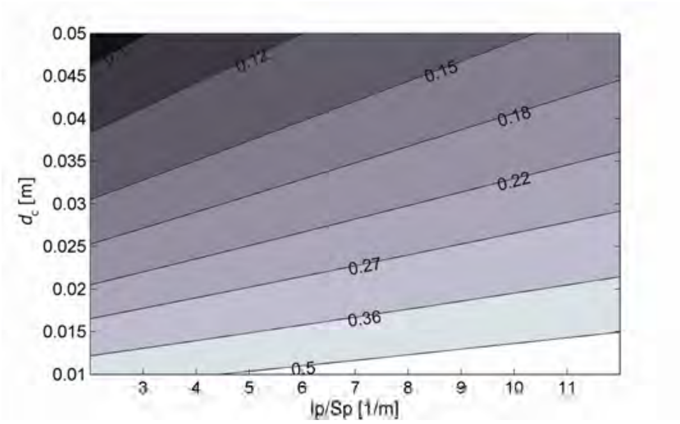

Figure A47.3b

Plot of the U_{eff}-value of a VIP-integrated building panel as function of thickness, d_c [m], and perimeter to surface area ratio, l_p/S_p [m^{-1}]. Values along the lines denote U_{eff} [$W{\cdot}m^{-2}{\cdot}K^{-1}$].

Spacer: non-metallic tape;
Face sheets: 1.5 mm steel;
VIP barrier: metallised film;
$\lambda_c = 4.0{\cdot}10^{-3}\ W{\cdot}m^{-1}{\cdot}K^{-1}$;
$\alpha_1 = 7.8\ m^2{\cdot}K{\cdot}W^{-1}$;
$\alpha_2 = 25\ m^2{\cdot}K{\cdot}W^{-1}$;

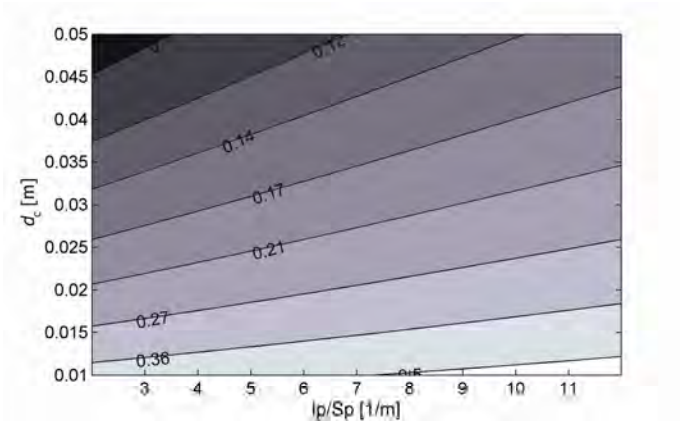

Figure A47.3c

Plot of the U_{eff}-value of a VIP-integrated building panel as function of thickness, d_c [m], and perimeter to surface area ratio, l_p/S_p [m^{-1}]. Values along the lines denote U_{eff} [$W{\cdot}m^{-2}{\cdot}K^{-1}$].

Spacer: non-metallic tape;
Face sheets: 3 mm polyester;
VIP barrier: metallised film;
$\lambda_c = 4.0{\cdot}10^{-3}\ W{\cdot}m^{-1}{\cdot}K^{-1}$;
$\alpha_1 = 7.8\ m^2{\cdot}K{\cdot}W^{-1}$;
$\alpha_2 = 25\ m^2{\cdot}K{\cdot}W^{-1}$;

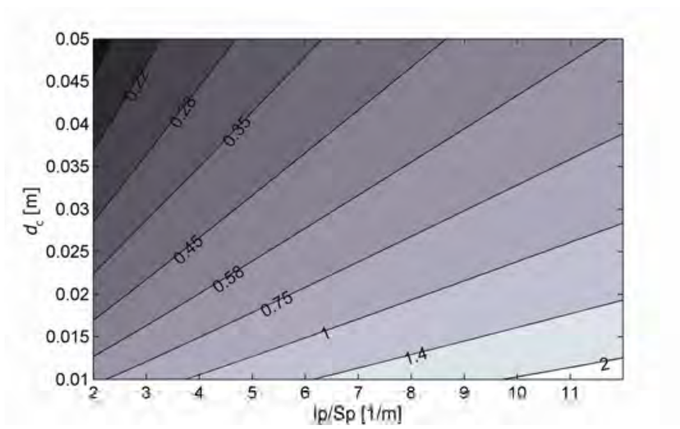

Figure A47.4a

Plot of the U_{eff}-value of a VIP-integrated building panel as function of thickness, d_c [m], and perimeter to surface area ratio, l_p/S_p [m^{-1}]. Values along the lines denote U_{eff} [$W{\cdot}m^{-2}{\cdot}K^{-1}$].

Spacer: optimised plastic;
Face sheets: 2 mm aluminium;
VIP barrier: metallised film;
$\lambda_c = 4.0{\cdot}10^{-3}\ W{\cdot}m^{-1}{\cdot}K^{-1}$;
$\alpha_1 = 7.8\ m^2{\cdot}K{\cdot}W^{-1}$;
$\alpha_2 = 25\ m^2{\cdot}K{\cdot}W^{-1}$;

Figure A47.4b

Plot of the U_{eff}-value of a VIP-integrated building panel as function of thickness, d_c [m], and perimeter to surface area ratio, l_p/S_p [m^{-1}]. Values along the lines denote U_{eff} [$W \cdot m^{-2} \cdot K^{-1}$].

Spacer: optimised plastic;
Face sheets: 3 mm polyester;
VIP barrier: metallised film;
$\lambda_c = 4.0 \cdot 10^{-3}$ $W \cdot m^{-1} \cdot K^{-1}$;
$\alpha_1 = 7.8$ $m^2 \cdot K \cdot W^{-1}$;
$\alpha_2 = 25$ $m^2 \cdot K \cdot W^{-1}$;

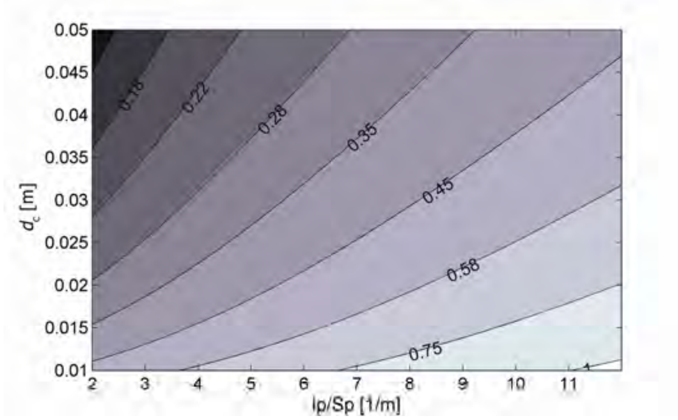

Figure A47.5a

Plot of the U_{eff}-value of a VIP-integrated building panel as function of thickness, d_c [m], and perimeter to surface area ratio, l_p/S_p [m^{-1}]. Values along the lines denote U_{eff} [$W \cdot m^{-2} \cdot K^{-1}$].

Spacer: alu. double-glazing;
Face sheets: 2mm aluminium;
VIP barrier: metallised film;
$\lambda_c = 8.0 \cdot 10^{-3}$ $W \cdot m^{-1} \cdot K^{-1}$;
$\alpha_1 = 7.8$ $m^2 \cdot K \cdot W^{-1}$;
$\alpha_2 = 25$ $m^2 \cdot K \cdot W^{-1}$;

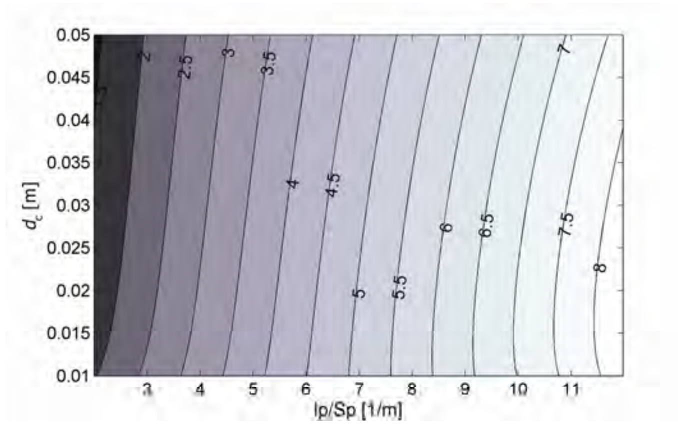

Figure A47.5b

Plot of the U_{eff}-value of a VIP-integrated building panel as function of thickness, d_c [m], and perimeter to surface area ratio, l_p/S_p [m^{-1}]. Values along the lines denote U_{eff} [$W \cdot m^{-2} \cdot K^{-1}$].

Spacer: alu. double-glazing;
Face sheets: 1.5 mm steel;
VIP barrier: metallised film;
$\lambda_c = 8.0 \cdot 10^{-3}$ $W \cdot m^{-1} \cdot K^{-1}$;
$\alpha_1 = 7.8$ $m^2 \cdot K \cdot W^{-1}$;
$\alpha_2 = 25$ $m^2 \cdot K \cdot W^{-1}$;

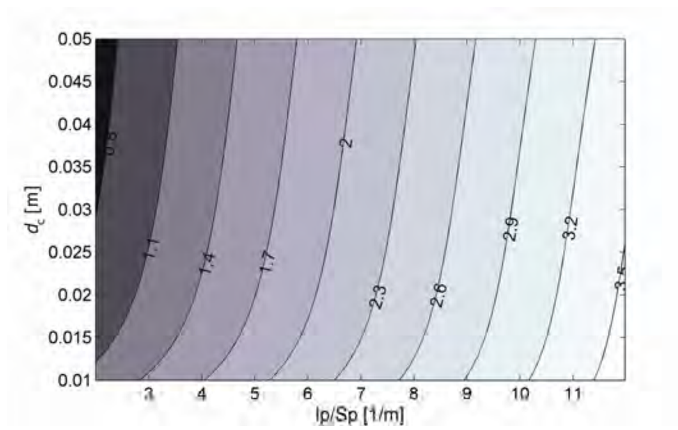

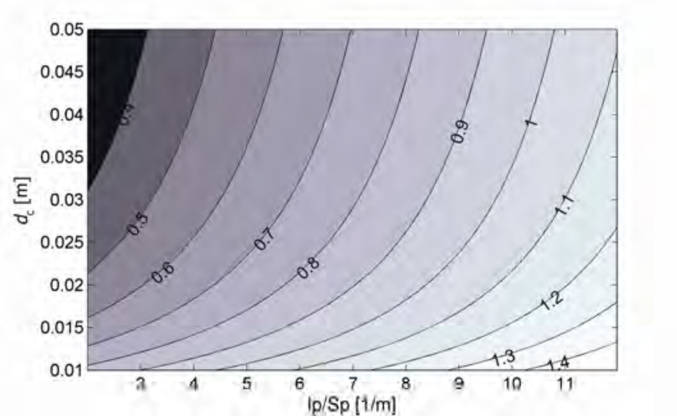

Figure A47.5c

Plot of the U_{eff}-value of a VIP-integrated building panel as function of thickness, d_c [m], and perimeter to surface area ratio, l_p/S_p [m^{-1}]. Values along the lines denote U_{eff} [$W \cdot m^{-2} \cdot K^{-1}$].

Spacer: alu. double-glazing;
Face sheets: 3 mm polyester;
VIP barrier: metallised film;
$\lambda_c = 8.0 \cdot 10^{-3}$ $W \cdot m^{-1} \cdot K^{-1}$;
$\alpha_1 = 7.8$ $m^2 \cdot K \cdot W^{-1}$;
$\alpha_2 = 25$ $m^2 \cdot K \cdot W^{-1}$;

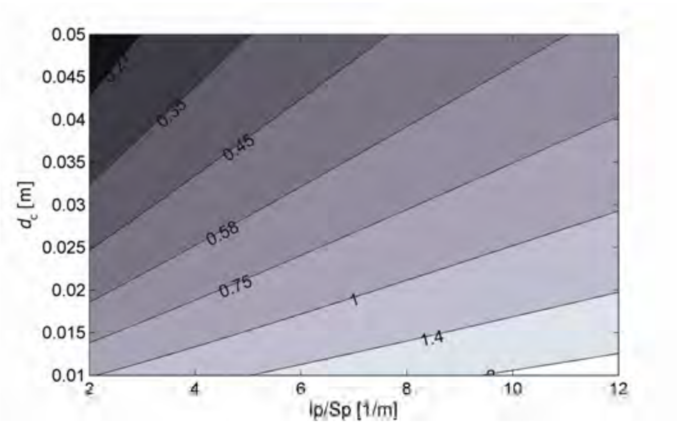

Figure A47.6a

Plot of the U_{eff}-value of a VIP-integrated building panel as function of thickness, d_c [m], and perimeter to surface area ratio, l_p/S_p [m^{-1}]. Values along the lines denote U_{eff} [$W \cdot m^{-2} \cdot K^{-1}$].

Spacer: folded edge spacer;
Face sheets: 2 mm aluminium;
VIP barrier: metallised film;
$\lambda_c = 8.0 \cdot 10^{-3}$ $W \cdot m^{-1} \cdot K^{-1}$;
$\alpha_1 = 7.8$ $m^2 \cdot K \cdot W^{-1}$;
$\alpha_2 = 25$ $m^2 \cdot K \cdot W^{-1}$;

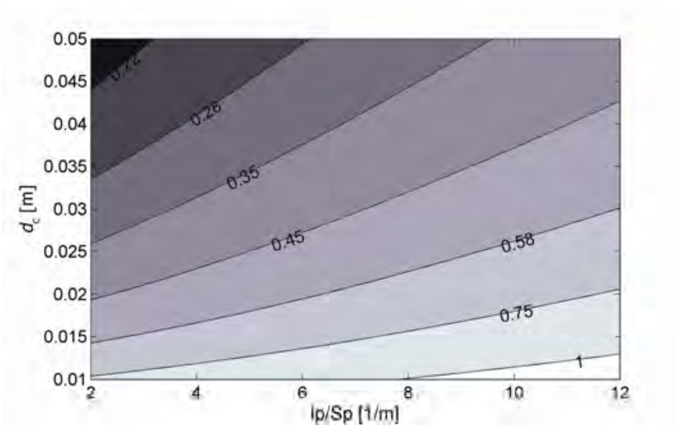

Figure A47.6b

Plot of the U_{eff}-value of a VIP-integrated building panel as function of thickness, d_c [m], and perimeter to surface area ratio, l_p/S_p [m^{-1}]. Values along the lines denote U_{eff} [$W \cdot m^{-2} \cdot K^{-1}$].

Spacer: folded edge spacer;
Face sheets: 3 mm polyester;
VIP barrier: metallised film;
$\lambda_c = 8.0 \cdot 10^{-3}$ $W \cdot m^{-1} \cdot K^{-1}$;
$\alpha_1 = 7.8$ $m^2 \cdot K \cdot W^{-1}$;
$\alpha_2 = 25$ $m^2 \cdot K \cdot W^{-1}$;

Figure A47.7a

Plot of the U_{eff}-value of a VIP-integrated building panel as function of thickness, d_c [m], and perimeter to surface area ratio, l_p/S_p [m^{-1}]. Values along the lines denote U_{eff} [$W \cdot m^{-2} \cdot K^{-1}$].

Spacer: non-metallic tape;
Face sheets: 2 mm aluminium;
VIP barrier: metallised film;
$\lambda_c = 8.0 \cdot 10^{-3}\ W \cdot m^{-1} \cdot K^{-1}$;
$\alpha_1 = 7.8\ m^2 \cdot K \cdot W^{-1}$;
$\alpha_2 = 25\ m^2 \cdot K \cdot W^{-1}$;

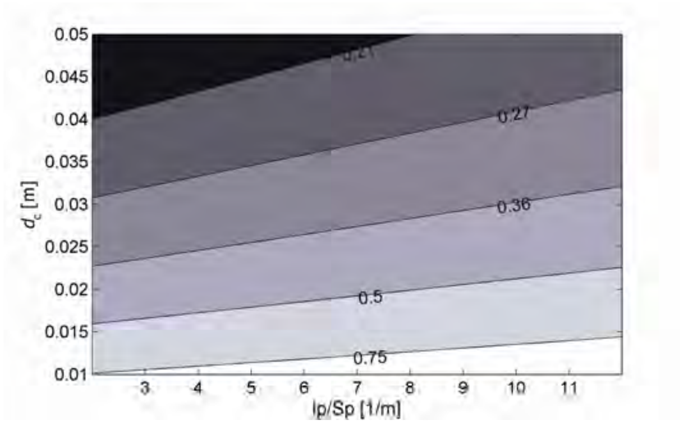

Figure A47.7b

Plot of the U_{eff}-value of a VIP-integrated building panel as function of thickness, d_c [m], and perimeter to surface area ratio, l_p/S_p [m^{-1}]. Values along the lines denote U_{eff} [$W \cdot m^{-2} \cdot K^{-1}$].

Spacer: non-metallic tape;
Face sheets: 1.5 mm steel;
VIP barrier: metallised film;
$\lambda_c = 8.0 \cdot 10^{-3}\ W \cdot m^{-1} \cdot K^{-1}$;
$\alpha_1 = 7.8\ m^2 \cdot K \cdot W^{-1}$;
$\alpha_2 = 25\ m^2 \cdot K \cdot W^{-1}$;

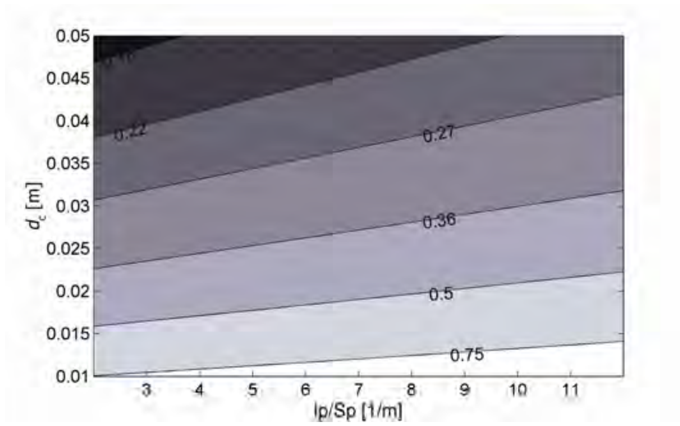

Figure A47.7c

Plot of the U_{eff}-value of a VIP-integrated building panel as function of thickness, d_c [m], and perimeter to surface area ratio, l_p/S_p [m^{-1}]. Values along the lines denote U_{eff} [$W \cdot m^{-2} \cdot K^{-1}$].

Spacer: non-metallic tape;
Face sheets: 3 mm polyester;
VIP barrier: metallised film;
$\lambda_c = 8.0 \cdot 10^{-3}\ W \cdot m^{-1} \cdot K^{-1}$;
$\alpha_1 = 7.8\ m^2 \cdot K \cdot W^{-1}$;
$\alpha_2 = 25\ m^2 \cdot K \cdot W^{-1}$;

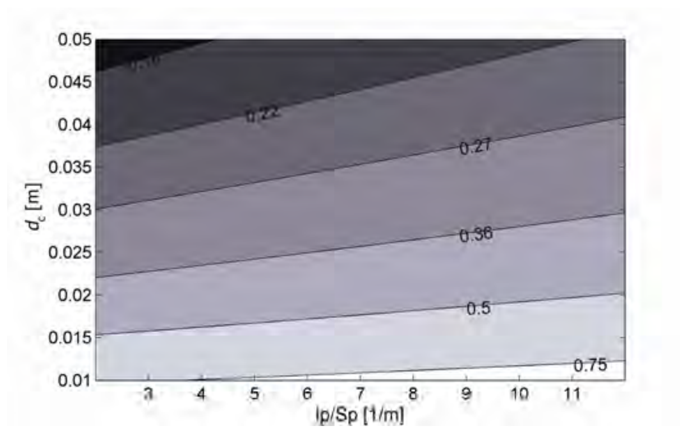

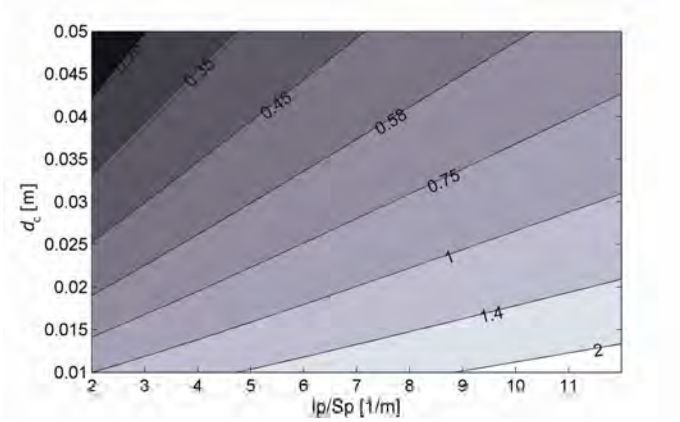

Figure A47.8a

Plot of the U_{eff}-value of a VIP-integrated building panel as function of thickness, d_c [m], and perimeter to surface area ratio, l_p/S_p [m^{-1}]. Values along the lines denote U_{eff} [$W\cdot m^{-2}\cdot K^{-1}$].

Spacer: optimised plastic;
Face sheets: 2 mm aluminium;
VIP barrier: metallised film;
$\lambda_c = 8.0\cdot 10^{-3}\ W\cdot m^{-1}\cdot K^{-1}$;
$\alpha_1 = 7.8\ m^2\cdot K\cdot W^{-1}$;
$\alpha_2 = 25\ m^2\cdot K\cdot W^{-1}$;

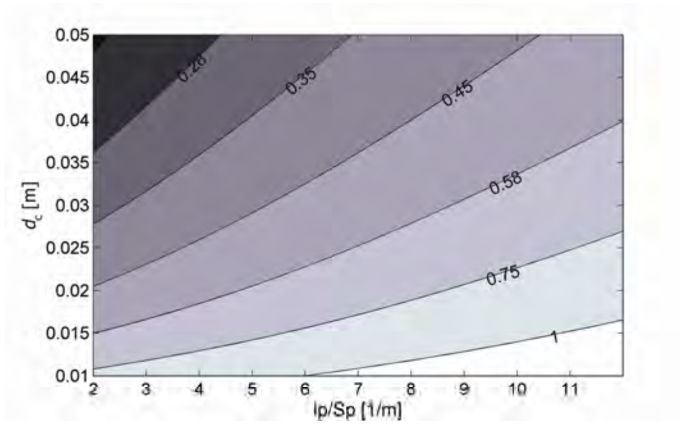

Figure A47.8b

Plot of the U_{eff}-value of a VIP-integrated building panel as function of thickness, d_c [m], and perimeter to surface area ratio, l_p/S_p [m^{-1}]. Values along the lines denote U_{eff} [$W\cdot m^{-2}\cdot K^{-1}$].

Spacer: optimised plastic;
Face sheets: 3 mm polyester;
VIP barrier: metallised film;
$\lambda_c = 8.0\cdot 10^{-3}\ W\cdot m^{-1}\cdot K^{-1}$;
$\alpha_1 = 7.8\ m^2\cdot K\cdot W^{-1}$;
$\alpha_2 = 25\ m^2\cdot K\cdot W^{-1}$;

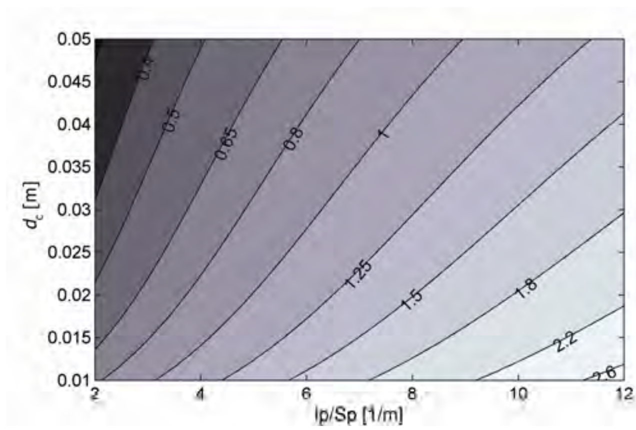

Figure A47.9a

Surface plot of the U_{eff}-value of a sheet-based VIP as function of core thickness, d_c [m], and perimeter to surface area ratio, l_p/S_p [m^{-1}]. Values along the lines denote U_{eff} [$W\cdot m^{-2}\cdot K^{-1}$].

Face sheets: 0.8 / 1.5 mm steel;
$\lambda_c = 4.0\cdot 10^{-3}\ W\cdot m^{-1}\cdot K^{-1}$;
$\alpha_1 = 7.8\ m^2\cdot K\cdot W^{-1}$;
$\alpha_2 = 25\ m^2\cdot K\cdot W^{-1}$;

Figure A47.9b

Surface plot of the U_{eff}-value of a sheet-based VIP as function of core thickness, d_c [m], and perimeter to surface area ratio, l_p/S_p [m^{-1}]. Values along the lines denote U_{eff} [$W \cdot m^{-2} \cdot K^{-1}$].

Face sheets: 0.8 / 4.0 mm steel;
$\lambda_c = 4.0 \cdot 10^{-3}$ $W \cdot m^{-1} \cdot K^{-1}$;
$\alpha_1 = 7.8$ $m^2 \cdot K \cdot W^{-1}$;
$\alpha_2 = 25$ $m^2 \cdot K \cdot W^{-1}$;

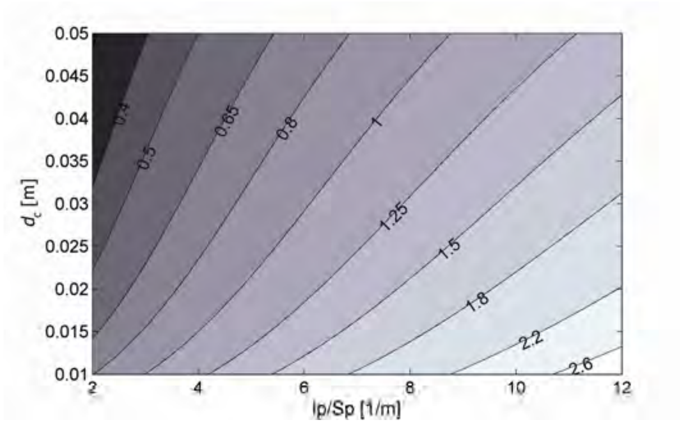

Figure A47.10a

Surface plot of the U_{eff}-value of a sheet-based VIP as function of core thickness, d_c [m], and perimeter to surface area ratio, l_p/S_p [m^{-1}]. Values along the lines denote U_{eff} [$W \cdot m^{-2} \cdot K^{-1}$].

Face sheets: 0.8 / 1.5 mm steel;
$\lambda_c = 8.0 \cdot 10^{-3}$ $W \cdot m^{-1} \cdot K^{-1}$;
$\alpha_1 = 7.8$ $m^2 \cdot K \cdot W^{-1}$;
$\alpha_2 = 25$ $m^2 \cdot K \cdot W^{-1}$;

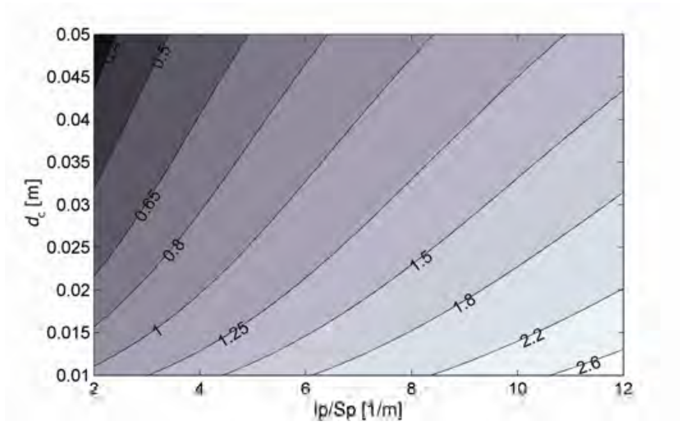

Figure A47.10b

Surface plot of the U_{eff}-value of a sheet-based VIP as function of core thickness, d_c [m], and perimeter to surface area ratio, l_p/S_p [m^{-1}]. Values along the lines denote U_{eff} [$W \cdot m^{-2} \cdot K^{-1}$].

Face sheets: 0.8 / 4.0 mm steel;
$\lambda_c = 8.0 \cdot 10^{-3}$ $W \cdot m^{-1} \cdot K^{-1}$;
$\alpha_1 = 7.8$ $m^2 \cdot K \cdot W^{-1}$;
$\alpha_2 = 25$ $m^2 \cdot K \cdot W^{-1}$;

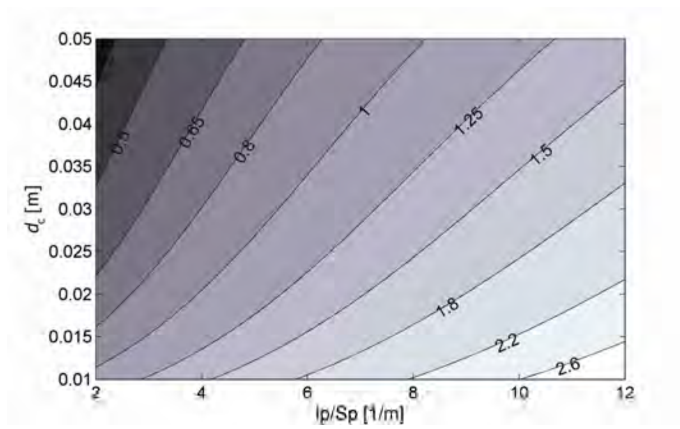

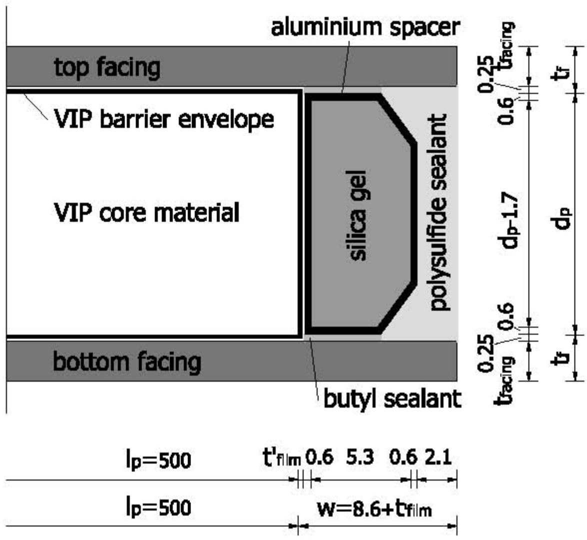

Figure 48.1a

Aluminium double-glazing type of spacer.

Dimensions in mm.

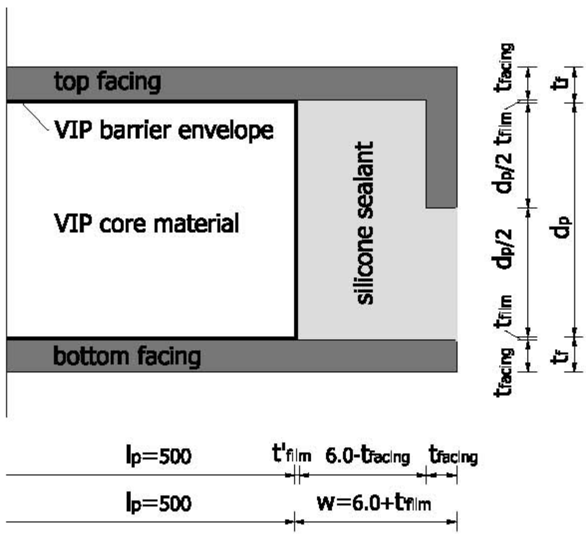

Figure 48.1b

Inwards folded edge type of spacer.

Dimensions in mm.

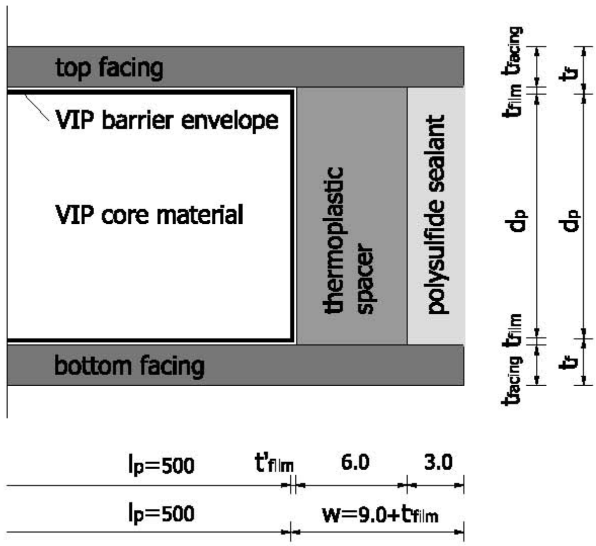

Figure 48.1c

Improved thermoplastic spacer.

Dimensions in mm.

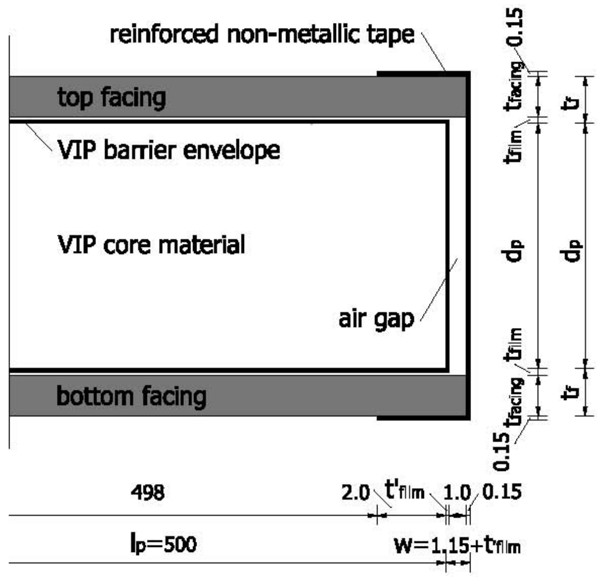

Figure 48.1d

Reinforced non-metallic tape.

Dimensions in mm.

APPENDIXES TO CHAPTER 5 A

A51 SORPTION-CURVE OF FUMED SILICA AND GLASS FIBRE INSULATION

For the use of VIPs in buildings, the most widely applied and most suited core material is fumed silica. During the IEA Annex 39 research project, the sorption-isotherm of fumed silica samples has been determined by three institutes: NRC, ZAE-Bayern and CSTB. This sorption-isotherm can be described with the following equation (Simmler et al., 2005):

$$u = \frac{c_1 \phi}{c_2 + \phi} e^{c_3 \phi^{c_4}} \qquad \text{(A51.1a)},$$

with c_1, c_2, c_3 and c_4 experimental parameters specified in Table 51.1a. The slope of the sorption-curve is either found by taking the derivative of equation (A51.1a) with respect to relative humidity or by a regression analysis of experimental data. In the relative humidity range between 0% and 80% this slope (using experimental data for regression) may be approximated with sufficient accuracy as

$$\frac{du}{d\phi} = 0.071 \pm 0.006 \qquad (0<\phi<0.8) \qquad \text{(A51.1b)},$$

although the average slope according to the derivative of Equation (A51.1a) within this interval is 0.107.

For glass fibre insulation with a dry density of 45 kg·m^{-3}, Hokoi and Kumaran (1993) found the following empirical relationship for the adsorption-isotherm

$$u = \left(c_1 + c_2 \phi + c_3 \phi^{c_4}\right) \frac{\rho_w}{\rho_{dry}} \qquad \text{(A51.2a)},$$

with c_1 to c_4 again regression parameters which are displayed in Table 51.1b and ρ_w [kg·m^{-3}] the density of water. The average slope of this sorption-isotherm between 0% and 95% relative humidity may be approximated as

$$\frac{du}{d\phi} = 0.013 \qquad (0<\phi<0.95) \qquad \text{(A51.2b)}.$$

It is important to mention that for glass fibre insulation with a dry density of 45 kg·m^{-3} and a porosity of 95%, Hokoi and Kumaran (1993) found that below 0.1 m^3·m^{-3} water content no significant effect of water content on thermal conductivity was measured. Since the moisture content in the hygroscopic range of this material is always below this value, the thermal conductivity for service life estimations of VIPs with a glass fibre core can be assumed independent of water content. However, water vapour pressure does account for an increase in thermal conductivity over time.

For open-celled polyurethane foams a sorption-isotherm was not found in literature. But due to the hydrophobic character of the materials it is assumed that no significant amount of water will be adsorbed within the pores.

Table 51.1a - *Parameters determining the sorption-isotherm of fumed silica (Simmler et al., 2005).*

c_1 [kg·kg^{-1}]	c_2 [-]	c_3 [-]	c_4 [-]
0.01721	0.08356	2.82429	2.26663

Table 51.1b - *Parameters determining the sorption-isotherm of glass fibre insulation (Hokoi and Kumaran, 1993)*.

c_1 [kg·kg^{-1}]	c_2 [kg·kg^{-1}]	c_3 [kg·kg^{-1}]	c_4 [-]
0.0015	0.0006	0.0179	900

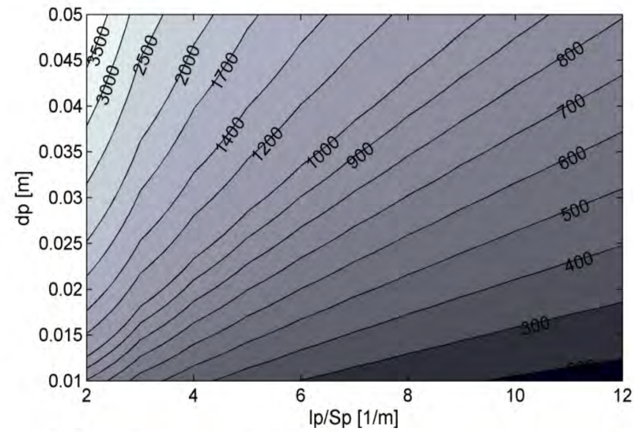

Figure A52.1a

Service life plot of a SiO_x-VIP as function of panel thickness and of panel perimeter to surface ratio.

Barrier: AF:8
T = 278 K
RH = 50%
$\lambda_{cr} = 8.0 \cdot 10^{-3}\ W \cdot m^{-1} \cdot K^{-1}$

Numbers on lines are t_{SL} [yr].

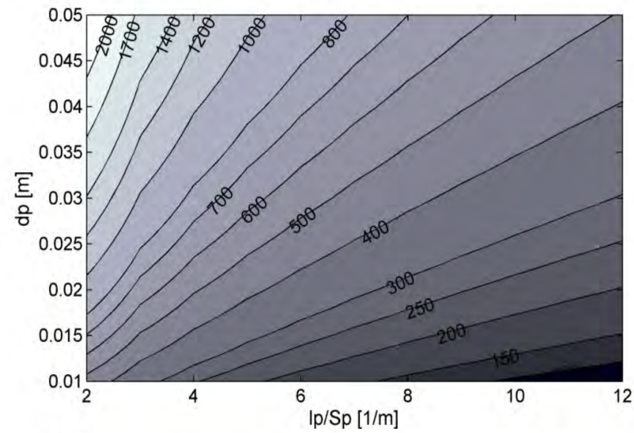

Figure A52.1b

Service life plot of a SiO_x-VIP as function of panel thickness and of panel perimeter to surface ratio.

Barrier: AF:8
T = 288 K
RH = 50%
$\lambda_{cr} = 8.0 \cdot 10^{-3}\ W \cdot m^{-1} \cdot K^{-1}$

Numbers on lines are t_{SL} [yr].

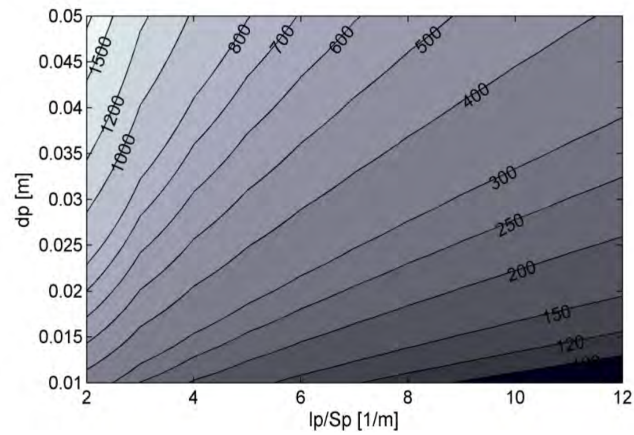

Figure A52.1c

Service life plot of a SiO_x-VIP as function of panel thickness and of panel perimeter to surface ratio.

Barrier: AF:8
T = 293 K
RH = 50%
$\lambda_{cr} = 8.0 \cdot 10^{-3}\ W \cdot m^{-1} \cdot K^{-1}$

Numbers on lines are t_{SL} [yr].

Figure A52.1d

Service life plot of a SiO_x-VIP as function of panel thickness and of panel perimeter to surface ratio.

Barrier: AF:8
T = 298 K
RH = 50%
$\lambda_{cr} = 8.0 \cdot 10^{-3}\ W \cdot m^{-1} \cdot K^{-1}$

Numbers on lines are t_{SL} [yr].

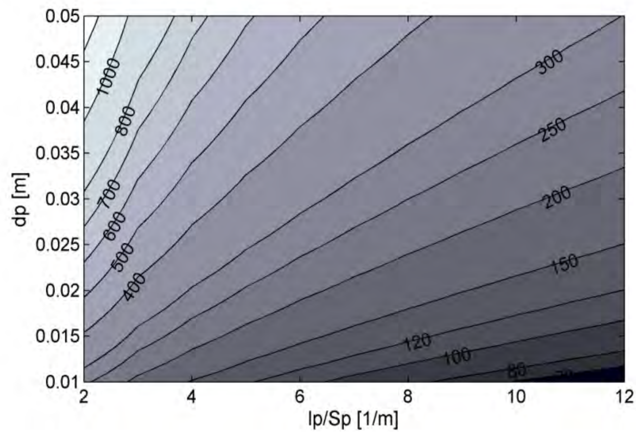

Figure A52.1e

Service life plot of a SiO_x-VIP as function of panel thickness and of panel perimeter to surface ratio.

Barrier: AF:8
T = 308 K
RH = 50%
$\lambda_{cr} = 8.0 \cdot 10^{-3}\ W \cdot m^{-1} \cdot K^{-1}$

Numbers on lines are t_{SL} [yr].

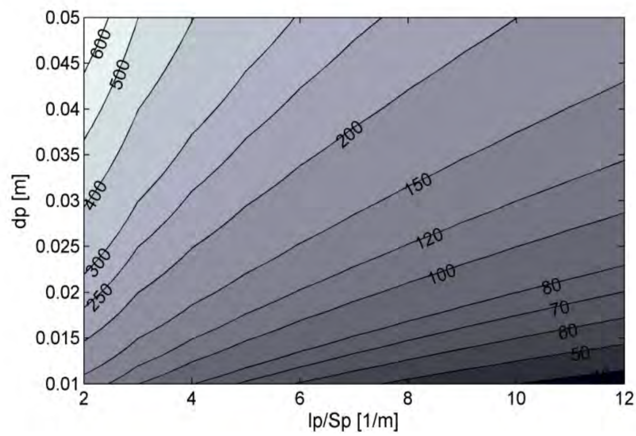

Figure A52.1f

Service life plot of a SiO_x-VIP as function of panel thickness and of panel perimeter to surface ratio.

Barrier: AF:8
T = 318 K
RH = 50%
$\lambda_{cr} = 8.0 \cdot 10^{-3}\ W \cdot m^{-1} \cdot K^{-1}$

Numbers on lines are t_{SL} [yr].

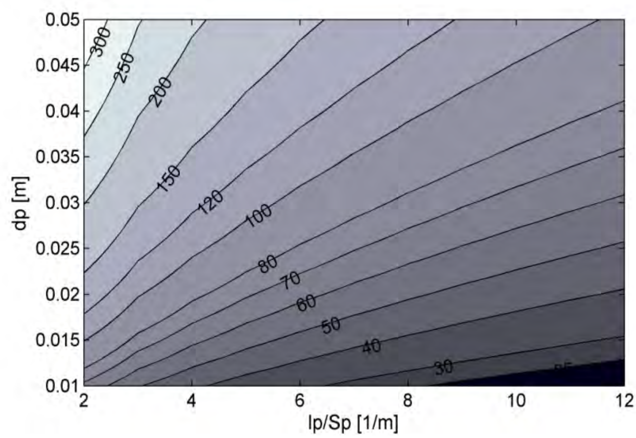

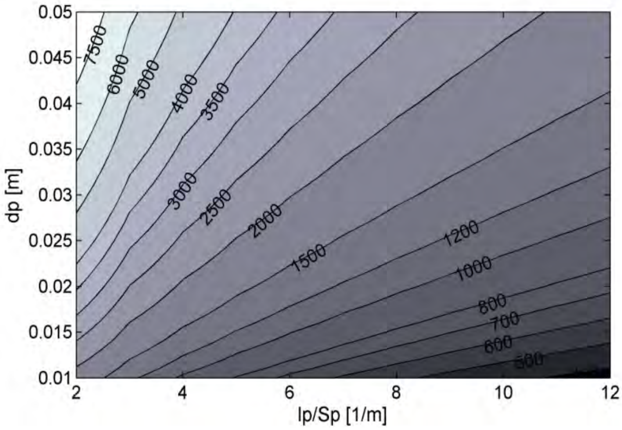

Figure A52.1g

Service life plot of a SiO_x-VIP as function of panel thickness and of panel perimeter to surface ratio.

Barrier: AF:8
T = 278 K
RH = 50%
$\lambda_{cr} = 11 \cdot 10^{-3}$ $W \cdot m^{-1} \cdot K^{-1}$

Numbers on lines are t_{SL} [yr].

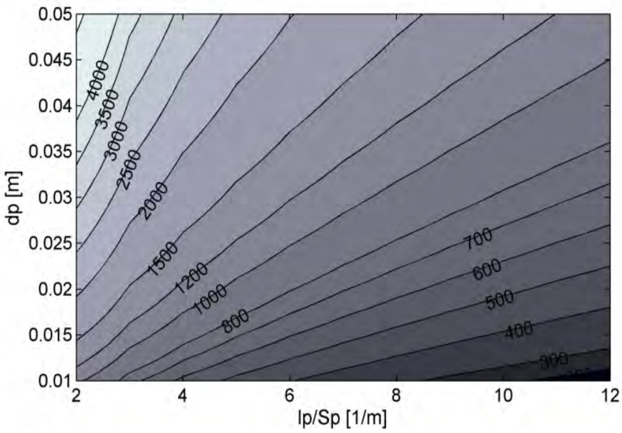

Figure A52.1h

Service life plot of a SiO_x-VIP as function of panel thickness and of panel perimeter to surface ratio.

Barrier: AF:8
T = 288 K
RH = 50%
$\lambda_{cr} = 11 \cdot 10^{-3}$ $W \cdot m^{-1} \cdot K^{-1}$

Numbers on lines are t_{SL} [yr].

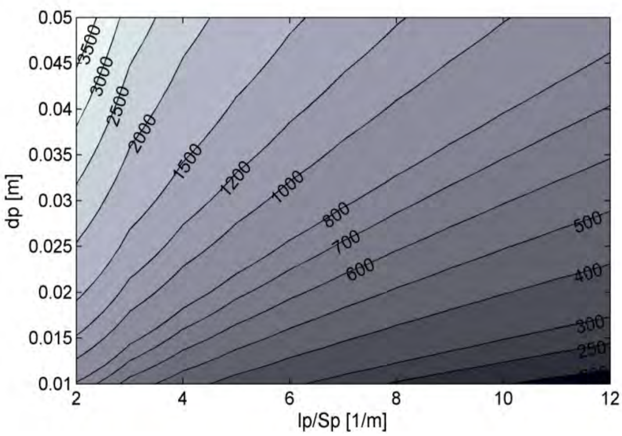

Figure A52.1i

Service life plot of a SiO_x-VIP as function of panel thickness and of panel perimeter to surface ratio.

Barrier: AF:8
T = 293 K
RH = 50%
$\lambda_{cr} = 11 \cdot 10^{-3}$ $W \cdot m^{-1} \cdot K^{-1}$

Numbers on lines are t_{SL} [yr].

Figure A52.1j

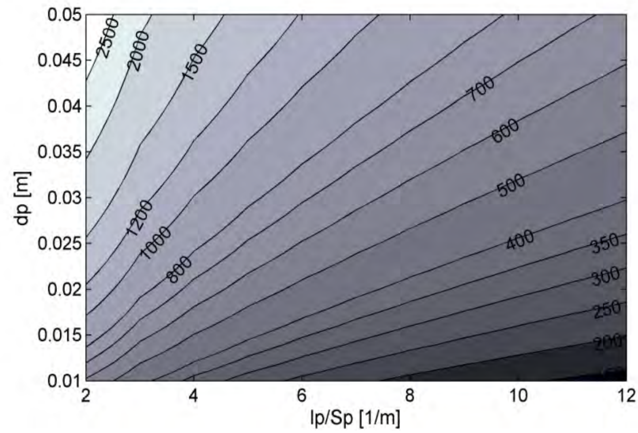

Service life plot of a SiO_x-VIP as function of panel thickness and of panel perimeter to surface ratio.

Barrier: AF:8
T = 298 K
RH = 50%
$\lambda_{cr} = 11 \cdot 10^{-3}\ W \cdot m^{-1} \cdot K^{-1}$

Numbers on lines are t_{SL} [yr].

Figure A52.1k

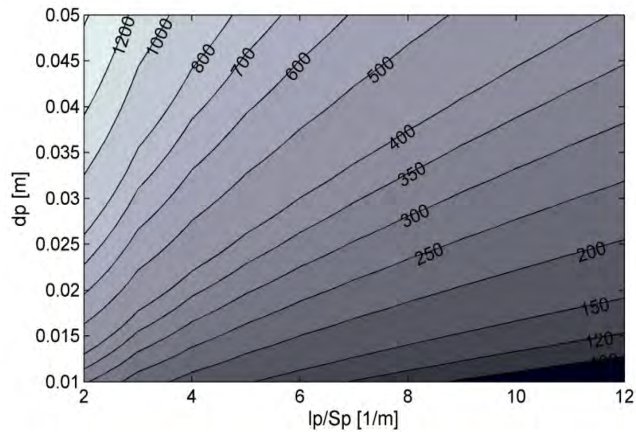

Service life plot of a SiO_x-VIP as function of panel thickness and of panel perimeter to surface ratio.

Barrier: AF:8
T = 308 K
RH = 50%
$\lambda_{cr} = 11 \cdot 10^{-3}\ W \cdot m^{-1} \cdot K^{-1}$

Numbers on lines are t_{SL} [yr].

Figure A52.1l

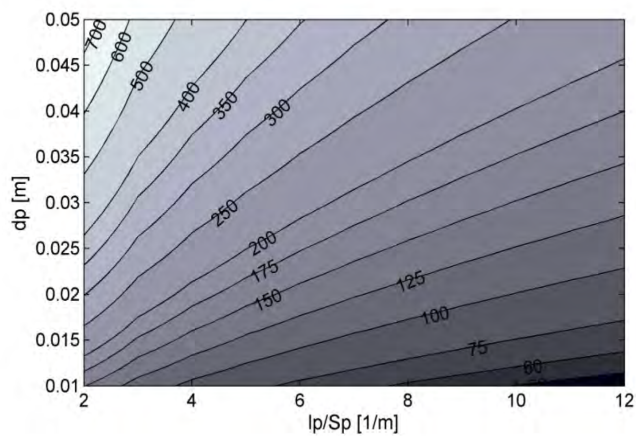

Service life plot of a SiO_x-VIP as function of panel thickness and of panel perimeter to surface ratio.

Barrier: AF:8
T = 318 K
RH = 50%
$\lambda_{cr} = 11 \cdot 10^{-3}\ W \cdot m^{-1} \cdot K^{-1}$

Numbers on lines are t_{SL} [yr].

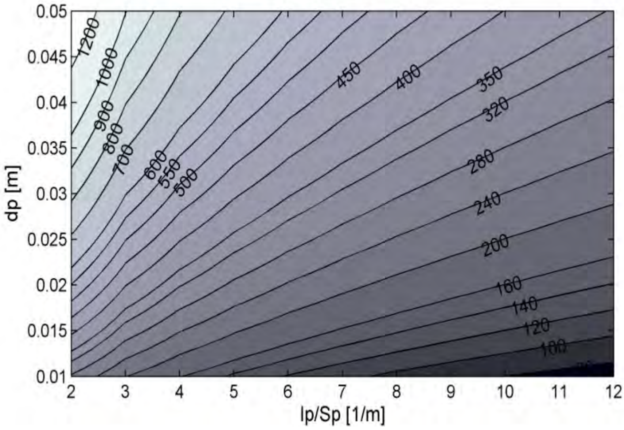

Figure A52.2a

Service life plot of a SiO_x-VIP as function of panel thickness and of panel perimeter to surface ratio.

Barrier: MF3
T = 278 K
RH = 50%
$\lambda_{cr} = 8.0 \cdot 10^{-3}\ W \cdot m^{-1} \cdot K^{-1}$

Numbers on lines are t_{SL} [yr].

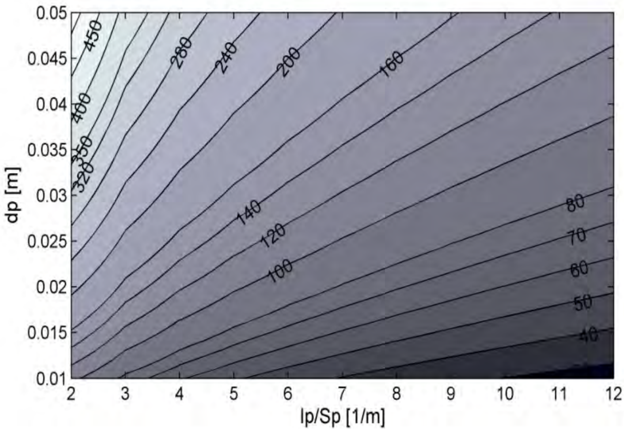

Figure A52.2b

Service life plot of a SiO_x-VIP as function of panel thickness and of panel perimeter to surface ratio.

Barrier: MF3
T = 288 K
RH = 50%
$\lambda_{cr} = 8.0 \cdot 10^{-3}\ W \cdot m^{-1} \cdot K^{-1}$

Numbers on lines are t_{SL} [yr].

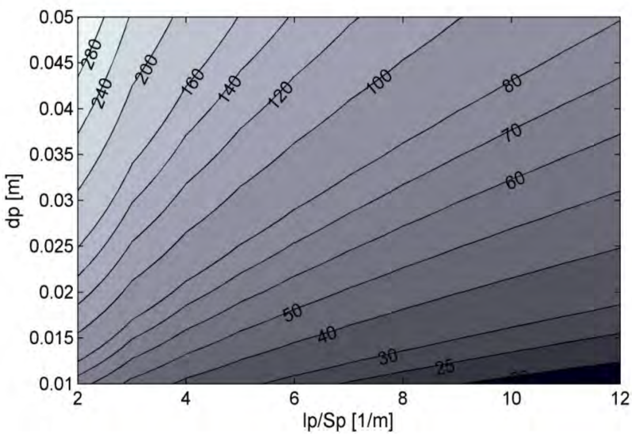

Figure A52.2c

Service life plot of a SiO_x-VIP as function of panel thickness and of panel perimeter to surface ratio.

Barrier: MF3
T = 293 K
RH = 50%
$\lambda_{cr} = 8.0 \cdot 10^{-3}\ W \cdot m^{-1} \cdot K^{-1}$

Numbers on lines are t_{SL} [yr].

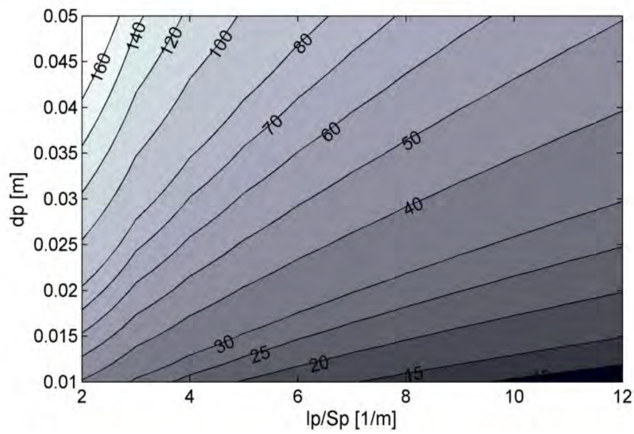

Figure A52.2d

Service life plot of a SiO_x-VIP as function of panel thickness and of panel perimeter to surface ratio.

Barrier: MF3
T = 298 K
RH = 50%
$\lambda_{cr} = 8.0 \cdot 10^{-3}\ W \cdot m^{-1} \cdot K^{-1}$

Numbers on lines are t_{SL} [yr].

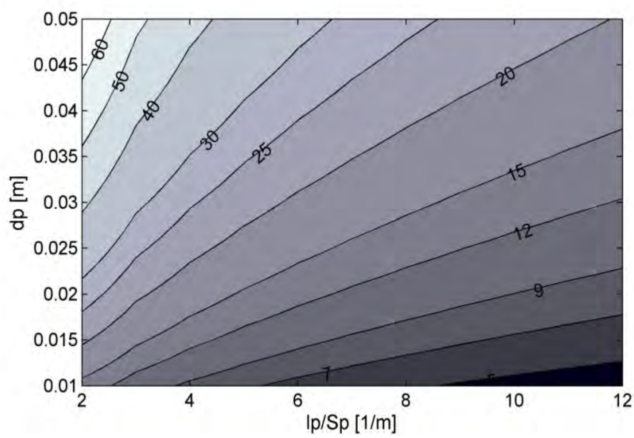

Figure A52.2e

Service life plot of a SiO_x-VIP as function of panel thickness and of panel perimeter to surface ratio.

Barrier: MF3
T = 308 K
RH = 50%
$\lambda_{cr} = 8.0 \cdot 10^{-3}\ W \cdot m^{-1} \cdot K^{-1}$

Numbers on lines are t_{SL} [yr].

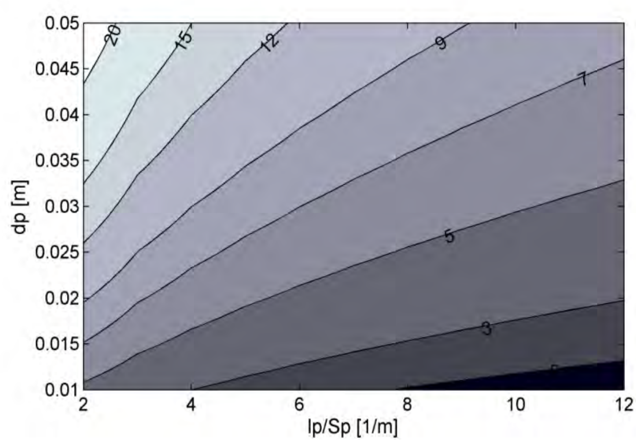

Figure A52.2f

Service life plot of a SiO_x-VIP as function of panel thickness and of panel perimeter to surface ratio.

Barrier: MF3
T = 318 K
RH = 50%
$\lambda_{cr} = 8.0 \cdot 10^{-3}\ W \cdot m^{-1} \cdot K^{-1}$

Numbers on lines are t_{SL} [yr].

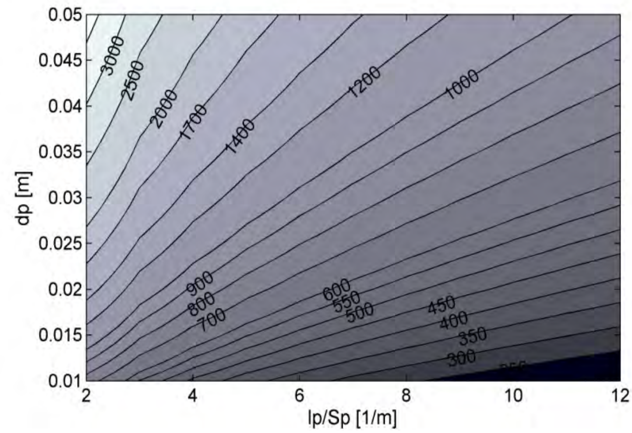

Figure A52.2g

Service life plot of a SiO_x-VIP as function of panel thickness and of panel perimeter to surface ratio.

Barrier: MF3
T = 278 K
RH = 50%
$\lambda_{cr} = 11 \cdot 10^{-3}\ W \cdot m^{-1} \cdot K^{-1}$

Numbers on lines are t_{SL} [yr].

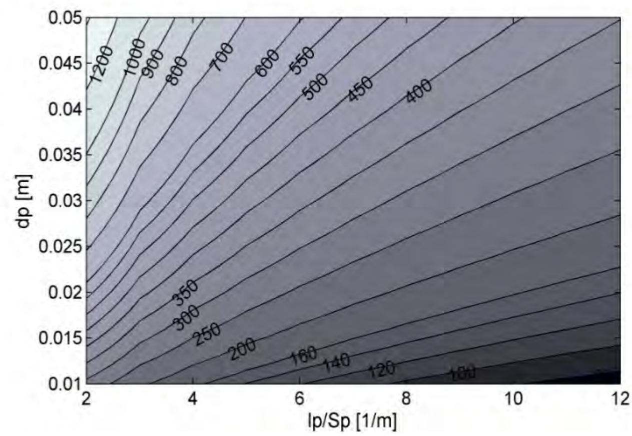

Figure A52.2h

Service life plot of a SiO_x-VIP as function of panel thickness and of panel perimeter to surface ratio.

Barrier: MF3
T = 288 K
RH = 50%
$\lambda_{cr} = 11 \cdot 10^{-3}\ W \cdot m^{-1} \cdot K^{-1}$

Numbers on lines are t_{SL} [yr].

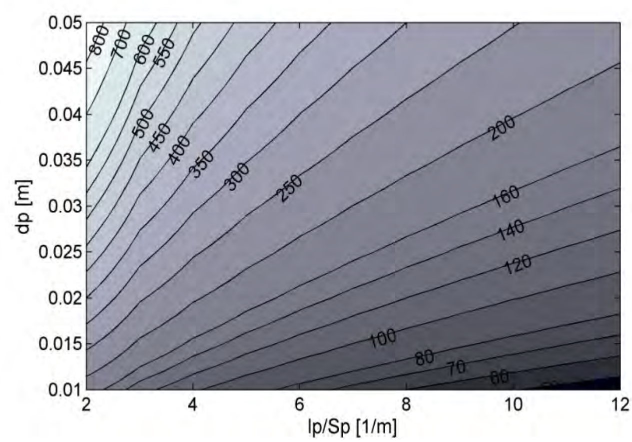

Figure A52.2i

Service life plot of a SiO_x-VIP as function of panel thickness and of panel perimeter to surface ratio.

Barrier: MF3
T = 293 K
RH = 50%
$\lambda_{cr} = 11 \cdot 10^{-3}\ W \cdot m^{-1} \cdot K^{-1}$

Numbers on lines are t_{SL} [yr].

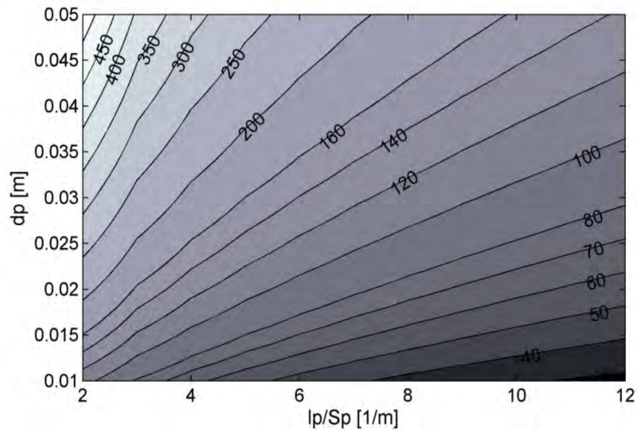

Figure A52.2j

Service life plot of a SiO$_x$-VIP as function of panel thickness and of panel perimeter to surface ratio.

Barrier: MF3
T = 298 K
RH = 50%
λ_{cr} = 11·10^{-3} W·m^{-1}·K^{-1}

Numbers on lines are t_{SL} [yr].

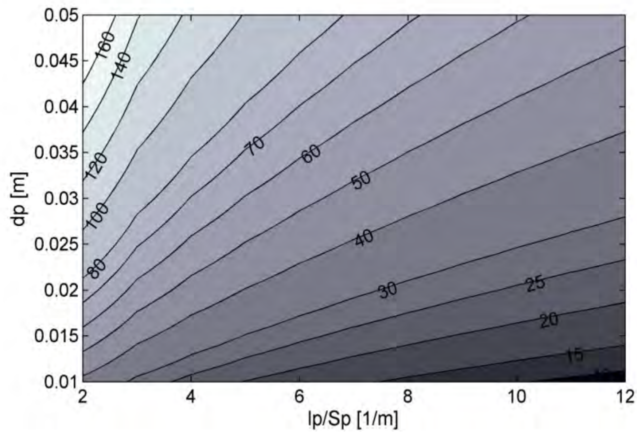

Figure A52.2k

Service life plot of a SiO$_x$-VIP as function of panel thickness and of panel perimeter to surface ratio.

Barrier: MF3
T = 308 K
RH = 50%
λ_{cr} = 11·10^{-3} W·m^{-1}·K^{-1}

Numbers on lines are t_{SL} [yr].

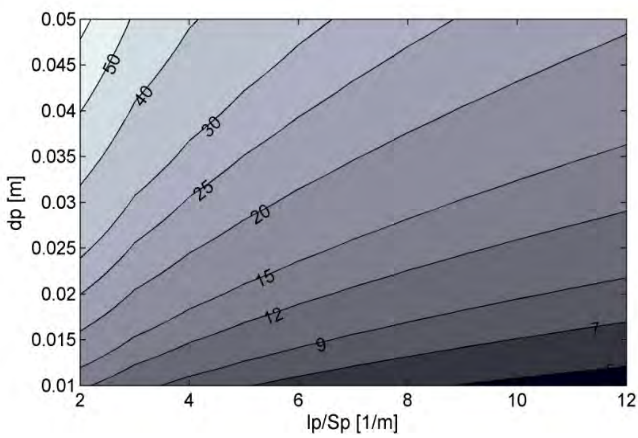

Figure A52.2l

Service life plot of a SiO$_x$-VIP as function of panel thickness and of panel perimeter to surface ratio.

Barrier: MF3
T = 318 K
RH = 50%
λ_{cr} = 11·10^{-3} W·m^{-1}·K^{-1}

Numbers on lines are t_{SL} [yr].

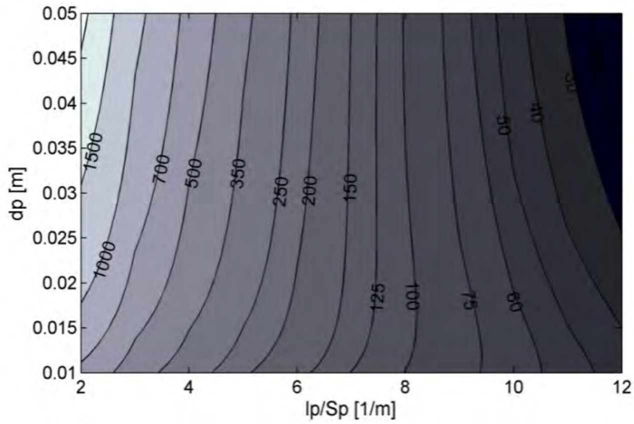

Figure A53.1a

Service life plot of a SiO_x-VIP as function of panel thickness and of panel perimeter to surface ratio including thermal edge effects.

Barrier: AF:8
Seam: type b (φ = 0.67)
T = 278 K; RH = 50%
$\lambda_{eff;cr} = 8.0 \cdot 10^{-3}$ W·m^{-1}·K^{-1}
$\alpha_1 = 7.8$ m^2·K·W^{-1};
$\alpha_2 = 25$ m^2·K·W^{-1}

Numbers on lines are t_{SL} [yr].

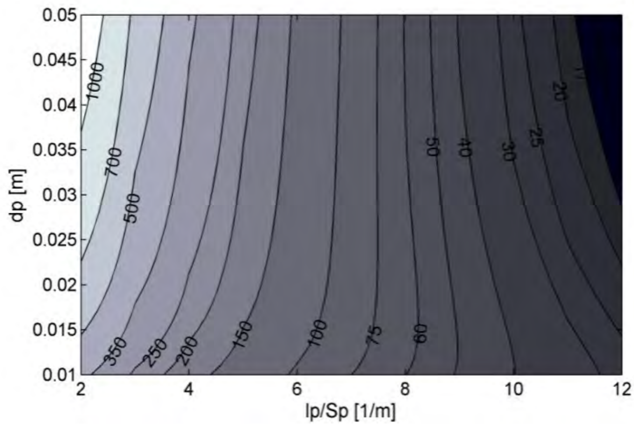

Figure A53.1b

Service life plot of a SiO_x-VIP as function of panel thickness and of panel perimeter to surface ratio including thermal edge effects.

Barrier: AF:8
Seam: type b (φ = 0.67)
T = 288 K; RH = 50%
$\lambda_{eff;cr} = 8.0 \cdot 10^{-3}$ W·m^{-1}·K^{-1}
$\alpha_1 = 7.8$ m^2·K·W^{-1}
$\alpha_2 = 25$ m^2·K·W^{-1}

Numbers on lines are t_{SL} [yr].

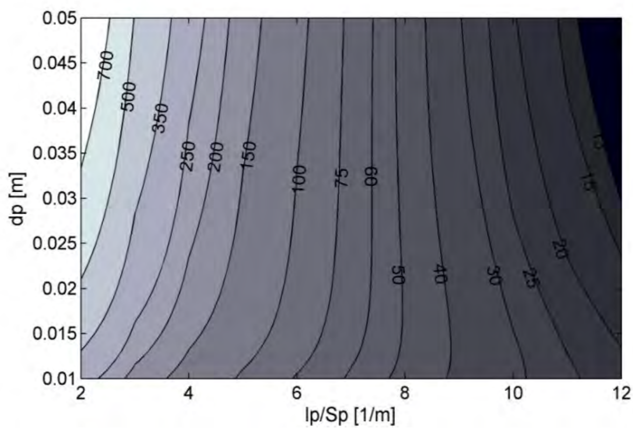

Figure A53.1c

Service life plot of a SiO_x-VIP as function of panel thickness and of panel perimeter to surface ratio including thermal edge effects.

Barrier: AF:8
Seam: type b (φ = 0.67)
T = 293 K; RH = 50%
$\lambda_{eff;cr} = 8.0 \cdot 10^{-3}$ W·m^{-1}·K^{-1}
$\alpha_1 = 7.8$ m^2·K·W^{-1}
$\alpha_2 = 25$ m^2·K·W^{-1}

Numbers on lines are t_{SL} [yr].

Figure A53.1d

Service life plot of a SiO_x-VIP as function of panel thickness and of panel perimeter to surface ratio including thermal edge effects.

Barrier: AF:8
Seam: type b ($\varphi = 0.67$)
T = 298 K; RH = 50%
$\lambda_{eff;cr} = 8.0 \cdot 10^{-3}$ W·m^{-1}·K^{-1}
$\alpha_1 = 7.8$ m^2·K·W^{-1}
$\alpha_2 = 25$ m^2·K·W^{-1}

Numbers on lines are t_{SL} [yr].

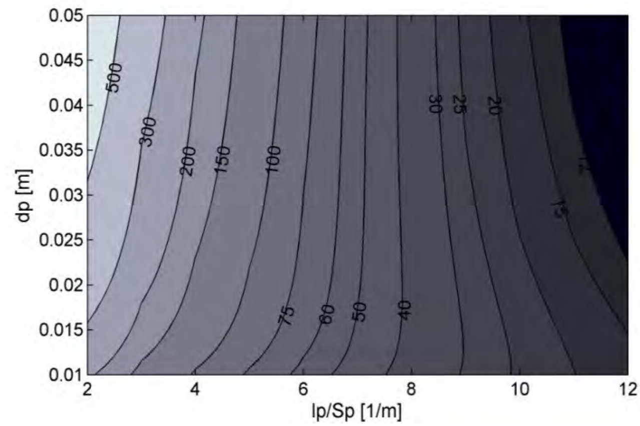

Figure A53.1e

Service life plot of a SiO_x-VIP as function of panel thickness and of panel perimeter to surface ratio including thermal edge effects.

Barrier: AF:8
Seam: type b ($\varphi = 0.67$)
T = 308 K; RH = 50%
$\lambda_{eff;cr} = 8.0 \cdot 10^{-3}$ W·m^{-1}·K^{-1}
$\alpha_1 = 7.8$ m^2·K·W^{-1}
$\alpha_2 = 25$ m^2·K·W^{-1}

Numbers on lines are t_{SL} [yr].

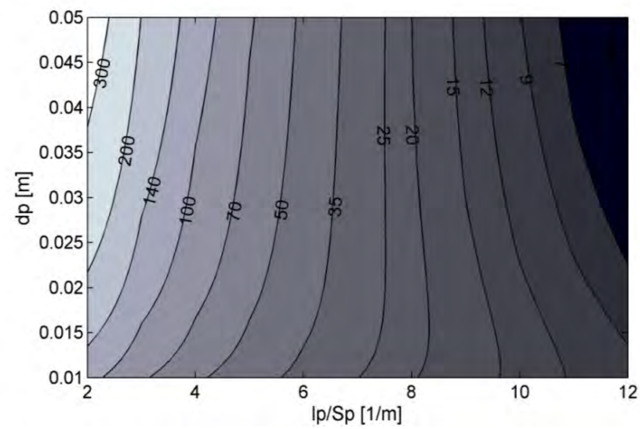

Figure A53.1f

Service life plot of a SiO_x-VIP as function of panel thickness and of panel perimeter to surface ratio including thermal edge effects.

Barrier: AF:8
Seam: type b ($\varphi = 0.67$)
T = 318 K; RH = 50%
$\lambda_{eff;cr} = 8.0 \cdot 10^{-3}$ W·m^{-1}·K^{-1}
$\alpha_1 = 7.8$ m^2·K·W^{-1}
$\alpha_2 = 25$ m^2·K·W^{-1}

Numbers on lines are t_{SL} [yr].

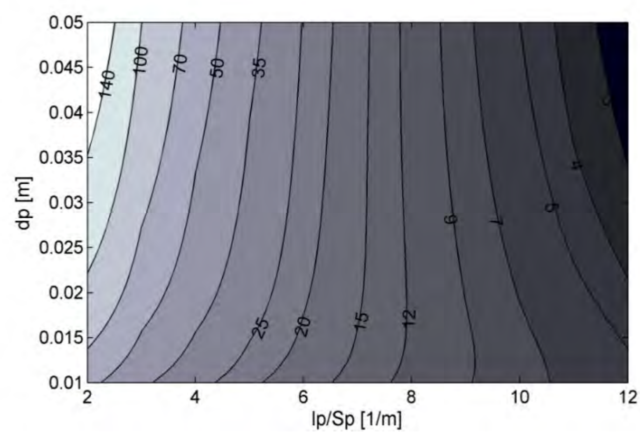

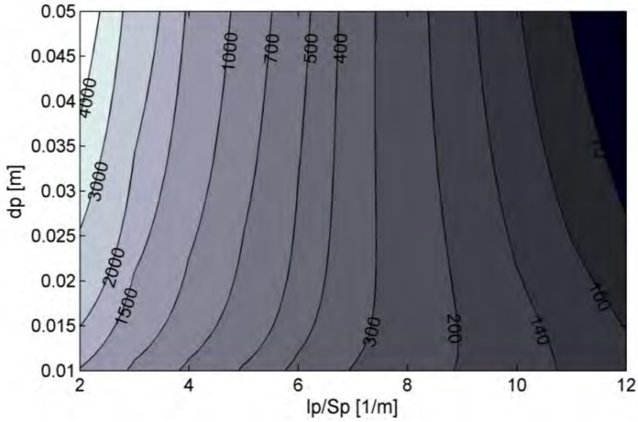

Figure A53.1g

Service life plot of a SiO_x-VIP as function of panel thickness and of panel perimeter to surface ratio including thermal edge effects.

Barrier: AF:8
Seam: type b ($\varphi = 0.67$)
T = 278 K; RH = 50%
$\lambda_{eff;cr} = 11 \cdot 10^{-3}$ $W \cdot m^{-1} \cdot K^{-1}$
$\alpha_1 = 7.8$ $m^2 \cdot K \cdot W^{-1}$;
$\alpha_2 = 25$ $m^2 \cdot K \cdot W^{-1}$

Numbers on lines are t_{SL} [yr].

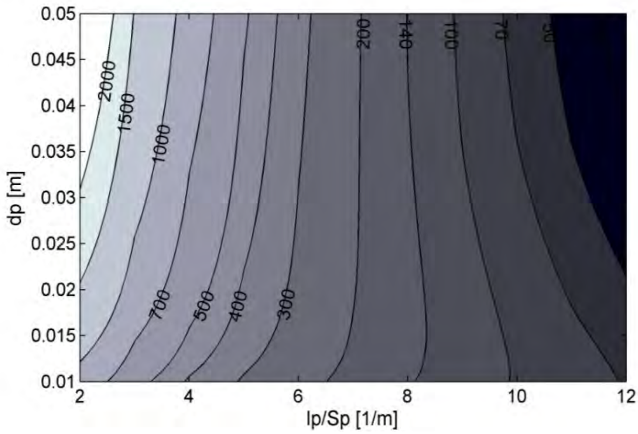

Figure A53.1h

Service life plot of a SiO_x-VIP as function of panel thickness and of panel perimeter to surface ratio including thermal edge effects.

Barrier: AF:8
Seam: type b ($\varphi = 0.67$)
T = 288 K; RH = 50%
$\lambda_{eff;cr} = 11 \cdot 10^{-3}$ $W \cdot m^{-1} \cdot K^{-1}$
$\alpha_1 = 7.8$ $m^2 \cdot K \cdot W^{-1}$
$\alpha_2 = 25$ $m^2 \cdot K \cdot W^{-1}$

Numbers on lines are t_{SL} [yr].

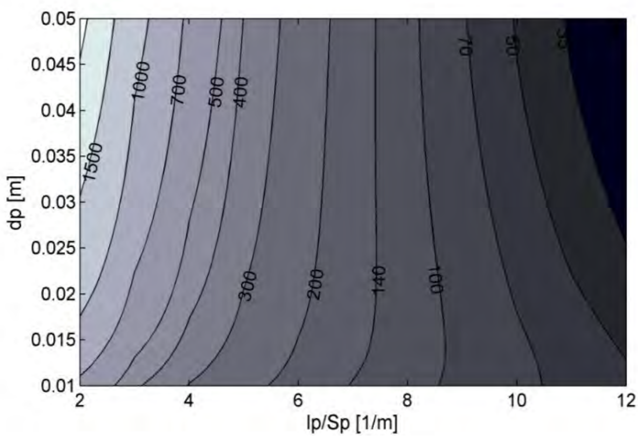

Figure A53.1i

Service life plot of a SiO_x-VIP as function of panel thickness and of panel perimeter to surface ratio including thermal edge effects.

Barrier: AF:8
Seam: type b ($\varphi = 0.67$)
T = 293 K; RH = 50%
$\lambda_{eff;cr} = 11 \cdot 10^{-3}$ $W \cdot m^{-1} \cdot K^{-1}$
$\alpha_1 = 7.8$ $m^2 \cdot K \cdot W^{-1}$
$\alpha_2 = 25$ $m^2 \cdot K \cdot W^{-1}$

Numbers on lines are t_{SL} [yr].

Figure A53.1j

Service life plot of a SiO_x-VIP as function of panel thickness and of panel perimeter to surface ratio including thermal edge effects.

Barrier: AF:8
Seam: type b ($\varphi = 0.67$)
$T = 298$ K; RH = 50%
$\lambda_{eff;cr} = 11 \cdot 10^{-3}$ $W \cdot m^{-1} \cdot K^{-1}$
$\alpha_1 = 7.8$ $m^2 \cdot K \cdot W^{-1}$
$\alpha_2 = 25$ $m^2 \cdot K \cdot W^{-1}$

Numbers on lines are t_{SL} [yr].

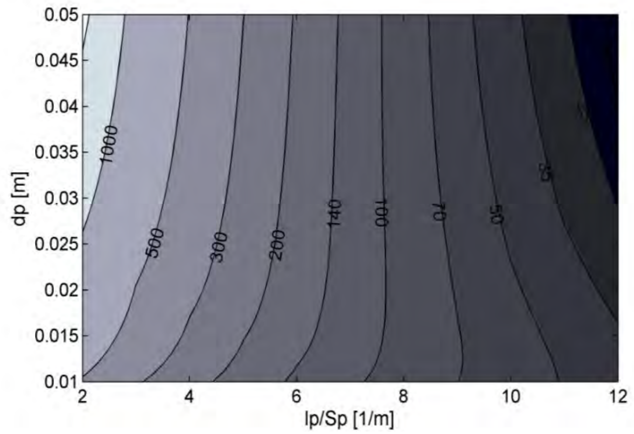

Figure A53.1k

Service life plot of a SiO_x-VIP as function of panel thickness and of panel perimeter to surface ratio including thermal edge effects.

Barrier: AF:8
Seam: type b ($\varphi = 0.67$)
$T = 308$ K; RH = 50%
$\lambda_{eff;cr} = 11 \cdot 10^{-3}$ $W \cdot m^{-1} \cdot K^{-1}$
$\alpha_1 = 7.8$ $m^2 \cdot K \cdot W^{-1}$
$\alpha_2 = 25$ $m^2 \cdot K \cdot W^{-1}$

Numbers on lines are t_{SL} [yr].

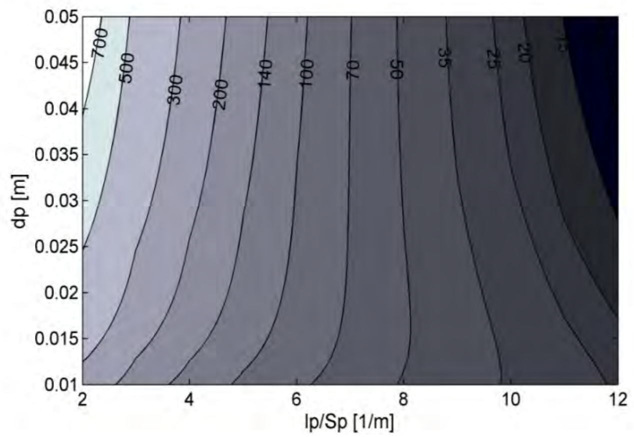

Figure A53.1l

Service life plot of a SiO_x-VIP as function of panel thickness and of panel perimeter to surface ratio including thermal edge effects.

Barrier: AF:8
Seam: type b ($\varphi = 0.67$)
$T = 318$ K; RH = 50%
$\lambda_{eff;cr} = 11 \cdot 10^{-3}$ $W \cdot m^{-1} \cdot K^{-1}$
$\alpha_1 = 7.8$ $m^2 \cdot K \cdot W^{-1}$
$\alpha_2 = 25$ $m^2 \cdot K \cdot W^{-1}$

Numbers on lines are t_{SL} [yr].

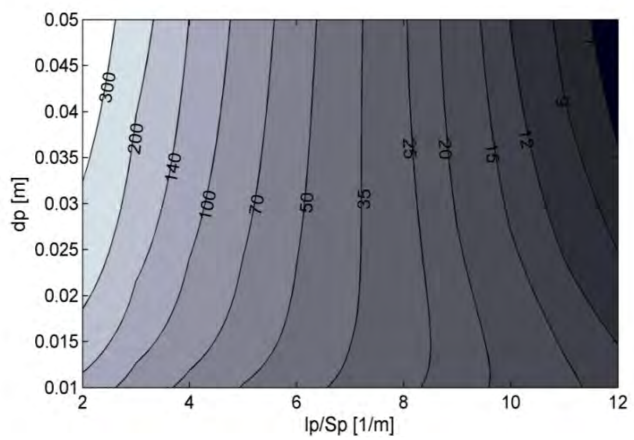

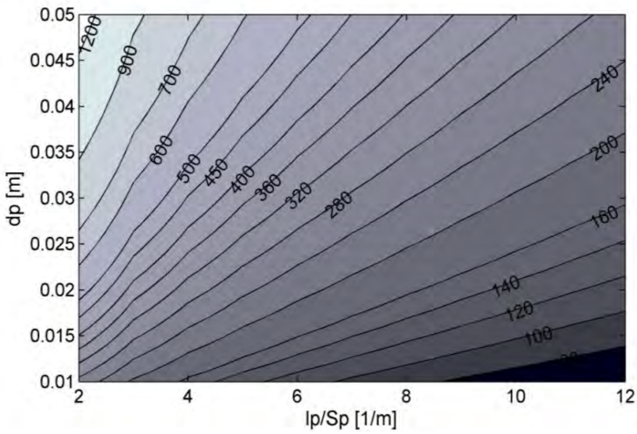

Figure A53.2a

Service life plot of a SiO_x-VIP as function of panel thickness and of panel perimeter to surface ratio including thermal edge effects.

Barrier: MF3
Seam: type b ($\varphi = 0.67$)
T = 278 K; RH = 50%
$\lambda_{eff;cr} = 8.0 \cdot 10^{-3}\ W \cdot m^{-1} \cdot K^{-1}$
$\alpha_1 = 7.8\ m^2 \cdot K \cdot W^{-1}$;
$\alpha_2 = 25\ m^2 \cdot K \cdot W^{-1}$

Numbers on lines are t_{SL} [yr].

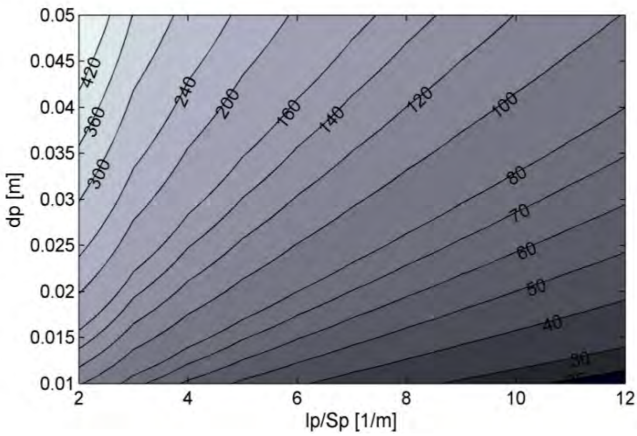

Figure A53.2b

Service life plot of a SiO_x-VIP as function of panel thickness and of panel perimeter to surface ratio including thermal edge effects.

Barrier: MF3
Seam: type b ($\varphi = 0.67$)
T = 288 K; RH = 50%
$\lambda_{eff;cr} = 8.0 \cdot 10^{-3}\ W \cdot m^{-1} \cdot K^{-1}$
$\alpha_1 = 7.8\ m^2 \cdot K \cdot W^{-1}$
$\alpha_2 = 25\ m^2 \cdot K \cdot W^{-1}$

Numbers on lines are t_{SL} [yr].

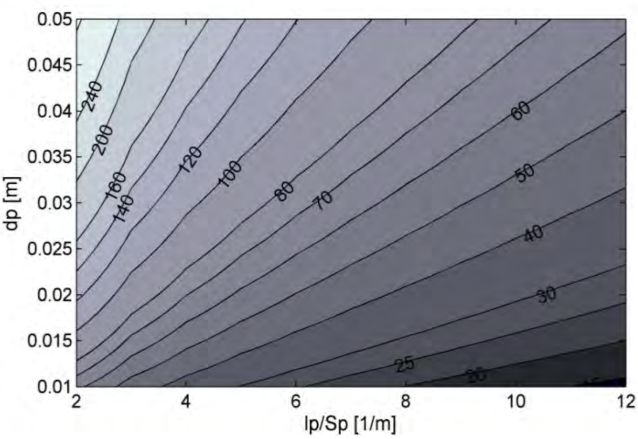

Figure A53.2c

Service life plot of a SiO_x-VIP as function of panel thickness and of panel perimeter to surface ratio including thermal edge effects.

Barrier: MF3
Seam: type b ($\varphi = 0.67$)
T = 293 K; RH = 50%
$\lambda_{eff;cr} = 8.0 \cdot 10^{-3}\ W \cdot m^{-1} \cdot K^{-1}$
$\alpha_1 = 7.8\ m^2 \cdot K \cdot W^{-1}$
$\alpha_2 = 25\ m^2 \cdot K \cdot W^{-1}$

Numbers on lines are t_{SL} [yr].

Figure A53.2d

Service life plot of a SiO_x-VIP as function of panel thickness and of panel perimeter to surface ratio including thermal edge effects.

Barrier: MF3
Seam: type b (φ = 0.67)
T = 298 K; RH = 50%
$\lambda_{eff;cr}$ = 8.0·10^{-3} W·m^{-1}·K^{-1}
α_1 = 7.8 m^2·K·W^{-1}
α_2 = 25 m^2·K·W^{-1}

Numbers on lines are t_{SL} [yr].

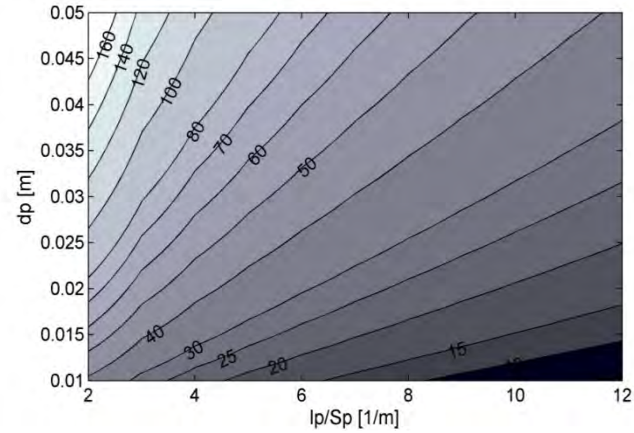

Figure A53.2e

Service life plot of a SiO_x-VIP as function of panel thickness and of panel perimeter to surface ratio including thermal edge effects.

Barrier: MF3
Seam: type b (φ = 0.67)
T = 308 K; RH = 50%
$\lambda_{eff;cr}$ = 8.0·10^{-3} W·m^{-1}·K^{-1}
α_1 = 7.8 m^2·K·W^{-1}
α_2 = 25 m^2·K·W^{-1}

Numbers on lines are t_{SL} [yr].

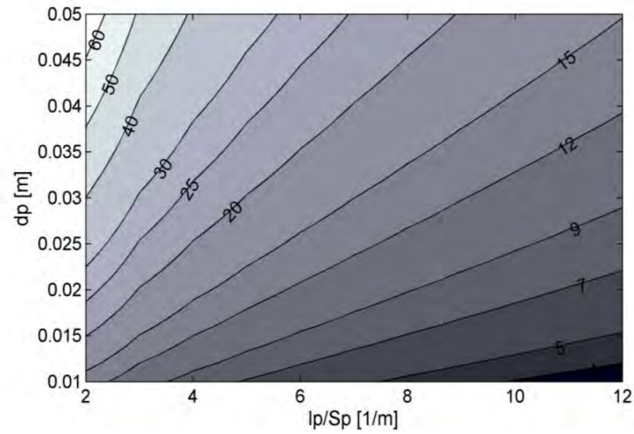

Figure A53.2f

Service life plot of a SiO_x-VIP as function of panel thickness and of panel perimeter to surface ratio including thermal edge effects.

Barrier: MF3
Seam: type b (φ = 0.67)
T = 318 K; RH = 50%
$\lambda_{eff;cr}$ = 8.0·10^{-3} W·m^{-1}·K^{-1}
α_1 = 7.8 m^2·K·W^{-1}
α_2 = 25 m^2·K·W^{-1}

Numbers on lines are t_{SL} [yr].

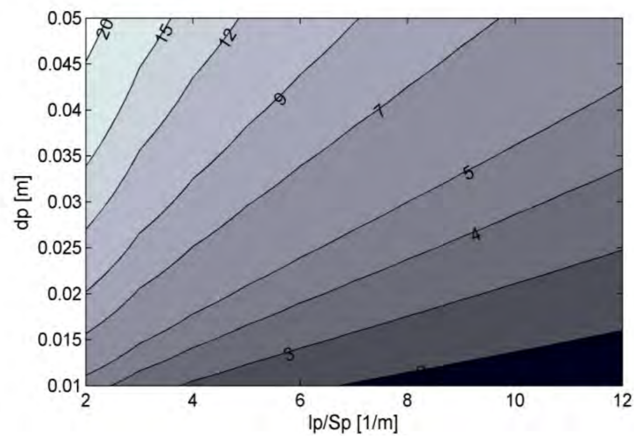

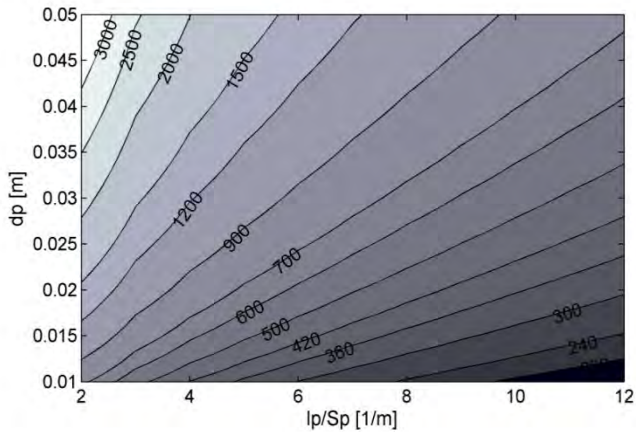

Figure A53.2g

Service life plot of a SiO_x-VIP as function of panel thickness and of panel perimeter to surface ratio including thermal edge effects.

Barrier: MF3
Seam: type b ($\varphi = 0.67$)
T = 278 K; RH = 50%
$\lambda_{eff;cr} = 11 \cdot 10^{-3}\ W \cdot m^{-1} \cdot K^{-1}$
$\alpha_1 = 7.8\ m^2 \cdot K \cdot W^{-1}$;
$\alpha_2 = 25\ m^2 \cdot K \cdot W^{-1}$

Numbers on lines are t_{SL} [yr].

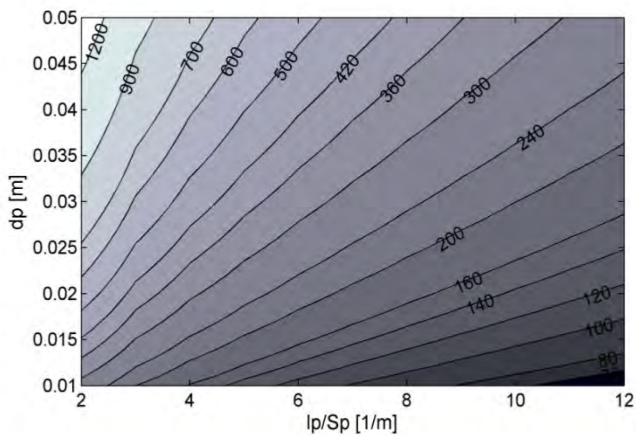

Figure A53.2h

Service life plot of a SiO_x-VIP as function of panel thickness and of panel perimeter to surface ratio including thermal edge effects.

Barrier: MF3
Seam: type b ($\varphi = 0.67$)
T = 288 K; RH = 50%
$\lambda_{eff;cr} = 11 \cdot 10^{-3}\ W \cdot m^{-1} \cdot K^{-1}$
$\alpha_1 = 7.8\ m^2 \cdot K \cdot W^{-1}$
$\alpha_2 = 25\ m^2 \cdot K \cdot W^{-1}$

Numbers on lines are t_{SL} [yr].

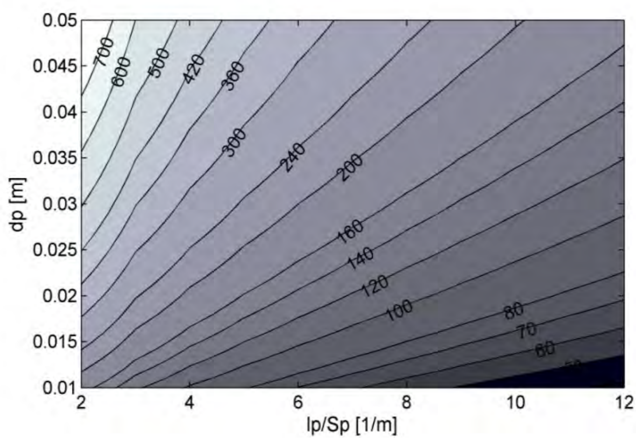

Figure A53.2i

Service life plot of a SiO_x-VIP as function of panel thickness and of panel perimeter to surface ratio including thermal edge effects.

Barrier: MF3
Seam: type b ($\varphi = 0.67$)
T = 293 K; RH = 50%
$\lambda_{eff;cr} = 11 \cdot 10^{-3}\ W \cdot m^{-1} \cdot K^{-1}$
$\alpha_1 = 7.8\ m^2 \cdot K \cdot W^{-1}$
$\alpha_2 = 25\ m^2 \cdot K \cdot W^{-1}$

Numbers on lines are t_{SL} [yr].

Figure A53.2j

Service life plot of a SiO_x-VIP as function of panel thickness and of panel perimeter to surface ratio including thermal edge effects.

Barrier: MF3
Seam: type b (φ = 0.67)
T = 298 K; RH = 50%
$\lambda_{eff;cr} = 11\cdot10^{-3}$ W·m^{-1}·K^{-1}
$\alpha_1 = 7.8$ m^2·K·W^{-1}
$\alpha_2 = 25$ m^2·K·W^{-1}

Numbers on lines are t_{SL} [yr].

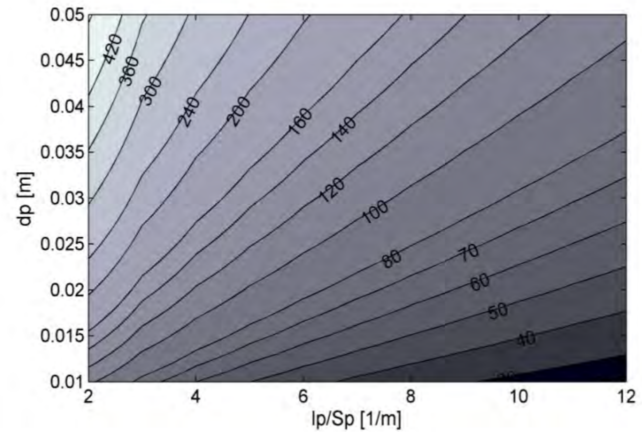

Figure A53.2k

Service life plot of a SiO_x-VIP as function of panel thickness and of panel perimeter to surface ratio including thermal edge effects.

Barrier: MF3
Seam: type b (φ = 0.67)
T = 308 K; RH = 50%
$\lambda_{eff;cr} = 11\cdot10^{-3}$ W·m^{-1}·K^{-1}
$\alpha_1 = 7.8$ m^2·K·W^{-1}
$\alpha_2 = 25$ m^2·K·W^{-1}

Numbers on lines are t_{SL} [yr].

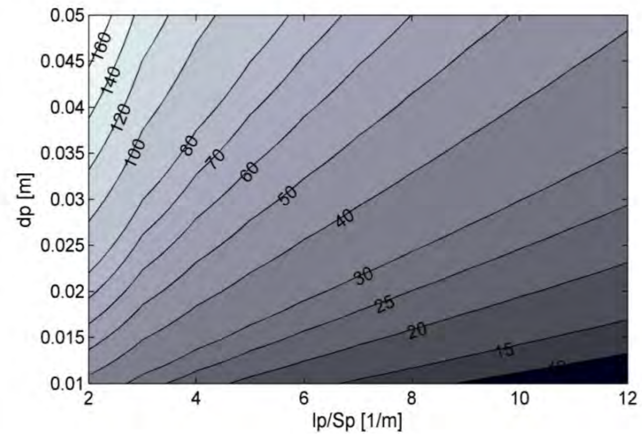

Figure A53.2l

Service life plot of a SiO_x-VIP as function of panel thickness and of panel perimeter to surface ratio including thermal edge effects.

Barrier: MF3
Seam: type b (φ = 0.67)
T = 318 K; RH = 50%
$\lambda_{eff;cr} = 11\cdot10^{-3}$ W·m^{-1}·K^{-1}
$\alpha_1 = 7.8$ m^2·K·W^{-1}
$\alpha_2 = 25$ m^2·K·W^{-1}

Numbers on lines are t_{SL} [yr].

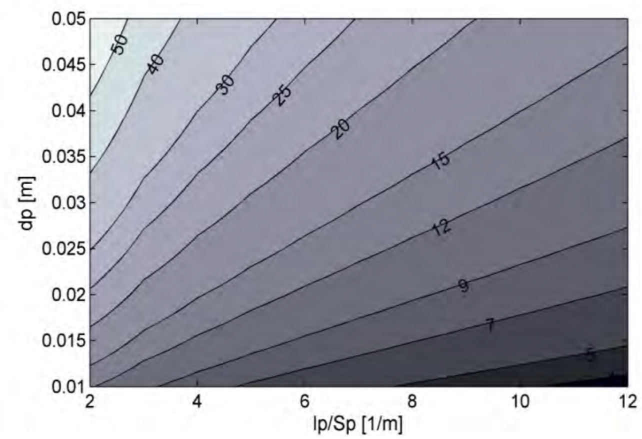

Equation (5.33) from the main text in conjunction with a modified version of Equation (5.36) from the main text can also be used to estimate the service life of a VIP incorporated building component. The model for estimating linear thermal transmittance values developed in chapter 4 should then be used. Based on that equation, the thermal conductivity criterion that should be used in can be written as

$$\lambda_{cr} = \frac{d_c}{\dfrac{S_{cop}}{U_{eff;cr}\left(S_{cop}+S_{edge}\right)-\psi_{edge}^{(c)} l_p} - \dfrac{1}{\alpha_1} - \dfrac{1}{\alpha_2} - \dfrac{t_{f1}}{\lambda_{f1}} - \dfrac{t_{f2}}{\lambda_{f2}}} \qquad \text{(A54.1),}$$

with d_c [m] the thickness of the core, S_{cop} [m²], the surface area of the centre-of-panel region, S_{edge} [m²] the surface area of the edge region, $U_{eff;cr}$ [$W \cdot m^{-2} \cdot K^{-1}$] the critical value of the effective thermal transmittance of the component, ψ_{edge} [$W \cdot m^{-1} \cdot K^{-1}$] the linear thermal transmittance of the edge calculated according to the models and procedures of chapter 4, l_p [m] the panel circumference, α_1 and α_2 [$W \cdot m^{-1} \cdot K^{-1}$] the boundary heat transfer coefficients of the warm respectively the cold side of the panel, t_{f1} and t_{f2} [m] the thickness of facing 1 and 2 and λ_{f1} and λ_{f2} [$W \cdot m^{-1} \cdot K^{-1}$] the thermal conductivity of facing 1 and 2 respectively. The value for the effective thermal transmittance, $U_{eff;cr}$, can again be set to any value higher than the initial value. Since the U-value of a panel depends on thickness, $U_{eff;cr}$ is defined as

$$U_{eff;cr} = \frac{1}{\dfrac{d_c}{\lambda_{eff;cr}} + \dfrac{1}{\alpha_1} + \dfrac{1}{\alpha_2} + \dfrac{t_{f1}}{\lambda_{f1}} + \dfrac{t_{f2}}{\lambda_{f2}}} \qquad \text{(A54.2),}$$

with $\lambda_{eff;cr}=8.0 \cdot 10^{-3}$ $W \cdot m^{-1} \cdot K^{-1}$ whereas the ratio (S_{cop} + S_{edge}) / S_{cop} is approximated as

$$\frac{S_{cop}+S_{edge}}{S_{cop}} \approx 1 + w\frac{l_p}{S_{cop}} + \left(\frac{wl_p}{8S_{cop}}\right)^2 \qquad \text{(A54.3),}$$

Equation (5.33) is however only valid as long as the following condition is fulfilled: $\lambda_{cr} > \lambda_0$, otherwise t_{sl}=0 years. For brief service lives which are more likely for building panels than for VIPs, however, Equation (5.33) might produces results which are even too inaccurate for use in practice. Therefore Equation (5.30) is used for determining service life plots of VIP incorporated building panels.

Using Equations (5.30) and (A54.1) several service life plots have been drawn for building components with a VIP core (fumed silica wrapped in a MF3 barrier), as presented in Figure A54.1. Building panels with an aluminium double-glazing spacer are not presented since they do not fulfill the requirement of the effective thermal transmittance criterion stated in the previous section. So, using that requirement the service life of these building components would be zero years. Table A54.1 presents an overview of building panels with an indication whether for architecturally practical sizes their service life is zero, less than ten years or more than ten years. If within the intervals [2,12] for l_p / S_{cop} [m^{-1}] and [0.01,0.05] for d_p [m] at least one panel size and thickness combination has a service life larger than 10 years, a Figure number is inserted in Table A54.1 corresponding to a service life plot for this component.

Table A54.1 *- Overview of service life plots of VIP incorporated building panels. (0 => $\lambda_{cr} < \lambda_0$; < 10=> within specified interval (almost) all service lives are shorter than 10 years).*

face sheet	T [K]	spacer type				
		aluminium double-glazing	folded edge	optimised thermo-plast	reinforced non-metallic tape	polymer U-section
2 mm aluminium	278	0	0	0	Fig. A54.4a	Fig. A54.6a
	288	0	0	0	Fig. A54.4b	Fig. A54.6b
	293	0	0	0	Fig. A54.4c	Fig. A54.6c
	298	0	0	0	Fig. A54.4d	Fig. A54.6d
	308	0	0	0	Fig. A54.4e	< 10
	318	0	0	0	< 10	< 10
3 mm polyester	278	Fig. A54.1a	Fig. A54.2a	Fig. A54.3a	Fig. A54.5a	Fig. A54.7a
	288	Fig. A54.1b	Fig. A54.2b	Fig. A54.3b	Fig. A54.5b	Fig. A54.7b
	293	Fig. A54.1c	Fig. A54.2c	Fig. A54.3c	Fig. A54.5c	Fig. A54.7c
	298	< 10	Fig. A54.2d	Fig. A54.3d	Fig. A54.5d	Fig. A54.7d
	308	< 10	Fig. A54.2e	< 10	Fig. A54.5e	Fig. A54.7e
	318	< 10	< 10	< 10	Fig. A54.5f	< 10

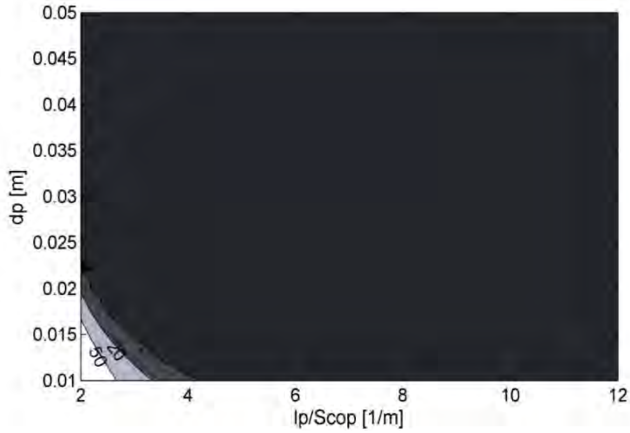

Figure A54.1a

Service life plot of a building panel with a SiO_x-VIP included as function of panel thickness and of panel perimeter to surface ratio including thermal edge effects.

spacer: alu. double-glazing
facings: 3 mm polyester
Barrier: MF3
T = 278 K; RH = 50%
$\lambda_{cr} = 8.0 \cdot 10^{-3}\ W \cdot m^{-1} \cdot K^{-1}$
$\alpha_1 = 7.8\ m^2 \cdot K \cdot W^{-1}$
$\alpha_2 = 25\ m^2 \cdot K \cdot W^{-1}$

Numbers on lines are t_{SL} [yr].

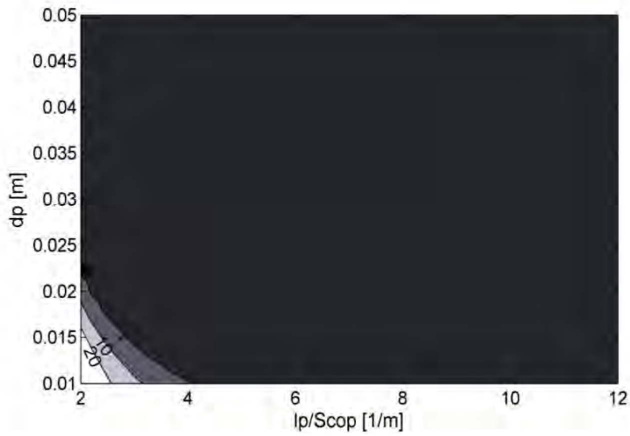

Figure A54.1b

Service life plot of a building panel with a SiO_x-VIP included as function of panel thickness and of panel perimeter to surface ratio including thermal edge effects.

spacer: alu. double-glazing
facings: 3 mm polyester
Barrier: MF3
T = 288 K; RH = 50%
$\lambda_{cr} = 8.0 \cdot 10^{-3}\ W \cdot m^{-1} \cdot K^{-1}$
$\alpha_1 = 7.8\ m^2 \cdot K \cdot W^{-1}$
$\alpha_2 = 25\ m^2 \cdot K \cdot W^{-1}$

Numbers on lines are t_{SL} [yr].

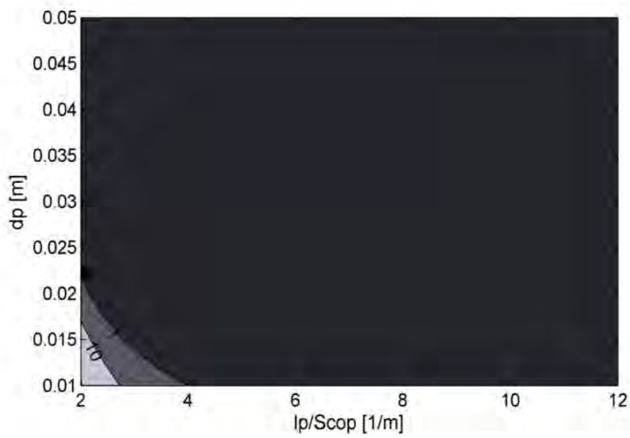

Figure A54.1c

Service life plot of a building panel with a SiO_x-VIP included as function of panel thickness and of panel perimeter to surface ratio including thermal edge effects.

spacer: alu. double-glazing
facings: 3 mm polyester
Barrier: MF3
T = 293 K; RH = 50%
$\lambda_{cr} = 8.0 \cdot 10^{-3}\ W \cdot m^{-1} \cdot K^{-1}$
$\alpha_1 = 7.8\ m^2 \cdot K \cdot W^{-1}$
$\alpha_2 = 25\ m^2 \cdot K \cdot W^{-1}$

Numbers on lines are t_{SL} [yr].

Figure A54.2a

Service life plot of a building panel with a SiO_x-VIP included as function of panel thickness and of panel perimeter to surface ratio including thermal edge effects.

spacer: folded edge
facings: 3 mm polyester
Barrier: MF3
T = 278 K; RH = 50%
$\lambda_{cr} = 8.0 \cdot 10^{-3}$ $W \cdot m^{-1} \cdot K^{-1}$
$\alpha_1 = 7.8$ $m^2 \cdot K \cdot W^{-1}$
$\alpha_2 = 25$ $m^2 \cdot K \cdot W^{-1}$

Numbers on lines are t_{SL} [yr].

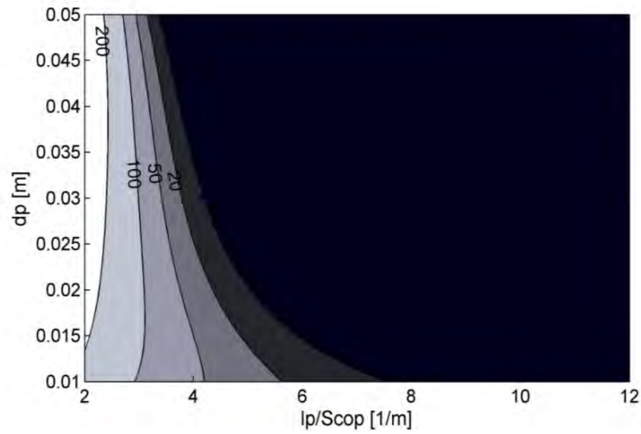

Figure A54.2b

Service life plot of a building panel with a SiO_x-VIP included as function of panel thickness and of panel perimeter to surface ratio including thermal edge effects.

spacer: folded edge
facings: 3 mm polyester
Barrier: MF3
T = 288 K; RH = 50%
$\lambda_{cr} = 8.0 \cdot 10^{-3}$ $W \cdot m^{-1} \cdot K^{-1}$
$\alpha_1 = 7.8$ $m^2 \cdot K \cdot W^{-1}$
$\alpha_2 = 25$ $m^2 \cdot K \cdot W^{-1}$

Numbers on lines are t_{SL} [yr].

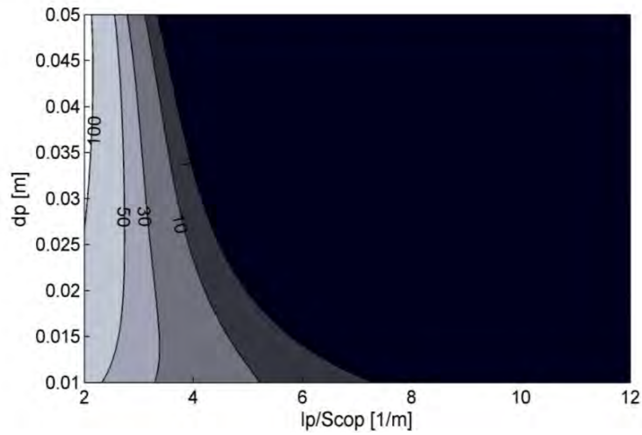

Figure A54.2c

Service life plot of a building panel with a SiO_x-VIP included as function of panel thickness and of panel perimeter to surface ratio including thermal edge effects.

spacer: folded edge
facings: 3 mm polyester
Barrier: MF3
T = 293 K; RH = 50%
$\lambda_{cr} = 8.0 \cdot 10^{-3}$ $W \cdot m^{-1} \cdot K^{-1}$
$\alpha_1 = 7.8$ $m^2 \cdot K \cdot W^{-1}$
$\alpha_2 = 25$ $m^2 \cdot K \cdot W^{-1}$

Numbers on lines are t_{SL} [yr].

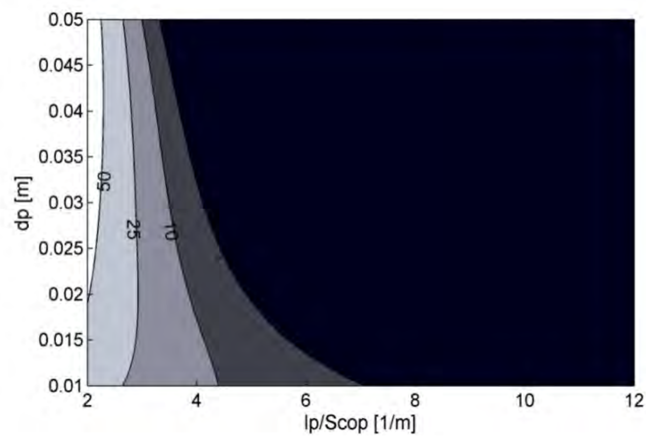

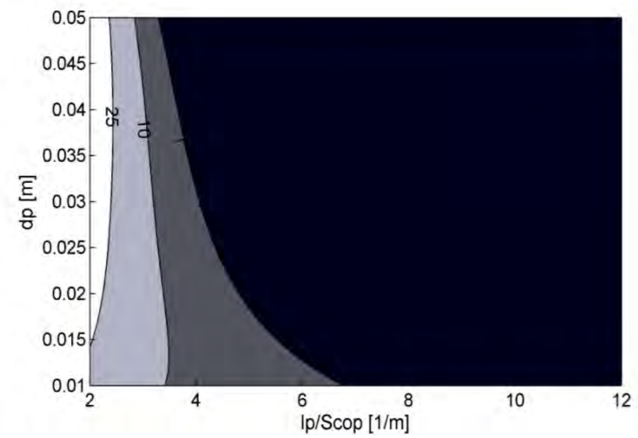

Figure A54.2d

Service life plot of a building panel with a SiO_x-VIP included as function of panel thickness and of panel perimeter to surface ratio including thermal edge effects.

spacer: folded edge
facings: 3 mm polyester
Barrier: MF3
T = 298 K; RH = 50%
$\lambda_{cr} = 8.0 \cdot 10^{-3}\ W \cdot m^{-1} \cdot K^{-1}$
$\alpha_1 = 7.8\ m^2 \cdot K \cdot W^{-1}$
$\alpha_2 = 25\ m^2 \cdot K \cdot W^{-1}$

Numbers on lines are t_{SL} [yr].

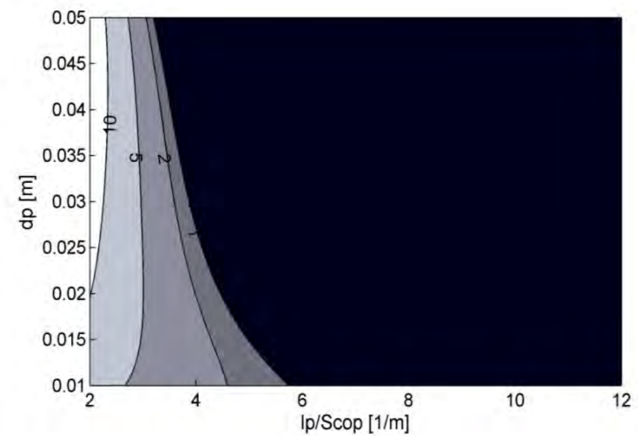

Figure A54.2e

Service life plot of a building panel with a SiO_x-VIP included as function of panel thickness and of panel perimeter to surface ratio including thermal edge effects.

spacer: folded edge
facings: 3 mm polyester
Barrier: MF3
T = 308 K; RH = 50%
$\lambda_{cr} = 8.0 \cdot 10^{-3}\ W \cdot m^{-1} \cdot K^{-1}$
$\alpha_1 = 7.8\ m^2 \cdot K \cdot W^{-1}$
$\alpha_2 = 25\ m^2 \cdot K \cdot W^{-1}$

Numbers on lines are t_{SL} [yr].

Figure A54.3a

Service life plot of a building panel with a SiO_x-VIP included as function of panel thickness and of panel perimeter to surface ratio including thermal edge effects.

spacer: optimised thermoplast
facings: 3 mm polyester
Barrier: MF3
T = 278 K; RH = 50%
$\lambda_{cr} = 8.0 \cdot 10^{-3}\ W \cdot m^{-1} \cdot K^{-1}$
$\alpha_1 = 7.8\ m^2 \cdot K \cdot W^{-1}$
$\alpha_2 = 25\ m^2 \cdot K \cdot W^{-1}$

Numbers on lines are t_{SL} [yr].

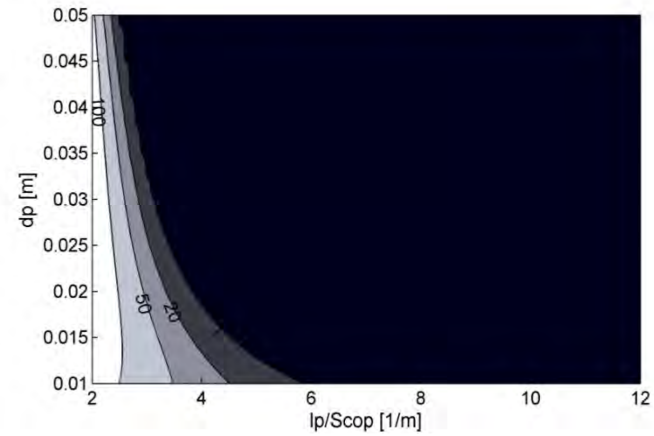

Figure A54.3b

Service life plot of a building panel with a SiO_x-VIP included as function of panel thickness and of panel perimeter to surface ratio including thermal edge effects.

spacer: optimised thermoplast
facings: 3 mm polyester
Barrier: MF3
T = 288 K; RH = 50%
$\lambda_{cr} = 8.0 \cdot 10^{-3}\ W \cdot m^{-1} \cdot K^{-1}$
$\alpha_1 = 7.8\ m^2 \cdot K \cdot W^{-1}$
$\alpha_2 = 25\ m^2 \cdot K \cdot W^{-1}$

Numbers on lines are t_{SL} [yr].

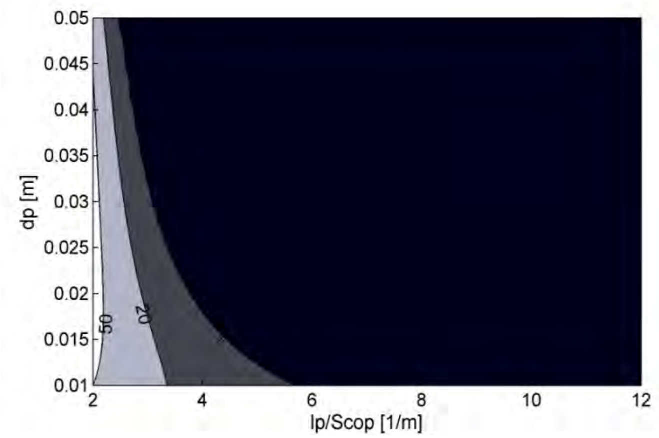

Figure A54.3c

Service life plot of a building panel with a SiO_x-VIP included as function of panel thickness and of panel perimeter to surface ratio including thermal edge effects.

spacer: optimised thermoplast
facings: 3 mm polyester
Barrier: MF3
T = 293 K; RH = 50%
$\lambda_{cr} = 8.0 \cdot 10^{-3}\ W \cdot m^{-1} \cdot K^{-1}$
$\alpha_1 = 7.8\ m^2 \cdot K \cdot W^{-1}$
$\alpha_2 = 25\ m^2 \cdot K \cdot W^{-1}$

Numbers on lines are t_{SL} [yr].

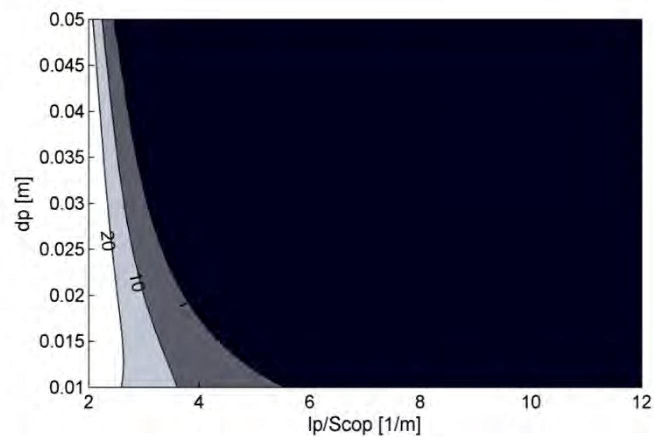

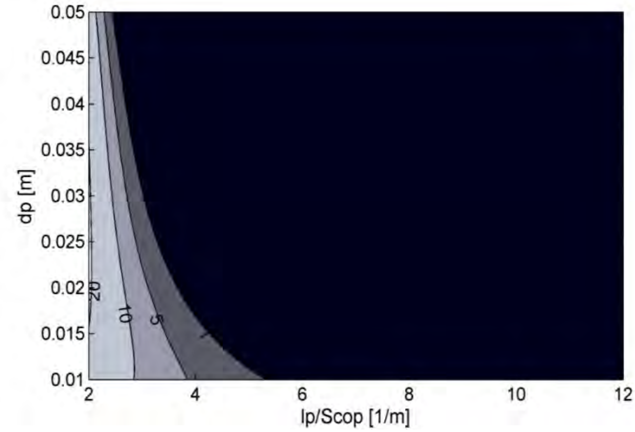

Figure A54.3d

Service life plot of a building panel with a SiO_x-VIP included as function of panel thickness and of panel perimeter to surface ratio including thermal edge effects.

spacer: optimised thermoplast
facings: 3 mm polyester
Barrier: MF3
T = 298 K; RH = 50%
$\lambda_{cr} = 8.0 \cdot 10^{-3}\ W \cdot m^{-1} \cdot K^{-1}$
$\alpha_1 = 7.8\ m^2 \cdot K \cdot W^{-1}$
$\alpha_2 = 25\ m^2 \cdot K \cdot W^{-1}$

Numbers on lines are t_{SL} [yr].

Figure A54.4a

Service life plot of a building panel with a SiO_x-VIP included as function of panel thickness and of panel perimeter to surface ratio including thermal edge effects.

spacer: non-metallic tape
facings: 2 mm aluminium
Barrier: MF3
T = 278 K; RH = 50%
$\lambda_{cr} = 8.0 \cdot 10^{-3}\ W \cdot m^{-1} \cdot K^{-1}$
$\alpha_1 = 7.8\ m^2 \cdot K \cdot W^{-1}$
$\alpha_2 = 25\ m^2 \cdot K \cdot W^{-1}$

Numbers on lines are t_{SL} [yr].

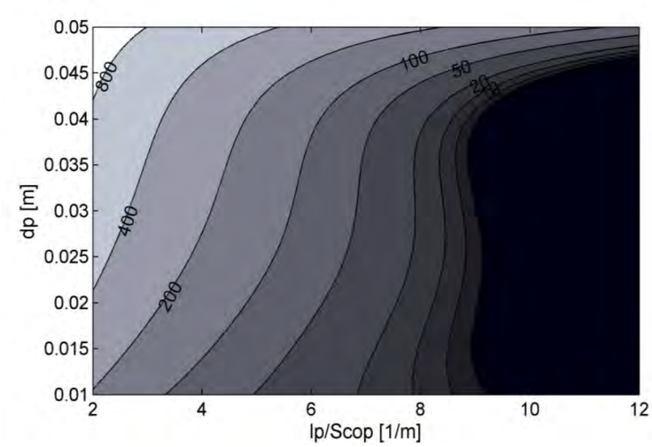

Figure A54.4b

Service life plot of a building panel with a SiO_x-VIP included as function of panel thickness and of panel perimeter to surface ratio including thermal edge effects.

spacer: non-metallic tape
facings: 2 mm aluminium
Barrier: MF3
T = 288 K; RH = 50%
$\lambda_{cr} = 8.0 \cdot 10^{-3}\ W \cdot m^{-1} \cdot K^{-1}$
$\alpha_1 = 7.8\ m^2 \cdot K \cdot W^{-1}$
$\alpha_2 = 25\ m^2 \cdot K \cdot W^{-1}$

Numbers on lines are t_{SL} [yr].

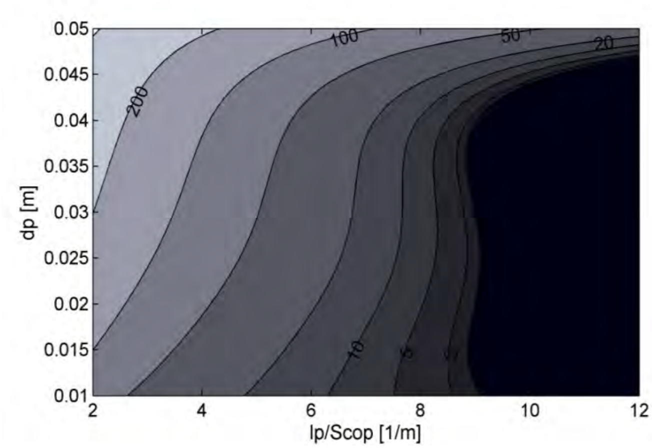

Figure A54.4c

Service life plot of a building panel with a SiO_x-VIP included as function of panel thickness and of panel perimeter to surface ratio including thermal edge effects.

spacer: non-metallic tape
facings: 2 mm aluminium
Barrier: MF3
T = 293 K; RH = 50%
$\lambda_{cr} = 8.0 \cdot 10^{-3}\ W \cdot m^{-1} \cdot K^{-1}$
$\alpha_1 = 7.8\ m^2 \cdot K \cdot W^{-1}$
$\alpha_2 = 25\ m^2 \cdot K \cdot W^{-1}$

Numbers on lines are t_{SL} [yr].

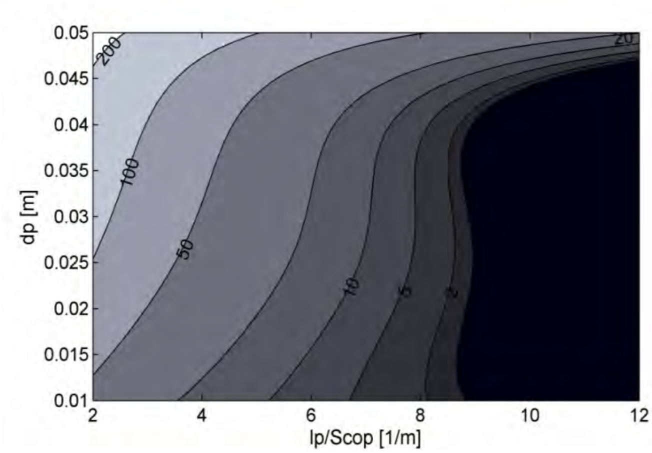

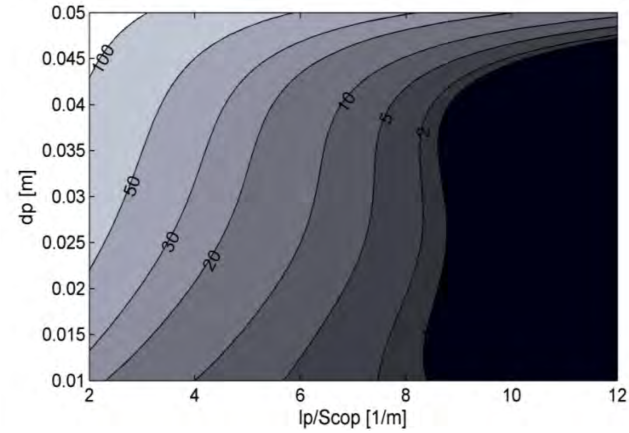

Figure A54.4d

Service life plot of a building panel with a SiO_x-VIP included as function of panel thickness and of panel perimeter to surface ratio including thermal edge effects.

spacer: non-metallic tape
facings: 2 mm aluminium
Barrier: MF3
T = 298 K; RH = 50%
$\lambda_{cr} = 8.0 \cdot 10^{-3}\ W \cdot m^{-1} \cdot K^{-1}$
$\alpha_1 = 7.8\ m^2 \cdot K \cdot W^{-1}$
$\alpha_2 = 25\ m^2 \cdot K \cdot W^{-1}$

Numbers on lines are t_{SL} [yr].

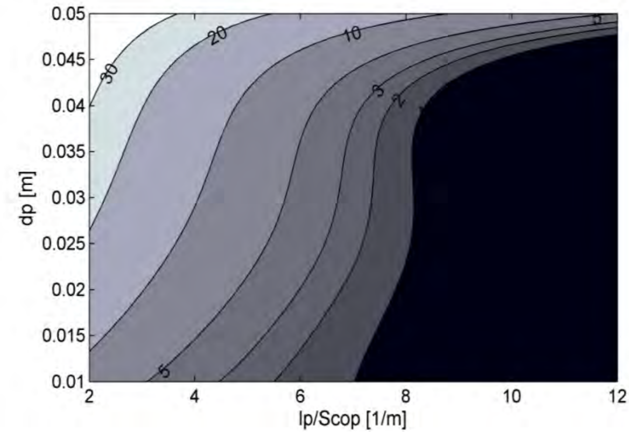

Figure A54.4e

Service life plot of a building panel with a SiO_x-VIP included as function of panel thickness and of panel perimeter to surface ratio including thermal edge effects.

spacer: non-metallic tape
facings: 2 mm aluminium
Barrier: MF3
T = 308 K; RH = 50%
$\lambda_{cr} = 8.0 \cdot 10^{-3}\ W \cdot m^{-1} \cdot K^{-1}$
$\alpha_1 = 7.8\ m^2 \cdot K \cdot W^{-1}$
$\alpha_2 = 25\ m^2 \cdot K \cdot W^{-1}$

Numbers on lines are t_{SL} [yr].

Figure A54.5a

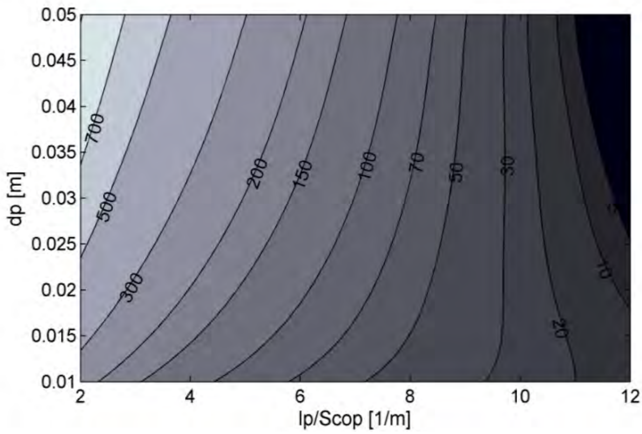

Service life plot of a building panel with a SiO_x-VIP included as function of panel thickness and of panel perimeter to surface ratio including thermal edge effects.

spacer: non-metallic tape
facings: 3 mm polyester
Barrier: MF3
T = 278 K; RH = 50%
$\lambda_{cr} = 8.0 \cdot 10^{-3}\ W \cdot m^{-1} \cdot K^{-1}$
$\alpha_1 = 7.8\ m^2 \cdot K \cdot W^{-1}$
$\alpha_2 = 25\ m^2 \cdot K \cdot W^{-1}$

Numbers on lines are t_{SL} [yr].

Figure A54.5b

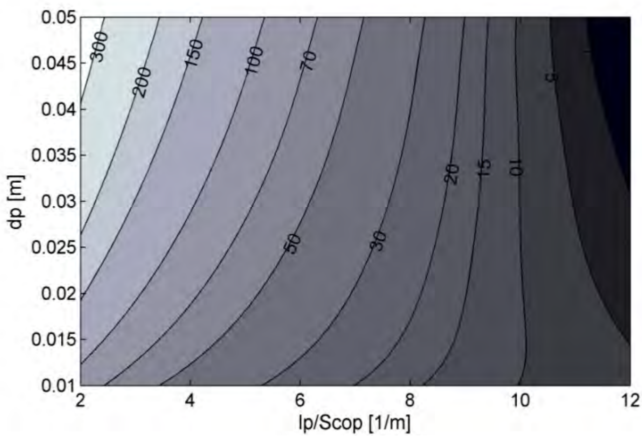

Service life plot of a building panel with a SiO_x-VIP included as function of panel thickness and of panel perimeter to surface ratio including thermal edge effects.

spacer: non-metallic tape
facings: 3 mm polyester
Barrier: MF3
T = 288 K; RH = 50%
$\lambda_{cr} = 8.0 \cdot 10^{-3}\ W \cdot m^{-1} \cdot K^{-1}$
$\alpha_1 = 7.8\ m^2 \cdot K \cdot W^{-1}$
$\alpha_2 = 25\ m^2 \cdot K \cdot W^{-1}$

Numbers on lines are t_{SL} [yr].

Figure A54.5c

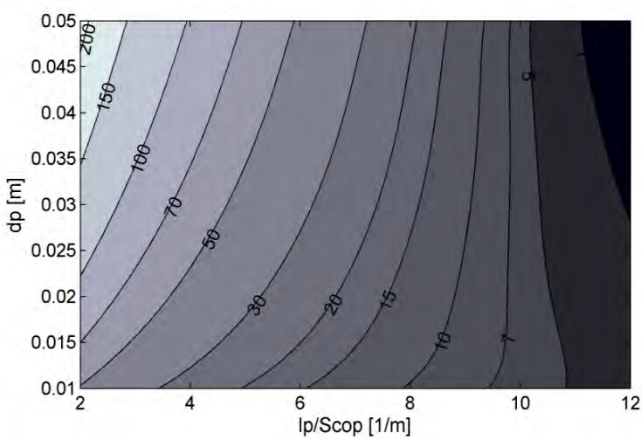

Service life plot of a building panel with a SiO_x-VIP included as function of panel thickness and of panel perimeter to surface ratio including thermal edge effects.

spacer: non-metallic tape
facings: 3 mm polyester
Barrier: MF3
T = 293 K; RH = 50%
$\lambda_{cr} = 8.0 \cdot 10^{-3}\ W \cdot m^{-1} \cdot K^{-1}$
$\alpha_1 = 7.8\ m^2 \cdot K \cdot W^{-1}$
$\alpha_2 = 25\ m^2 \cdot K \cdot W^{-1}$

Numbers on lines are t_{SL} [yr].

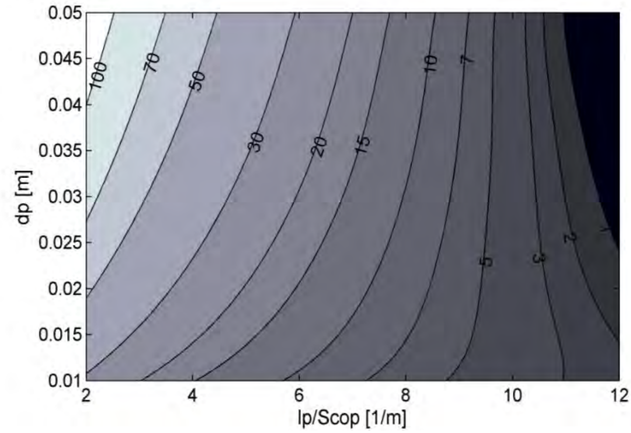

Figure A54.5d

Service life plot of a building panel with a SiO_x-VIP included as function of panel thickness and of panel perimeter to surface ratio including thermal edge effects.

spacer: non-metallic tape
facings: 3 mm polyester
Barrier: MF3
T = 298 K; RH = 50%
$\lambda_{cr} = 8.0 \cdot 10^{-3}\ W \cdot m^{-1} \cdot K^{-1}$
$\alpha_1 = 7.8\ m^2 \cdot K \cdot W^{-1}$
$\alpha_2 = 25\ m^2 \cdot K \cdot W^{-1}$

Numbers on lines are t_{SL} [yr].

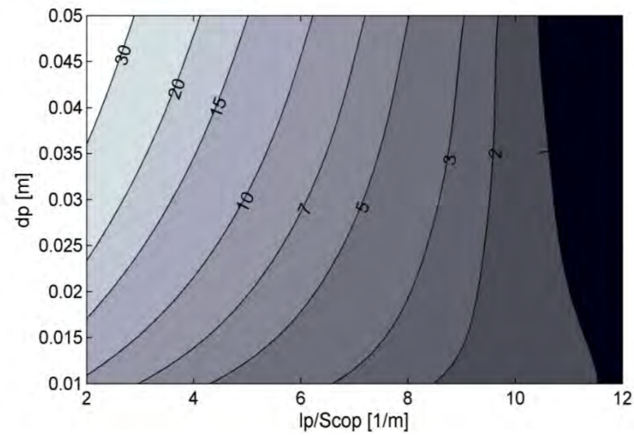

Figure A54.5e

Service life plot of a building panel with a SiO_x-VIP included as function of panel thickness and of panel perimeter to surface ratio including thermal edge effects.

spacer: non-metallic tape
facings: 3 mm polyester
Barrier: MF3
T = 308 K; RH = 50%
$\lambda_{cr} = 8.0 \cdot 10^{-3}\ W \cdot m^{-1} \cdot K^{-1}$
$\alpha_1 = 7.8\ m^2 \cdot K \cdot W^{-1}$
$\alpha_2 = 25\ m^2 \cdot K \cdot W^{-1}$

Numbers on lines are t_{SL} [yr].

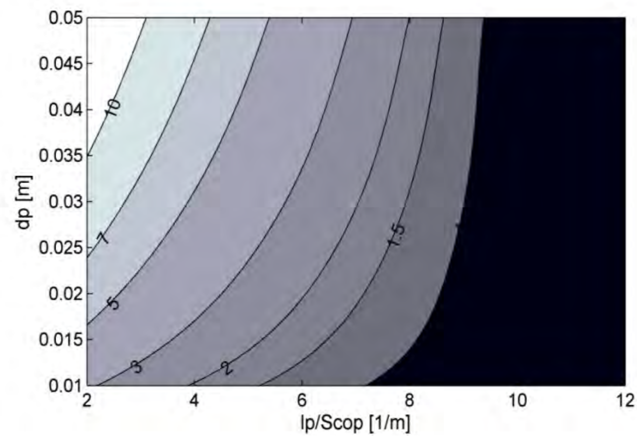

Figure A54.5f

Service life plot of a building panel with a SiO_x-VIP included as function of panel thickness and of panel perimeter to surface ratio including thermal edge effects.

spacer: non-metallic tape
facings: 3 mm polyester
Barrier: MF3
T = 308 K; RH = 50%
$\lambda_{cr} = 8.0 \cdot 10^{-3}\ W \cdot m^{-1} \cdot K^{-1}$
$\alpha_1 = 7.8\ m^2 \cdot K \cdot W^{-1}$
$\alpha_2 = 25\ m^2 \cdot K \cdot W^{-1}$

Numbers on lines are t_{SL} [yr].

Figure A54.6a

Service life plot of a building panel with a SiO_x-VIP included as function of panel thickness and of panel perimeter to surface ratio including thermal edge effects.

spacer: polymer U-section
facings: 2 mm aluminium
Barrier: MF3
T = 278 K; RH = 50%
$\lambda_{cr} = 8.0 \cdot 10^{-3}\ W \cdot m^{-1} \cdot K^{-1}$
$\alpha_1 = 7.8\ m^2 \cdot K \cdot W^{-1}$
$\alpha_2 = 25\ m^2 \cdot K \cdot W^{-1}$

Numbers on lines are t_{SL} [yr].

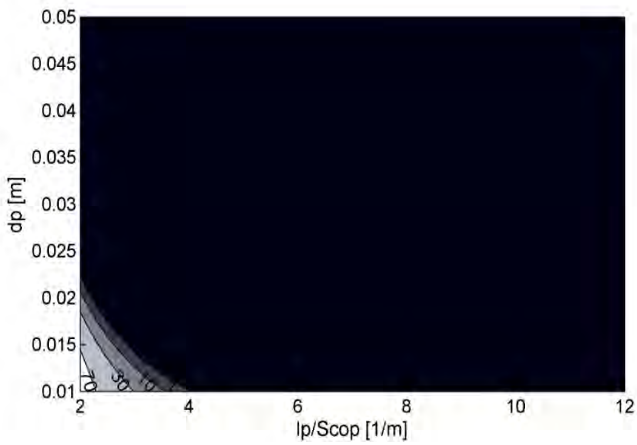

Figure A54.6b

Service life plot of a building panel with a SiO_x-VIP included as function of panel thickness and of panel perimeter to surface ratio including thermal edge effects.

spacer: polymer U-section
facings: 2 mm aluminium
Barrier: MF3
T = 288 K; RH = 50%
$\lambda_{cr} = 8.0 \cdot 10^{-3}\ W \cdot m^{-1} \cdot K^{-1}$
$\alpha_1 = 7.8\ m^2 \cdot K \cdot W^{-1}$
$\alpha_2 = 25\ m^2 \cdot K \cdot W^{-1}$

Numbers on lines are t_{SL} [yr].

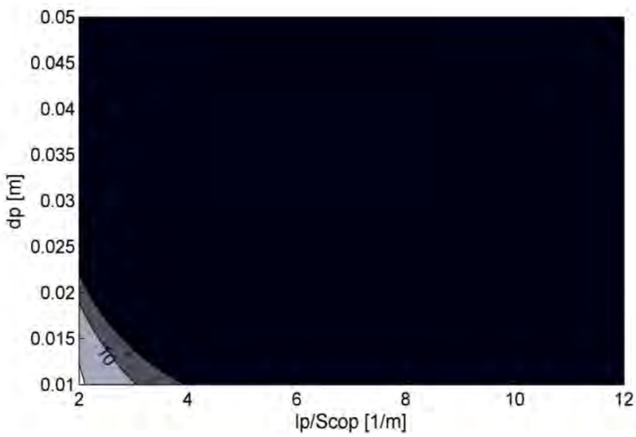

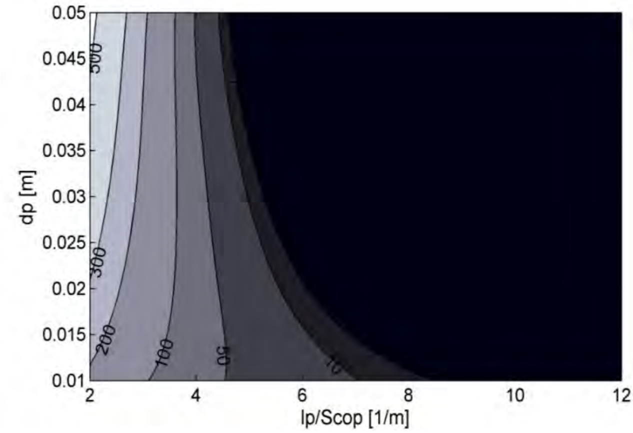

Figure A54.7a

Service life plot of a building panel with a SiO_x-VIP included as function of panel thickness and of panel perimeter to surface ratio including thermal edge effects.

spacer: polymer U-section
facings: 3 mm polyester
Barrier: MF3
T = 278 K; RH = 50%
$\lambda_{cr} = 8.0\cdot10^{-3}\ W\cdot m^{-1}\cdot K^{-1}$
$\alpha_1 = 7.8\ m^2\cdot K\cdot W^{-1}$
$\alpha_2 = 25\ m^2\cdot K\cdot W^{-1}$

Numbers on lines are t_{SL} [yr].

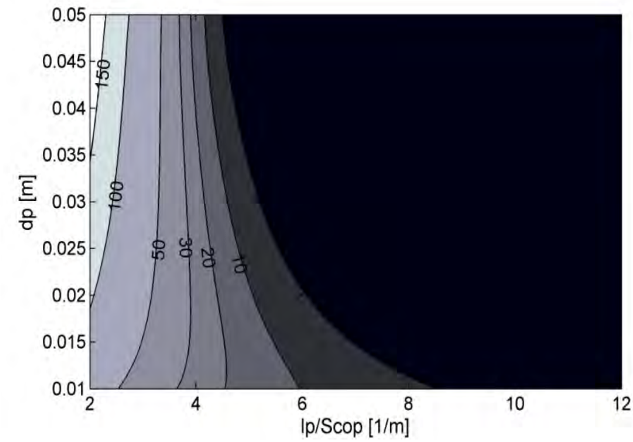

Figure A54.7b

Service life plot of a building panel with a SiO_x-VIP included as function of panel thickness and of panel perimeter to surface ratio including thermal edge effects.

spacer: polymer U-section
facings: 3 mm polyester
Barrier: MF3
T = 288 K; RH = 50%
$\lambda_{cr} = 8.0\cdot10^{-3}\ W\cdot m^{-1}\cdot K^{-1}$
$\alpha_1 = 7.8\ m^2\cdot K\cdot W^{-1}$
$\alpha_2 = 25\ m^2\cdot K\cdot W^{-1}$

Numbers on lines are t_{SL} [yr].

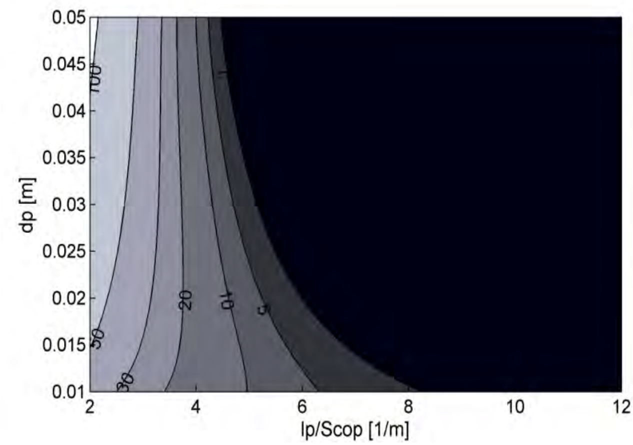

Figure A54.7c

Service life plot of a building panel with a SiO_x-VIP included as function of panel thickness and of panel perimeter to surface ratio including thermal edge effects.

spacer: polymer U-section
facings: 3 mm polyester
Barrier: MF3
T = 293 K; RH = 50%
$\lambda_{cr} = 8.0\cdot10^{-3}\ W\cdot m^{-1}\cdot K^{-1}$
$\alpha_1 = 7.8\ m^2\cdot K\cdot W^{-1}$
$\alpha_2 = 25\ m^2\cdot K\cdot W^{-1}$

Numbers on lines are t_{SL} [yr].

Figure A54.7d

Service life plot of a building panel with a SiO_x-VIP included as function of panel thickness and of panel perimeter to surface ratio including thermal edge effects.

spacer: polymer U-section
facings: 3 mm polyester
Barrier: MF3
T = 298 K; RH = 50%
$\lambda_{cr} = 8.0 \cdot 10^{-3}$ W·m^{-1}·K^{-1}
$\alpha_1 = 7.8$ m^2·K·W^{-1}
$\alpha_2 = 25$ m^2·K·W^{-1}

Numbers on lines are t_{SL} [yr].

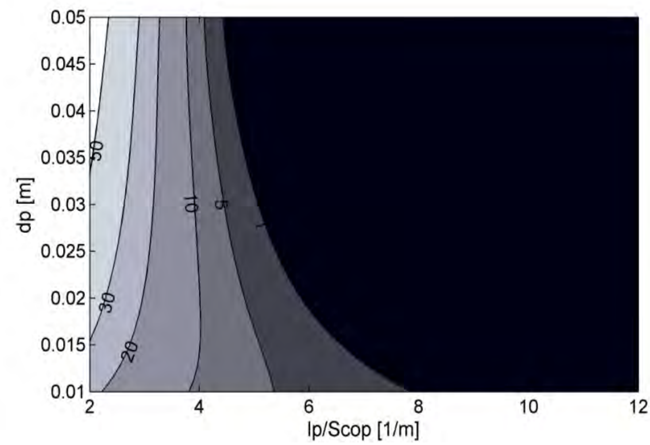

Figure A54.7e

Service life plot of a building panel with a SiO_x-VIP included as function of panel thickness and of panel perimeter to surface ratio including thermal edge effects.

spacer: polymer U-section
facings: 3 mm polyester
Barrier: MF3
T = 308 K; RH = 50%
$\lambda_{cr} = 8.0 \cdot 10^{-3}$ W·m^{-1}·K^{-1}
$\alpha_1 = 7.8$ m^2·K·W^{-1}
$\alpha_2 = 25$ m^2·K·W^{-1}

Numbers on lines are t_{SL} [yr].

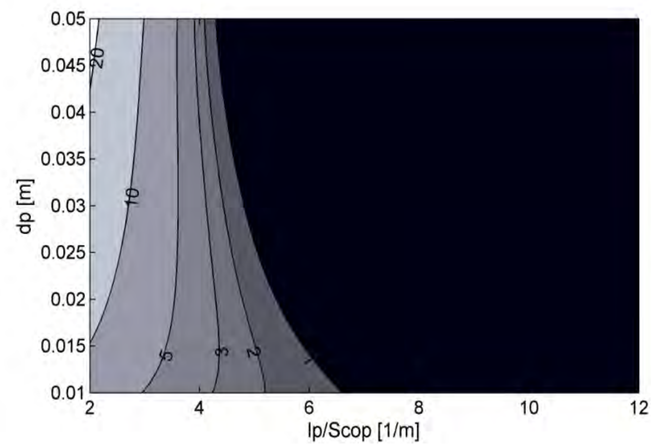

As can be seen from Table A54.1, an aluminium spacer, a folded edge spacer and a optimized thermoplastic spacer combined with 2 mm thick aluminium facings (or facings which have a $\lambda_f t_f$ higher than 0.3 W·K^{-1}) are not suitable for application in building panels if λ_{cr} is chosen $8.0 \cdot 10^{-3}$ W·m^{-1}·K^{-1} or below. For all these panels within the intervals specified in the previous section, the critical value of the thermal conductivity of the core material is lower than its initial thermal conductivity, as a result of which the service life of a VIP is 0 years. Within the specified intervals for panel size and under the studied temperature conditions, the aluminium double-glazing spacer is even practically hardly suitable in combination with low thermal conductivity facings like polyester ($\lambda_f t_f = 8 \cdot 10^{-3}$ W·K^{-1}). Only very large thin panels have a service life which goes beyond that required for office buildings (25 to 30 years).

Since all building components studied in this paragraph are equipped with SiO_x-VIP with a MF3 envelope and thus generally exhibit the same behaviour with respect to thermal conductivity ageing, thermal bridge effects are responsible for the differences in service life between panel typologies. As a consequence, the panel typologies exhibiting the smallest thermal edge effect have the highest service lives. Considering these observations, spacer performance regarding service life is ranked from best to worst as reinforced non-metallic tape, polymer U-section, folded edge spacer, optimised thermoplastic spacer, aluminium double-glazing spacer. A comparison of Figures A54.1 to A54.5 substantiates this ranking. A panel of 1.0x1.0x0.020 m^3 with a SiO_x-VIP enveloped by a MF3 laminate and two face sheets of 3 mm polyester at a temperature of 293 K and a relative humidity of 50% using a critical thermal conductivity of $8.0 \cdot 10^{-3}$ $W \cdot m^{-1} \cdot K^{-1}$, for example, has a service life of 43, 17, 8, 0, 0 years if a reinforced non-metallic tape, a polymer U-section, a folded edge spacer, an optimised thermoplastic spacer and an aluminium double-glazing spacer is used respectively.

As can be seen from a comparison of service life plots of VIPs without considering thermal bridge effects (Figures A52.2a t/m f) and building components in which these effects are taken into account (Figures A54.1 to A54.7), the influence of panel thickness on service life becomes less important when thermal edge effects are considered, i.e. the lines denoting equal service life are becoming more vertical in the service life plots. This can be explained as follows. Since the thermal conductivity criterion of the core, $\lambda_{c;cr}$ depends on the thickness of the VIP inside, d_c, and since it decreases with increasing thickness, the difference between the panel initial thermal conductivity and critical value decreases as well, i.e. λ_{cr} - λ_0 becomes smaller. Both Equations (5.30) and (5.33) show that if this difference reduces, then the service life reduces as well. This implies that, for a certain panel size and thickness, the service life becomes shorter if thermal edge effects are taken into account. This again implies that the lines denoting equal service life become more vertical in service life plots with panel thickness along the ordinate. Apparently, this effect is so strong for building components with a strong thermal edge effect that from a certain panel thickness these lines become almost vertical. For panels with a lesser thermal bridge effect (Figures A54.4 and A54.5), this effect is less strong as a consequence of which panel thickness still influences the service life. A similar effect can also be observed by comparing the service life, which both includes thermal conductivity ageing and thermal edge effects, of a SiO_x-VIP with an AF:8 envelope (Figure A52.1) to a SiO_x-VIP with a MF3 envelope (Figure A52.2).

The increase in thermal conductivity, or actually the increase in pore gas pressure and water content, is principally determined by the properties of the core material (1) as explained in previous paragraph, the presence of getters and desiccants (2), the initial vacuum and water content (3), degassing of the core material and the barrier laminate (4), the envelope permeance for atmospheric gases and water vapour (5), the panel's dimensions (6) and the environmental conditions, like temperature, relative humidity and partial water vapour pressure (7) (Porextherm, 2004). Since, the first five factors are product-related and can hardly be influenced by architects and building engineers, especially the last two are interesting from the perspective of construction design. Yet, all influences will be discussed briefly in this appendix, except for the properties of the core material and the initial vacuum and water content since they have already been discussed in chapters 3 and 5.

GAS AND VAPOUR TIGHTNESS OF THE BARRIER LAMINATES AND SEAMS[26]

The change in thermal conductivity over time, $\mathrm{d}\lambda/\mathrm{d}t$, and as a consequence the service life depends on the rate at which the gas pressure in the core material, $\mathrm{d}p_{g;i}/\mathrm{d}t$, and the water content of the core material, $\mathrm{d}u/\mathrm{d}t$, increase. These rates of change of internal gas pressure and water content in turn depend for a large part on the permeability properties of the high barrier envelope. Foil manufacturers specify a water vapour transmission rate (WVTR in $g\cdot m^{-2}\cdot day^{-1}$) and an oxygen transmission rate (O_2TR in cm^3 (STP)$\cdot m^{-2}\cdot day^{-1}\cdot bar^{-1}$ or cm^3 (STP)$\cdot m^{-2}\cdot day^{-1}$)[27]. These rates are

[26] Gas and water vapour tightness of the barrier envelope and seal are important parameters influencing the length of the service life of a vacuum insulation panel. As a consequence, service life predictions are practically only interesting for foil- and film-based vacuum insulation panels, since their service life will in most cases be less than 100 years. Sheet-based VIPs (VIS) however have a relatively thick stainless steel casing and welded edge membrane, resulting in very low, non-detectable permeation rates. The service life of a sheet-based VIP can therefore be several hundreds of years or even thousands of years. For practical purposes in buildings, the thermal conductivity of those panels may thus be considered constant, provided that no significant damage is afflicted during the production, installation and mounting processes.

[27] STP stands for standard temperature and pressure. It is important to realise that during O_2TR or WVTR measurements other gases than oxygen and water vapour respectively are not included in the measurements. Detection occurs on the molecules and not on pressure.

defined as the amount of water vapour or oxygen respectively which comes through the laminate per unit area, per day (and per bar pressure difference)[28,29].

The gases and vapours that are most important for permeation through barrier films for vacuum insulated panels are oxygen (O_2), nitrogen (N_2) and water vapour (H_2O). Since the transmission rate for nitrogen molecules (N_2TR) through most materials and under standard conditions is about 25% of the oxygen transmission rate (O_2TR) (Brunner and Simmler, 2003) and since in case of vacuum insulation panels the partial pressure difference on both sides of the barrier is for nitrogen approximately 4 times as high as for oxygen under normal circumstances, the internal pressure increase in the core due to nitrogen ingression almost equals the pressure increase due to oxygen. So both gases are more or less equally important.

In general, however, permeation rates are measured for the laminate itself and not for an entire envelope around a VIP. This is the principal reason that the values for the transmission rates declared by manufacturers are not quite representative for the amount of gases and water vapour penetrating a complete barrier envelope of a vacuum insulation panel. Not only are the seals weak spots in this envelope but also the corners at which the laminate is folded. These effects must certainly be accounted for when considering the total permeability of a barrier envelope.

Other reasons that the transmission rates specified by manufacturers cannot always directly be used for service life estimates are (Brunner and Simmler, 2003):

- The presence of non-linear behaviour in laminate permeation mechanisms. Permeation rates strongly depend on relative humidity and temperature (Brunner and Simmler, 2005a). With increasing temperature or relative humidity the permeation rates for polymers increase exponentially (van 't Hoff, 1884; Arrhenius, 1889).
- The water vapour transmission rate normally is not constant during the service life of a vacuum insulated panel. Water vapour permeation is a fast process relative to gas permeation and on a long-term basis equilibrium of the internal partial water vapour pressure with the environment may be reached well within the range of standard service lives for thin vacuum insulation panels.

---

[28] The values stated by foil and film manufacturers must be treated with caution, because they strongly depend on the environmental conditions under which the tests have been conducted (relative humidity and temperature). Standard measurement conditions are a temperature of 23°C and a relative humidity of 90% on one side and of 0% on the other side of the laminate.

[29] These two rates, however, stand for more than water vapour and oxygen alone. The water vapour transmission rate is representative for water vapour and all polaric gases present in air, while the oxygen transmission rate represents all non-polaric gases. Often foils that have high barrier qualities against polaric gases are less optimal for non-polaric gases, vice versa.

- On a long-term basis physical and mechanical ageing mechanisms occur as well. Polymer degradation, delaminating, corrosion, UV-radiation and mechanical stresses can have a profound influence on transmission rates. At this moment not much information on the long-term behaviour of VIP barrier envelopes under these conditions is available.

AMOUNT AND EFFECTIVENESS OF GETTERS AND DESICCANTS

Getters are substances or devices capable of absorbing and bonding gasses, whereas desiccants are substances capable of absorbing water molecules. Gas or water vapour molecules that have penetrated the barrier envelope and have entered the core material pores will thus be absorbed by the getter or desiccant and will therefore not raise the internal gas pressure or partial water vapour pressure, at least for as long as the getter or desiccant is not saturated. This means that the thermal conductivity of the VIP does not immediately start increasing, but stays more or less constant until the getter and/or desiccant are saturated. The amount and effectiveness determines the length of this initial stable period. Getters and desiccants are, however, quite costly but can lengthen the service life of a panel or give the possibility to start at a higher initial internal vacuum pressure, if the service life is a value set a priori.

GAS RELEASE OF CORE MATERIAL AND BARRIER FILM

Gases not just enter the core material via permeation through the high barrier film and seam, but can also be released by the core material or by the barrier envelope. These gases can raise the internal gas pressure and thus the thermal conductivity in the same manner as permeated gases do. Under standard conditions, the gas release of most modern barrier materials can more-or-less be neglected. The gas release of the core material, however, can have a significant influence on the internal gas pressure, especially just after production. The effect of core material gas release however is only of importance in the initial weeks after production, in which a new equilibrium between adsorbed gas and pore gas is established.

PANEL DIMENSIONS

For the effect of panel dimensions on service life, both the thickness and the ratio of panel circumference to surface area need to be considered, since both factors influence the volume in which gases can be stored and the envelope or edge area through which gases can permeate. In general, thick and large panels have a longer expected service life than thin and small panels. So, in the design process of building constructions with vacuum insulation panels, panels need to be designed as large as possible with an aspect ratio, which is the ratio of length to width, close to one; also because of the reduction of the thermal edge effect[30].

ENVIRONMENTAL OPERATING CONDITIONS

The environmental operating conditions comprise environmental conditions as well as mechanical conditions. The most important environmental conditions are the temperature and the moisture conditions directly outside the VIP.

Temperature can have several effects on a VIP:

- with increasing temperature, the gas and water vapour permeability of barrier laminates and seams increases almost exponentially;
- with increasing temperature, in general the relative humidity of air decreases because of increased vapour saturation pressure;
- with increasing temperature, gas release of polymer foams increases;
- at a certain temperature polymer foams melt. For polyurethane and polystyrene foam this melt temperature, T_m, is somewhere near 120°C and 70°C respectively. This might especially be important for application of VIPs in façade panels subjected to insolation;
- with increasing temperature, the rate of degradation processes on barrier films and seams might increase as well. These degradation processes are corrosion on metal foils, polymer degradation and delaminating.

[30] To discuss the effect of panel dimensions on service life in more detail, we must distinguish between the effect of water vapour and the effect of atmospheric gases. Since the permeance of high barrier films for oxygen and nitrogen is very low (in the order of $5 \cdot 10^{-4}$ $cm^3 \cdot m^{-2} \cdot day^{-1}$ for oxygen for a triple layer metallized film) (Hanita, 2004), oxygen and nitrogen permeation primarily occurs through the seam, implying that both panel thickness and the ratio of circumference to surface area are important. In case of very large panels, though, the amount of dry gas permeating through the surface of a VIP and through its seam can be in the same order of magnitude. With respect to water vapour, however, permeation through the surface area and through the seam are of equal importance for typical panel sizes due to the higher permeance for water vapour through barrier laminates (in the order of $1 \cdot 10^{-2}$ $g \cdot m^{-2} \cdot day^{-1}$ for a triple layer metallized film) (Hanita, 2004). This implies that especially for larger panels the thickness is important, while for small panels both the thickness and the panel's circumference (or ratio of circumference to surface area) are equally important.

The second important environmental condition concerns partial water vapour pressure (and relative humidity) around the VIP. The partial water vapour pressure and relative humidity also have several effects on a VIP:

- with increasing relative humidity, the permeability of barrier laminates and seams for atmospheric gas but especially for water vapour permeation increases;
- with increasing water vapour pressure, the driving potential Δp increases as well;
- with increasing moisture levels, the rate of corrosion processes on non-protected metal foils increases. This is not a linear relation.

The mechanical conditions under which the VIP has to operate finally can be subdivided into two categories:

- external loads that might cause damage to the barrier film or to a complete VIP. Puncture or rupture of the barrier envelope creates an easy path for gas and water vapour molecules to enter the VIP. The service life of a panel is than expired some seconds to months after damage, depending on the degree of damage;
- internal stresses in the high barrier film, especially the stresses near edges and corners. Internal stresses in the barrier film may increase the permeation rates for gases and water vapour. Moreover, stresses beyond a certain limit may cause micro-cracks to form in the barrier layer which tremendously deteriorate the barrier quality of the laminate. The exact effect of such internal stresses in not yet completely understood at this moment.

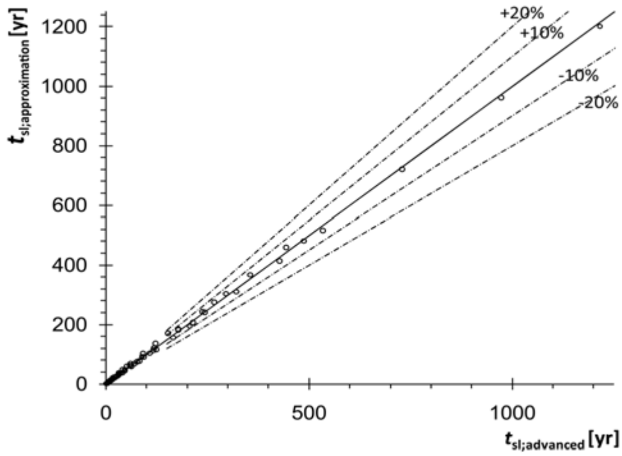

Figure A56.1a MF3

Error plot: plot of the service life calculated with the approximation model as function of the service life calculated with the advanced model for film-based vacuum insulation panels with a ***core of fumed silica and an MF3 barrier****. No thermal bridging.*

λ_{cr} = 7.0·10^{-3} W·m^{-1}·K^{-1};
ϕ = 50%; thickness: 1 to 5 cm;
size: 0.25x0.25 m^2 to 2x2 m^2;
T: 5^{o}C to 45^{o}C.

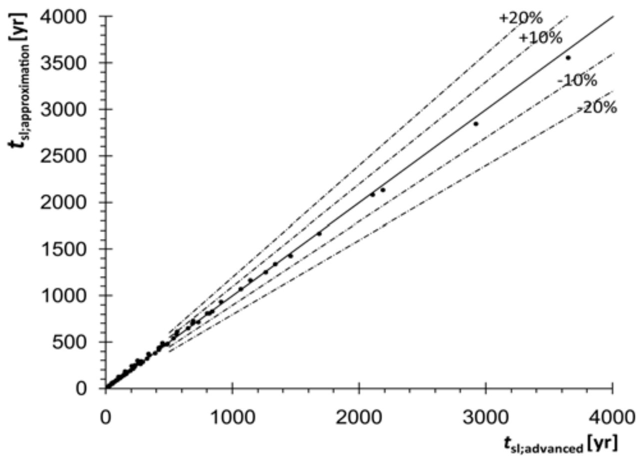

Figure A56.1b AF:8

Error plot: plot of the service life calculated with the approximation model as function of the service life calculated with the advanced model for film-based vacuum insulation panels with a ***core of fumed silica and an AF:8 barrier****. No thermal bridging.*

λ_{cr} = 7.0·10^{-3} W·m^{-1}·K^{-1};
ϕ = 50%; thickness: 1 to 5 cm;
size: 0.25x0.25 m^2 to 2x2 m^2;
T: 5^{o}C to 45^{o}C.

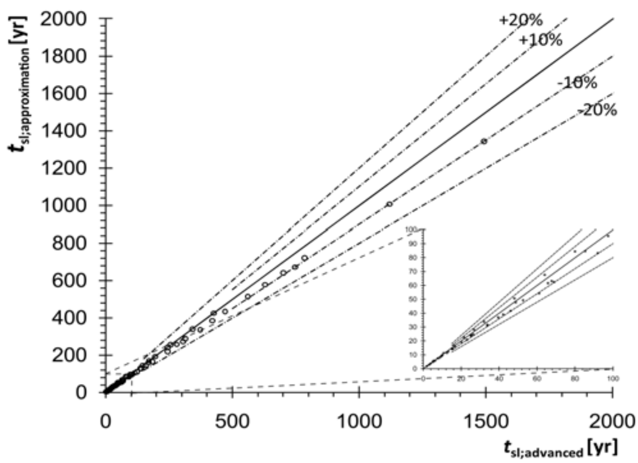

Figure A56.2a MF3

Error plot: plot of the service life calculated with the approximation model as function of the service life calculated with the advanced model for film-based vacuum insulation panels with a ***core of fumed silica and an MF3 barrier****. No thermal bridging.*

λ_{cr} = 8.0·10^{-3} W·m^{-1}·K^{-1};
ϕ = 50%; thickness: 1 to 5 cm;
size: 0.25x0.25 m^2 to 2x2 m^2;
T: 5^{o}C to 45^{o}C.

Figure A56.2b AF:8

*Error plot: plot of the service life calculated with the approximation model as function of the service life calculated with the advanced model for film-based vacuum insulation panels with a **core of fumed silica and an AF:8 barrier**. No thermal bridging.*

λ_{cr} = 8.0·10^{-3} W·m^{-1}·K^{-1};
ϕ = 50%; thickness: 1 to 5 cm; size: 0.25x0.25 m^2 to 2x2 m^2;
T: 5^{o}C to 45^{o}C.

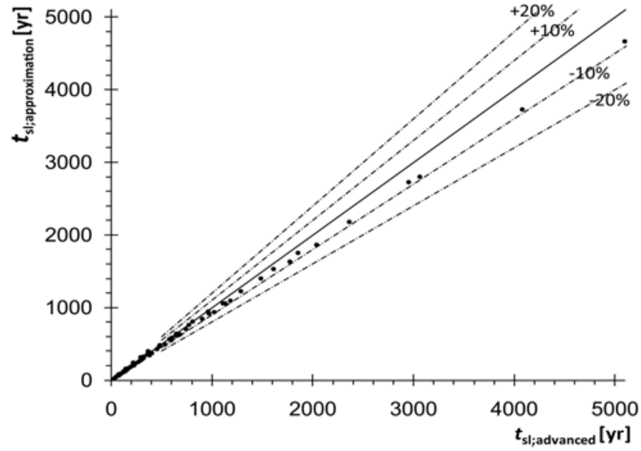

Figure A56.3a MF3

*Error plot: plot of the service life calculated with the approximation model as function of the service life calculated with the advanced model for film-based vacuum insulation panels with a **core of fumed silica and an MF3 barrier**. No thermal bridging.*

λ_{cr} = 11·10^{-3} W·m^{-1}·K^{-1};
ϕ = 50%; thickness: 1 to 5 cm; size: 0.25x0.25 m^2 to 2x2 m^2;
T: 5^{o}C to 45^{o}C.

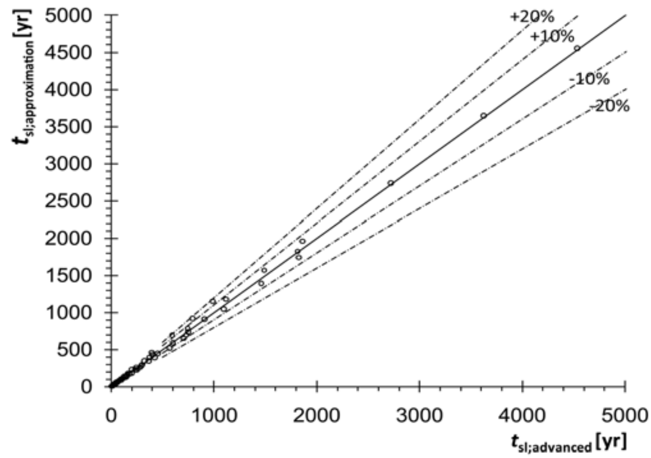

Figure A56.3b AF:8

*Error plot: plot of the service life calculated with the approximation model as function of the service life calculated with the advanced model for film-based vacuum insulation panels with a **core of fumed silica and an AF:8 barrier**. No thermal bridging.*

λ_{cr} = 11·10^{-3} W·m^{-1}·K^{-1};
ϕ = 50%; thickness: 1 to 5 cm; size: 0.25x0.25 m^2 to 2x2 m^2;
T: 5^{o}C to 45^{o}C.

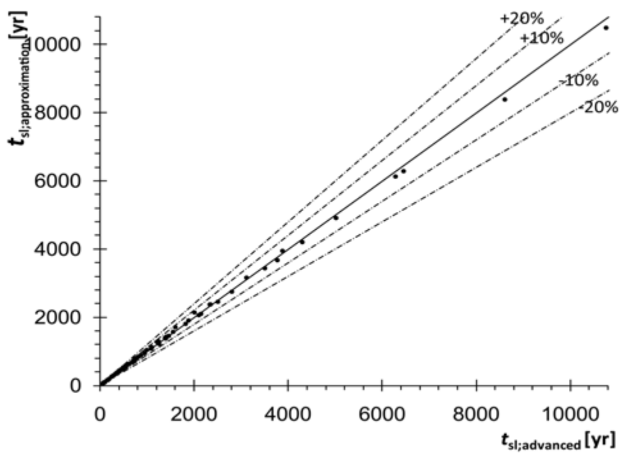

APPENDIXES TO CHAPTER 6 A

A61 BUCKLING OF TOP BARRIER LAMINATE (BEFORE BUCKLING)

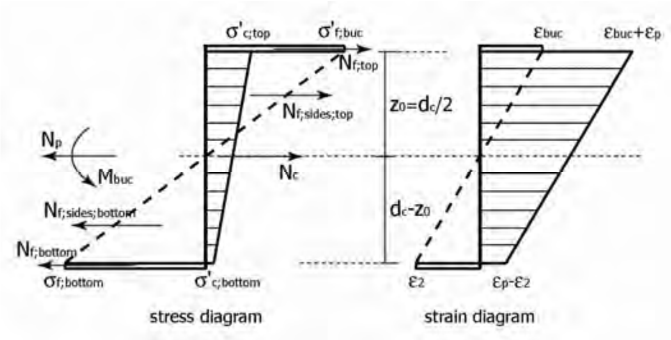

Figure A61

Stress and strain diagrams for the load case buckling of top barrier laminate (right before buckling).

Forces

$$N_p = \Delta p d_c w_c \qquad \text{(A61.1a)} \qquad N_c = \frac{\varepsilon_{buc} - \varepsilon_2 + 2\varepsilon_p}{2\varepsilon'_{c;pl}} f'_{c;y} w_c d_c \qquad \text{(A61.1b)}$$

$$N_{f;top} = \frac{\varepsilon_{buc}}{\varepsilon_{f;pl}} f_{f;y} t_f w_c \qquad \text{(A61.1c)} \qquad N_{f;bottom} = \frac{\varepsilon_2}{\varepsilon_{f;pl}} f_{f;y} t_f w_c \qquad \text{(A61.1d)}$$

$$N_{f;sides;top} = \frac{\varepsilon_{buc}}{2\varepsilon_{f;pl}} f_{f;y} t_f d_c \qquad \text{(A61.1e)} \qquad N_{f;sides;bottom} = \frac{\varepsilon_2}{2\varepsilon_{f;pl}} f_{f;y} t_f d_c \qquad \text{(A61.1f)}$$

Force equilibrium

$$N_p + N_{f;bottom} + N_{f;sides;bottom} - N_c - N_{f;top} - N_{f;sides;top} = 0 \qquad \text{(A61.2)}$$

Strains (Davies, 2001)

$$\varepsilon_2 = \varepsilon_{buc} = \frac{3}{2}\left[\frac{2(1-\nu_c)^2}{3(1+\nu_c)^2(3-4\nu_c)^2(1-\nu_f^2)}\right]^{1/3}\left(E_c^2 E_f\right)^{1/3}\frac{\varepsilon_{f;pl}}{f_{f;y}} \qquad \text{(A61.3a)}$$

$$\varepsilon_p = \frac{\Delta p}{E'_c} \qquad \text{(A61.3b)}$$

Bending Moment

$$M_{buc} = N_{f;top}\left(d_c + t_f\right) + \frac{2}{3}N_{f;sides;top} d_c + \frac{1}{12}\frac{\varepsilon_{buc} + \varepsilon_2}{\varepsilon'_{c;pl}} f'_{c;y} w_c d_c^2 \qquad \text{(A61.4)}$$

Curvature

$$\kappa_{buc;1} = \frac{\left|\varepsilon_{buc}\right| + \varepsilon_2}{d_c} \qquad \text{(A61.5)}$$

A62 BUCKLING OF TOP BARRIER LAMINATE (AFTER BUCKLING)

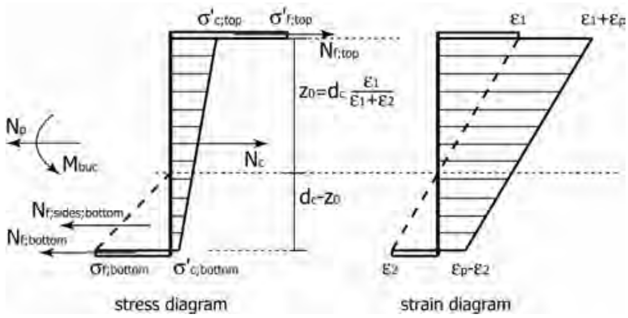

Figure A62

Stress and strain diagrams for the load case buckling of top barrier laminate (immediately after buckling).

Forces

$$N_p = \Delta p d_c w_c \tag{A62.1a}$$

$$N_c = \frac{\varepsilon_1 - \varepsilon_2 + 2\varepsilon_p}{2\varepsilon'_{c;pl}} f'_{c;y} w_c d_c \tag{A62.1b}$$

$$N_{f;bottom} = \frac{\varepsilon_2}{\varepsilon_{f;pl}} f_{f;y} t_f w_c \tag{A62.1c}$$

$$N_{f;sides;bottom} = \frac{\varepsilon_2}{\varepsilon_{f;pl}} f_{f;y} t_f d_c \left(1 - \frac{\varepsilon_1}{\varepsilon_1 + \varepsilon_2}\right) \tag{A62.1d}$$

$$N_{f;top} = \frac{\varepsilon_1}{\varepsilon_{f;pl}} f_{f;y} t_f w_c \left(1 - c_{buc}\right) \tag{A62.1e}$$

Force equilibrium

$$N_p + N_{f;bottom} + N_{f;sides;bottom} - N_c - N_{f;top} = 0 \tag{A62.2}$$

Bending moments

$$M_{f;bottom} = N_{f;bottom}\left(0.5 \cdot t_f + d_c\left(1 - \frac{\varepsilon_1}{\varepsilon_1 + \varepsilon_2}\right)\right) \tag{A62.3a}$$

$$M_{f;top} = N_{f;top}\left(0.5 \cdot t_f + d_c\left(1 - \frac{\varepsilon_2}{\varepsilon_1 + \varepsilon_2}\right)\right) \tag{A62.3b}$$

$$M_{f;sides;bottom} = \frac{2}{3} N_{f;sides;bottom} d_c \left(1 - \frac{\varepsilon_1}{\varepsilon_1 + \varepsilon_2}\right) \tag{A62.3c}$$

$$M_c = \frac{1}{3} \frac{\varepsilon_1}{\varepsilon'_{c;pl}} f'_{c;y} w_c d_c^2 \left(\frac{\varepsilon_1}{\varepsilon_1 + \varepsilon_2}\right)^2 + \frac{1}{3} \frac{\varepsilon_2}{\varepsilon'_{c;pl}} f'_{c;y} w_c d_c^2 \left(1 - \frac{\varepsilon_1}{\varepsilon_1 + \varepsilon_2}\right)^2 \tag{A62.3d}$$

Bending moment equilibrium

$$M_{f;bottom} + M_{f;top} + M_{f;sides;bottom} + M_c - M_{buc} = 0 \tag{A62.4}$$

Strains

$$\varepsilon_1 = k\varepsilon_2 \tag{A62.5a}$$

$$\varepsilon_2 = F \frac{1 + 2k + k^2}{D + Ek + Gk^2 + Hk^3} \tag{A62.5b}$$

$$\varepsilon_p = \frac{\Delta p}{E'_c} \tag{A62.5c}$$

$$k = -\frac{B + \sqrt{B^2 - 4AC}}{2A} \tag{A62.6}$$

$$A = -\varepsilon'_{c;pl} f_{f;y} w_c t_f (1 - c_{buc}) - \frac{1}{2} \varepsilon_{f;pl} f'_{c;y} w_c d_c \tag{A62.7a}$$

$$B = \varepsilon'_{c;pl} f_{f;y} w_c t_f c_{buc} \tag{A62.7b}$$

$$C = \varepsilon'_{c;pl} f_{f;y} t_f (w_c + d_c) + \frac{1}{2} \varepsilon_{f;pl} f'_{c;y} w_c d_c \tag{A62.7c}$$

$$D = \frac{1}{2} \varepsilon'_{c;pl} f_{f;y} t_f^2 w_c + \varepsilon'_{c;pl} f_{f;y} t_f w_c d_c + \frac{2}{3} \varepsilon'_{c;pl} f_{f;y} t_f d_c^2 + \frac{1}{3} \varepsilon_{f;pl} f'_{c;y} w_c d_c^2$$

$$E = \varepsilon'_{c;pl} f_{f;y} t_f^2 w_c + \varepsilon'_{c;pl} f_{f;y} t_f w_c d_c + \frac{1}{2} \varepsilon'_{c;pl} f_{f;y} t_f^2 w_c (1 - c_{buc}) \tag{A62.7e}$$

$$F = \varepsilon_{f;pl} \varepsilon'_{c;pl} M_{buc} \tag{A62.7f}$$

$$G = \varepsilon'_{c;pl} f_{f;y} t_f^2 w_c \left(\frac{3}{2} - c_{buc}\right) + \varepsilon'_{c;pl} f_{f;y} t_f d_c w_c (1 - c_{buc}) \tag{A62.7g}$$

$$H = \frac{1}{2} \varepsilon'_{c;pl} f_{f;y} t_f^2 w_c (1 - c_{buc}) + \varepsilon'_{c;pl} f_{f;y} t_f d_c w_c (1 - c_{buc}) + \frac{1}{3} \varepsilon_{f;pl} f'_{c;y} w_c d_c^2 \tag{A62.7h}$$

Curvature

$$\kappa_{buc;2} = \frac{\left|\varepsilon_1\right| + \varepsilon_2}{d_c} \tag{A62.8}$$

A63 PHYSICAL FAILURE

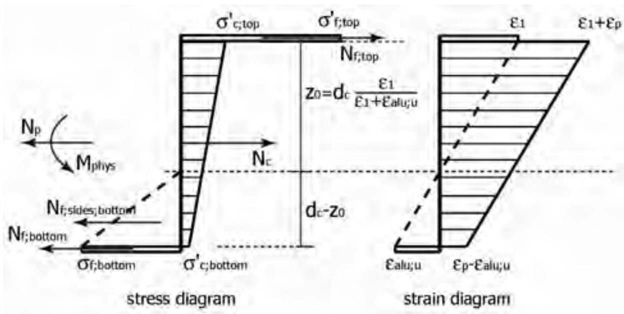

Figure A63

Stress and strain diagrams for the load case physical failure (crack initiation in metallic barrier layer).

Forces

$$N_p = \Delta p d_c w_c \tag{A63.1a}$$

$$N_c = \frac{\varepsilon_1 - \varepsilon_{alu;u} + 2\varepsilon_p}{2\varepsilon'_{c;pl}} f'_{c;y} w_c d_c \tag{A63.1b}$$

$$N_{f;bottom} = \frac{\varepsilon_{alu;u}}{\varepsilon_{f;pl}} f_{f;y} t_f w_c \tag{A63.1c}$$

$$N_{f;sides;bottom} = \frac{\varepsilon_{alu;u}}{\varepsilon_{f;pl}} f_{f;y} t_f d_c \left(1 - \frac{\varepsilon_1}{\varepsilon_1 + \varepsilon_{alu;u}}\right) \tag{A63.1d}$$

$$N_{f;top} = \left[f_{f;y} + \left(f_{f;u} - f_{f;y}\right) \frac{\varepsilon_1 - \varepsilon_{f;pl}}{\varepsilon_{f;u} - \varepsilon_{f;pl}} \right] t_f w_c \left(1 - c_{buc}\right) \tag{A63.1e}$$

Force equilibrium

$$N_p + N_{f;bottom} + N_{f;sides;bottom} - N_{f;top} - N_c = 0 \tag{A63.2}$$

Bending moments

$$M_{f;bottom} = N_{f;bottom} \left(0.5 \cdot t_f + d_c \left(1 - \frac{\varepsilon_1}{\varepsilon_1 + \varepsilon_{alu;u}}\right)\right) \tag{A63.3a}$$

$$M_{f;sides;bottom} = \frac{2}{3} N_{f;sides;bottom} d_c \left(1 - \frac{\varepsilon_1}{\varepsilon_1 + \varepsilon_{alu;u}}\right) \tag{A63.3b}$$

$$M_{f;top} = N_{f;top}\left(0.5 \cdot t_f + d_c\left(\frac{\varepsilon_1}{\varepsilon_1 + \varepsilon_{alu;u}}\right)\right) \tag{A63.3c}$$

$$M_c = \frac{1}{3}\frac{\varepsilon_1}{\varepsilon'_{c;pl}} f'_{c;y} w_c d_c^2 \left(\frac{\varepsilon_1}{\varepsilon_1 + \varepsilon_{alu;u}}\right)^2 + \frac{1}{3}\frac{\varepsilon_{alu;u}}{\varepsilon'_{c;pl}} f'_{c;y} w_c d_c^2 \left(1 - \frac{\varepsilon_1}{\varepsilon_1 + \varepsilon_{alu;u}}\right)^2 \tag{A63.3d}$$

Bending moment equilibrium

$$M_{phys} = M_{f;bottom} + M_{f;sides;bottom} + M_{f;top} + M_c \tag{A63.4}$$

Strains

$$\varepsilon_1 = \frac{-B - \sqrt{B^2 - 4AC}}{2A} \tag{A63.5a}$$

$$\varepsilon_p = \frac{\Delta p}{E'_c} \tag{A63.5b}$$

$$A = -\frac{1}{2}\varepsilon_{f;pl}\left(\varepsilon_{f;u} - \varepsilon_{f;pl}\right) f'_{c;y} w_c d_c - \varepsilon_{f;pl}\varepsilon'_{c;pl}\left(f_{f;u} - f_{f;y}\right) t_f w_c \left(1 - c_{buc}\right) \tag{A63.6a}$$

$$\begin{aligned} B = {} & \varepsilon_{alu;u}\varepsilon'_{c;pl}\left(\varepsilon_{f;u} - \varepsilon_{f;pl}\right) f_{f;y} t_f w_c \\ & - \varepsilon_{f;pl}\varepsilon'_{c;pl}\left(\varepsilon_{f;u} - \varepsilon_{f;y}\right) f_{f;y} t_f w_c \left(1 - c_{buc}\right) \\ & + \varepsilon_{f;pl}\varepsilon'_{c;pl}\left(\varepsilon_{f;pl} - \varepsilon_{alu;u}\right)\left(f_{f;u} - f_{f;y}\right) t_f w_c \left(1 - c_{buc}\right) \end{aligned} \tag{A63.6b}$$

$$\begin{aligned} C = {} & \varepsilon_{alu;u}^2\varepsilon'_{c;pl}\left(\varepsilon_{f;u} - \varepsilon_{f;pl}\right) f_{f;y} t_f \left(w_c + d_c\right) \\ & + \tfrac{1}{2}\varepsilon_{alu;u}^2\varepsilon_{f;pl}\left(\varepsilon_{f;u} - \varepsilon_{f;pl}\right) f'_{c;y} w_c d_c \\ & - \varepsilon_{f;pl}\varepsilon_{alu;u}\varepsilon'_{c;pl}\left(\varepsilon_{f;u} - \varepsilon_{f;pl}\right) f_{f;y} t_f w_c \left(1 - c_{buc}\right) \\ & + \varepsilon_{f;pl}^2\varepsilon_{alu;u}\varepsilon'_{c;pl}\left(f_{f;u} - f_{f;y}\right) t_f w_c \left(1 - c_{buc}\right) \end{aligned} \tag{A63.6c}$$

Curvature

$$\kappa_{phys} = \frac{\left|\varepsilon_1\right| + \varepsilon_{alu;u}}{d_c} \tag{A63.7}$$

A64 YIELD OF LOWER BARRIER LAMINATE

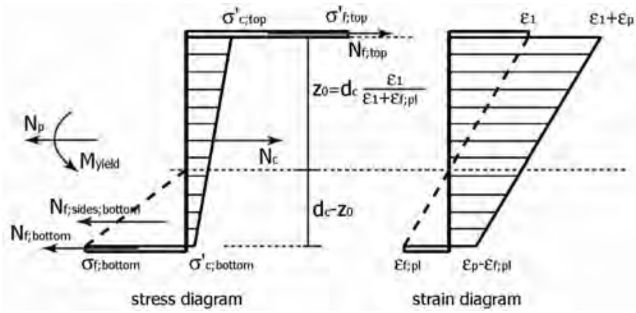

Figure A64

Stress and strain diagrams for the load case start of yield in lower barrier laminate. Diagrams are valid before the occurrence of cracks in the core material.

Forces

$$N_p = \Delta p d_c w_c \tag{A64.1a}$$

$$N_c = \frac{\varepsilon_1 - \varepsilon_{f;pl} + 2\varepsilon_p}{2\varepsilon'_{c;pl}} f'_{c;y} w_c d_c \tag{A64.1b}$$

$$N_{f;bottom} = f_{f;y} t_f w_c \tag{A64.1c}$$

$$N_{f;sides;bottom} = f_{f;y} t_f d_c \left(\frac{\varepsilon_{f;pl}}{\varepsilon_1 + \varepsilon_{f;pl}} \right) \tag{A64.1d}$$

$$N_{f;top} = \left[f_{f;y} + \left(f_{f;u} - f_{f;y} \right) \frac{\varepsilon_1 - \varepsilon_{f;pl}}{\varepsilon_{f;u} - \varepsilon_{f;pl}} \right] t_f w_c \left(1 - c_{buc} \right) \tag{A64.1e}$$

Force equilibrium

$$N_p + N_{f;bottom} + N_{f;sides;bottom} - N_{f;top} - N_c = 0 \tag{A64.2}$$

Bending moments

$$M_{f;bottom} = N_{f;bottom} \left(0.5 \cdot t_f + d_c \left(\frac{\varepsilon_{f;pl}}{\varepsilon_1 + \varepsilon_{f;pl}} \right) \right) \tag{A64.3a}$$

$$M_{f;sides;bottom} = \frac{2}{3} N_{f;sides;bottom} d_c \left(\frac{\varepsilon_{f;pl}}{\varepsilon_1 + \varepsilon_{f;pl}} \right) \tag{A64.3b}$$

$$M_{f;top} = N_{f;top}\left(0.5 \cdot t_f + d_c\left(\frac{\varepsilon_1}{\varepsilon_1 + \varepsilon_{f;pl}}\right)\right) \quad \text{(A64.3c)}$$

$$M_c = \frac{1}{3}\frac{\varepsilon_1}{\varepsilon'_{c;pl}} f'_{c;y} w_c d_c^2 \left(\frac{\varepsilon_1}{\varepsilon_1 + \varepsilon_{f;pl}}\right)^2 + \frac{1}{3}\frac{\varepsilon_{f;pl}}{\varepsilon'_{c;pl}} f'_{c;y} w_c d_c^2 \left(\frac{\varepsilon_{f;pl}}{\varepsilon_1 + \varepsilon_{f;pl}}\right)^2 \quad \text{(A64.3d)}$$

Bending moment equilibrium

$$M_{yield} = M_{f;bottom} + M_{f;sides;bottom} + M_{f;top} + M_c \quad \text{(A64.4)}$$

Strains

$$\varepsilon_1 = \frac{-B - \sqrt{B^2 - 4AC}}{2A} \quad \text{(A64.5a)}$$

$$\varepsilon_p = \frac{\Delta p}{E'_c} \quad \text{(A64.5b)}$$

$$A = -\frac{1}{2}\varepsilon_{f;pl}\left(\varepsilon_{f;u} - \varepsilon_{f;pl}\right) f'_{c;y} w_c d_c - \varepsilon_{f;pl}\varepsilon'_{c;pl}\left(f_{f;u} - f_{f;y}\right) t_f w_c \left(1 - c_{buc}\right) \quad \text{(A64.6a)}$$

$$B = \varepsilon_{f;pl}\varepsilon'_{c;pl}\left(\varepsilon_{f;u} - \varepsilon_{f;pl}\right) f_{f;y} t_f w_c c_{buc} \quad \text{(A64.6b)}$$

$$\begin{aligned} C = {} & \varepsilon_{f;pl}^2 \varepsilon'_{c;pl}\left(\varepsilon_{f;u} - \varepsilon_{f;pl}\right) f_{f;y} t_f \left(w_c c_{buc} + d_c\right) \\ & + \tfrac{1}{2}\varepsilon_{f;pl}^3\left(\varepsilon_{f;u} - \varepsilon_{f;pl}\right) f'_{c;y} w_c d_c + \varepsilon_{f;pl}^3 \varepsilon'_{c;pl}\left(f_{f;u} - f_{f;y}\right) t_f w_c \left(1 - c_{buc}\right) \end{aligned} \quad \text{(A64.6c)}$$

Curvature

$$\kappa_{yield} = \frac{\left|\varepsilon_1\right| + \varepsilon_{f;pl}}{d_c} \quad \text{(A64.7)}$$

A65 CRACK INITIATION IN CORE MATERIAL (BEFORE RUPTURE)

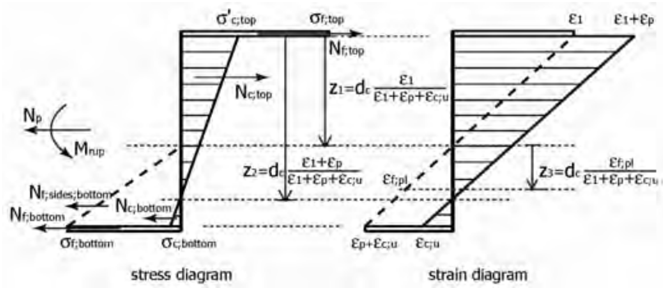

Figure A65

Stress and strain diagram for the load case crack initiation in the tension zone of the core material (immediately before rupture). Diagrams are valid after start of yield in lower barrier envelope.

Forces

$$N_p = \Delta p d_c w_c \tag{A65.1a}$$

$$N_{c;top} = \frac{(\varepsilon_1 + \varepsilon_p)^2}{2\varepsilon'_{c;pl}(\varepsilon_1 + \varepsilon_p + \varepsilon_{c;u})} f'_{c;y} w_c d_c \tag{A65.1b}$$

$$N_{c;bottom} = \frac{\varepsilon_{c;u}}{2(\varepsilon_1 + \varepsilon_p + \varepsilon_{c;u})} f_{c;u} w_c d_c \tag{A65.1c}$$

$$N_{f;bottom} = \left[f_{f;y} + \frac{\varepsilon_p + \varepsilon_{c;u} - \varepsilon_{f;pl}}{\varepsilon_{f;u} - \varepsilon_{f;pl}} \left(f_{f;u} - f_{f;y} \right) \right] t_f w_c \tag{A65.1d}$$

$$\begin{aligned} N_{f;sides;bottom} = {} & \frac{\varepsilon_{f;pl}}{\varepsilon_1 + \varepsilon_p + \varepsilon_{c;u}} f_{f;y} t_f d_c \\ & + \left[f_{f;y} + \frac{\varepsilon_p + \varepsilon_{c;u} - \varepsilon_{f;pl}}{2(\varepsilon_{f;u} - \varepsilon_{f;pl})} \left(f_{f;u} - f_{f;y} \right) \right] 2 t_f d_c \frac{\varepsilon_p + \varepsilon_{c;u} - \varepsilon_{f;pl}}{\varepsilon_p + \varepsilon_{c;u} + \varepsilon_1} \end{aligned} \tag{A65.1e}$$

$$N_{f;top} = \left[f_{f;y} + \frac{\varepsilon_1 - \varepsilon_{f;pl}}{\varepsilon_{f;u} - \varepsilon_{f;pl}} \left(f_{f;u} - f_{f;y} \right) \right] t_f w_c (1 - c_{buc}) \tag{A65.1f}$$

Force equilibrium

$$N_p + N_{f;bottom} + N_{f;sides;bottom} + N_{c;bottom} - N_{f;top} - N_{c;top} = 0 \tag{A65.2}$$

Strains

$$\varepsilon_1 = \frac{-B - \sqrt{B^2 - 4AC}}{2A} \tag{A65.3a}$$

$$\varepsilon_p = \frac{\Delta p}{E_c^{'}} \tag{A65.3b}$$

$$A = -\frac{1}{2}\left(\varepsilon_{f;u} - \varepsilon_{f;pl}\right) f_{c;y}^{'} w_c d_c - \varepsilon_{c;pl}^{'}\left(f_{f;u} - f_{f;y}\right) t_f w_c \left(1 - c_{buc}\right) \tag{A65.4a}$$

$$\begin{aligned} B = {} & \left(\varepsilon_p + \varepsilon_{c;u} - \varepsilon_{f;pl}\right)\varepsilon_{c;pl}^{'}\left(f_{f;u} - f_{f;y}\right) t_f w_c c_{buc} \\ & + \left(\varepsilon_{f;u} - \varepsilon_{f;pl}\right)\varepsilon_{c;pl}^{'} f_{f;y} t_f w_c c_{buc} \end{aligned} \tag{A65.4b}$$

$$\begin{aligned} C = {} & \left(\varepsilon_p + \varepsilon_{c;u} - \varepsilon_{f;pl}\right)\left(\varepsilon_p + \varepsilon_{c;u}\right)\varepsilon_{c;pl}^{'}\left(f_{f;u} - f_{f;y}\right) t_f w_c \\ & + \left(\varepsilon_{f;u} - \varepsilon_{f;pl}\right)\left(\varepsilon_p + \varepsilon_{c;u}\right)\varepsilon_{c;pl}^{'} f_{f;y} t_f w_c c_{buc} \\ & + \left(\varepsilon_{f;u} - \varepsilon_{f;pl}\right)\varepsilon_{f;pl}\varepsilon_{c;pl}^{'} f_{f;y} t_f d_c \\ & + \left(\varepsilon_p + \varepsilon_{c;u} - \varepsilon_{f;pl}\right)^2 \varepsilon_{c;pl}^{'}\left(f_{f;u} - f_{f;y}\right) t_f d_c \\ & + 2\left(\varepsilon_p + \varepsilon_{c;u} - \varepsilon_{f;pl}\right)\left(\varepsilon_{f;u} - \varepsilon_{f;pl}\right)\varepsilon_{c;pl}^{'} f_{f;y} t_f d_c \\ & + \tfrac{1}{2}\varepsilon_{c;u}\varepsilon_{c;pl}^{'}\left(\varepsilon_{f;u} - \varepsilon_{f;pl}\right) f_{c;u} w_c d_c \\ & + \left(\varepsilon_{f;u} - \varepsilon_{f;pl}\right)\left(\tfrac{1}{2}\varepsilon_p + \varepsilon_{c;u}\right)\varepsilon_{c;pl}^{'}\Delta p w_c d_c \\ & + \varepsilon_{f;pl}\varepsilon_{c;pl}^{'}\left(\varepsilon_p + \varepsilon_{c;u}\right)\left(f_{f;u} - f_{f;y}\right) t_f w_c \left(1 - c_{buc}\right) \end{aligned} \tag{A65.4c}$$

Bending moments

$$M_{c;top} = \frac{1}{3}\frac{\varepsilon_1^3}{\varepsilon_{c;pl}^{'}\left(\varepsilon_1 + \varepsilon_p + \varepsilon_{c;u}\right)^2} f_{c;y}^{'} w_c d_c^2 \tag{A65.5a}$$

$$\begin{aligned} M_{c;bottom} = {} & \frac{1}{3}\frac{\left(\varepsilon_p + \varepsilon_{c;u}\right)^3}{\varepsilon_{c;pl}^{'}\left(\varepsilon_1 + \varepsilon_p + \varepsilon_{c;u}\right)^2} f_{c;y}^{'} w_c d_c^2 \\ & + \frac{1}{2}\frac{\varepsilon_{c;u}\left(\varepsilon_p + 2/3\varepsilon_{c;u}\right)}{\left(\varepsilon_1 + \varepsilon_p + \varepsilon_{c;u}\right)^2}\left(f_{c;u} - \frac{\varepsilon_{c;u}}{\varepsilon_{c;pl}^{'}} f_{c;y}^{'}\right) w_c d_c^2 \end{aligned} \tag{A65.5b}$$

$$M_{f;bottom} = N_{f;bottom}\left[\frac{1}{2}t_f + d_c\left(\frac{\varepsilon_p + \varepsilon_{c;u}}{\varepsilon_1 + \varepsilon_p + \varepsilon_{c;u}}\right)\right] \tag{A65.5c}$$

$$\begin{aligned} M_{f;sides;bottom} = {} & \frac{2}{3}\frac{\varepsilon_{f;pl}^2}{\left(\varepsilon_1 + \varepsilon_p + \varepsilon_{c;u}\right)^2} f_{f;y} t_f d_c^2 \\ & + \left[f_{f;y} + \frac{\varepsilon_p + \varepsilon_{c;u} - \varepsilon_{f;pl}}{2\left(\varepsilon_{f;u} - \varepsilon_{f;pl}\right)}\left(f_{f;u} - f_{f;y}\right)\right] t_f d_c^2 \frac{\left(\varepsilon_p + \varepsilon_{c;u} - \varepsilon_{f;pl}\right)^2}{\left(\varepsilon_p + \varepsilon_{c;u} + \varepsilon_1\right)^2} \end{aligned} \tag{A65.5d}$$

$$M_{f;top} = N_{f;top}\left[\frac{1}{2}t_f + d_c\left(\frac{\varepsilon_1}{\varepsilon_1 + \varepsilon_p + \varepsilon_{c;u}}\right)\right] \tag{A65.5c}$$

$$M_{rup} = \sum_{i=1}^{5} M_i \tag{A65.5e}$$

Curvature

$$\kappa_{rup} = \frac{|\varepsilon_1| + \varepsilon_p + \varepsilon_{c;u}}{d_c} \tag{A65.6}$$

A66 Crack Initiation in Core Material (After Rupture)

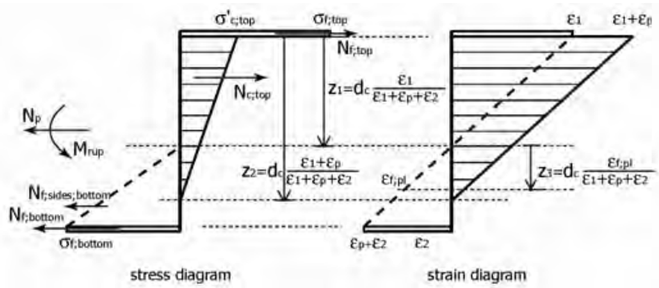

Figure A66

Stress and strain diagram for the load case crack initiation in the tension zone of the core material (immediately after rupture).

Forces

$$N_p = \Delta p d_c w_c \tag{A66.1a}$$

$$N_{c;top} = \frac{(\varepsilon_1 + \varepsilon_p)^2}{2\varepsilon'_{c;pl}(\varepsilon_1 + \varepsilon_p + \varepsilon_2)} f'_{c;y} w_c d_c \tag{A66.1b}$$

$$N_{c;bottom} = 0 \tag{A66.1c}$$

$$N_{f;bottom} = \left[f_{f;y} + \frac{\varepsilon_p + \varepsilon_2 - \varepsilon_{f;pl}}{\varepsilon_{f;u} - \varepsilon_{f;pl}} \left(f_{f;u} - f_{f;y} \right) \right] t_f w_c \tag{A66.1d}$$

$$\begin{aligned} N_{f;sides;bottom} &= \frac{\varepsilon_{f;pl}}{\varepsilon_1 + \varepsilon_p + \varepsilon_2} f_{f;y} t_f d_c \\ &+ \left[f_{f;y} + \frac{\varepsilon_p + \varepsilon_2 - \varepsilon_{f;pl}}{2(\varepsilon_{f;u} - \varepsilon_{f;pl})} \left(f_{f;u} - f_{f;y} \right) \right] 2 t_f d_c \frac{\varepsilon_p + \varepsilon_2 - \varepsilon_{f;pl}}{\varepsilon_1 + \varepsilon_p + \varepsilon_2} \end{aligned} \tag{A66.1e}$$

$$N_{f;top} = \left[f_{f;y} + \frac{\varepsilon_1 - \varepsilon_{f;pl}}{\varepsilon_{f;u} - \varepsilon_{f;pl}} \left(f_{f;u} - f_{f;y} \right) \right] t_f w_c (1 - c_{buc}) \tag{A66.1f}$$

Force equilibrium

$$N_p + N_{f;bottom} + N_{f;sides;bottom} + N_{c;bottom} - N_{f;top} - N_{c;top} = 0 \tag{A66.2}$$

Bending moments

$$M_{c;top} = \frac{1}{3} \frac{\varepsilon_1^3 + \varepsilon_p^3}{\varepsilon_{c;pl}^{'} \left(\varepsilon_1 + \varepsilon_p + \varepsilon_2\right)^2} f_{c;y}^{'} w_c d_c^2 \qquad \text{(A66.3a)}$$

$$M_{c;bottom} = 0 \qquad \text{(A66.3b)}$$

$$M_{f;bottom} = N_{f;bottom} \left[\frac{1}{2} t_f + d_c \left(\frac{\varepsilon_p + \varepsilon_2}{\varepsilon_1 + \varepsilon_p + \varepsilon_2} \right) \right] \qquad \text{(A66.3c)}$$

$$M_{f;sides;bottom} = \frac{2}{3} \frac{\varepsilon_{f;pl}^2}{\left(\varepsilon_1 + \varepsilon_p + \varepsilon_2\right)^2} f_{f;y} t_f d_c^2 + \left[f_{f;y} + \frac{\varepsilon_p + \varepsilon_2 - \varepsilon_{f;pl}}{2\left(\varepsilon_{f;u} - \varepsilon_{f;pl}\right)} \left(f_{f;u} - f_{f;y} \right) \right] t_f d_c^2 \frac{\left(\varepsilon_p + \varepsilon_2 - \varepsilon_{f;pl}\right)^2}{\left(\varepsilon_p + \varepsilon_2 + \varepsilon_1\right)^2} \qquad \text{(A66.3d)}$$

$$M_{f;top} = N_{f;top} \left[\frac{1}{2} t_f + d_c \left(\frac{\varepsilon_1}{\varepsilon_1 + \varepsilon_p + \varepsilon_2} \right) \right] \qquad \text{(A66.3e)}$$

Bending moment equilibrium

$$M_{f;bottom} + M_{f;sides;bottom} + M_{f;top} + M_{c;bottom} + M_{c;top} - M_{rup} = 0 \qquad \text{(A66.4)}$$

NB: M_{rup} is calculated from equation (A65.5e).

Strains

$$\varepsilon_p = \frac{\Delta p}{E_c^{'}} \qquad \text{(A66.5)}$$

ε_1 and ε_2 are determined from simultaneously solving eq. (A66.2) and (A66.4).

Curvature

$$\kappa_{rup} = \frac{\left|\varepsilon_1\right| + \varepsilon_p + \varepsilon_2}{d_c} \qquad \text{(A66.6)}$$

A67 UPSETTING OF CORE MATERIAL

Figure A67

Stress and strain diagram for the load case upsetting of the core material in the compression zone. Diagrams are valid after start of yield in lower barrier envelope and crack occurrence in core material.

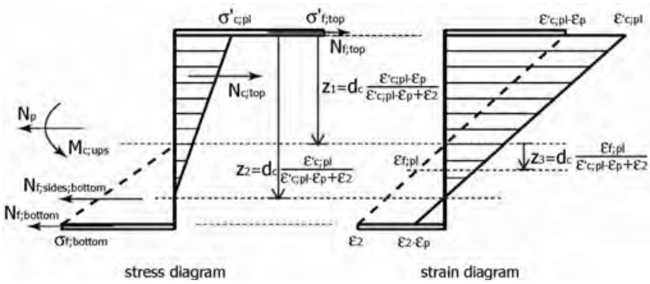

Forces

$$N_p = \Delta p d_c w_c \tag{A67.1a}$$

$$N_{c;top} = \frac{\varepsilon'_{c;pl}}{2\left(\varepsilon'_{c;pl} - \varepsilon_p + \varepsilon_2\right)} f'_{c;y} w_c d_c \tag{A67.1b}$$

$$N_{f;bottom} = \left[f_{f;y} + \frac{\varepsilon_2 - \varepsilon_{f;pl}}{\varepsilon_{f;u} - \varepsilon_{f;pl}} \left(f_{f;u} - f_{f;y} \right) \right] t_f w_c \tag{A67.1c}$$

$$\begin{aligned} N_{f;sides;bottom} &= \frac{\varepsilon_{f;pl}}{\varepsilon'_{c;pl} - \varepsilon_p + \varepsilon_2} f_{f;y} t_f d_c \\ &+ \left[f_{f;y} + \frac{\varepsilon_2 - \varepsilon_{f;pl}}{2\left(\varepsilon_{f;u} - \varepsilon_{f;pl}\right)} \left(f_{f;u} - f_{f;y} \right) \right] 2 t_f d_c \frac{\varepsilon_2 - \varepsilon_{f;pl}}{\varepsilon'_{c;pl} - \varepsilon_p + \varepsilon_2} \end{aligned} \tag{A67.1d}$$

$$N_{f;top} = \left[f_{f;y} + \frac{\varepsilon'_{c;pl} - \varepsilon_p - \varepsilon_{f;pl}}{\varepsilon_{f;u} - \varepsilon_{f;pl}} \left(f_{f;u} - f_{f;y} \right) \right] t_f w_c \left(1 - c_{buc}\right) \tag{A67.1e}$$

Force equilibrium

$$N_p + N_{f;bottom} + N_{f;sides;bottom} - N_{f;bottom} - N_{c;top} = 0 \tag{A67.2}$$

Strains

$$\varepsilon_2 = \frac{-B + \sqrt{B^2 - 4AC}}{2A} \tag{A67.3a}$$

$$\varepsilon_p = \frac{\Delta p}{E'_c} \tag{A67.3b}$$

$$A = \left(f_{f;u} - f_{f;y}\right)t_f\left(w_c + d_c\right) \tag{A67.4a}$$

$$\begin{aligned} B = &\left(\varepsilon_{f;u} - \varepsilon_{f;pl}\right)\Delta p d_c w_c + \left(\varepsilon'_{c;pl} - \varepsilon_p - \varepsilon_{f;pl}\right)\left(f_{f;u} - f_{f;y}\right)t_f w_c c_{buc} \\ &+ \left(\varepsilon_{f;u} - \varepsilon_{f;pl}\right)f_{f;y}t_f w_c c_{buc} + 2\left(\varepsilon_{f;u} - \varepsilon_{f;pl}\right)f_{f;y}t_f d_c \\ &- 2\varepsilon_{f;pl}\left(f_{f;u} - f_{f;y}\right)t_f d_c \end{aligned} \tag{A67.4b}$$

$$\begin{aligned} C = &\left(\varepsilon_{f;u} - \varepsilon_{f;pl}\right)\left(\varepsilon'_{c;pl} - \varepsilon_p\right)\Delta p w_c d_c - \varepsilon_{f;pl}\left(\varepsilon'_{c;pl} - \varepsilon_p\right)\left(f_{f;u} - f_{f;y}\right)t_f w_c \\ &+ \left(\varepsilon_{f;u} - \varepsilon_{f;pl}\right)\left(\varepsilon'_{c;pl} - \varepsilon_p\right)f_{f;y}t_f w_c c_{buc} - \varepsilon_{f;pl}\left(\varepsilon_{f;u} - \varepsilon_{f;pl}\right)f_{f;y}t_f d_c \\ &+ \varepsilon^2_{f;pl}\left(f_{f;u} - f_{f;y}\right)t_f d_c - \tfrac{1}{2}\varepsilon'_{c;pl}\left(\varepsilon_{f;u} - \varepsilon_{f;pl}\right)f'_{c;y}w_c d_c \\ &- \left(\varepsilon'_{c;pl} - \varepsilon_p\right)\left(\varepsilon'_{c;pl} - \varepsilon_p - \varepsilon_{f;pl}\right)\left(f_{f;u} - f_{f;y}\right)t_f w_c\left(1 - c_{buc}\right) \end{aligned} \tag{A67.4c}$$

Bending moments

$$\begin{aligned} M_{c;top} = &\frac{1}{3}\frac{\left(\varepsilon'_{c;pl} - \varepsilon_p\right)^3}{\varepsilon'_{c;pl}\left(\varepsilon'_{c;pl} - \varepsilon_p + \varepsilon_2\right)^2} f'_{c;y}w_c d_c^2 \\ &+ \frac{1}{3}\frac{\varepsilon_p^3}{\varepsilon'_{c;pl}\left(\varepsilon'_{c;pl} - \varepsilon_p + \varepsilon_2\right)^2} f'_{c;y}w_c d_c^2 \end{aligned} \tag{A67.5a}$$

$$M_{f;bottom} = N_{f;bottom}\left[\frac{1}{2}t_f + d_c\left(\frac{\varepsilon_2}{\varepsilon'_{c;pl} - \varepsilon_p + \varepsilon_2}\right)\right] \tag{A67.5b}$$

$$\begin{aligned} M_{f;sides;bottom} = &\frac{2}{3}\frac{\varepsilon^2_{f;pl}}{\left(\varepsilon'_{c;pl} - \varepsilon_p + \varepsilon_2\right)^2} f_{f;y}t_f d_c^2 \\ &+ \left[f_{f;y} + \frac{\varepsilon_2 - \varepsilon_{f;pl}}{2\left(\varepsilon_{f;u} - \varepsilon_{f;pl}\right)}\left(f_{f;u} - f_{f;y}\right)\right]t_f d_c^2 \frac{\left(\varepsilon_2 - \varepsilon_{f;pl}\right)^2}{\left(\varepsilon'_{c;pl} - \varepsilon_p + \varepsilon_2\right)^2} \end{aligned} \tag{A67.5c}$$

$$M_{f;top} = N_{f;top}\left[\frac{1}{2}t_f + d_c\left(\frac{\varepsilon'_{c;pl} - \varepsilon_p}{\varepsilon'_{c;pl} - \varepsilon_p + \varepsilon_2}\right)\right] \tag{A67.5b}$$

$$M_{c;ups} = \sum_{i=1}^{4} M_i \tag{A67.5e}$$

Curvature

$$\kappa_{c;ups} = \frac{\left|\varepsilon'_{c;pl} - \varepsilon_p\right| + \varepsilon_2}{d_c} \tag{A67.6}$$

Figure A68

Stress and strain diagram for the load case structural failure of the core material in the compression zone. Diagrams are valid after start of yield in lower barrier envelope and crack occurrence in core material.

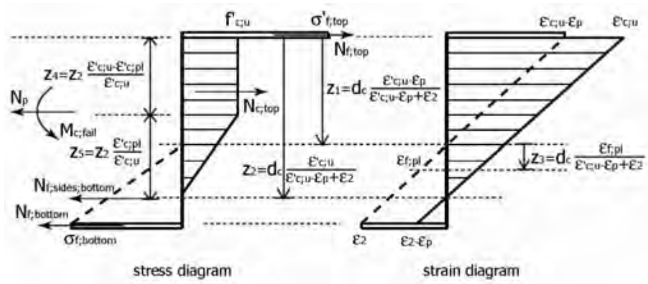

Forces

$$N_p = \Delta p d_c w_c \tag{A68.1a}$$

$$N_{c;top} = \frac{\varepsilon'_{c;u} - \varepsilon'_{c;pl}/2}{\varepsilon'_{c;u} - \varepsilon_p + \varepsilon_2} f'_{c;u} w_c d_c \tag{A68.1b}$$

$$N_{f;bottom} = \left[f_{f;y} + \frac{\varepsilon_2 - \varepsilon_{f;pl}}{\varepsilon_{f;u} - \varepsilon_{f;pl}} \left(f_{f;u} - f_{f;y} \right) \right] t_f w_c \tag{A68.1c}$$

$$\begin{aligned} N_{f;sides;bottom} = {} & \frac{\varepsilon_{f;pl}}{\varepsilon'_{c;u} - \varepsilon_p + \varepsilon_2} f_{f;y} t_f d_c \\ & + \left[f_{f;y} + \frac{\varepsilon_2 - \varepsilon_{f;pl}}{2\left(\varepsilon_{f;u} - \varepsilon_{f;pl}\right)} \left(f_{f;u} - f_{f;y} \right) \right] 2 t_f d_c \frac{\varepsilon_2 - \varepsilon_{f;pl}}{\varepsilon'_{c;u} - \varepsilon_p + \varepsilon_2} \end{aligned} \tag{A68.1d}$$

$$N_{f;top} = \left[f_{f;y} + \frac{\varepsilon'_{c;u} - \varepsilon_p - \varepsilon_{f;pl}}{\varepsilon_{f;u} - \varepsilon_{f;pl}} \left(f_{f;u} - f_{f;y} \right) \right] t_f w_c \left(1 - c_{buc}\right) \tag{A68.1e}$$

Force equilibrium

$$N_p + N_{f;bottom} + N_{f;sides;bottom} - N_{f;top} - N_{c;top} = 0 \tag{A68.2}$$

Strains

$$\varepsilon_2 = \frac{-B + \sqrt{B^2 - 4AC}}{2A} \tag{A68.3a}$$

$$\varepsilon_p = \frac{\Delta p}{E_c^{'}} \tag{A68.3b}$$

$$A = \left(f_{f;u} - f_{f;y}\right)t_f\left(w_c + d_c\right) \tag{A68.4a}$$

$$\begin{aligned} B = &\left(\varepsilon_{f;u} - \varepsilon_{f;pl}\right)\Delta p d_c w_c + \left(\varepsilon_{c;u}^{'} - \varepsilon_p - \varepsilon_{f;pl}\right)\left(f_{f;u} - f_{f;y}\right)t_f w_c c_{buc} \\ &+ \left(\varepsilon_{f;u} - \varepsilon_{f;pl}\right)f_{f;y} t_f w_c c_{buc} + 2\left(\varepsilon_{f;u} - \varepsilon_{f;pl}\right)f_{f;y} t_f d_c \\ &- 2\varepsilon_{f;pl}\left(f_{f;u} - f_{f;y}\right)t_f d_c \end{aligned} \tag{A68.4b}$$

$$\begin{aligned} C = &\left(\varepsilon_{f;u} - \varepsilon_{f;pl}\right)\left(\varepsilon_{c;u}^{'} - \varepsilon_p\right)\Delta p w_c d_c - \varepsilon_{f;pl}\left(\varepsilon_{c;u}^{'} - \varepsilon_p\right)\left(f_{f;u} - f_{f;y}\right)t_f w_c \\ &+ \left(\varepsilon_{f;u} - \varepsilon_{f;pl}\right)\left(\varepsilon_{c;u}^{'} - \varepsilon_p\right)f_{f;y} t_f w_c c_{buc} - \varepsilon_{f;pl}\left(\varepsilon_{f;u} - \varepsilon_{f;pl}\right)f_{f;y} t_f d_c \\ &+ \varepsilon_{f;pl}^2\left(f_{f;u} - f_{f;y}\right)t_f d_c - 2\varepsilon_{f;pl}\left(\varepsilon_{f;u} - \varepsilon_{f;pl}\right)f_{f;y} t_f d_c \\ &- \left(\varepsilon_{c;u}^{'} - \varepsilon_{c;pl}^{'}/2\right)\left(\varepsilon_{f;u} - \varepsilon_{f;pl}\right)f_{c;u}^{'} w_c d_c \\ &- \left(\varepsilon_{c;u}^{'} - \varepsilon_p - \varepsilon_{f;pl}\right)\left(\varepsilon_{c;u}^{'} - \varepsilon_p\right)\left(f_{f;u} - f_{f;y}\right)t_f w_c\left(1 - c_{buc}\right) \end{aligned} \tag{A68.4c}$$

Bending moments

$$\begin{aligned} M_{c;top} = &\left(f_{c;u}^{'} - \frac{\varepsilon_p}{\varepsilon_{c;pl}^{'}} f_{c;y}^{'}\right)\frac{\left(\varepsilon_{c;u}^{'} - \varepsilon_{c;pl}^{'}\right)\left(\varepsilon_{c;u}^{'} + \varepsilon_{c;pl}^{'} - 2\varepsilon_p\right)}{2\left(\varepsilon_{c;u}^{'} - \varepsilon_p + \varepsilon_2\right)^2} w_c d_c^2 \\ &+ \frac{1}{3}\left(f_{c;u}^{'} - \frac{\varepsilon_p}{\varepsilon_{c;pl}^{'}} f_{c;y}^{'}\right)\frac{\left(\varepsilon_p - \varepsilon_{c;pl}^{'}\right)^2}{\left(\varepsilon_{c;u}^{'} - \varepsilon_p + \varepsilon_2\right)^2} w_c d_c^2 \\ &+ \frac{1}{3}\frac{\varepsilon_p^3}{\varepsilon_{c;pl}^{'}\left(\varepsilon_{c;u}^{'} - \varepsilon_p + \varepsilon_2\right)^2} f_{c;y}^{'} w_c d_c^2 \end{aligned} \tag{A68.5a}$$

$$M_{f;bottom} = N_{f;bottom}\left[\frac{1}{2}t_f + d_c\left(\frac{\varepsilon_2}{\varepsilon_{c;u}^{'} - \varepsilon_p + \varepsilon_2}\right)\right] \tag{A68.5b}$$

$$\begin{aligned} M_{f;sides;bottom} = &\frac{2}{3}\frac{\varepsilon_{f;pl}^2}{\left(\varepsilon_{c;u}^{'} - \varepsilon_p + \varepsilon_2\right)^2} f_{f;y} t_f d_c^2 \\ &+ \left[f_{f;y} + \frac{\varepsilon_2 - \varepsilon_{f;pl}}{2\left(\varepsilon_{f;u} - \varepsilon_{f;pl}\right)}\left(f_{f;u} - f_{f;y}\right)\right]t_f d_c^2 \frac{\left(\varepsilon_2 - \varepsilon_{f;pl}\right)\left(\varepsilon_{c;u}^{'} - \varepsilon_p + \varepsilon_{f;pl}\right)}{\left(\varepsilon_{c;u}^{'} - \varepsilon_p + \varepsilon_2\right)^2} \end{aligned} \tag{A68.5c}$$

$$M_{f;top} = N_{f;top}\left[\frac{1}{2}t_f + d_c\left(\frac{\varepsilon_{c;u}^{'} - \varepsilon_p}{\varepsilon_{c;u}^{'} - \varepsilon_p + \varepsilon_2}\right)\right] \tag{A68.5b}$$

$$M_{c;fail} = \sum_{i=1}^{4} M_i \tag{A68.5e}$$

Curvature

$$\kappa_{c;fail} = \frac{\left|\varepsilon'_{c;u} - \varepsilon_p\right| + \varepsilon_2}{d_c} \tag{A68.6}$$

In section 6.3 the bending stiffness of a vacuum insulation panel as a whole, $(EI)_{vip}$, was defined as

$$
\begin{aligned}
(EI)_{vip} &= E_f \frac{w_c\left(d_p^3 - d_c^3\right)}{12\cdot(1-\nu_f^2)} + E_c \frac{w_c d_c^3}{12\cdot(1-\nu_c^2)} \\
&= E_f \frac{w_c t_f^3}{6\cdot(1-\nu_f^2)} + E_f \frac{w_c t_f\left(t_f + d_c\right)^2}{2\cdot(1-\nu_f^2)} + E_c \frac{w_c d_c^3}{12\cdot(1-\nu_c^2)}
\end{aligned}
\qquad (69.1),
$$

with E_f [Pa] the Young's modulus of the barrier film, E_c [Pa] the Young's modulus of the core material, ν_f the Poission's ratio of the film, ν_c the Poission's ratio of the core, d_c [m] the thickness of the core, w_c [m] the width of the core and t_f [m] the thickness of the barrier envelope. In this equation, the effect of the barrier envelope at the panel's sides was not included since these were added later to the equations. If we add the effect of the barrier envelope at the sides to the equation, we obtain

$$
(EI)_{vip} = E_f \frac{w_c t_f^3}{6\cdot(1-\nu_f^2)} + E_f \frac{w_c t_f\left(t_f + d_c\right)^2}{2\cdot(1-\nu_f^2)} + E_f \frac{t_f\left(2t_f + d_c\right)^3}{6\cdot(1-\nu_f^2)} + E_c \frac{w_c d_c^3}{12\cdot(1-\nu_c^2)} \qquad (A69.2).
$$

If in this equation Poisson's ratios are neglected and if $t_f << d_c$, then it reduces to

$$
(EI)_{vip} = E_f \frac{w_c t_f d_c^2}{2} + E_f \frac{t_f d_c^3}{6} + E_c \frac{w_c d_c^3}{12} \qquad (A69.3).
$$

Based upon the equations derived for the (M,k)-diagram, it is also possible to determine $(EI)_{vip}$ since this quantity is defined as bending moment divided by curvature. This bending stiffness can thus be written as

$$
\begin{aligned}
(EI)_{vip} = \frac{M}{\kappa} &= \frac{N_{f;top}\left(t_f + d_c\right) + \frac{2}{3} N_{f;sides} d_c + \frac{1}{12}\frac{\left(\varepsilon_1 + \varepsilon_2\right)}{\varepsilon_{c;pl}^{'}} f_{c;y}^{'} w_c d_c^3}{\frac{\left(\varepsilon_1 + \varepsilon_2\right)}{d_c}} \\
&= \frac{\varepsilon_1 t_f w_c d_c\left(t_f + d_c\right)\frac{f_{f;y}}{\varepsilon_{f;pl}} + \frac{1}{3}\varepsilon_1 t_f d_c^3 \frac{f_{f;y}}{\varepsilon_{f;pl}} + \frac{1}{6}\varepsilon_1 w_c d_c^3 \frac{f_{c;y}^{'}}{\varepsilon_{c;pl}^{'}}}{2\varepsilon_1} \\
&= E_f \frac{t_f w_c d_c\left(t_f + d_c\right)}{2} + E_f \frac{t_f d_c^3}{6} + E_c \frac{w_c d_c^3}{12}
\end{aligned}
\qquad (A69.4).
$$

If again t_f <<d_c, then the same equation as equation (A69.3) is obtained. This shows that both methods should more-or-less result in the same values of the bending stiffness and thus the Young's modulus of a vacuum insulation panel system. Small deviations occur due to the use of Poisson's ratios and due to the assumption of t_f <<d_c.

A610 DERIVATION OF $E_{EQ;EFF}$ FOR 4-POINT BENDING

The deflection of a beam under four-point flexion at mid span can be calculated as

$$\delta_{mid} = \frac{Fa\left(3l^2 - 4a^2\right)}{24(EI)_{vip}} + \frac{Fa}{(GA)_{vip}} \qquad \text{(A610.1)},$$

in which δ_{mid} [m] is the deflection of the beam/plate at mid span, F [N] the load acting upon the beam/plate, l [m] the span, a [m] the distance from the point of action of the load to the supports, $(EI)_{vip}$ [N·m^2] and $(GA)_{vip}$ [N], the bending and shear stiffness respectively (including Poisson's ratios). The first term on the right hand side of the equation represent pure bending while the second term represents shear. A similar equation can be obtained from literature for the deflection at the point of action of the load

$$\delta_F = \frac{Fa^2\left(3l - 4a\right)}{6(EI)_{vip}} + \frac{Fa}{(GA)_{vip}} \qquad \text{(A610.2)}.$$

In case shear effects are included in the bending stiffness, or Young's modulus, the deflection at mid span can be written as

$$\delta_{mid} = \frac{Fa\left(3l^2 - 4a^2\right)(1 - \overline{\nu^2})}{24E_{eff}I_{vip}} \qquad \text{(A610.3)},$$

with E_{eff} [N·m^{-2}] an effective Young's modulus including shear effects and I_{vip} [m^4] the area moment of inertia of a VIP. Since both deflections should be the same, equating formulae (A610.1) and (A610.3) results in an expression for E_{eff}

$$E_{eff} = \frac{(EI)_{vip}(1 - \overline{\nu^2})}{I_{vip}} \frac{1}{1 + \frac{24}{\left(3l^2 - 4a^2\right)} \frac{(EI)_{vip}}{(GA)_{vip}}} \qquad \text{(A610.4)}.$$

For the deflection at the point of action of the load, a similar equation can be derived yielding

$$E_{eff} = \frac{(EI)_{vip}(1 - \overline{\nu^2})}{I_{vip}} \frac{1}{1 + \frac{6}{a\left(3l - 4a\right)} \frac{(EI)_{vip}}{(GA)_{vip}}} \qquad \text{(A610.5)}.$$

Both equations can be written in a general form as

$$E_{eff} = \frac{(EI)_{vip}(1-\overline{\nu^2})}{I_{vip}} \frac{1}{1+\xi \dfrac{(EI)_{vip}}{(GA)_{vip}}} \qquad \text{(A610.6),}$$

with ξ [m^{-2}] a factor depending on span, load-to-span distance and the type of loading. Figure 6.3 gives an overview of this ξ-factor for several load cases.

A611 PRACTICAL CONSIDERATION: INCREASING THE VIP'S BENDING STIFFNESS

As shown previously, the bending stiffness of a vacuum insulation panel primarily depends on the Young's modulus and thickness of the core material and the Young's modulus and thickness of the barrier envelope. Most of these properties are however determined by other reasons than structural reasons.

To minimise thermal bridge effects, the thickness of the barrier laminate is chosen as thin as possible, as a trade-off between high thermal performance and low gas transmission rates. For vacuum insulation panels, special barrier laminates have therefore been developed by industry, several of which were discussed in chapter 2. From a thermal perspective, the most favourable laminates are those based upon (metallised) polymers while from a service life perspective the most favourable laminates contain an aluminium or stainless steel foil. The thickness and Young's modulus of the barrier laminate are therefore not determined by structural reasons.

Besides, the type of core material is primarily determined by a combination of thermal performance and desired service life. A fine pore size and optimal pore size distribution result in favourable thermal behaviour, an open pore structure results in the ability to evacuate the system while sufficient structural cohesion enables the core to withstand a 1 bar pressure difference. As a result of these considerations, fumed silica and aerogels are good solutions to serve as VIP core. The type of core material in general is thus not determined by preferred bending behaviour either.

Moreover, the thickness of the core material is mainly determined by a trade-off between thermal behaviour and service life on the one hand and minimised material use and architectural appearance on the other hand. High Thermal performance and increased service life require the panel to be as thick as possible whereas minimised material use requires the panel to be as thin as possible. Another factor might be added too: structural behaviour. For high bending stiffness, the core material should be as thick as possible since it then increases the distance between the centroids of the top and bottom barrier laminate. Apart from structural performance the core material should therefore be chosen as thin as possible with thermal behaviour (and service life) as minimum requirement. However, in case a panel is structurally loaded in flexion, bending stiffness should be considered as well.

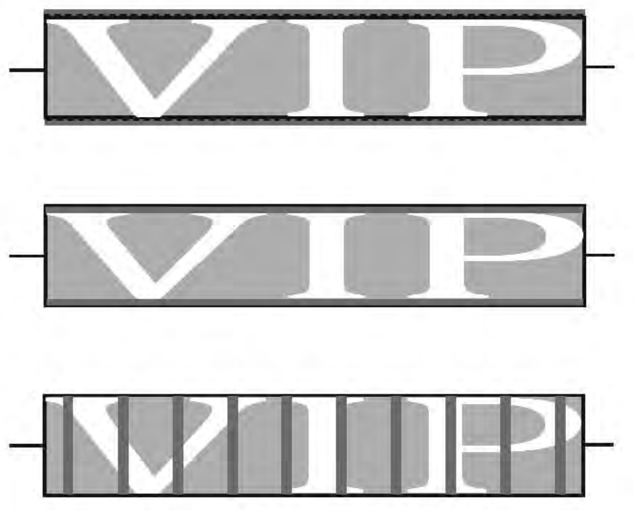

Figure A611.1

Methods of stiffening a vacuum insulation panel: glued plates outside the barrier envelope (top); in-plane plates inside the barrier envelope (middle); perpendicular plates inside the barrier envelope (bottom).

If we are now interested in keeping the VIP as thin as possible while still giving it sufficient bending stiffness to withstand wind pressure, we must seek other ways of increasing the bending stiffness than increasing the core's thickness or changing the materials used to make up a VIP. If the shape of a panel is beyond consideration, one way of increasing the stiffness would then be adding stiffening elements. Such stiffening elements could be conceived in three ways.

The first type of stiffening element would be a thin metal plate glued on top of the VIP's barrier laminate outside its perimeter, as presented in Figure A611.1 (top). If the connection between the plate and the barrier laminate is perfect (perfect adhesion) and friction between core and laminate is high, no sliding of this plate over the laminate and of this laminate over the core occurs and the composite system might phenomenologically be considered as a regular VIP with increased thickness of the top and bottom barrier laminate[31]. The model for calculating the bending stiffness of a VIP developed in section 6.3 could now be used for calculating the bending stiffness of this type of stiffened VIP, as long as the thickness of the top and barrier laminate is the sum of the thickness of the barrier laminate and the stiffening plate and its Young's modulus is an area-weighted average of both the laminate and the plate. However, a good connection between plate and laminate is necessary but difficult to obtain, as we will see in chapter 8.

The second type of stiffening element is similar to the one described in the previous paragraph, however with a different position. It no longer is outside the

[31] Or alternatively as a sandwich panel.

perimeter of the VIP but placed between the core material and the barrier envelope, as can be seen from Figure A611.1 (middle). No adhesive is required as long as friction between core and plate on the one hand and plate and laminate on the other hand is sufficient to connect all elements to a structural composite. Also for this model, the E-model developed in section 6.3 can be used for calculating the bending stiffness of this structurally improved VIP with the same modifications as made in the previous paragraph.

The third type of stiffening element consists of a series of (equidistantly spaced) plates perpendicular to the main surface of the VIP, as can be seen from Figure A611.1 (bottom). However, safe structural behaviour is not certain since again friction is required to keep the plates aligned with the core material. If friction is insufficient the core between the stiffening elements might deflect more under a bending load than the stiffening elements as a consequence of which these stiffening elements might puncture and damage the barrier envelope. Moreover, the stiffening plates form a direct high thermal conductivity connection from one side of the panel to the other side, thus forming a thermal bridge which significantly reduces the thermal performance of the entire panel. This option is therefore no viable solution.

Since the second option for stiffening a vacuum insulation panel seems to be most promising, it is theoretically studied in more detail here. A 4 cm thick vacuum insulation panel with a fumed silica core and a three-layer metallised barrier laminate is used as an example. The bending stiffness of such a vacuum insulation panel[32] under four-point loading with a span of 1200 mm and loads acting at quarter span distance, would according to section 6.3 approximately be $1.44 \cdot 10^2$ N·m² or $1.43 \cdot 10^2$ N·m² based upon E_{eq} (26.7 MPa) or $E_{eq;eff}$ (26.4 MPa) respectively[33]. If now a 1 mm thick aluminium plate is added between the both the top and bottom barrier laminate and the core, the bending stiffness increases to approximately $5.03 \cdot 10^4$ N·m² or $1.12 \cdot 10^4$ N·m² based upon E_{eq} ($9.30 \cdot 10^3$ MPa) or $E_{eq;eff}$ ($2.08 \cdot 10^3$ MPa) respectively[34]. Adding a 1 mm thick aluminium stiffener according to type 2, thus increases the bending stiffness approximately one to two orders of magnitude. It must however be noted that this considerable increase only occurs if friction results in good adhesion between the stiffener and the laminate on the one hand and the stiffener and the core on the other hand. In all other cases the bending stiffness will lie between the bending stiffness of the non-stiffened and perfectly stiffened VIP. In any case, the bending stiffness of the composite system will increase.

---

[32] The material properties of the constituents are discussed previously in this chapter.

[33] w_c = 1 m.

[34] It is important to realise that the thickness of the core decreases from 40 mm to 38 mm.

Table A611.1 *– Flexion modulus of several insulation materials (Simmler et al., 2005; http://www.matweb.com/)*

Core material	Flexion Modulus (MPa)
Extruded Polystyrene foam	1 - 3
Expanded Polystyrene foam	6 - 10
Polyurethane foam	3 - 8
Pressed fumed silica powder board	2.3 – 8.9

Notwithstanding improved structural behaviour, the panel's thermal performance is affected negatively by adding a highly thermally conducting layer on top and at the bottom of a VIP. This stiffening plate increases the heat deflection from the surface of the panel towards the corner and thus increases the thermal bridge effect. The extent of this bridge effect, i.e. the change in linear thermal transmittance, can be calculated either using the thermal bridge model for VIPs developed in chapter 3 or for building panels derived in chapter 4. If the same vacuum insulation panel without stiffening plates as described in the previous paragraph is used, a linear thermal transmittance of $1.65 \cdot 10^{-3}$ $W \cdot m^{-1} \cdot K^{-1}$ is obtained using either model[35]. The effective U-value thus becomes: $U_{eff} = 9.83 \cdot 10^{-2} + 1.65 \cdot 10^{-3}\ l_p/S_p$ $W \cdot m^{-2} \cdot K^{-1}$. If on both sides of the panel between the barrier laminate and the core a 1 mm thick aluminium plate is added, the linear thermal transmittance increases to $1.98 \cdot 10^{-3}$ $W \cdot m^{-1} \cdot K^{-1}$ according to model 1 and $1.99 \cdot 10^{-3}$ $W \cdot m^{-1} \cdot K^{-1}$ according to model 2[36]. As a result the effective U-value of the panel has increased to[37] $U_{eff} = 1.03 \cdot 10^{-1} + 1.99 \cdot 10^{-3}\ l_p/S_p$ $W \cdot m^{-2} \cdot K^{-1}$, which is moderately higher. As can be observed, though, this increase, which is in the order of 20%, is acceptable since a significant increase in bending stiffness is obtained while only a moderate decrease in thermal performance is observed. Stiffening a vacuum insulation panel by adding two 1 mm thick aluminium plates between the barrier laminate and the core might thus be a good solution if improved bending stiffness is required and provided that friction results in sufficient ability to transfer shear stresses between all constituents.

---

[35] $\lambda_c = 4 \cdot 10^{-3}$ $W \cdot m^{-1} \cdot K^{-1}$; $\alpha_i = 7.8$ $W \cdot m^{-2} \cdot K^{-1}$; $\alpha_e = 25$ $W \cdot m^{-2} \cdot K^{-1}$; $\varphi = 0.67$.

[36] $\lambda_c = 4 \cdot 10^{-3}$ $W \cdot m^{-1} \cdot K^{-1}$; $\alpha_i = 7.8$ $W \cdot m^{-2} \cdot K^{-1}$; $\alpha_e = 25$ $W \cdot m^{-2} \cdot K^{-1}$; $\varphi = 0.67$; $\lambda_{alu} = 225$ $W \cdot m^{-1} \cdot K^{-1}$.

[37] Due to the added stiffening plates the thickness of the core is reduced with 2 mm.

A612 Excerpts from Movie: The Effect of a Vacuum on Stiffness

0:00:01.74

0:00:05.49

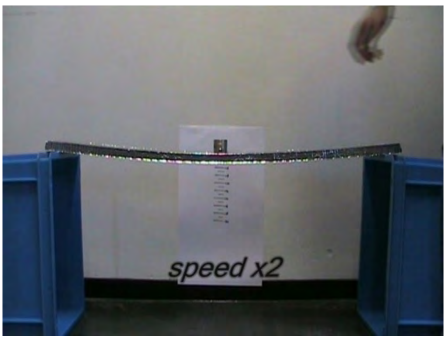

0:00:12.68

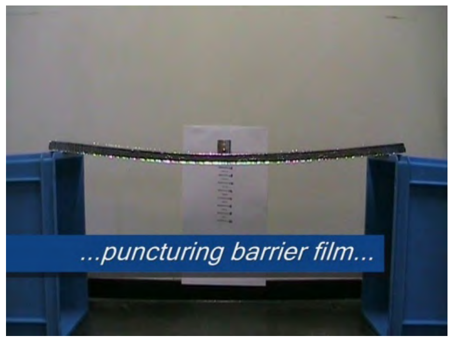

0:00:14.18

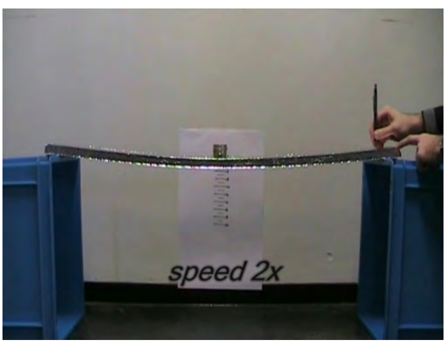

0:00:21.77

0:00:27.15

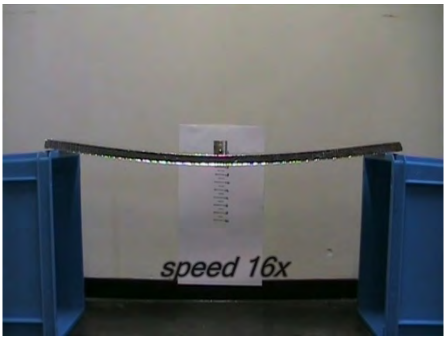

0:00:38.26

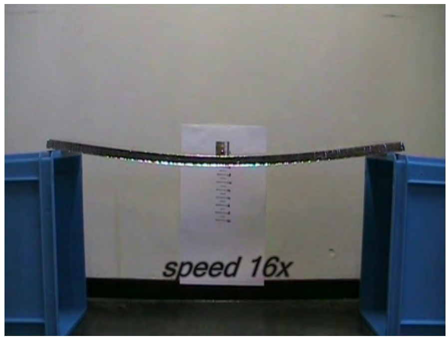

0:00:43.11

0:00:47.52

0:00:52.95

0:00:58.21

0:01:02.75

Time indicated is virtual (movie) time and not actual time. In real time the entire process took about 9 minutes.

A613 MECHANICAL PROPERTIES OF FUMED SILICA: COMPRESSION

One of the main constituents of a vacuum insulation panel is the core. Core materials must fulfil several requirements in a VIP:

- It must be 100% open-porous so that it can be evacuated completely;
- It must have small pore sizes so that a relatively high gas pressure is allowed before the service life expires;
- It must have the ability to take up opacifiers so that radiation heat transfer is reduced;
- It must have sufficient compressive strength so that a pressure force of 1 mbar (=100 kPa) is absorbed without mechanical failure and too high dimensional changes.

In this appendix, the last requirement will be subject of study. The mechanical properties of fumed silica as a VIP core material both determined during compression and flexion tests are presented. 'Dynamic' mechanical properties like dynamic Young's modulus and dynamic stiffness, which are relevant for acoustic applications, are discussed in chapter 9.

Compression

During the IEA/ECBCS Annex 39 project (Simmler et al., 2005), compression tests on two types of fumed silica (specimen sizes were 60x50x20 mm^3) according to French standard NF T 56 101 (1976) have been conducted at CSTB in Grenoble. The specimens were tested at two different conditions:

- Condition 1: tests immediately after opening the high barrier envelope (dry);
- Condition 2: tests after storing the samples at 23°C and 50% RH for 13 days.

Table A613.1 *- Compression behaviour of two types of fumed silica (Simmler et al., 2005).*

condition	Material	compressive stress [kPa] at x% compression		
		10%	25%	40%
1	SIL 1	142	408	835
	SIL 2	108	325	630
2	SIL 1	92	264	555
	SIL 2	90	274	521

NB: test speed is 10 $mm \cdot min^{-1}$

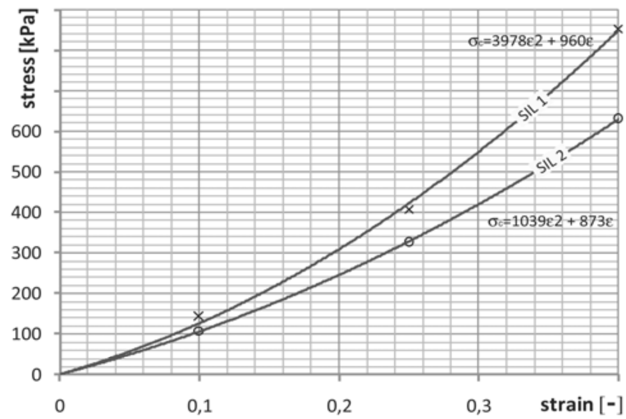

Figure A613.1

Compression behaviour of fumed silica samples under condition 1 (data from Simmler et al., 2005).

Table A613.1 and figure A613.1 present the results of these compression tests. At least two effects can be seen from Table A613.1. First, the effect of water / water vapour inside the core material is clearly visible by a reduction of the compressive stress by about 35% for SIL1 and 20% for SIL2. It is thus important to realise that stress relaxation will occur during the service life of a VIP as the water content of and water vapour pressure inside the core will increase to equilibrium with its surroundings. Second, due to evacuation a pressure will act upon the core material equal to 100 kPa resulting in a deformation of the panel of about 10%. As a consequence, the thickness of a fumed silica board will decrease with this same amount during the evacuation process. This effect clearly needs to be considered by VIP manufacturers.

APPENDIXES TO CHAPTER 7 A

A71 MATHEMATICAL SUBSTANTIATION OF EXISTENCE OF MAXIMUM IN THERMAL PERFORMANCE FOR EPS ENCAPSULATED VIPS

It was observed that for EPS encapsulated VIPs a local maximum in thermal performance exists at a certain thickness of the VIP inside. So, there is a local minimum in total heat flow through such a component at a specific VIP thickness. Mathematically, such a minimum in heat flow should occur where the derivative of the total heat flow to the VIP thickness equals zero. Since the linear thermal transmittance model developed in chapter 4 is far too complex to determine this derivative, the following is assumed:

- As a simplification, the heat flow through the thermal bridge can be calculated using the equation for calculating the linear thermal transmittance of a VIP with λ_c = 0 W·m^{-1}·K^{-1}.

Using this assumption, the heat flow through the thermal bridge then becomes:

$$\frac{\phi_{q,kobru}}{\Delta T} = \psi_{vip,edge,0} = \frac{1}{\dfrac{d_p}{t_f' \lambda_f'} + \dfrac{1}{\sqrt{\alpha_1^* t_f \lambda_f}} + \dfrac{1}{\sqrt{\alpha_2^* t_f \lambda_f}}} \qquad \text{(A71.1)},$$

with α_j^* [W·m^{-2}·K^{-1}] modified boundary heat transfer coefficients calculated as

$$\alpha_j^* = \left(\frac{1}{\alpha_j} + \frac{0.1 - d_p}{2\lambda_{eps}} \right)^{-1} \qquad \text{(A71.2)}.$$

In this linear thermal transmittance both the effect of the aluminium foil based barrier laminate and the EPS strip at the component's edge are included. They are included in the product $\lambda_f' t_f'$ according to the method specified in section 3.3.5 for air gaps at the edge of a VIP.

The heat flow trough the centre-of-panel area can be determined from

$$\frac{\phi_{q,cop}}{\Delta T} = \frac{b}{R_{cop}} \approx b \left(\frac{d_p}{\lambda_c} + \frac{1}{\alpha_1^*} + \frac{1}{\alpha_2^*} \right)^{-1} \qquad \text{(A71.3)},$$

Total heat flow through the EPS encapsulated VIP now equals the sum of both heat flows. If we now take the derivative of this total heat flow divided by ΔT to the VIP thickness, d_p, we obtain

$$\frac{d}{dd_p}\left(\frac{\phi_q}{\Delta T}\right) = -\psi^2_{vip,edge,0}\left(\frac{1}{t'_f\lambda'_f} - \frac{\sqrt{\alpha_1^*}+\sqrt{\alpha_2^*}}{4\lambda_{eps}\sqrt{t_f\lambda_f}}\right) - b\left(\frac{1}{\lambda_c}-\frac{1}{\lambda_{eps}}\right)\left(\frac{d_p}{\lambda_c}+\frac{1}{\alpha_1^*}+\frac{1}{\alpha_2^*}\right)^{-2} \quad \text{(A71.4).}$$

A local maximum in thermal performance can now be found where this derivative equals zero, or

$$\frac{d}{dd_p}\left(\frac{\phi_q}{\Delta T}\right) = 0 \quad \text{(A71.5).}$$

As shown in Figure 7.13 in the main body of the text, for certain components this derivative indeed equals zero at a certain thickness of the vacuum insulation panel. Bearing in mind the simplifying assumption made in this appendix, this derivative thus proofs the existence of a local maximum in thermal performance of certain EPS encapsulated VIPs at a certain thickness of the VIP. For complex 3-dimensional components, the position of this local maximum value in thermal performance should be determined using numerical simulation software.

APPENDIXES TO CHAPTER 8

A

A81 MODEL FOR COMPUTING RELATIVE HUMIDITY IN AIR CAVITY OF M-PANEL

To investigate the changes in relative humidity of the air inside the cavity between a vacuum insulation panel incorporated into a building component and the membrane of an M-panel, a prediction model based on mass balance equations was derived. This prediction model is based on the following assumptions:

- The air inside the cavity is perfectly mixed as a result of which a one-node model can be used to estimate the relative humidity of the thin air layer.

- The air cavity can be schematized as a water-vapour tight system, i.e. no interaction between the water vapour inside the system (wooden encasing, membrane and air gap) and outside the system (surrounding air) occurs. This assumption is plausible because the panels investigated have a 0.5 mm thick membrane sealing of the air cavity. A small amount of air exchange might in practice though occur through the wooden encasing along the component's perimeter. This effect is neglected. Moreover, due to a temperature increase or decrease of the air inside this cavity, the air volume will increase or decrease likewise. This effect which changes the relative humidity inside the air cavity is neglected, too.

- The sorption curve of the encasings is temperature dependent. It is assumed that the sorption-curve of Accoya wood equals the one of Radiata Pine, which is the species of wood used for producing Accoya. This sorption-curve can be described as (Ball et al., 2001)

  $$u \cdot 100\% = \left[-\frac{\log(1-\phi)}{A} \right]^{1/B} \qquad \text{(A81.1a)},$$

  with

  $$A = \exp(-5.30)\left(\frac{T}{300}\right)^{12.0} \qquad \text{(A81.1b)},$$

  $$B = \exp(2.21)\left(\frac{T}{300}\right)^{-1.36} \qquad \text{(A81.1c)},$$

  and ϕ [-] the relative humidity, u [kg·kg^{-1}] the water content, and T [K] the temperature.

- The condition of thermodynamic equilibrium is always fulfilled.

This closed system can be schematically represented as in Figure A81.1.

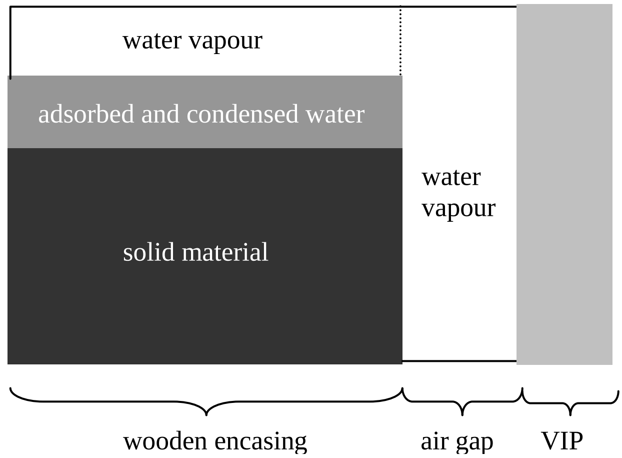

Figure A81.1

Schematic representation of vapour closed moisture system with volume equations.

volume wooden encasing:	V_{wood}
volume air cavity:	V_{airgap}
volume solid material:	$V_s = (1-\varepsilon)\cdot V_{wood}$
volume 'liquid' water:	$V_l = u\dfrac{\rho_{dry}}{\rho_w}\cdot V_{wood}$
pore volume:	$V_p = \varepsilon \cdot V_{wood}$
volume water vapour:	$V_v = (V_p - V_l) + V_{airgap}$

The total amount of water present in the closed system, m_w [kg], consists of water vapour, m_v [kg], and adsorbed and condensed water, m_l [kg]:

$$m_w = m_v + m_l \qquad \text{(A81.2).}$$

The amount of water vapour and adsorbed and condensed water can be obtained from multiplying the volume with the water vapour concentration, $c_{w;v}$ [kg m^{-3}], or water density, ρ_w [kg m^{-3}], respectively, resulting in

$$m_w = V_v \cdot c_{w;v} + V_l \cdot \rho_w \qquad \text{(A81.3).}$$

Combining the volume equations with equation (A81.3) yields

$$m_w = \left[(\varepsilon - u\frac{\rho_{dry}}{\rho_w})V_{wood} + V_{airgap} \right] c_{w;v} + u\frac{\rho_{dry}}{\rho_w}\rho_w V_{wood} \quad \text{(A81.4)},$$

in which ε [-] is the porosity (assumed 0.4), ρ_{dry} [kg·m^{-3}] is the density of dry Accoya wood (between 450 and 550 kg·m^{-3} (Titan Wood, 2009)) and ρ_w [kg·m^{-3}] is the density of water (ρ_w = 1000 kg·m^{-3}). Finally, the water vapour concentration, $c_{w;v}$, can according to the perfect gas law be written as a function of relative humidity, ϕ, and saturation pressure, p_{sat}, leading to

$$m_w = \left[(\varepsilon - u\frac{\rho_{dry}}{\rho_w})V_{wood} + V_{airgap} \right] \frac{\phi p_{sat} M_w}{RT} + u\rho_{dry}V_{wood} \quad \text{(A81.5)},$$

with R [J·mol^{-1}·K^{-1}] the universal gas constant (R = 8.31 J·mol^{-1}·K^{-1}), M_w [kg·mol^{-1}] the molar mass of water ($M_w = 1.8 \cdot 10^{-2}$ kg·mol^{-1}) and T [K] the absolute temperature. Since no water exchange with the environment occurs, m_w is constant for each time step. If for each time step the temperature is known, then the relative humidity inside the cavity can be computed for each time step, too.

Originally vacuum insulation panels have been developed for consumer goods and transport boxes. Required long service lives for buildings and the fragility of the product, however, among others impeded architectural applications. Yet, over the last few years, several buildings have been erected in Europe in which VIPs have been applied. In most of these buildings, the original core material of the VIP, open-porous polymer foam, was replaced by fumed silica, outperforming polymer foams on service life by several decades. Table A82.1 presents an overview of demonstration projects in Europe in which VIPs are applied[38]. Two of these projects will be discussed in more detail below.

Apartment and office block in München, Germany, by Pool Architekten

In the summer of 2004, the first building in Europe completely insulated with vacuum insulation panels was completed. The combined apartment and office block is located in the city centre of München (Germany) and is designed by Martin Pool from Pool Architekten. Despite the location in a densely urban environment, the building lot provides sufficient possibility for daylight and sun penetration into the building, even at the first floor. Figure A82.1 presents an image of the appearance of the building.

Figure A82.1

Office and apartment building in München designed by Pool Architekten (Pool, 2005).

[38] A detailed description of these projects can be found in the sources mentioned in the table.

Table A82.1 *– Selection of demonstration projects in which VIPs have been applied.*

nr	building	location	year	application area
01	test façade, building ZAE-Bayern	Würzburg (D)	1998	
02	semi-detached house	Nürnberg (D)	2000	façade insulation in rail system
03	Single-family house	Leimbach (CH)	2000	terrace insulation (in EPS)
04	passive houses	Wolfurt (A)	2000	terrace insulation
05	Single-family house	Meilen (CH)	2000	Roller-blind boxes
06	Cepheus project (dwellings)	Kassel (D)	2000	filler panels in doors
07	Extension of hospital	Erlenbach (D)	2001	prefab façade panels
08	Allgäu Energy and Environment Centre (eza! House)	Kempten (D)	2001	floor
09	one-family house Sunny Woods	Zürich (CH)	2001	at several critical places
10	gymnastics hall	Gemünden (D)	2001	floor
11	office building	Allgäu (D)	2001	façade system
12	terraced house	München (D)	2001	complete building envelope
13	semi-detached wooden house: 2-liter-house	München (D)	2002	outside walls, roof and door
14	historic court house	Schaffhausen (D)	2002	floor
15	passive house	Bersenbrück (D)	2002/3	façade
16	multi-family house	Zürich (CH)	2003	Façade, dormer window
17	multi-family houses	Kerzers (CH)	2003	terrace insulation
18	Single-family house	Landschlacht(CH	2003	non-load bearing sandwich panels
19	former church	Wernfeld (D)	2003	wall heating system
20	terraced passive house in Petrisberg	Trier (D)	2004	façade
21	apartment and office block	München (D)	2004	roof and façade
22	Kindertagesstätte Plappersnut	Wismar (D)	2004	prefab façade elements
23	Building of Fraunhofer ISE	Freiburg (D)	2004	façades
24	Single-family house	Zossen (D)	2004	terrace insulation
25	gymnastics hall	Nürnberg (D)	2004	floor insulation
26	fire station	Gerbrunn (D)	2004	window parapet insulation
27	dwelling with office	Ravensburg (D)	2004	insulated prefab concrete elements
28	terraced houses	Binningen (CH)	2005	prefab façade panels
29	multi-family houses	Hofheim (D)	2005	façade (large prefab comp)
30	Sonnenschiff	Freiburg (D)	2006	Façade elements
31	Education room for factory Hasit	Schwarzenfeld(D)	2007	floor insulation / heating
32	Single-family house	Doorn (NL)	2008	part of facade

***Table A82.1** – Continuation of table (R=refurbishment; N=new building).*

nr		architects / planners	sources
01	R	prof. Volz	Schwab et al, 2003 / Fricke et al., 2006
02	R	fa. Schös Trockenbau	Binz et al., 2005 / Fricke et al., 2006 / Schwab et al., 2003
03	R		Materna, 2001
04	N	G. Zweier	Materna, 2001 / Eicher et al., 2000
05	R		Materna, 2001
06	N	prof. Schneider / HHS / ASP	Feist, 2001
07	N	fa. Glaskeil GmbH & Co	Binz et al., 2005 / Schwab et al., 2003
08	R	Bayosan Wachter / Prill & Schurr Architects	Binz et al., 2005 / Schwab et al., 2003
09	N	B. Kämpfen	Kämpfen, 2003
10	R	Rosel Engineering	Binz et al., 2005 / Schwab et al., 2003
11	N		Noware, 2005
12	R	M. Neumann (Lichtblau Architekten)	Binz et al., 2005 / Lichtblau and Jendges, 2005 / Schwab et al., 2003 / Beck et al., 2007
13	N	N. Jendges (Lichtblau Architekten)	Binz et al., 2005 / Lichtblau and Jendges, 2005 / Fricke et al., 2006 / Schwab et al., 2003
14	R	Mion AG / Arch. Rolf Lüscher	Binz et al., 2005
15	N	Sto AG	Binz et al., 2005 / Zwerger, 2005
16	R	A. Büsser (Viridén & Partner)	Binz et al., 2005 / Viriden et al., 2004
17	N	P. Kunz (3D Architecten)	Binz et al., 2005
18	N	Architecturbüro Beat Consoni	Binz et al., 2005
19	R	W. Haase (Architekturbüro Haase + Partner)	Binz et al., 2005 / Va-Q-tec brochure / Schwab et al., 2003
20	N	Lamberty/Schmitz & Hoffmann Architecten	Binz et al., 2005 / Ferle, 2005 / Zwerger, 2005
21	N	M. Pool (Pool Architekten)	Binz et al., 2005 / Pool, 2005 / Pool, 2009
22	R		Winkler, 2005
23	R		Zwerger, 2005
24	R		Hasse, 2005
25	R	Va-Q-tec AG	Va-Q-tec brochure
26	N		Va-Q-tec brochure / Schwab et al., 2003
27	N	Weinbrenner.Single / Hangleiter GmbH	Binz et al., 2005 / Hangleiter, 2005 / Hangleiter and Weismann, 2006
28	N	Feiner and Pestalozzi	Binz et al., 2005 / Noware, 2005
29	R	Planungsgruppe Drei	Grossklos, 2005 / Diefenbach and Grossklos, 2007
32	N	Architekturbüro Rolf Disch	Disch, 2007
31	R	Effidur GmbH	Wieleba, 2007
32	N	M. Thijssen	Direct contact to architect

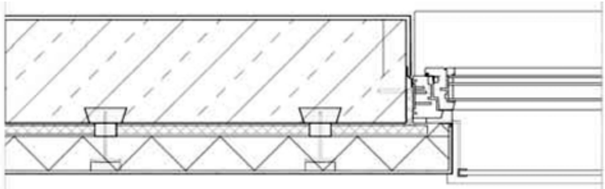

Figure A82.2

Construction detail of the façade of the office and apartment building in München designed by Pool Architekten (Pool, 2005).

Figure A82.3

Checking the internal vacuum of the VIPs (Binz et al., 2005).

In this project the application of vacuum insulation panels was favoured over conventional insulation materials allowing a maximisation of usable built volume or floor space area at the same time creating a highly energy-efficient building. The energy consumption of the building for heating and hot water preparation lays around 20 kWh per square meter usable floor space area per year, which is substantially below the average annual energy consumption of office and apartment buildings in München (200 $kWh \cdot m^{-2} \cdot yr^{-1}$) and even below regional low energy standards (30 to 70 $kWh \cdot m^{-2} \cdot yr^{-1}$) (Pool, 2005). Not only vacuum insulation contributes to this low energy demand but also the compact shape of the building, the optimised position and size of windows, balanced ventilation with heat recovery and natural cooling using groundwater. Due to the application of VIPs, the thickness of the insulation layer in the façade could be reduced from about 25 cm with conventional materials to only 11 cm with VIPs (2 cm VIP + 9 cm additional insulation). In total this resulted in additional floor space area of about 250 m^2 which is about 10% of the total usable floor area of the building (Pool, 2005).

In this project, vacuum insulation panels are applied as thermal insulation of the façades and of the roof terraces. For both application areas VIPs are applied in-situ, so that careful handling of the panels was required. In general, prefabricated applications are preferred to in-situ application since the risk of damage is reduced in that way. Figures A82.2 and A82.3 give a detailed drawing of a cross-section through a piece of the façade and a photograph of the construction process. The advantages of using VIPs in this project are among others the increased usable floor space area and thin window frames allowing maximum daylight and sun penetration. Drawbacks are among others risk of applying an unconventional building material, higher investment costs, additional construction time, more careful design and planning and the risk of damage because of in-situ application. Despite these drawbacks, the overall balance of the application of VIPs in this project was evaluated positively by the architects and contractor (Binz et al., 2005).

Office with apartment in Ravensburg, Germany, by Weinbrenner.Single Architects

This demonstration building, shown in Figure A82.4, was more-or-less the outcome of a research project aimed at developing VIP-integrated prefabricated concrete elements suitable for application in buildings complying to passivhaus standard. These prefabricated insulated concrete elements, designed by Matthias Hangleiter, consist of a concrete layer of 15 cm on top of which a sandwich of 3 cm PU-foam, 3 cm VIP and a watertight film is laid. Within the seams, several anchors are placed serving as supports for vertical laths that keep the insulation layer in place and as the connecting points for the façade cladding, as can be seen from Figure A82.5. These concrete façade elements are 27 to 35 cm thick in total and have an average U-value of 0.15 $W \cdot m^{-2} \cdot K^{-1}$ (Hangleiter, 2005).

This demonstration building designed by Weinbrenner.Single Architects consists of a dwelling and an office and was completed at the start of 2005. The building is located in Ravensburg, a small city in the southern part of Germany. The façades of the building are either made of glass or of the aforementioned concrete components placed strictly in a grid to allow for standardisation of façade components.

The main advantages of applying VIPs in this project are again thin façade constructions (resulting in more usable space and psychological effects) and high thermal performance of the building skin. Hangleiter (2005) even shows that in a single-family house of approximately 150 m^2 the application of VIPs could reduce the effective building costs, despite the relatively high costs of the insulation material. Prefabrication of VIPs into building components in a manufacturing plant has several advantages over on-site application. First, by integrating a VIP into a component in the manufacturing plant already, the VIP is inherently protected

Figure A82.4

Drawing of the west-façade of the Ravensburg office and dwelling (Hangleiter, 2005).

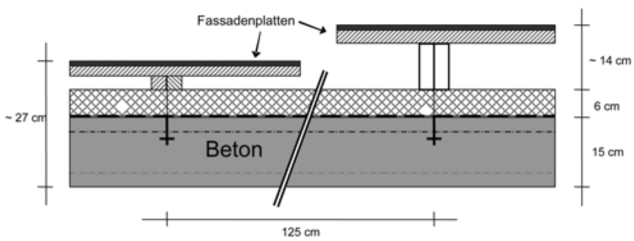

Figure A82.5

Detailed drawing of the prefab VIP-integrated concrete components of the Ravensburg building (Hangleiter, 2005).

during transportation to the building site and subsequent storage. Second, the VIP can be integrated into a building construction under controlled environmental conditions, with high quality equipment and with smaller tolerances. Third, high skilled labour is transferred from the building site to the manufacturing plant. And fourth, the VIPs incorporated in many components are replaceable thus guaranteeing the possibility of 'repairing' a façade from a thermal perspective. Prefabrication is therefore preferred to on-site application.

Disadvantages of this concrete component however relate to the impossibility of checking the quality of the panels after installation, i.e. checking whether the core is still under vacuum. Typical on-site quality assurance tools use infrared thermography, which requires that the individual VIPs can be 'seen' by the camera, which is impossible if the panels are installed behind a thick well-conducting material or in a back-ventilated façade.

Non-Project Related Building Products

Since integration of vacuum insulation panels in prefabricated components is favoured over in-situ application, several manufacturers have developed such components. An excerpt of these products available on the market is presented in Table A82.2. The advantages of such prefabricated components are among others the protection of the VIP inside, smaller dimensional tolerances, less labour on the building site and a controlled production environment with highly skilled labourers. As an example, one of these VIP incorporated products, is discussed below: a façade design by Jan Cremers. This design is briefly discussed since it fundamentally considers the properties of VIPs and tries to use the advantages and considerately overcome the disadvantages of the application of VIPs in façade systems.

Moreover, Skottke and Willems (2009) attempt to develop a glass coated vacuum insulation sandwich consisting of a core of micro fibre or polymeric foam insulation, two glass sheets and an edge of polymeric foam and adhesive. The advantages of this system are that no VIP needs to be additionally integrated into a component – the system already is a component -, that it is hardly damageable, and that it has a high thermal performance according to calculations (Skottke and Willems, 2009). Disadvantages might be that a high quality seal is hard to obtain by the spacer along the component's edge made of polymeric foam and that as with sheet-based vacuum insulation panels high cost might be involved.

***Table A82.2** – Selection of sheet-VIP integrated products for the construction sector available on the market already (except for number 12).*

nr	product type	manufacturer	sources
01	Vakupaneel - VIP in double-glazing type of system	Metallbau Ralf Boetker GmbH	Ebert, 2003
02	Klimapaneel - integrated façade element with radiator	Metallbau Ralf Boetker GmbH	Binz et al., 2005 / Ebert, 2003 / Ebert, 2005
03	Vacupur - VIPs foamed into PU-insulation for sandwich panels and doors	Fa. Variotec GmbH &Co KG	Stölzel, 2003
04	Energyframe – VIP integrated window frames	Fa. Variotec GmbH &Co KG	Stölzel, 2003/ Variotec, 2007
05	Qasa – VIP integrated products as problem solver	Fa. Variotec GmbH &Co KG	Forstner, 2007 / Eberlein, 2007 / Stölzel, 2007 / Variotec, 2007
07	vacuum insulated bricks	Fa. Georg Rimmele KG	Schupp, 2003
07	VIP in double-glazing type of system	Linzmeier Bauelemente GmbH	Luib, 2005
08	VIP in double-glazing type of system	Schüco GmbH	Schneider, 2003
09	Brunex doors	Brunegg AG	
10	insulated boiler		
11	roller blinds	fa. Denk-Rolladentechnik aus Gangkofen	Cremers, 2006
12	Thermobel VIP - façade panels	AGC Flat Glass Europe	Mooi, 2009
13	conceptual façade design for large span membrane walls	J. Cremers	Cremers, 2006 / Cremers, 2006

PRINCIPAL DESIGN OF MEMBRANE FAÇADE BY JAN CREMERS

In the framework of a PhD study at the Technical University of München (Cremers, 2006), Jan Cremers designed a membrane-like wall consisting of two layers of VIP on both sides protected by a metallic or polymeric sheet, and stabilised by either a cable or a membrane structure. Three different variants were conceptually developed, one of which was then manufactured as a prototype. These variants are presented in Figure A82.6. In variant 1, no external protective sheet is present, while in variants 2 (Figure A82.7) and 3 an external sheet protects the VIP against environmental influences and mechanical damage. The difference between variants 2 and 3 results from the way in which the façade is stabilised: variant 2 uses a pre-stressed cable structure, while variant 3 uses a thin pre-stressed membrane.

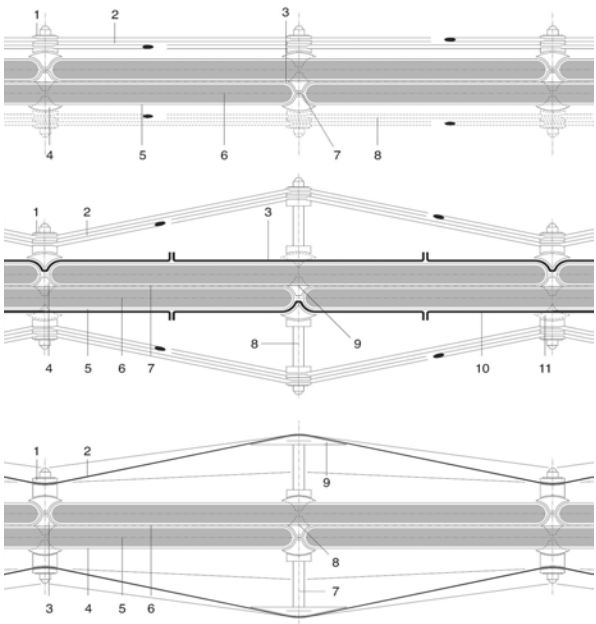

Figure A82.6

Principal designs by Cremers for a thin membrane-like building skin based upon vacuum insulation panels (Cremers, 2006).

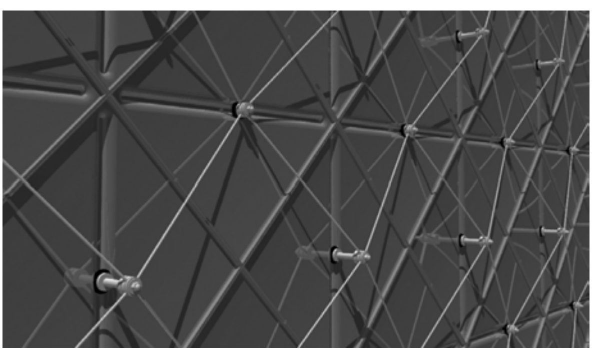

Figure A82.7

Artist impression by Cremers of principal façade design variant 2 (Cremers, 2006).

The advantages of applying VIPs in this façade system are that a very slim but thermally highly performing membrane-like wall is obtained[39] and that the properties of VIPs are considered thoughtfully. Disadvantages of this system are the impossibility of or at least difficulty with creating windows, the complexity of the details at the edge of the wall and the special requirements on the load bearing structure resulting from pre-stresses (Cremers, 2006). Moreover, acceptation by the construction industry might be slow due to the novelty of the system.

[39] The initial overall *U*-value of the façade systems lies between 0.10 and 0.12 $W \cdot m^{-2} \cdot K^{-1}$ if two layers of 30 mm VIP are used and between 0.08 and 0.10 $W \cdot m^{-2} \cdot K^{-1}$ if two layers of 40 mm VIP are used (Cremers, 2006).

A83 STRUCTURAL BOND BETWEEN VIP AND FACE SHEETS

At the laboratory of an adhesive supplier (Lubbinge, 2004), the possibility of adhering vacuum insulation panels with a metallized barrier film to different component facings, aimed at making sandwich components with a VIP core, was investigated. First, polyurethane adhesives commonly used by the façade industry and suitable for use with the barrier film were selected: Dynol U480 and U440. Peel strength tests with these glues resulted in peel strength values of 0.4 to 0.52 $N \cdot mm^{-1}$, which more-or-less equals the value stated by the manufacturer, but is significantly lower than the for panel fabrication desired value of more than 1.0 $N \cdot mm^{-1}$. This low peel strength is caused by delaminating of the polymer-aluminium interface within the barrier film. Different samples have also been tested on tensile strength in their flatwise plane according to ASTM C297 (1992), for which Dynol U480 was used as adhesive and Trespa as facing. During these measurements the vacuum insulation panels stay intact, while the adhesive between facing and VIP fails at normal stresses of 0.05 $N \cdot mm^{-2}$ to 0.11 $N \cdot mm^{-2}$ for panels of 110x110 mm^2. These same tests were not only performed with the adhesive U480, but also with U440, U462, UD400 UD402 and E202, resulting in similar failure behaviour. Even surface modifications of the barrier film, like oxidizing and priming, for better adhesion, do not change the failure behaviour significantly. Possibly, a UV/ozone treatment of the barrier film may improve the bonding between film and adhesive. This treatment may however damage or age the barrier laminate resulting in a reduced service life of the vacuum insulation panel. Another potential surface treatment less risky might be a corona surface treatment. Since a thorough study of creating a perfect bond between face sheets and barrier laminate is outside the scope of this dissertation, the influence of such surface treatments on adhesion is not investigated further.

A84 Accoya® Wood

Accoya® wood is a type of wood recently introduced in the Netherlands by Titan Wood (Titan Wood, 2008). Starting point for producing Accoya® is a Pinus Radiata wood. By a process called wood acetylation (using Acetic Acid), the durability of this Pinus Radiata wood is increased considerable. According to Titan Wood (2008), Accoya® wood combines high durability (class 1), dimensional stability and UV resistance without compromising the material's strength, stiffness and thermal conductivity. According to Delichatsios et al. (2003), the thermal conductivity of Radiata Pine is 0.19 $W \cdot m^{-1} \cdot K^{-1}$. Titanwood (2008) states that the thermal conductivity of Accoya® wood is less than that of similar types of wood. For calculation purposes 0.19 $W \cdot m^{-1} \cdot K^{-1}$ will be used. According to Kamke (2006) the flexural Young's modulus of untreated Radiata Pine is approximately 9 GPa while treatments might increase it to over 15 GPa. According to Dutch standards however (NEN6760:2008) softwoods with a specific mass between 450 and 550 $kg \cdot m^{-3}$ have a representative flexural modulus of 16 GPa (class C50). This value will be used for calculation purposes.